https://ntrs.nasa.gov/search.jsp?R=19660005979 2018-05-25T16:43:40+00:00Z

2 copies left

GPO PRICE $ _____

CFSTI PRICE(S) $ _____

Hard copy (HC) 7.00

Microfiche (MF) 2.00

ff 653 July 65

FACILITY FORM 602

N66 15268 (ACCESSION NUMBER)

(THRU)

384 (PAGES)

1 (CODE)

CR 69235 (NASA CR OR TMX OR AD NUMBER)

31 (CATEGORY)

JET PROPULSION LABORATORY
CALIFORNIA INSTITUTE OF TECHNOLOGY
PASADENA, CALIFORNIA

RE-ORDER NO. 64-524

CONCEPTUAL DESIGN STUDIES OF AN ADVANCED MARINER SPACECRAFT

Volume IV

Flyby Bus Design

Prepared by

RESEARCH AND ADVANCED DEVELOPMENT DIVISION
AVCO CORPORATION
Wilmington, Massachusetts

This work was performed for the Jet Propulsion Laboratory, California Institute of Technology, sponsored by the National Aeronautics and Space Administration under Contract NAS7-100.

RAD-TR-64-36
Contract 950896

28 October 1964

Prepared for

CALIFORNIA INSTITUTE OF TECHNOLOGY
JET PROPULSION LABORATORY
4800 Oak Grove Drive
Pasadena, California

360 PAGES
INCLUDES
(17 ROMAN NUMERIALS)

RE-ORDER No. 64-524

This document consists of 362 pages,
200 copies, Series A

CONCEPTUAL DESIGN STUDIES OF AN ADVANCED MARINER SPACECRAFT

Volume IV
Flyby Bus Design

Prepared by

RESEARCH AND ADVANCED DEVELOPMENT DIVISION
AVCO CORPORATION
Wilmington, Massachusetts

RAD-TR-64-36
Contract 950896

28 October 1964

Prepared for

CALIFORNIA INSTITUTE OF TECHNOLOGY
JET PROPULSION LABORATORY
4800 Oak Grove Drive
Pasadena, California

II

RE-ORDER No. 64-524

CONTENTS

1.0 Design Study 1

1.1 Scope of Study 1
1.2 Design Objectives 3
1.3 Design Contraints 3
1.4 Design Evaluation 6
1.5 Conceptual Design 14
1.6 Parametric Design Study 25

2.0 Scientific Payload 37

2.1 Mission Objectives Analysis 37
2.2 Instrumentation List 47
2.3 Landing Site and Mapping Corridor 51
2.4 TV Mapping System 55
2.5 Gimbaled Payload Platform 71

3.0 Power Supply System 87

3.1 System Description 87
3.2 Battery 87
3.3 Solar Array 93

4.0 Communication System 103

4.1 Command Link 103
4.2 Tracking Link 108
4.3 Telemetry Link 110
4.4 Communication System Hardware 149

5.0 Command and Control 167

5.1 Guidance 167
5.2 Flight Command Subsystem 168

6.0 Propulsion System 174

6.1 Performance and Design Requirements 174
6.2 Parametric Design Data 175
6.3 Propulsion System Selection 175

RE-ORDER No. 64-524

CONTENTS (Concl'd)

7.0 Stabilization and Control System 188

7.1 Characteristics of Selected System 188
7.2 Rating System for Design Alternatives 194
7.3 Impulse Requirements 202
7.4 Subsystem Design 215

8.0 Structure 235

8.1 Conceptual Design 235
8.2 Parametric Variation 241

9.0 Thermal Control 243

9.1 Design Approach 243
9.2 Analytical Procedure 243
9.3 Design Parameters 246
9.4 Thermal Control During Mission Modes 250

10.0 Lander Separation System 265

10.1 Design Concept 265
10.2 Physical Arrangement 269
10.3 Sterilization 269
10.4 Separation Mechanism 272
10.5 Lander Stabilization 277
10.6 Lander Propulsion 279

A. Equations of Gimbal Motion 281
B. Comparative Reliability Analyses 309
C. Battery Weight Requirements as Determined by Maneuver Mode Operations 322
D. Separation Spring Analysis 334

4

RE-ORDER No. 64-524

TABLES

Table 1	Booster Launch Weight Capability	3
2	Periapsis Passing Distance	5
3	Characteristics and Performance of Flyby/Bus System	26
4	Flyby/Bus Weight Summary	27
5	Lander Separation System Weight Summary	29
6	Advanced Mariner Spacecraft Weights	29
7	Spacecraft Center of Gravity Location	35
8	Spacecraft Moments of Inertia	36
9	Flyby/Bus Science Measurements -- Atmosphere	39
10	Flyby/Bus Science Measurements -- Biosphere	41
11	Flyby/Bus Science Measurements -- Lithosphere	43
12	Flyby/Bus Science Measurements	45
13	JPL Instrumentation List for Flyby/Bus	48
14	Instrumentation For Advanced Flyby/Bus	50
15	TV Mapping System Parameters	56
16	Camera Parameters as a Function of Resolution	66
17	Glossary of Terms	89
18	Flyby/Bus Power System and Power Consumption List	90
19	Component Performance Data Supplied by Vendors	91
20	Components of Power Supply System	92
21	Glossary of Terms	104

5

RE-ORDER No. 64-524

TABLES (Cont'd)

Table 22 DSIF S-band Transmitter Capabilities 105

23 Assumed DSIF Receiver Characteristics 105

24 Telecommunications Design Control Chart -- DSIF to Flyby/Bus Command 106

25 Telecommunications Design Control Chart -- DSIF to Flyby/Bus Doppler Track 111

26 Telecommunications Design Control Chart -- Flyby/Bus to DSIF Doppler Track 112

27 Telecommunication Design Control Chart -- Flyby/Bus to DSIF Telemetry Playout 114

28 Component Performance Data Supplied by Vendors 151

29 Components of Communication System..... 152

30 Abridged Advanced Mariner Spacecraft Mission Profile..... 171

31 Propellant Characteristics 181

32 Characteristics of Flyby/Bus Propulsion System 186

33 Propulsion System Weight Breakdown 187

34 Operational Requirements 190

35 Description of ACS Modes 192

36 ACS Components Used During Each Mode of Operation 193

37 Matrix Used for Rating ACS Reaction Control Concepts ... 196

38 Matrix Used for Rating TVC System 197

39 ACS Total Impulse Summary for Cruise Mode ACS Operation 213

40 Cold Gas Leakage Summary 223

6

RE-ORDER No. 64-524

TABLES (Concl'd)

Table 41 System Weight Without TVC 225

42 Size and Weight for Reaction Control System 230

43 Gyro and Electronics Package Characteristics 233

44 ACS Size, Weight, and Power Summary 234

45 Structural Weight Summary 240

46 Variation of Lander Weight and Ejected Weight 241

47 Radiative Properties of Typical Surface Coatings 247

48 Lander Separation System Weight Summary 266

49 Characteristics of Lander-Retro-Propulsion System 280

B-1 Reliability Evaluation of Alternative Design Concepts Summary of Results 313

B-2 Inherent Reliability of Lander Separation and Stabilization Alternatives 316

B-3 Relative Rankings of Lander Separation and Sterlization System Alternatives Summary of Results..... 319

C-1 Power Consuming Equipment 325

C-2 Pre-Launch Through Initial Cruise Mode Sequence 326

C-3 Power Consumption Analysis - Pre-Launch through Initial Mode Sequence 327

C-4 Midcourse Maneuver Sequence 328

C-5 Power Consumption Analysis -- First Midcourse Maneuver Sequence 329

C-6 Separation and Bus Slowdown Sequence 330

C-7 Power Consumption Analysis -- Bus/Lander Separation and Slowdown Sequence 331

7

RE-ORDER No. 64-524

ILLUSTRATIONS

Figure 1 Static Envelope - Surveyor 4

2 Advanced Mariner Design Concepts 7

3 Spacecraft Configuration with Flyby/Bus Mounted on Top of Lander - 96-Inch-Diameter Lander 9

4 Spacecraft Configuration with Lander Mounted on Top of Flyby/Bus - 85-inch-Diameter Lander..... 10

5 Diametric Drawing of Advanced Mariner Spacecraft ... 12

6 Design Layout of Advanced Mariner Flyby/Bus Reference Design 13

7 Gimbaled Payload Platform 16

8 Spacecraft - Mars Cone Angle Variation 17

9 Spacecraft - Mars Clock Angle Variation 18

10 Spacecraft -- Earth Cone Angle Variation 21

11 Spacecraft -- Earth Clock Angle Variation 22

12 Simplified Layout of Spacecraft..... 33

13 Advanced Mariner Lander Geometry - 1969 Launch 52

14 Advanced Mariner Flyby Geometry - 1969 Launch 54

15 Altitude Variation During Advanced Mariner Mars Flyby..... 63

16 Time from Periapsis Passage During Advanced Mariner Mars Flyby 65

17 Target Resolution of Optical System 67

18 Camera Head Weight as a Function of Resolution 68

19 Gimbaled Payload Platform 72

8

RE-ORDER No. 64-524

ILLUSTRATIONS (Cont'd)

Figure 20 Smear Velocity While Maintaining the Local Vertical 75

21 Smear Velocity While Maintaining the Direction of Initial Local Vertical Fixed in Space - V_∞ = 3.70 km/sec.. 76

22 Smear Velocity While Maintaining the Direction of Initial Local Vertical Fixed in Space - V_∞ = 4.34 km/sec.. 77

23 Single Axis Component Block Diagram 80

24 Payload Position Control System Block Diagram 82

25 Power Subsystem 88

26 Battery Weight 94

27 Solar Array Area and Weight 95

28 DC-DC Converter Weight -- 500 c Germanium Transistors 97

29 DC-DC Converter Weight -- 2 kc Germanium Transistors 98

30 DC-DC Converter Weight -- 2 kc Silicon Transistors 99

31 DC-DC Converter Volume -- 500 c Germanium Transistors 100

32 DC-DC Converter Volume -- 2 kc Germanium Transistors 101

33 DC-DC Converter Volume -- 500 c Silicon Transistors 102

34 Flyby/Bus Command Link Performance Margin - 100 kw Transmitter 109

35 Transmitter Power/Net Antenna Gain Product 117

36 High Gain Antenna Fixity 118

9

RE-ORDER No. 64-524

ILLUSTRATIONS (Cont'd)

Figure 37 High Gain Antenna Polar and Azimuthal Angles 118

38 Relative Antenna Gain, Major Diamter 2 Feet, Axis Ratio 0.5 119

39 Relative Antenna Gain, Major Diameter 2 Feet, Axis Ratio 0.6 120

40 Relative Antenna Gain, Major Diameter 2 Feet, Axis Ratio 0.8 121

41 Relative Antenna Gain, Major Diameter 2 Feet, Axis Ratio 1.0 122

42 Relative Antenna Gain, Major Diameter 3 Feet, Axis Ratio 0.5 123

43 Relative Antenna Gain, Major Diameter 3 Feet, Axis Ratio 0.6 124

44 Relative Antenna Gain, Major Diameter 3 Feet, Axis Ratio 0.8 125

45 Relative Antenna Gain, Major Diameter 3 Feet, Axis Ratio 1.0 126

46 Relative Antenna Gain, Major Diameter 4 Feet, Axis Ratio 0.5 127

47 Relative Antenna Gain, Major Diameter 4 Feet, Axis Ratio 0.6 128

48 Relative Antenna Gain, Major Diameter 4 Feet, Axis Ratio 0.8 129

49 Relative Antenna Gain, Major Diameter 4 Feet, Axis Ratio 1.0 130

50 Relative Antenna Gain, Major Diameter 5 Feet, Axis Ratio 0.5 131

51 Relative Antenna Gain, Major Diameter 5 Feet, Axis Ratio 0.6 132

15

RE-ORDER No. 64-524

ILLUSTRATIONS (Cont'd)

Figure 52 Relative Antenna Gain, Major Diameter 5 Feet, Axis Ratio 0.8 133

53 Relative Antenna Gain, Major Diameter 5 Feet, Axis Ratio 1.0 134

54 Relative Antenna Gain, Major Diameter 6 Feet, Axis Ratio 0.5 135

55 Relative Antenna Gain, Major Diameter 6 Feet, Axis Ratio 0.6 136

56 Relative Antenna Gain, Major Diameter 6 Feet, Axis Ratio 0.8 137

57 Relative Antenna Gain, Major Diameter 6 Feet, Axis Ratio 1.0 138

58 Relative Antenna Gain, Major Diameter 8 Feet, Axis Ratio 0.5 139

59 Relative Antenna Gain, Major Diameter 8 Feet, Axis Ratio 0.6 140

60 Relative Antenna Gain, Major Diameter 8 Feet, Axis Ratio 0.8 141

61 Relative Antenna Gain, Major Diameter 8 Feet, Axis Ratio 1.0 142

62 Antenna Gain (On Axis) 144

63 Transmitter Power - High Gain Antenna Combinations, Axis Ratio 0.5 145

64 Transmitter Power - High Gain Antenna Combinations, Axis Ratio 0.6 146

65 Transmitter Power - High Gain Antenna Combinations, Axis Ratio 0.8 147

66 Transmitter Power - High Gain Antenna Combinations, Axis Ratio 1.0 148

11

RE-ORDER No. 64-524

ILLUSTRATIONS (Cont'd)

Figure 67 Communication System 150

68 Mesh Antenna Weight 155

69 Circularly Polarized Horn 156

70 Spiral Antenna 157

71 Typical Radiation Pattern of a Spiral Antenna (No Ground Plane) 158

72 Tape Recorder Weight 159

73 Tape Recorder Volume 160

74 Tape Recorder Power Consumption as a Function of Storage Capacity 161

75 Tape Recorder Power Consumption as a Function of Recording Rate 162

76 Solid State Core Memory Weight 163

77 Solid State Core Memory Volume 164

78 Solid State Memory Power Consumption 165

79 Spacecraft-Bus Flight Command Subsystem - Typical Functional Diagram 170

80 Propellant Requirement -10 to 100 ft/sec V 176

81 Propellant Requirement -100 to 1000 ft/sec V 177

82 Propellant Requirement -1000 to 10,000 ft/sec V 178

83 Propulsion System Mass Fraction 179

84 Schematic of Flyby/Bus Propulsion System 184

85 Vehicle-Centered Coordinate System 189

86 Reaction System Weight As a Function of Total Impulse 195

12

RE-ORDER No. 64-524

ILLUSTRATIONS (Cont'd)

Figure 87 Thrust Vector Control System Weight 201

88 Total Impulse Expended for Stabilization and Orientation .. 205

89 Total Impulse Expended in Cruise Limit Cycling 207

90 Total Impulse Expended in Flyby Limit Cycling 208

91 Impulse Expenditure Due to Meteoroid Impacts - Cruise Phase..... 211

92 Impulse Expenditure Due to Meteoroid Impacts - Flyby Phase 212

93 Minimum Control Thrust 214

94 Thrust Vector Control System Total Impulse 216

95 Stabilization and Control System Block Diagram - Sun Acquisition Mode 217

96 Stabilization and Control System Block Diagram- Transit Cruise Mode 218

97 Stabilization and Control System Block Diagram - Orientation Command Mode 219

98 Reaction System Functional Diagram 227

99 Block Diagram of Control Electronics..... 228

100 Block Diagram of Gyro/Electronics Package 229

101 Flyby/Bus Structural Elements 236

102 Bus Structural Weight as a Function of Lander Ejected Weight At Separation 242

103 Surface Temperature as a Function of Distance From Sun..... 248

104 Typical Louver Characteristics 249

13

RE-ORDER No. 64-524

ILLUSTRATIONS (Cont'd)

Figure 105 Thermal Conductance as a Function of No. of Mylar Layers 251

106 Contact Resistance for Typical Metal Joints 252

107 Node Number of 60-degree Vector 254

108 Temperature Levels Near Earth 255

109 Temperature Levels Near Mars 256

110 Temperature Levels Near Mars Port Separation 257

111 Transient Characteristics During a 90-degree Turning Maneuver m = 4 lb/ft^2 Attached to Node 10, Near Earth 259

112 Temperature Excursions for Node 10 During a Turning Maneuver with Different Masses Attached to the Louvers, Sun Exposed Section, Near Earth 260

113 Transient Characteristics During a 90-degree Turning, Node 10, Near Mars 261

114 Transient Characteristics During a 90-degree Turning Maneuver, m = 4 lb/ft^2 Attached to Node 9, Near Earth 262

115 Transient Characteristics During a 90-degree Turning Maneuver, Node 8, Near Earth 263

116 Separation Sequence 267

117 Lander Sequence After Separation 268

118 Alternate Bus/Lander Arrangements 270

119 Spin-Off of Canister -- Two Pieces 273

120 Spin-Off of Canister -- Three Pieces and Four Pieces... 274

121 Bus/Lander Separation Joint Detail..... 276

14

RE-ORDER No. 64-524

ILLUSTRATIONS (Cont'd)

Figure A-1 Mission Geometry 282

A-2 Gimbal Geometry 283

A-3 Resolver Diagrams 285

A-4 Outer Gimbal Time History 288

A-5 Inner Gimbal Time History 289

A-6 Geometry for 1-22-69 Launch Date 291

A-7 Outer Gimbal Angle Time History, 14 Jan 1969, i = 45° 292

A-8 Inner Gimbal Angle Time History, 14 Jan 1969, i = 45° 293

A-9 Outer Gimbal Angle Time History, 22 Jan 1969, i = 45° 294

A-10 Inner Gimbal Angle Time History, 22 Jan 1969, i = 45° 295

A-11 Outer Gimbal Angle Time History, 30 Jan 1969, i = 45° 296

A-12 Inner Gimbal Angle Times History 30 Jan 1969, i = 45° 297

A-13 Outer Gimbal Angle Time History, 7 Feb 1969, i = 45° 298

A-14 Inner Gimbal Angle Time History, 7 Feb 1969, i = 45° 299

A-15 Outer Gimbal Angle Time History, 14 Jan 1969 i = 28.95° 300

A-16 Inner Gimbal Angle Time History, 14 Jan 1969, i = 28.95° 301

A-17 Outer Gimbal Angle Time History, 22 Jan 1969, i = 31.31° 302

15

RE-ORDER No. 64-524

ILLUSTRATIONS (Concl'd)

Figure A-18 Inner Gimbal Angle Time History, 22 Jan 1969, i = 31.31° 303

A-19 Outer Gimbal Angle Time History 30 Jan 1969, i = 33.85° 304

A-20 Inner Gimbal Angle Time History, 30 Jan 1969, i = 33.85° 305

A-21 Outer Gimbal Angle Time History, 7 Feb 1969, i = 36.59° 306

A-22 Inner Gimbal Angle Time History, 7 Feb 1969, i = 36.59° 307

C-1 Flyby/Bus Battery Weight Required as a Function of Flyby/Bus Engine Thrust Level 333

D-1 Two Mass System 334

D-2 Initial Total Spring Load as a Function of Individual Spring Rate - 3 Spring Configuration 336

D-3 Initial Total Spring Load as a Function of Individual Spring Rate - 1 Spring Configuration 337

D-4 Force Diagram 335

D-5 Frequency, Period, and Separation Pulse Duration as a Function of Spring Rate 340

D-6 Spring Force as a Function of Time 341

D-7 $\omega^2 \theta_{max}$ and $\omega \dot{\theta}_{max}$ as a Function of Initial Total Spring Load 342

16

RE-ORDER No. 64-524

SUMMARY

This report presents the results of a four-month parametric analysis and conceptual design study conducted by the Research and Advanced Development Division of Avco Corporation for the Jet Propulsion Laboratory. The study objectives included a parametric analysis of the unmanned Flyby Bus/Lander concept for scientific investigation of Mars during the 1969 and 1971 launch opportunities, a conceptual design of the selected configuration, and a development and cost plan indicating the program leading to development and first flight of the Advanced Mariner Vehicle in 1969.

The flyby/lander concept utilizes a 1493 pound spacecraft launched on an Atlas Centaur launch vehicle. The scientific capability of the lander and flyby bus vehicles were determined to obtain a balance between scientific data and overall systems complexity commensurate with the first landing mission to Mars.

The lander vehicle separates from the flyby bus vehicle prior to planet encounter, enters the planetary atmosphere, and descends to the surface on a parachute. During atmospheric entry, parachute descent, and surface operations, the lander analyzes the Martian atmosphere; and for five hours after impact determines wind velocity as well as performing a simple life detection experiment. The information is transmitted to Earth via both a direct transmission link to the DSIF and is also relayed through the flyby bus which has been placed on a delayed flyby trajectory for this purpose. The flyby bus also collects interplanetary data and maps the planet. The lander vehicle has been designed to accommodate the minimum projected atmosphere for Mars (11-millibar surface pressure) and surface winds gusting to 200 ft/sec resulting in impact loads of up to 1500 g for a landed payload protected by crushable material. The lander is to be dry heat sterilized to avoid contamination of Mars with Earth organisms while the flyby bus is placed on a biased trajectory providing a small probability of entering the planetary atmosphere and therefore is not required to be sterilized.

The development plan shows a minimum of three launch attempts are necessary to achieve an 84 percent chance of a successful mission in the 1969 and 1971 launch opportunities; requiring that hardware development begin in early 1965 to meet a 1969 launch date.

17

RE-ORDER No. 64-524

1.0 DESIGN STUDY

1.1 SCOPE OF STUDY

The Advanced Mariner flyby/bus-lander parametric and conceptual design study for the 1969 and 1971 launch opportunities towards Mars has been completed, and the flyby/bus information generated is presented herein. The primary objective of this study has been to arrive at a spacecraft configuration that would maximize the lander vehicle dimension. To perform the study the basic ground rules that were set were 1) the spacecraft, that is the flyby/bus-lander combination, shall not exceed the static envelope of the Surveyor shroud, and 2) the launch weight of the spacecraft shall not exceed the injection capability of an Atlas Centaur booster. Launch weight can range from the performance of an unfloxed Atlas-Centaur to that of a 30-percent floxed Atlas-Centaur booster. In principle, the upper launch weight boundary should govern the spacecraft mission goals; however, the lower launch weight boundary also is an interesting constraint for it represents the spacecraft weight that can be launched on an unmodified booster. Floxing of the Atlas must await a development program, and so imposes the penalty of integrating a spacecraft development with a booster development program.

This study also was conducted with the objective of providing a worthwhile return of scientific information, with a design approach for spacecraft and systems selection that allowed for a low risk mission. The spacecraft mission and resulting design was not directed towards either utilizing all the weight available to the 30-percent floxed Atlas-Centaur, or meeting the minimum weight limitations of an unfloxed Atlas-Centaur. The conceptual design of the Advanced Mariner Spacecraft generated a vehicle weight that lay between the launch capability of the unfloxed and 30-percent floxed Atlas-Centaur.

It has been the intent of this study to identify the significant parameters that can vary within each system. The first goal of the study was to provide parametric data about the significant subsystems. The objective of this parametric study was to provide sufficient data so that once system characteristics were selected, both weight and performance of the system could be rapidly determined. Thus, it would be possible to arrive at a set of flyby/bus vehicle system weight and performance with a minimum of effort. In conducting the study it soon became apparent that parametric configurational studies were not feasible and that a configuration would have to be evolved during the parametric study. It should also be observed that the configurational study also helped to mold the parametric study in that it provided bounding estimates for the size of solar panels, lander, high gain antenna, main propulsion thrust chamber, moments of inertia, and gimbaled payload platform.

Upon completion of the two month parametric phase of the study, work was begun on the conceptual design phase of the flyby/bus. During this phase, which also lasted for two months, the effort was concentrated on refining the design of the flyby/bus, and also checking the breadth and validity of the parametric information generated.

18

The results presented show the conceptual design of an Advanced Mariner flyby/bus with sufficient parameteric data to permit modifications in the major subsystems.

1.2 DESIGN OBJECTIVES

The conceptual design of the flyby/bus has been directed towards achieving, primarily, the delivery of a lander to Mars. Experiments performed after landing have the possibility of determining whether life forms exist. This combined with the determination of atmospheric composition and properties, and winds in situ will provide valuable future data for the design of a more efficient lander mission, that is, a mission for which the design contingencies are minimized.

A secondary design objective is to obtain topographical information. This phase of the mission, unlike the lander which performs its measurements while immersed in the media being studied, is performed by passive measurements at an external point. The characteristics of the planet are deduced by the study of electromagnetic signatures of ultra-violet, visible, and infra-red emission from the surface. The combination of the lander and flyby/bus experiments affords a potentially interesting experiment. Flyby/bus measurements which have broad coverage are limited by the relatively gross resolving power of the instruments. Lander instruments can resolve fine detail but are limited by their narrow field of coverage. Simultaneous measurements carried out while the flyby/bus passes over the landing site can enhance the natural limitations of both spacecraft and lander to provide more information than either vehicle could provide independent of the other.

The third objective is to measure the particles and fields at planetary encounter. It will be shown later that the payload penalties resulting for the addition of these instruments is minimal since they are, in general, light in weight, and consume small quantities of power relative to other spacecraft components. When the flyby/bus measures particles and fields at encounter it is measuring phenomena in situ, like the lander. It is also possible to determine topological information by noting anomalies in these measurements and relating these anomalies to surface phenomena.

Once the third objective has been met, the same set of instruments can be used to achieve the fourth objective, the measurement of particles and field during the cruise from Earth to Mars. The main limitation of the measurements is that they are spatial and do not provide temporal variations at a given point. However, the spatial and temporal variation of interplanetary space can be built up from data telemetred by many spacecraft.

RE-ORDER No. 64-524

1.3 DESIGN CONSTRAINTS

Achievement of the design objectives is limited by a multiple number of external constraints. These constraints include the injected weight capability of the Atlas-Centaur, the dimensional limitations of the Surveyor shroud, the requirement of not exceeding one chance in ten-thousand of allowing a viable organism to contaminate the planet, performance characteristics of the Deep Space Information Facility, and the booster launch environment.

The injected weight capability of the unfloxed Atlas-Centaur for the selected 1969 launch opportunity, which extends from 10 January to 11 February is 1342 pounds; for the selected 1971 opportunity which extends from 2 May to 3 June the spacecraft launch weight is 1965 pounds. The launch weights used are the minimum ones for the opportunity since the spacecraft must be designed to be launched at any time during the opportunity. The summary of launch weights for the 1969 and 1971 launch opportunity, for both the floxed and unfloxed Atlas-Centaur is presented in table 1.

TABLE 1

BOOSTER LAUNCH WEIGHT CAPABILITY

	Unfloxed Atlas-Centaur (pounds)	30 Percent Floxed Atlas-Centaur (pounds)
1969	1342 lbs.	1965 lbs.
1971	1550 lbs.	2215 lbs.

The spacecraft weight, (which includes the lander, flyby/bus, the lander separation system, and the spacecraft-booster adapter), must satisfy the 1969 launch opportunity, and so the lower value serves as the design goal. Additional weight allowances for the 1971 opportunity can be utilized by providing additional scientific payload to the flyby/bus, and also by providing redundancy for the systems. (If the sea-level pressure of Mars is found to be greater than the 11-millibar value on which the lander design is based, it would then be possible to increase the lander m/C_DA. This would increase the lander weight, and so reflect as a weight increase for the spacecraft.)

Dimensional constraints are provided by the Surveyor shroud. Figure 1 shows the dimensions of the shroud. Although the nominal base dimension of the shroud is 104 inches, the largest body of revolution that can be designed into this shape is one whose dimension does not exceed 96 inches. This reduction is caused by the fact that the shroud is not a body of revolution, but rather has two flats that reduce the dimension, and clearance must be allowed for storing the deployable solar panels. The actual shroud envelope that was used is a

20

RE-ORDER No. 64-524

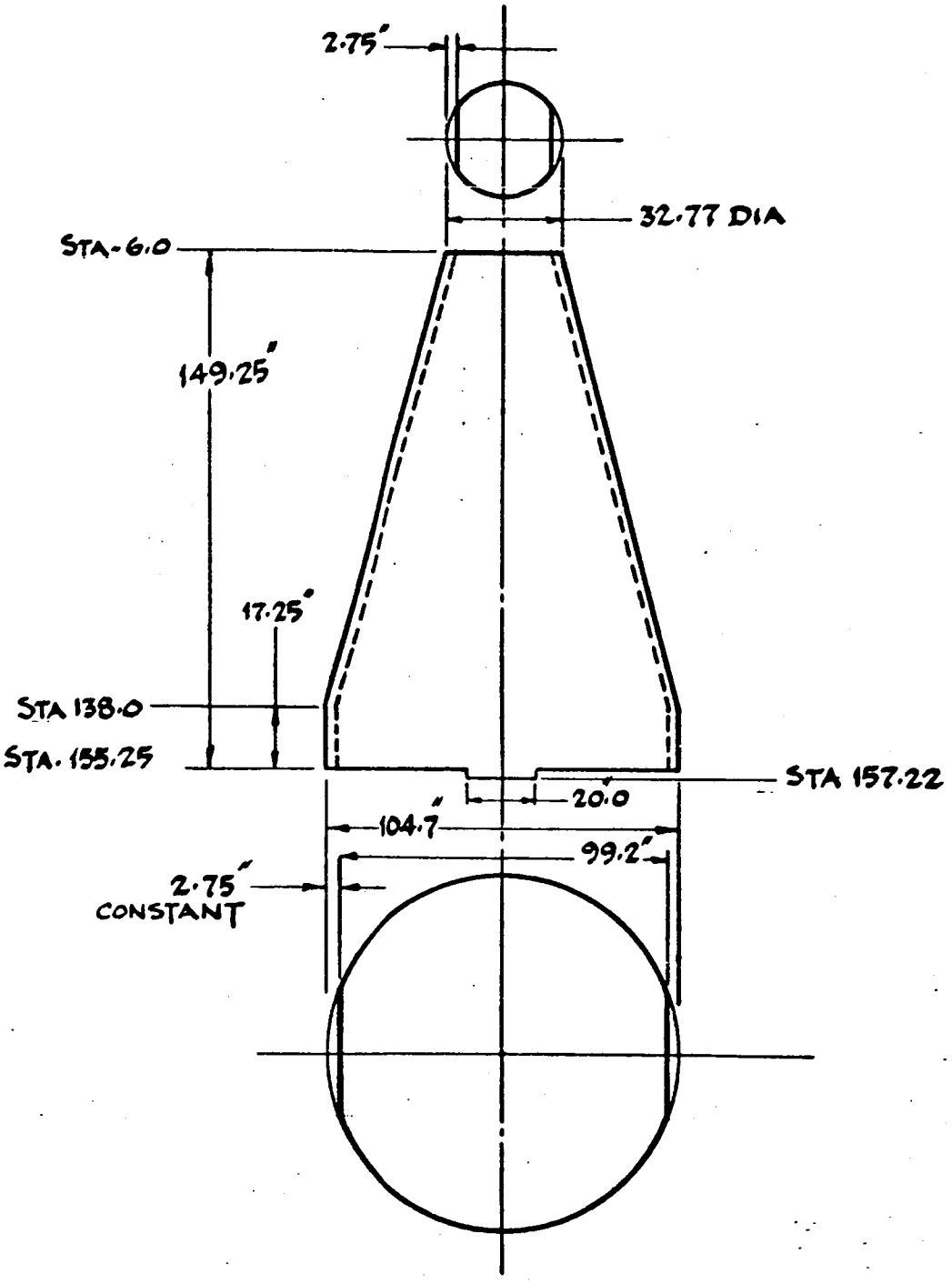

64-11308

Figure 1 STATIC ENVELOPE-SURVEYOR

21

slight modification of the one shown in figure 1. It was found that the flyby-bus configuration could be simplified if the vertical length of the shroud were increased. This change amounted to an increase of 11 inches. The requirements that led to this modification are discussed in section 1.4.

Achievement of the final sterilization goals has been approached by design of a system that minimizes the number of elements that have to be sterilized and maintained in sterile condition. The lander is sterilized and maintained with a sterile canister. This canister is attached to the flyby/bus, which is not sterilized. The trajectory of the flyby/bus is biased away from the planet so that the closest approach is at a 4σ value greater in altitude than the altitude at which planetary contamination will occur. (The altitude below which contamination is possible was arbitrarily chosen to be 1,500 kilometers.) It should be pointed out that a 4σ bias away from the 1500-kilometer distance statistically more than satisfies the sterilization requirements. For the 1969 launch, sterilization requirements constrain the closest approach. In 1971 the flyby altitude is constrained by an occultation limit.

DSIF performance constrains the design of the communication system and the guidance accuracy of the spacecraft to the planet. The DSIF tracking accuracy combined with the number of midcourse corrections, position of corrections, and precision, that is, control of the magnitude and direction of the velocity correction, will yield a guidance error. Table 2 shows the predicted periapsis passing distance, for the advanced Mariner with two midcourse connections.

TABLE 2

PERIAPSIS PASSING DISTANCE

	Lower Bound	Nominal	Upper Bound
1969	2707	6328	9949
1971	4000	5521	7024

DSIF characteristics also influence the command and telemetry performance of the flyby/bus by providing a firm constraint at the Earth end of the communication link. These characteristics are the DSIF transmitter power, antenna gain, and system noise temperature.

The acceleration profile experienced during launch determines the structure that must be provided to support the inertia loads and transmit these loads to the Atlas-Centaur. Launch loads and subsequent stress levels also influence the design and/or selection of components.

1.4 DESIGN EVALUATION

The primary objective of the flyby/bus conceptual design study has been to provide a bus for the lander. To achieve this objective, the spacecraft configuration has strived to accommodate a lander with a larger diameter, that is, a lander with a diameter nearly equal to the shroud dimension near the booster.

Early inthe parametric study a multitude of spacecraft concepts were investigated. These concepts are shown in figure 2. Various configurational arrangements were studied from the viewpoint of maximizing the lander dimension. These preliminary studies indicated that in the arrangement with the flyby/bus supporting the lander and transmitting the launch loads to the booster, an 84-inch-diameter lander could be accommodated. An arrangement was also investigated which placed the lander in contact with the booster and the flyby/bus atop the lander. In this configuration it would be possible to place the largest diameter of the Apollo shape, a 96-inch-diameter vehicle, at the maximum available cross section in the Surveyor shroud. Also considered were arrangements of two equal diameter landers with a flyby/bus. Two landers would enhance the probability of mission success. Two equal diameter landers would be of interest for then the design and manufacture would be limited to just one vehicle configuration. It was found that two 66-inch-diameter landers could be designed into the shroud. Finally, two unequal diameter landers were also considered. For the configuration it would be found that the maximum landers that could be accommodated were 96 and 50 inches in diameter. In the early part of the study, the lander diameter was not known; however, preliminary assessment of the required dimension indicated that more than 80 inches would be needed to land a minimum acceptable weight. This, in effect, removed multiple landers from consideration, since the addition of the second lander always recuced the dimension of one of the landers below this 80-inch limit. Upon further investigation the multiple lander arrangements shown in figure 2 created attachment and separation problems that would compromise the success of the lander mission. For this additional reason it was decided that the stacking of landers would not be allowed.

Design arrangements were studied, keeping in mind (1) the requirements to separate the lander, which would subject the vehicle to a large shift in the position of the center of gravity, (2) arrangement of propulsion tanks to account for the shift in the center of gravity during and after propellant expulsion (unlike the Mariner C, the propulsion system for the Advanced Mariner has to provide for flyby/bus slowdown after separation of the lander, so that the lander can arrive at the planet, perform a 5-hour biological experiment, and be able to relay the data acquired to the flyby/ bus as it passes over), (3) location of the main thrust chamber so as to minimize effects of alterations in the center of gravity, so as not to complicate a thrust vector control system, (4) deployment of solar panels, gimbaled payload platform which supports the relay horn antenna and flyby mapping equipment, deployment of solar panels, and if necessary, deployment of a high gain antenna, and (5) provision for proper look angle

23

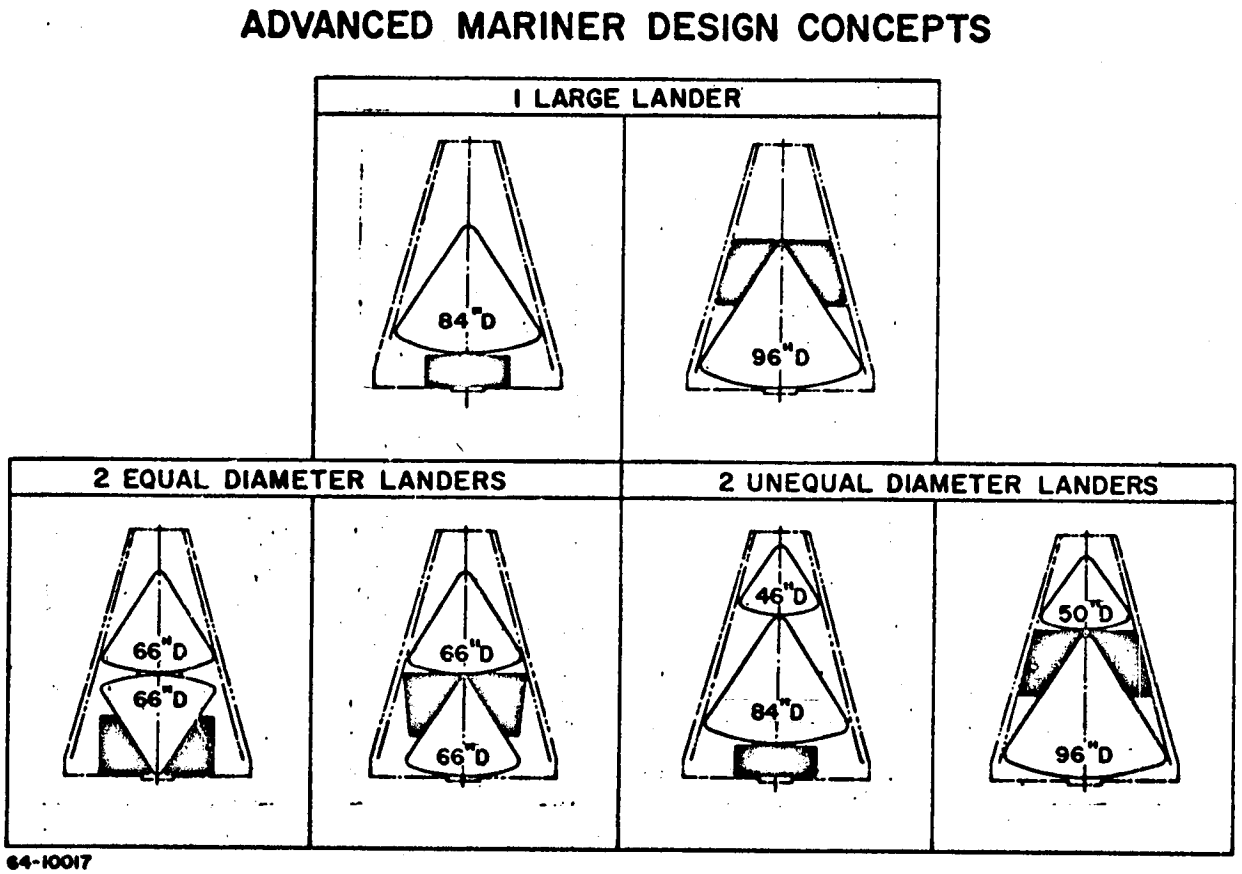

Figure 2 ADVANCED MARINER DESIGN CONCEPTS

RE-ORDER No. 64-524

location and unobstructed view for attitude control sensors, gimbaled payload platform, low gain antenna system, and high gain antenna system. During the parametric phase of the study conceptual designs were studied so as to provide bounds for the generation of parametric system weights and performance data.

Since the configuration with the lander making contact with the launch vehicle led to the largest lander dimensions within the Surveyor shroud, this arrangement was initially carried along and is shown in figure 3. It was found that this configuration was compatible with meeting the requirements of the deployable sensors and integration of the propulsion system. The major difficulty was the attachment of the flyby/bus. It terms of simplicity the flyby/bus was at first attached directly to the lander, so that the lander structure would provide load paths for the flyby/bus launch inertia loads. This resulted in two penalties. First, the inertia loads from the flyby/bus would design part of the aft section structure of the lander. This would detract from the weight that might have otherwise been available for the lander payload since the structural weight would increase. (The purpose of placing the flyby/bus atop the lander was to provide a greater lander dimension and a resulting greater lander payload.) Second, the increase in the weight of the aft structure would also move the center of gravity of the lander rearward, which would aggravate the lander stability problem. For these reasons it was decided to provide the flyby/bus with a load path independent of the lander. It was recognized that this would lead to a structural weight penalty in the flyby/bus. It was soon determined that the major limitation of this new design arrangement was that the lander was now encased in six structural members. To separate the lander, it would be necessary to cut through this structure, a much more complicated procedure than just a simple release, which would be possible if another design were considered.

To facilitate lander separation, the configuration in which the lander was placed on top of the flyby/bus was reconsidered. The objective of this new effort was to look for techniques to increase the lander diameter. Figure 4 shows the final conceptual design and serves as a good reference for the discussion of techniques of increasing the lander diameter. The 85-inch diameter lander shown atop the flyby/bus was the largest lander that could be accommodated under the existing ground rules. In this configuration, the diameter of the lander is prescribed by the height of the flyby/bus. The objective was to shrink the flyby/bus. Certain restrictions were imposed. Sufficient bus volume must be maintained for the propulsion tanks, black boxes, and attitude control system cold gas bottles. The next limitation was the location of the lander propulsion unit and the flyby/bus propulsion thrust chamber. It was found desirable to strap the lander propulsion to the forebody, because at separation the lander could be ejected and accelerated onto an impact trajectory with the planet, without flyby/bus position changes after separation. If the propulsion system were located at the apex of the lander, then upon separation, it would be necessary to maneuver the flyby/bus away from the path of the lander; an unwanted complication. Location of the flyby/bus propulsion system thrust

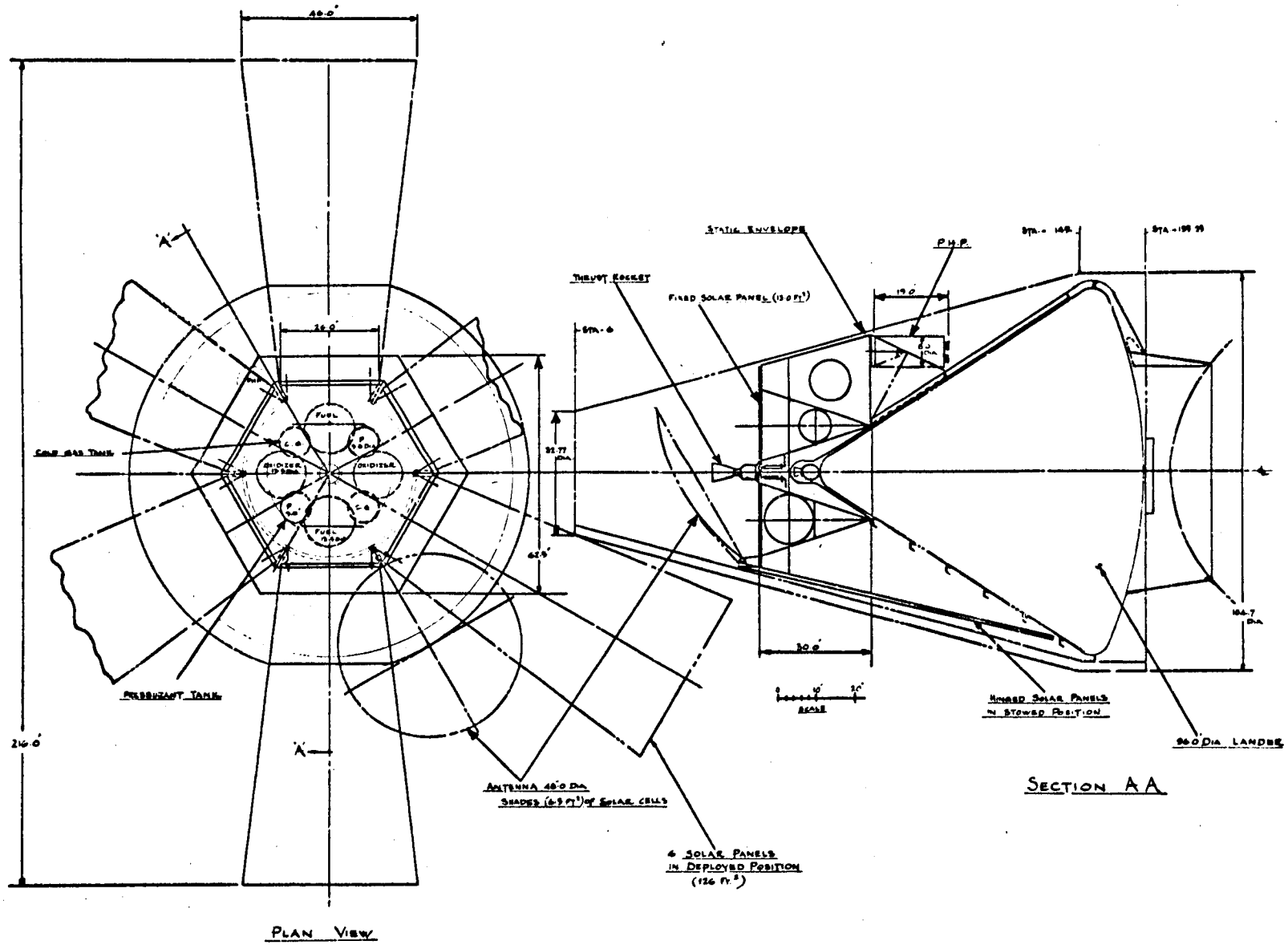

Figure 3 SPACECRAFT CONFIGURATION WITH FLYBY/BUS MOUNTED ON TOP OF LANDER - 96-INCH-DIAMETER LANDER

RE-ORDER No. 64-524

26

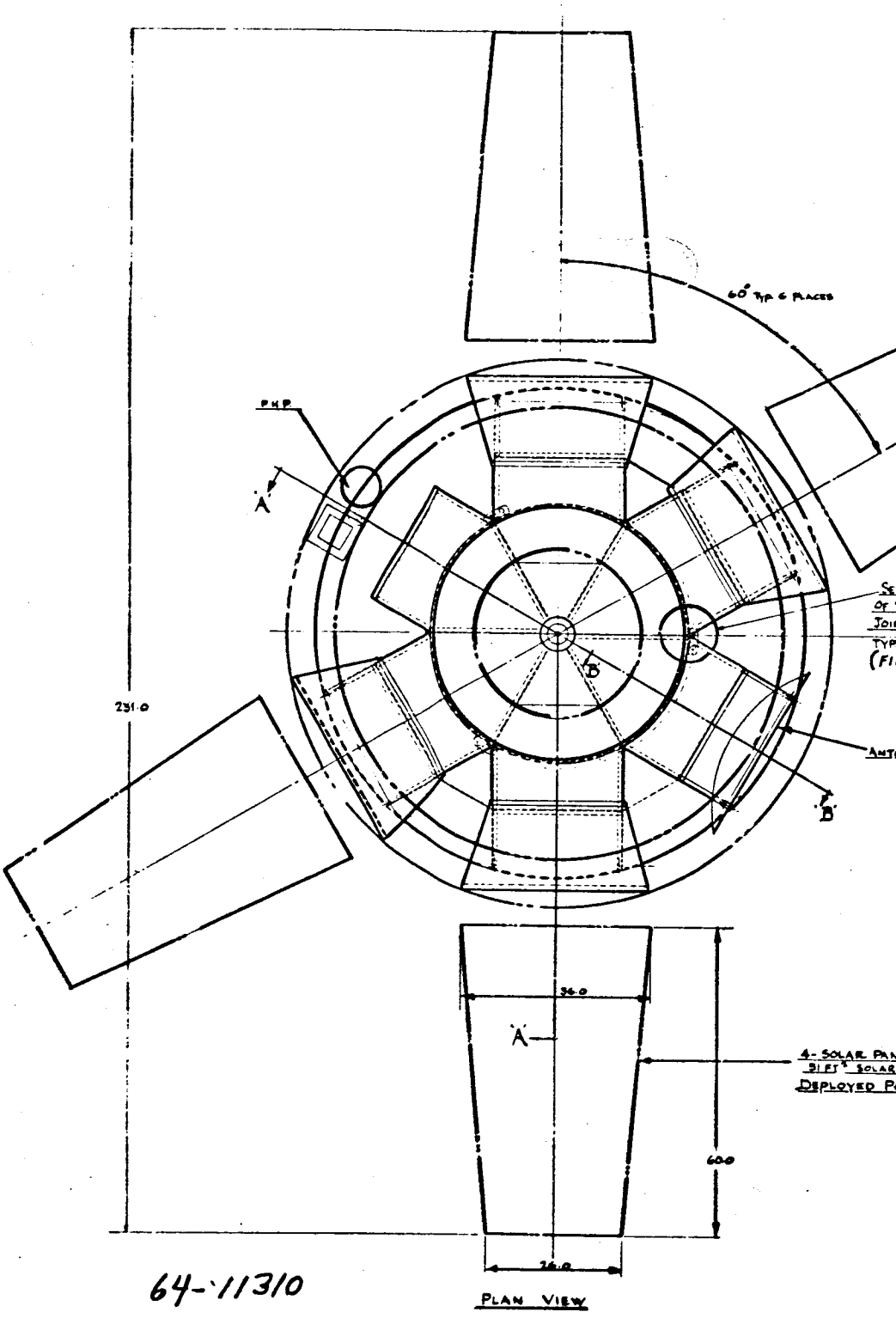

64-11310

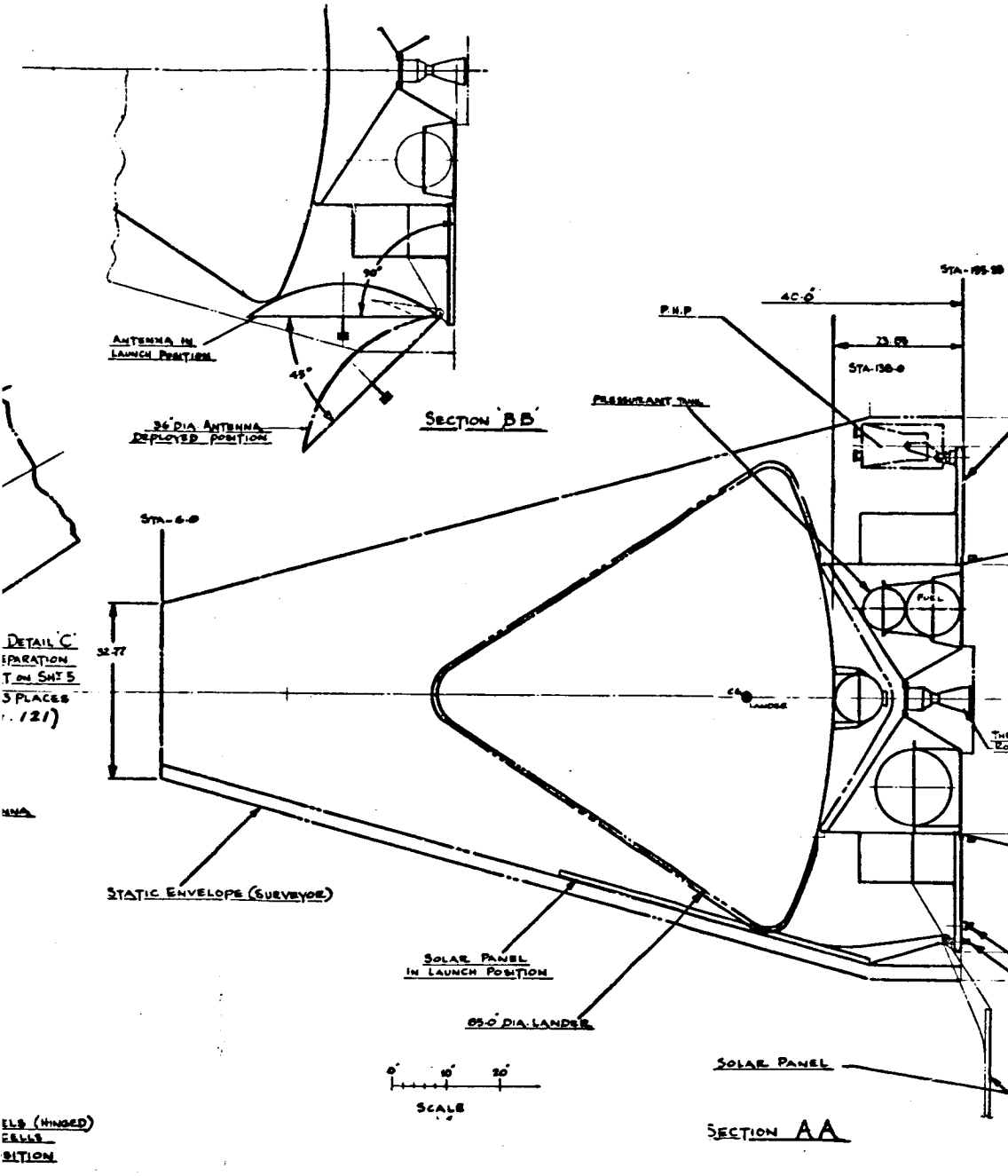

Figure 4 SPACECRAFT CONFIGURATION WITH LANDER MOUNTED ON TOP OF FLYBY/BUS - 85-INCH-DIAMETER LANDER

2 #

RE ORDER No. 64-524

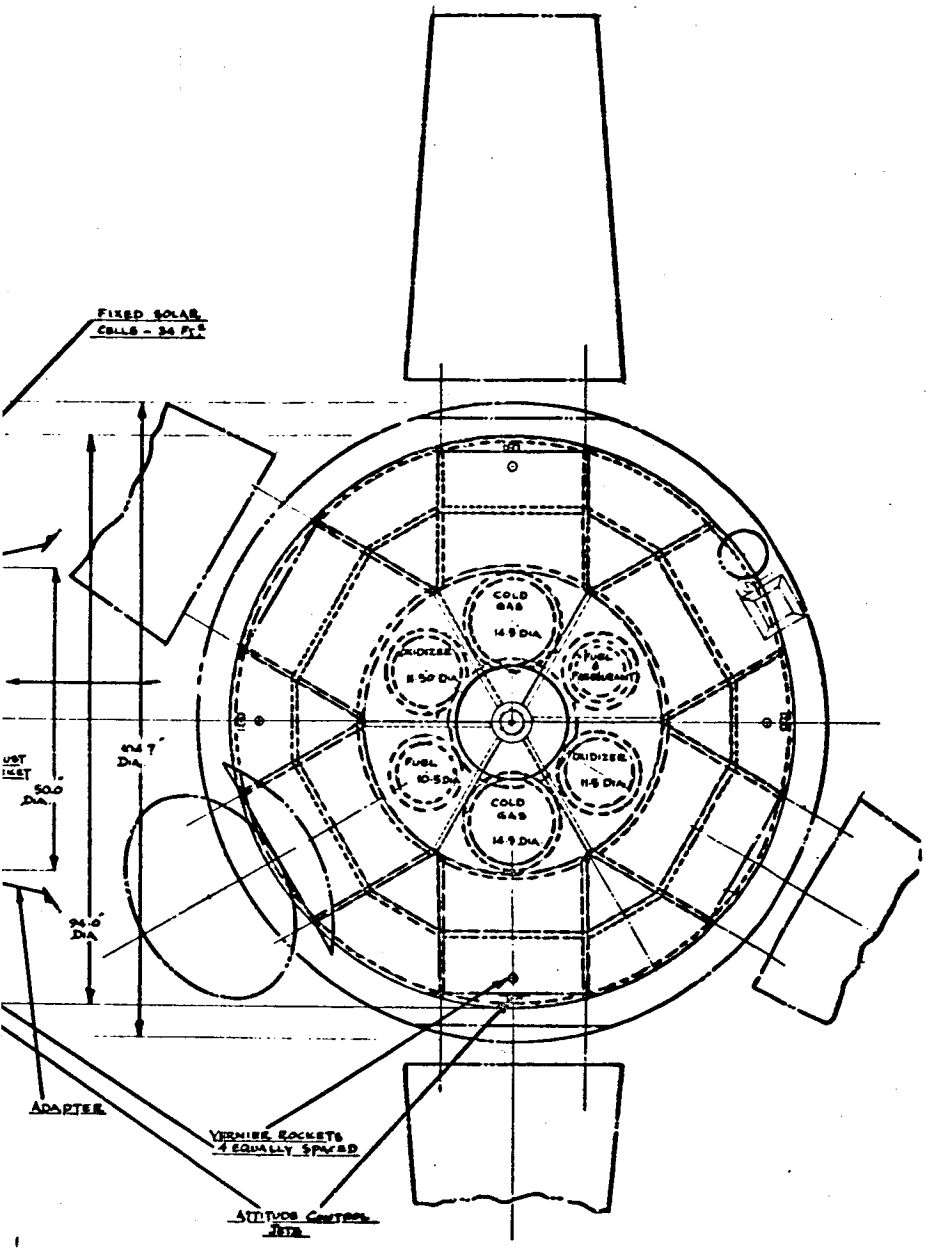

VIEW IN DIRECTION OF ARROW

3#

27

chamber along the same axis as the lander propulsion system that is, the longitudinal axis of the spacecraft and booster, was advantageous from the viewpoint of simplicity of design. Since after lander separation, the center of gravity of the flyby/bus shifts about one foot down the longitudinal axis towards the thrust chamber, it is desirable to have a single thrust chamber propulsion system located along this center of gravity shift axis. For Mariner C, where the mass change is very small (only propellants for two midcourse corrections are required), it was possible to locate the thrust axis normal to the longitudinal axis and passing through the center of gravity. Because of the large mass loss at lander separation this arrangement was not feasible for advanced Mariner. To reduce the length of the thrust chamber, a low thrust level was selected. These design decisions set the height of the flyby/bus, and the maximum lander dimension. Further design studies were conducted that altered the thrust chamber arrangement. In one configuration the single thrust chamber would be hinged at an angle of 90 degrees to the longitudinal axis. The nozzle would be stored in this position from launch to separation of the spacecraft from the booster. Upon separation, the thrust chamber would be pivoted through an angle of 90 degrees, until the thrust chamber was along the longitudinal axis and then it would be locked in place. Using this approach, the height of the flyby/bus could be reduced, and an 89-inch diameter lander could be placed within the shroud. Another concept removed the thrsut chamber from the longitudinal center line axis, and would place four thrust chambers 90 degrees apart along the edge of the rigid solar panel. The major objection to this scheme was the additional propulsion system complexity and anticipated lower reliability. It was found that this modification allowed for the mounting of a 92-inch diameter lander.

Upon completion of these modification studies, the concept of shroud modification was introduced. Also, the lander study had been carried to sufficient depth to arrive at definite requirements for a 90-inch diameter vehicle. It was found that the 90-inch lander could be accommodated if the 17.25-inch vertical section (see figure 1) of the Surveyor shroud were increased by 7 inches. At this point in the study of the Advanced Mariner spacecraft, it appeared to be unrealistic to compromise spacecraft design to meet the Surveyor shroud envelope. It was felt that a minor modification could be justified on the basis that the trade-offs between shroud and spacecraft should be considered. It was found necessary to increase the depth of the bus by an additional four inches to accommodate the necessary operational excursions of the gimbaled payload platform. This resulted in a total 11-inch extension of the vertical section of the shroud.

The final reference design is shown in perspective in figure 5 and in layout of figure 6. The design shown in figures 5 and 6 incorporate the shroud modification. The features of this reference design are expanded in the following section.

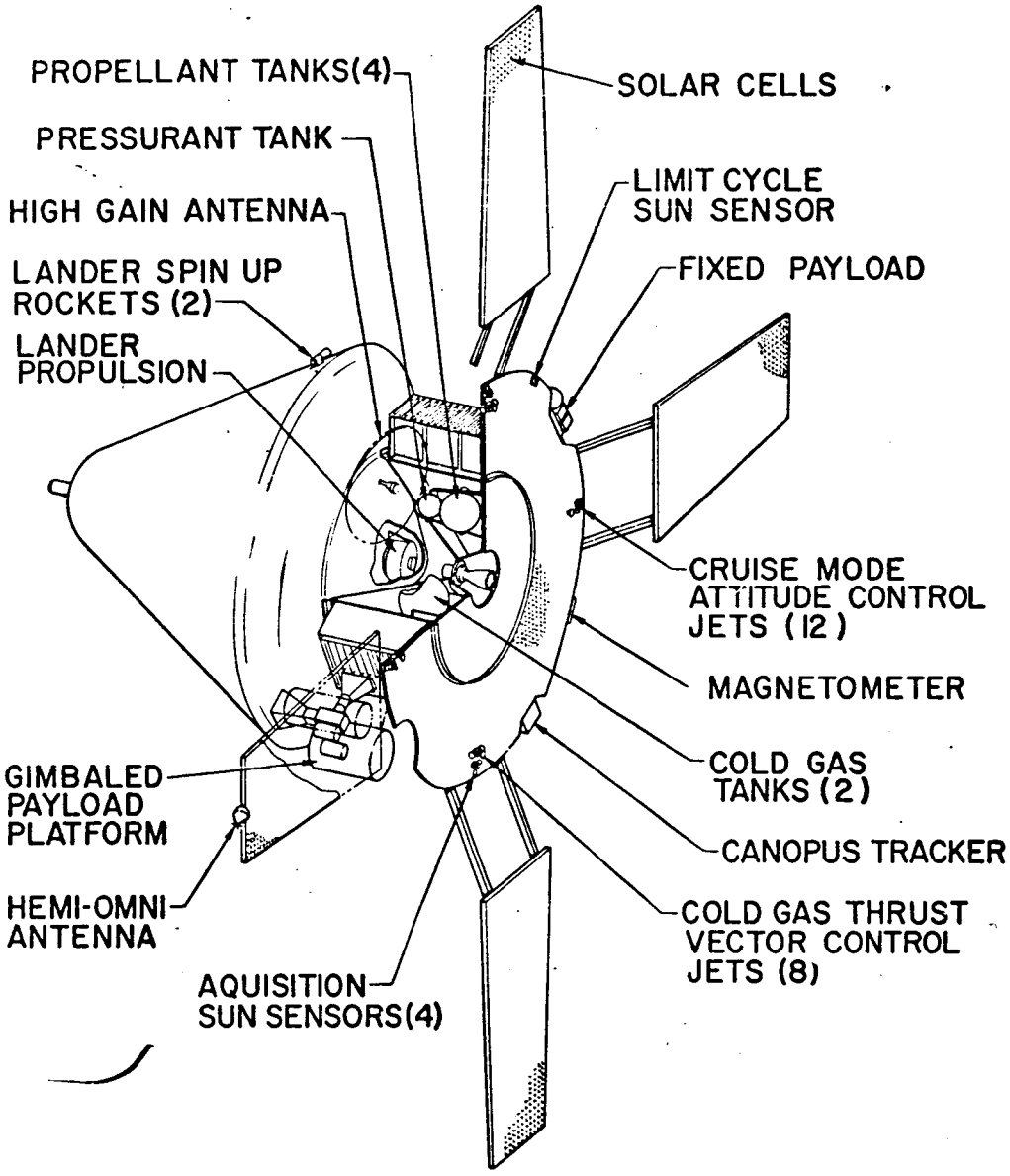

ADVANCED MARINER SPACECRAFT
CUTAWAY OF FLY BY / BUS - LANDER

64-9909-2

Figure 5 DIAMETRIC DRAWING OF ADVANCED MARINER SPACECRAFT

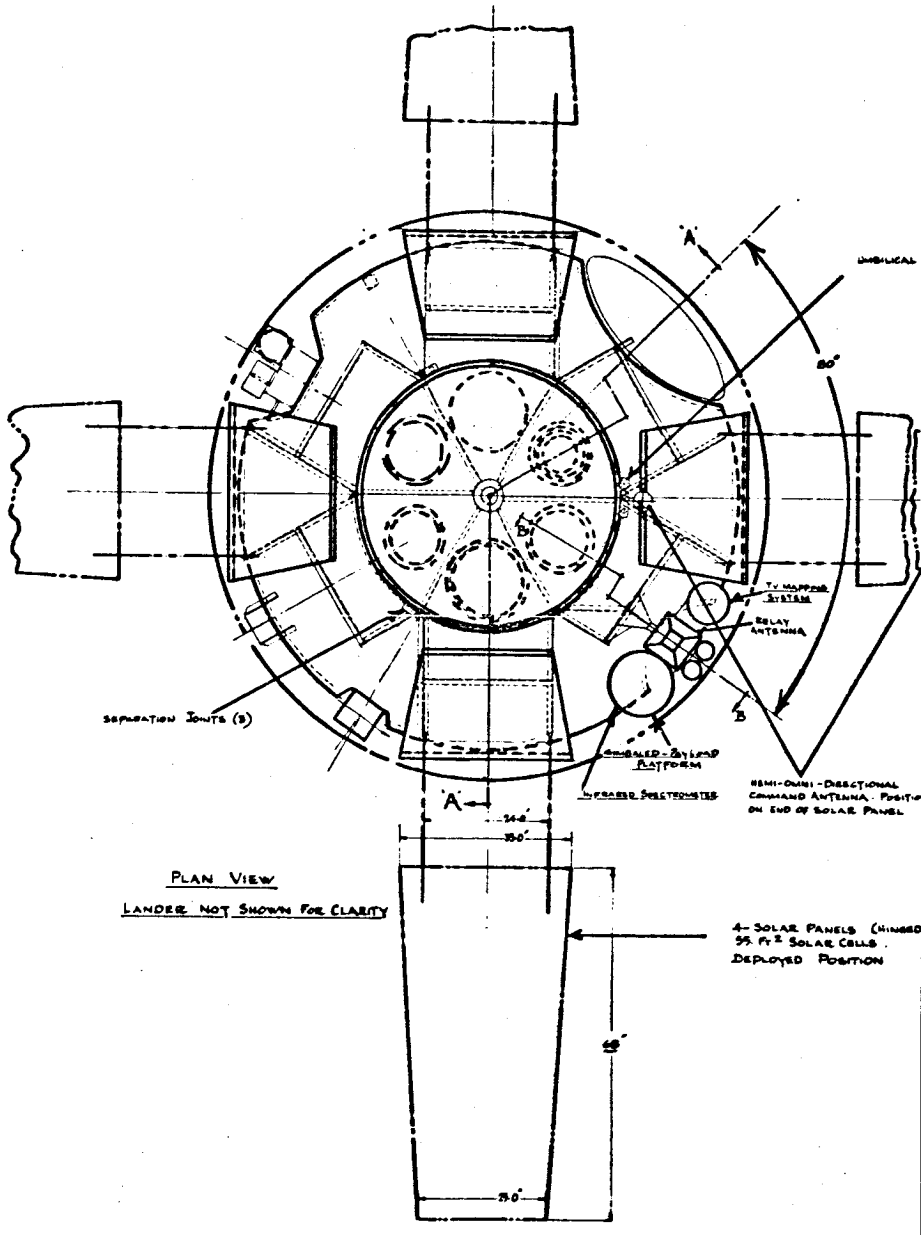
'A'
UMBILICAL
80°
TV MAPPING SYSTEM
RELAY ANTENNA
SEPARATION JOINTS (3)
GIMBALED-BY-LEAD PLATFORM
INFRARED SPECTROMETER
SEMI-OMNI-DIRECTIONAL COMMAND ANTENNA - POSITION ON END OF SOLAR PANEL
'A'
14.0'
15.0'
PLAN VIEW
LANDER NOT SHOWN FOR CLARITY
4- SOLAR PANELS (HINGED
55 Ft² SOLAR CELLS.
DEPLOYED POSITION
15.0'

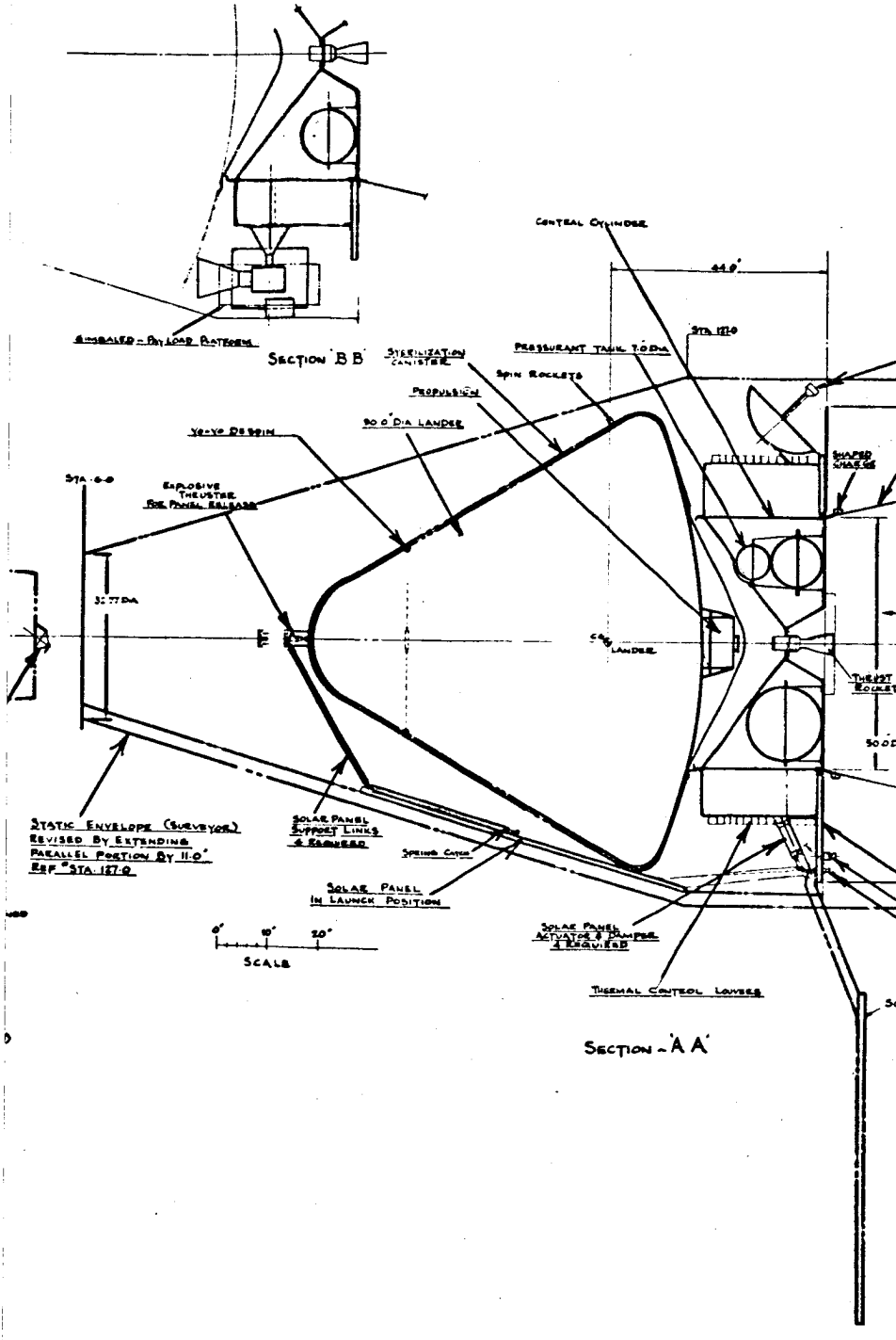

Figure 6 DESIGN LAYOUT OF ADVANCED MARINER FLYBY/BUS REFERENCE DESIGN

RE-ORDER No. 64-524

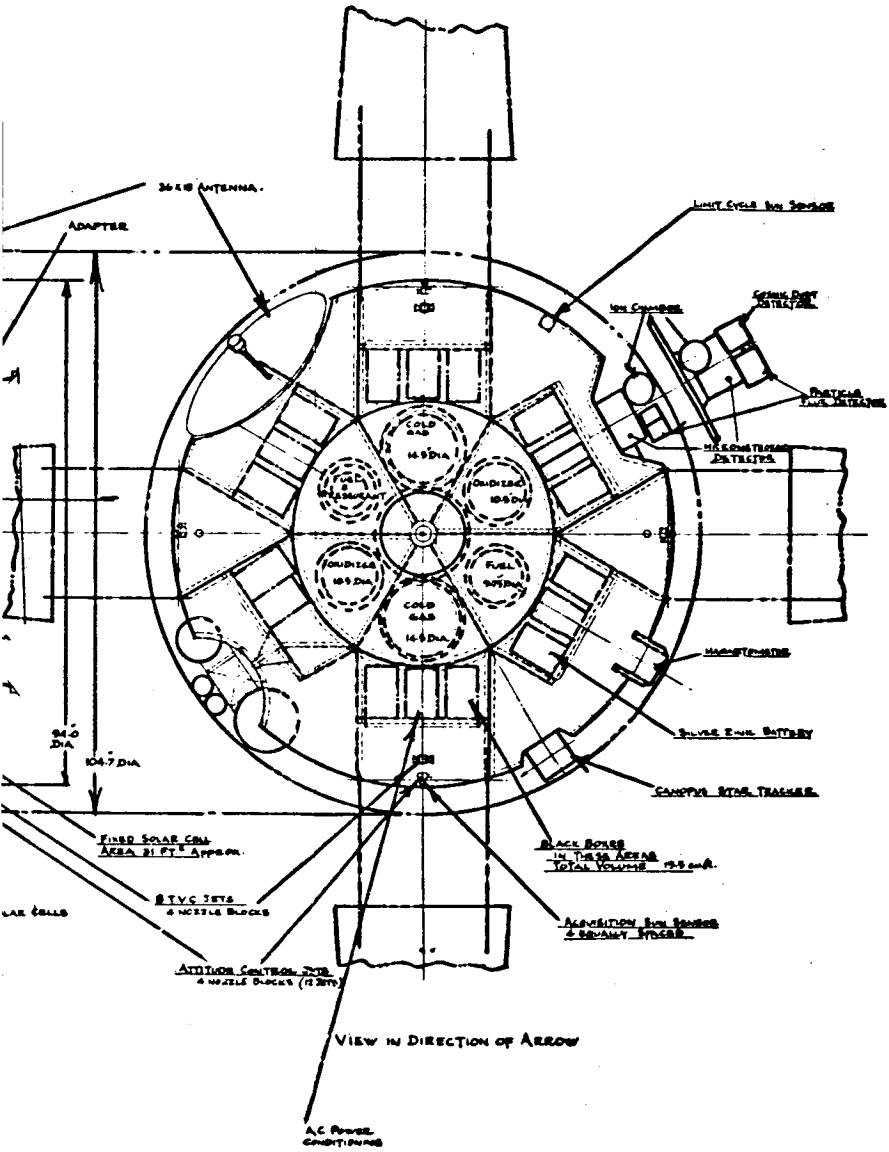

3#

30

1.5 CONCEPTUAL DESIGN

The design evolution was dominated by the spacecraft mission objective of delivering a 90-inch diameter lander to Mars. In this section the reasons behind the systems selection will be discussed and the extent of parametric supporting data will be detailed.

1. Scientific Payload

For this Advanced Mariner spacecraft, the secondary mission objective is the topographical mapping of Mars during planetary encounter, third and fourth mission objectives are measurements of near-planetary particles and fields at encounter, and measurements of particles and fields during interplanetary transfer, respectively. It was of interest in the parametric phase of the study to arrive at a rationale that would allow for the maximization of information during flyby. Rather than treat each instrument as an independent recording device, the approach was taken to see how combinations of scientific instruments could be used to increase the information gathering potential of the flyby mission. From this study it would also be possible to obtain a ranking of instrumentation so that instruments could be added or removed from the flyby/bus in an optimal fashion. To this end the planet was divided into a number of spheres of interest, particularly, the biosphere, endosphere, lithosphere, and atmosphere. Each sphere was divided into a number of regimes. For example, the lithosphere was divided into six regimes. The first order regime would describe the grossest feature; for increasing order, the feature dimension would be reduced. A first-order regime corresponded to the rotational bulge; second-order regime to features of continental dimensions; third order regime to features the size of mountain ranges or oceanic rifts; fourth order regime to features the dimensions of volcanic cones or meteor craters; fifth order regime to features the size of boulders; and sixth order regime to bodies of sand grain dimensions. The phenomena that can be measured with sensors, detectors, etc., correspond to (1) electromagnetic signatures ranging from X-radiation through visible to radar, (2) detection of gravitational, electric, and magnetic fields, and (3) detection of particles ranging from corpuscular to molecular to dust. In some cases, the instruments are external to the phenomenon e. g. mapping, in other cases the instruments are immersed in the phenomena, e. g. magnetic fields. The object of the parametric study was to match the regime and physical phenomenon so that geophysical data about Mars could be deduced. The instrument list for the flyby bus includes a cosmic dust detector, micrometeoroid detector, ion chamber, and particle flux detector. These instruments are mounted together on a cut-out in the rigid solar panel. The cosmic dust detector and micrometeoroid detector are required to be mounted in planes parallel to and perpendicular to the ecliptic. For a 1969 launch it was found that the clock angle position of the ecliptic varied over 24 degrees or that the maximum error in orientation would be about 12 degrees for a fixed instrument. The magnetometer is also located on the rigid solar panel,

removed from the other instruments and sources of magnetic disturbance. If in the final design analysis, the magnetometer cannot be shielded from stray magnetic fields, it will then be necessary to provide a boom, so as to place the magnetometer further away from disturbances. The gimbaled payload platform supports the television mapping system and the infrared spectrometer. Also located on the platform is the relay horn antenna. The relay antenna is mounted to the gimbaled payload platform so that it will point to the planetary local vertical. The local vertical will insure a preferred direction and so allow for an improvement in relay antenna performance. (The relay antenna is designed to receive the data that are transmitted from the lander, these data are subsequently transmitted by the flyby / bus.)

The gimbaled payload platform shown in figure 7 is designed to accommodate the 1969 launch opportunity. For this opportunity the periapsis point lies near the Sun line, so the cone angle varies over 180 degrees during the flyby; there is a small variation in clock angle. Figures 8 and 9 show the cone and clock angle variations, respectively. These variations can be translated into gimbal motion and this analysis was conducted in section 2.5. Essentially the cone angle variation can be represented by the excursion in the outer gimbal. In figure 7 the gimbal is shown at the position that it would have near the Sun line and periapsis for the 1969 launch. The gimbal moves 90 degrees in each direction about the axis. For example, at the beginning of encounter, the gimbal is 90 degrees away from the position shown in figure 7. At the termination of encounter it will have to rotate through 180 degrees and so point in the opposite direction. The gimbal motion required to satisfy the clock angle variation is smaller than the motion required for the cone angle variation. In the design arrangement the outer gimbal satisfies the cone angle variation, and the inner gimbal, the clock angle variation. Near encounter a command will be sent from the central computer and sequencer unit to commence a search mode. The outer gimbal will swing to the appropriate stop and the inner gimbal will nod until the planet disc is sensed by the horizon scanner, at which time the gimbal will lock on the planet and track. Two control systems were considered, a continuous position control, and a gimbal lock system. In the former system the platform would maintain the local vertical during picture frame exposure.

Smear would be induced by a geometrical shift in position of the local vertical and tracking errors in the control system. In the latter system the gimbal is locked during television exposure and the error induced results only from the change in the position of the initial local vertical. The geometrical smear caused by the shift in the local vertical for the locking system is greater than the geometrical smear resulting from the shift in the local vertical in the position control system. However, for the periapsis altitudes considered, the error contributed by the position control system is greater than the differences in geometrical smear; for this reason a fixed

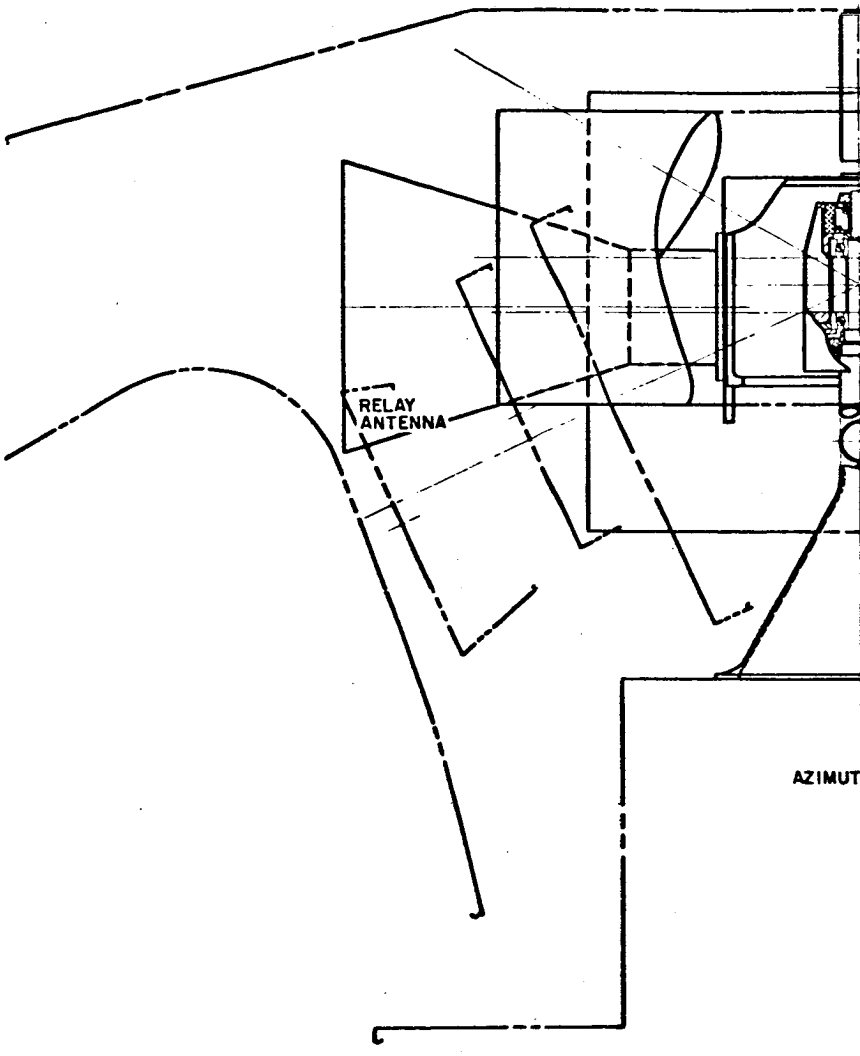

64-11312

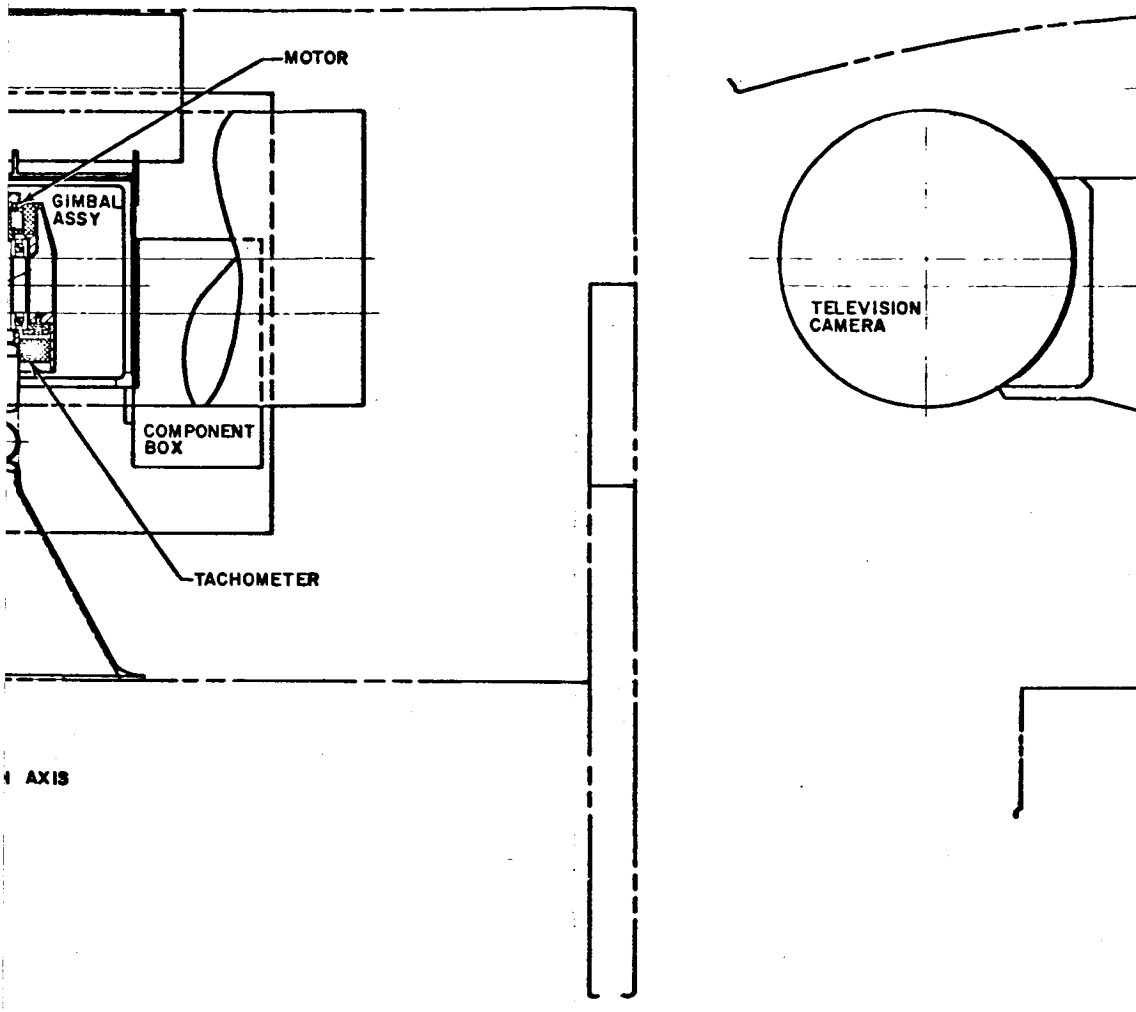

GIMBALED PAYLOAD PLATFORM

Figure 7 GIMBALLED PAYLOAD PLATFORM

RE-ORDER No. 64-524

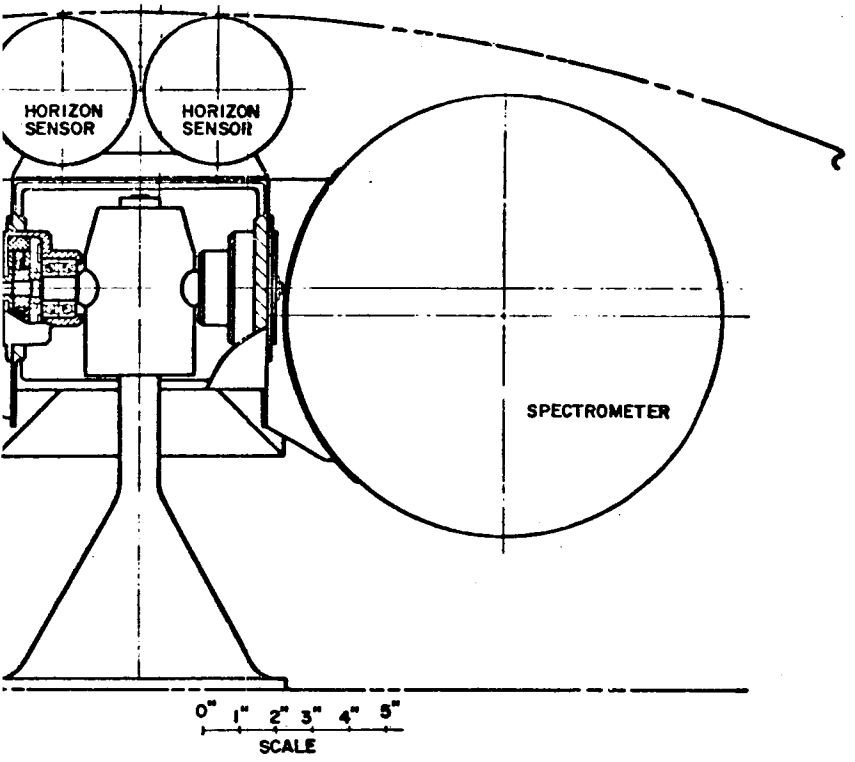

ELEVATION AXIS

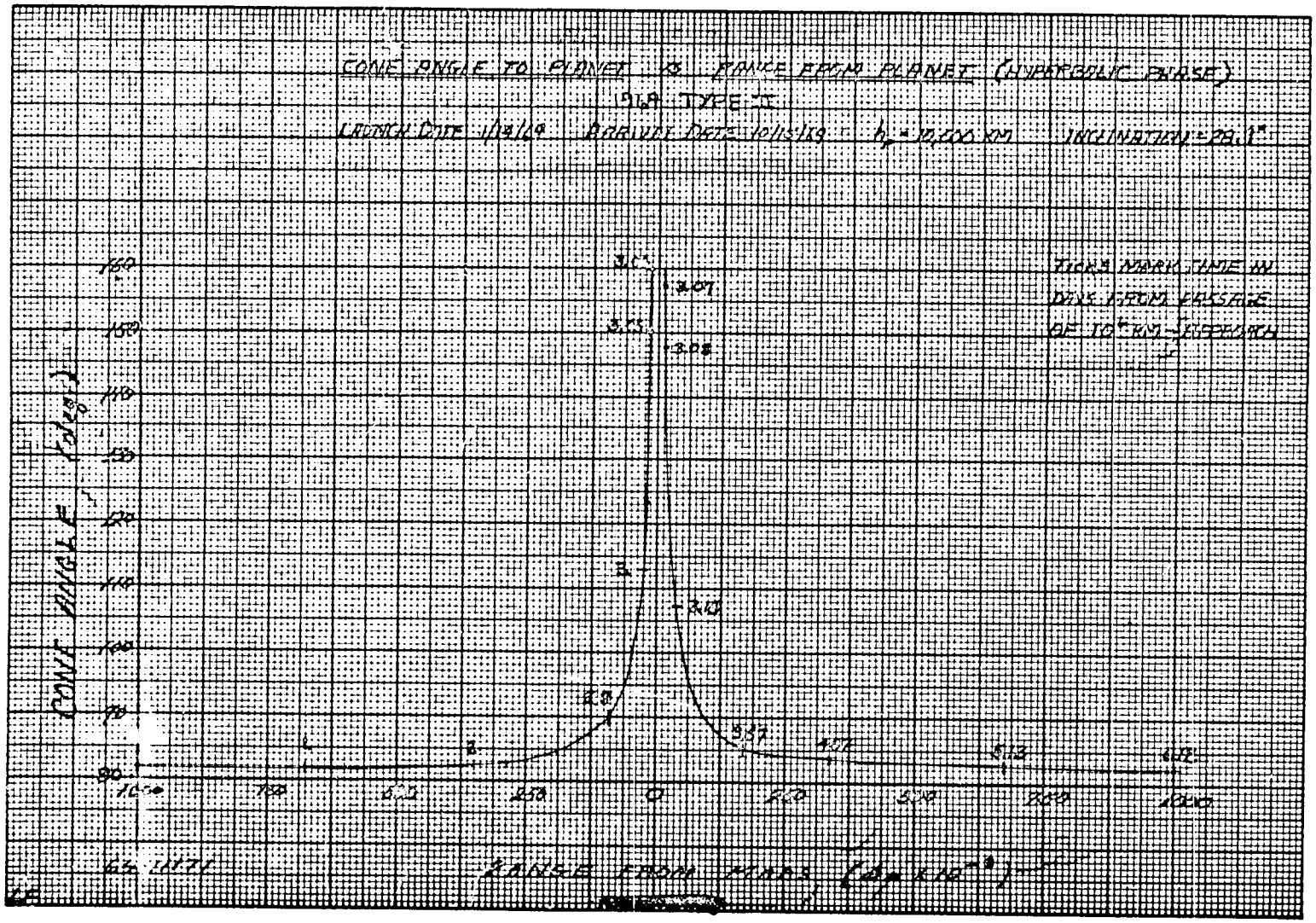

Figure 8 SPACECRAFT - MARS CONE ANGLE VARIATION

RE-ORDER No. 64-524

34

gimbal system was selected. The gimbal was located at zero clock angle. This choice was based on the variation in clock angle as shown in figure 9. where the mean position of the gimbal is at zero clock angle. It also appeared from the drawing that the spacecraft interference would be minimum in this location.

The television system that was considered utilizes modified Cassegrain optics, a focal length of 12 inches and a relative aperture of 8. The vidicon used is an improved version of the Mariner C sensor. The line density is 1,360 lines per inch, compared to Mariner C 910 lines per inch, and the tube is twice as photosensitive as the one used on Mariner C. At an altitude of 12,000 kilometers, the system yields a resolution of 1 kilometer with a 220-kilometer field of view. It was assumed, as in the case of Mariner C, that the allowable smear would not exceed 50 percent of the resolution element or in this case 1/2 kilometer. Parametric design data are presented in section 2.4, for determining mapping system weight and performance.

2. Power Supply

The power supply for the flyby/bus is based on the use of (1) solar cells for primary power generation, (2) silver-zinc batteries as a secondary power source, and (3) an ac power distribution system. Solar cells were selected because of the comparative ease of integrating this type of source into a spacecraft design. It was determined that the raw power requirements would not exceed 300 watts. Using a solar cell performance figure of 4 watts/ft^2 at the Martian distance from the sun, this led to a total solar panel area requirement of 75 ft^2. The actual power requirement came out to be 240 watts of raw power, or translated into terms of panel area, only 60 ft^2. For the conceptual design there exists a total of 85 ft^2 of panel area with the capability of providing 340 watts of raw power. This additional 25 ft^2 of panel area causes a weight increase of 30 pounds based on panel weight of 1.2 lb/ft^2. This larger area was selected because of 1) anticipated growth in power requirements, 2) redundancy in the event of cell failure and 3) it provided an allowance for degradation of solar cells anticipated for a spacecraft that operates near the asteroid belt. This is of particular importance for the 1969 Type II trajectory, which requires greater periods of operating time in this region of high meteoroid flux. The solar cells are arranged in five panels. Four panels are deployed after launch with each panel area being 13.75 ft^2, for a total of 55 ft^2. The rigid solar panel supports 30 ft^2 of panel area. It is to be noted that based on the minimum power requirements without any allowance, the deployable panels support 55 ft^2 out of the total requirement of 60 ft^2. The deployable panels are not at their maximum envelope-allowable size. The secondary power source is provided by silver-zinc batteries. A performance figure of 37 w-hrs/lb is used for sizing the battery. Since the battery will be discharged only three times, (at first midcourse correction, and during the lander separation and flyby/bus slowdown maneuver), it is possible to use the higher performance of silver-zinc batteries. If there had been a great many cycles of charging and discharging, nickel-cadmium

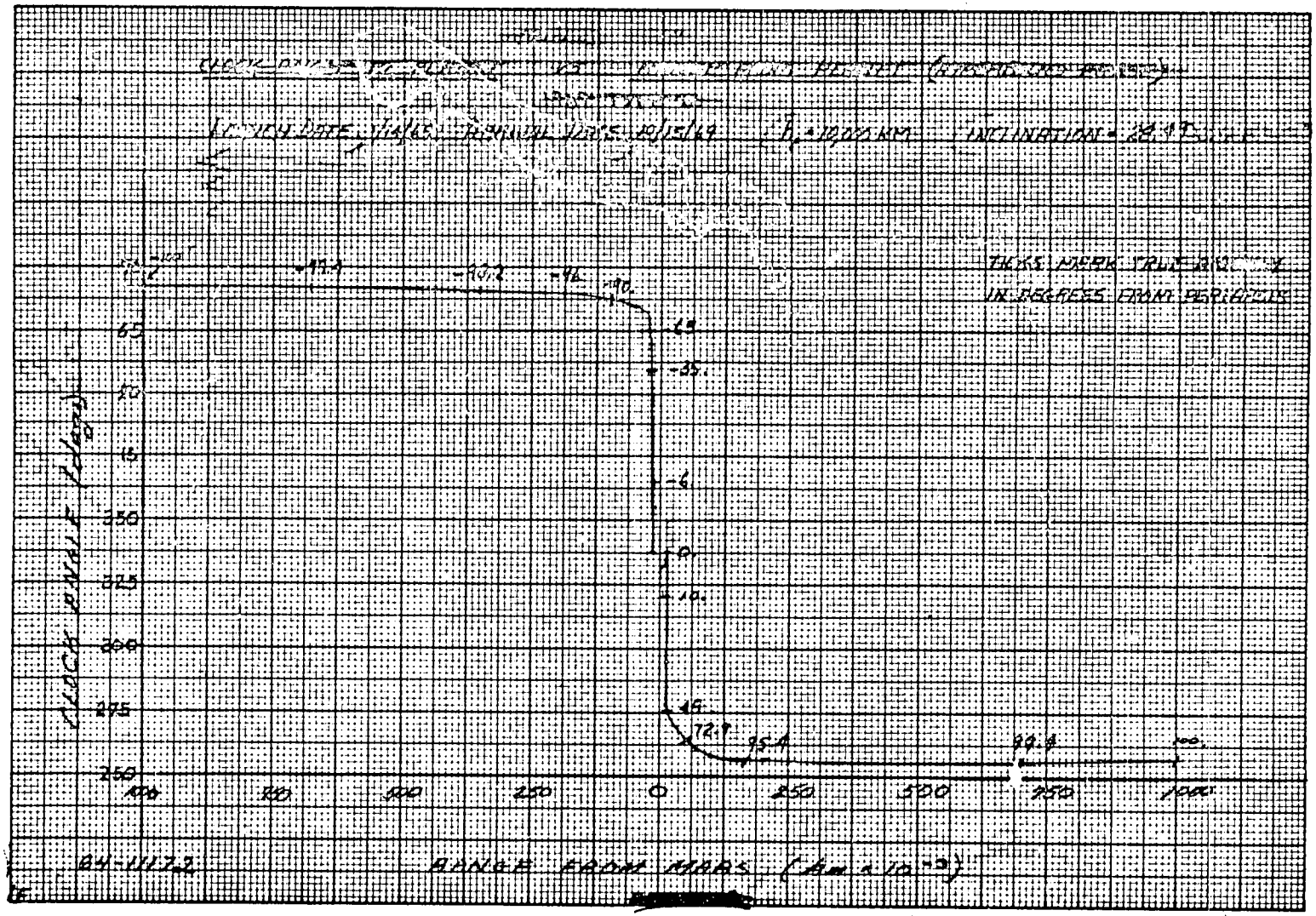

Figure 9 SPACECRAFT - MARS CLOCK ANGLE VARIATION

RE-ORDER No. 64-524

35

batteries with a performance figure of 6 w-hrs/lb would have to be used. An ac power distributing system was selected since it has a higher reliability. The greater inefficiencies in power conversion of the distribution system can be absorbed because of the noncritical relation between power demand and solar cell area for power generation.

3. Communication

All flyby/bus communication is carried out at S band, 2295 mc. The Mariner C transmitter and triode power tube have been incorporated into the Advanced Mariner communication system. System performance is based on 10 watts of radiated power. The communication system provides ranging information for guidance trajectory determination, a command link, and a telemetry link. It has been shown that if the command and telemetry links are satisfied, then the up and down ranging links are satisfied. From launch to 43 million km a low gain hemi-omni antenna is used. (Based on an 8-1/3 bps data rate and 10 watts of transmitted power, the hemi-omni antenna could be used out to a range of about 70 million kilometers). At this point it is necessary to crossover to a high gain antenna. Figures 10 and 11 show the Earth cone and clock angle variation. It is to be noted that the variation of both the cone and clock angle is quite large near Earth; at a great distance from Earth these variations become quite small. The hemi-omni antenna is located at a clock angle of 45 degrees at the end of one of the deployed solar panels (for the configuration shown in figure 6, clock angle is measured in a clockwise direction about the circumference of the rigid solar panel on the side opposite the sun). To meet the clock angle variation, the axis of the hemi-omni antenna is canted so as to be parallel to the zero clock angle line. Since the cone and clock angle variation is small, past ranges of 40 million kilometers, the possibility of fixing the high gain antenna to the spacecraft was examined and found feasible. Near Earth the low gain of the hemi-omni antenna can be tolerated. To maintain the bit rate of 8-1/3 bps and the transmitted power at 10 watts, the antenna gain must be increased as the distance from the earth increases. A high gain antenna fixed to the spacecraft provides the capability and is shown in figure 6. The antenna feed axis is located so that it points towards Earth at encounter. The antenna minor axis is located in a plane formed by the spacecraft-sun vector and spacecraft-Earth vector and at an angle of 90 degrees to the feed axis. Since the cone angle variation is slightly greater than the clock angle variation, it was expedient to resort to an elliptical antenna and take advantage of the improved gain. The minor axis of the antenna covers the cone angle variation. With a 3-foot x 1-1/2-foot antenna it is possible to crossover at 43 million kilometers from the Earth and maintain a bit rate of 8-1/3 bps until encounter, at which time, with the feed axis pointing towards Earth, the bit rate can be increased to 133-1/3 bps and maintained for 10 days past encounter.

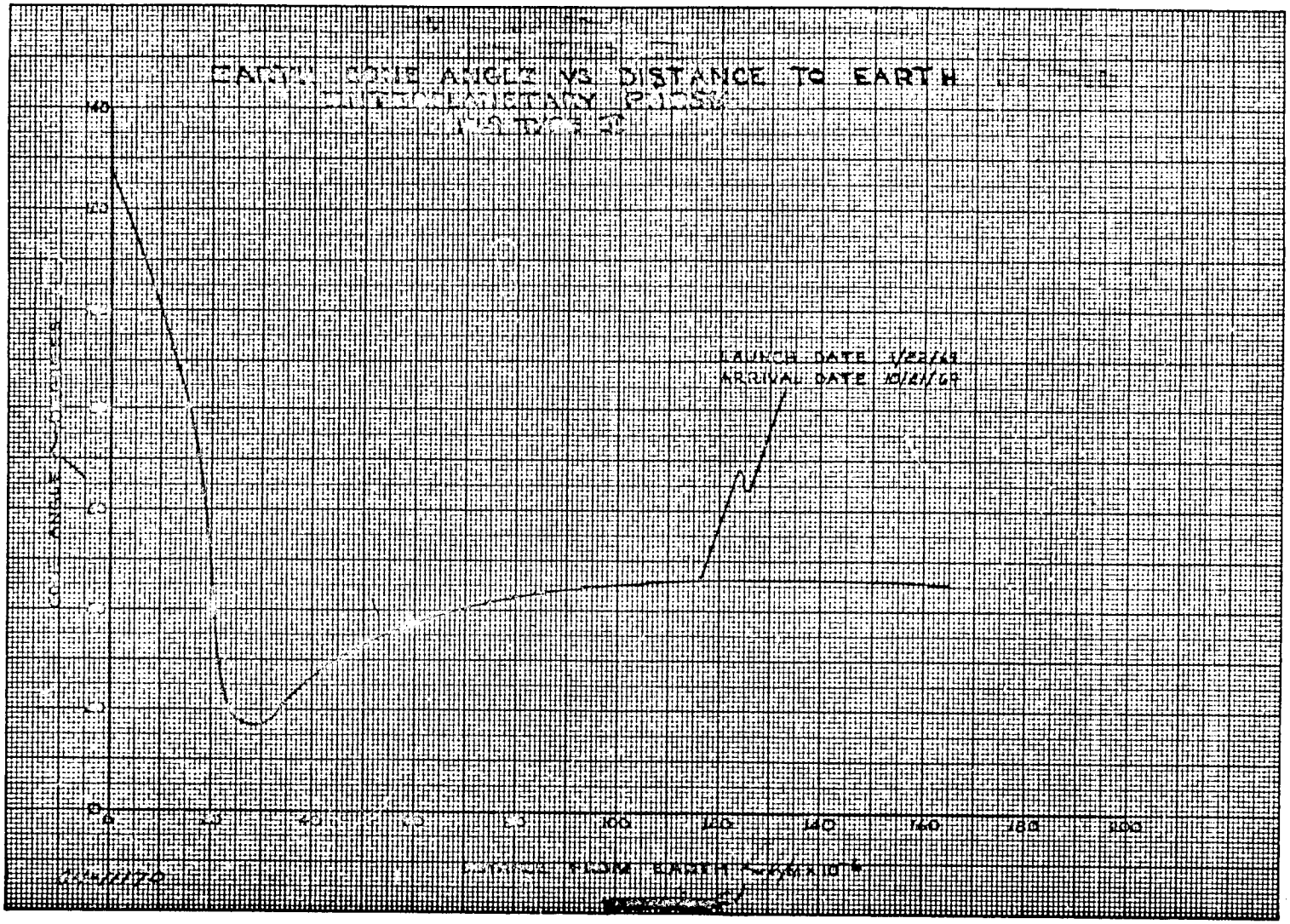

Figure 10 SPACECRAFT -- EARTH CONE ANGLE VARIATION

RE-ORDER No. 64-524

30

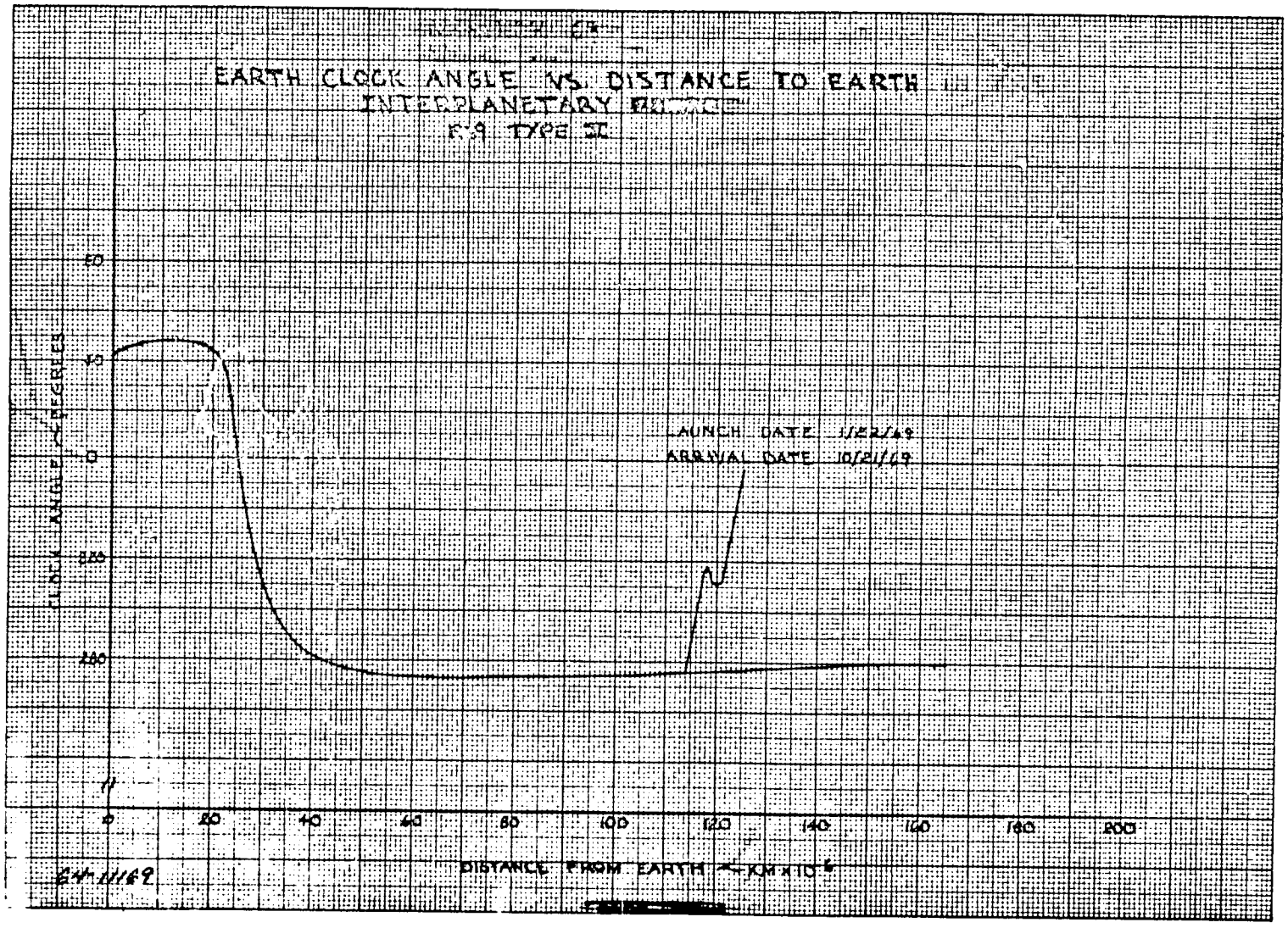

Figure 11 SPACECRAFT -- EARTH CLOCK ANGLE VARIATION

RE-ORDER No. 64-524

The gimbaled payload platform also supports a 34-degree half power beam-width horn antenna, which is used to receive data transmitted from the lander.

4. Stabilization and Control

The stabilization and control system provides attitude control during the cruise mode and maneuver mode of operation. During cruise, the attitude reference is the Sun and Canopus; during a maneuver, gyros are used to provide attitude reference. For cruise mode operation several different types of reaction control systems were investigated. Cap pistols, subliming gas, and cold gas were considered and rated. Based on reliability, weight, development problems, vehicle interface, operating history and cost, a nitrogen cold gas system was selected. Total impulse requirements were based on initial acquisition, limit cycle operation during cruise, maneuver orientations, meteoroid perturbations, solar radiation pressure, and lander separation disturbances. A safety factor of three was used in the total impulse requirement determination. The reaction control system is arranged in four nozzle blocks containing three jets each. The thrust vector control system is a nitrogen cold gas reaction control and is fed by the same cold gas tanks as the cruise mode reaction control jets. Early in the study it appeared that the Mariner C propulsion system would be used for the Advanced Mariner. Although the system utilized a monopropellant with lower performance, this could be justified by utilization of a proven system. A jet vane thrust vector control system was developed for this monopropellant propulsion system and was to be used for the Advanced Mariner. Unlike the Mariner C, which performs two velocity corrections near Earth, where the spacecraft operating temperature is high, (that is, above the +35 °F freezing point of hydrazine), the Advanced Mariner performs a slowdown maneuver near Mars. A thermal control analysis determined that the temperature of the propulsion system would be about 0 °F. Rather than resort to propellant heaters, it was decided to use a bipropellant system and a cold gas reaction control system. There are eight TVC jets. Two jets provide yaw control; two jets provide pitch control; and two couples of jets provide roll control during main engine burning.

5. Propulsion

The propellants selected are IRFNA as the oxidizer and UDMH as the fuel. The allowable operational temperature range for these propellants extends from -56 to + 146 °F. The tanks are arranged in pairs -- Two tanks each of UDMH and IRFNA. This configuration was selected so as to maintain the position of the center of gravity along the longitudinal axis of the spacecraft during propellant depletion. Because of lander diameter requirements, as discussed in section 1.4, it was not possible to consider two tanks -- one placed on top of the other. Two tanks perpendicular to the longitudinal axis were also considered. In this configuration the oxidizer

tank was placed close to the longitudinal axis and the fuel tank was removed a sufficient distance so that the moments of the two tanks about the longitudinal axis would be equal. It was found that the fuel tank fell outside the Surveyor shroud envelope. A low thrust level was necessitated by the requirement of accommodating a large lander diameter. A low thrust level was also required to achieve the velocity increment accuracy of the second midcourse correction, that is, 0.1 ft/sec. Also, this thrust level corresponded to a minimum battery weight requirement. If the thrust level were less than about 20 pounds, the battery requirement would be increased. It was found that the pre-launch through initial acquisition maneuver sequence sized the battery. A 25-pound thrust level was selected because of availability of a developed thrust chamber.

6. Structure

The overall dimension of the flyby/bus are 94 inches in diameter and a height of 26 inches. Lander loads are transmitted to the flyby/bus through an aluminum cylindrical shell. Propellant and cold gas tanks are housed within this shell, and the black boxes are housed in six compartments located external to the shell. Total compartment volume available is 15.5 ft^3. It has been determined that the total volume of black boxes to be housed within the six compartments is 4.5 $ft.^3$ The resulting low volumetric efficiency will ease the problem of center of gravity balance, and thermal control balance.

7. Thermal Control

Thermal control is maintained by the use of surface coatings and louvers. The louvers are attached to the exterior of the compartments and the black boxes are located within the compartment and attached to the same skin as the louvers. Temperature excursions of the black boxes during transit will range from + 94°F near Earth to + 20°F near Mars. Certain components such as batteries, gyros, and cryogenic liquids for the infrared detector will have to be provided with special active control devices, so as to maintain their temperature within prescribed bounds.

8. Separation System

Lander sterilization objectives have been met by placing the lander within a rigid canister. Near planetary encounter the separation sequence is initiated. Lander and canister tiedowns are released; spring forces separate the lander and flyby/bus. Spin rockets attached to the exterior of the canister spin the lander and canister to 20 rpm. A shaped charge cuts the canister into four equal segments causing these segments to fly off radically with respect to the lander. The lander propulsion system is ignited and accelerates the lander so as to place it on an impact trajectory with Mars. After burnout a yo-yo system is used to despin the lander.

41

Characteristics and performance of the flyby/bus systems are summarized in table 3. Flyby/bus conceptual design weights are summarized in table 4, and lander separation system weights are summarized in table 5. The Advanced Mariner spacecraft weight is summarized in table 6. Note that the spacecraft weight is in excess of the 1,342-pound launch weight capability of the unfloxed Atlas-Centaur for the selected 1969 launch opportunity and well below the 1964-pound launch weight capability of the 30-per-cent floxed Atlas-Centaur.

1.6 PARAMETRIC DESIGN STUDY

One of the major goals of this study was to provide sufficient parametric information to allow for significant variations in the final conceptual design. In this section (1) the characteristics of the conceptual design of the systems selected will be noted, and (2) the parametric data that is available and the method of using it for flyby/bus vehicle design will be outlined.

The major constraints that enter into the design of a new flyby/bus are the shroud envelope and the launch booster injected weight capability. The constraints of DSIF on the communication system, guidance error, and the aiming point bias away from planet to meet sterilization requirements have been incorporated into the design and are reflected in the parametric performance curves. To arrive at a new flyby/bus configuration, it is necessary to meet only the weight and dimensional limitations.

Meeting the weight constraint with the parametric data is a straight-forward process. Either the weight is under or over the allowable limit. The envelope constraint is more difficult to define because of the fact that for most subsystems there is not a simple answer. For example, if the maximum shroud constraint was based on the 105-inch diameter of the shroud (the largest body of revolution that could be accommodated is about 96 inches due to two flats on the Surveyor shroud), then it would be clear that a lander with a diameter greater than 96 inches could not be accommodated. The problem is not as clear cut for an increase in the 1) diameter of the fixed high gain antenna, 2) length of the deployable solar panels, 3) length and diameter of the gimbaled payload platform, 4) length of the main propulsion thrust chamber. It is not possible to suggest easily the combinations of previously mentioned alterations that can be accommodated. It must be pointed out that for any change in configuration, a check must be made that the (1) lander can separate without interference, (2) gimbaled payload platform can be allowed the required excursion, (3) solar panels can be deployable, and (4) gimballed payload platform, attitude control sensors, and antennas are mounted so that their view is not obstructed by other elements of the spacecraft. A crude layout would be most helpful to ensure that the new dimensional arrangement can be accommodated.

The discussion will now be centered about the weight constraint and how to develop a new spacecraft. First the booster launch injection weight for the particular mission must be established. This information can be found in the

4r

RE-ORDER No. 64-524

TABLE 3

CHARACTERISTICS AND PERFORMANCE OF FLYBY/BUS SYSTEM

System	
Scientific Instrumentation	Television mapping system; 12-inch focal length; f8 relative aperture; 1-Kilometer resolution at 12,000 kilometers; 330 pictures (2×10^8 bits)
	Charged particle detector, ion chamber, cosmic dust detector, micrometeoroid detector, infrared spectrometer.
Communication	From launch to 43 million kilometers, 10 watts, S-band, hemi-omni antenna, 33-1/3 to 8-1/3 bps; from 43 million kilometers, to encounter, 10 watts S-Band, 3-ft x 1 1/2-ft fixed antenna, 8 1/3 bps; from encounter to encounter + 10 days, 10 watts, S-band, 3 x 1-1/3-foot fixed antenna, 133-1/3 bps; S-Band relay link 34-degrees half-power beam-width horn antenna.
Power Supply	Solar cells, 85 feet^2; silver-zinc batteries.
Guidance	DSIF and two midcourse corrections.
Stabilization and Control	Cruise mode: ACS, Sun-Canopus reference, nitrogen cold gas, limit cycle ± 0.1 degree, 88-minute nominal limit cycle period; propulsion mode: gyro reference, nitrogen cold gas TVC.
Propulsion	UDMH and IRFNA; 280-I_{sp}; mass fraction 0.7 nitrogen pressurant; surface tension baffles to expel propellants; 25-pound thrust level.
Thermal Control	Surface coatings and louvers.
Structure	Aluminum shell with six black box compartments.

43

RE-ORDER No. 64-524

TABLE 4

FLYBY/BUS WEIGHT SUMMARY

Scientific Payload		
Cosmic Dust Detector	2.5 Pounds	
Micrometeoroid Detector	8.0	
Ion Chamber	1.3	
Particle Flux Detector	2.5	
Magnetometer	5.0	
Infrared Spectrometer	29.0	
Television Mapping System	20.0	
	68.3 Pounds	68.3
Gimbaled Payload Platform		20.6
Power Supply		
Batteries	20.0	
Solar Panels	102.0	
Power Conditioning	22.5	
	144.5	144.5
Communications		
Antennas	3.5	
S-Band Power Amplifier	8.0	
S-Band Transponder	28.5	
Telemetry Subsystem	23.0	
Television Tape Recorder	40.0	
Command Subsystem	11.0	
	114.0	114.0
Relay Antenna, Receiver, and Recorder		23.5
Data Automation System		8.0
Central Computer and Sequencer		15.0

14

RE-ORDER No. 64-524

TABLE 4 (Concl'd)

Stabilization and Control		
Gyro Electronics Package	10.0	
Control Electronics Package	3.0	
Canopus Star Tracker	7.0	
Limit Cycle Sun Sensor	1.5	
Acquisition Sun Sensors	0.4	
Plumbing and Nozzles	13.0	
Tankage	31.0	
Cold Gas	31.0	
	96.9	96.9
Propulsion		
Propellants	93.0	
Tankage	14.0	
Pressurant Bottle	2.7	
Thrust Chamber	2.1	
Plumbing, Valves, Residuals	21.2	
	133.0	133.0
Thermal Control		
Insulation	10.0	
Louvers	21.0	
Surface Coatings	5.0	
	36.0	36.0
Structures		
Booster-Spacecraft Adapter	17.0	
Flyby/Bus-Lander Support Structure	13.5	
Panel Support Ribs	11.1	
Propulsion System Support Structure	23.0	
Black Box Structure	43.0	
Accessories	16.4	
	124.0	124.0
Bracketry and Fittings		25.0
Cabling		58.0
		866.8

45

TABLE 5

LANDER SEPARATION SYSTEM WEIGHT SUMMARY

Sterilization Canister	66.5 Pounds
Separation Joints	3.3
Spin Rockets	2.8
Propulsion	23.0
Yo-Yo Despin	9.5
Bracketry, Fittings, and Leads	5.5
	110.6 Pounds

TABLE 6

ADVANCED MARINER SPACECRAFT WEIGHTS

Lander	516 Pounds
Separation System	110
Flyby/Bus	867
	1,493 Pounds

Systems Analysis Volume, Volume 2. The mission selection will give rise to (1) a transfer time, (2) predicted guidance error, (3) communication range, and (4) approach velocity. The transfer time is required to establish the cruise mode cold gas requirements; the guidance error is used to determine the dispersion in the flyby passing distance; the communication range is used to establish the allowable telemetry bit rate; and the approach velocity taken in combination with a required lander lead time will establish the velocity increment requirements of the propulsion system.

Lander weight comprises the largest payload item for the flyby/bus. The lander dimension and weight can be determined from the parametric material presented in the Lander Design Study, Volume 3. Instrumentation for the flyby/bus can be selected from data presented in section 2.2. Justification for the selection can be found in section 2.1, where there is to be found a discussion of planetary observables and associated physical phenomena that would aid in the selection of instrumentation. In section 2.4 there is presented a parametric analysis of television mapping system performance. Since the periapsis passing altitude is known after the launch trajectory is selected, the focal length and aperture can be determined for a required resolution. From the focal length and aperture, the dimension, weight, and power consumption of the TV mapping system can be calculated. In a similar fashion the payload for the flyby/bus can be selected, and the weight and power requirements can be determined. The power will be converted to a power supply weight figure after the total spacecraft power requirements have been established. It will be assumed that the gimbaled payload platform weight is constant. A discussion of the platform can be found in section 2.5.

The next element considered is the structure. It has been assumed that the lander comprises the greatest single weight acting on the flyby/bus and that the loads imposed during the launch phase by the lander will have the greatest effect on structural weight, to the exclusion of all other system load variations.

The flyby/bus structure must be designed to carry the lander and lander separation system. The separation system includes the sterilization canister, propulsion system, spin rockets, despin yo-yo, separation joints, and bracketry. A description of the separation system is to be found in section 10.1. Only the sterilization canister and propulsion system weight will vary significantly. It can be assumed that the canister weight is proportional to the square of the lander diameter. The weight of the propulsion unit can be determined after the propellant mass fraction and specific impulse have been selected as shown in section 10.6. The velocity increment to place the lander on an impact trajectory can be determined from work accomplished in the Systems Analysis Volume, Volume 2. Using performance charts developed in section 6.2, the mass of the lander propulsion can be determined. The flyby/bus structural weight can then be determined from the parametric structural weight chart to be found in section 8.2.

Sizing of the communication system depends upon the total number of bits to be collected and the bit rate requirements. During encounter, the time when a large quantity of bits are collected, the decision must be made whether to transmit data in real time, (to minimize the recorder storage capacity), or to store and playback the data after planetary encounter. In the case of real time transmission the power/antenna gain product of the telemetry link must be large, so that the transmitted bit rate equals the rate of acquisition of bits. For the playback after encounter case, the tape recorder must be large enough to store all bits during encounter, and then the bit rate and time allowed for transmission can be traded off. Account must be taken of changes in the antenna slant range and look angles after encounter. The parametric information presented in section 4.3 allows for playback for periods as much as 10 days after encounter. With this parametric data, both transmitted power and antenna dimensions can be determined. The characteristics of the low gain antenna, (which must be used during the initial phases of the mission due to large excursions in the cone and clock angle), are presented in section 4.2. Using the data in section 4.1, it is possible to determine the cross-over range from the low gain antenna to the high gain antenna. The weights, volumes, power consumption of the electronic equipment associated with communications systems can be determined from Section 4.4. Sufficient information is provided with which to determine the weight variation of those components which are sensitive to performance.

In section 7.0 there is to be found the stabilization and control system parametric design data and conceptual design. The power requirements of the system are invariant, and so the performance figures given in section 7.4 will yield the power that must be supplied. Cold gas requirements, however, are variable. For the reference conceptual design, the cold gas system provides for attitude control during cruise mode and maneuver mode. Section 7.3 has both parametric data and design equations to allow for estimates to be made of the total required impulse. Account must be taken of requirements for initial acquisition, limit cycling, maneuver orientation, meteoroid impacts, lander separation disturbances, gimbaled payload platform inertia torques, and solar radiation pressure. To establish the impulse requirements for initial acquisition, limit cycling, and maneuver orientation, the reaction jet moment arm and spacecraft moments of inertia must be established.

At this point the power consumers have been identified, and the power supply system can be sized. According to the procedures outlined in section 3.0, the power conditioning equipment weight, the batteries, and solar panels can be sized. Margins of safety for panel area and battery capacity should be included.

The next items that must be accounted for are the fixed weights. These items include bracketry and fittings and have been assumed to be 20 percent of the structural weight (see table 4). The fixed weight also includes cabling. The 58 pound weight allowance shown in table 4 for the reference design has been arrived at by (1) determining the number of leads, (2) assuming a mean length of lead, i.e., radial distance to the outer edge of black box compartment, and

(3) a total number of connectors. The 25-pound estimate for bracketry and fittings and 58 pounds for cabling should be nearly invariant for spacecraft designed within the weight limitation of the Atlas-Centaur and dimensional limitations of the modified Surveyor shroud.

At this point in the design an iterative process must be conducted.

There is an interrelationship between the cold gas, propulsion system, and moments of inertia. To determine the size of the propulsion system, the cold gas must be known; but the cold gas depends on the moment of inertia, and to establish the moment of inertia, the cold gas and propulsion system mass must be known.

To proceed, an estimate should be made of the cold gas requirement for both TVC and cruise mode ACS. The figure used for the reference design (see table 4) is a good starting point.

The total mass of the spacecraft has been established save for the mass of the propulsion system. Using the ΔV for the midcourse corrections (see section 6.1) and the ΔV established by mission considerations for the flyby/bus slowdown maneuver, the mass of the propulsion system can be determined from the parametric information presented in section 6.2. Since the mass of propellants and the specific impulse are known, the product of these two parameters, the total impulse, is known. After the moments of inertia are established, the cold gas required for TVC can be determined from section 7.3. Propellant tanks can be determined from data presented in section 6.3 to insure that the tank dimensions are within reasonable bounds.

A simplified spacecraft configuration can be used to establish the moments of inertia. Figure 12 shows a simplified layout of the reference design shown in figure 6. The spacecraft has been divided into seven components. Items 1, 2, 3, and 4 refer to the deployable solar panels. The moments of inertia can be determined by assuming that the panels are rectangular and are two-dimensional. A moment of inertia about the center of gravity of the panel can be approximated by the product of the area moment and the mass per unit area of the panel. Item 5, the fixed solar panel, can be treated as a two-dimensional annulus. Item 6 represents the flyby/bus cylinder which houses the cold gas tanks and propellant tanks and the six (only two are shown) black box compartments. It can be assumed that these spacecraft components can be packaged to form a homogeneous cylinder and a mass moment of inertia established. Item 7 is the lander; the moments of inertia and center of gravity location can be determined from the lander design study, Volume 3. These inertias should be increased to account for the inertia contribution of the separation system. Determine the radii of gyration of the lander and multiply by the sum of the masses of the lander and separation system. It was also assumed that the pitch and yaw moments of inertia of the lander are equal. Table 7 shows how the center of gravity of the spacecraft is established. The spacecraft moments of inertia are presented in Table 8, where $I_{x'_n}$, $I_{y'_n}$, $I_{z'_n}$ is the moment of inertia of the spacecraft elements about their own center of gravity, and $I_{x''_n}$, $I_{y''_n}$, $I_{z''_n}$ is the moment of inertia of the spacecraft elements about the spacecraft center of gravity.

RE-ORDER No. 64-524

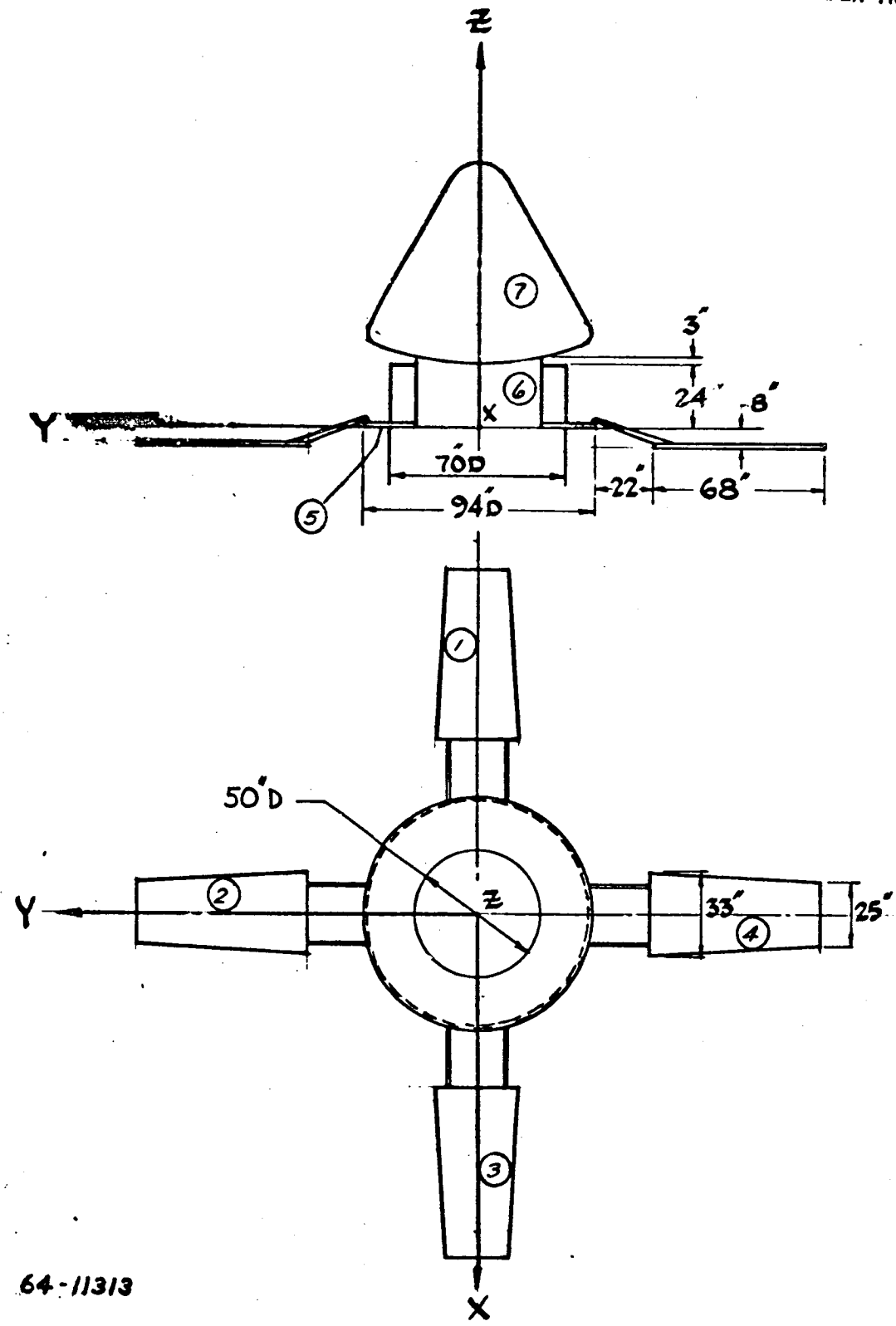

Figure 12 SIMPLIFIED LAYOUT OF SPACECRAFT

50

These moments of inertia can now be used to determine the cold gas requirements according to Section 7.3. If the cold gas weight determined is significantly different than the one assumed, the propulsion system will have to be sized again, and the calculations repeated until convergence occurs.

RE-ORDER No. 64-524

TABLE 7

SPACECRAFT CENTER OF GRAVITY LOCATION

PRE-SEPARATION CONFIGURATION

Item, n	w_n (lb)	m_n (slugs)	x_n (in)	$w_n x_n$	y_n (in)	$w_n y_n$	z_n (in)	$w_n z_n$
1	16.5	0.513	-103.	-1700.	0	0	+ 8.0	+132.
2	16.5	0.513	0	0	+103.	+1700.	+ 8.0	+132.
3	16.5	0.513	+103.	+1700.	0	0	+ 8.0	+132.
4	16.5	0.513	0	0	-103.	-1700.	+ 8.0	+132.
5	36.0	1.12	0	0	0	0	0	0
6	765.0	23.8	0	0	0	0	-12.0	-9180.
7	626.0	19.4	0	0	0	0	-46.0	-28,796.

$\sum w_n = 1493.0$ $\quad \sum w_n x_n = 0$ $\quad \sum w_n y_n = 0$ $\quad \sum w_n z_n = -37,448.$ in-lb

$\bar{x} = 0$ $\quad \bar{y} = 0$ $\quad \bar{z} = 25.1$ in.

POST-SEPARATION CONFIGURATION

1	16.5	0.513	-103.	-1700.	0	0	+ 8.	+132.
2	16.5	0.513	0	0	+103.	+1700.	+ 8.	+132.
3	16.5	0.513	+103.	+1700.	0	0	+ 8.	+132.
4	16.5	0.513	0	0	-103.	-1700.	+ 8.	+132.
5	36.0	1.12	0	0	0	0	0	0
6	765.0	23.8	0	0	0	0	-12.	-9180.

$\sum w_n = 867.$ $\quad \sum w_n x_n = 0$ $\quad \sum w_n y_n = 0$ $\quad \sum w_n z_n = 8652.$

$\bar{x} = 0$ $\quad \bar{y} = 0$ $\quad \bar{z} = -9.98$ in.

where

$$\bar{x} = \frac{\sum w_n x_n}{\sum w_n} \quad \bar{y} = \frac{\sum w_n y_n}{\sum w_n} \quad \bar{z} = \frac{\sum w_n z_n}{\sum w_n}$$

52

TABLE 8

SPACECRAFT MOMENTS OF INERTIA
PRE-SEPARATION CONFIGURATION

Item, n	$I_{x'n}$*	$I_{y'n}$	$I_{z'n}$	$\bar{x}_n - \bar{x}$	$\bar{y}_n - \bar{y}$	$\bar{z}_n - \bar{z}$	$(\bar{x}_n - \bar{x})^2$	$(\bar{y}_n - \bar{y})^2$	$(\bar{z}_n - \bar{z})^2$	$m_n d^2_{z_n}$	$m_n d^2_{y_n}$	$m_n d^2_{x_n}$	$I_{x''n}$	$I_{y''n}$	$I_{z''n}$
1	36.	198.	234.	-103.	0	+33.	10,609.	0	1094.	561.	6004.	5442.	597.	6202.	5676.
2	198.	36.	234.	0	+103.	+33.	0	10,609.	1094.	6004.	561.	5442.	6202.	597.	5676.
3	36.	198.	234.	+103.	0	+33.	10,609.	0	1094.	561.	6004.	5442.	597.	6202.	5676.
4	198.	36.	234.	0	-103.	+33.	0	10,609.	1094.	6004.	561.	5442.	6202.	597.	5676.
5	444.	444.	887.	0	0	+25.	0	0	629.	705.	705.	0	1148.	1148.	887.
6	8432.	8432.	14,578.	0	0	+13.	0	0	171.	4072.	4072.	0	12,505.	12,505.	14,578.
7	6584.	6584.	6329.	0	0	-21.	0	0	438.	8489.	8489.	0	15,073.	15,073.	6329.
												ΣI =	42,323.	42,323.	44,497.

I_x = 294. slug-ft^2
I_y = 294.
I_z = 309.

POST-SEPARATION CONFIGURATION

1	36.	198.	234.	-103.	0	+18.	10,609.	0	323.	166.	5608.	5442.	202.	5806.	5676.
2	198.	36.	234.	0	+103.	+18.	0	10,609.	323.	5608.	166.	5443.	5806.	202.	5676.
3	36.	198.	234.	+103.	0	+18.	10,609.	0	323.	166.	5608.	5442.	202	5806.	5676.
4	198.	36.	234.	0	-103.	+18.	0	10,609.	323.	5608.	166.	5442.	5806.	202.	5676.
5	444.	444.	887.	0	0	+10.	0	0	100.	112.	112.		555.	555.	887.
6	8432.	8432.	14,578.	0	0	-2.	0	0	4.	97.	97.	0	8529.	8529.	14,578.
												ΣI =	21,100.	21,100.	38,169.

I_x = 147.
I_y = 147.
I_z = 265.

where:

$$d^2_{z_n} = (\bar{y}_n - \bar{y})^2 + (\bar{x}_n - \bar{x})^2$$
$$d^2_{y_n} = (\bar{x}_n - \bar{x})^2 + (\bar{z}_n - \bar{z})^2$$
$$d^2_{x_n} = (\bar{z}_n - \bar{z})^2 + (\bar{y}_n - \bar{y})^2$$

*slugs-in^2

RE-ORDER No. 64-524

43

2.0 SCIENTIFIC PAYLOAD

2.1 MISSION OBJECTIVES ANALYSIS

The analysis of possible science returns from the Mars environment through use of the flyby/bus portion of the Advanced Mariner system is based on the division of the planet into zones. The zones are as follows:

1. Atmosphere:

Taken as the volume bounded by the solar wind and the surface of the planet; this volume is subdivided in table 9.

2. Biosphere:

Taken as the distribution of ecologies and individuals in the Mars environment. They may be in a viable or post-biotic (fossil) state. (See table 10.)

3. Lithosphere:

Taken as the solid crust of the planet, bounded by the atmosphere (there are no oceans), and the interior, where rocks change from solid to stress-fluid states. (See table XI.)

4. Endosphere:

Taken as the interior of the planet where earthquake energies are generated and released (See table 12.)

It can be seen that matter composed of atoms can be combined in various ways in all of the four spheres. In some spheres, more combinations are possible than in others. It is manifest that the most complex combinations are possible in the vicinity of the lithosphere, particularly in its upper parts. The most complex groupings of elements are expected to be organic, if there is life on Mars. This is the case on Earth.

The four, somewhat arbitrary, zones listed above can be further subdivided into geomorphic orders of magnitude. Nine subdivisions have been made; these range from hemispheric and circumplanetary features of the first order through ninth order corpuscular (atomic fragment) features. The orders are best seen by referring to the four charts. Interaction between the four planetary zones has been considered in attempting to optimize the position of flyby vehicles surface track. For example, a steep dark mountain of the lithosphere, which in all probability has brought materials from depth to surface, can be expected to be the locale of a maximum number of diverse elemental nutrients. Such a

54

prominence can also be expected to be the site at which the maximum number per unit area and variety of weathered forms may be expected, and therewith shelters of a sort. Such a mountain will also be the site of maximum variety in temperature per unit linear distance across the geoid of Mars and also the site above which there will be the maximum variety in weather changes in the atmosphere. Telescopic observations suggest that such sites will cause cloud banks to form. Terrestrial experience and telescopic observation of post cloud bank darkness at dark areas suspected to be topographic prominences, suggest that sublimination and/or precipitation will be at a maximum in such areas. It is thought that such sites will provide optimum variety in conditions and therefore an optimum probability of finding living forms. Living forms may be much more extensively developed in more monotonous areas; however, the presence of Sinton bands, waxing and waning of dark areas, reestablishment of dark areas after dust storms, and the improved possibility of precipitation suggest the dark areas as an optimum location to look for life. The variety of atmospheric and lithospheric (geological) features in such areas as opposed to the more monotonously regular areas is obvious.

The target signatures which include the electromagnetic spectrum, fields, and materials have been tabulated across the top of the charts. The instruments which may be used to measure the feature will be listed later. Contours have been drawn about the rating of each source of information from geomorphic features in each zone from the flyby/bus. The subdivisions used are nil, fair, good, and excellent. The reader should note that the contours would be quite different if the instruments were in a vehicle 10 to 100 km above the surface of Mars as opposed to the flyby height of 5,000 to 15,000 km or as compared with surface measurements. In the notes accompanying each table below, only those contours rated good and excellent have been amplified with brief explanations.

The atmospheric chart has not been contoured because there is a multiplicity of zones on a single sheet. The density of information is higher, however, concerning the first through fourth orders because the features are more easily resolved than the smaller geometries and temporal sequences of the fifth through ninth orders.

Evidences concerning the endosphere from the flyby vehicle will be indirect. They can be secured primarily by magnetic measurements and gravitational variations as evidenced in the flyby trajectory.

Very little concerning the detailed nature of the biosphere can be seen from a flyby vehicle; however, the presence may be suggested. Proof would probably have to be secured on the surface. A strong suggestion of a biosphere would immediately suggest the presence of highly complex structures in the sixth,

RE-ORDER No. 64-524

TABLE 9

FLYBY/BUS SCIENCE MEASUREMENTS -- ATMOSPHERE

	sub zones	GAMMA	X-RAY	UV	OPTICAL	IR	RADAR	RADIO		GRAVITY	MAGNETIC	ELECTRIC	CORPUSCULAR	MOLECULAR
1st Order circumplanetary & hemispheric	Troposphere		F	F	E	G	F							
	Stratosphere			G	G	F								
	Mesosphere				F						F		F	
	Exosphere													F
	Magnetosphere										E		G	
2nd Order hemispheric convection and standing waves	Troposphere			F	E	G	F							
	Stratosphere			G	G	F								
	Mesosphere						F	G			G		G	
	Exosphere													
	Magnetosphere										G		G	
3rd Order high pressure & low pressure vorticies	Troposphere			F	G	F								
	Stratosphere			F	F									
	Mesosphere						F	F			F		F	
	Exosphere													
	Magnetosphere													
4th Order major cloud structures such as individual local thunderstorm	Troposphere			G	F	G	F							
	Stratosphere			F	F	F								
	Mesosphere										F			
	Exosphere													
	Magnetosphere													
5th Order turbulent regime as wind shear, cloud structures	Troposphere				F	F	F							
	Stratosphere				F									
	Mesosphere													
	Exosphere													
	Magnetosphere													
6th Order Viscous regime vorticies can no longer form	Troposphere													
	Stratosphere													
	Mesosphere													
	Exosphere													
	Magnetosphere													
7th Order suspended solid and liquid particles	Troposphere													
	Stratosphere													
	Mesosphere													
	Exosphere													
	Magnetosphere													
8th Order molecular	Troposphere													
	Stratosphere			F										
	Mesosphere													
	Exosphere													
	Magnetosphere													
9th Order corpuscular regime	Troposphere													
	Stratosphere													
	Mesosphere						F	F						
	Exosphere													
	Magnetosphere													

56

RE-ORDER No. 64-524

TABLE 9 NOTES

ATMOSPHERE

1st Order

Optical: First under banding at the horizon should be detectable by optical TV. Optical occultation of sun and/or stars would also be of value in defining the general structure with altitude of the atmosphere.

UV and IR: TV photography in these short and long wavelength regions could enhance the optical horizon studies above.

Magnetic: First order shape of a possible magnetosphere may be able to be obtained, depending on flyby geometry.

Corpuscular: Additional evidence on magnetosphere.

2nd Order

Optical: Cloud patterns by optical TV provides information on hemispheric or circumplanetary atmospheric waves.

UV and IR: UV enhances optical becuase of spectrally dependent transparencies and albedo of various cloud particles. IR mapping replaces optical on night side of planet.

Radiowaves: Various frequencies valuable for top-side sounding of ionosphere variations of first order.

Magnetic: Second order features of magnetosphere may be discerned.

3rd Order

Optical: Essentially as for 2nd order above. 3rd order features are more completely covered by limited area photography.

4th Order

Optical: As above. Large numbers of 4th order cloud features should be observed.

TABLE 10

FLYBY/BUS SCIENCE MEASUREMENTS -- BIOSPHERE

	GAMMA	X-RAY	UV	OPTICAL	IR	RADAR	RADIO		GRAVITY	MAGNETIC	ELECTRIC	CORPUSCULAR	MOLECULAR
1st Order (Geoidal Regime) circumplanetary and hemispheric distributions of living matter			F	E	G								
2nd Order (Differentiation Regime) continental and oceanic distributions of living matter, or wet/dry, hot/cold patterns less than hemispheric or circumplanetary			F	E	G								
3rd Order (Provincial Regime) local ecologies, say a coastal plain of a continent or single desert of Mars			F	G	F								
4th Order (Differential Regime) zones on single mountain like terrestial timberline, or in dry/drier zones of Mars deserts				F									
5th Order (Localized Regimes) largely related to minor shelter, nutrients, water, etc.													
6th Order distribution of zooplankton & phytoplanktom about minor sedimentary features, as single grains & nodules													
7th Order (Colloidal-Molecular Regime) association of organisms with clays and small particles				G									
8th Order (Geochemical Regimes) ability of life (particularly microorganisms) to concentrate compounds and elements													
9th Order (Corpuscular Regime) cosmic flux and mutation rates of DNA gene codes													

TABLE 10 NOTES

BIOSPHERE

1st Order

Optical: TV photography should map major portion of dark belt during flyby if sufficient photos are taken.

IR: Spectroscopy of dark maria will supplement 1st order optical mapping, possibly distinguishing wide scale variation in composition of presumed vegetative life.

2nd Order

Optical: TV photography of one or more domains of continental extent should be covered.

IR: Spectroscopy as above.

3rd Order

Optical: TV photography of local ecologies, features in size just below earthbased resolution limitations. Information may be obtained on contacts between vegetation and adjacent relatively lifeless areas.

7th Order

Optical: Polarization measurements can provide information on particulate nature of biotic entities.

RE-ORDER No. 64-524

TABLE 11

FLYBY/BUS SCIENCE MEASUREMENTS -- LITHOSPHERE

	GAMMA	X-RAY	UV	OPTICAL	IR	RADAR	RADIO		GRAVITY	MAGNETIC	ELECTRIC	CORPUSCULAR	MOLECULAR
1st Order (Geoidal Regime) circumplanetary rotational bulge, hemispheric tidal bulges	F	F	F	G					F			F	F
2nd Order (Differentiation Regime) continents, ocean-basins, major impacts with melting over +5° of planets arc		F	F	G	F				G	F	F	F	
3rd Order (Provincial Regime) mountain ranges, old-lands, coastal plain, continental shelves, all phases of geosynclinal complexes craters which break crust of a planet			G	E	E	G			F	F			
4th Order (Differential Topographic Regime) single mountains			G	E	E	G							
5th Order (Mass Waste Regime) mass waste sequence			F	G	F								
6th Order (Sedimentary Regime) sedimentary series from mass waste product to sedimentary grains			F	G	F								
7th Order (Colloidal-Molecular Regime) sedimentary grains to colloids													F
8th Order (Geochemical Regime) base exchange, hydrolyzate exchange, PT-changes													
9th Order (Nuclear-Corpuscular Regime) lithospheric nuclear chemistry from endogenetic sources and exogenetic sources													

60

RE-ORDER No. 64-524

TABLE 11 NOTES

LITHOSPHERE

1st Order

Optical:	As for biosphere, TV photography, if coverage is achieved, will map geological aspects of hemispherical or circumplanetary extent.

2nd Order

Optical:	TV photography of regions of continental extent will receive somewhat more complete coverage.
Gravity:	Continents may be discernible by gravitational anomalies. (See Endosphere notes.)

3rd Order

Optical and IR:	TV photography will provide excellent coverage. IR will supplement through spectral differences of various third order features. Major circular deserts should be included in flyby coverage.
UV and Microwave:	Additional spectral information by broad band mapping in these electromagnetic regions.
4th Order	As above. Large numbers of 4th order features such as impact craters, mountains, etc., should be seen. 5th and 6th orders depending on resolution of instruments.

61

seventh, and eighth orders. If such life should be based on a code like that in DNA of terrestrial life, there is an implication of vast numbers of information bits in these orders.

The coutours of the lithospheric table include a large area. From our knowledge of the Earth's lithosphere, we can project numbers of bits needed to describe first to sixth order geomorphic features and know that the data yielded in the first through third orders is rather high while the data yielded in the fourth through ninth orders are progressively more difficult to resolve from a flyby vehicle.

2.2 INSTRUMENTATION LIST

The analysis in the previous section provided an evaluation of the possible observations from the planetary flyby. Table 13 is the list of instruments as provided by the Jet Propulsion Laboratory that were to be considered in this flyby study.

By considering both the results obtained in the mission objective analysis and by performing an optimization analysis as developed during the Voyager Program, the final payload (table 14, was selected from table 13.

This selected payload satisfied both interplanetary and planet flyby science.

RE-ORDER No. 64-524

TABLE 12

FLYBY/BUS SCIENCE MEASUREMENTS--ENDOSPHERE

	GAMMA	X-RAY	UV	OPTICAL	IR	RADAR	RADIO	GRAVITY	MAGNETIC	ELECTRIC	CORPUSCULAR	MOLECULAR
1st Order (Geoidal Regime) rotational circumplanetary, tidal hemispheric				F				G	G			
2nd Order (Differentiation Regime) convective up/down drafts major thermal, seismic, gravity anomalies, shields & cratons				F				F	F			
3rd Order (Provincial Regime) earthquake zones: margin & mid-continental, isostatic balance of geomorphic provinces			F	G	F							
4th Order (Differential Regime) concentration of earthquake foci thermal, gravity anomalies at intersecting geomorphic provinces; single foci, thermal anomalies, etc.				F								
5th Order (Xenolithic Regime) sub-crustal stopeing												
6th Order ("Sedimentary" Regime) single crystal differentiation and growth in magma or migma												
7th Order (Molecular Regime) decrease in silicate polymerization with depth, gravity differentiation carrier-ion differentiation												
8th Order (Geochemical Regime) differentiation of elements												
9th Order (Nuclear-Fission-Corpuscular Regime) decay schemes breeder-reactions												

62

RE-ORDER No. 64-524

TABLE 12 NOTES

ENDOSPHERE

1st Order

Gravity: Accurate altimetry will enable gravitational effects on flyby trajectories to be analyzed in terms of rotational and possibly tidal bulge of endosphere.

Magnetic: Mapping of planetary field will allow determination of location and sense of magnetic poles.

63

TABLE 13

JPL INSTRUMENTATION LIST FOR FLYBY/BUS

Instrument	Experimental Objectives	Weight (pounds)	Power (watts)	Volume or Dimensions (inches)	Bits/Sample	Total Bits	Additional Constraints
Infrared spectrometer	Planetary -- determination of those minor constituents of the upper cloud structure whose absorption spectra are in the infrared region. Measurement of the atmospheric profile of temperature and pressure.	29	7	12 (dia) x 15	5000	To be maximized	Aligned toward planet vertical; required detector cooling
Ultraviolet photometer	Planetary -- determination of the presence of particular constituents of the upper atmosphere by means of filter spectroscopy.	1.5	1.5	3 (dia) x 5	4 bits/second/photometer	Continuous	Aligned toward planet vertical
Magnetometer	Planetary -- to establish the existence of a planetary field and to determine its characteristics; magnitude, direction, multipolarity, and orientation. To investigate the nature of the interface between planetary and interplanetary magnetic fields.	5	5	4 x 4 x 6	24	Sampled every minute	Reduction of spacecraft magnetic field required; orientation in planetary coordinates must be known.
Particle flux detector	Interplanetary -- used in conjunction with the ion chamber to monitor the energetic particle and photon radiation in interplanetary space. Provides semi-quantitative information about the energy and particle types composing radiation.	2.5	0.35	4 x 5 x 6	N/A	N/A	Close to ion chamber, spacecraft to subtend minimum solid angle.
Ion chamber	Interplanetary -- to measure the total ionizing radiation (cosmic rays) and the variation with time and position in the solar system.	1.3	0.10	6" sphere	N/A	N/A	Close to particle flux; spacecraft to subtend minimum solid angle.
Trapped radiation detector	Planetary -- to search for magnetically trapped, charged particles, if present, to study their intensity and directional and spatial distributions; also cosmic rays.	4	0.7	4 x 5 x 5	N/A	N/A	30-degree cone angles, toward and away from the sun.
High-energy proton directional monitor	Interplanetary -- to provide information about the temporal, spatial and directional variations of galactic cosmic ray flux.	4	0.5	3 x 4 x 4	N/A	N/A	60-degree angle visibility parallel to ecliptic. 60-degree cone angle visibility perpendicular to ecliptic. 60-degree cone angle toward the sun.

RE-ORDER No. 64-524

65

TABLE 13 (Concl'd)

Instrument	Experimental Objectives	Weight (pounds)	Power (watts)	Volume or Dimensions (inches)	Bits/Sample	Total Bits	Additional Constraints
Cosmic ray spectrum analyzer	Interplanetary -- to investigate the intensity and the gradient of flux of charged particles in space as functions of nuclear species and time.	18	2	18 x 6 x 6	N/A	N/A	Four mutually perpendicular telescopes. 30 - to 60-degree cone angles.
Plasma instrument (electrostatic analyzer)	Interplanetary -- to measure the flux of positive and negative components of solar plasma travelling outward from the sun with good energy and directional resolution. To correlate these data with the magnetic field and the low energy plasma.	7	1.25	6 x 8 x 8	N/A	N/A	Covers seven sections of a solid angle of 4 sterad centered on the sun.
Plasma instrument (Faraday cup)	Interplanetary -- to determine the particle number density, the distribution of velocity vector, and the temporal and spatial distributions of the interplanetary plasma. To correlate these data with the magnetic field measurements.	20	4	36 x 10 x 10	N/A	N/A	Four 60-degree cone angles, toward, away, and perpendicular to the sun.
Cosmic dust (A)	Interplanetary -- to measure the flux of cosmic dust particles as a function of direction, distance from the sun, and momentum with respect to the spacecraft.	2.5	0.2	5 x 5 x 5	N/A	N/A	One plate perpendicular to ecliptic.
Micrometeoroid detector (A)	Interplanetary -- direct measurement of the velocity and cumulative mass distribution of the cosmic dust of the Zodiacal cloud and in the vicinity of the planets.	8	0.5	10 x 10 x 6	N/A	N/A	Three tubes in ecliptic plane, toward, away from, and 90-degrees from the sun. One tube perpendicular to ecliptic.
Bistatic radar	Interplanetary -- to obtain information on the absolute electron density in inter-planetary space and the fluctuation of this density as a function of time.	6-8	2	4 x 4 x 12 excluding antennas	Cruise: 0.2 bit/sec Encounter: 1.2 bit/sec.	Continuous	Occulting of spacecraft by planet required. Antennas to be oriented to Earth. Antennas: 40-cm, 300-cm dipoles.
Infrared spectrometer	Simultaneous mapping of composition of surface and correct radiation and correct radiation from orbiting vehicle.	12	15	12 (dia) x 15	500 bit/sec.	To be maximized	Point to vertical

RE-ORDER No. 64-524

66

TABLE 14

INSTRUMENTATION FOR FLYBY/BUS

Scientific Instrument	Weight (pounds)	Power Consumption (watts)	Dimensions (inches)	Bits of Information Generated		
				Acquisition to Encounter	Encounter	Post Encounter
Cosmic Dust Detector	2.5	0.2	5 x 5 x 5	Bits collected will be assumed to fill the available capacity of the telemetry system, and so cannot exceed 8-1/3 bits/sec.		
Micrometeoroid Detector	8.0	0.5	10 x 10 x 6			
Ion Chamber	1.3	0.1	6 inch sphere			
Particle Flux Detector	2.5	0.35	4 x 5 x 6			
Magnetometer	5.0	5.0	4 x 4 x 6	Sampled every minute.		
Infrared Spectrometer	29.0	7.0	12 inch diameter x 15 inches	5000 bits/sample. Number of samples will equal number of TV pictures.		
TV Mapping System	20.0	15.0	Optics and camera: 6 inch diameter x 12 inches Electronics: about five packages, 4 x 5 x 6	600,000 bits/picture.		

RE-ORDER No. 64-524

2.3 LANDING SITE AND MAPPING CORRIDOR

The planetary approach geometry, among other criteria, controls the selection of landing sites and flyby mapping corridors for each mission. The results presented in this section are necessary but not sufficient to select the entry angle and azimuth of the lander and the flyby azimuth for the television mapping. Several other system considerations place further constraints on the parameters considered here, and must be combined with these results to determine the total constraints.

In figure 13 are presented the geometrical aspects of the lander geometry for the 3.75 km/sec departure velocity case, as based on computations of the planetary transfer trajectory. The coordinate system used here is a Mercator projection of a latitude-longitude grid which is conventional in its definition except that the zero of longitude is chosen as that meridian directed towards the sun. The actual planetary surface may then be considered as rotating beneath this grid once each Martian solar day. Each contour in the figure is given as a set of four curves, corresponding to the arrival conditions for four launch dates as indicated in the caption.

The sunlit hemisphere is bounded by the symmetrical set of curves for which sunrise and sunset are indicated. The -90° entry point of impact can be seen in the upper left quadrant to be situated on or very near the sunrise line. The landing contours for selected entry angles of -70, -50 and -30 degrees are shown as shaded bands swept out by the changing conditions during the arrival window. Also shown in figure 13 are the curves defining the locations for which, at the landing time, the Earth is just on the local horizon, and for which it is 20 degrees above the horizon. If the latter earth elevation and a minimum entry angle of 30 degrees are selected as constraints, then it can be seen for example that the latitude limits for the lander extend from 55 degrees north to 45 degrees south at the beginning of the window and from 45 degrees north to 35 degrees south at the end of the launch window, and thus from 45 degrees north to 35 degrees south for the entire window.

The longitude constraints on the lander depend on the precise time of the landing. If that time could be freely selected by small Earth orbit departure and midcourse guidance adjustments, then any landing site within the above latitude limits could be achieved. In northern latitude cases, considerable freedom of choice of entry angle is possible. For example, Syrtis Major, a desirable landing site for this mission, is at 10 degrees north and can be reached with entry angles ranging from about -70 to -20 degrees.

The flyby geometry also enters into the selection of the landing site since it would be highly desirable to obtain flyby photographs of the area in which the lander is located. In figure 14 are shown paths along the planet surface which should be traced out directly below the spacecraft for typical flyby azimuths. The curves were calculated with two approximations. It was assumed that the

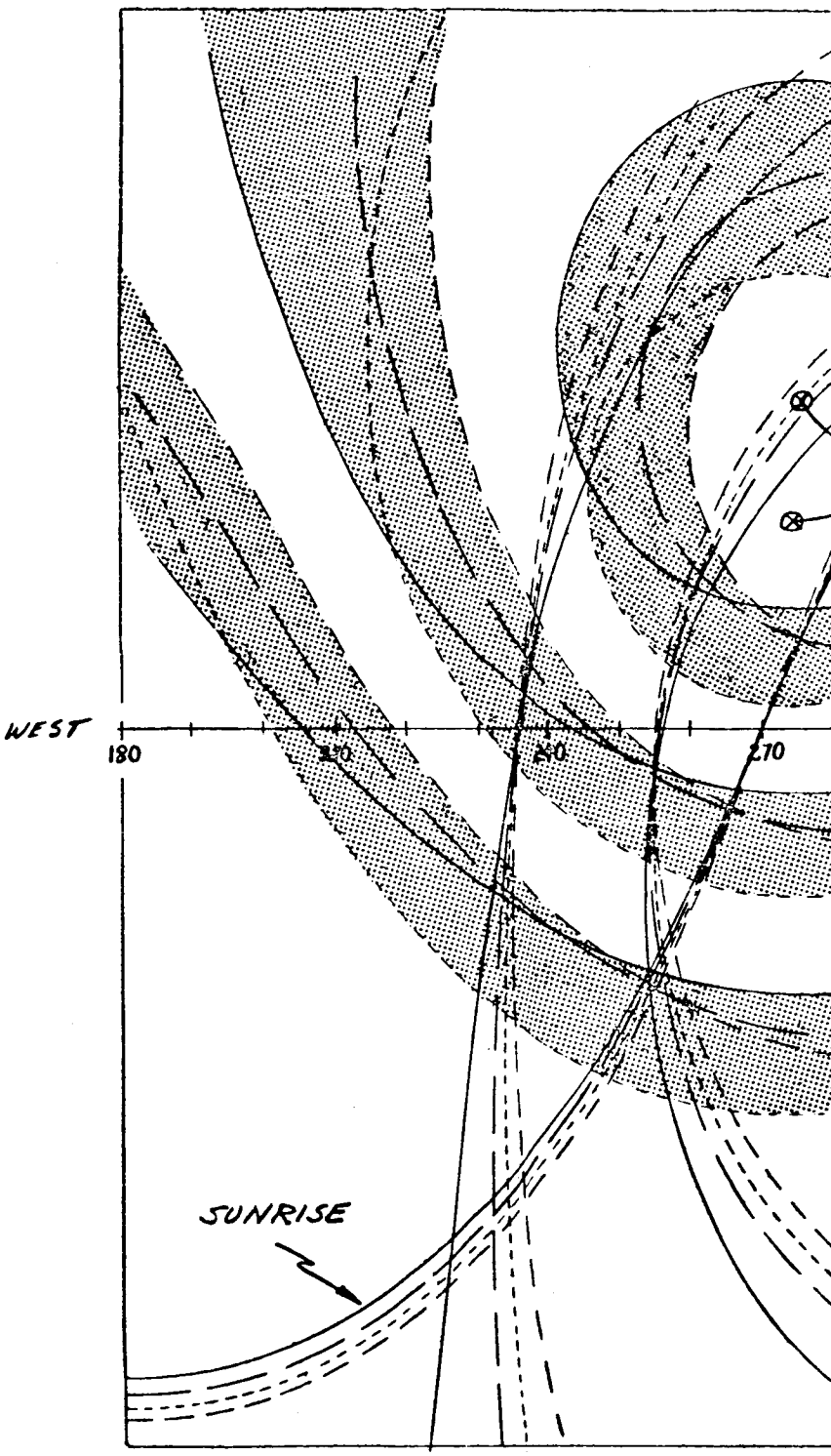

64-11314

1d

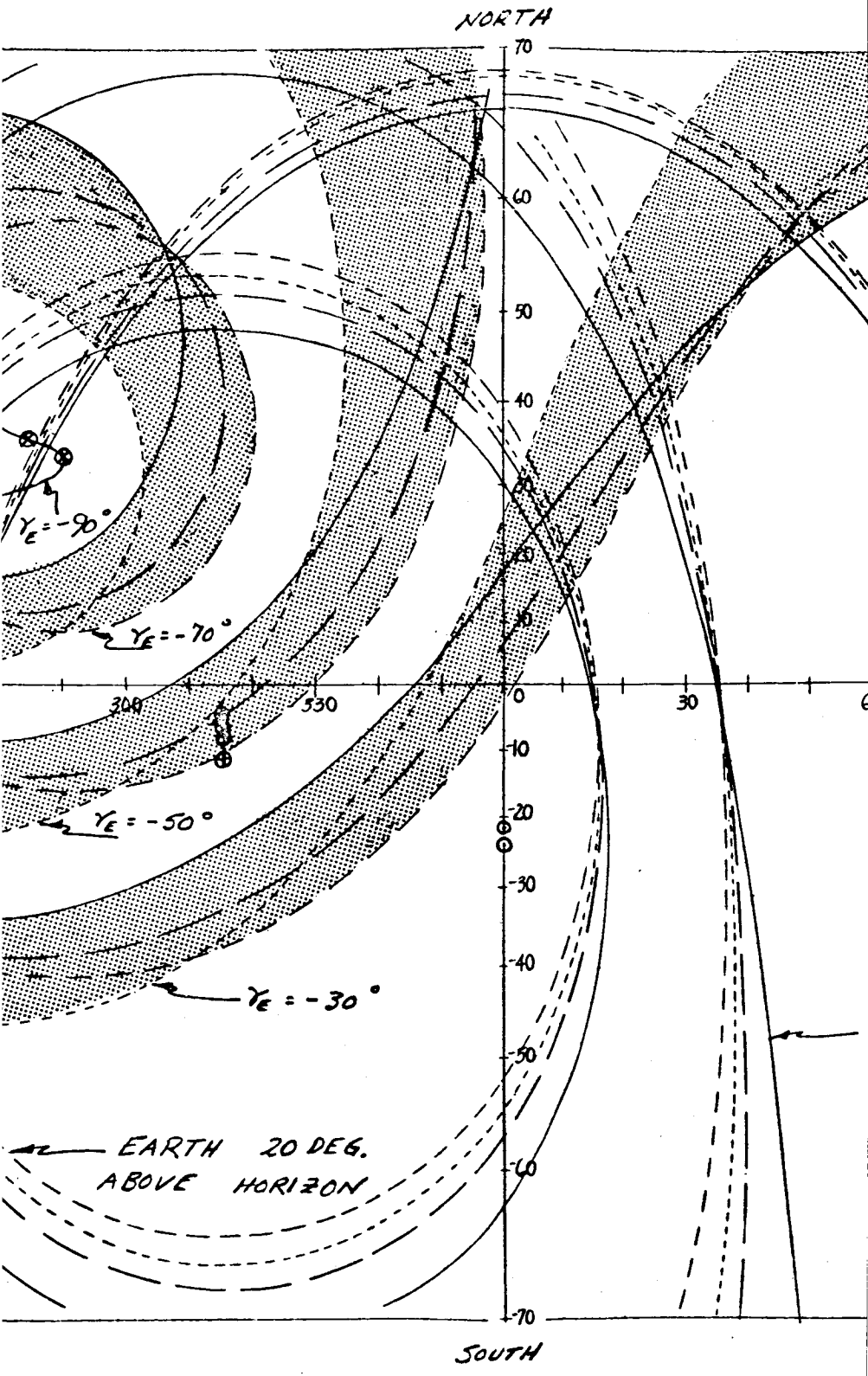

Figure 13 ADVANCED MARINER LANDER GEOMETRY - 1969 LAUN

2#

RE-ORDER No. 64-524

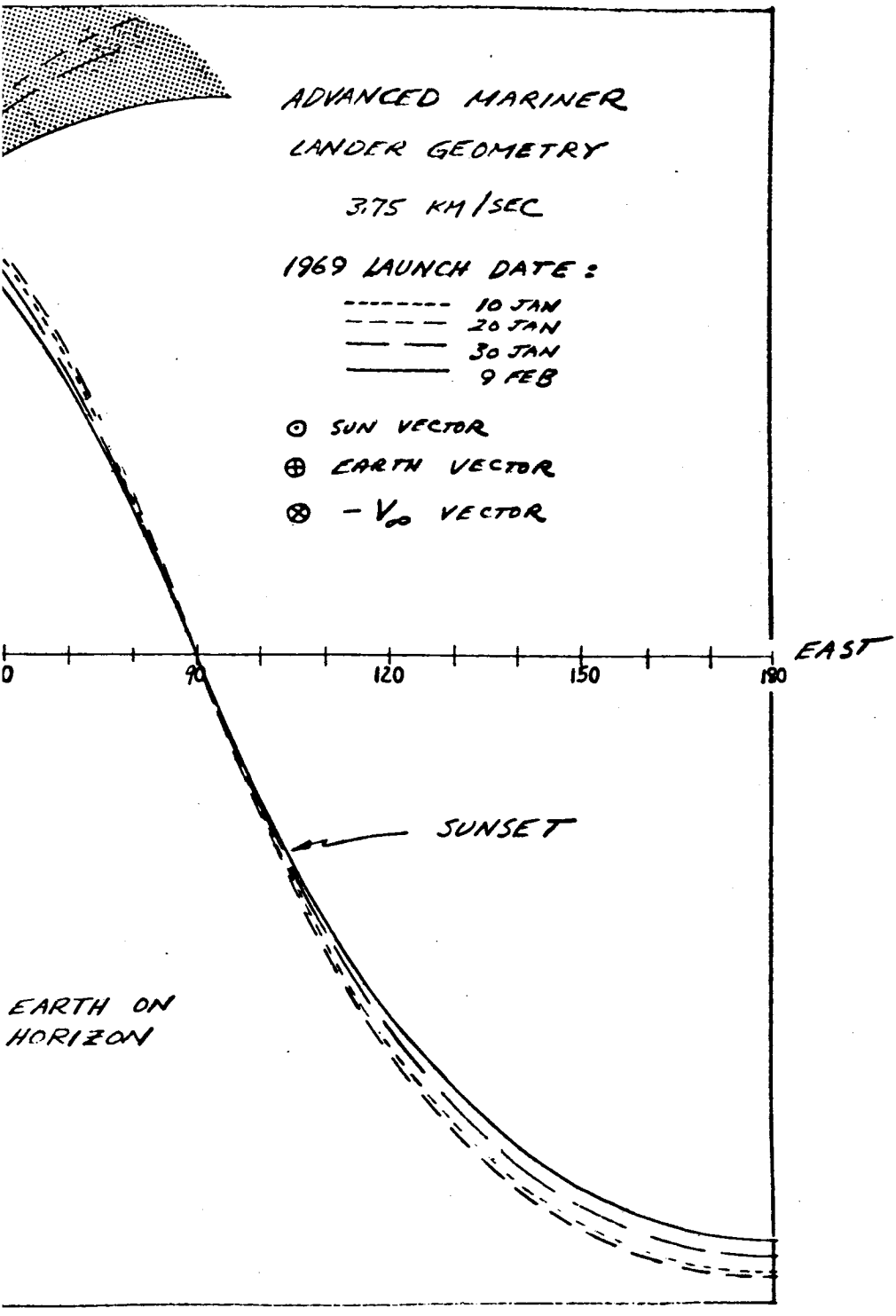

:H

3#

69.

planet did not rotate during flyby. Rotation would shorten the ground track shown in figure 14. In addition, planetary attraction, which would tend to extend the path of the flyby a few degrees depending on the velocity and distance of closest approach, was also neglected. These corrections, both small in themselves, tend to cancel each other and would not significantly affect the conclusions derived below.

The shaded portions of each typical flyby azimuth mark the arc on the planet surface directly below the spacecraft from 30 degrees before until 30 degrees after the point of closest approach. This is the optimum time for photographic work, since rapidly increasing distance becomes troublesome before and after this interval. It can be seen from figure 14 that sunlit latitudes from about 65 degrees north (which would include the continuous polar region cloud cover at this time of the Martian season) to 85 degrees south could be achieved by proper selection of the flyby azimuth. Due to the circumstance that the approach velocity vector lies essentially on the terminator, optical television photographs and radiometer measurements of the dark hemisphere surface temperature cannot both be obtained from the flyby spacecraft.

If the time of arrival of the flyby can independently be controlled relative to the time of the capsule landing, the point directly below the spacecraft at its time of closest approach can be made to coincide with the landing site. This procedure is recommended since the interpretation of the flyby photographs will be strongly aided if they cover the area of the landing capsule.

Utilizing the results shown in figures 13 and 14, the following recommendations can now be made, based on the scientific mission objectives:

1. Incorporate in Advanced Mariner a capability to adjust the time of arrival of the lander over a 24-hour time period.

2. Incorporate a capability to adjust the entry angle over a wide range in order to make possible target site selection.

3. Select Syrtis Major, at 10 degrees north latitude, as the first priority landing site, and adjust the landing time to be one hour after local sunrise. This places the landing at 288 degrees longitude on figure 13, and requires entry angles ranging from -72 to -63 degrees depending on the day of launch. A circle of 8 degrees radius around this target point lies entirely within Syrtis Major.

4. For this landing site, select a flyby delay of 5 hours and a flyby azimuth of 90 degrees (clockwise, in a plane normal to V_∞, from a zero azimuth flight over the north pole of the planet). This happens to be the minimum inclination flyby, and places Syrtis Major at 354 degrees longitude on figure 14. The surface track of this flyby intersects Syrtis Major from 20 to 30 degrees before periapsis, which degrades the resolution for that

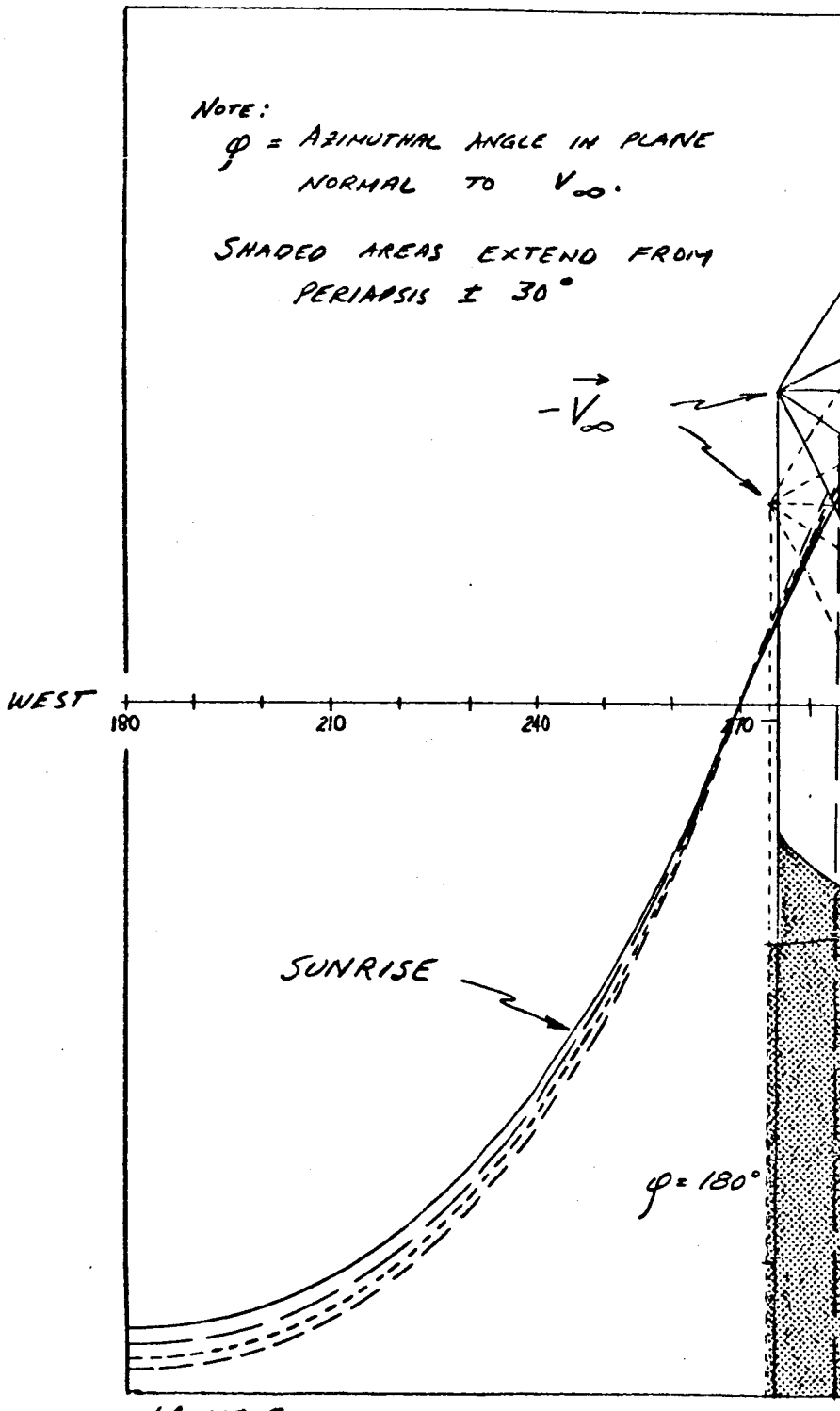
NOTE:
φ = AZIMUTHAL ANGLE IN PLANE NORMAL TO V_∞.
SHADED AREAS EXTEND FROM PERIAPSIS ± 30°
$-\vec{V}_\infty$
WEST
180
210
240
270
SUNRISE
φ = 180°

64-11315

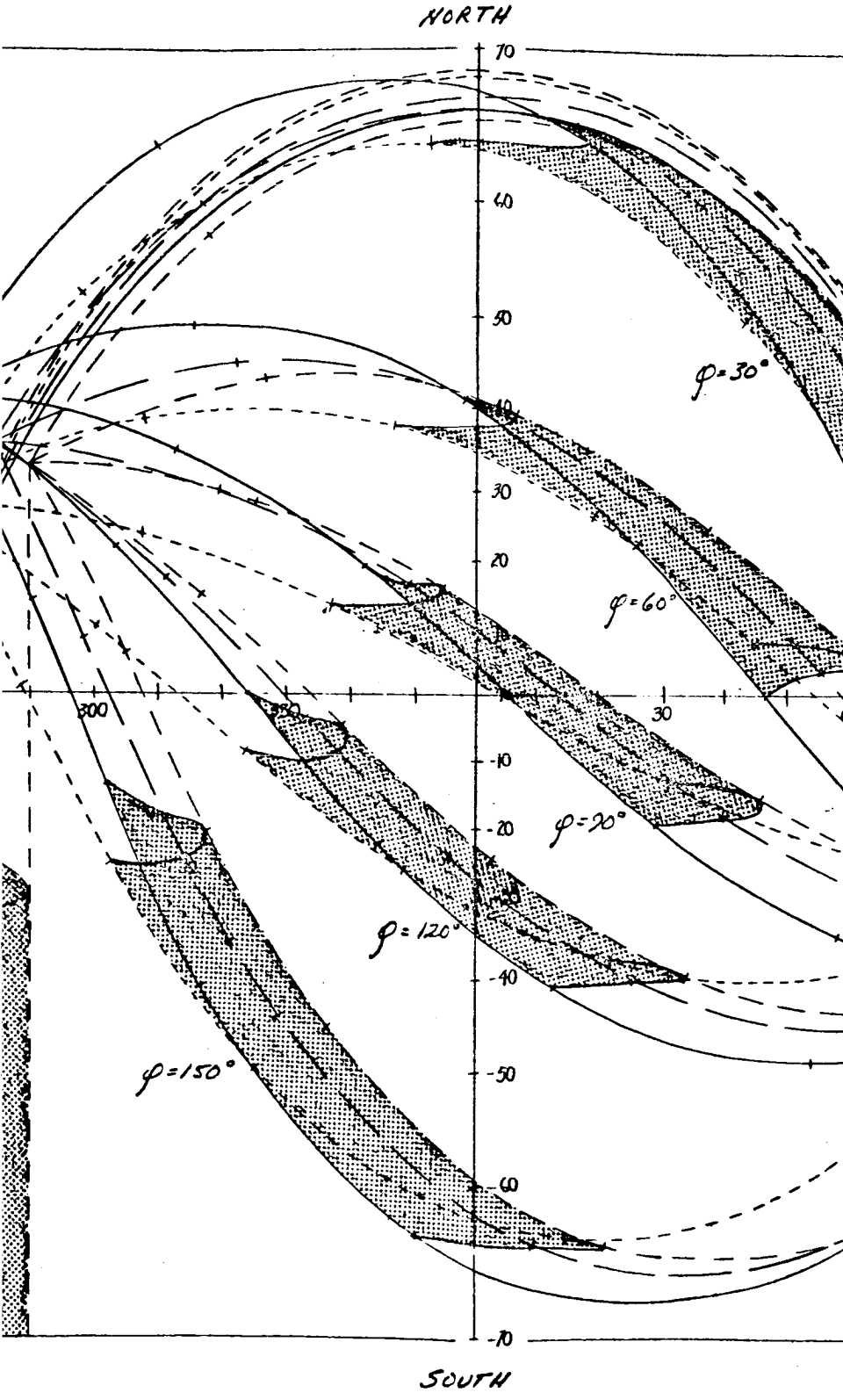

Figure 14 ADVANCED MARINER FLYBY GEOMETRY - 1969 LAUNCH

RE-ORDER No. 64-524

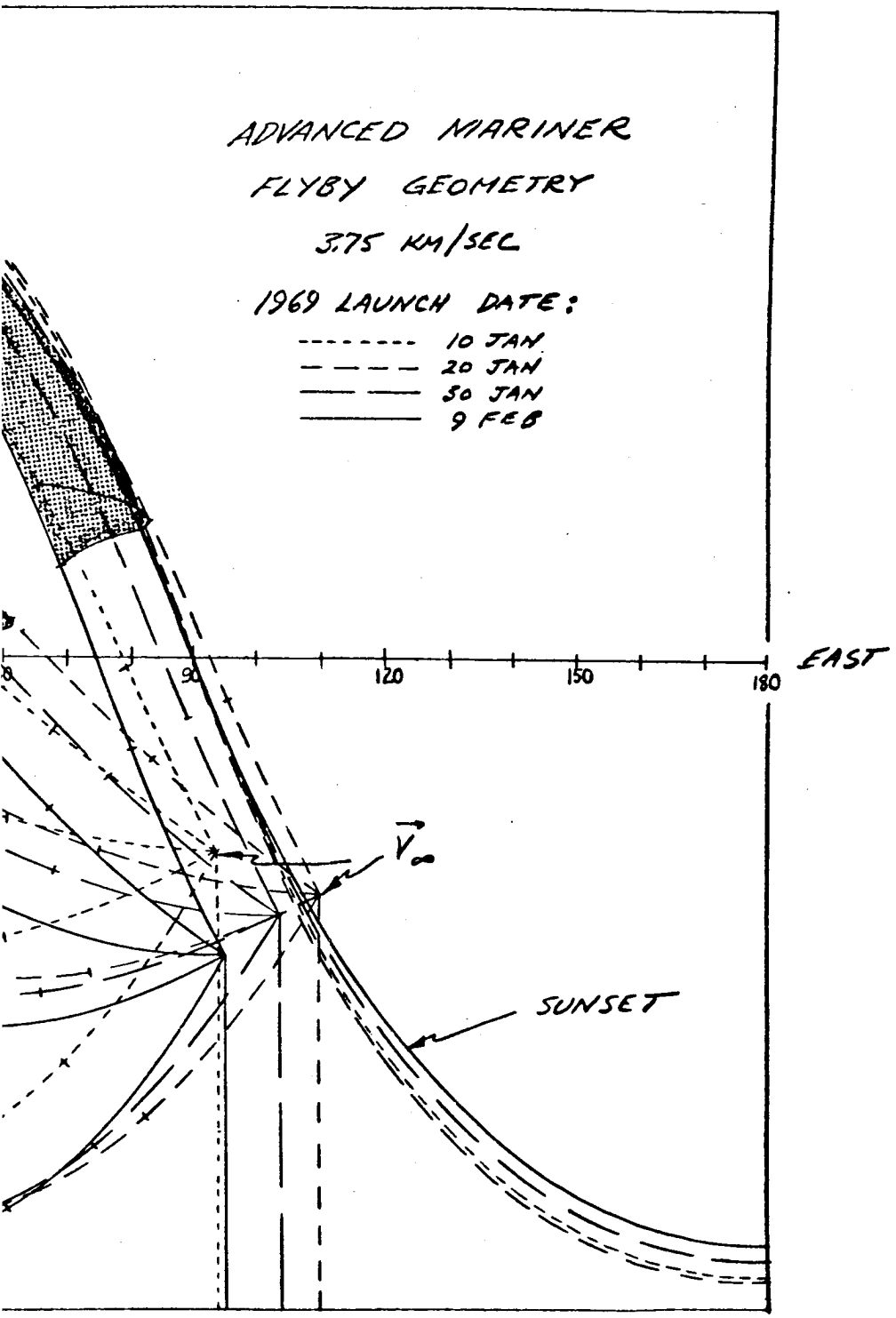

3#

target only slightly. However, this path continues through a region on the northern edge of Mare Tyrrhenum which is desirable for photographic purposes.

Alternative sites at other longitudes could be selected to meet other possible constraints. Landing at Solis Lacus at 25 degrees south latitude, requires an entry angle as low as -38 to -48 degrees, a lander dispersion radius of 3 degrees, and a flyby delay time of 5-1/2 hours for satisfactory flyby photography of the landing site. The northern latitude approach direction for 1969 makes the selection of even adequate landing sites extremely difficult.

2.4 TV MAPPING SYSTEM

1. Objectives

The purpose of this analysis is to determine the relationships between the television system component characteristics and the quality or information content of the pictures to be taken. From these relationships and the practical constraints imposed by hardware availability and reliability a conceptual system design for an arbitarary mission is formulated. A completely general analysis will not be attempted largely because the important relationships change form if different types of equipment are used. It will therefore be assumed that the TV system components are similar types to those used on the Mariner C Program. This restriction is justified because the primary system constraints of reliability and ruggedness are the same for both the Mariner C and Mariner Mars 1969 missions, and breakthroughs in equipment, which will enhance reliability, cannot be predicted for the development time period for a 1969 mission.

2. Parameters

The parameters which are of interest in designing the television subsystem have been broken into four groups (in a somewhat arbitrary, but useful, manner). These groups are: 1) the input parameters or those which define the quality or usefullness of the final received pictures, 2) the parameters which will exist as constraints imposed on the system, 3) the design parameters of the system which define how the input parameters relate to the final output parameters, and 4) the output parameters which describe the effects of the effects of the TV system on the spacecraft as a whole.

Table 15 lists the parameters according to the groupings described above.

TABLE 15

TV MAPPING SYSTEM PARAMETERS

Input	Constraints	Design	Output
Target Size	Smear Effects	Image Size	Total Bits
Resolution	Illumination	Tube Resolution (Lines/In)	Size
Brightness Level Resolution	Sun-Spacecraft Planet Angle	Focal Length Lens Aperture	Weight
	Altitude	Shutter Speed Tube Sensitivity	

a. Relationships (Input-Design)

The two fundamental relationships in this analysis relate the target size and resolution to the basic design parameters. These are

$$W = h \frac{L}{F} \tag{1}$$

$$R = h \frac{L}{nF} \tag{2}$$

where

W = Side of target area (km) (square image assumed)

L = Side of image area (inches) (i.e., side of largest square image possible on tube)

h = Vehicle distance from target (km)

F = Lens focal length (inches)

R = Side of target resolution cell (km)

n = Number of lines or samples per line in a picture

It should be noted that $\frac{L}{F}$ and $\frac{L}{nF}$ are the instrument parameters and as such are the only parameters that are under the designer's control.

Thus it is useful to rewrite equations (1) and (2) as

$$\frac{W}{h} = \frac{L}{F} \tag{3}$$

$$\frac{R}{h} = \frac{L}{nF} \tag{4}$$

Another important quantity to the system designer is the amount of light or illuminance of the picture tube. This can be shown to be

$$E_{pc} = \frac{I_s}{\pi} \rho \cos \alpha \frac{T}{4 r_o^2 f^2} \text{ (foot-candles)} \tag{5}$$

where

I_s = Illuminance at 1 AV (lumens/m^2)

$\frac{I_s}{\pi}$ = Average brightness (lamberts)

ρ = Geometrical albedo ($\sim$0.15)

α = Included angle between incident and collected light rays

T = Lens efficiency (80 percent)

r_o = Distance between planet and Sun (AU)

f = f number = (ratio of focal length to aperture distance)

Substituting the values for ρ and I_s which are applicable for Mars, equation (5) can be simplified to

$$E_{pc} = \frac{376 \cos \alpha}{r_o^2 f^2}$$

where

$$1.38 < r_o < 1.66$$

Taking

r_o = 1.52, we get

$$E_{pc} = \frac{163 \cos \alpha}{f^2} \tag{6}$$

74

If it assumed that the maximum value of α is 75 degrees, then

$$E_{pc} = \frac{42.5}{f^2}$$

The use of this value of α for the calculations does not imply that attempts should not be made to obtain photographs at angle approaching 90 degrees. The actual light levels available at these large angles is a function of surface composition and the terrain being photographed and therefore cannot be predicted.

However, this in itself indicates that very useful information will be obtained by trying to photograph at these high angles.

For a given type of storage camera tube, there is a threshold value of average integrated plate illumination below which a satisfactory picture cannot be attained. The exposure time required is thus determined by the relation

$$\Delta t = \frac{K}{E_{pc}} \qquad (7)$$

Where

Δt is the required exposure time

and K is a tube constant measured in average foot-candle seconds. It is very difficult to determine the value of K for a particular type of tube, especially in the case of the vidicon, where the voltage response to brightness is non-linear. The satisfactory average light level will be determined by the minimum resolvable brightness level desired for the "low-light" portions of the picture. This is determined by the effective signal-to-noise ratio out of the tube, which is in turn a function of the temperature and target voltage at which the tube is operated. Thus the value of K is determined not only by the tube characteristics but also by the way it is used and the information desired from it.

If we let $E_{pc} = \dfrac{\frac{I_s}{\pi}}{f^2}$

then,

$$\Delta t = \frac{K}{\frac{I_s}{\pi}} f^2 \qquad (7)$$

75

From the above analysis it can be seen that the following component parameters determine the system performance:

1) Focal length (F)

2) Aperture or f number (f)

3) Size of image on tube (L)

4) Number of lines on tube (n)

5) Duration of shutter opening (Δt)

b. Constraints

The ranges of allowable design parameters are constrained by the choice of trajectory for a particular mission. The most important effect is termed smear and results from the change in the position or apparent size of the target during the exposure time. The relationship between the smear velocity for a given exposure time and the optimum size of a resolution cell is somewhat subjective. It seems apparent that decreasing the size of the resolution cell will result in increased information despite the effects of smear; however, the rate of increase of information will decrease sharply as the resolution cell is made smaller than the total smear during an exposure. For Mariner C the allowable total smear was one-half of the resolution cell size. Expressing this criterion in equation form:

$$R = 2\dot{S}(\Delta t) \tag{8}$$

The parameters which relate to the acheived resolution can now be expressed follows:

$$R = \frac{Lh}{hF} \tag{9}$$

$$R = 2\dot{S}(\Delta t) \tag{10}$$

$$\Delta t = \frac{K}{B} f^2 \tag{11}$$

$$R = \frac{2\dot{S}Kf^2}{B} \tag{12}$$

76

Equation (9) is the straightforward optical geometry condition which must be met, and equation (12) describes the effect on resolution of the light level available as a function of optical, picture tube, and trajectory parameters.

e. Output Parameter Relationships

Of the three output parameters mentioned previously, only the number of total bits can easily be related to resolution. The key relationship is

$$B = n^2 \times \log_2 b \tag{13}$$

where

B = total number of bits/picture

n = number of lines/picture

b = number of brightness levels

The determination of satisfactory number of brightness levels or equivalently the number of bits in the grey scale is largely subjective. It will be tacitly assumed that a six-bit grey scale will be used largely because a six-bit grey scale corresponds closely to human ability (to resolve brightness levels). It must be pointed out, however, that the human eye need not be the only data processer available to evaluate the received pictures of Mars. It is conceivable that geologists could find finer brightness level information useful, or alternatively it might be possible to get nearly as much information with a coarser grey scale. The weight of the data storage system will vary with the required storage capacity, but the weight variation is more sensitive to the type of design than to small changes in capacity. It appears that a recorder of 2×10^8 bit capacity can be provided in a reasonable configuration. It the camera raster is fixed by the tube type, it is then possible to trade off brightness resolution against the total number of pictures. The weight and size of the camera system will be affected by each of the design parameters. The general proportionality relationships can be derived; however, exact determination of weight and size are determined by the designs of the devices themselves. An approach which can be used is to define the proportionality relationships and then to pick the device types of interest (e.g., vidicon, orthicon, etc.) to establish actual design constants. The resolution achievable can then be determined as a function of the over-all system size and weight.

For the purposes of weight analysis the television system will consist of two packages. The first is the camera head, which includes the lens, camera tube, supporting structures, and possible preamplifier electronics. The second package is the electronics, which will not vary appreciably with any of the parameters which have been discussed. Also associated with the television system are the buffer storage and the final storage systems. These have been discussed as parts of other vehicle subsystems.

The camera head weight will be a function of the lens focal length and aperture. The camera tube weight will be largely a function of the type of tube selected rather than the tube parameters discussed above. An approximate relation for the camera lead weight can be shown to be

$$\text{Head Weight} = C_1 + \frac{C_2 L^3}{f^2} \tag{14}$$

where C_1 is the weight of the camera tube, and any supporting electronics in the head and C_2 is a constant determined by the type of lens and the structural materials used.

3. Design Considerations

The parameteric approach to design implies that the relations derived in the analysis will be used to select the design parameters for a final system design. In many cases, however, the types of designs are selected on the basis of factors not considered in the parametric evaluation. For the case of the television system, these factors are reliability, and noninterference with other spacecraft systems. Consideration of these factors is particularly important in the selection of the camera tube. At present two types of devices are in wide use. These are the image orthicon, and the vidicon. In general, orthicons are more complex and larger, and for space use, the choice is at least at present restricted to vidicon-type tubes. There are several new types of vidicons being studied and evaluated throughout industry. These include all electrostatic tubes, devices using image intensifier tubes with fiber optics coupling to the vidicons and tubes using various new materials, including "ferro electric" collectors. Most of these new devices exhibit increased sensitivity as their major improvement. As will be seen from further analysis, the practical limit to achievable resolution is not the tube sensitivity, but rather is the line density of the tube. For this reason, the remaining analysis is based upon using a tube very similar to that presently being used for Mariner C. This is an all-electrostatic, slow scan vidicon using a selenium compound photo conductor.

The choice of the type of lens system is to a large extent governed by the limitations to the system imposed by the choice of camera tubes. Because of vidicon has a relatively small usable target area and compared to image orthicons or film devices, a relatively poor resolving capability, only moderate resolving power is needed in the lens. Thus it is possible to use a Dall-Kirkam or a simplified Cassegrain lens system with no degradation of the system performance. The approximate weight relationship introduced earlier is based upon using a lens system of this type.

a. Design Data

As discussed above, the parameteric relations which are useful in designing the television system are

$$R = \frac{Lh}{nF} \tag{9}$$

$$R = \frac{2\dot{S}\,K\,f^2}{I_s/\pi} \tag{12}$$

$$\text{Head Weight} = \frac{C_1 + C_2\,L^3}{f^2} \tag{14}$$

The parameters $\frac{L}{h}$ and K are camera tube characteristics and as discussed previously, are a function only of the type of tubes selected. Data from the manufacturer of these tubes, General Electrodynamic Corporation, indicate that for a 1969 mission, tubes with an $\frac{L}{h}$ value of 1360 for target area of 0.22 x 0.22 inch can be manufactured using an improved version of the deflectron electrostatic deflection system. A value of K = 0.03 appears to be an achievable sensitivity threshold for the type of slow-scan tube under consideration, and a value of $\frac{I_s}{\pi}$ = 40 lamberts is taken as the worst case illumination.

The constant C_1 refers to the weight of the camera tube and any supporting electrons required. For an all-electrostatic tube this weight should be approximately 0.5 pound. The constant C_2 is determined by the lens design and the materials used. For a system such as that used in Mariner C, where considerable use was made of beryllium and beryllium alloys, the value of C_2 is approximately 0.15.

For the 1969 mission the periapsis altitude will vary from 2,707 to 9,949 kilometers. A conservative smear velocity, $\dot{S}$, of 5 km/sec for this mission was selected. The lens apertures are derived for this smear velocity. The change of altitude during flyby is shown in figure 15.

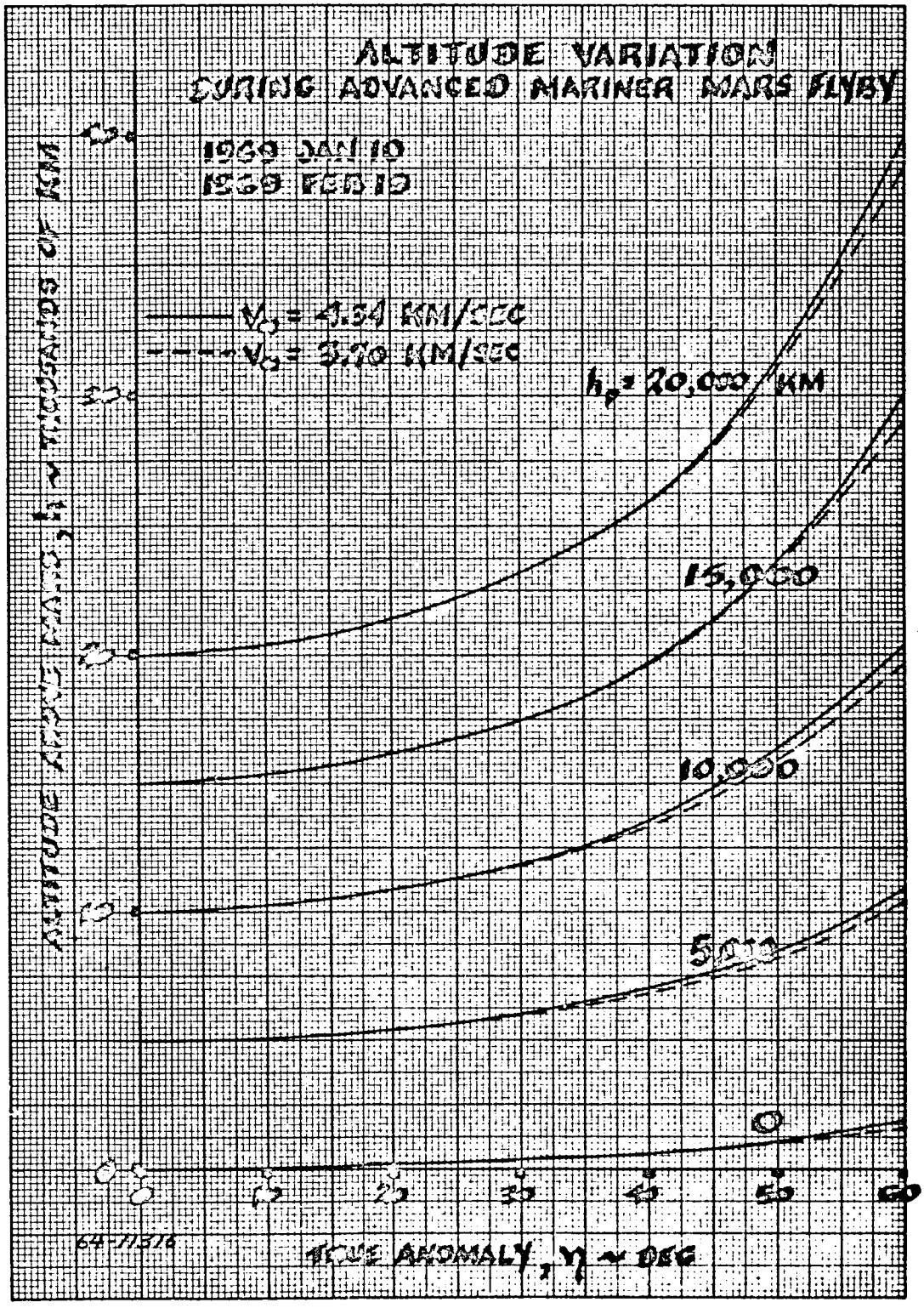

Figure 15 ALTITUDE VARIATION DURING ADVANCED MARINER MARS FLYBY

80

The data storage capacity of the telecommunication system is expected to be about 2×10^8 bits as a reasonable maximum. The television system as described so far will provide about 600,000 bits/pictures including synchronizing and identification words. Thus capacity for about 330 pictures will be available. The slow-scan vidicon, which will be used, has the capability of taking a picture every 30 seconds if special fast erase circuits are used. Assuming that only one camera is used, about 160 minutes will be required to take all of the pictures possible. The possibility of using more than one camera is not considered in this analysis; however, it should be noted that such an approach could be attractive for reliability and rapid picture taking but would increase the weight for a given resolution. The 80 minutes on either side of periapsis needed for mapping altitude, varying between 10,000 kilometers and 20,000 kilometers, depending on the actual periapsis altitude. A value of 12,000 kilometers will be used as the average altitude. Figure 16, shows the time variation during flyby for the 1969 launch opportunity.

The parametric equations listed above may now be written with their constants evaluated as follows:

$$R = \frac{8.8}{F} \tag{15}$$

$$R = 0.0075\, f^2 \tag{16}$$

$$\text{Head Weight} = 0.5 + 0.148\, \frac{L^3}{f^2} \tag{17}$$

One other factor which has not been taken into account is the Kell factor, which takes into account the fact that resolvable elements of the planet's surface may not coincide with the resolution cells of the camera tube target. The value of this factor has been taken as 0.7. Thus equation (15) becomes

$$R = \frac{12.6}{F} \tag{18}$$

The size of the camera head is also a function of the lens parameters for a given type of lens. For the type of modified cassegrain being considered here the length is approximately:

$$L = 7.5 + \frac{F}{3} \text{ inches}$$

where

7.5 = length of camera tube + fixture

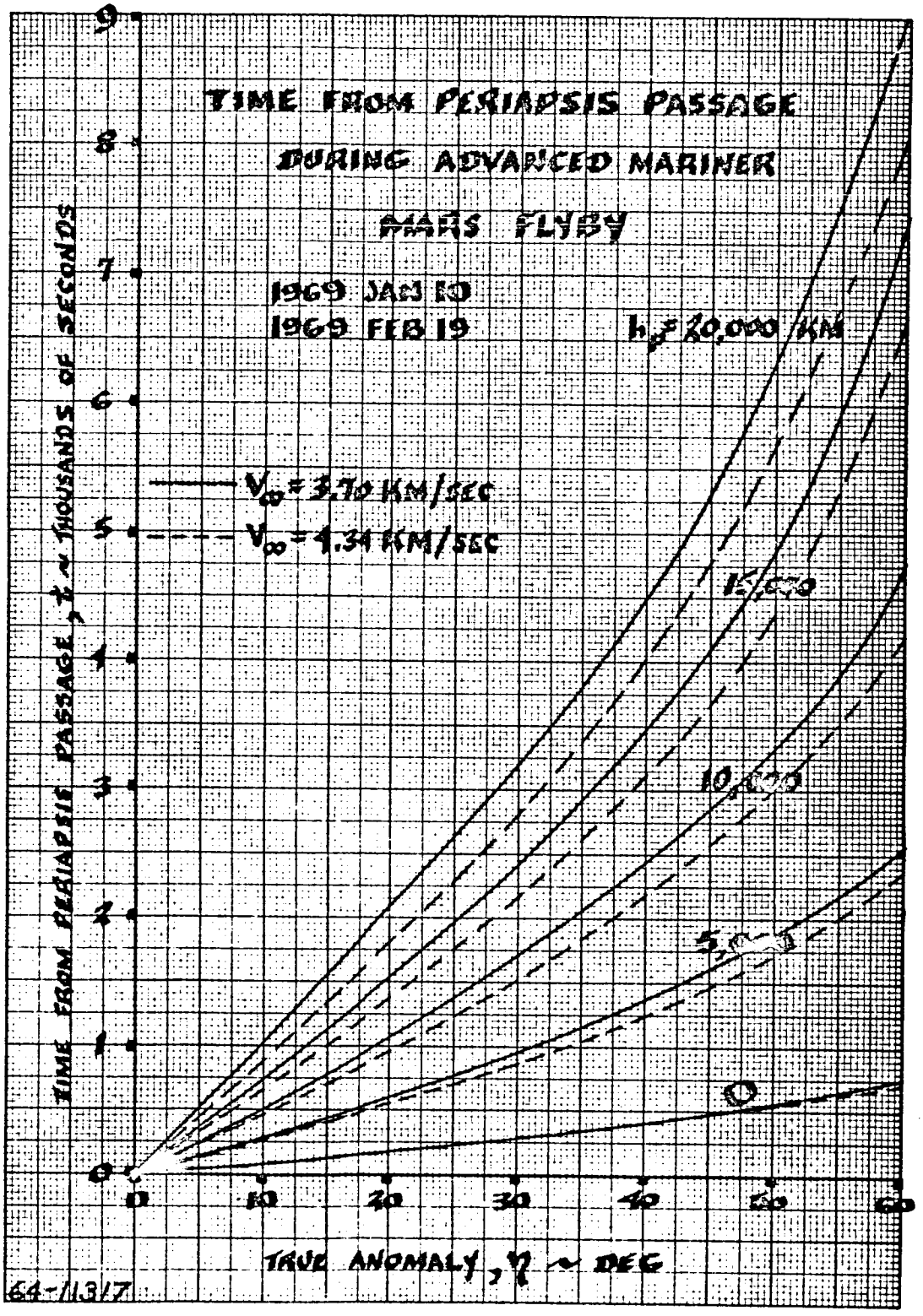

Figure 16 TIME FROM PERIAPSIS PASSAGE DURING ADVANCED MARINER MARS FLYBY

82

Table 16, shows the variation of the various design parameters with the size of a resolution cell. Figures 17, and 18, show the variation of focal length, aperture, and camera head weight with resolution as determined in table 16. The weights are calculated on the basis of using an aperture safety factor of about 2.

TABLE 16

CAMERA PARAMETERS AS A FUNCTION OF RESOLUTION

R (KM)	f^2	f	F	F^3	Length	Weight	f^{2*}	f^*
0.1	13.3	3.65	126.0	large	large	large	7	2.7
0.3	40.0	6.35	42.0	74,088	21.5	550.0	20	4.5
0.5	67.0	8.20	25.0	15,625	15.8	75.0	33	5.8
0.8	117.0	10.8	15.8	3,920	12.7	9.5	59	7.66
1.0	133.0	11.5	12.6	2,000	11.7	5.1	67	8.2
1.5	200.0	14.3	8.4	700	10.3	1.5	100	10.0
2.0	267.0	16.4	6.3	395			0.35	11.5

*f stop with safety factor of 2

b. Conceptual Design -- Television System

The design of television camera systems for space use is a relatively new discipline, and as a result, the components and techniques available are in a continual state of flux. In attempting to project the state-of-the-art for a 1969 mission, the designer is tempted to take advantage of the latest laboratory developments and thereby evolve a system which would provide vastly improved performance relative to presently existing systems. Such a procedure is not, however, justified when planning for as difficult a mission as the Mariner Mars mission under consideration. The main problem is that the reliability requirement for a system to provide a reasonable probability of successful operation is so stringent that the required confidence in components and techniques can only be obtained by careful refinement of well-known principles and devices.

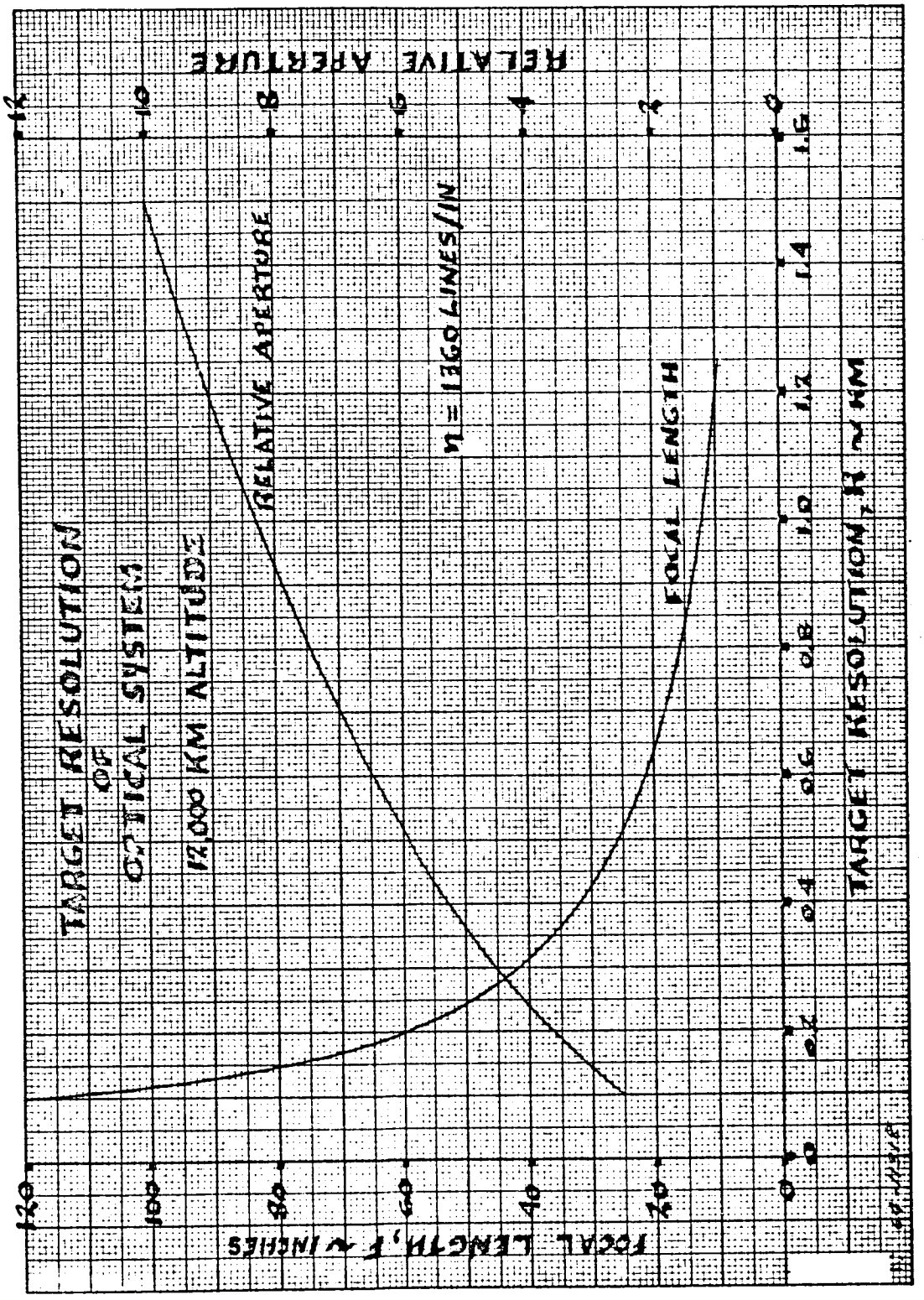

Figure 17 TARGET RESOLUTION OF OPTICAL SYSTEM

84

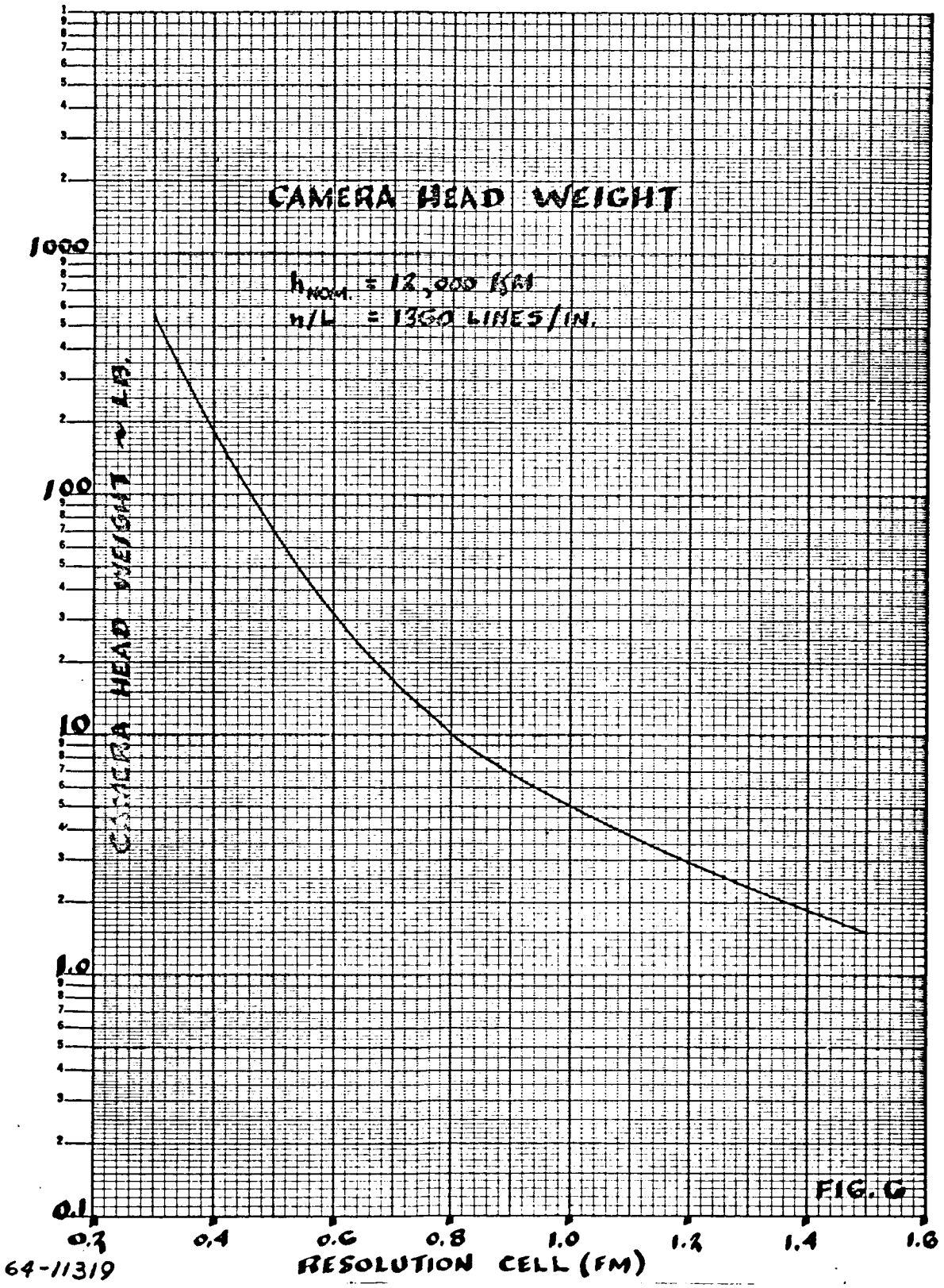

Figure 18 CAMERA HEAD WEIGHT AS A FUNCTION OF RESOLUTION

85

The changes to the existing Mariner C that are recommended include the use of a slightly improved vidicon camera tube and slight modifications to the electronics to allow for the different programming and line synchronization requirements.

1) Camera Tube

The vidicon proposed for consideration is essentially the same all electrostatic unit used on Mariner C. It is expected that refinement of the deflection structure, however, will allow the use of a 300-line raster in the 0.22-inch image height rather than the 200 line raster presently being used. It also appears that the effective sensitivity of the tube can be improved by at least a factor of 2. The curves displayed in the parametric section are based upon the use of this improved vidicon.

2) Optical System

The lens design is rather a more subjective problem, in that relatively small changes in design can result in large improvements in performance. It is certain that a lens system exactly like that of Mariner C would be adequate in terms of resolution capability, since the edge resolution capability of that lens is greater than sixty lines/mm for the 0.22-inch image side being considered. This optical system would also be properly matched as far as speed of aperture is concerned, for as can be seen, a 12-inch focal lens would have to be about f 8 to compensate for smear effects. This lens system with the camera tube discussed above will provide resolving capability of better than one kilometer at 12,000 kilometers.

Longer focal length lenses of the same type can be used in this system if desired with no changes to other system components because for longer focal length lenses, the angle of view becomes smaller and hence resolution of the lens will increase. For shorter focal length lenses it is possible that either the screen size would have to be decreased or the quality of the lens increased to allow for the larger angle of view inherent in a short focal length lens.

3) Electronics

The changes required to the television system electronics are in the areas of the camera control computer, encoder and synchronizer. The computer changes are required to enable more pictures to be taken more quickly and more accurately in time. The changes required in the encoder and synchronizer are to account for an increased number of lines and an increase in the number of samples per line. The system need not change functionally, however, and it is likely that the major modification required is increased buffer storage capacity in the DAS.

4) Shutter Mechanism

The decision to design a system with minimum changes from the existing Mariner C television system is most questionable in dealing with the shutter and filter selection mechanism. Substantial improvements in system ruggedness and reliability could be achieved if the mechanical part of the system could be eliminated. This might be possible by using an image converter tube in front of the vidicon. The converter would have to be fiber optics coupled to the vidicon and would provide a light intensifying function as well as a mechanical shuttering capability. Such devices are being evaluated for classified military programs and may actually be in use in space. The disadvantage of these devices is that there is no way of changing filters, and so unless two complete cameras are used mechanical switching would still have to be performed. This being the case it appears that even in this area it is worthwhile to spend the maximum effort in refining and improving the existing shutter design.

5) Weight and Power Considerations

If the Mariner C lens and head design is used for Mariner 1969, the system will physically be almost identical with the Mariner C system. The head weight will be about 4-1/2 pounds and the electronics package will weigh about 9 pounds. The system power consumption will not exceed 9 watts during picture taking.

If a different lens design is used to achieve greater or lesser resolution only the camera head weight will change as shown above, the electronics weight and system power consumption remaining unaffected.

2.5 Gimbaled Payload Platform

1. General

The Advanced Mariner planetary payload platform is a servo-controlled mounting platform serving as a base for planet oriented payload instrumentation and detection equipment. The platform has been designed with freedom to rotate about two orthogonal axes as shown in figure 19. By controlling angular position of the platform about both axes, it is possible to hold the payload in a fixed orientation with respect to the planet. A two-channel horizon sensor mounted on the platform will detect payload orientation with respect to the planet local vertical and will supply error information to position the platform about its azimuth and elevation axes. In this way the payload will be oriented to continuously monitor the surface of the planet, while the vehicle is on the flyby section of its flight path.

2. Planet Oriented Payload Instrumentation

The Advanced Mariner payload will consist of a television camera, an infrared spectrometer and a relay antenna. The following dimensions and weights have been used for platform geometry and performance considerations.

	Weight (pounds)	Size
a. Television Camera optical head	10	8-inch diameter by 10 inches long
b. Infrared Spectrometer	10	12-inch diameter by 15 inches long
c. Relay Antenna	3	Horn with 6 inch square maximum aperture by 12 inches long

Each of these instruments are shown mounted on the gimballed payload platform in figure 7.

In addition to payload instrumentation, a two axis horizon sensor and associated electronics will be mounted on the platform. The horizon sensor is shown as two separate conical scan, single axis sensors mounted with their reference axes mutually perpendicular to permit two-axis detection of the planetary horizon. These units each weigh 3 pounds, have a diameter of 4 inches and a length of 5 inches.

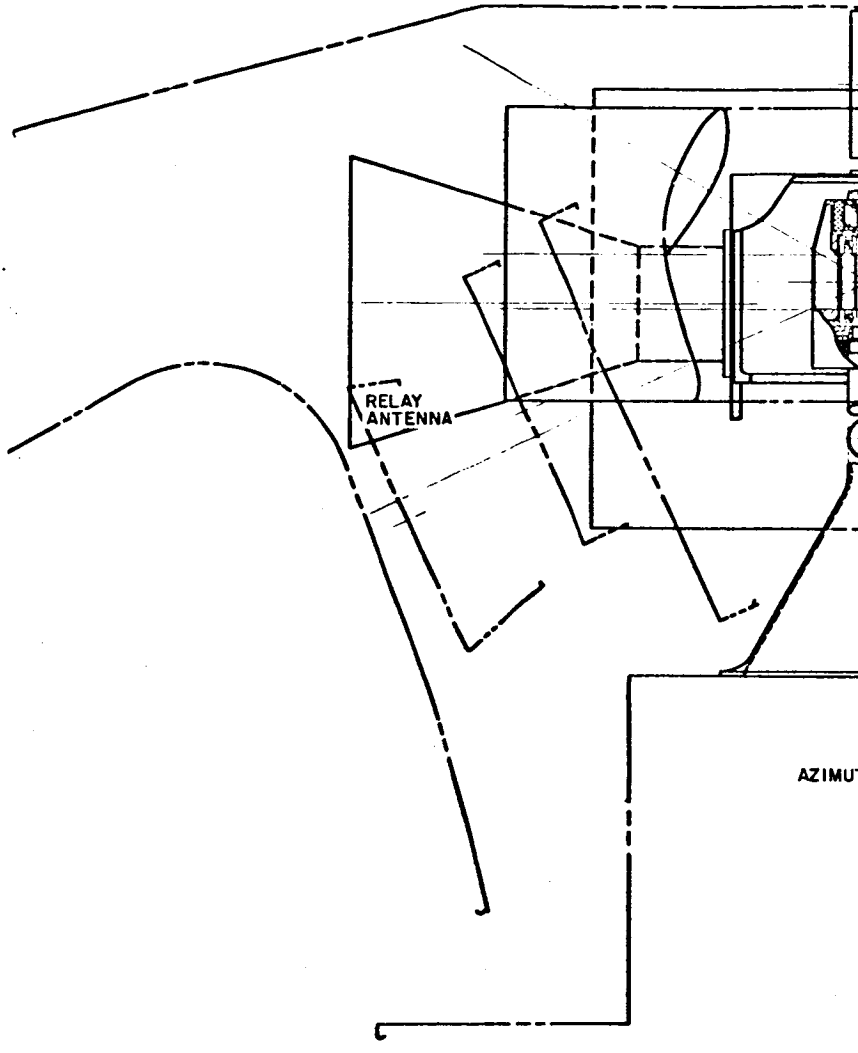

64-11312

1#

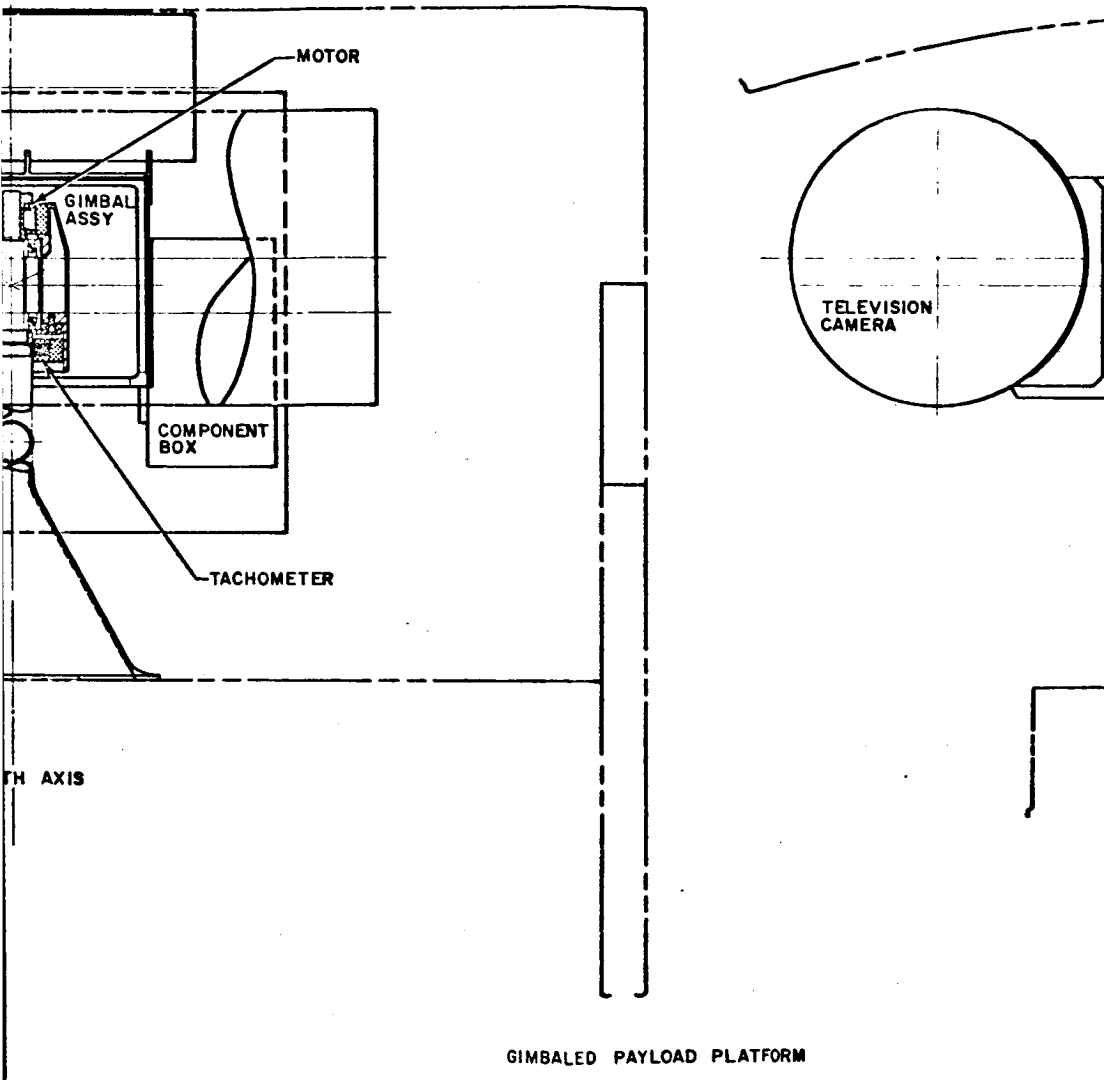

Figure 19 GIMBALLED PAYLOAD PLATFORM

RE-ORDER No. 64-524

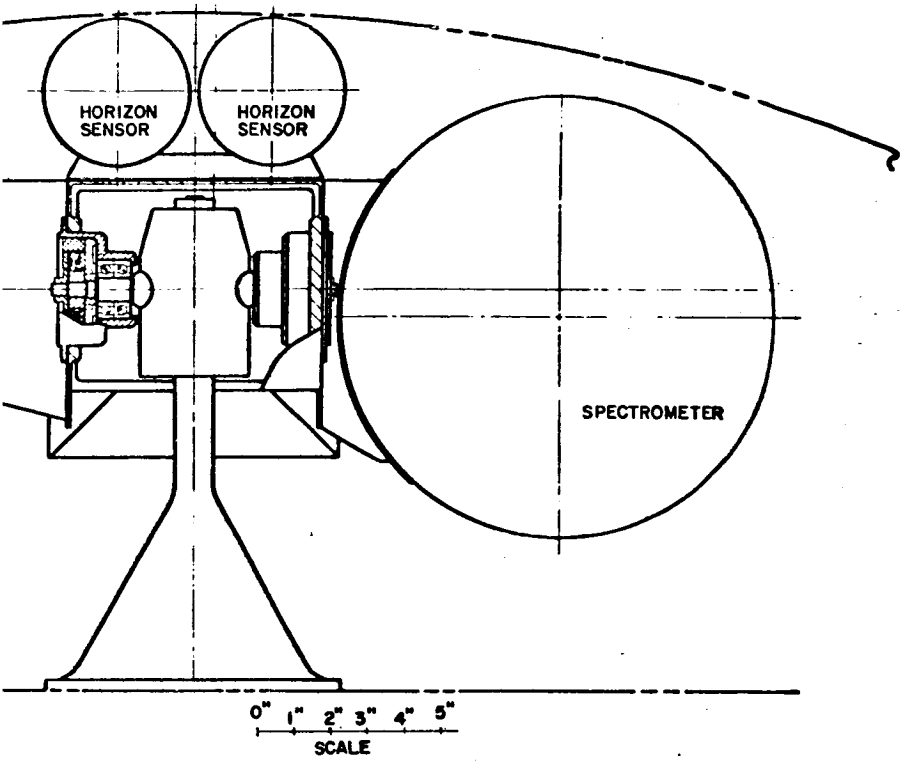

ELEVATION AXIS

3#

3. Performance Requirements

a. Optical Axis Position Accuracy

There are two basic requirements for payload optical axis position accuracy. These are:

1) Absolute payload optical axis pointing accuracy

The payload optical axis must be held on the planet local vertical with a permissable angular accuracy of 0.5 degree. This angular accuracy is determined in part by horizon sensor accuracy capability.

2) Short time payload optical axis accuracy

The short time accuracy requirement is imposed to limit optical axis motion during periods when the camera shutter is open so that picture smear will be held within acceptable levels. While the camera shutter is open, optical axis angular motion must be limited to hold picture smear within 50 percent of one resolution element.

b. Shock and Acceleration Loadings

The size and weight of the payload platform will be determined to a large extent by the structure and bearings required to withstand the Launch environment without failure. The Atlas-Centaur launch environment was used for this study.

4. System Considerations

a. TV Camera Picture Smear

Two techniques have been investigated for controlling the position of the planet oriented payload optical axis with respect to the planet local vertical. The first of these considers continuous active position control for each axis of the two-axis gimbal system to hold the payload optical axis on the planet local vertical at all times. The second approach uses a braking technique to lock both platform gimbal axes (and hence the payload optical axis) to the flyby/bus during periods when the television camera shutter is open, using the periods between camera shutter operation to realign the platform optical axis with the planet local vertical. Both of these approaches will result in television camera picture smear.

Television camera picture smear can result due to the following effects:

1) Effect of optical axis motion with respect to the planet surface due to flyby vehicle limit cycle rates.

2) Effect of optical axis motion due to payload platform error rates with respect to the flyby/bus (control system rates).

3) Effect of optical axis motion with respect to the planet surface due to relative motion between the planet and the flyby/bus (flyby/bus velocity). This smear, which is due to the geometry of the flyby, can be subdivided into contributions due to:

a) Change in direction of the initial local vertical while the camera shutter is open.

b) Displacement of the initial local vertical while the camera shutter is open.

The graphical representation (see insert) is helpful in visualizing the effects of smear due to geometrical effects.

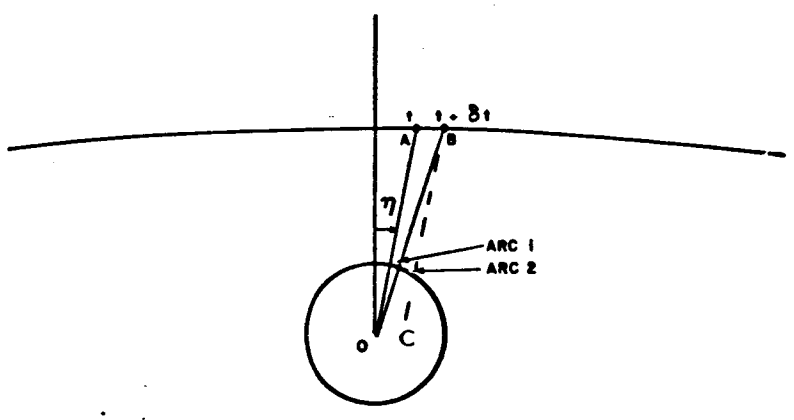

S_v = arc 1 = change in direction of initial local vertical, and corresponds to the case where the TV optical axis maintains the local vertical when the camera shutter is open. S_I = arc 1 + arc 2 = displacement of initial local vertical, and corresponds to the case of latching the television platform to the flyby when the camera shutter is open; that is, (OA is parallel to BC.) S_I variation is shown in figure 20, and variation is shown in figures 21 and 22.

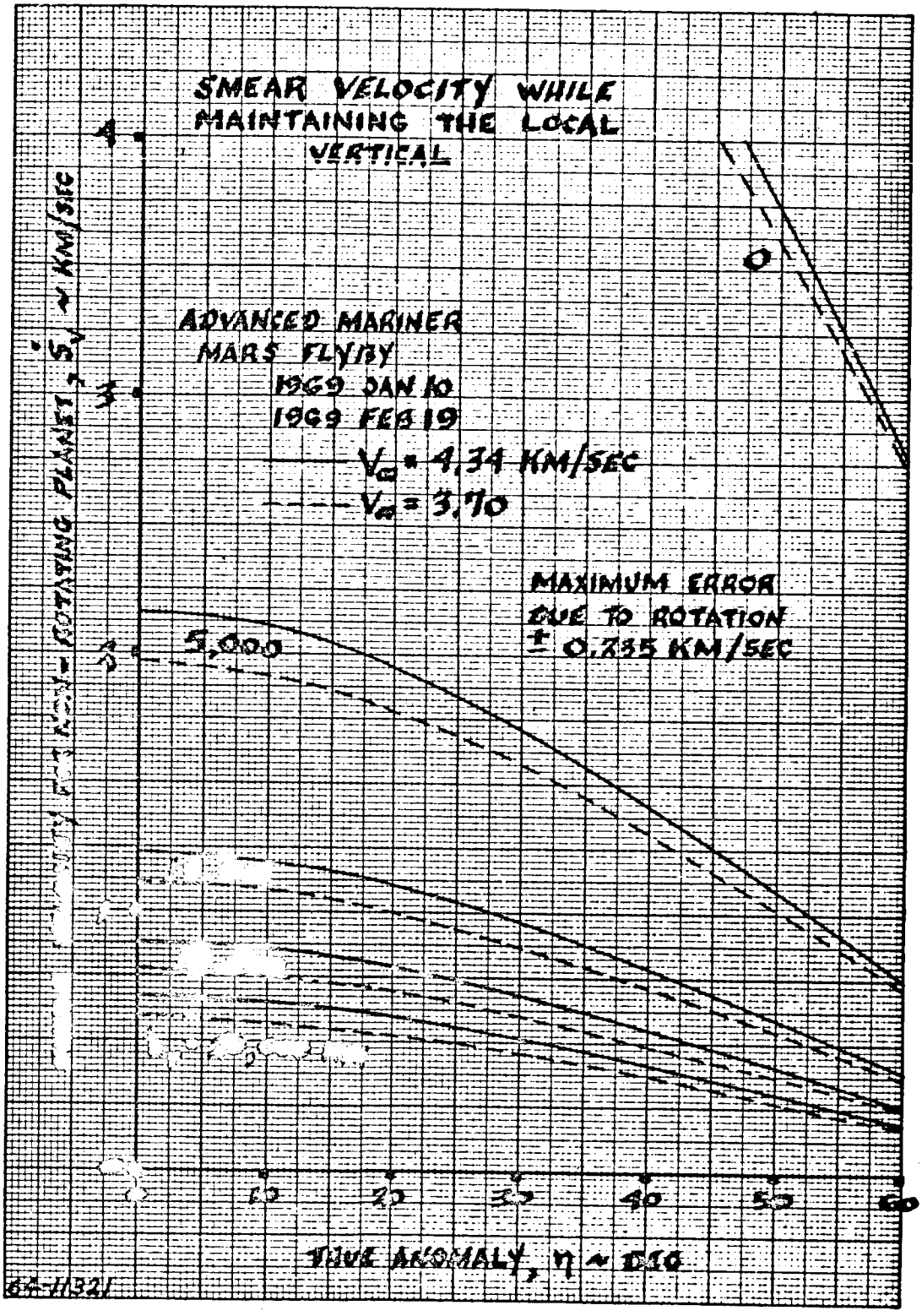

Figure 20 SMEAR VELOCITY WHILE MAINTAINING THE LOCAL VERTICAL

92

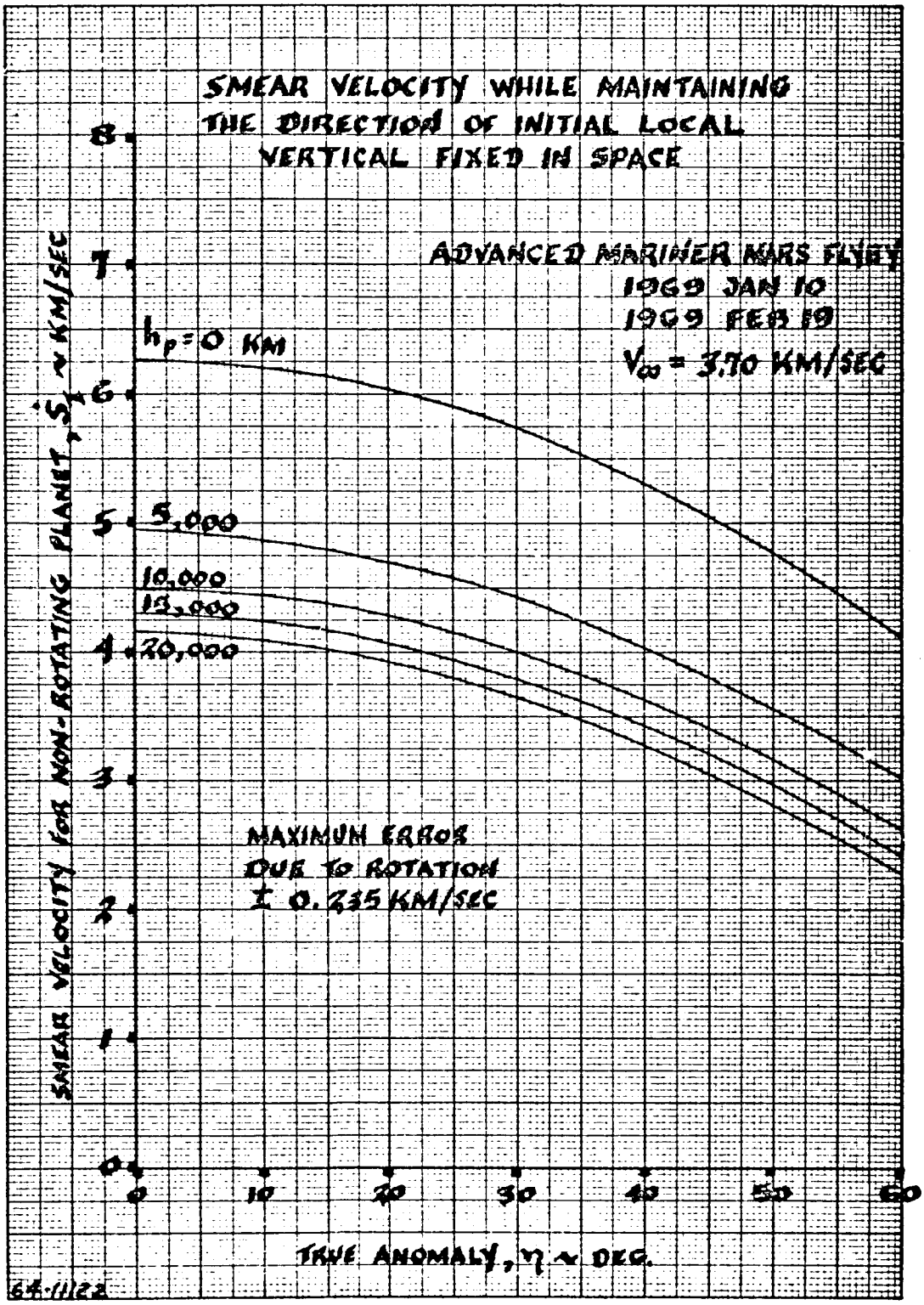

Figure 21 SMEAR VELOCITY WHILE MAINTAINING THE DIRECTION OF INITIAL LOCAL VERTICAL FIXED IN SPACE - V_∞ = 3.70 km/sec

RE-ORDER No. 64-524

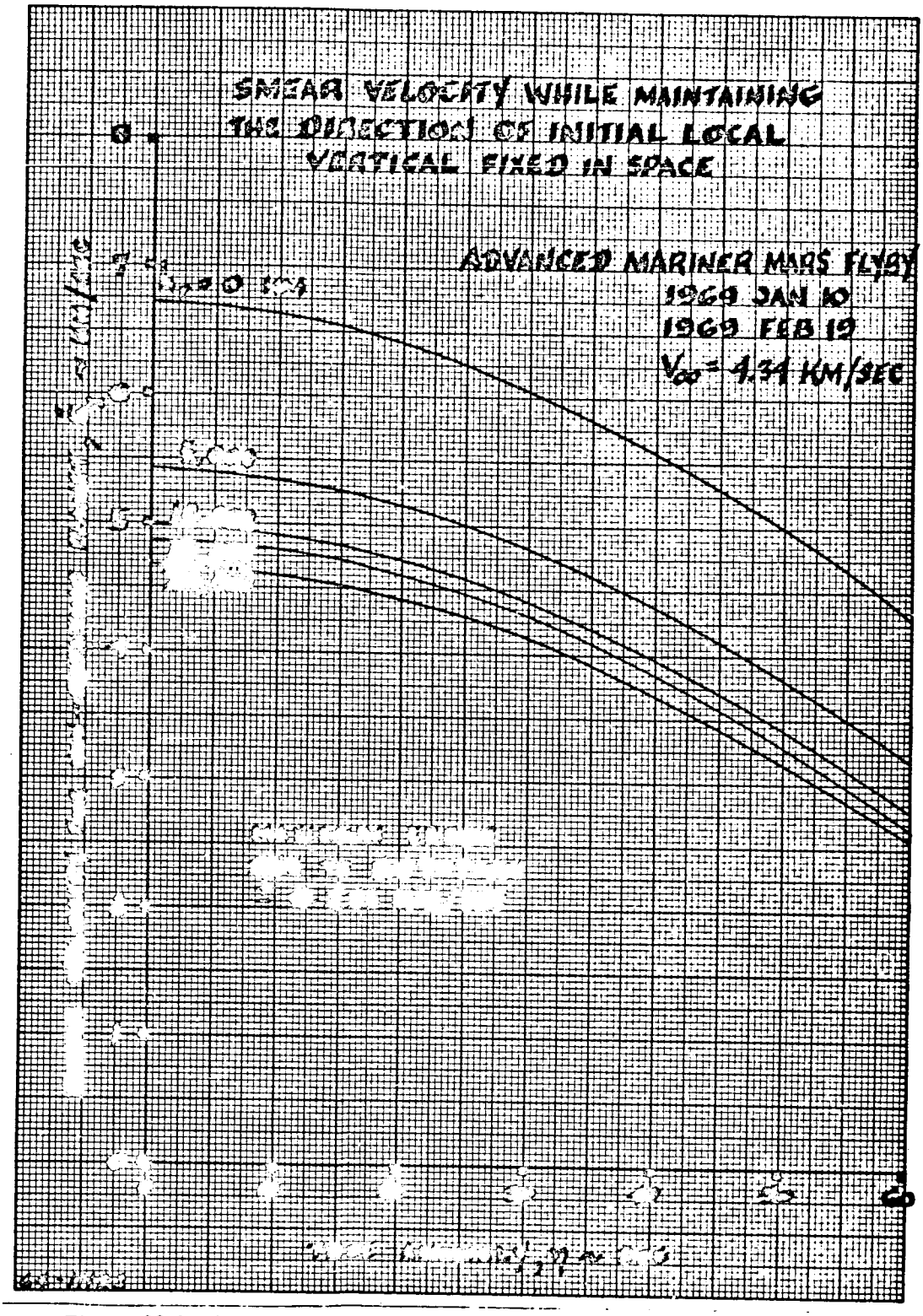

Figure 22 SMEAR VELOCITY WHILE MAINTAINING THE DIRECTION OF INITIAL LOCAL VERTICAL FIXED IN SPACE - V_∞ = 4.34 km/sec

94

The maximum error due to Mars axial rotation cannot exceed ±0.235 km/sec. The absolute error is dependent upon the angle between the flyby great circle track and the minor circle of latitude at the instantaneous ground track point. The choice of sign depends on the direction of the orbit relative to the direction of rotation; minus for a direct orbit and positive for a retrograde orbit.

For this analysis it is assumed that smear effects lie in the plane of the trajectory of the flyby.

1) Continuous Position Control

With the continuous position control technique planetary horizon sensors would be used to detect position of the planet local vertical developing an error signal used to command payload platform position. Under these conditions the optical axis would be under active control at all times including periods when the television camera shutter is open.

Considering the smear errors discussed above, it has been calculated that flyby/bus position control system limit cycle rates are very low, compared with the errors under consideration (10^{-5} deg/sec) and can be neglected. The effects of payload platform error rates with respect to the flyby/bus and effects generated by the bus flyby velocity with respect to the planet are, however, large enough to cause appreciable TV camera picture smear. Smear velocities on the planet surface caused by bus flyby velocity are shown in figure 20 for this case with varying anomaly and periapsis altitude. Refering to figure 20, it may be seen that the maximum smear velocity is generated at zero anomaly. With a periapsis altitude of 5000 kilometers, the smear rate will be 2.16 km/sec. With a TV camera shutter time of 0.1 second, picture smear will be 0.216 kilometer. It should be noted that this error does not include the effect of platform error rates with respect to the flyby bus. However, since permissable smear has been specified at 0.5 kilometer, 0.284 kilometer of the allowable smear error remains for this effect. The 0.284 kilometer permissable smear for attitude control system error rates will result in an allowable payload platform position change of 11.7 seconds of arc during the 0.1-second period in which the camera shutter is open. It appears reasonable that a position control system having an accuracy of this order can be developed. However, the problems associated with achievement of this type accuracy under operational conditions need not become a burden for the design if the payload platform gimbal axes can be locked to the flyby bus during periods when the TV camera shutter is open.

2) Gimbal Axis Locking System

As outlined above, performance within specified smear limits can be achieved by locking the payload platform rigidly to the flyby bus during periods when the TV camera shutter is open. Using this technique, the payload platform (and hence the payload optical axis) will be aligned with the planet local vertical within a specified absolute accuracy of 0.5 degree during the interval of time between each TV camera shutter operation. Prior to camera shutter operation a gimbal axis braking system will lock the platform to the flyby bus eliminating all motion between the bus and the optical axis. This operation eliminates the effect of systematic and random platform control error rates with respect to the bus but also introduces a new error since the position control system is effectively disengaged allowing the optical axis to gradually move off the planet local vertical. The data contained in figures 21 and 22 have been corrected to include this additional element of smear. It is evident from inspection of these curves that the maximum smear rate with zero anomaly and periapsis altitude of 5000 kilometers will be 4.95 km/sec. With a shutter time of 0.1 second the picture smear will be 0.495 kilometer or within the 0.5 kilometer absolute accuracy requirement.

Locking the optical axis to the flyby bus during "open shutter" periods has a number of distinct advantages. First, attaining and maintaining very tight payload platform position control accuracies will not be necessary. Second, it is probable that the gimbal position control systems can be lightened if the accuracy requirement is relaxed to the absolute level shown in the requirements. Finally, and perhaps of dominant importance, the locking system will prove to be substantially more reliable.

b. Position Control Concept

The automatic position control system required to maintain payload orientation with respect to the planet will consist of a servomechanism controlling rotation about each of the two platform axes (see figure 19). A component block diagram of the system configuration for the azimuth axes is shown in figure 23. The platform elevation axes system will be similar.

As illustrated by figure 19, position of the payload with respect to the planet local vertical will be detected by a horizon sensor mounted on the platform. Output from the horizon sensor is a voltage proportional to the payload optical axis angular displacement from the local vertical. This voltage is summed with position command information from the

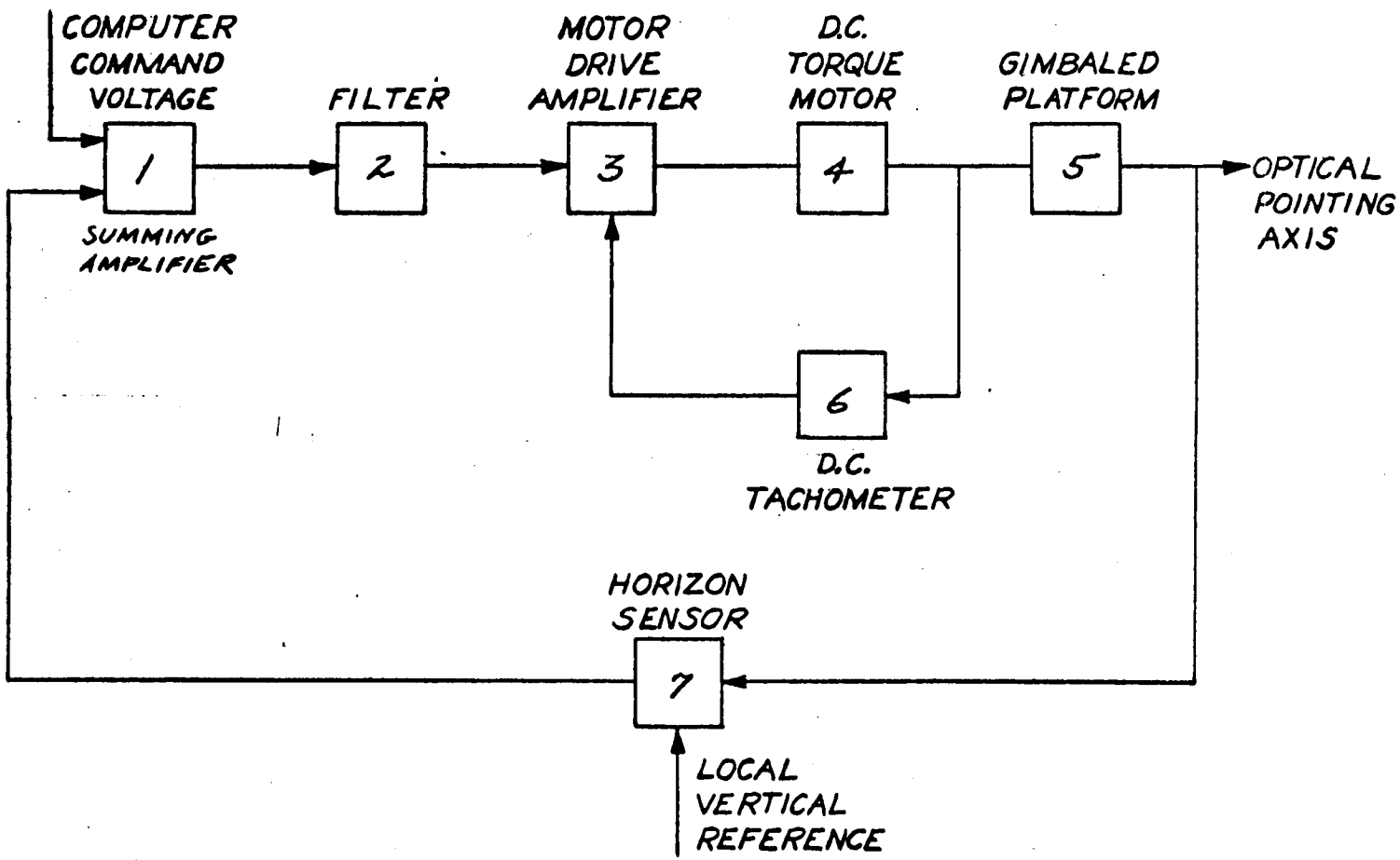

SINGLE AXIS
COMPONENT BLOCK DIAGRAM

64-11324

Figure 23 SINGLE AXIS COMPONENT BLOCK DIAGRAM

RE-ORDER No. 64-524

computer and operated on by compensation networks to provide an input signal for the motor drive amplifier. The amplifier will provide controlled DC power to the gimbal axis drive motor. The drive motor is coupled to the gimballed platform axis. A DC tachometer will sense motor shaft velocity developing a voltage signal proportional to velocity which is fed back to the motor drive amplifier for stabilization. Deviation of platform position from that commanded by the computer will result in drive motor rotation to restore the desired position. Under normal operating conditions the computer input signal will be zero so that the control system will orient the payload along the planet local vertical. It is anticipated that payload pointing errors generated by motion of the vehicle past the planet will be compensated for primarily through operation of the rotation axes. However, the servomechanisms on both axes will provide whatever torques are necessary to maintain command platform attitude.

c. Acquisition

Acquisition of the planet by the planetary payload platform will be accomplished through use of the gimbal position control systems discussed above. As the vehicle approaches the planet a scan mode of operation will be initiated. A command signal from the CC & S will cause the azimuth gimbal axis drive to swing the payload optical axis at a slow scan rate through its full 180 degrees of travel recycling at each extreme. At the same time the elevation axis will be cycled through an angle of ±40 degrees at a substantially faster rate setting up a search grid for detection of planet position. The horizon sensors will be used to detect the planet location. When a threshold signal is received from the planetary horizon sensors indicating the presence of the planet, command logic will discontinue the search mode and initiate the position control mode to lock the payload optical axis on the planet local vertical. After acquisition, the gimbal position servomechanisms will operate to minimize error between platform optical axis and the planet local vertical permitting initiation of mapping functions and their continuation throughout the remainder of the flyby mission.

d. The Basic System

A system block diagram is shown in figure 24 describing the dynamic and static relationships existing between components to be used for a single axes of the payload position control system. As shown, payload angle θ_L will be detected by the horizon sensor and compared with the angle of the planet local vertical θ_v to establish platform attitude error θ_e. Error voltage V_1 will be generated by the horizen sensor. This voltage is statically proportional to platform attitude error θ_e. However, the relationship is frequency dependent as a result of energy storage

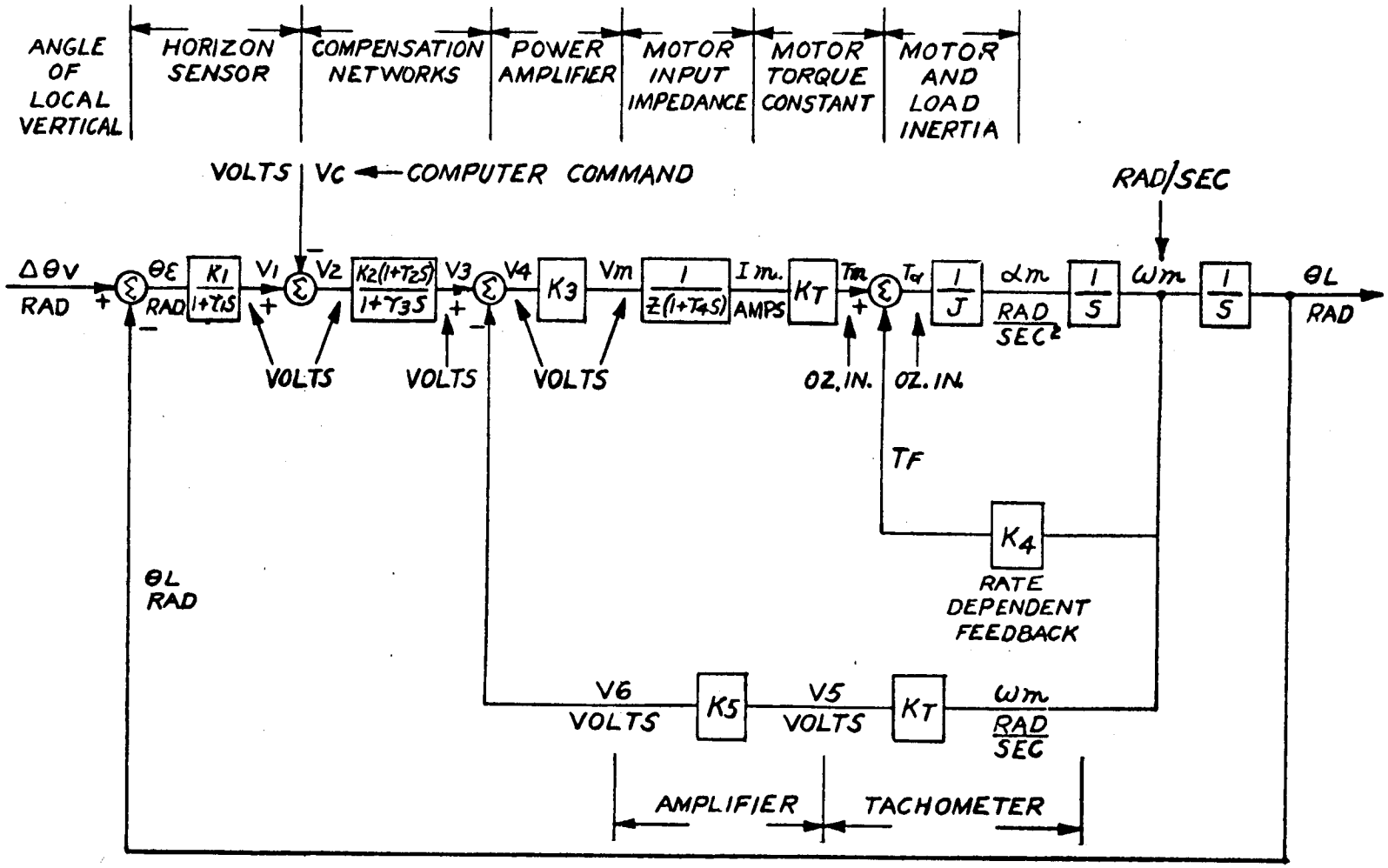

PAYLOAD POSITION CONTROL SYSTEM BLOCK DIAGRAM

64-11325

Figure 24 PAYLOAD POSITION CONTROL SYSTEM BLOCK DIAGRAM

RE-ORDER No. 64-524

elements in the sensor and output filter. It is anticipated that the horizon sensor will have a static gain of approximately 14 volts per radian per second and a first order band pass of 10 radians per second. Horizon sensor output voltage V_1 will be summed with computer command voltage V_c to provide system error voltage V_2. A frequency dependent network is shown operating on error voltage V_2 and will be designed to provide a high system velocity constant. It is possible that more detailed analysis of changes in bus flyby rate will show that the system low frequency gain can be made high enough without use of this compensation.

DC output voltage, V_3, from the compensation network will be summed with tachometer feedback signal V_6 forming summation voltage, V_4, which in turn will be amplified by K_3 and used to drive a DC torque motor. Motor drive voltage V_m is operated on by motor input impedance to form armature current I_m. This current will function through the motor torque constant to provide total generated motor torque T_m. The generated torque is summed with velocity dependent feedback torque T_f to form acceleration torque T_a, accelerating the motor and load through total inertia J. Motor armature acceleration a_m is integrated to provide armature angular rate W_m. W_m is used for motor velocity dependent feedback and as input for the tachometer loop. Motor or gimbal axis rate is integrated to form platform position closing the control loop.

Motor input impedance time constant T_4 will be approximately 0.001 second for the motor selected and can likely be neglected.

A tachometer loop has been added to the system to substantially increase the magnitude of the motor inertia break frequency allowing higher open loop gains to be employed. In addition, the tachometer feedback loop will subordinate the effect of rotating equipment random input torques due to mechanical friction providing smoother system performance. In the final analysis, however, the necessity of using a tachometer loop will be determined by more detailed analysis of the system gain requirement, velocity accuracy characteristic, and component error contributions. It is important to note that in this analysis, dynamics of the gimbal structure have not been discussed although they will obviously have a pronounced effect on the performance of the system. Since structural considerations have been left for the design stage of the program, no effort will be made here to evaluate their effect on system performance.

e. Payload Platform Gimbal Orientation and Gimbal Motion Equations

In determining an optimum orientation for the two gimbal platform on the flyby bus, it is necessary to determine gimbal excursion requirements over the complete flyby mission. This analysis is covered in detail in appendix A.

6. Components

a. Gimbal System

The gimbal system (see figure 19) will be a two axis precision suspension system capable of positioning a payload platform in any position commanded by input signals from the computer and horizon sensors. Each axis will be driven by a DC torquing position control servomechanism consisting of a DC Torque drive motor, a DC precision tachometer, a horizon sensor, stabilizing networks and amplifiers.

There are two basic problems associated with gimbal system design aside from those resulting from accuracy considerations. The first is operation of gimbal bearings and DC torque motor and tachometer commutators in the vacuum of space; and the second is design of a structure that will not impose unacceptable resonant characteristics on the gimbal axes position control servomechanisms.

b. Drive Motors

A drive motor will be used on each of the two orthogonal payload platform gimbal axes. The motor will be similar to the Inland type T-1342-D with a weight of 10 ounces and an average power consumption of 1.6 watts. Motor peak torque will be 0.2 pound/feet. It is interesting to note that the peak torque requirement for the DC servo motor under free fall operating conditions in the flyby trajectory will be very small, limited to random bearing loads and extremely light acceleration loadings. Design requirements for the motor are established on the basis of grounded test where normal loadings associated with operation in the earth's gravitational field will be necessary. Bearings used for support for the motor rotor and the motor commutator will be protected from the space vacuum environment through application of the VACKOTE process.

c. Tachometer

A DC tachometer will be used on each of the two gimbal axes for stabilization of the position control servomechanisms and to increase the system torque constant. Each tachometer will weigh 10 ounces and will have a power consumption of 0.01 watt. The size of the tachometer will be approximately the same as the motor. Again, the tachometer commutator will be treated with the VACKOTE process to prevent performance degradation when in operation under the vacuum of space.

d. Bearings

Bearings used for support of each gimbal axis will be similar to the New Departure QOLO3DTX7 440 stainless units and will be used in duplexed pairs. Bearings will weigh 0.17 pound per pair. Each bearing will be treated with the VACKOTE process to prevent spalling under the balls and races under hard vacuum operation.

e. Horizon Sensors

The horizon sensor to be used for detection of the planet local vertical will be of the scan type constructed to detect the planetary horizon in the CO_2 band, developing a signal proportional to angular error between the planet local vertical and the position of the sensor. A number of different types of horizon sensors have been developed to date and new passive devices are under development at the present time. However, the conical scan design is the only approach that has been used effectively to date under operating conditions where reasonable accuracy is required. The sensor consists of two conical scan heads mounted so that they create mutually orthogonal patterns to establish a two-axis coordinate frame. These units develop an output signal used in control of the two mutually perpendicular gimbal axes. The detectors will have a static gain of approximately 14 volts per radian per second and will have a first order band pass of 10 radians per second. The two-axis package will weigh approximately 7-1/2 pounds with electronics and may be housed as two independent sensors or in a dual package as space, balance, and weight requirements of the final design dictate. A Rosette scanner developed for two-axis control in a single package is also a scan type sensor which will be investigated for this application.

f. Amplifiers

A number of amplifiers will be required for each gimbal axis position control system. These will consist of a tachometer loop voltage amplifier amplifying tachometer output, a position loop voltage amplifier amplifying horizon sensor output, a summing preamplifier and a DC torque motor drive amplifier. These units would be designed with completely passive elements with welded modular construction. The electronic elements will have a composite weight of 37 ounces.

g. Operation of Sliding Parts in a Vacuum

A major state of the art problem associated with past space vehicle missions has been cold welding encountered on sliding and rolling metallic surfaces operating in the vacuum of space. A number of

solutions have been used to counter this problem and some have been successful on long term space missions. Special solid lubricant coatings have been used on bearing, gear teeth, and slip-ring surfaces on a number of programs including the Midas satellite. Gold plating of contracting bearing and gear tooth surfaces was used on other satellites including Advent and Nimbus. An O-ring grease seal technique was used on the Mariner satellite to retain critical components under a low pressure. Still other applications, including the Midas satellite, used hermetic sealing of rotating parts within an inert atmosphere through application of the Harmonic Drive transmission. Development work going on at the present time (NASA - Lewis, NASA-Goddard and in many industrial areas) stress the use of special retainer materials for bearing lubrication consisting essentially of filled teflon. These approaches depend on the lubrication quality of a film of Teflon picked up from the bearing retainer by the balls. Another approach uses close tolerance baffeling to create a pressure drop between parts to be lubricated and the vacuum of space thus holding liquid lubricants around the bearing for extended periods of time. All of these techniques appear to have significant merit but in each case are limited by a lack of detailed earth based and space test experience. Perhaps the only lubrication treatment that has been exposed to extensive ground and space testing is the VACKOTE process developed by Ball Brothers. This process was used on the OSO satellite with results reported to be excellent over an extended period of time under Earth orbiting conditions.

h. Component Weight and Power Requirements

Component	No. of Units	Weight (pounds)	Power (watts)
D. C. Torque Motors	2	1.80	3.2
Tachometers	2	1.30	0.1
Bearings	6	0.50	---
Preamplifiers	2	1.50	0.5
Power Amplifier	2	0.40	2.2
Structure	1	6.00	---
Brakes	2	0.40	0.5
Summing Amplifiers	2	0.40	0.5
Horizon Sensors	2	6.00	4.0
Horizon Sensor Electronics	1	1.5	2.0
Wiring Harness	1	0.40	---
Brackets	5	0.40	---
Totals		20.6 lbs.	13.0 watts

Note: Weights and power consumptions do not include those required for the payload.

3.0 POWER SUPPLY

3.1 SYSTEM DESCRIPTION

The power system selected for this study is similar to the one used on Mariner C, namely a silver-zinc battery and solar array with an ac power distribution system. Figure 25 shows a block diagram of this system. The main differences between this and the system used on Mariner C are the capability of trickle charging the lander battery and supplying heater power to the lander while in the cruise modes. The power demands on the various inverters will be similar to those in Mariner C. The power conversion efficiencies assumed for the inverters and regulators are assumed constant in this study to simplify the power calculations. Assumed values are:

Power Switching and Logic	97 percent
Main Booster Regulator	80 percent
Maneuver Booster Regulator	80 percent
Main Inverter	90 percent
Maneuver Inverter	90 percent
400 Cycle 1 ϕ Inverter	70 percent
400 Cycle 3 ϕ Inverter	75 percent
Battery Charger Efficiency	87 percent

During the cruise and maneuver modes, the total power conversion efficiency is a function of the power switching and logic, booster regulators and inverters. Table 17 is a glossary of terms used in this section. Table 18 lists the power users for each inverter and the power consumption during each phase. Table 19 lists the manufacturers of power sources and equipment contacted in this study. Table 20 is a parts list of the conceptual design power system.

3.2 BATTERY

A silver-zinc battery was selected to provide power to the spacecraft during launch, erection and sun acquisition, midcourse maneuvers and the separation maneuver. To minimize the battery size, it will be completely recharged between each maneuver. The battery size required is then a function of the maximum watt hours required during the phases mentioned above. In any of these phases, the total watt-hours required are mainly a function of the power required by the guidance science, and communication subsystems. This total

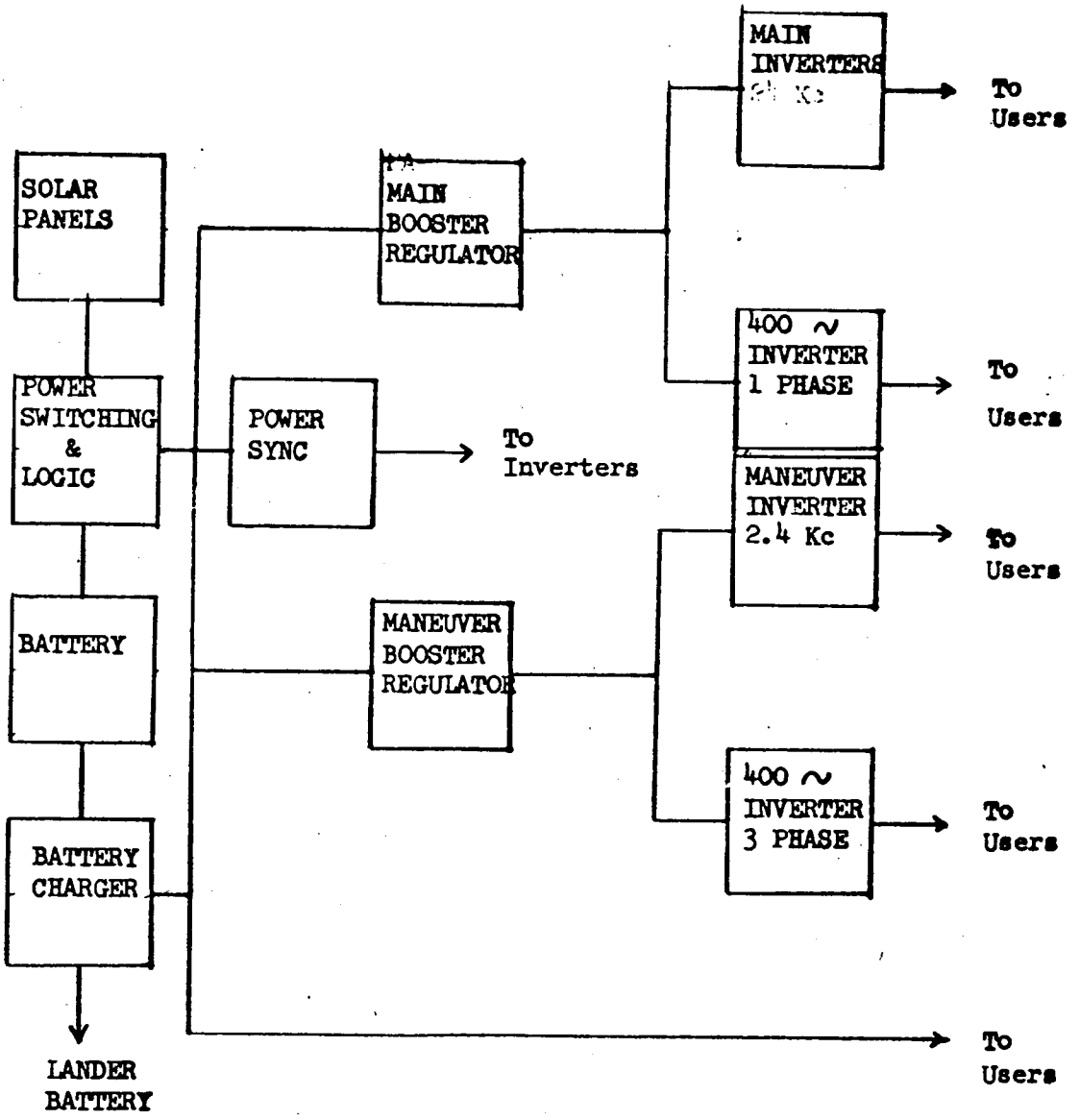

Figure 25 POWER SUBSYSTEM

TABLE 17

GLOSSARY OF TERMS

K	Battery watt-hour per pound conversion factor
P_{fc}	Communication power less transmitter (watts)
P_H	Lander heater power (watts)
P_g	Guidance Power (watts)
P_s	Science Power (watts)
P_T	Transmitter power (watts)
P_{tot}	Total Power Consumption (watts)
T_B	Duration of battery power consumption (hours)
W_B	Weight of battery (pounds)
n_1	Conversion efficiency for guidance power
n_2	Conversion efficiency for science power
n_3	Conversion efficiency for fixed communication power
n_4	Battery charger efficiency

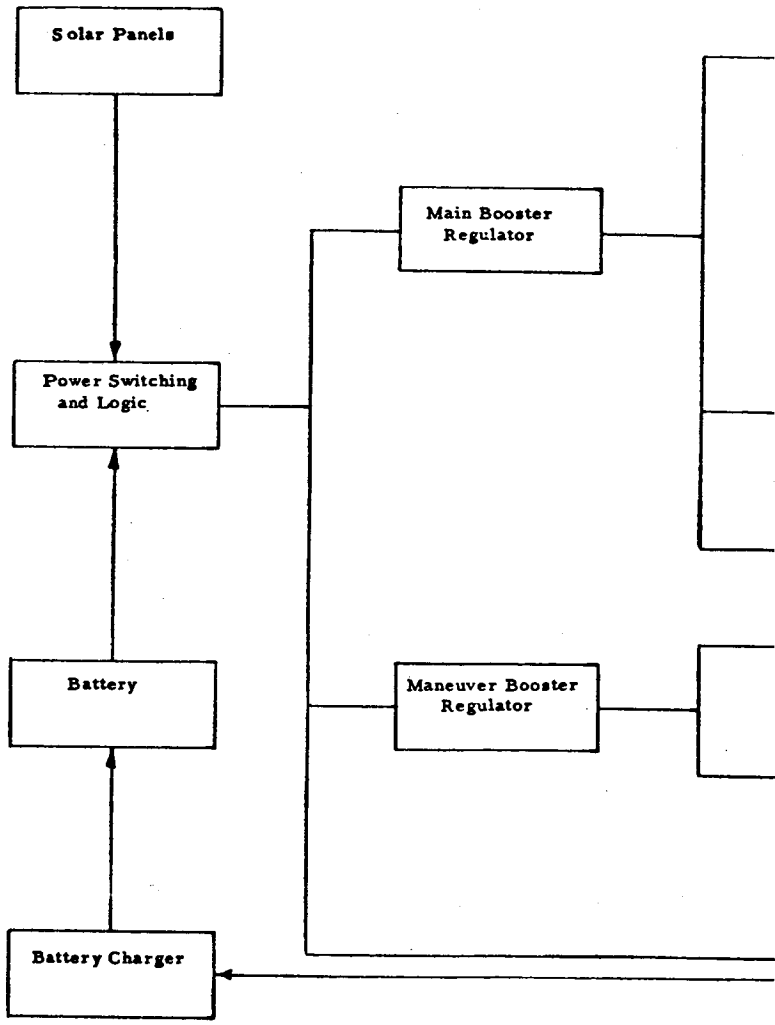
Solar Panels
Main Booster Regulator
Power Switching and Logic
Battery
Maneuver Booster Regulator
Battery Charger

#

FLYBY/BUS POWER SYST

	NOMENCLATURE	At Launch
Main Inverter 2.4 KC	Cosmic Dust Detector	---
	Magnetometer	---
	Micrometeoroid Detector	---
	Ion Chamber	---
	Particle Flux Detector	---
	TV Camera	---
	Narrow Angle Planet Sensor	---
	Canopus Star Tracker	7.2
	Limit Cycle Sun Sensor	0.5
	Course Acquisition Sun Sensor	0.35
	ACS Control Electronics	2.5
	ACS Thruster Solenoid	---
	Valves (2 per one axis, at one time) (12 valves total)	
	S-Band Transponder	16.0
	Telemetry	13.0
	Command	4.5
	CC and S	7.0
	DAS	8.0
	Recorder Electronics	---
	Planetary Horiz. Platform	---
	Antenna Pointing Control*	---
	Power Switching and Logic	2.0
	Total From Main Inverter	61.05
	Total Into Main Inverter	67.83
400 Cycle 1Ø Inverter	Infrared Spectrometer	---
	Recorder Transport	---
	Wide Angle Planet Sensor	---
	Total From 400 Cycle 1Ø Inverter	0
	Total Into 400 Cycle 1Ø Inverter	0
	Power Synchronization	1.0
	Total From Main Booster Regulator	63.83
	Total Into Main Booster Regulator	86.04
400 Cycle 3Ø Inverter	Gyros and Gyro Electronics	10.0
	Total From 400 Cycle 3Ø Inverter	10.0
	Total Into 400 Cycle 3Ø Inverter	13.33
Maneuver Inverter 2.4 KC	Gyros and Gyro Electronics	13.0
	Total From Maneuver Inverter	13.0
	Total Into Maneuver Inverter	15.30
	Total From Maneuver Booster Regulator	28.66
	Total Into Maneuver Booster Regulator	23.72
	Power Amplifier Power Supply	---
	Battery Charger (24 hrs/cycle)	---
	Capsule Heater Power (Nominal)	15
	Total From Power Switching and Logic	134.76
	Max. Total Demand on Solar Panels or Battery	138.93

*Low duty cycle. Do not consider for total power, only

** Assume 10 lbs. of Battery; @ 37. w-hrs/lb. $\frac{370 \text{ w-hrs}}{24 \text{ hrs}} \times \frac{1}{.87} = 17.7$

2#

RE-ORDER No. 64-524

TABLE 18

EM AND POWER CONSUMPTION LIST

MISSION PHASE					
Initial Erect. and Acquis.	Cruise	Midcourse Maneuver	Separation and Slowdown	Encounter	Post Encounter
0.2	0.2	0.2	0.2	0.2	0.2
5.0	5.0	5.0	5.0	5.0	5.0
0.5	0.5	0.5	0.5	0.5	0.5
0.1	0.1	0.1	0.1	0.1	0.1
0.35	0.35	0.35	0.35	0.35	0.35
---	---	---	---	15.0	---
---	---	---	---		---
7.2	7.2	7.2	7.2	7.2	7.2
0.5	0.5	0.5	0.5	0.5	0.5
0.35	0.35	0.35	0.35	0.35	0.35
2.5	2.5	2.5	2.5	2.5	2.5
6.0 (3.0/valve)*	6.0*	6.0*	6.0*	6.0*	6.0*
16.0	16.0	16.0	16.0	16.0	16.0
13.0	13.0	13.0	13.0	13.0	13.0
4.5	4.5	4.5	4.5	4.5	4.5
7.0	7.0	7.0	7.0	7.0	7.0
8.0	8.0	8.0	8.0.	8.0	8.0
---	---	---	---	1.4	---
---	---	---	---	20.0	---
---	---	---	---	---	---
2.0	2.0	2.0	2.0	2.0	2.0
72.85	72.85	72.85	72.85	111.25	72.85
80.95	80.95	80.95	80.95	123.61	80.95
---	---	---	---	7.0	---
---	---	---	---	1.5	---
---	---	---	---	4.5	---
0	0	0	0	13.0	0
0	0	0	0	18.57	0
1.0	1.0	1.0	1.0	1.0	1.0
81.95	81.95	81.95	81.95	143.18	81.95
102.44	102.44	102.44	102.44	178.98	102.44
10.0	---	10.0	10.0	---	---
10.0	---	10.0	10.0	---	---
13.33	---	13.33	13.33	---	---
21.0	---	50.0 (13. during warmup)	50.0 (13. during warmup)	---	---
21.0	---	50.0	50.0	---	---
24.71	---	58.82	58.82	---	---
38.04	---	72.15	72.15	---	---
47.55	---	90.19	90.19	---	---
30.0	30.0	30.0	30.0	30.0	30.0
---	17.72**	---	---	---	---
15	15	15	---	---	---
194.99	165.16**	237.63	237.63	208.98	132.44
201.02	170.26**	244.98	244.98	215.44	136.54

or instantaneous max. power.

w) Max. is 1st 24 hrs. of each cruise mode only.

TABLE 19

COMPONENT PERFORMANCE DATA SUPPLIED BY VENDORS

Subsystem	Manufacturer
Battery	Electric Storage Battery Co. Missile Battery Division 2510 Louisburg Road Raleigh, North Carolina
Solar Cells	Textron Electronics Heliotek Division 12500 Gladstone Avenue Sylman, Calif.
Solar Panels	Ryan Aeronautical Co. Lindbergh Field San Diego, Calif.
Power Conditioning Equipment	Westinghouse Electric Corp. Aerospace Electrical Division Lima, Ohio

TABLE 20

COMPONENTS AT POWER SUPPLY SYSTEM

	Weight (pounds)	Volume (in.^{3})	Dimensions (inches)	Power (watts)
Main Inverter	2.5	80	5 x 4 x 4	7.0
Maneuver Inverter	2.5	80	5 x 4 x 4	7.0
400 C 1 ϕ Inverter	3.5	80	5 x 4 x 4	1.5
400 C 3 ϕ Inverter	4.0	80	5 x 4 x 4	3.0
Main Booster Regulator	2.0	80	5 x 4 x 4	7.0
Maneuver Booster Regulator	2.0	80	5 x 4 x 4	7.0
Power Switching and Logic	2.0	80	5 x 4 x 4	1.5
Power Synchronizer	2.0	48	3 x 4 x 4	1.0
Power Distribution Subassembly	2.0	80	5 x 4 x 4	1.5
Battery Assembly	20.0	300	10 x 6 x 5	---
Battery Charger Subassembly	2.0	80	5 x 4 x 4	5.0
Solar Panel Assembly	102	85 ft^2	---	---
Battery Temp. Transducer	.03	---	---	---
Solar Panel Temp. Transducer	.03	---	---	---

may be expressed as

$$P_{tot.} = P_g/n_1 + P_s/n_2 + P_{fc}/n_3 + 3P_T$$

where n_1, n_2, and n_3 are the total power conversion efficiencies attained by routing the raw battery power through the appropriate regulators and inverters. The power required by the power amplifier ($3 P_T$) implies a conversion efficiency of 33 percent and could be expected with a highly efficient amplifier tube and converter. In the conceptual design the power amplifier efficiency is on the order of 20 percent due to the selection of the Resdel amplifier used in Mariner C. The battery weight can be expressed as

$$W_B = P_{tot.} T_B/K$$

where K is the energy density of the battery. In this study, K is 37 watt hours per pound as used in Mariner C. Figure 26 shows battery weight parametrically as a function of total power consumption and duration of battery power consumption.

In the conceptual design, the battery size is determined from the maneuver phase where the total watt hours required are 180. This results in a battery weight requirement of 5 pounds (see appendix C for analysis). 20 pounds are actually used to allow for a possible failure in the battery charger.

3.3 SOLAR ARRAY

The solar cells will be the primary source of power and will be used during all cruise, encounter and post encounter modes. The total power required from the solar array at any one time is

$$P_{tot.} = P_g/n_1 + P_s/n_2 + P_{fc}/n_3 + KW_B/24\, n_4 + 3P_T + P_H$$

where the conversion efficiencies are determined in the same manner as the battery case. The fourth item in this equation represents the power required to recharge the battery in 24 hours; 24 hours being the minimum time between maneuvers and occuring between sun acquisition and the first midcourse maneuver. The last item represents the heater power.

Figure 27 shows solar array weight and area as a function of P_{tot}. Four watt/ft^2 and 1.2 lb/ft^2 are the estimated conversion factors used in the solar array parametric studies. The maximum demand on the solar panels occurs during the maneuver mode and is approximately 245 watts of raw power (see table 18). In the conceptual design, a total active cell area of 85 ft^2 or 340 watts of raw power is used to provide 1) redundancy, 2) growth in power requirements and 3) performance margin in the event of solar cell degradation in the vicinity of Mars due to unexpectedly high meteoroid flux.

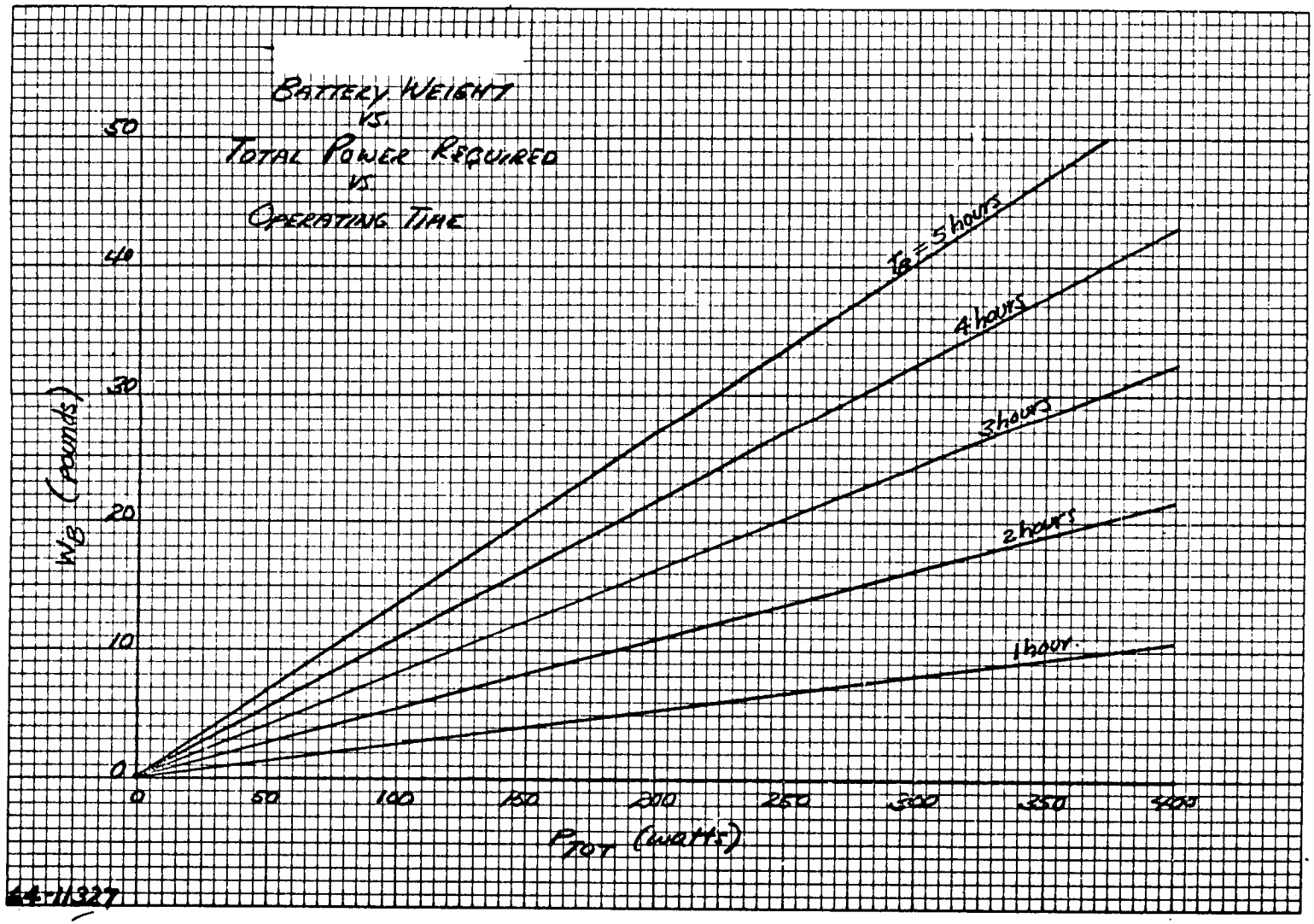

Figure 26 BATTERY WEIGHT

RE-ORDER No. 64-524

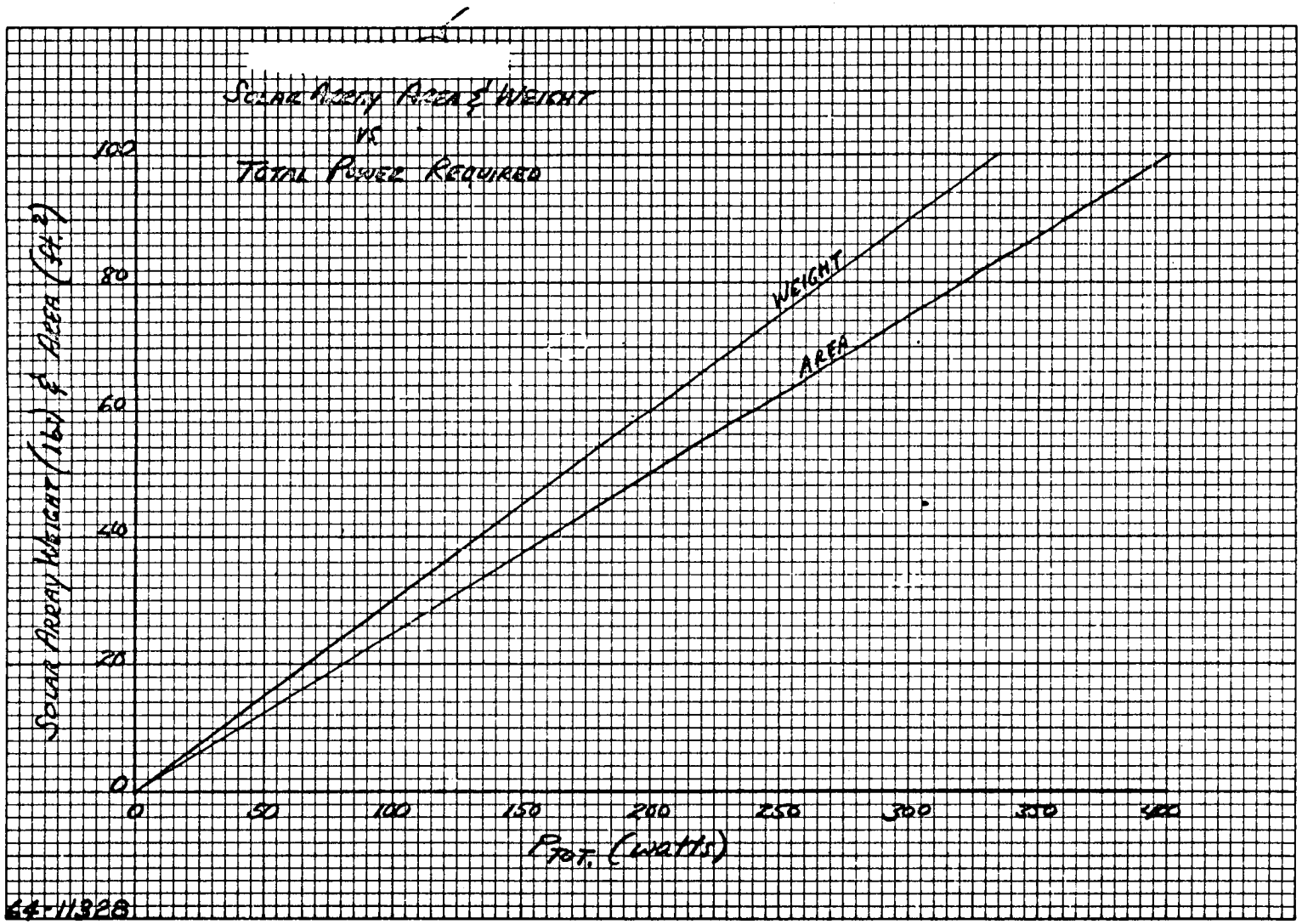

Figure 27 SOLAR ARRAY AREA AND WEIGHT

RE-ORDER No. 64-524

112

The unit weight for solar arrays on the order of 125 ft^2 or greater is estimated to be 1.4 lb/ft^2 by Ryan Aeronautical Co. For smaller areas where fewer support struts are needed, the unit weight approaches 1.2 lb/ft^2. These figures include both structure and cell weights.

The power density assumed is 4 $watts/ft^2$. This number has been checked in detail by extrapolating solar array performance at Earth, extrapolating Mariner II data, and performing a direct calculation. All methods yield the same result, 4.85 $watts/ft.^2$ 4 $watts/ft^2$ is assumed as a conservative estimate.

3.4 POWER CONDITIONING

Although it is reasonable to assume that the existing Mariner C power conditioning equipment, or modifications thereof, could be used for most Advanced Mariner concepts, expected variations in weight and volume were determined by examining similar equipment.

A silicon transistor converted operating at a frequency of 2 kc and a germanium transistor converter operating at 500 and 2000 cycles were examined. The results are presented in figures 28 through 33 as a function of input voltage and power.

The major contributions of weight and volume in the converters comes from the transformer and transistor switching circuits and associated heat sinks. As the frequency increases, the size and weight of the transformer decreases while the transistor heat sinks increase. An optimum frequency of operation in terms of minimizing weight and volume of a system has not been determined since this will vary with individual transistors.

For germanium transistors, operating at 500 cycles and silicon transistors operating at 2000 cycles, the converter volume and weight are found to rise linearly with input power. Above 5 volts, the weight and volume is essentially constant with input voltage. Germanium transistors operating at 2 kc show decreases in weight and volume with decreases in input voltage.

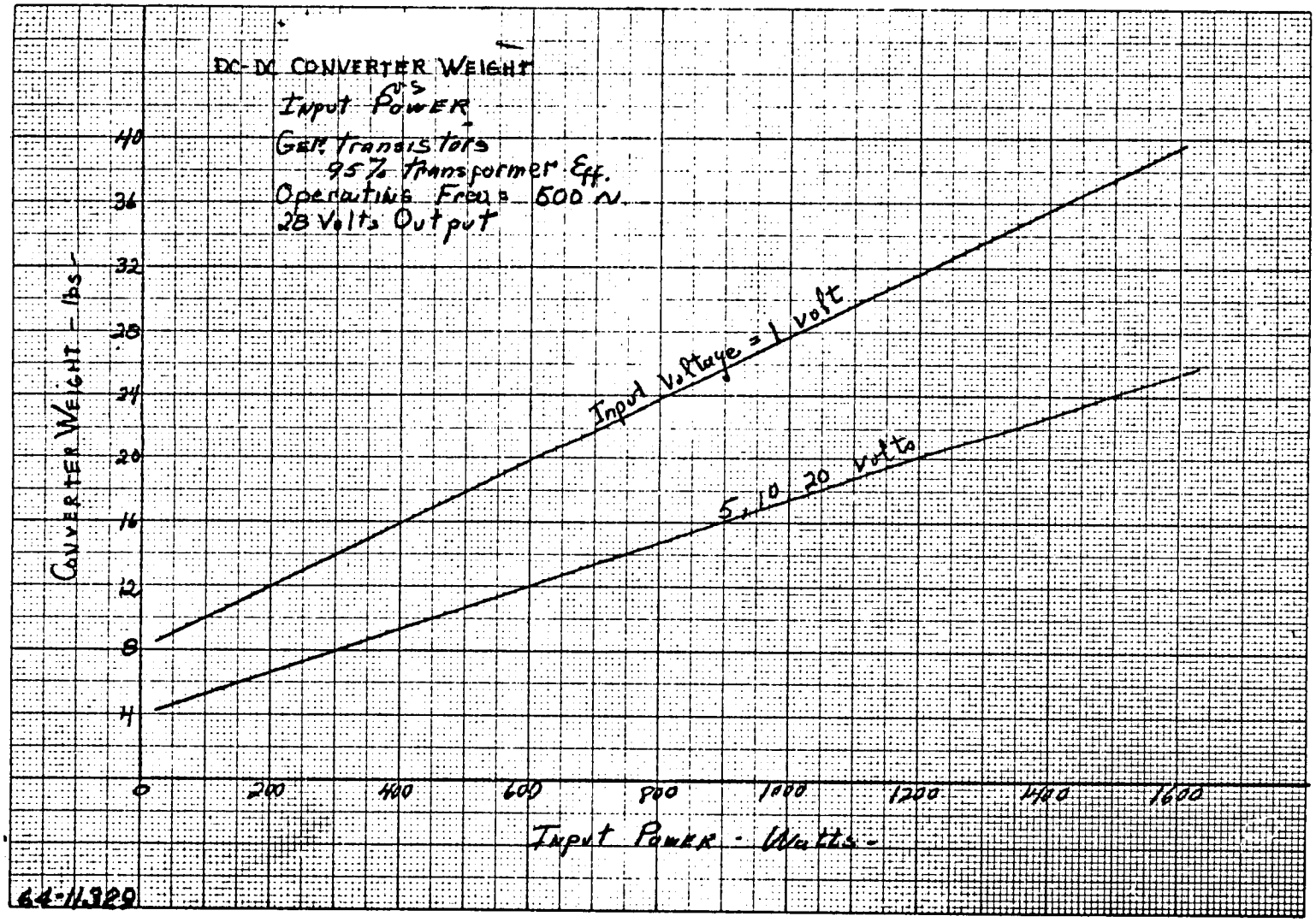

Figure 28 DC-DC CONVERTER WEIGHT -- 500 c GERMANIUM TRANSISTORS

RE-ORDER No. 64-524

114

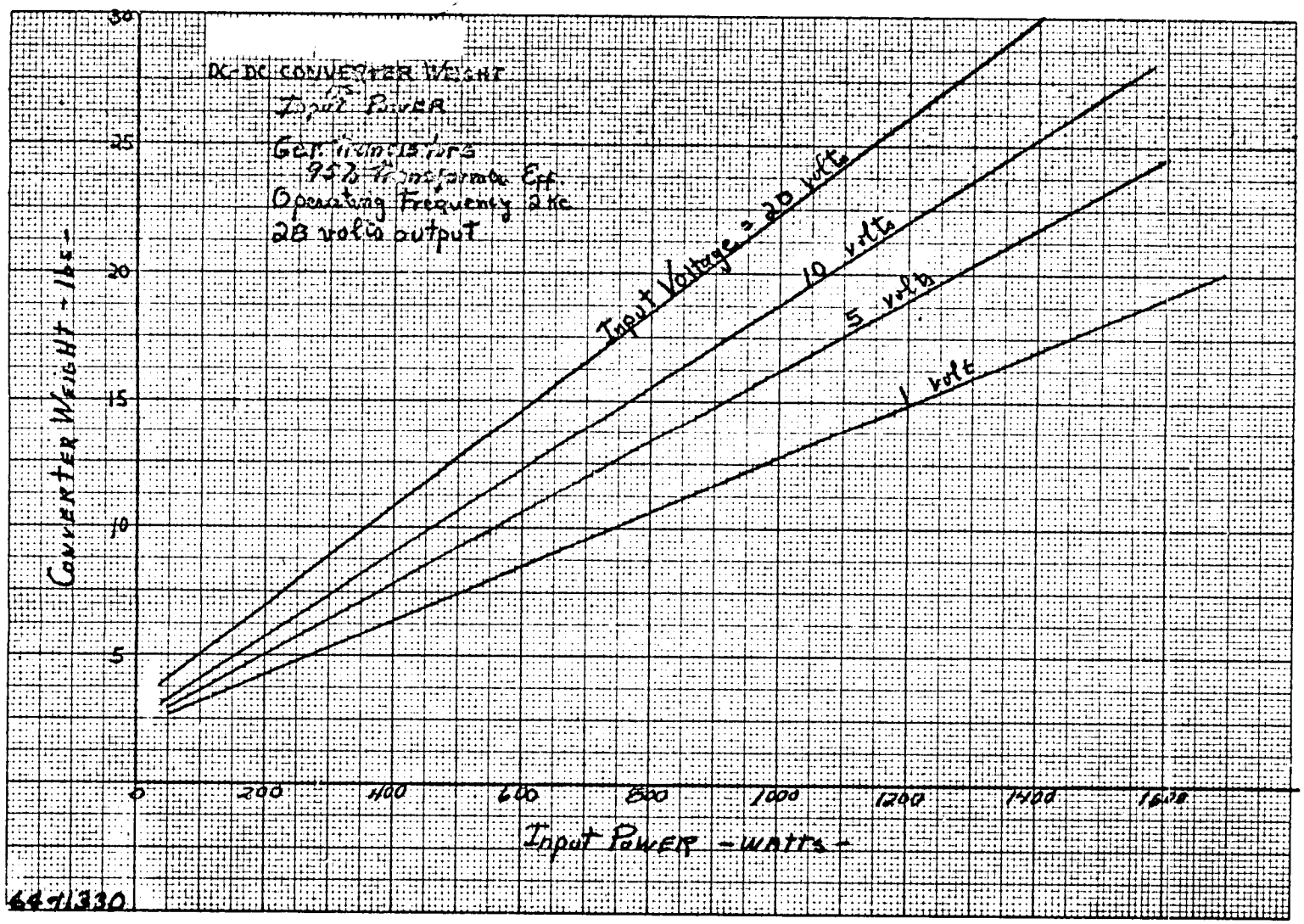

Figure 29 DC-DC CONVERTER WEIGHT -- 2 kc GERMANIUM TRANSISTORS

RE-ORDER No. 64-524

115

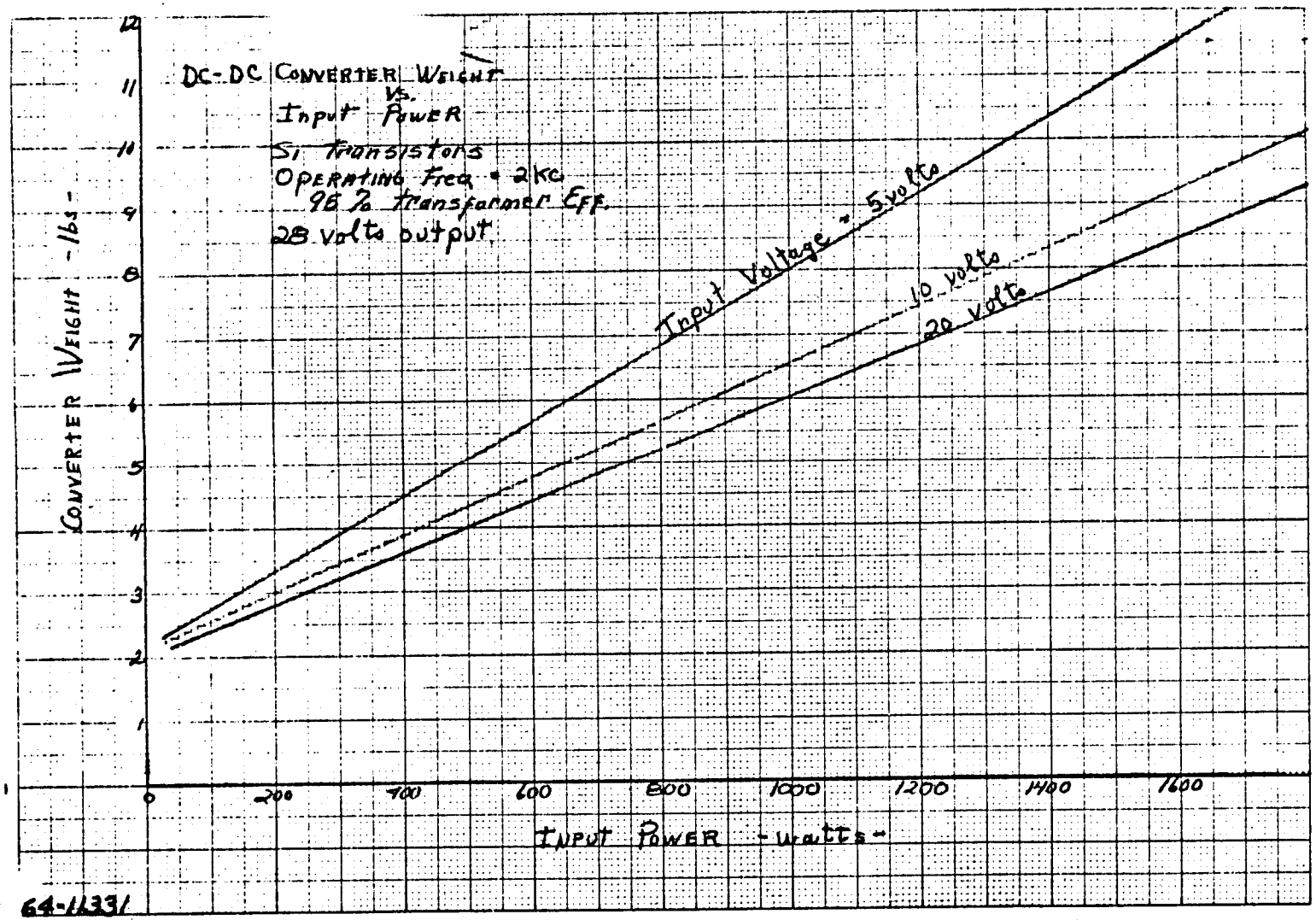

Figure 30 DC-DC CONVERTER WEIGHT --2 kc SILICON TRANSISTORS

RE-ORDER No. 64-524

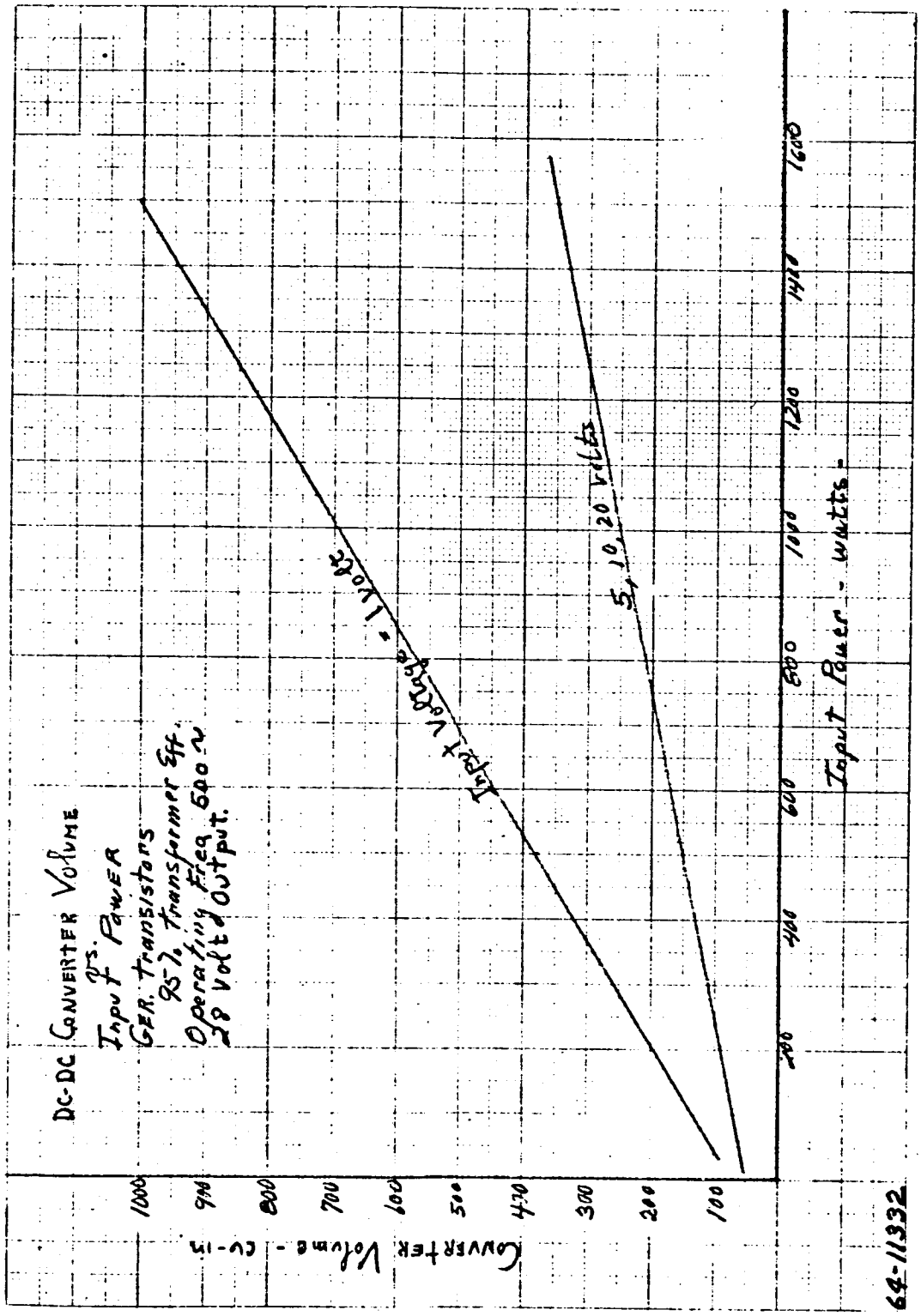

Figure 31 DC-DC CONVERTER VOLUME -- 500c - GERMANIUM TRANSISTORS

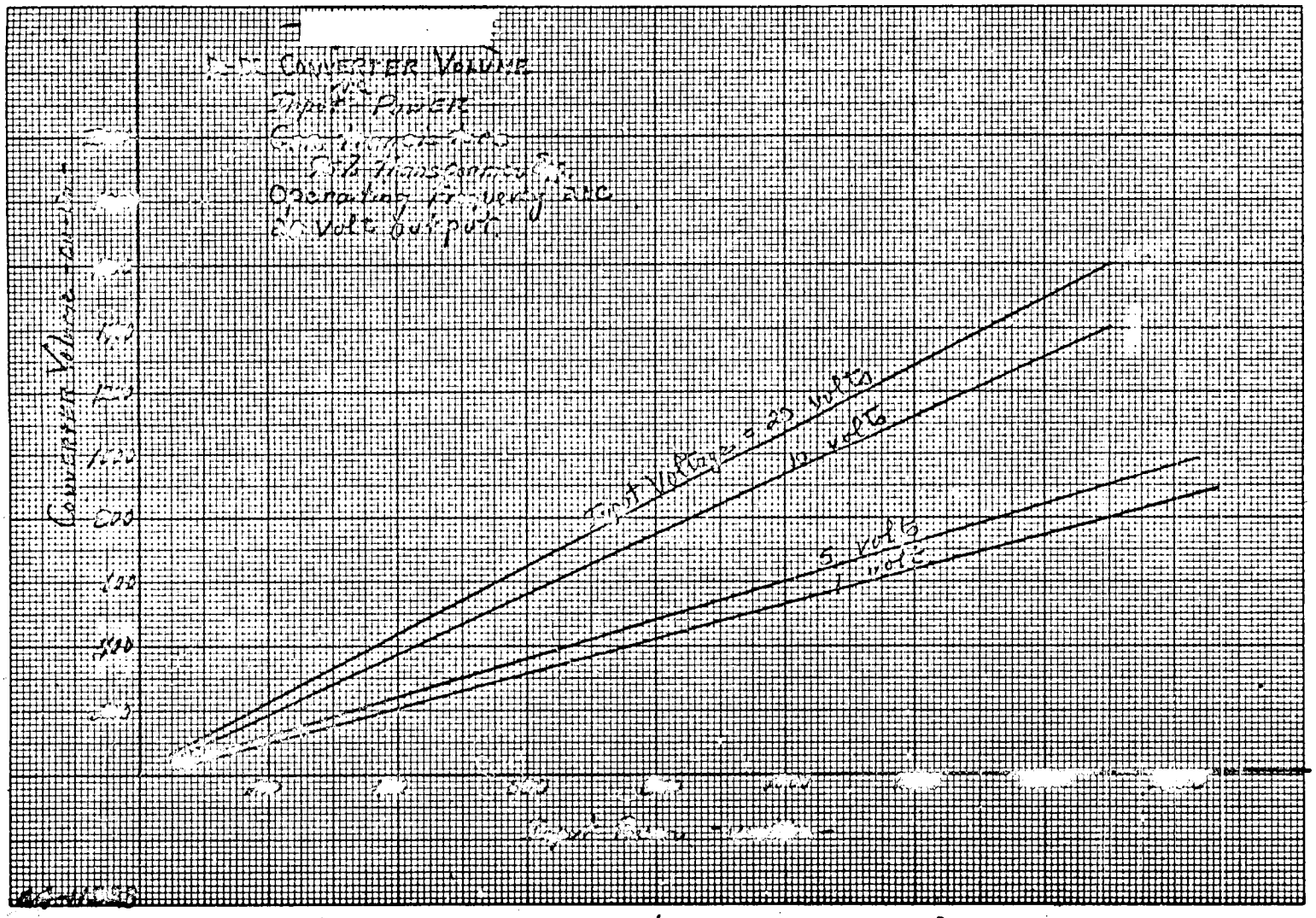

Figure 32. DC-DC CONVERTER VOLUME - 2 kc GERMANIUM TRANSISTORS

RE-ORDER No. 64-524

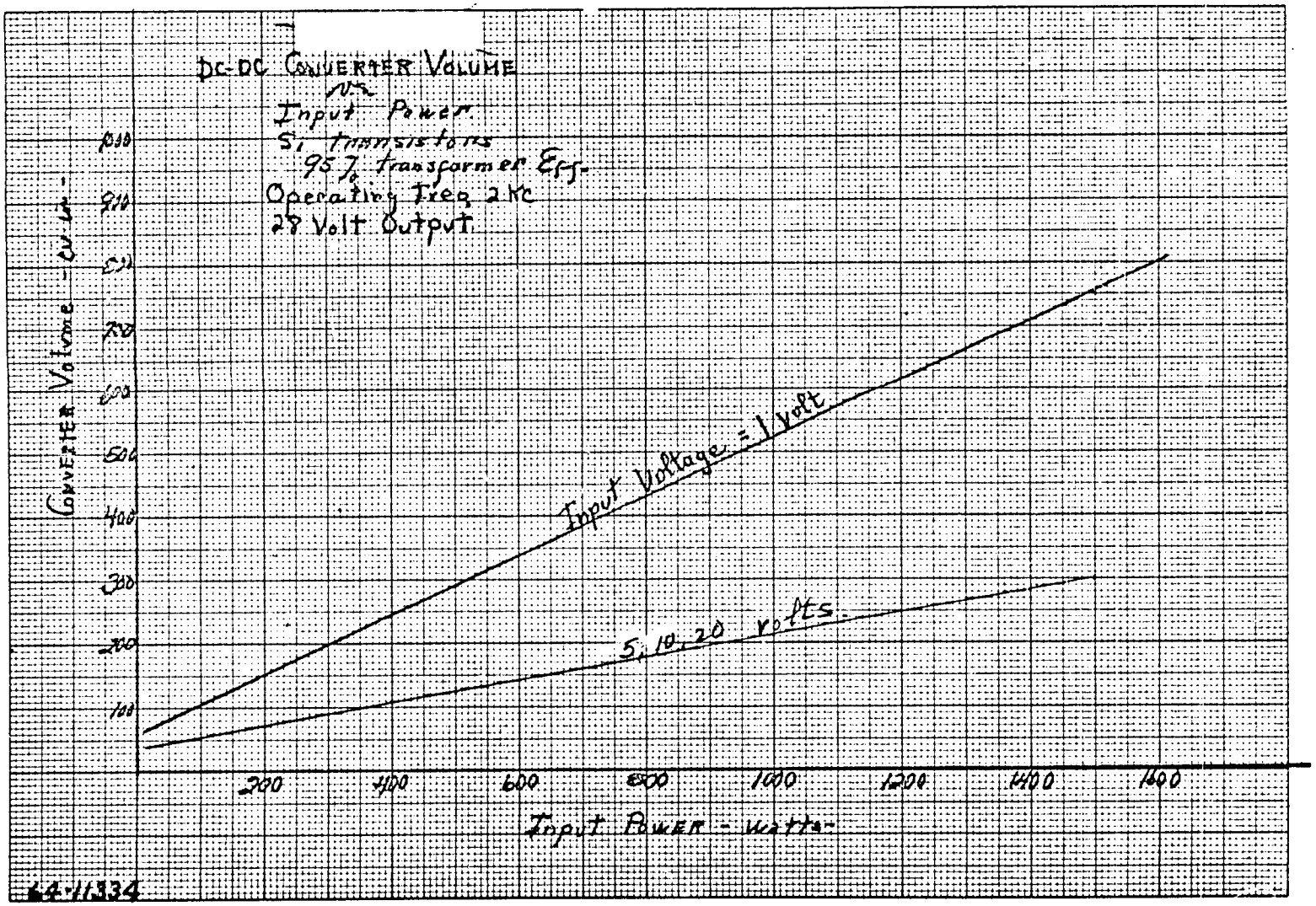

Figure 33 DC-DC CONVERTER VOLUME -- 500 c SILICON TRANSISTORS

RE-ORDER No. 64-534

RE-ORDER No. 64-524

4.0 COMMUNICATIONS

The communications system requirements for the flyby/bus were studied using the Mariner C system as a guide. Command, two-way doppler tracking, precision ranging and telemetry subsystems requirements were determined. The same precision ranging system used on Mariner C was assumed in these studies. Table 21 is a glossary of terms used in this section. Table 22 and 23 list the assumptions made concerning the DSIF characteristics.

4.1 COMMAND LINK

The transmitting and receiving techniques used on Mariner C for transfer of command data are applicable for the Advanced Mariner studies. Expected variations are an increase in the number of discrete commands, associated with lander separation. Table 24 lists all pertinent parameters affecting the performance of a command link between the DSIF and the flyby/bus. The receiving antenna provides hemi-omni coverage and would be used near Earth, i.e., out to some tens of millions of kilometers. The performance margin in this link can be determined as follows:

1. Carrier Power

P_{tc} = Threshold carrier power - net circuit loss

= -134.2 dbm + 191.1 db

= +56.9 dbm

= 490 watts

2. Data Power

P_{td} = Threshold subcarrier power - net circuit loss

= -142.4 dbm + 191.1 db

= +48.7 dbm

= 74 watts

120

TABLE 21

GLOSSARY OF TERMS

P_{tc}	Carrier power at threshold
P_{td}	Data power at threshold
P_{ts}	Sync. power at threshold
D	Major diameter of high gain antenna (feet)
$\dot{B}$	Bit rate (bits per second)
P_t	Total radiated power (watts)
R_s	Slant range (kilometers)
R	Ratio of Minor-to-Major diameters of high gain antennas.

TABLE 22

DSIF S-BAND TRANSMITTER CAPABILITIES (JPL TM 33-83)

Frequency (mc)	Output Power (watts)	Antenna (diameter)	Gain (db)	Feedline Loss (db)	Polarization	Approximate Beamwidth (degrees)	Location		
							GS	W	J
2115 ± 5 Channels	10K	85 ft HA-Dec.	53.5 (a)	0.4	Right Circ.	0.44	**	**	**
(1) 2110 - 2111 13/16 (2) 2111 13/16 - 2114 13/16 (3) 2114 13/16 - 2120	100K	85 ft A-El	53.5 (a)	0.4	Right Circ.	0.44	**		

GS = Goldstone, Calif., USA

W = Woomera, Australia

J = Johanesburg, South Africa

(a) = SPS 37-24 pg. 2

TABLE 23

ASSUMED DSIF RECEIVER CHARACTERISTICS

Receiving Frequency (mc)	Reflector Diameter (feet)	Reflector Gain (db)	Circuit Loss (db)	Noise Temperature (°K)	Noise Bandwidth (cps)	Polarization	Beamwidth (degrees)	Location
2290 - 2293 1/3 2293 1/3 - 2296 2/3 2296 2/3 - 2300	210	61 ± 1	0.03 max.	28 ± 5	(3-250)	Right Circ.	0.2	All Stations

122

RE-ORDER No. 64-524

RE-ORDER No. 64-524

TABLE 24

TELECOMMUNICATIONS DESIGN CONTROL CHART

PROJECT: Advanced Mariner
CHANNEL: DSIF to Flyby/Bus
MODE: Command

No.	Parameter	Nominal Value (db)	Tolerance (db)	Worst Value (db)	Source
1.	Transmitting circuit loss	-0.5	+0.0 -0.3	-0.8	
2.	Transmitting antenna gain	+53.7	±0.2	±53.5	SPS37-24 Vol. III
3.	Transmitting antenna pointing loss	---	---	---	
4.	Space loss = 32.46 + 20 log F + 20 log R F = 2120 mc, R = 10^7 km	-239.7	---	-239.7	
5.	Polarization loss	0.0	+0.0 -3.0	-3.0	
6.	Atmospheric absorption loss	---	---	---	
7.	Receiving antenna gain (hemi-omni)	+3.0	+0.0 -1.0	+2.0	
8.	Receiving antenna pointing loss	0.0	+0.0 -3.0	-3.0	
9.	Receiving circuit loss	-0.1	max.	-0.1	
10. 11.					
12.	Net circuit loss	-183.6	+0.2	-191.1	
13.	Total transmitter power	+80.0*	+0.0 -0.1	+79.9*	TM 33-83
14.	Total received power	-103.6*	+0.2 -7.6	-111.2*	

*dbm

123

TABLE 24 (Concl'd)

No.	Parameter	Nominal Value	Tolerance	Worst Value	Source
15.	Receiver noise spectral density (N/B) T System _____ NF 10 $\pm^{2}_{1}$ db	-162.0*	±1.1	-160.9*	mc 320
	Carrier Loop				
16.	Carrier APC noise BW ($2B_{LO}$ = 20 cps)	+13.0	---	+13.0	
17.	Required Threshold SNR in $2B_{LO}$	+12.7	±1.0	+13.7	mc 322
18.	Threshold carrier power	-136.3*	±2.1	-134.2*	
19.	Total received power				
20.	Carrier modulation loss				
21.	Received carried power				
22.	Performance margin				
	Data or Command Channel				
23.	Bit rate (1/t) = 1 bps	0.0	---	0.0	
24.	Required ST/N/B	+17.5	±1.0	+18.5	mc 322
25.	Threshold subcarrier power	-144.5*	±2.1	-142.4*	
26.	Total received power				
27.	Modulation loss				
28.	Received data subcarrier power				
29.	Performance margin				
	SYNC Channel				
30.	SYNC APC noise BW ($2B_{LO}$ = 2 cps)	+3.0	---	+3.0	
31.	Threshold SNR in $2B_{LO}$	+15.7	±1.0	+16.7	mc 322
32.	Threshold subcarrier power	-143.3*	±2.1	-141.2*	
33.	Total received power				
34.	Modulation loss				
35.	Received SYNC subcarrier power				
36.	Performance margin				

*dbm

124

3. Sync Power

P_{ts} = Threshold subcarrier power - net circuit loss

= -141.2 dbm + 191.1 db

= +49.9 dbm

= 97.6 watts

4. Total Power

$P_T = P_{tc} + P_{ts} + P_{td}$

= 490 + 74 + 97.6

= 661.6 watts

5. Performance Margin at 10^7 km

$$\text{Performance margin} = 10 \log \frac{100,000}{661.6}$$

$$= +17.9 \text{ db}$$

6. Performance Margin versus Range

$$\text{Performance margin} = +17.9 - 20 \log \frac{\text{Range}}{10^7}$$

Figure 34 shows performance margin as a function of range and antenna. In the conceptual design, the selected cross over range (cross over from low gain to high gain antenna) was 43 x 10^6 kilometers. The resultant performance margin, from figure 34, is +5.2 db. Also, in the conceptual design, a 3 foot by 1 1/2 foot parabolic antenna was selected for the high gain antenna system. The gain of this antenna, from figure 62 is +21 db. The performance margin in the command link will exceed +10 db with this antenna through the post encounter range.

4.2 TRACKING LINK

The tracking capability of the DSIF consists of angle tracking, one-way and two-way doppler measurement and precision ranging using psuedo -random noise codes (PN codes).

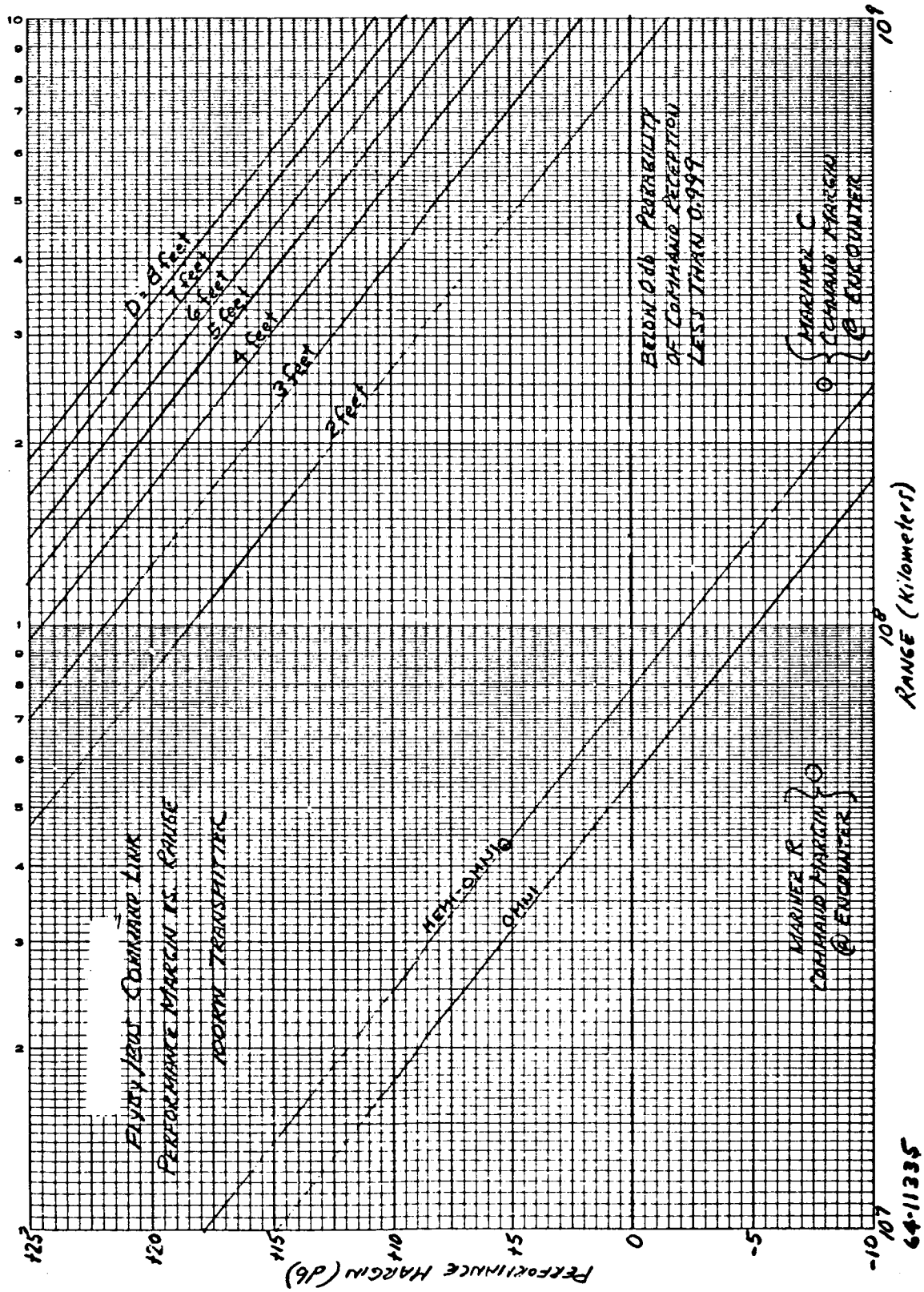

Figure 34 FLYBY/BUS COMMAND LINK PERFORMANCE MARGIN - 100-kw TRANSMITTER

126

1. Doppler

One-way and two-way doppler measurement capability is included at all DSIF stations. At S-band, the approximate accuracy of one-way doppler data is 30 m/sec. The accuracy of one-way doppler is limited primarily to predictable spacecraft oscillator drift. The approximate accuracy of two-way doppler data is 0.2 m/sec. The improved accuracy of the two-way system is the result of using a ground transmitter in the vicinity of the DSIF receiver. The spacecraft, by means of a phase-locked loop receiver, "locks" onto the carrier component of the received signal from the DSIF transmitter. This action switches the fixed frequency oscillator in the spacecraft transponder out of the circuit and replaces it with an exact multiple of the signal received from the DSIF transmitter. This signal is then retransmitted to the DSIF where it can easily be compared with the original signal from the DSIF transmitter. If the carrier can be locked in both directions two-way doppler can be made available.

Table 25 is the design control chart for the DSIF to flyby/bus link. A comparison of the carrier threshold requirements for the doppler tracking and the carrier threshold requirements for the command link shows that for two-way carrier track the ranging link is always 10 db better than the command link.

Table 26 is the design control chart for the flyby/bus to DSIF link. A comparison of the carrier threshold requirements for doppler tracking and the carrier threshold requirement for telemetry showed that the two-way carrier track link is always better than the telemetry link. Designing the telemetry and command links to operate throughout the mission automatically specifies that 2-way doppler track is attainable.

4.3 TELEMETRY LINK

The flyby/bus antenna system used two antennas; a low gain (wide beamwidth) antenna near Earth and a high gain (narrow beamwidth) antenna from some tens of millions of kilometers from Earth through post encounter. To maintain telemetry reception capability over the total mission, the telemetry link cross-over point (low gain to high gain antenna) can only occur when the worst case performance margin in both links is at or above 0.0 db. All pertinent parameters affecting the performance of a telemetry link between the flyby/bus and the DSIF are listed in table 27. The assigned values of these parameters are based on ground rules received regarding the DSIF, assumptions made regarding the performance of typical hardware, and direct calculation. The modulation scheme selected for this link is the same as the one used in the Mariner R Venus flyby experiment and the Mariner C spacecraft; namely, pulse code modulation (PCM) phase shift keying (PSK) a subcarrier which phase modulates (PM) a carrier.

RE-ORDER No. 64-524

TABLE 25

TELECOMMUNICATIONS DESIGN CONTROL CHART

PROJECT: Advanced Mariner
CHANNEL: DSIF to Flyby/Bus
MODE: Doppler Track

No.	Parameter	Nominal Value (db)	Tolerance (db)	Worst Value (db)	Source
1.	Transmitting circuit loss	-0.5	0.0 -0.3	-0.8	
2.	Transmitting antenna gain	53.7	-0.2	53.5	SPS 37-24 Vol. III p. 2
3.	Transmitting antenna pointing loss	---	---	---	
4.	Space loss = 32.46 20 log F 20 log R F = 2120 mc, R = 10^7 km	-239.7	---	-239.7	
5.	Polarization loss	0.0	0.0 -3.0	-3.0	
6.	Atmospheric absorption loss	---	---	---	
7.	Receiving antenna gain (hemi-omni)	3.0	0.0 -1.0	2.0	
8.	Receiving antenna pointing loss	0.0	0.0 -3.0	3.0	
9.	Receiving circuit loss	-0.1	max.	-0.1	
10. 11.					
12.	Net circuit loss	-183.6	0.2 -7.5	-191.1	
13. 14.	Total transmitter power Total received power				
15.	Receiver noise spectral density (N/B) NF = 10db $^{1.0}_{-2.0}$ db	-162.0*	-1.1	-160.9*	
16.	Carrier APC noise BW ($2B_{LO}$ = 20 -4 cps)	13	0.8 -1.0	13.8	
	Carrier Track-Oneway				
17.	Threshold SNR in $2B_{LO}$	0.0	---	0.0	
18.	Threshold Carrier Power	-149.0*	1.9 -2.1	-147.1*	
	Carrier Track - Two Way				
19.	Threshold SNR in $2B_{LO}$	3.0	---	3.0	
20.	Threshold Carrier power	-146.0*	1.9	-144.1*	

*dbm

128

RE-ORDER No. 64-524

TABLE 26

TELECOMMUNICATIONS DESIGN CONTROL CHART

PROJECT: Advanced Mariner
CHANNEL: Flyby/Bus to DSIF
MODE: Doppler Track

No.	Parameter	Nominal Value (db)	Tolerance (db)	Worst Value (db)	Source
1.	Transmitting circuit loss	-1.2	-0.3 0.0	-1.5	
2.	Transmitting antenna gain (hemi-omni)	3.0	-1.0	2.0	
3.	Transmitting antenna pointing loss	-1.5	-1.5	-3.0	
4.	Space loss = 32.46 20 log F 20 log R F = 2295 mc, R= 10^8km	-259.7	---	-259.7	
5.	Polarization loss	0.0	0.0 -0.1	-0.1	
6.	Atmospheric absorption loss	---	---	---	
7.	Receiving antenna gain/ 85 foot	54.4	-0.2	54.2	SPS 37-24 Nov. 63 p.2
8.	Receiving antenna pointing loss	---	---	---	
9.	Receiving circuit loss	-0.1	max.	-0.1	
10. 11.					
12.	Net circuit loss	-205.2	-3.4	-208.6	
13. 14.	Total transmitter power Total received power				
15.	Receiver noise spectral density (N/B) T System 28°K-5°K NF _____	-183.9*	-0.7	-183.2*	Mars 66 Gnd Rules from JPL
16.	Carrier APC Noise BW ($2B_{LO}$= 20 - 4 cps)	13	0.8 -1.0	13.8	
	Carrier Track - One Way				
17.	Threshold SNR in $2B_{LO}$	0.0	---	0.0	
18.	Threshold Carrier power	-170.9*	1.5 -1.7	-169.4*	
	Carrier Track - Two Way				
19.	Threshold SNR in $2B_{LO}$	3.0	---	3.0	
20.	Threshold Carrier power	-167.9*	1.5 -1.7	-166.4*	

*dbm

129

The low gain (wide beamwidth) link is used near Earth primarily for the reason that large clock and cone angle variations and most of the critical maneuvers by the bus occur in this region.

The high gain link is used when the communication distance increases to a point where continued use of the low gain link would require prohibitive transmitter power. A fixed body high gain link can be used if the aximuth and polar angle changes due to clock-cone angle variations do not reduce the effective gain of the antenna to a point where the link performance margin drops below 0 db. If this cannot be done, a steerable high gain antenna must be used.

1. DSIF Assumptions

Assumptions concerning the DSIF receiver are listed in table 23.

2. Telemetry Link Parameters

Assigned values of telemetry link parameters are based on the same reasoning used in the lander direct link.

3. Transmitter Power Calculations

The following calculations are based on table 27. All results are worst case values and are plotted parametrically in figure 35 as a function of power and net antenna gain.

a. Carrier Power

P_{tc} = Threshold Carrier Power Net Circuit Loss

= -164.1 dbm + 207.7 db

= +43.6 dbm

= 22.9 watts

b. Data Power

P_{td} = Threshold Subcarrier Power - Net Circuit Loss

= -175.2 dbm + 207.7 db

= +32.5 dbm

= 1.78 watts/bps

RE-ORDER No. 64-524

TABLE 27

TELECOMMUNICATIONS DESIGN CONTROL CHART

PROJECT: Advanced Mariner
CHANNEL: Flyby/Bus to DSIF
MODE: Telemetry Playout

No.	Parameter	Nominal Value (db)	Tolerance (db)	Worst Value (db)
1.	Transmitting circuit loss	-1.0	+0.0	-1.5
2.	Transmitting antenna gain	---	---	0.0
3.	Transmitting antenna pointing loss	---	---	0.0
4.	Space loss = 32.46 + 20 log F + 20 log R F = 2295 mc, R = 2×10^8 km	-265.7	---	-265.7
5.	Polarization loss	-0.3	+0.3 -0.2	-0.5
6.	Atmospheric absorption loss	---	---	---
7.	Receiving antenna gain (210 Dish)	+61.0	±1.0	+60.0
8.	Receiving antenna pointing loss	---	---	---
9.	Receiving circuit loss	-0.02	±0.01	-0.03
10. 11.				
12.	Net circuit loss	-206.0	+1.3 -1.7	-207.7
13.	Total transmitter power			
14.	Total received power			
15.	Receiver noise spectral density (N/B) T System = 28°K ± 5°K	-183.9*	±0.7	-183.2*

131

RE-ORDER No. 64-524

TABLE 27 Concl'd)

COMMUNICATIONS DESIGN CONTROL CHART

No.	Parameter	Nominal Value (db)	Tolerance (db)	Worst Value (db)
	Carrier Loop			
16.	Carrier APC noise BW ($2B_{LO}$ = 20 cps)	+13.0	---	+13.0
17.	Required Threshold SNR in $2B_{LO}$	+6.0	±0.1	+6.1
18.	Threshold Carrier power	-164.9*	±0.8	-164.1*
19.	Total received power			
20.	Carrier modulation loss			
21.	Received carrier power			
22.	Performance margin			
	Data Channel			
23.	Bit rate (1/t) = 1 bps	+0.0	---	+0.0
24.	Required ST/N/B ($P_e = 10^{-3}$	+7.4	±0.6	+8.0
25.	Threshold subcarrier power	-176.5*	±1.3	-175.2*
26.	Total received power			
27.	Modulation loss			
28.	Received data subcarrier power			
29.	Performance margin			
	SYNC Channel			
30.	SYNC APC noise BW ($2B_{LO}$ = 2 cps)	+3.0	---	+3.0
31.	Threshold SNR in $2B_{LO}$	+8.0	±1.0	+9.0
32.	Threshold received power	-172.9*	±1.7	-171.2*
33.	Total received power			
34.	Modulation loss			
35.	Received SYNC subcarrier power			
36.	Performance margin			

*dbm

132

c. SYNC Power

P_{tc} = Threshold Subcarrier Power - Net Circuit Loss

= -171.2 dbm + 207.7 db

= +36.5 dbm

= 4.47 watts

d. Total Power

$$P_T = P_{tc} + P_{ts} + P_{td}$$

$$= 27.37 + 1.78\ \dot{B}$$

The following is an example of the use of figure 35. At a range of 200 million kilometers and for a bit rate 10 bps, a power gain product of +16.5 dbw is required. If the net antenna gain is determined to be +6.5 db, then the transmitter power required is 10.0 dbw, or 10 watts.

4. Antenna/Transmitter Selection

The fixity of the high gain antenna on the bus was typically chosen from a Mariner C design. The feed axis of the antenna is positioned along the vehicle-earth vector at encounter. The minor axis is positioned in plane formed by the vehicle-sun and vehicle-earth vectors, 90 degrees from the feed. (See figure 36.)

The cone angle, θ, and clock angle, γ, variations can be resolved into polar and azimuthal angles by a co-ordinate transformation. The polar angle (ϕ) is measured from the feed of the antenna while the azimuthal angle (α) is measured from the antenna minor axis. (See figure 37.)

A set of antenna gain-contour curves have been plotted which indicate antenna pointing loss versus polar angle and azimuth angle for antenna diameters of 2, 3, 4, 5, 6, and 8 feet, and for antenna axis ratios of 0.5, 0.6, 0.8, and 1.0. Using these curves in combination with the polar and azimuthal variations along the flight trajectory, a new set of curves showing relative antenna gain versus slant range can be plotted for the antenna sizes and shapes mentioned above. Figures 38 through 61 are the results of the preceeding analysis. The polar and azimuthal angle variations along the flight trajectory have been computed for 4 mission opportunities in 1969 and 5 mission opportunities in 1971. In this analysis only 4 missions will be evaluated; the 2 extreme launch dates in '69 and the 2 extremes in '71. All other launch dates yield results of relative antenna gain which fall within the two extremes.

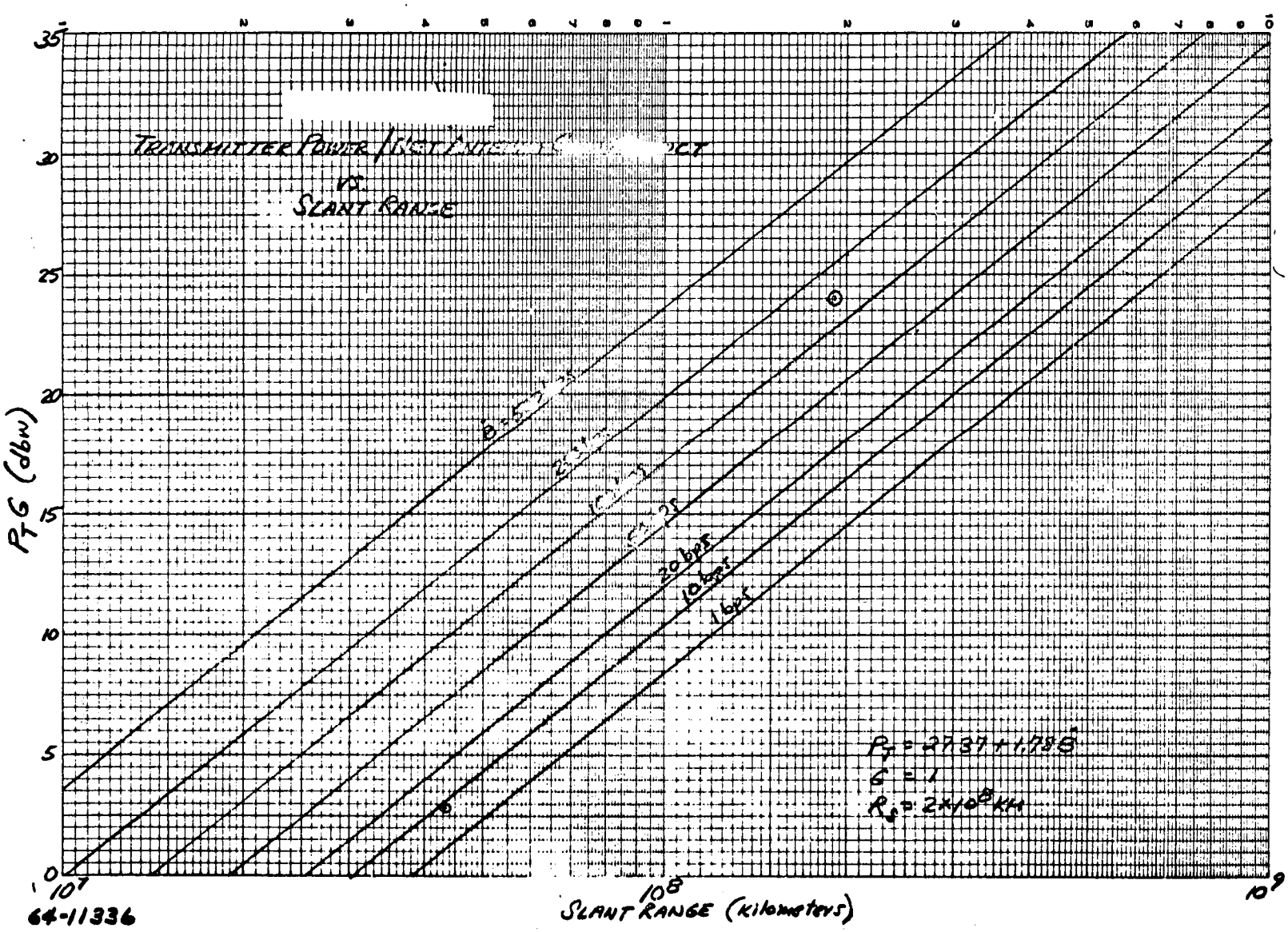

Figure 35 TRANSMITTER POWER/NET ANTENNA GAIN PRODUCT

RE-ORDER No. 64-524

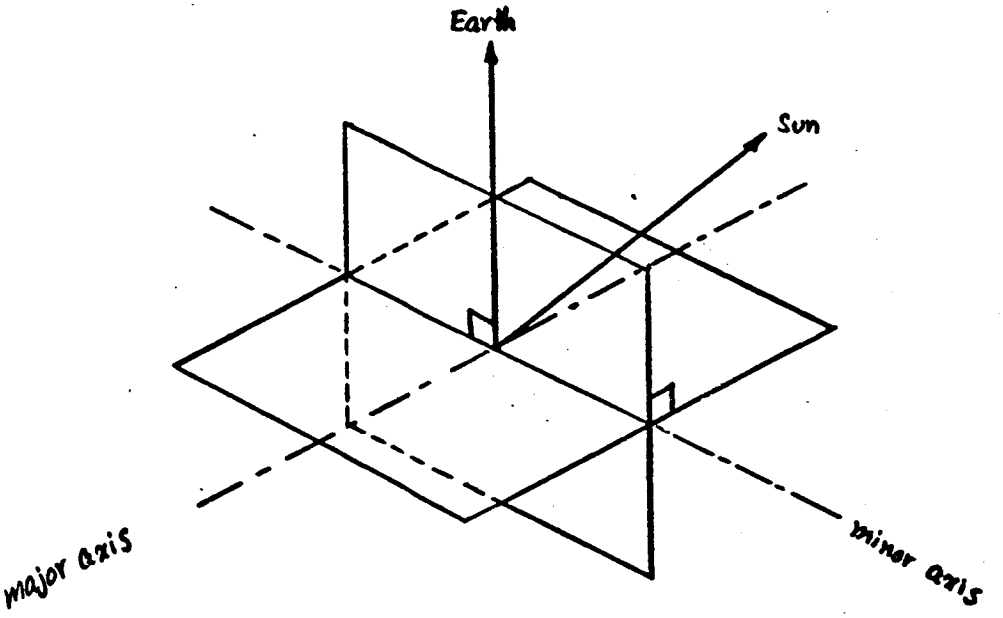

Figure 36 HIGH GAIN ANTENNA FIXITY

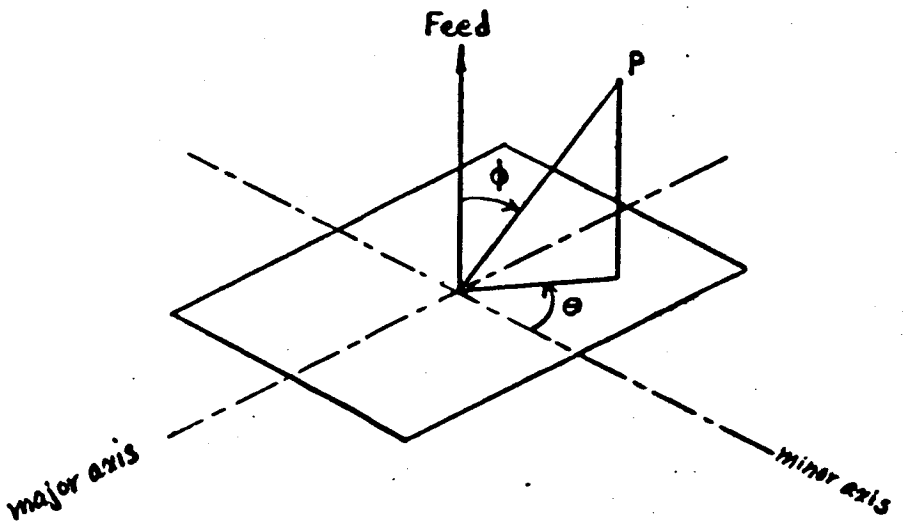

Figure 37 HIGH GAIN ANTENNA POLAR AND AZIMUTHAL ANGLES

64-11337

135

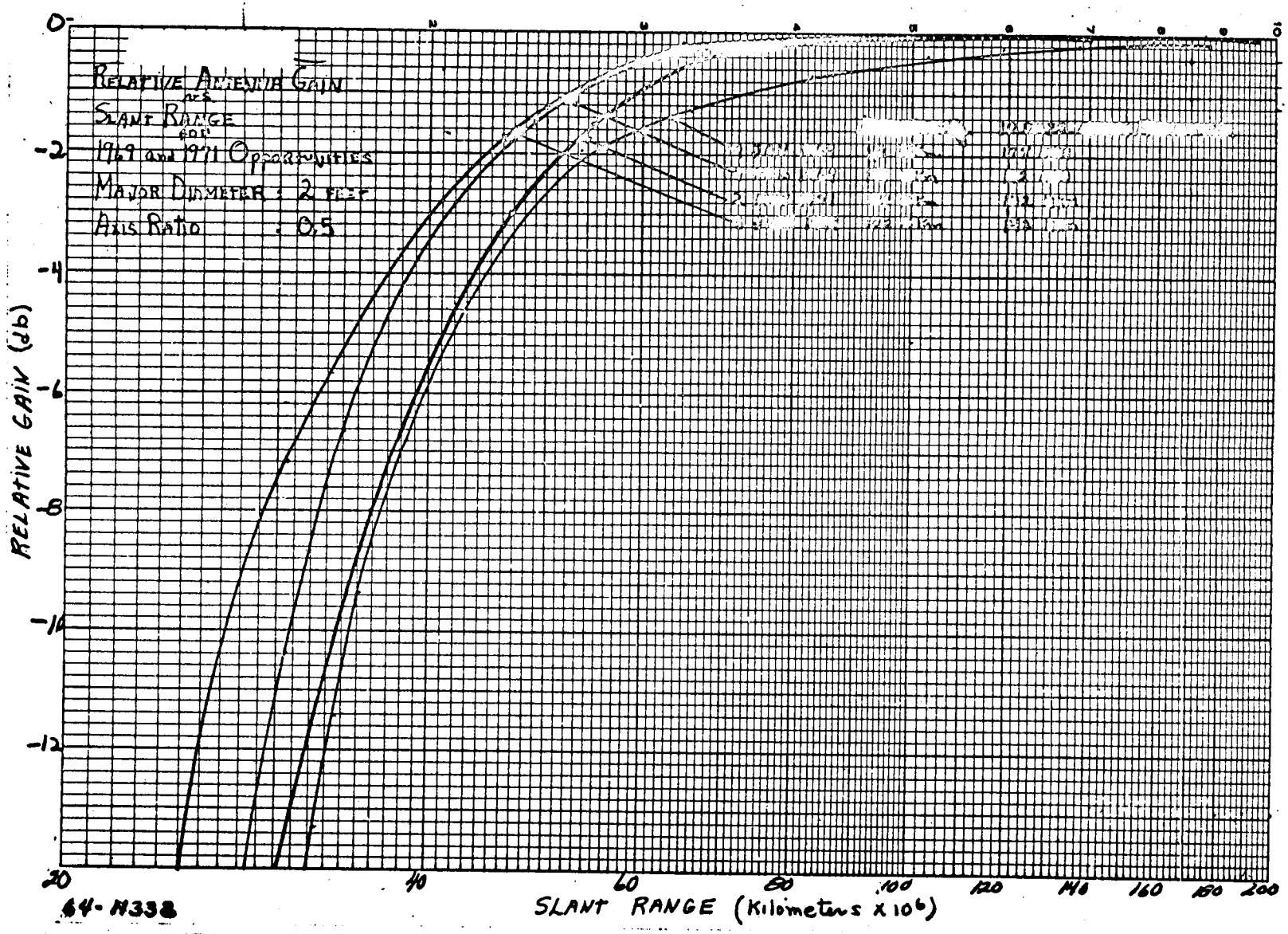

Figure 38 RELATIVE ANTENNA GAIN, MAJOR DIAMETER 2 FEET, AXIS RATIO 0.5

RE-ORDER No. 64-524

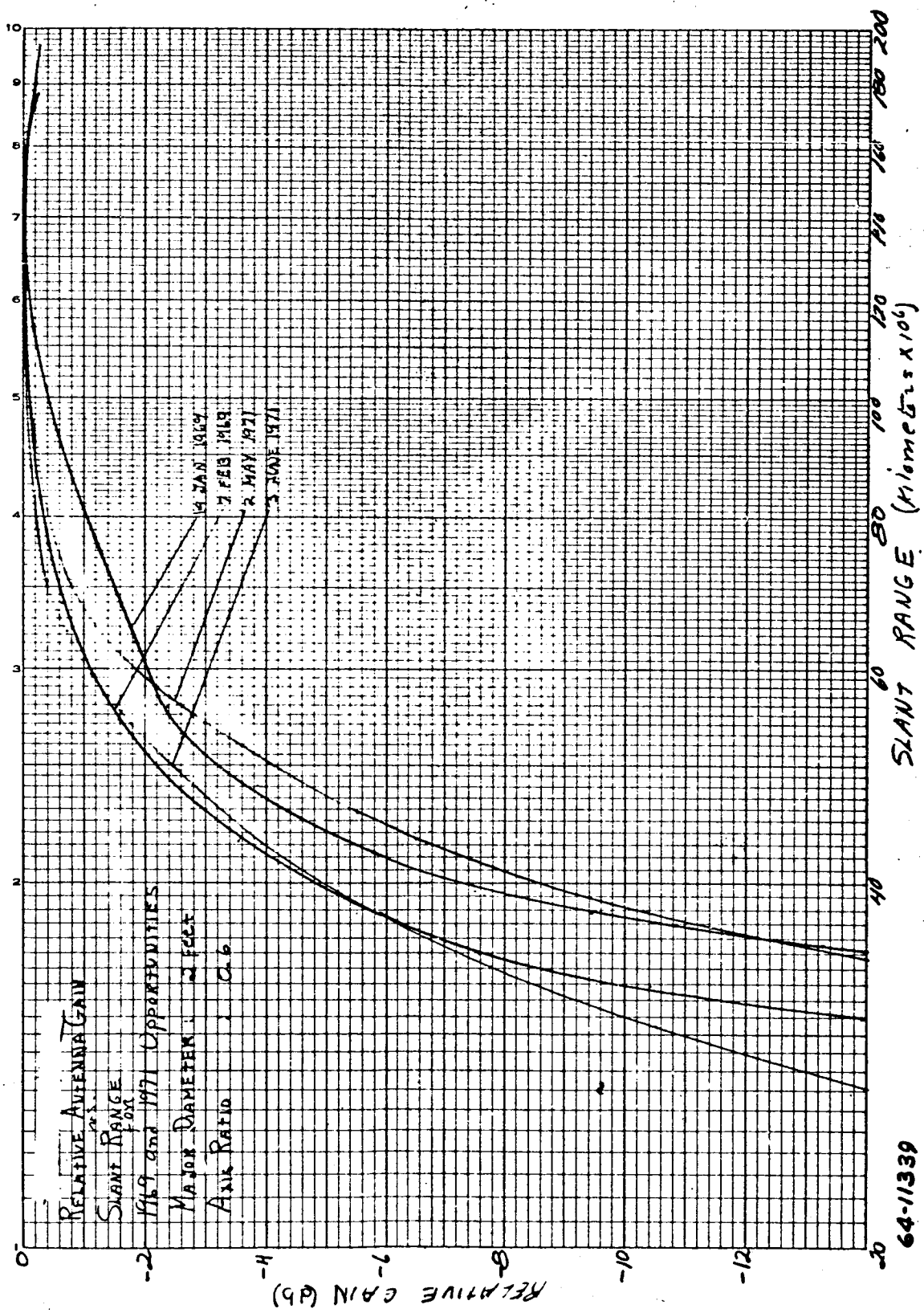

Figure 39 RELATIVE ANTENNA GAIN, MAJOR DIAMETER 2 FEET, AXIS RATIO 0.6

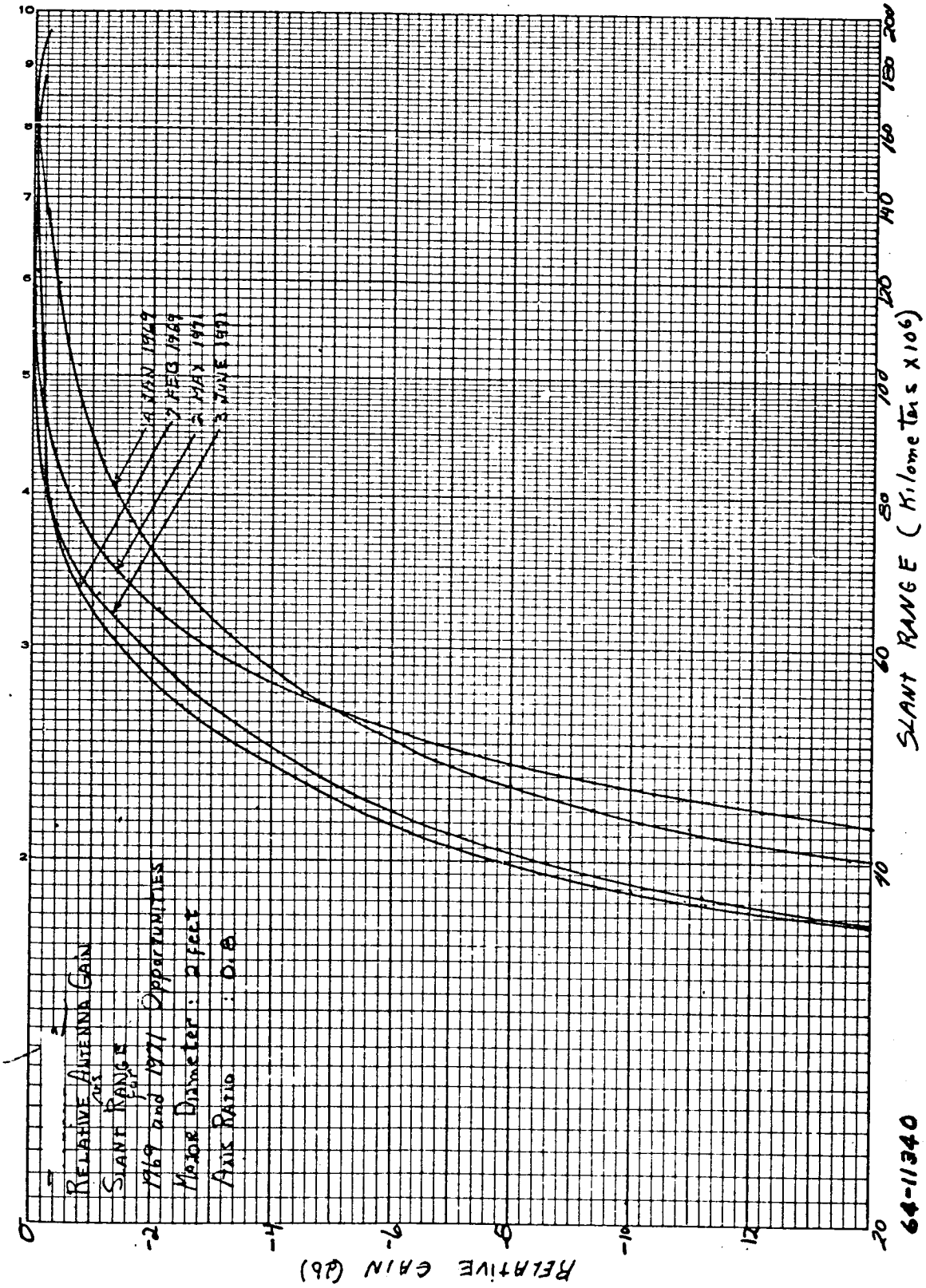

Figure 40 RELATIVE ANTENNA GAIN, MAJOR DIAMETER 2 FEET, AXIS RATIO 0.8

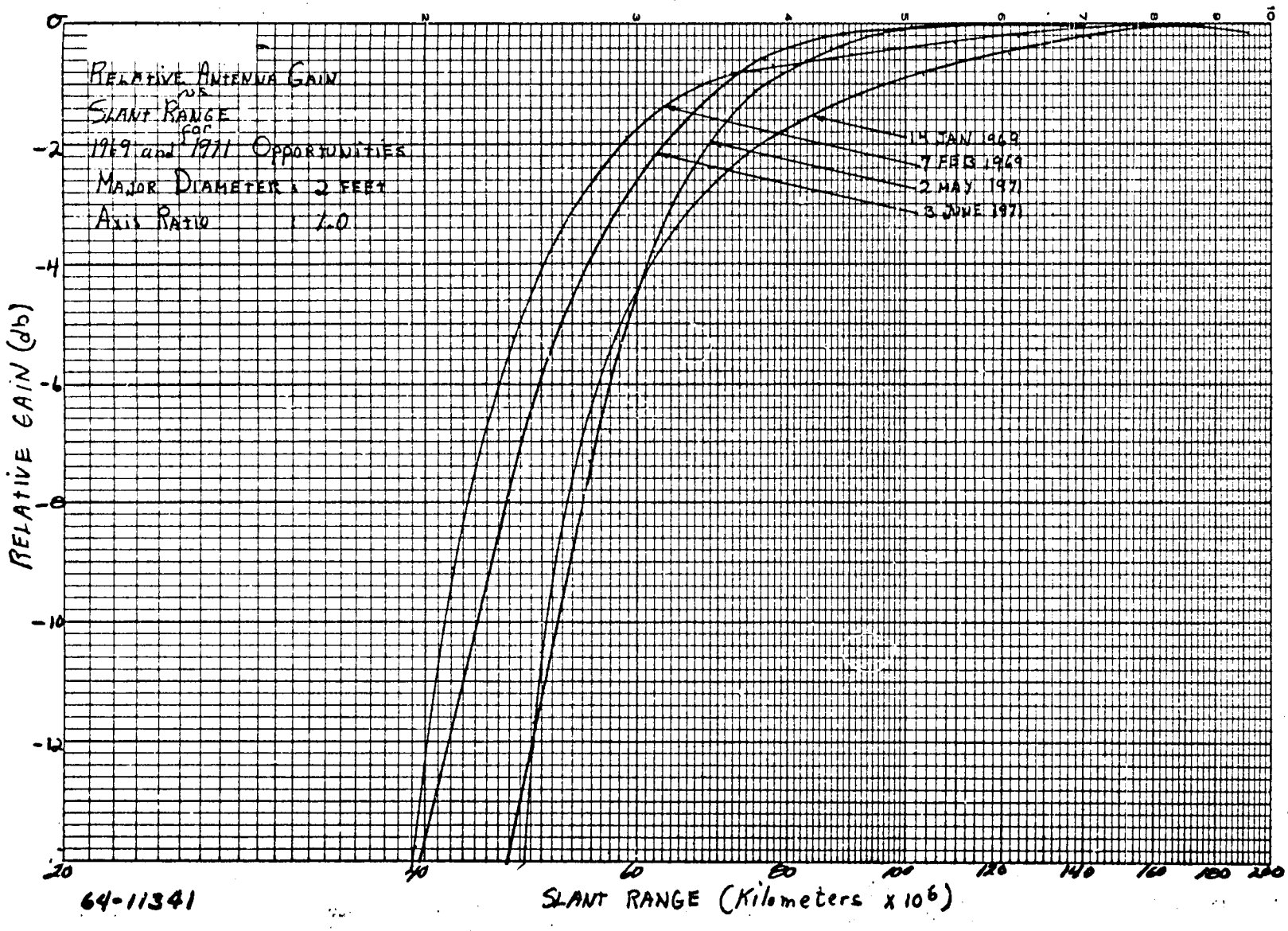

Figure 41 RELATIVE ANTENNA GAIN, MAJOR DIAMETER 2 FEET, AXIS RATIO 1.0

RE-ORDER No. 64-524

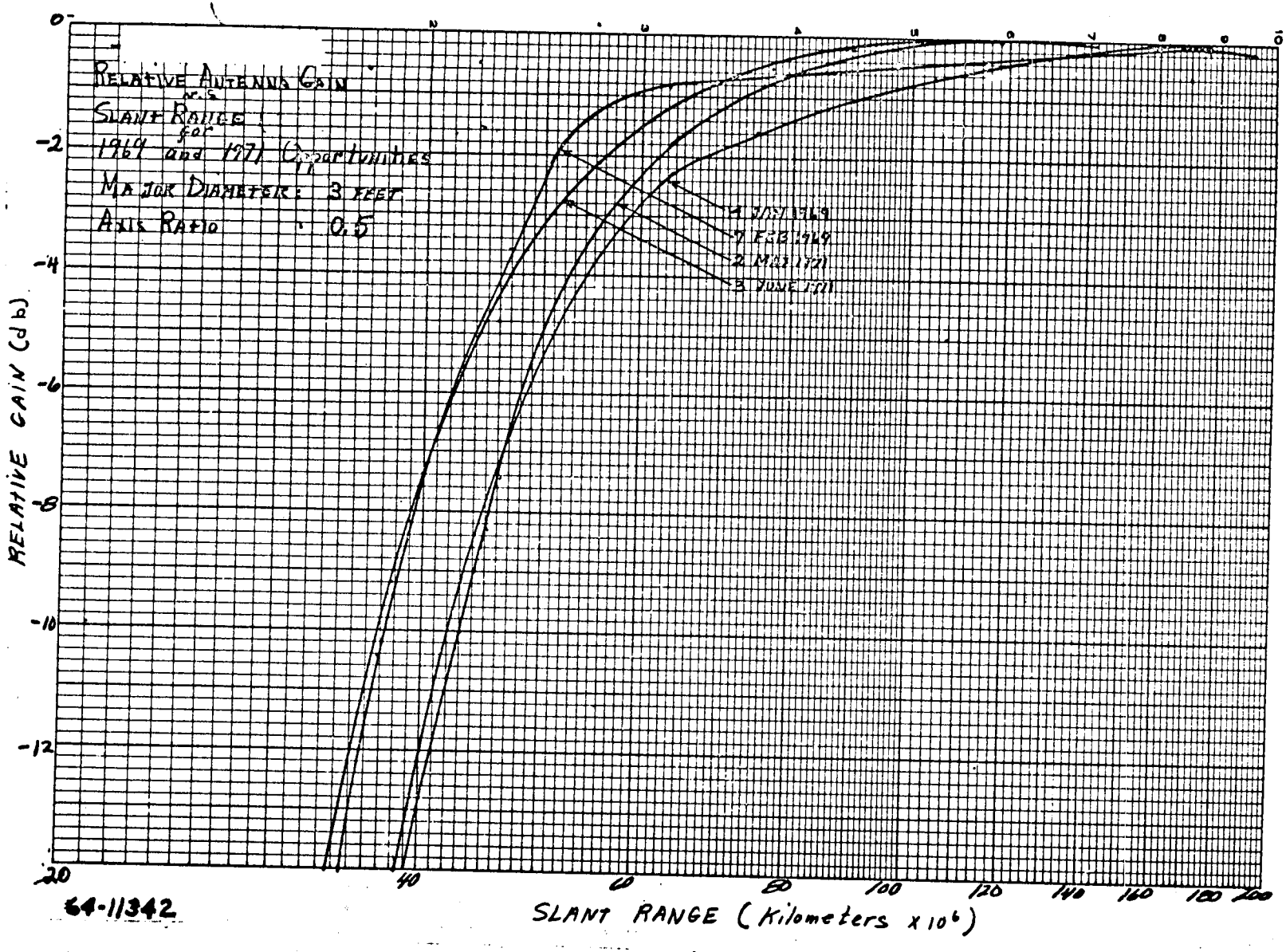

Figure 42 RELATIVE ANTENNA GAIN, MAJOR DIAMETER 3 FEET, AXIS RATIO 0.5

RE-ORDER No. 64-524

140

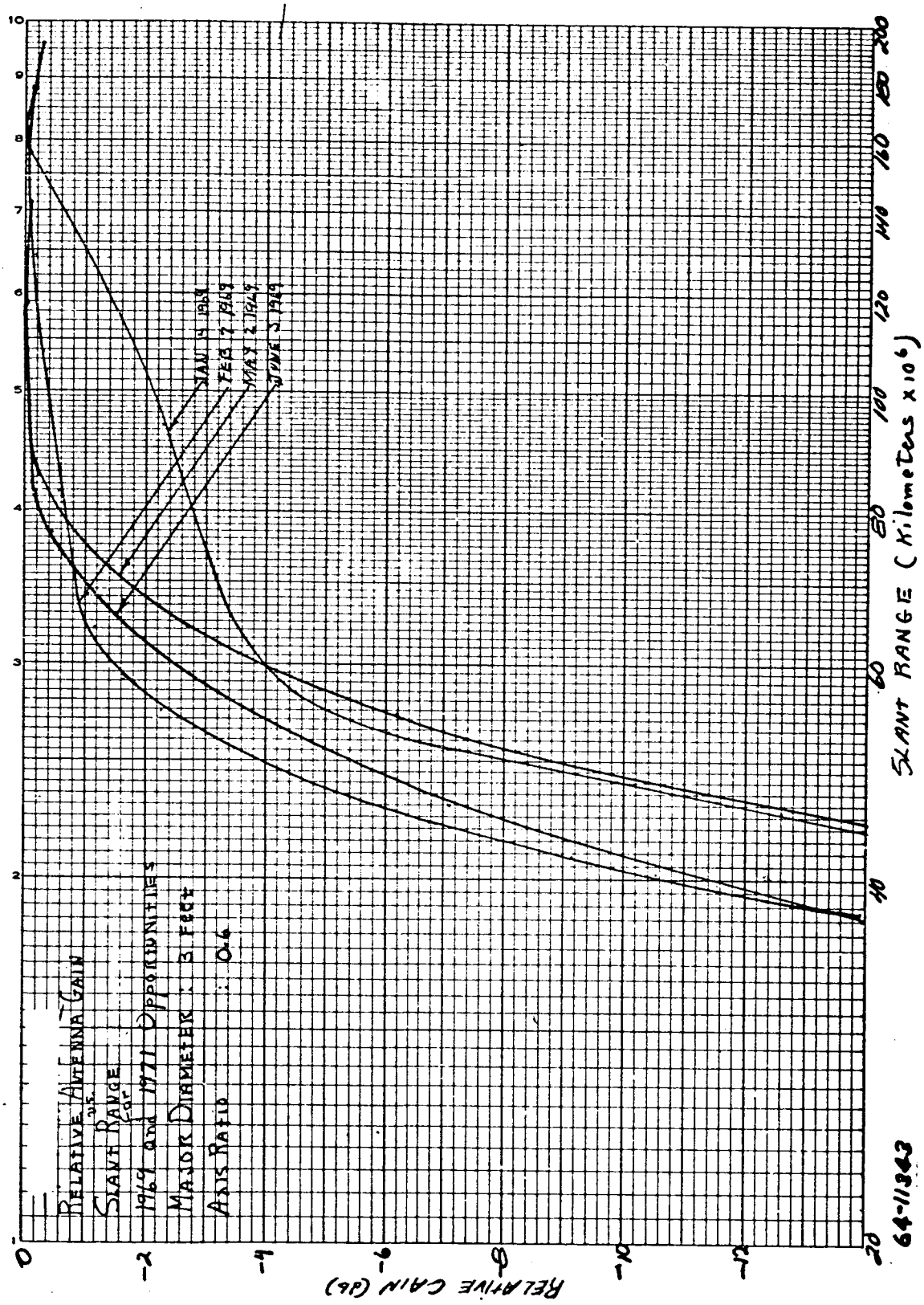

Figure 43 RELATIVE ANTENNA GAIN, MAJOR DIAMETER 3 FEET, AXIS RATIO 0.6

141

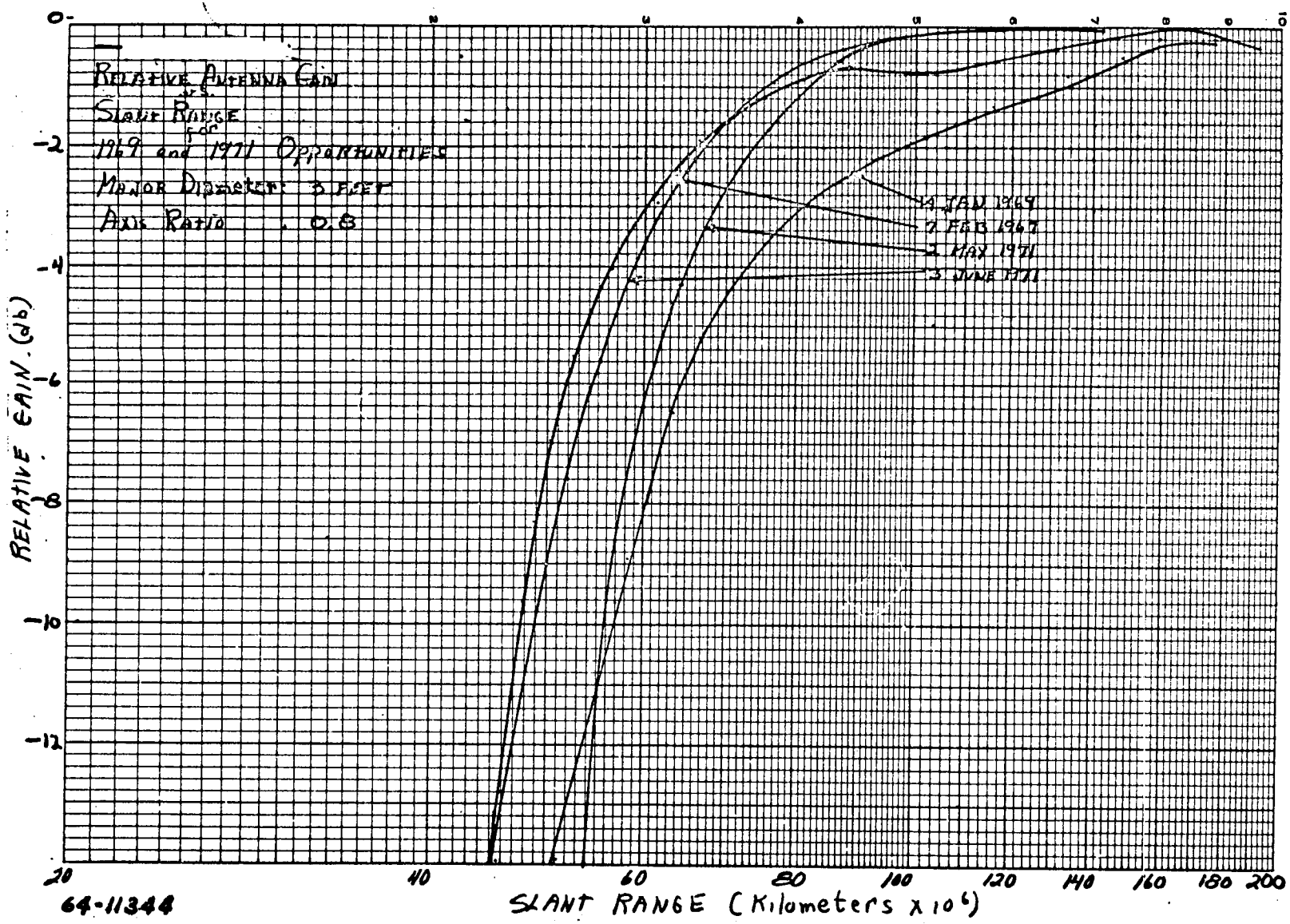

Figure 44 RELATIVE ANTENNA GAIN, MAJOR DIAMETER 3 FEET, AXIS RATIO 0.8

RE-ORDER No. 64-53

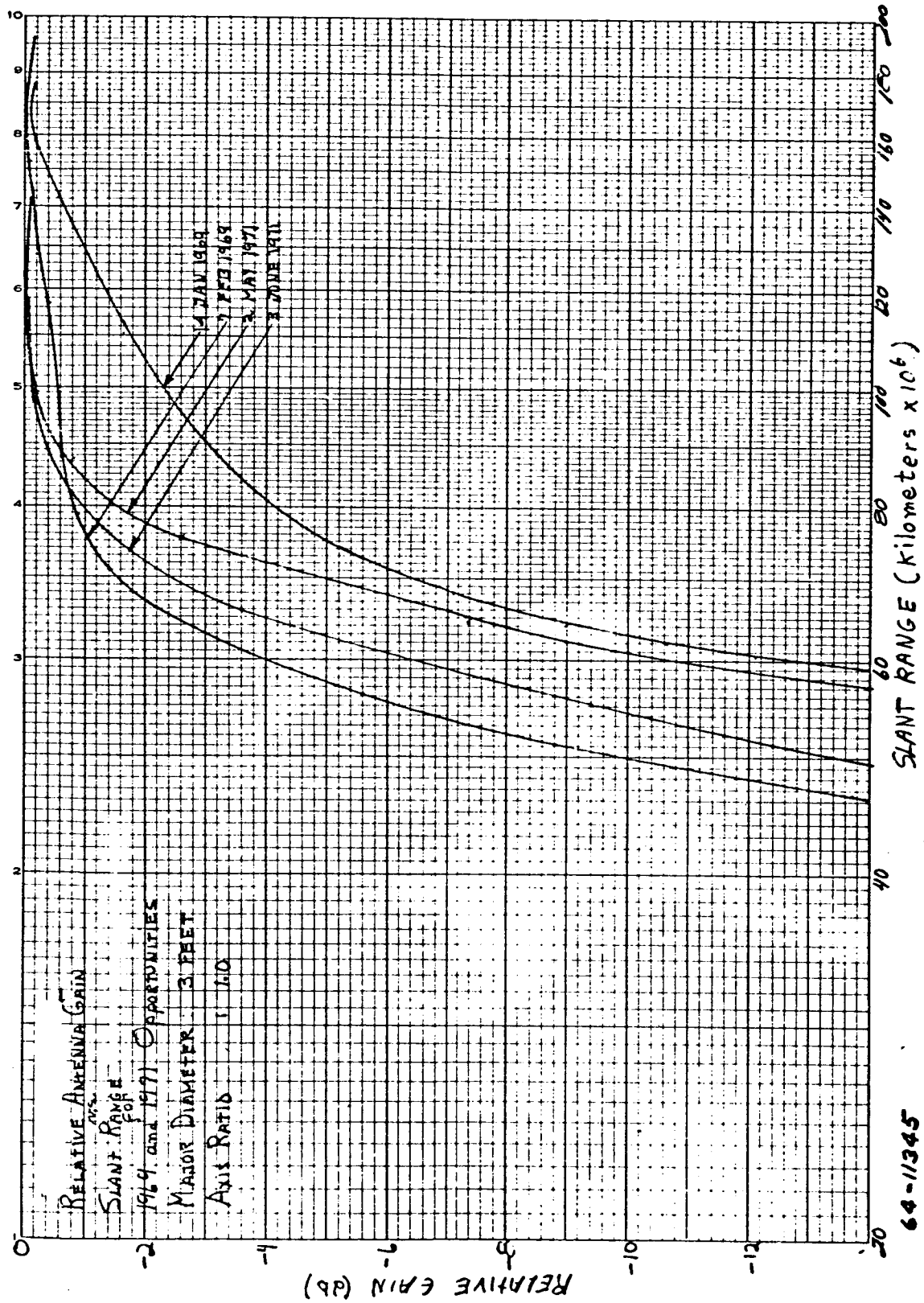

Figure 45 RELATIVE ANTENNA GAIN, MAJOR DIAMETER 3 FEET, AXIS RATIO 1.0

143

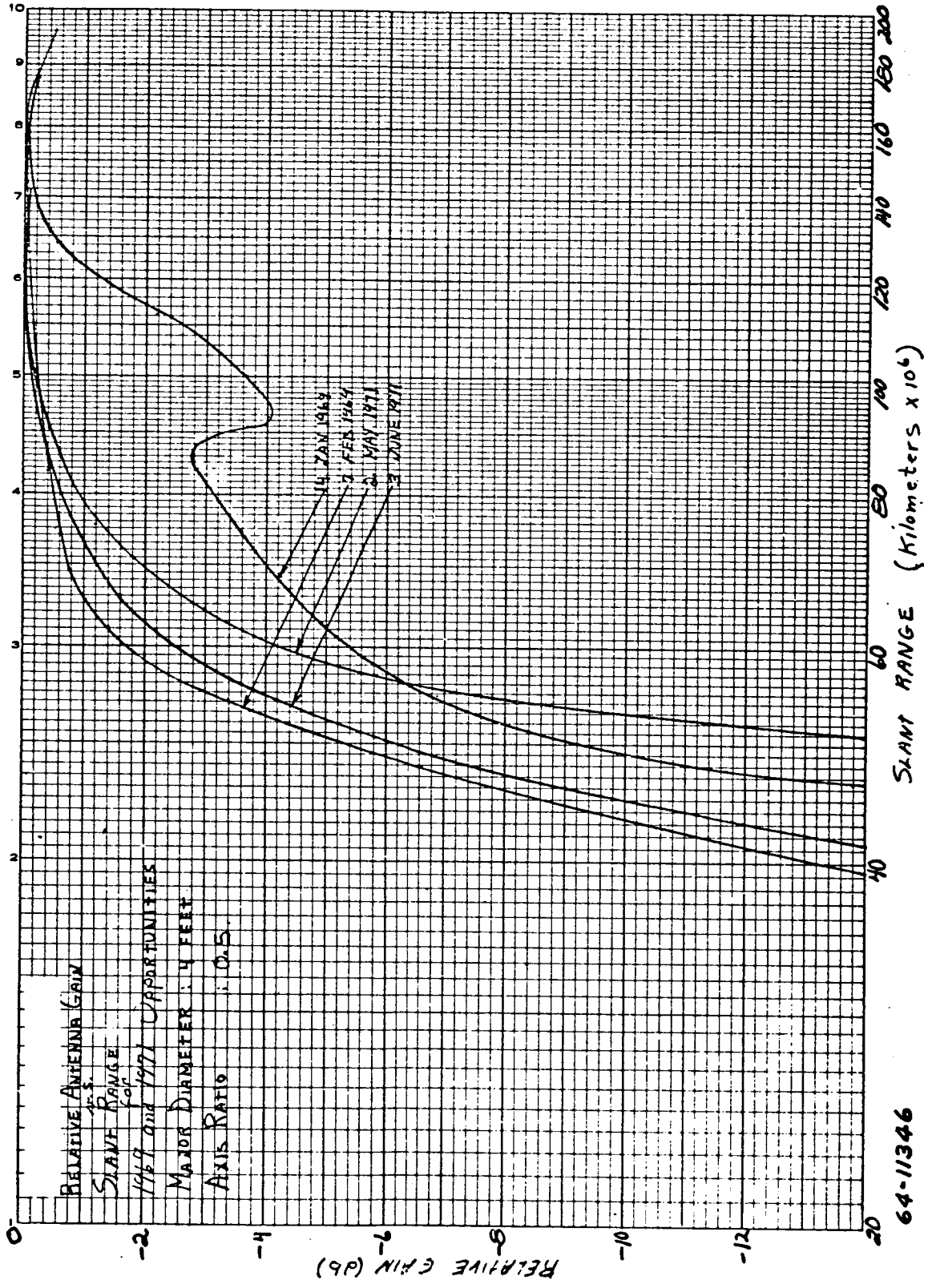

Figure 46 RELATIVE ANTENNA GAIN, MAJOR DIAMETER 4 FEET, AXIS RATIO 0.5

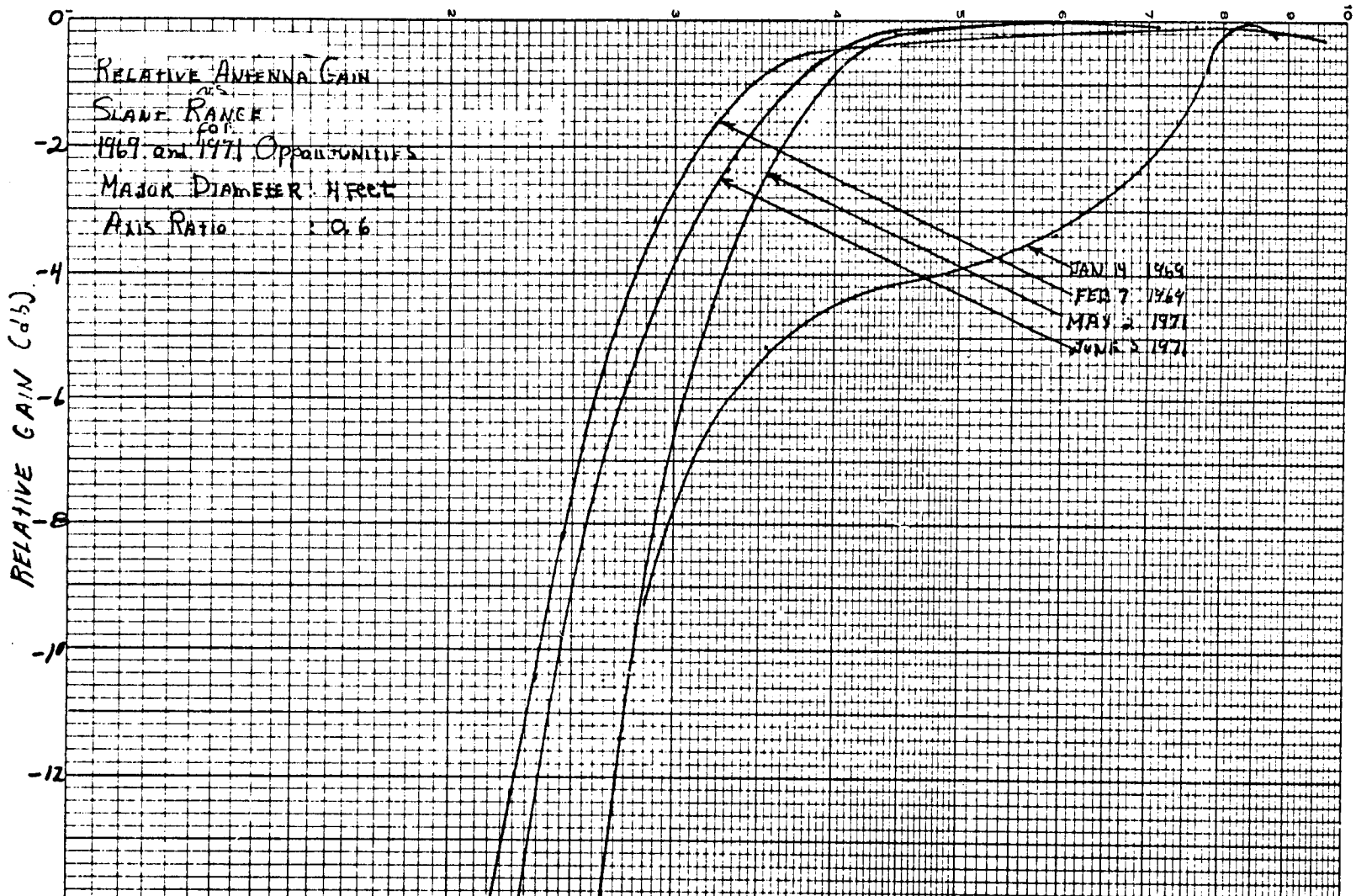

Figure 47 RELATIVE ANTENNA GAIN, MAJOR DIAMETER 4 FEET, AXIS RATIO 0.6

RE-ORDER No. 64-523

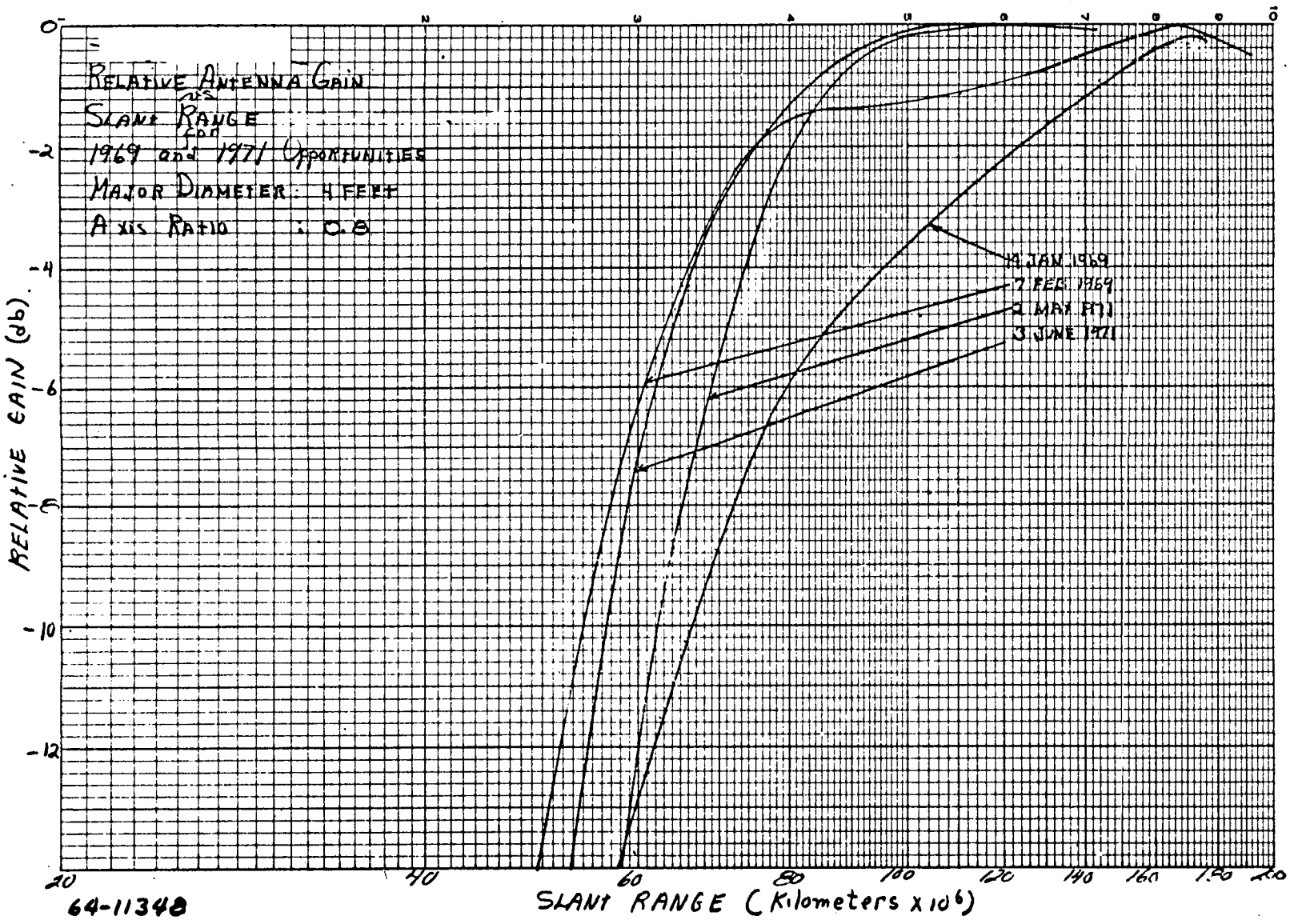

Figure 48 RELATIVE ANTENNA GAIN, MAJOR DIAMETER 4 FEET, AXIS RATIO 0.8

RE-ORDER No. 64-5244

146

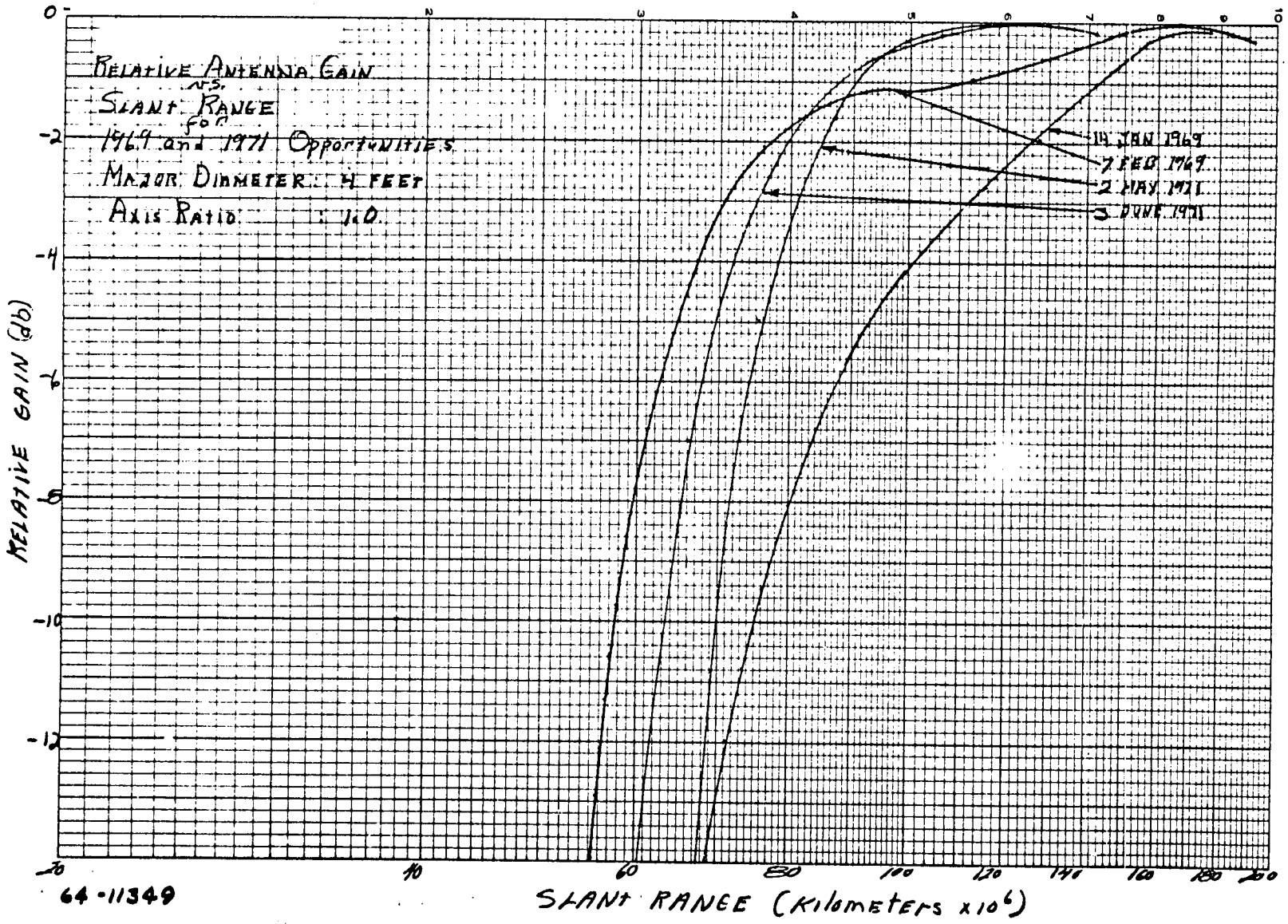

Figure 49 RELATIVE ANTENNA GAIN, MAJOR DIAMETER 4 FEET, AXIS RATIO 1.0

RE-ORDER No. 64-524

147

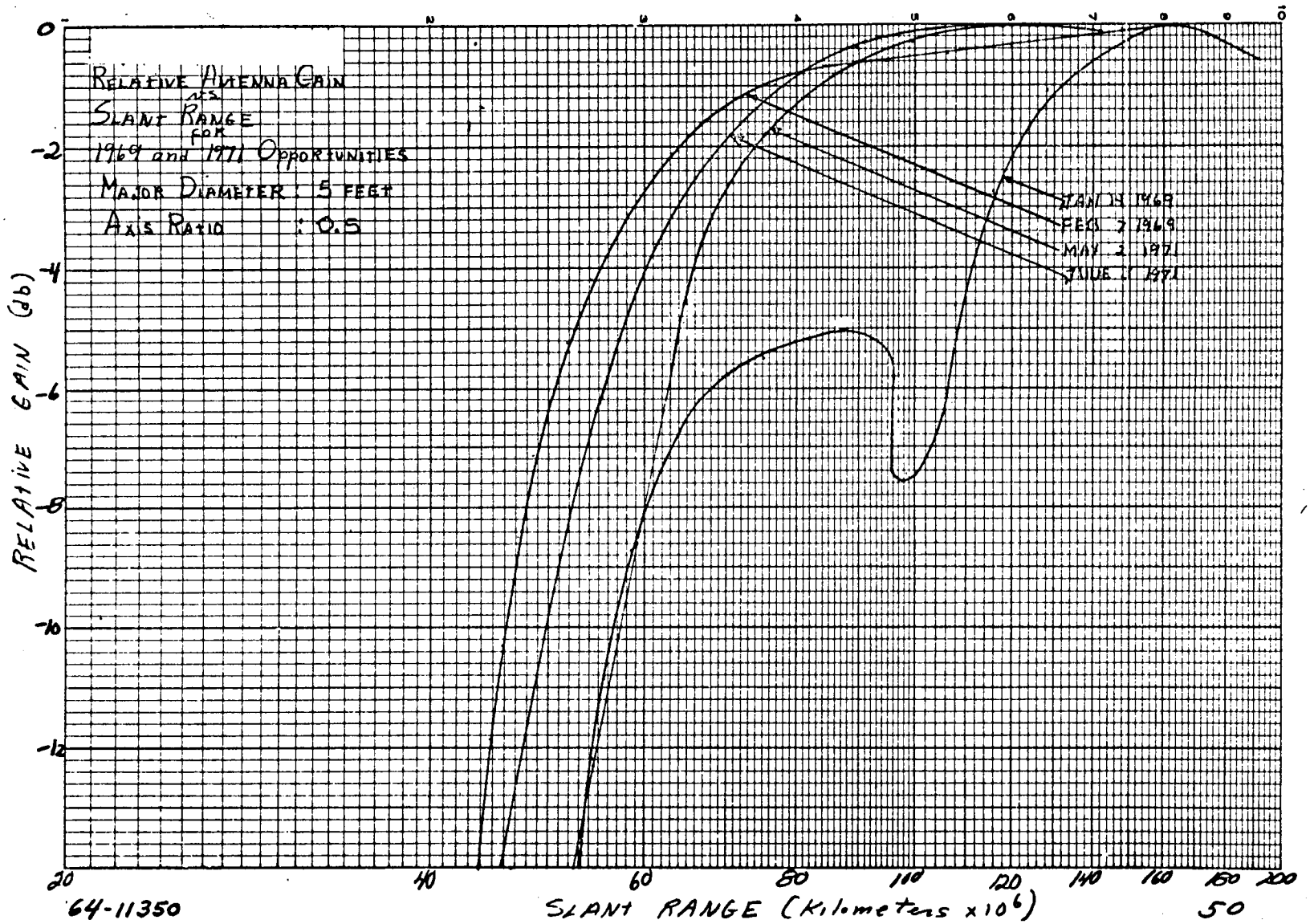

Figure 50 RELATIVE ANTENNA GAIN, MAJOR DIAMETER 5 FEET, AXIS RATIO 0.5

RE-ORDER No. 64-524

148

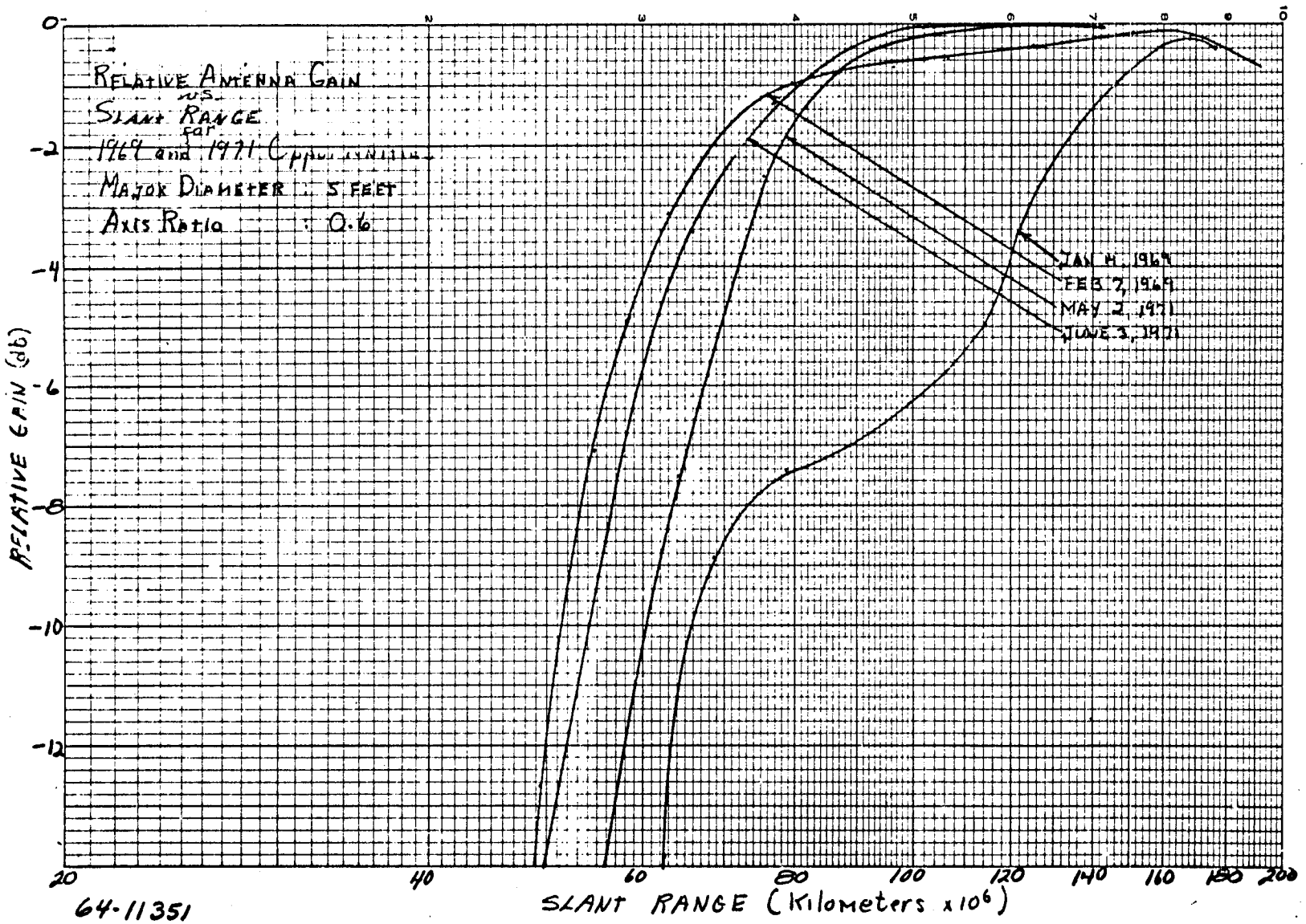

Figure 51 RELATIVE ANTENNA GAIN, MAJOR DIAMETER 5 FEET, AXIS RATIO 0.6

RE-ORDER No. 64-5-24

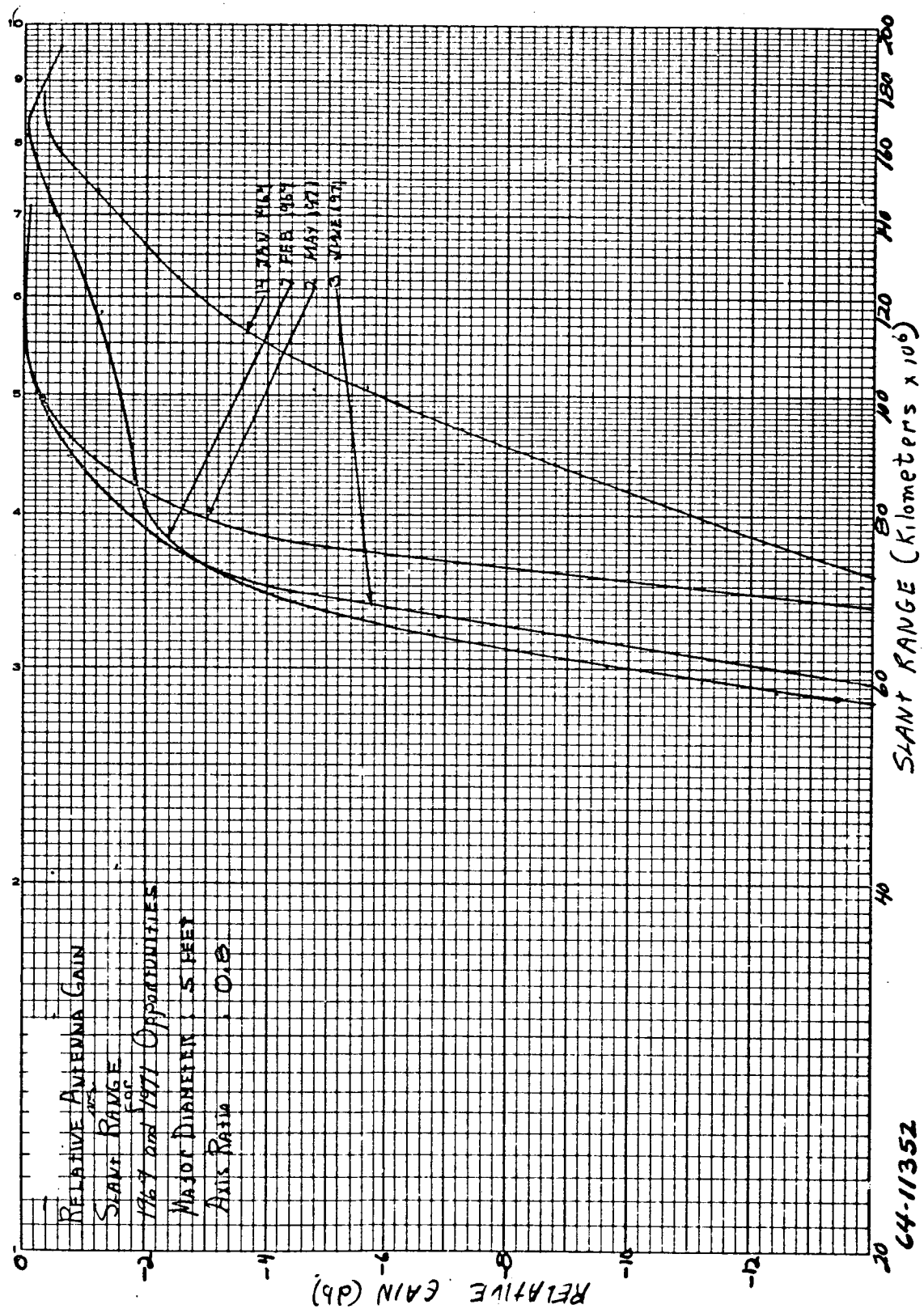

Figure 52 RELATIVE ANTENNA GAIN, MAJOR DIAMETER 5 FEET, AXIS RATIO 0.8

150

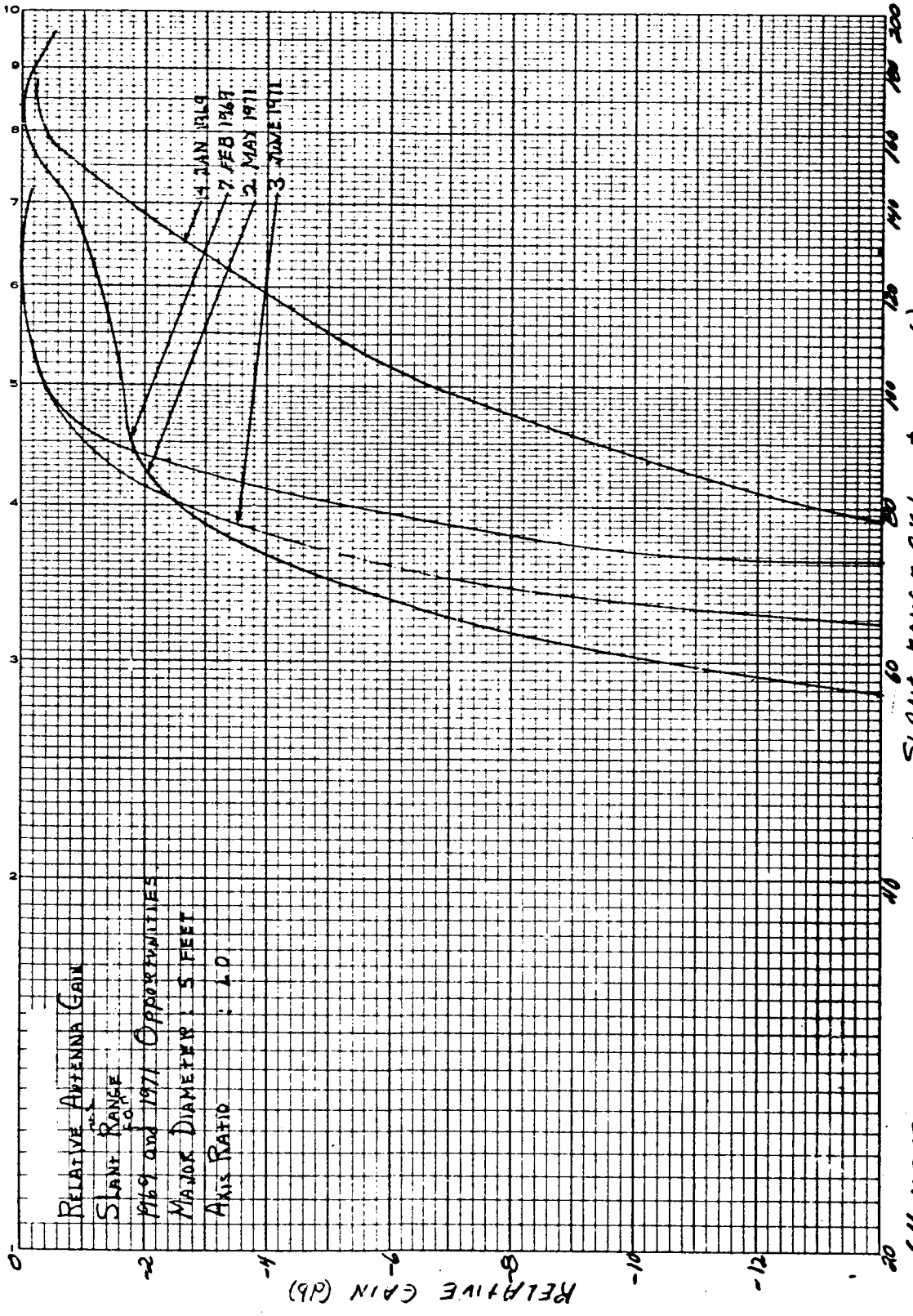

Figure 53 RELATIVE ANTENNA GAIN, MAJOR DIAMETER 5 FEET, AXIS RATIO 1.0

151

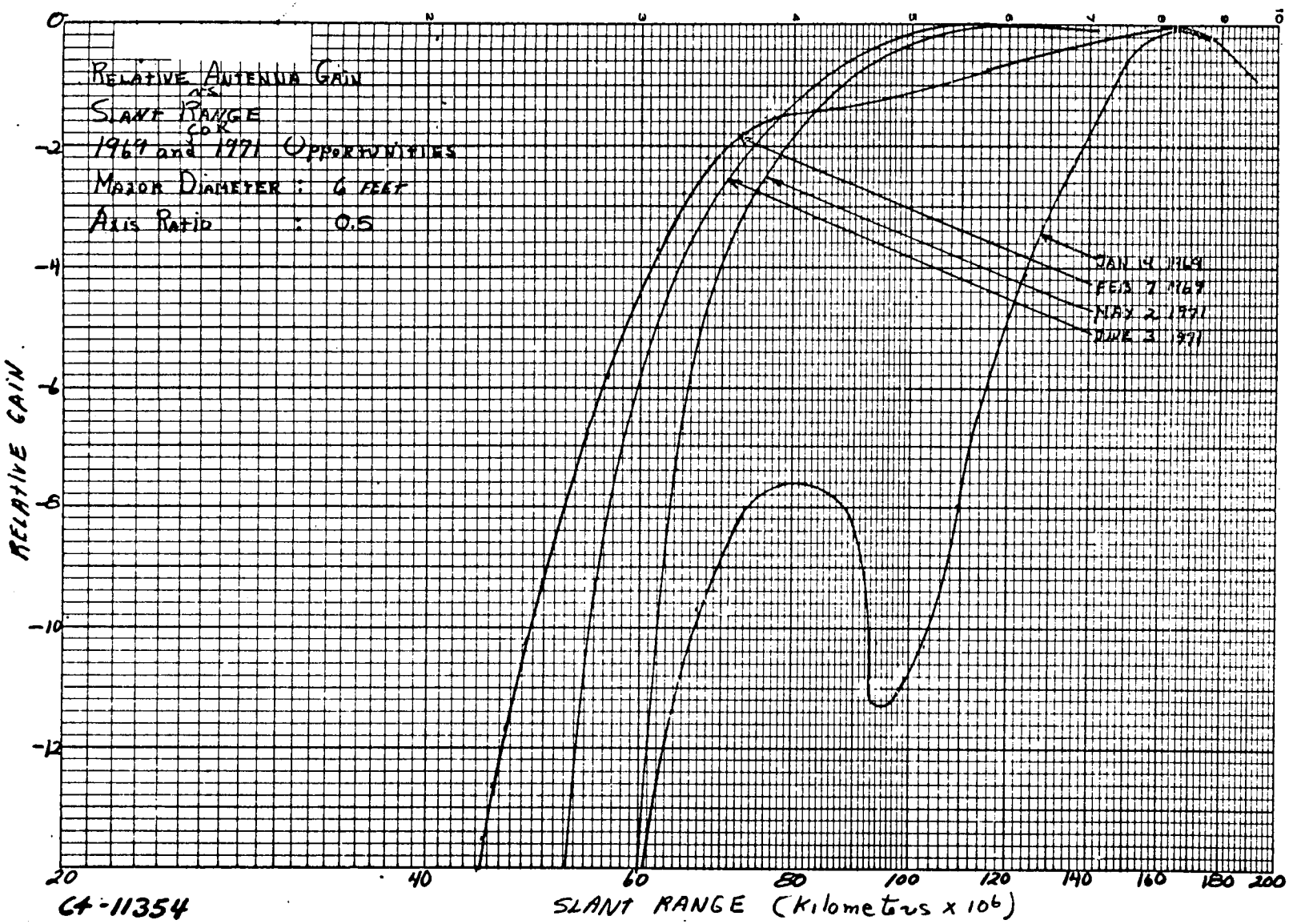

Figure 54 RELATIVE ANTENNA GAIN, MAJOR DIAMETER 6 FEET, AXIS RATIO 0.5

RE-ORDER No. 64-524

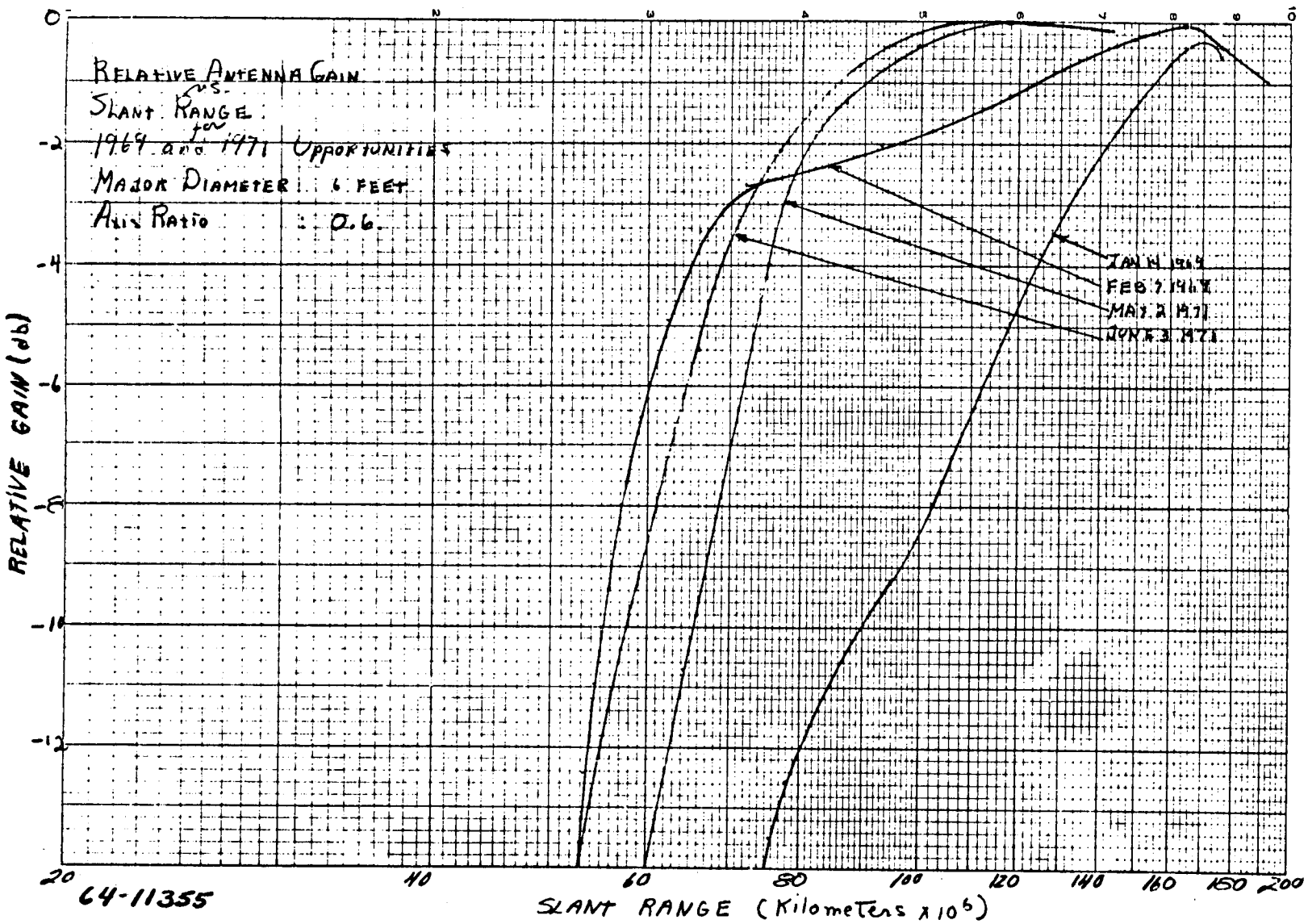

Figure 55 RELATIVE ANTENNA GAIN, MAJOR DIAMETER 6 FEET, AXIS RATIO 0.6

RE-ORDER NO. 64-524

153

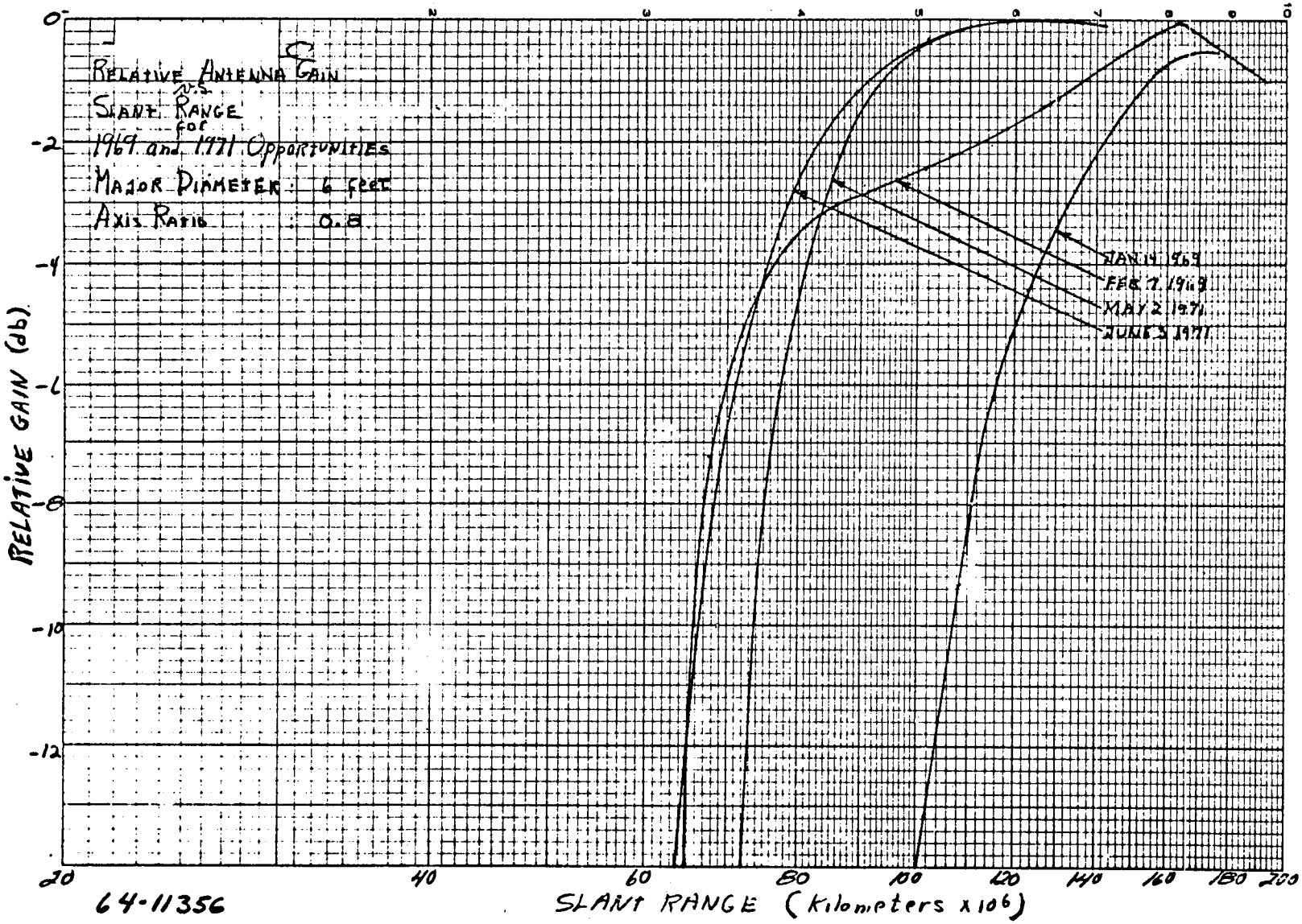

Figure 56 RELATIVE ANTENNA GAIN, MAJOR DIAMETER 6 FEET, AXIS RATIO 0.8

RE-ORDER No. 64-524

154

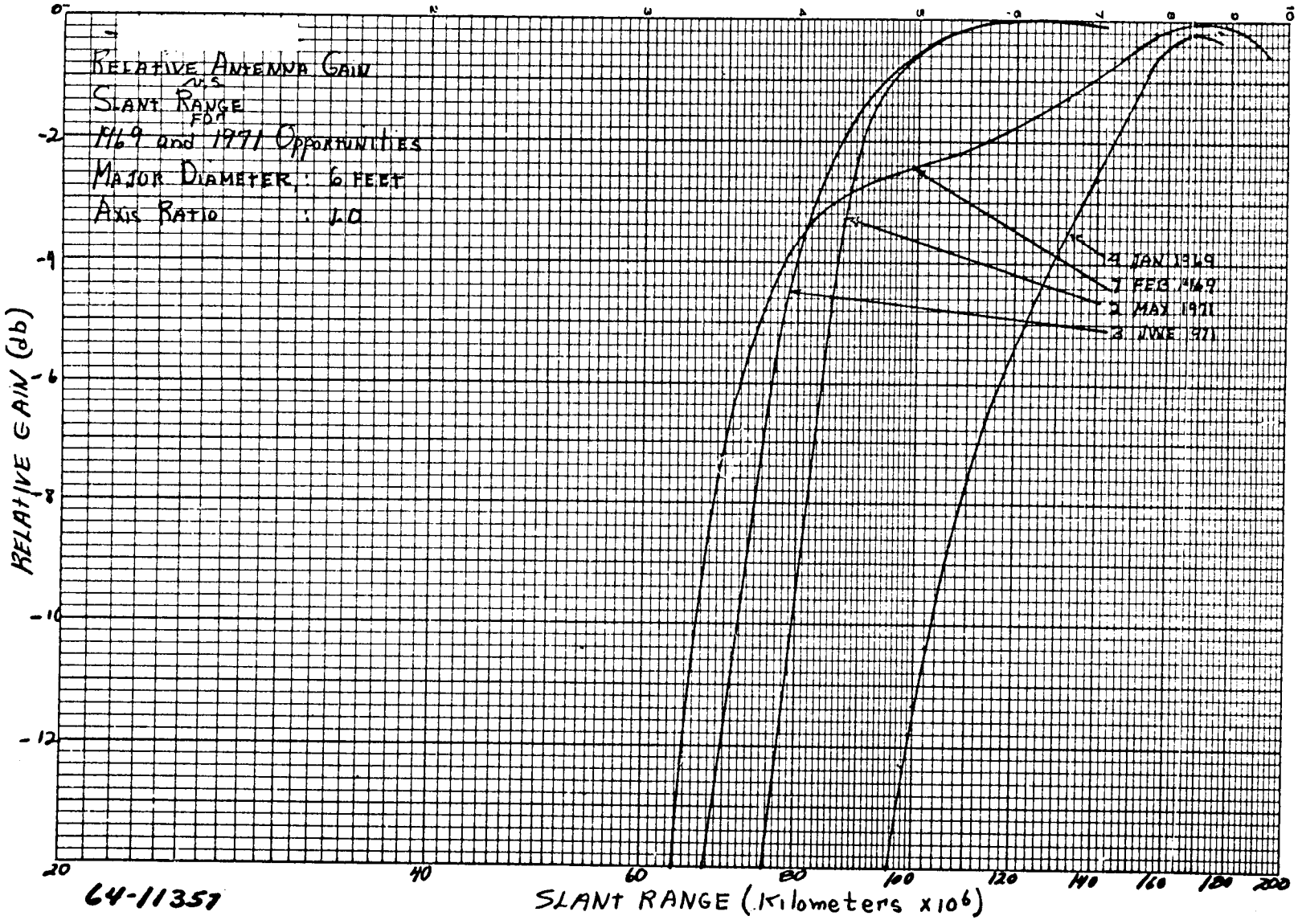

Figure 57 RELATIVE ANTENNA GAIN, MAJOR DIAMETER 6 FEET, AXIS RATIO 1.0

RE-ORDER No. 64-524

155

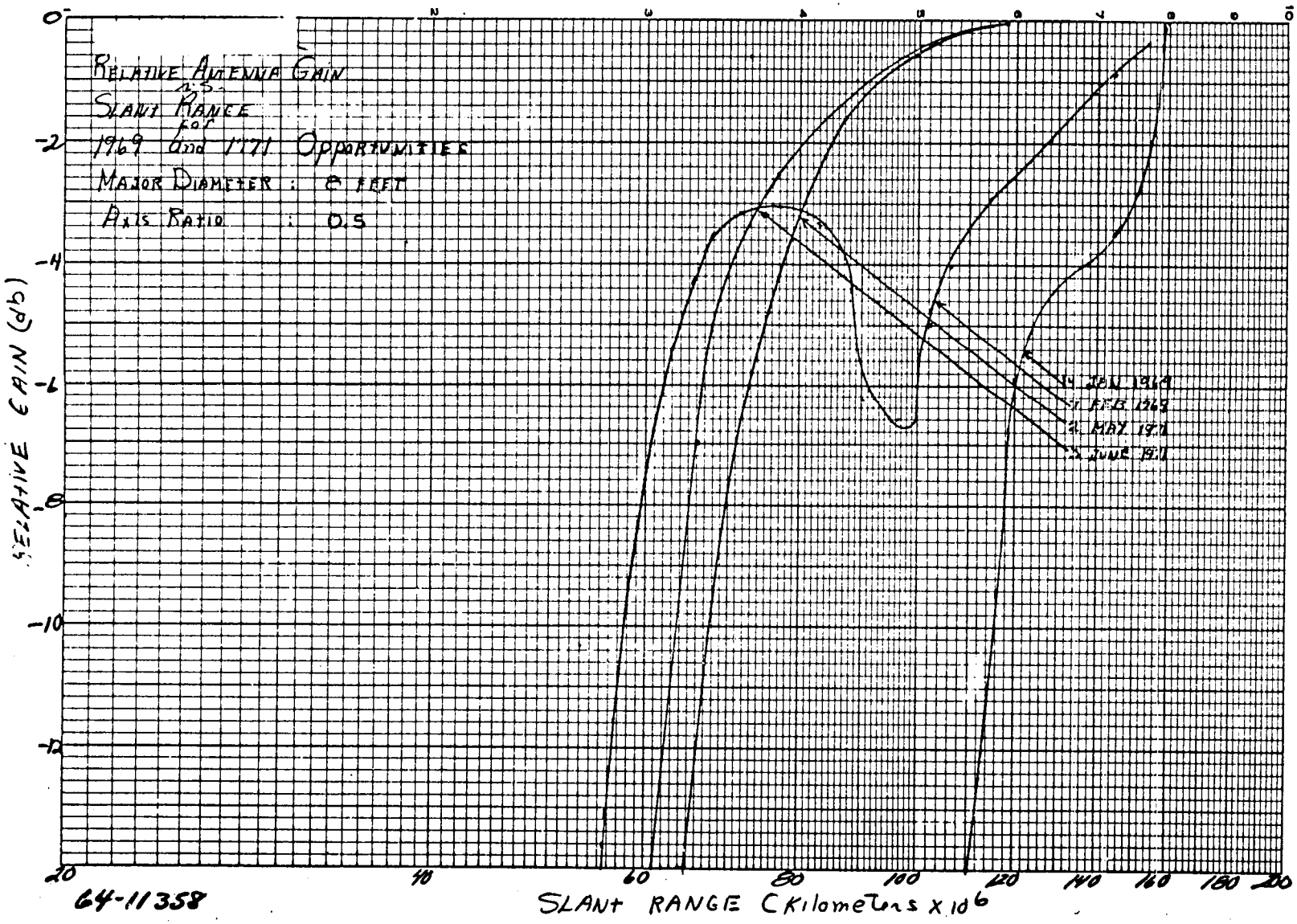

Figure 58 RELATIVE ANTENNA GAIN, MAJOR DIAMETER 8 FEET, AXIS RATIO 0.5

RE-ORDER No. 64-524

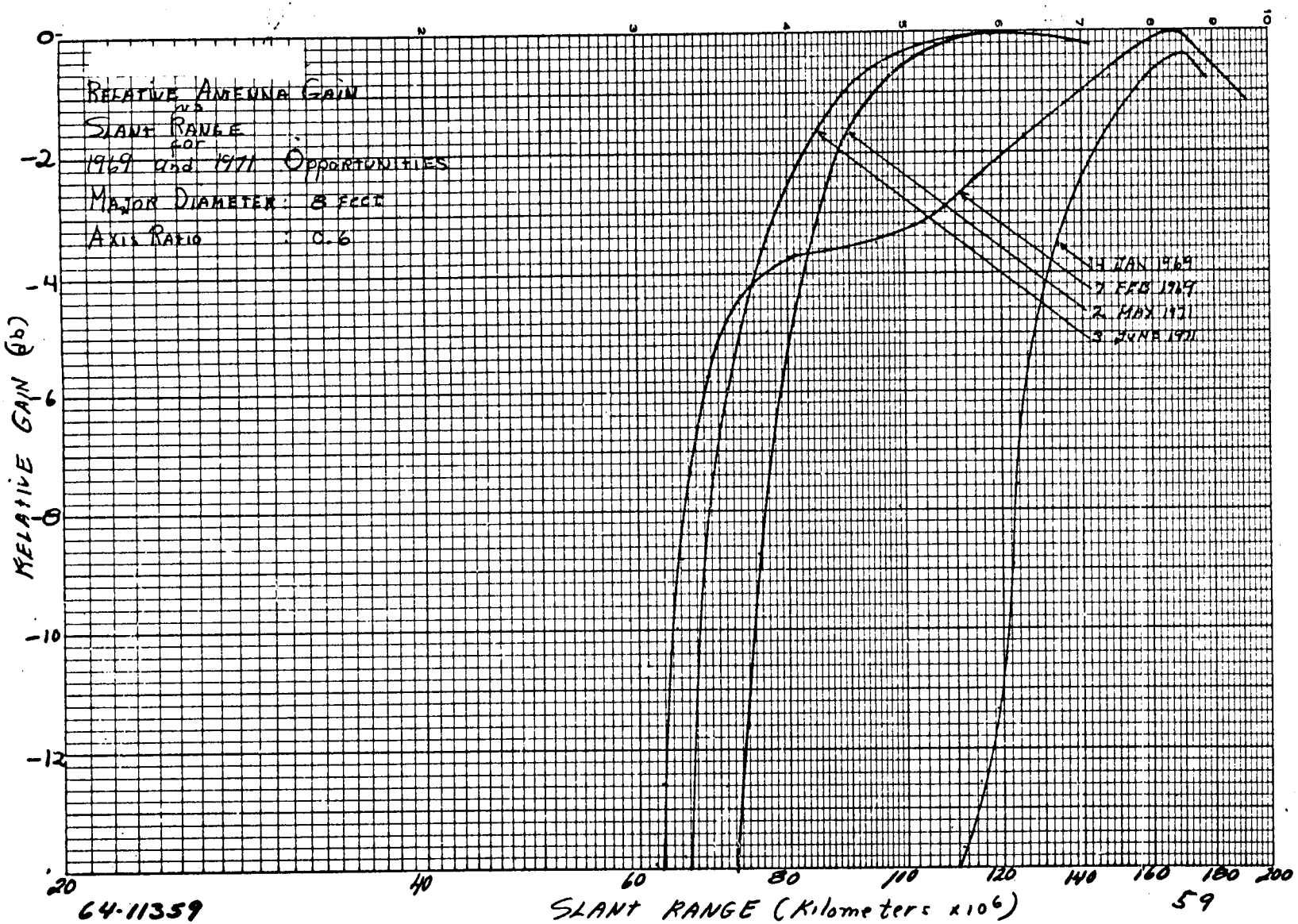

Figure 59 RELATIVE ANTENNA GAIN, MAJOR DIAMETER 8 FEET, AXIS RATIO 0.6

RE-ORDER No. 64-524

157

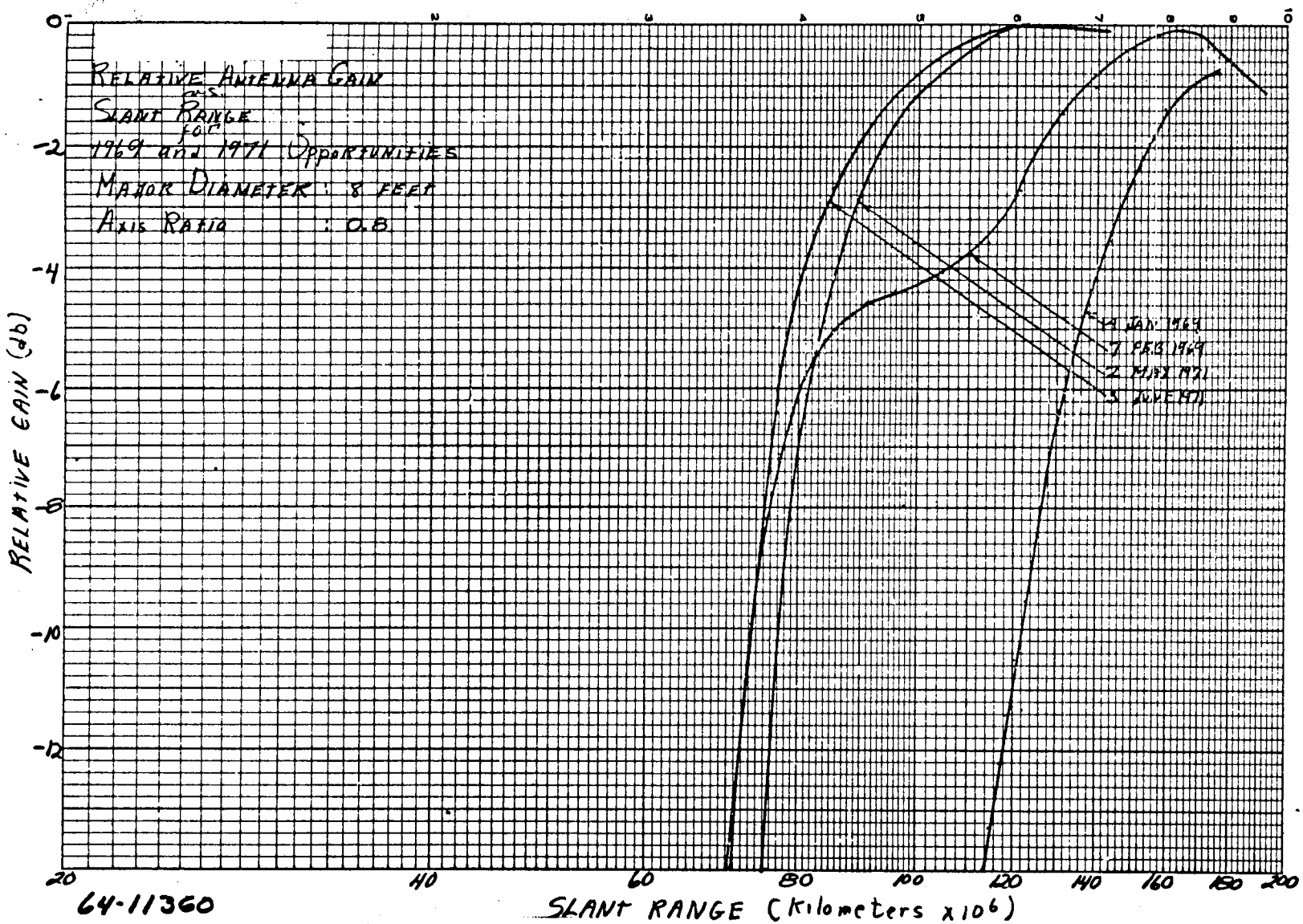

Figure 60 RELATIVE ANTENNA GAIN, MAJOR DIAMETER 8 FEET, AXIS RATIO 0.8

RE-ORDER No. 64-524

158

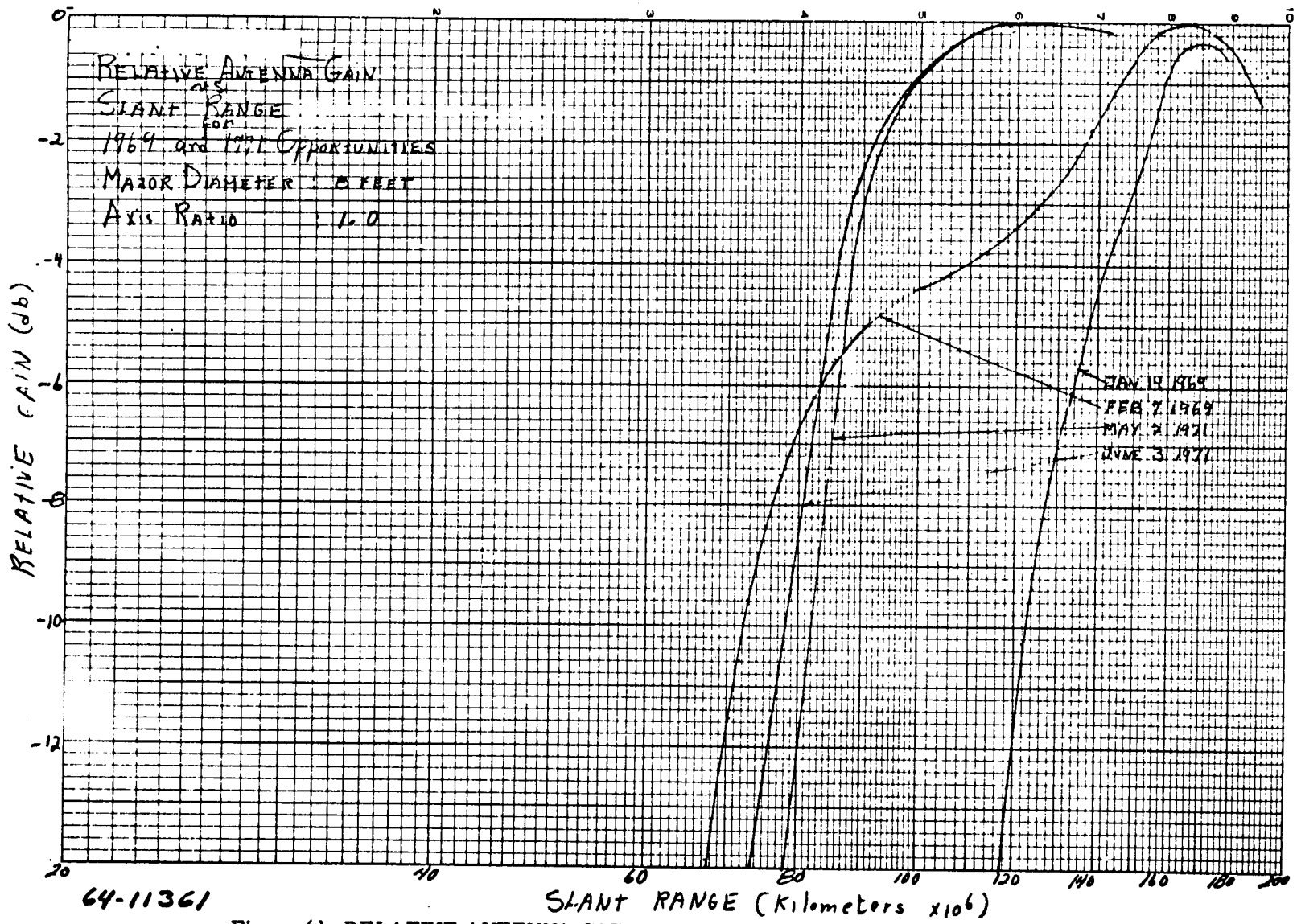

Figure 61 RELATIVE ANTENNA GAIN, MAJOR DIAMETER 8 FEET, AXIS RATIO 1.0

RE-ORDER No. 64-524

159

The launch windows to be evaluated are the first and last launch days of the 1969 and 1971 mission opportunities. (14 January 1969, 7 February 1969, 2 May 1971, 3 June 1971. Figures 38 through 61 indicate the relative antenna gain along the flight trajectory up to 10 days after periapsis for the previously mentioned launch dates. The pointing accuracy requirements are a function of the antenna half power beamwidth but for antennas up to 8 feet in diameter, the requirement is well within the attitude control system capabilities. Antenna pointing loss is assumed predictable up to 10 db off axis.

With this assumption, the crossover range between the low gain and high gain telemetry links can be determined. From figures 38 through 61, a relationship between the antenna size and the corresponding range along the 10 db cutoff line can be derived. Assuming a 0 db worst case gain on the low gain link, figure 35 can be used to determine P_T at each crossover range for any $\dot{B}$. The previous information leads to a set of relationships between transmitter power and maximum high gain antenna diameter which will also satisfy the low gain telemetry requirements at crossover. The relationship between transmitter power and maximum antenna diameter has been plotted in figures 63 through 66 for the four aforementioned mission opportunities.

The minimum antenna boundary condition arises in the high gain link at post encounter where the severest power requiremements (high $\dot{B}$) will occur. From fig. 34, the power gain requirements to transmit a given bit rate at post encounter can be determined. The gain of the antenna in the high gain link is a function of its size and shape as shown in figure 62. By utilizing the antenna curves and the power-gain requirements at post encounter a relation between transmitter power and minimum antenna diameter can be shown for various bit rates at post encounter. The relation of these two variables is shown in figures 63 to 66 for bit rates of 100 bps, 200 and 500 bps.

The selection of a transmitter power-antenna diameter combination must be made within the boundaries of the minimum and maximum antenna restrictions for the specific bit rate and mission launch date. The minimum transmitter power-antenna combination (0 db performance margin) is located on figures 63-66 at the intersection of the two antenna boundary conditions. Operation anywhere else within the boundary conditions will give rise to a performance margin at the crossover range and/or the post encounter range. The performance margin at crossover or post encounter can be measured directly on the curves by subtracting the power requirements at crossover or post encounter from the selected transmitter power.

As an example, assume a 3-foot diameter antenna with an axis ratio of 0.5. From figure 42 this particular antenna has a 10-db pointing loss at a range of 43×10^6 kilometers for the 2 May 1971 mission. This range automatically

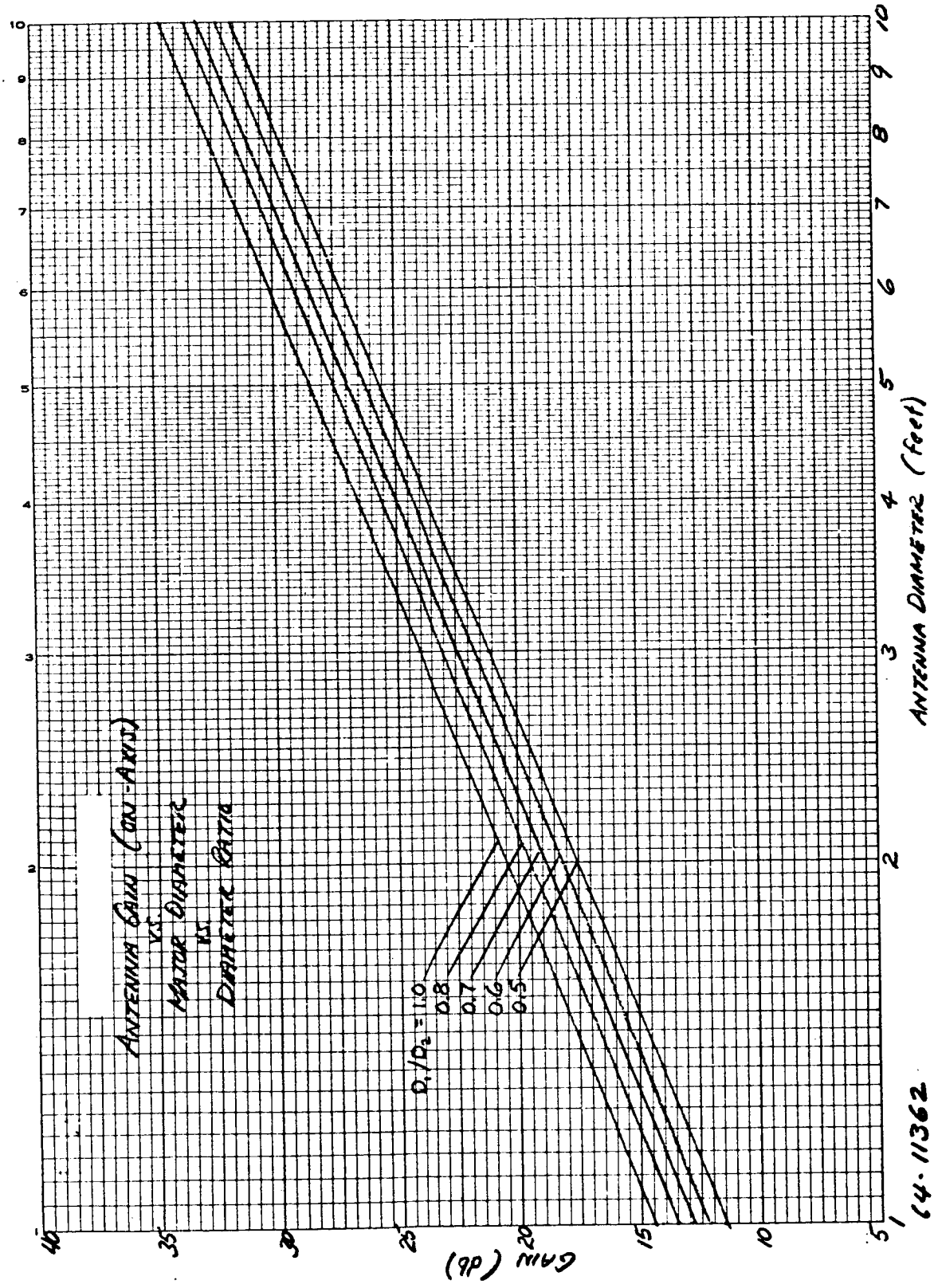

Figure 62 ANTENNA GAIN (ON AXIS)

161

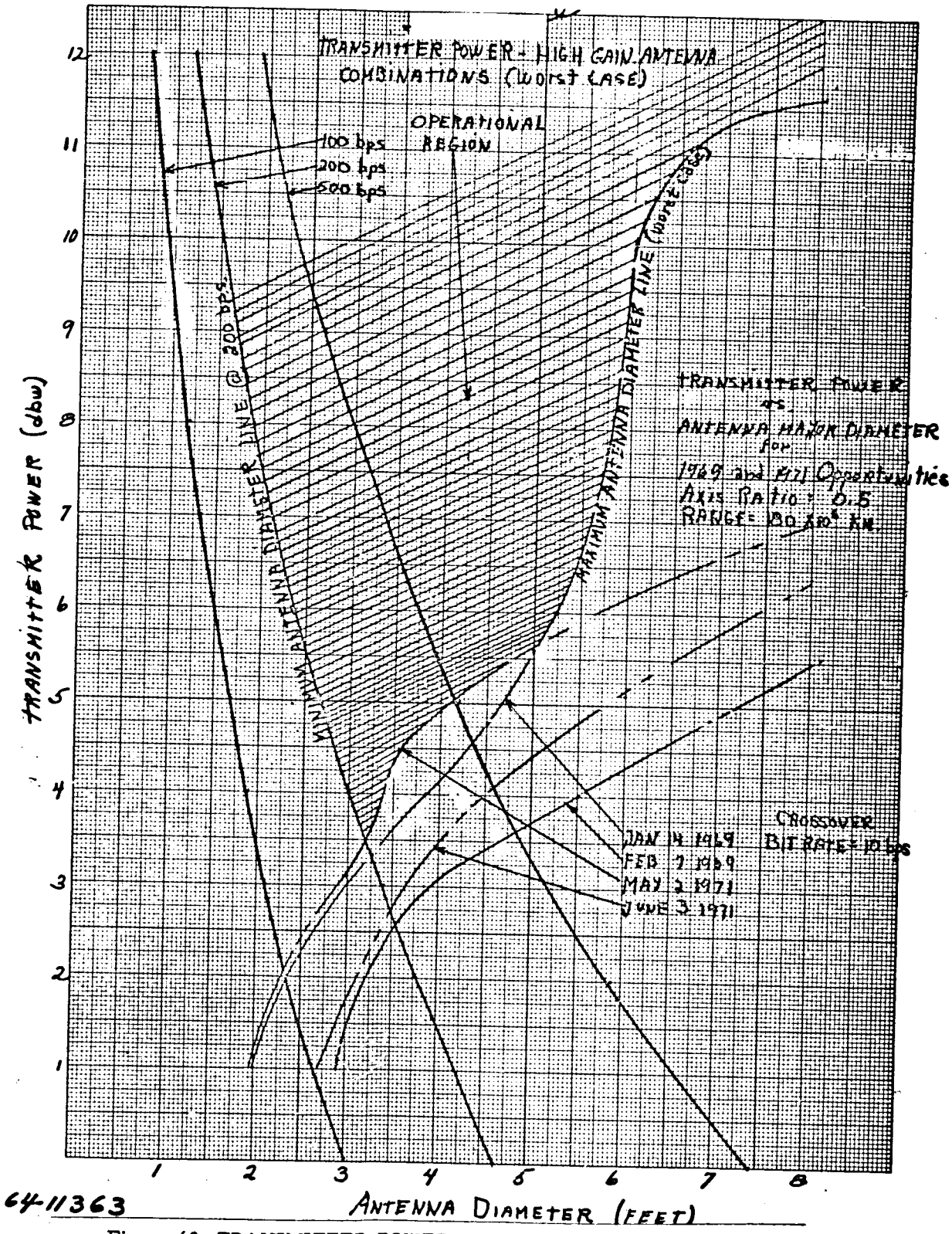

Figure 63 TRANSMITTER POWER - HIGH GAIN ANTENNA COMBINATIONS, AXIS RATIO 0.5

RE-ORDER No. 64-524

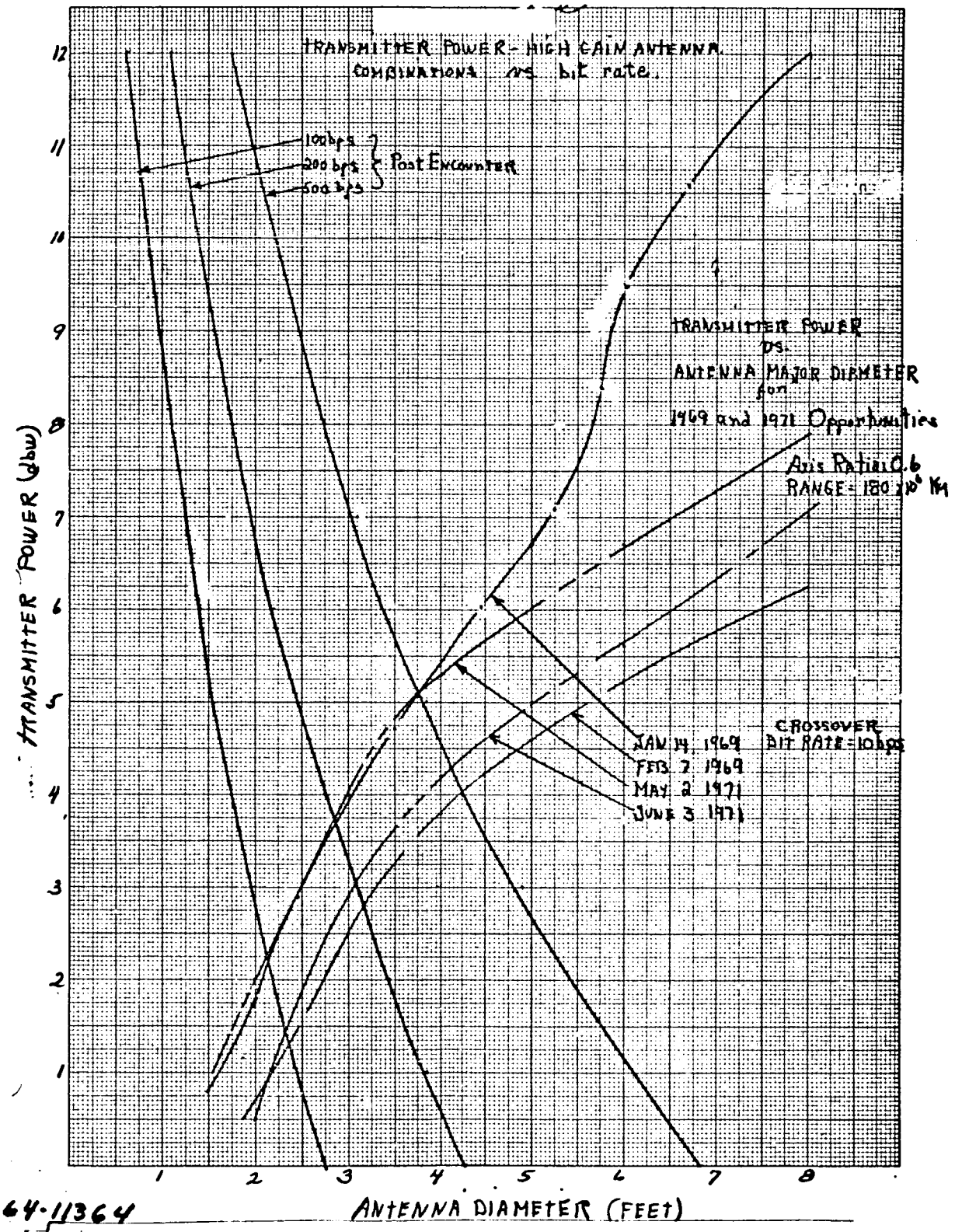

Figure 64 TRANSMITTER POWER - HIGH GAIN ANTENNA COMBINATIONS, AXIS RATIO 0.6

163

RE-ORDER No. 64-524

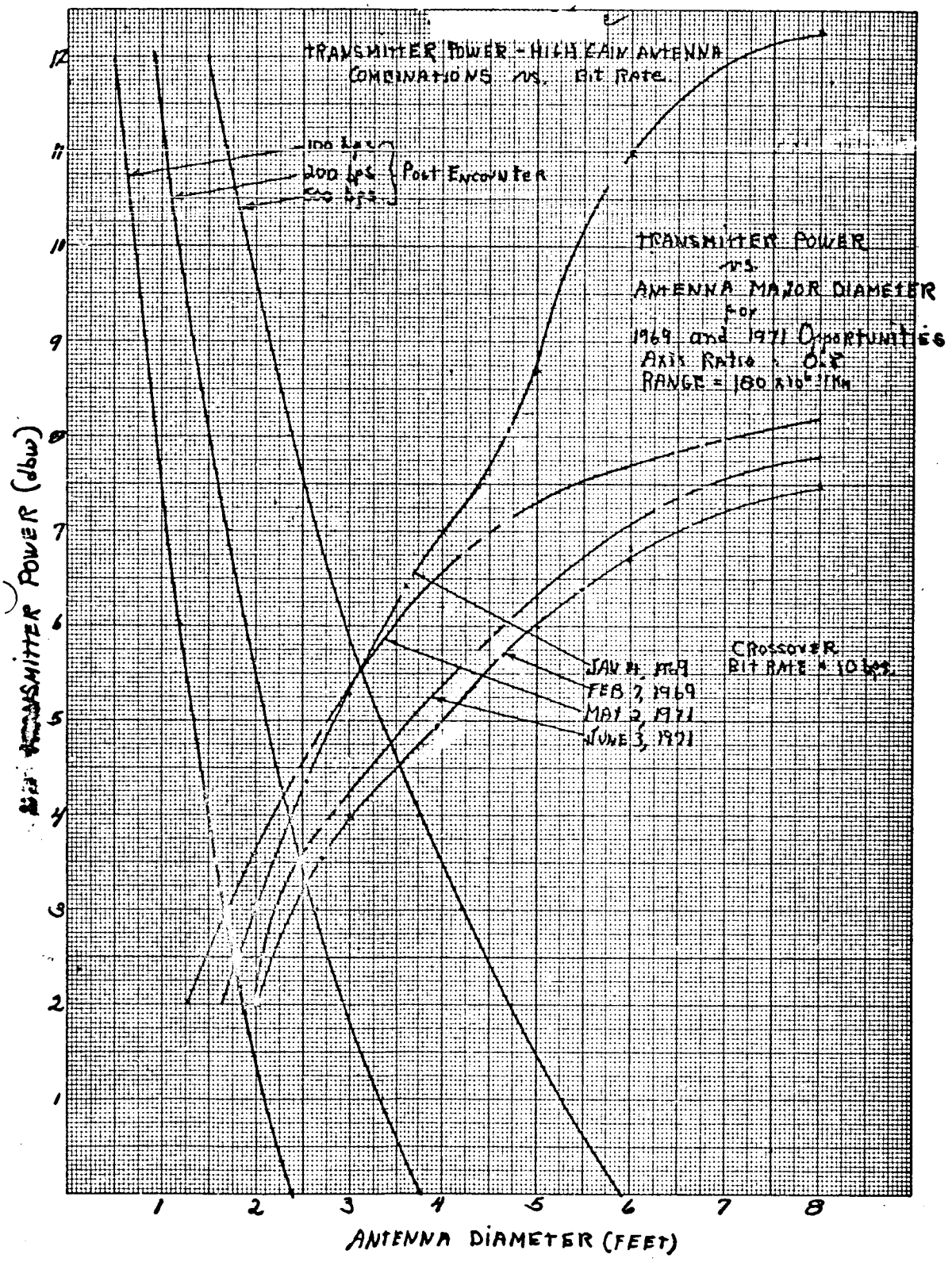

Figure 65 TRANSMITTER POWER - HIGH GAIN ANTENNA COMBINATIONS, AXIS RATIO 0.8

164

RE-ORDER No. 64-524

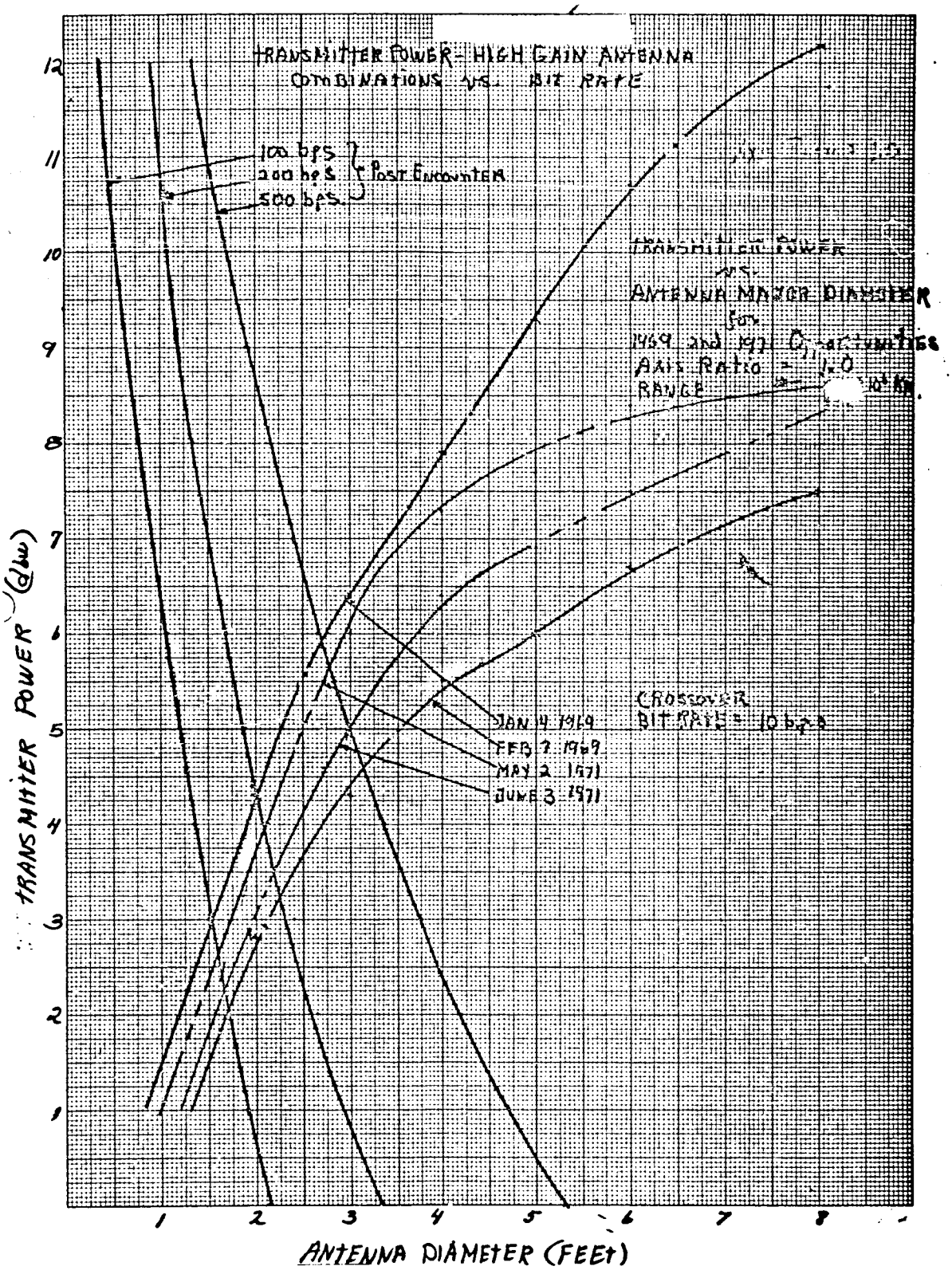

Figure 66 TRANSMITTER POWER - HIGH GAIN ANTENNA COMBINATIONS, AXIS RATIO 1.0

165

becomes the crossover range and requires that the low gain link function up to this range. The low gain link operating at a bit rate of 10 bps requires 3-dbw of power gain product at 43 x 10^6 kilometers as seen from figure 35. The gain of the hemi-omni antenna in the low gain link is assumed to be at 0 db (worst case value). The transmitter must therefore supply at least 3 dbw of power at crossover. The severest power requirements in the high gain link occur at post encounter. If we assume a post encounter range of 180 x 10^6 kilometers and a bit rate of 200 bps, figure 35 indicates that the P_TG requirement is 25 dbw. From figure 62, it can be determined that a 3-foot, 0.5 axis ratio antenna has an on-axis gain of 21 db. The resultant transmitter power requirement at post encounter must be at least 4 dbw. Therefore, the transmitter power is dictated in this case by the high gain link and is 4 dbw. The same results could have been achieved with figure 63. Figure 63 indicates that a 3-foot antenna requires at least 4 dbw of transmitter power before it is within the operational region. The shaded portion on the figure indicates the transmitter power-antenna diameter combinations that can be used.

In the conceptual design, the 10 watt power amplifier used on Mariner C was selected. The bit rates assumed during interplanetary transfer were 33 - 1/3 bps to approximately 20 million kilometer range and 8-1/3 bps to 43 million kilometer range for the low gain antenna. At 43 million kilometers, crossover to the high gain antenna occurred, the bit rate remained constant at 8-1/3 bps till encounter at which point the bit rate was increased to 133-1/3 bps. Mariner C uses an 8-1/3 bps data rate during post encounter. In Advanced Mariner, the large increase in TV data required a higher data rate to minimize the playout time. By using the preceeding parametric curves, the performance margins at cross-over and post encounter can be determined. Proceeding as in the example, the performance margin at crossover will be 7 db at 8-1/3 bps (low gain link) and at 190 million kilometers and 133-/1/3 bps using the 3 x 1-1/2 foot antenna, also 7 db.

4.4 COMMUNICATION SYSTEM HARDWARE

The flyby/bus communication system includes all subsystems associated with the collection storage and transmission of data. These subsystems include the antennas, transmitter, storage subsystem, data handling subsystems, command subsystem, telemetry subsystem and the relay link receiver. The data presented for these subsystems was obtained from the Mariner C functional specifications (13 July 1963) and from the manufacturers listed in table 28. The communication system hardware parts list is a minor modification of the Mariner C specifications and is listed in table 29.

Figure 67 is a block diagram of the Advanced Mariner flyby/bus communications system. The communication system includes the rf electronics, the telemetry subsystem, the command subsystem, the DAS, and the storage subsystem.

RE-ORDER No. 64-524

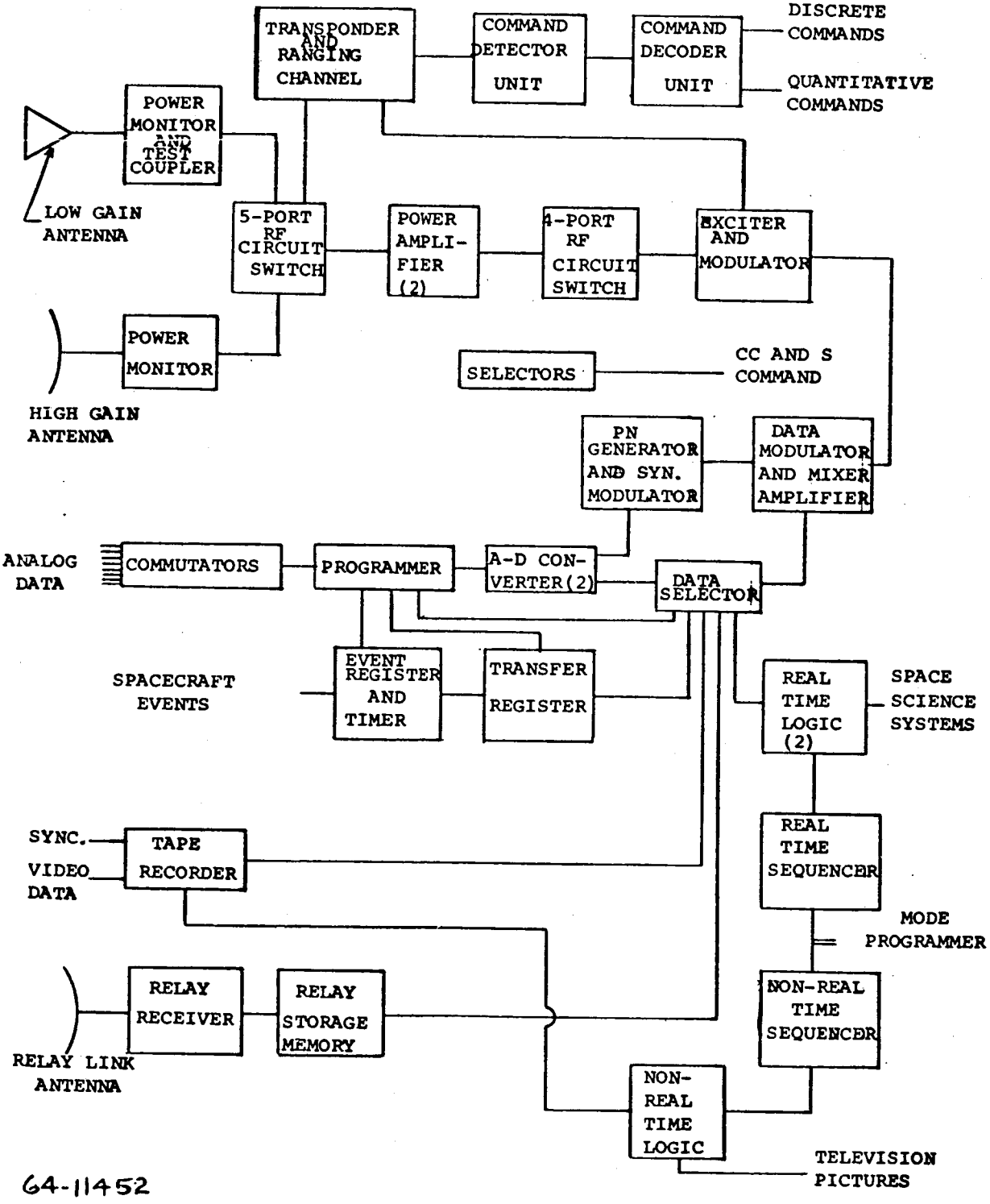

Figure 67 COMMUNICATION SYSTEM

167

RE-ORDER No. 64-524

TABLE 28

COMPONENT PERFORMANCE DATA SUPPLIED BY VENDORS

Subsystem	Manufacturer
Low Gain Antenna Relay Link Antenna	Avco/RAD Lowell Street Wilmington, Mass.
High Gain Antenna	Ryan Aeronautical Co. Lindbergh Field San Diego 12, Calif.
Tape Recorders	Raymond Engineering Lab. Inc. Magnetic Tape Recorder/Repro. Div. Smith Street Middletown, Conn.
Relay Memory	Electronic Memories Inc. 12621 Chadron Avenue Hawthorne, Calif.
Power Amplifier	Resdel Engineering Corp. 990 South Fair Oaks Pasadena, Calif.
RF Circulator Switches	Rantec Corporation 23999 Ventura Blvd. Calabassas, Calif.
Transponder	Motorola Inc. Military Electronic Div. 8201 East McDowell Road Scottsdale, Arizona
Relay Receiver	Avco Electronics Division 2630 Glendale - Milford Road Cincinnati 41, Ohio
Telemetry Subsystem	Texas Instruments Inc. Apparatus Division 6000 Lemon Avenue PO Box 6015 Dallas 22, Texas
DAS Subsystem	Computer Controls Co. Inc. Old Connecticut Path Framingham, Mass.
Command Subsystem	Motorola Inc. Military Electronics Div. 8201 East McDowell Road Scottsdale, Arizona

162

RE-ORDER No. 64-524

TABLE 29

COMPONENTS OF COMMUNICATION SYSTEM

I. RF Electronics Subsystem	Weight (pounds)	Volume (in.^{3})	Dimensions	Power (watts)
Power Amplifiers	3.0	440	11 x 10 x 4	36.0
Exciters	4.5	250	10 x 5 x 5	6.5
Receiver	9.5	250	10 x 5 x 5	5.5
Relay Receiver	20.0	500	10 x 10 x 5	5.0
P. A. Power Supplies	5.0	100	4 x 5 x 5	56.0
Exciter TR Unit	1.5	250	10 x 5 x 5	8.0
Receiver TR Unit	1.0			6.9
Control Unit	2.5	200	8 x 5 x 5	1.0
4 Part Circulator Switch				
5 Part Circulator Switch				
High Gain Power Monitor	5.0	500	10 x 10 x 5	2.0
Low Gain Power Monitor				
RF Test Coupler				
High Gain Antenna	2.5	---	---	---
Low Gain Antenna	1.0	---	---	---
Relay Antenna	1.5	---	---	---
Fixed Osc Xstal Temp. Transducer	0.03	---	---	---
Coax Cables (5)	1.5	---	---	1.50 db
Radio Cabling (5)	4.0	---	---	---

169

RE-ORDER No. 64-524

TABLE 29 (Concl'd)

II. Telemetry Subsystem	Weight (pounds)	Volume (in.^{3})	Dimensions (in.)	Power (Watts)
Commutators	12.0			
AD Converter	3.5			4.8
Event Counters	1.8	500	10 x 10 x 5	
Low Level Amplifier	1.5			
Gen, Mod, Mix, Sel, Reg.	1.8			
Switching CKTS	1.6			
TR Power Supply	2.3			13.0
III. Command Subsystem				
Command Detector				
Command Decoder	8.0	250	10 x 5 x 5	1.0
Command Program Control				
Command Decoder & Power Supply				4.5
IV. Storage Subsystem				
Video Tape Recorder	40.0	1440	12 x 12 x 10	20.0
Relay Memory	2.0	75	5 x 5 x 3	5.0
V. DAS				
DAS Memory				
DAS Rt Logic	12.0	200	8 x 5 x 5	8.0
DAS NRt Logic				
DAS TR Converter				

170

1. Antennas

a. High Gain Antenna

Figure 68 shows parabolic antenna weight versus major diameter in feet and ratio of minor to major diameters. These data are extrapolated from Report 63B077, Ryan Aeronautical Co., 15 August 1963.

b. Relay Link Antenna

The receiving antenna selected for the relay link is a horn located on the gimbaled payload platform. Parametric data are given in the lander section. (See figure 69.)

c. Low Gain Antenna

The low gain antenna chosen will be a spiral antenna (see figure 70) which is circularly polarized and has a polarization loss on axis of ±0.1 db and a polarization loss, at the 3-db points of ±0.7 db. These ellipticity losses are typical over the 200 mc bandwidth required to receive commands and transmit data (2100 to 2300 mc). The half power beamwidth is from 95 to 105 degrees. The gain is 4 db above isotropic and the estimated weight is 3/4 pound. Figure 71 is a typical radiation pattern of this spiral antenna.

2. Tape Recorders

Parametric data on recorder weight, volume and power consumption as a function of storage capacity and record rate is shown in figures 72 through 75. This tape recorder records video data from the science DAS and plays back to the transponder through the data encoder.

The tape recorder will have a maximum weight of 40 pounds, a volume of 1440 in.^{3} and a maximum storage capacity of 1.5×10^8 bits. The power requirements will be no greater than 20 watts.

3. Solid State Memories

For lander missions having low storage requirements (less than 50,000 bits) a solid state memory would be used in the bus to store the bit content of the relay link instead of a separate tape recorder (in addition to the TV data recorder). Parametric data on solid state memories is given in figures 76 through 78.

The solid state memory (ferrite core or plated wire) will have a storage capacity of 30,000 bits, a maximum weight of 2.0 pounds and a volume of 75 in.^{3}. The maximum power input will be 5 watts.

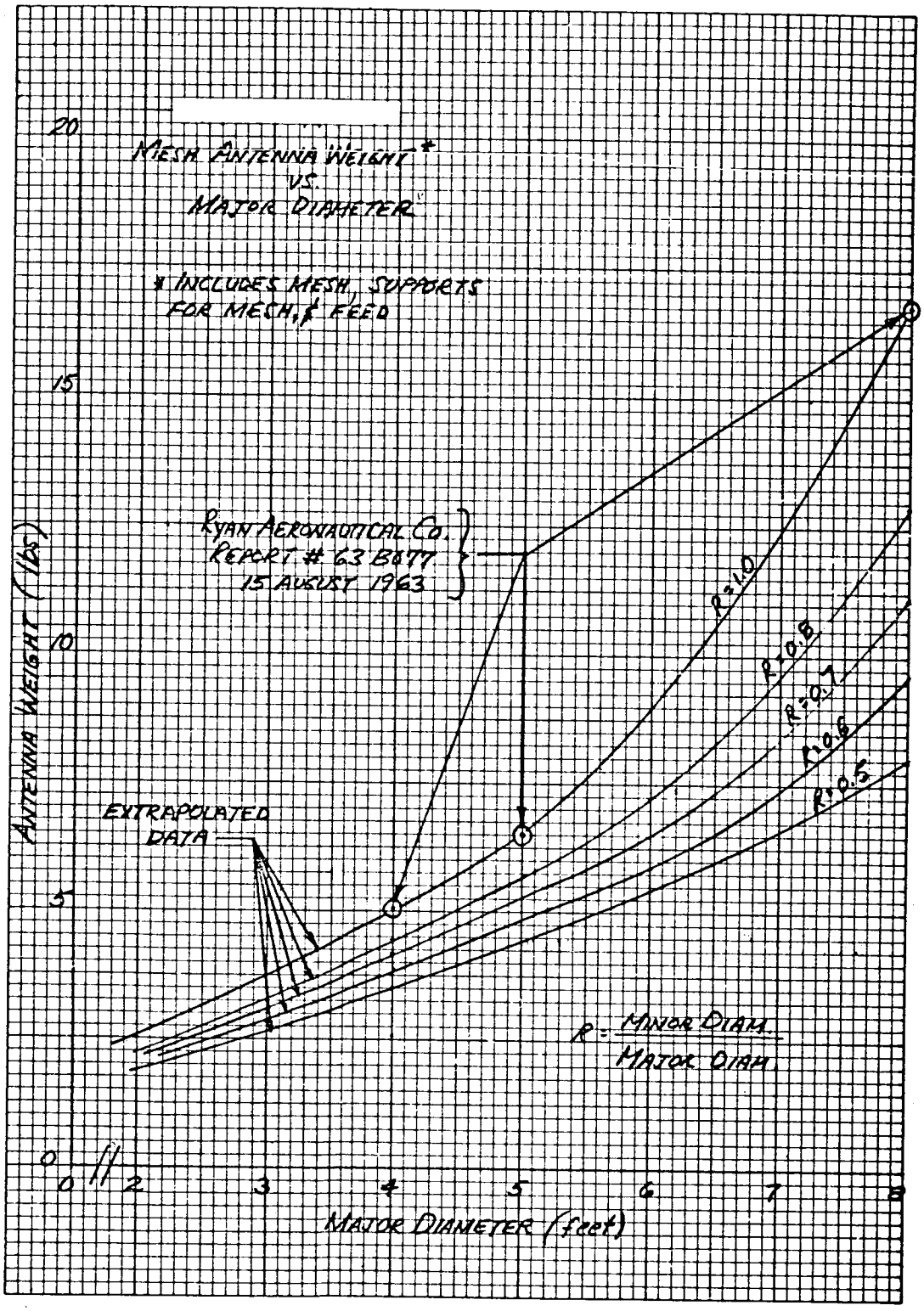

64-11367

Figure 68 MESH ANTENNA WEIGHT

172

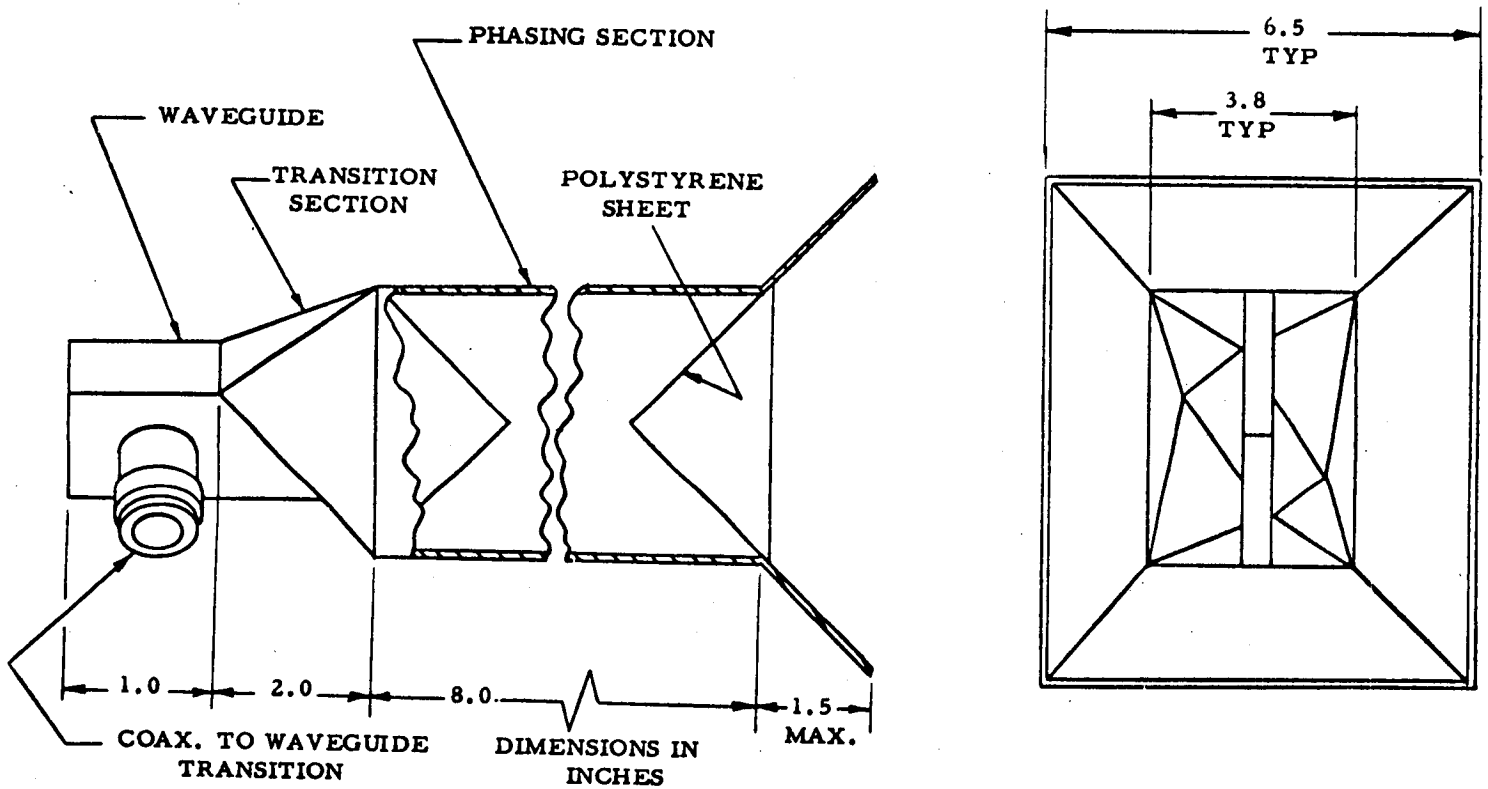

64-11453

Figure 69 CIRCULARLY POLARIZED HORN

RE-ORDER No. 64-524

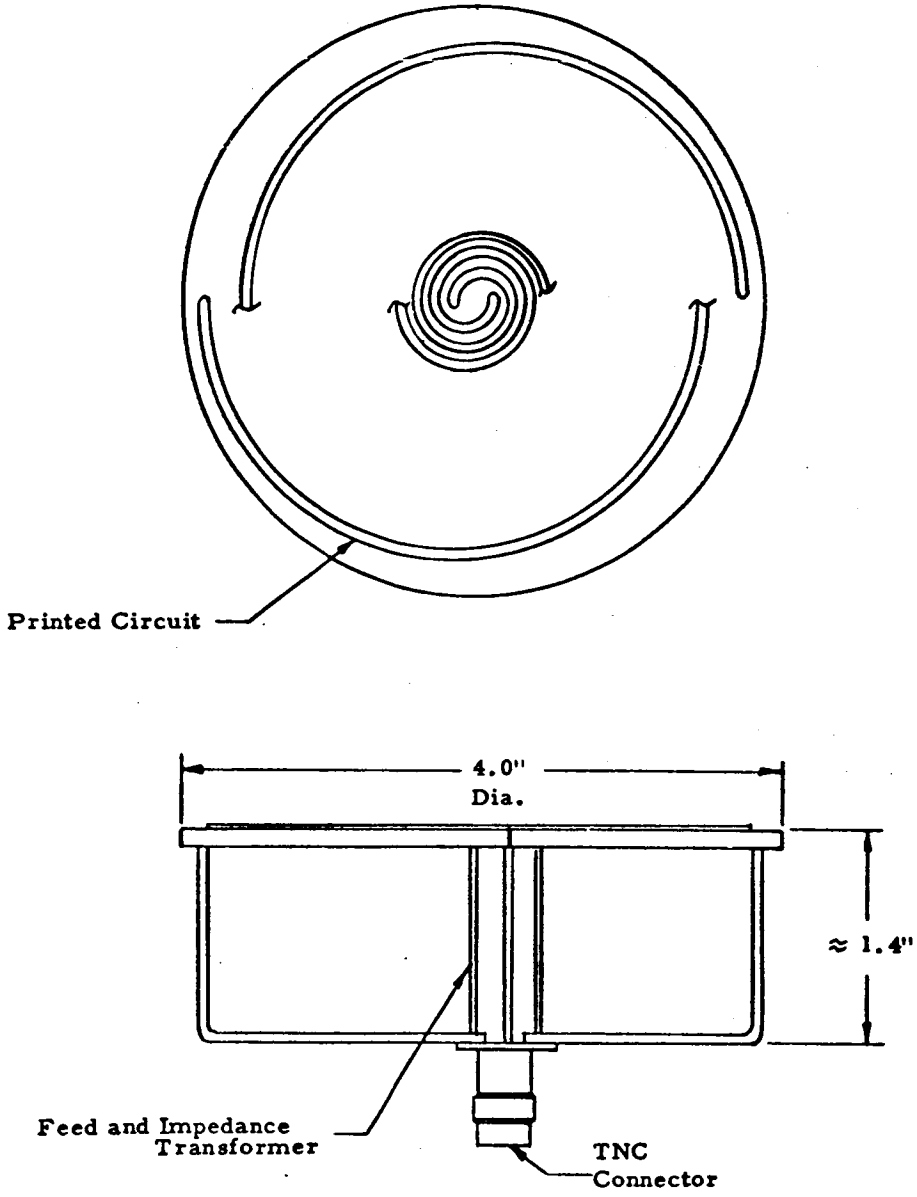

64-11454

Figure 70 SPIRAL ANTENNA

174

RE-ORDER No. 64-524

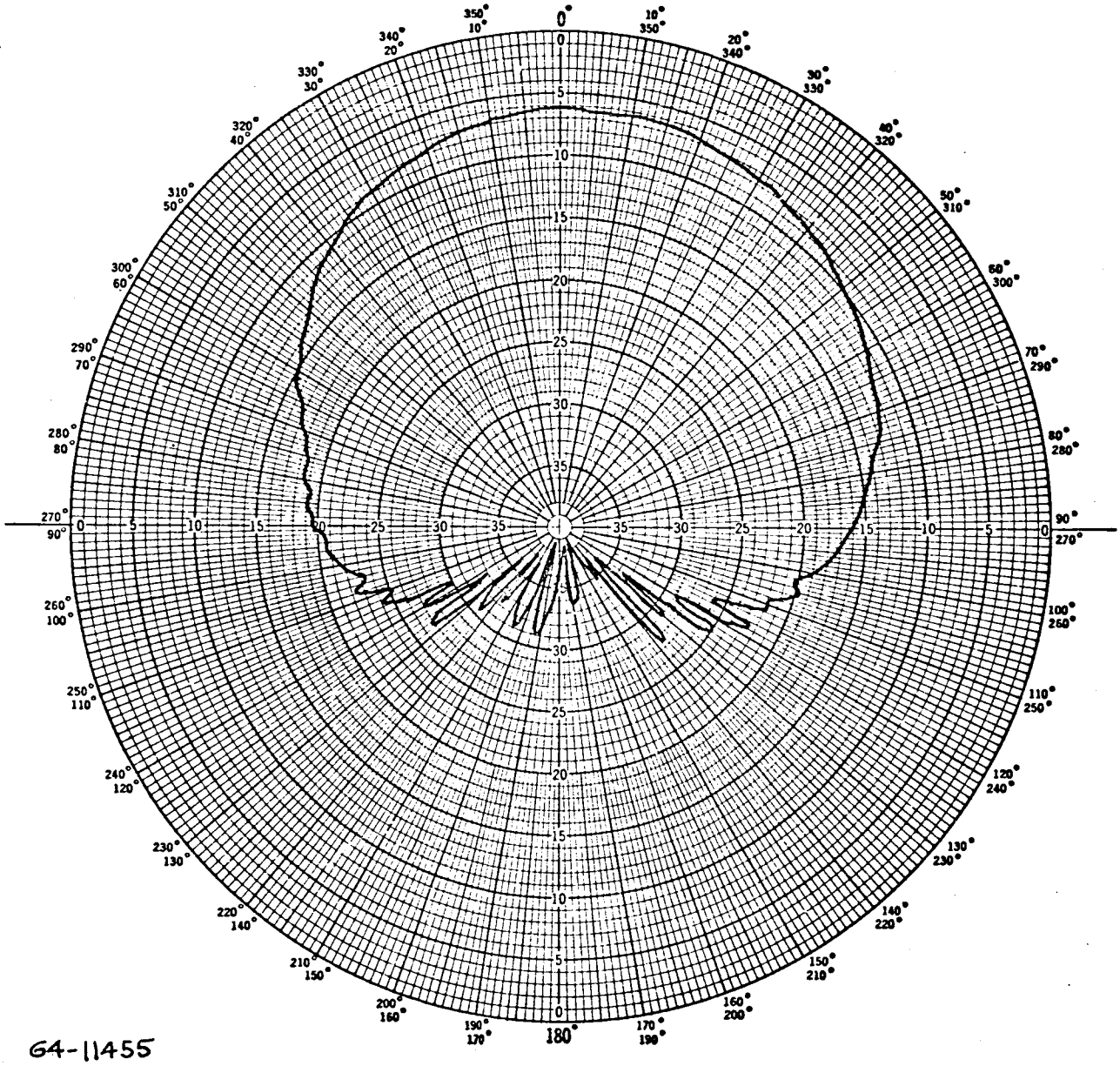

Figure 71 TYPICAL RADIATION PATTERN OF A SPIRAL ANTENNA
(NO GROUND PLANE)

175

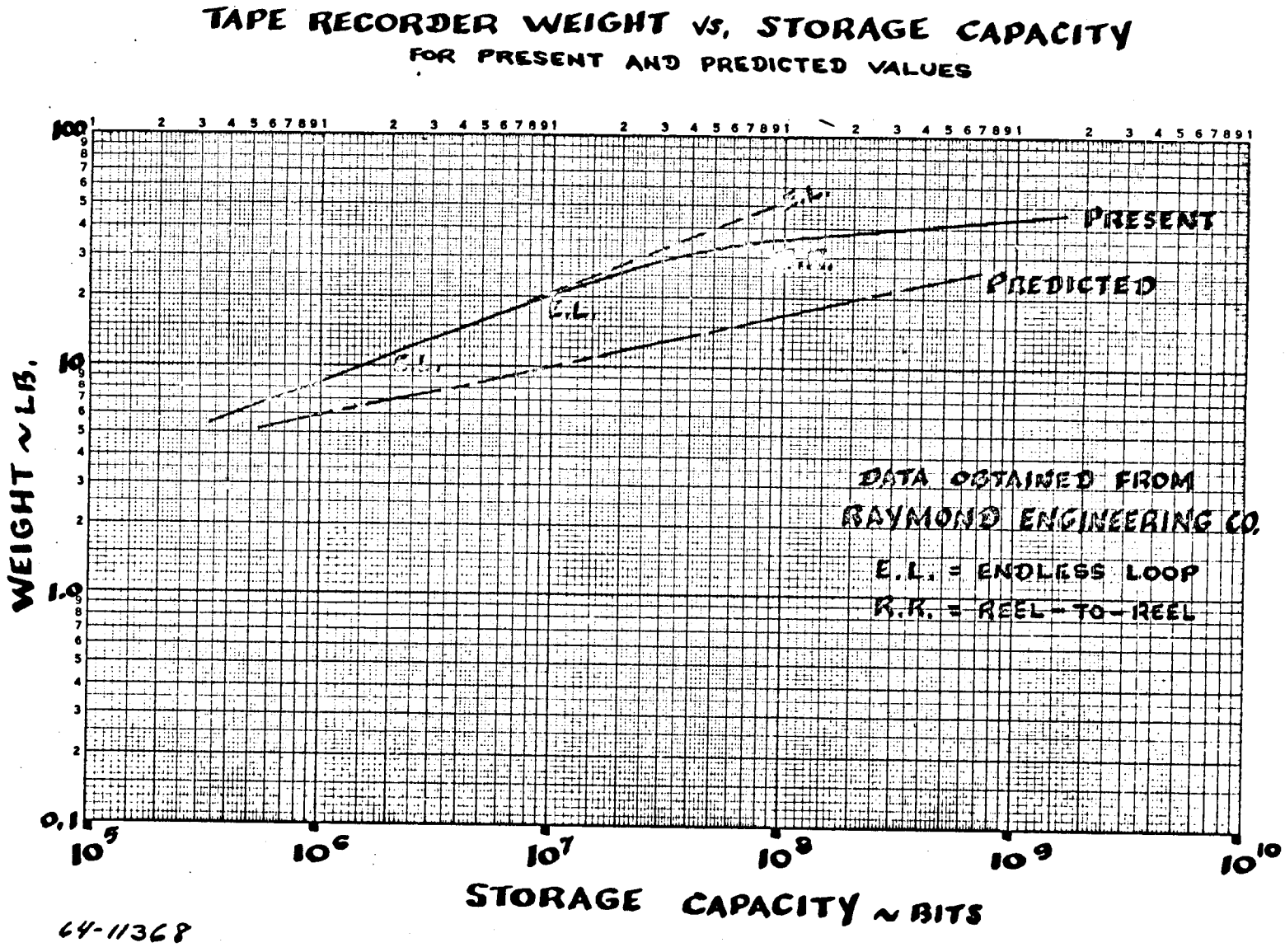

Figure 72 TAPE RECORDER WEIGHT

RE-ORDER NO. 64-524

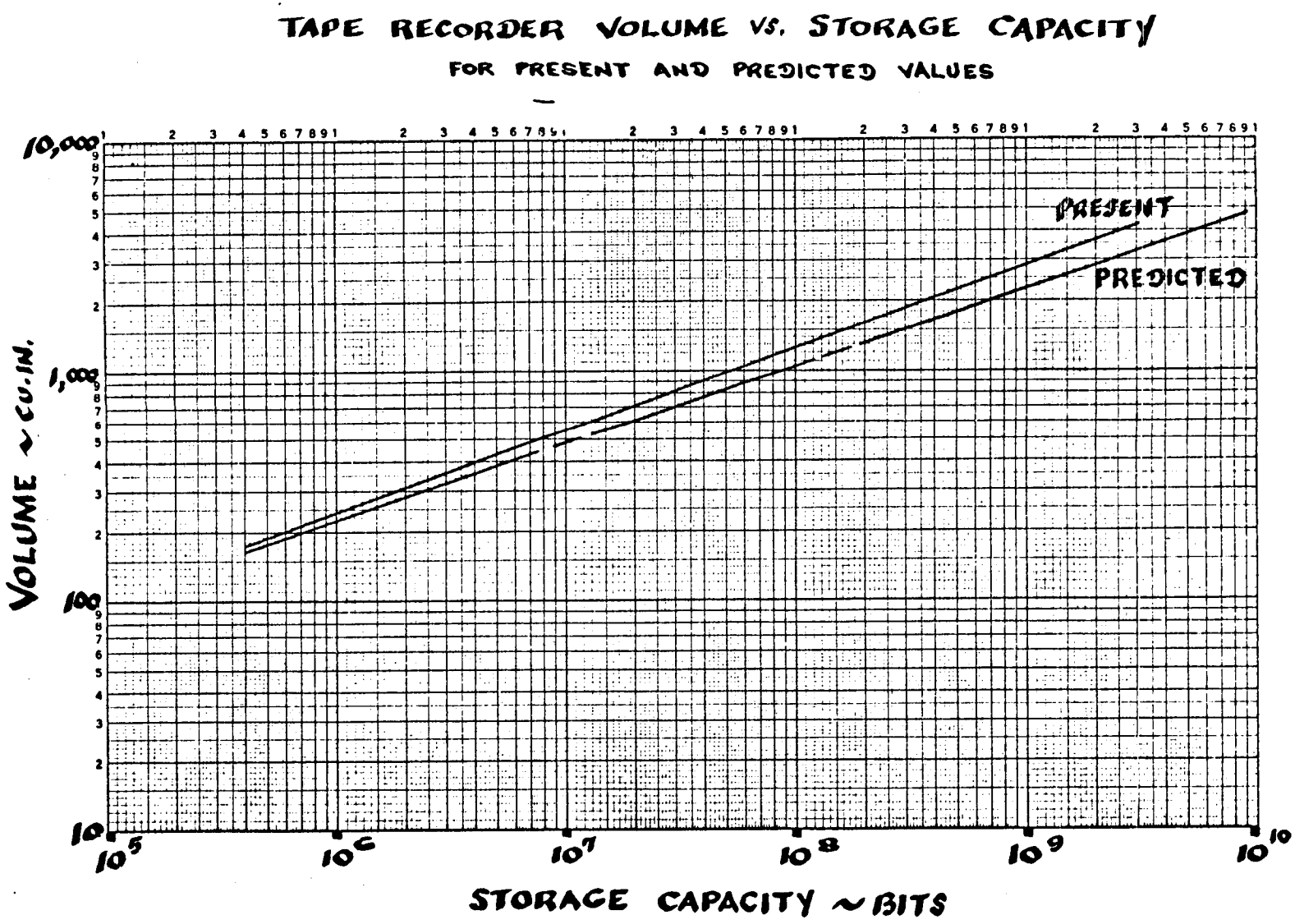

64-11369

Figure 73 TAPE RECORDER VOLUME

RE-ORDER No. 64-524

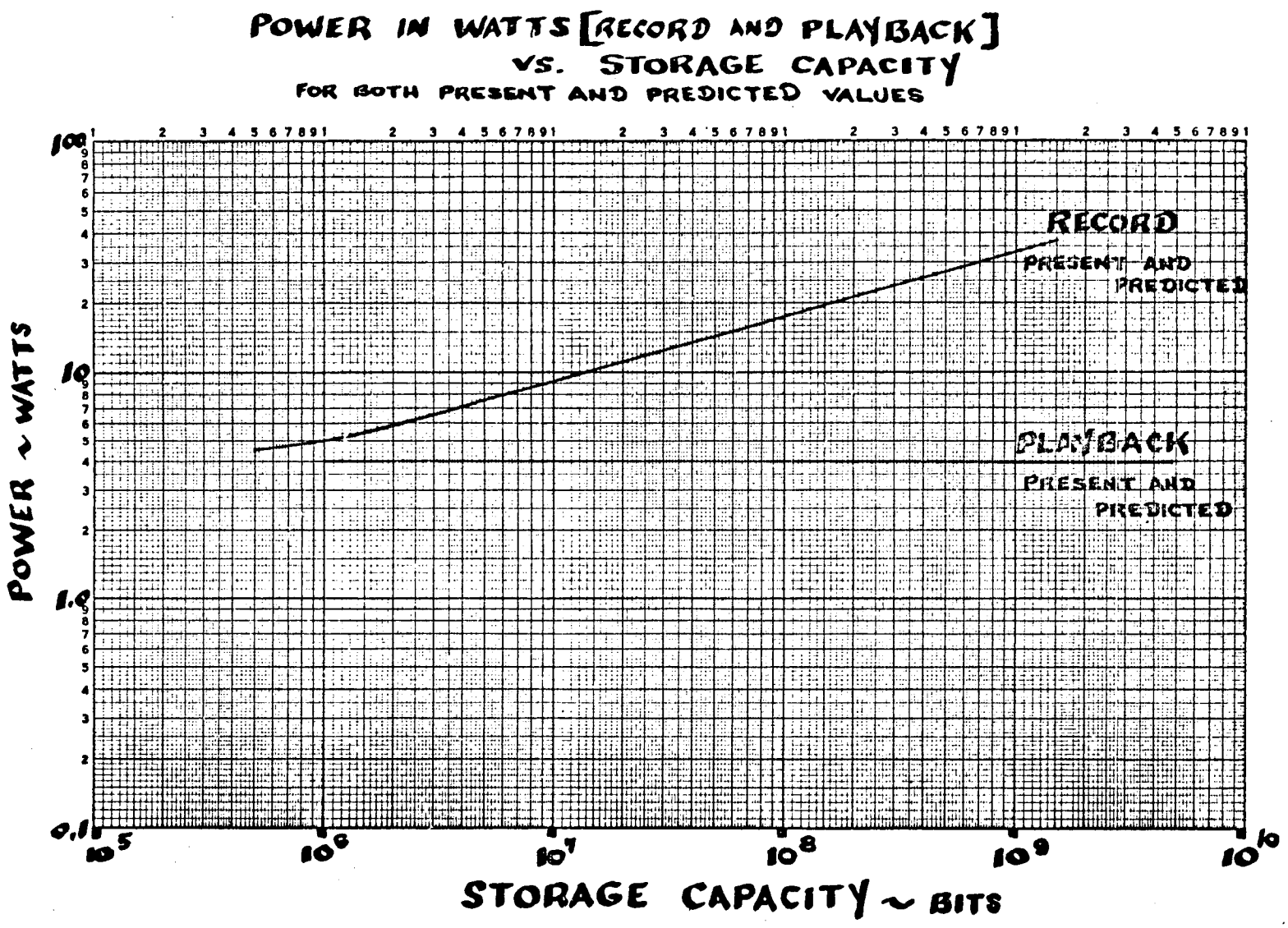

64-11370

Figure 74 TAPE RECORDER POWER CONSUMPTION AS A FUNCTION OF STORAGE CAPACITY

RE-ORDER No. 64-524

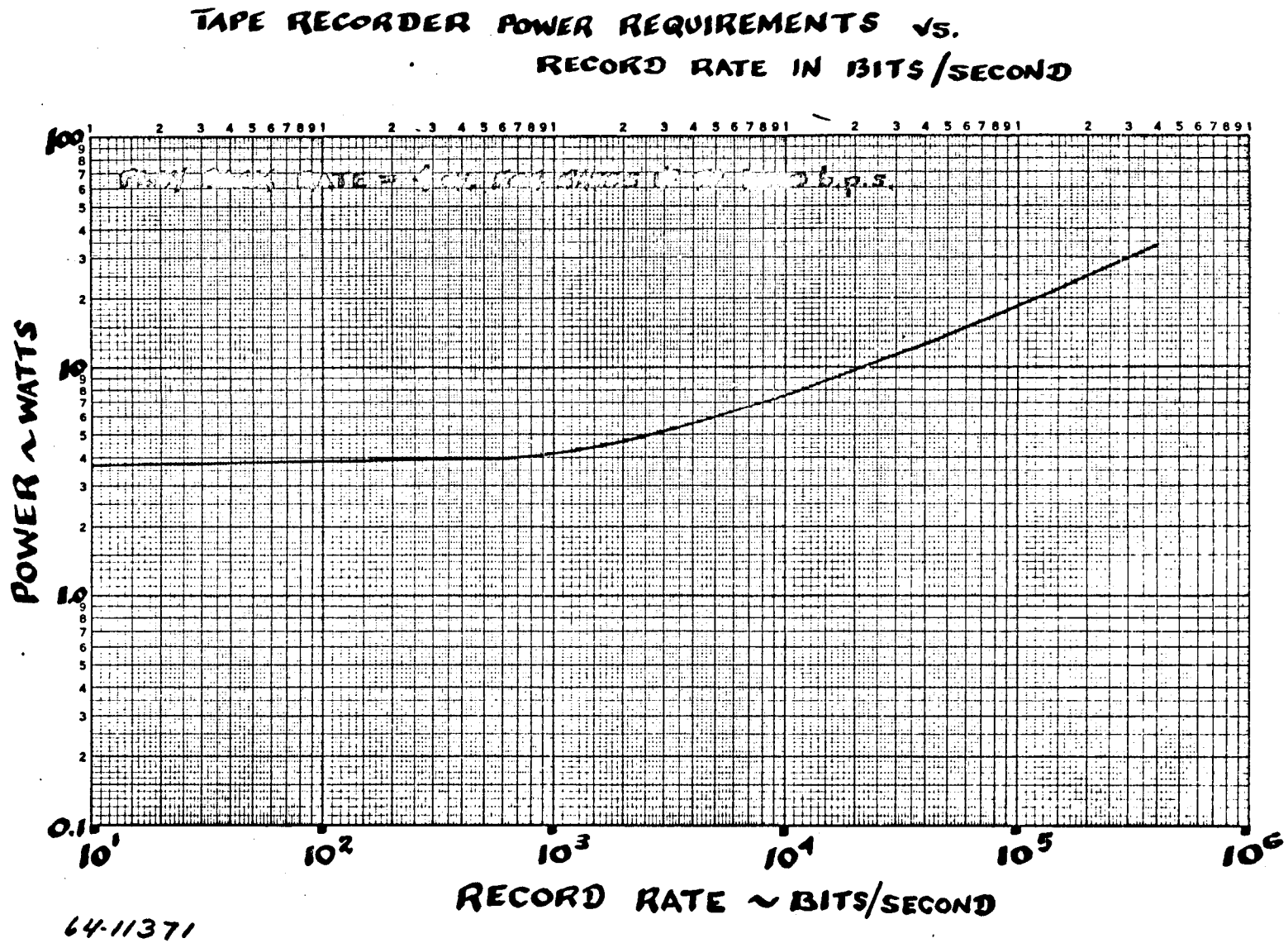

Figure 75 TAPE RECORDER POWER CONSUMPTION AS A FUNCTION OF RECORDING RATE

RE-ORDER No. 64-52

179

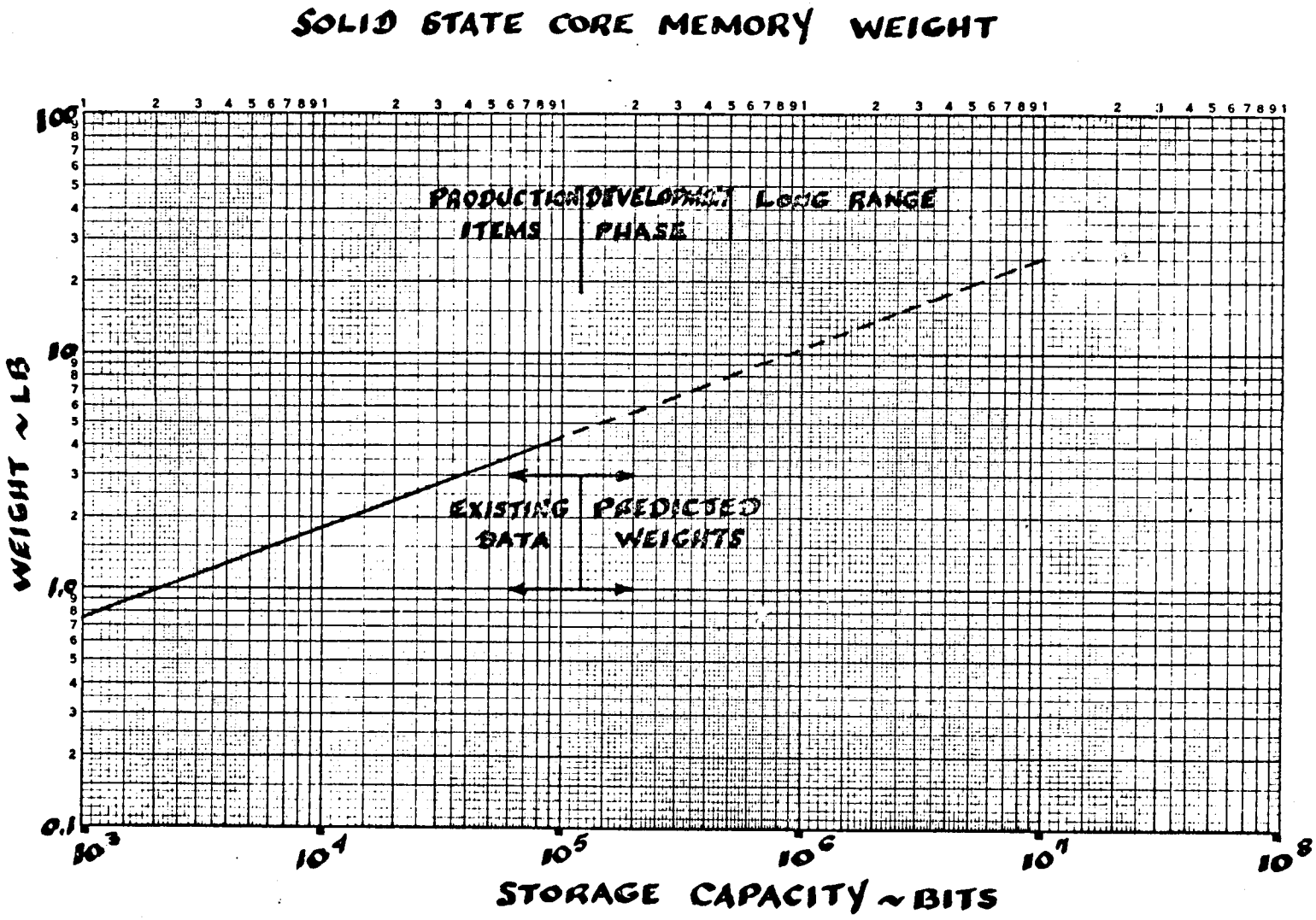

64-11372

Figure 76 SOLID STATE CASE MEMORY WEIGHT

RE-ORDER No. 64-534

180

RE-ORDER No. 64-524

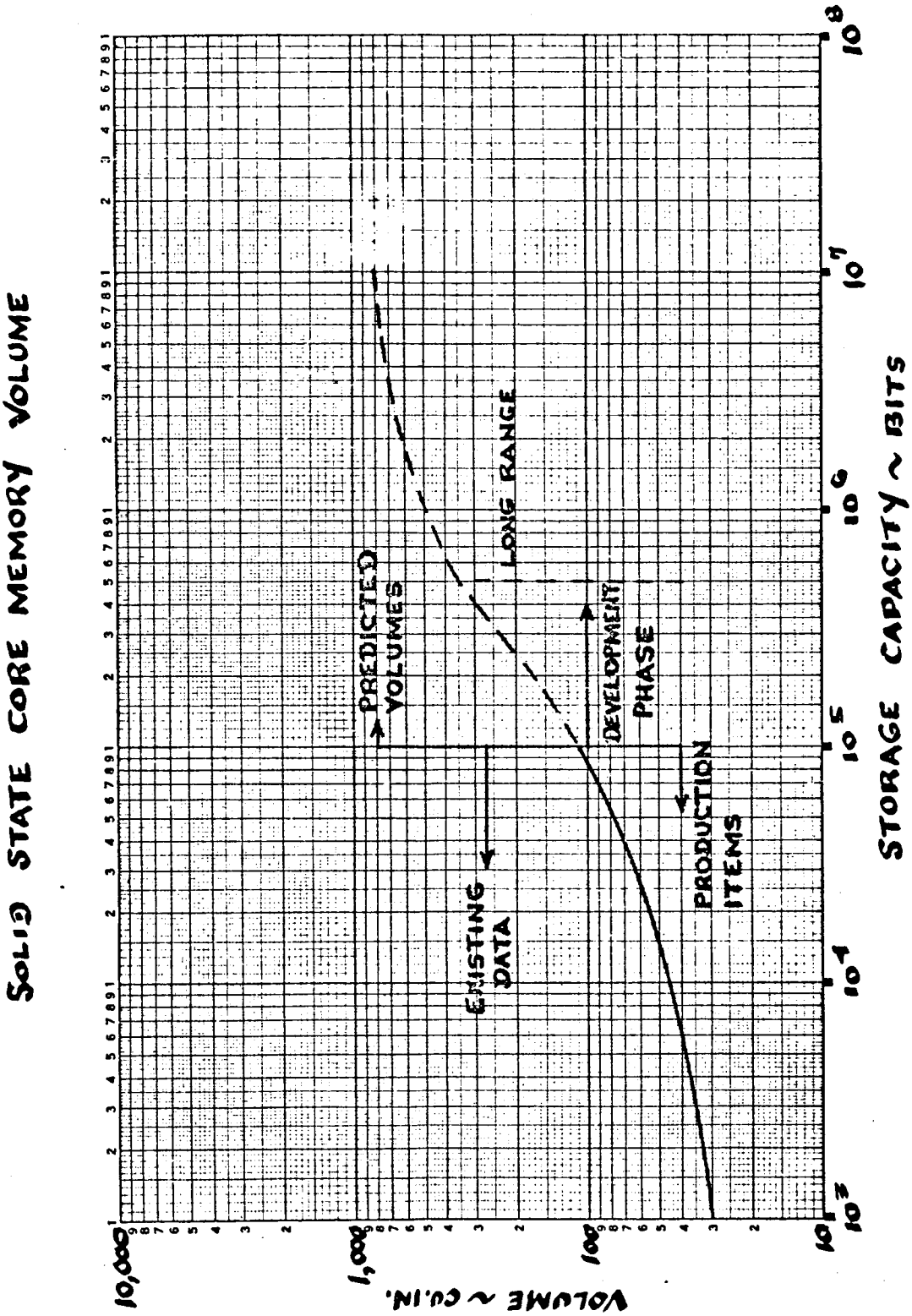

64-11373

Figure 77 SOLID STATE CASE MEMORY VOLUME

181

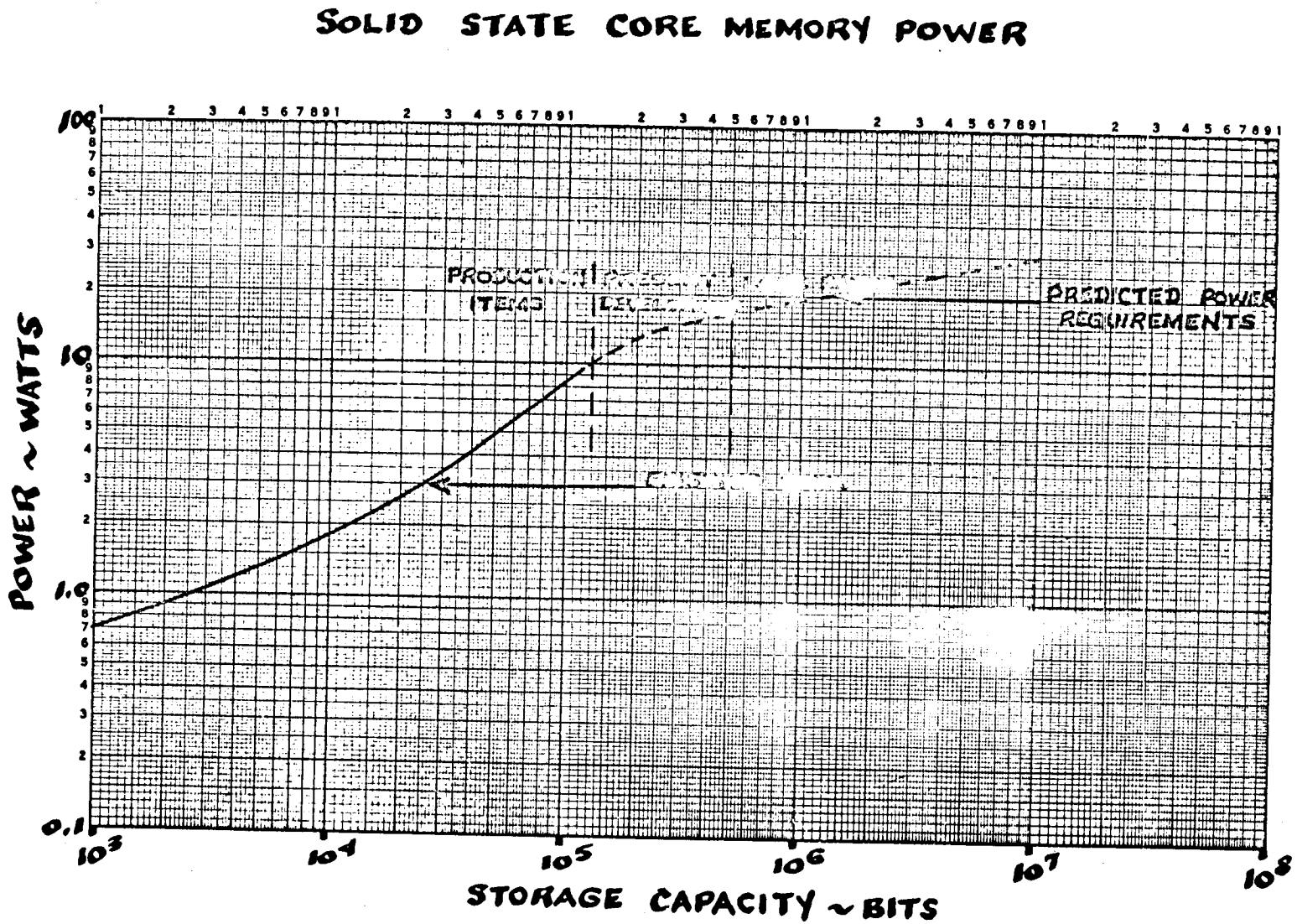

Figure 78 SOLID STATE MEMORY POWER CONSUMPTION

RE-ORDER No. 64-534

4. Power Amplifiers

Above 10 watts, the power amplifier supplied by Resdel Engineering Corp. for the Mariner C spacecraft could not be used. (Higher power could be obtained but not for periods up to 10,000 hours as required in these missions. Data on other power amplifiers are shown in the lander section.

5. Relay Receiver

The relay link receiver selected for this study employs a tunnel diode preamplifier with a noise figure of 4.5 ± 0.5 db. The receiver will require automatic (frequency swept) acquisition in the carrier and sync channels. A low pass filter noise bandwidth of 100 cps for the descent mode and a noise bandwidth of 20 cps for the lander and preentry mode are required in the conceptual design. The sync loop, accordingly will have a low pass filter with a noise bandwidth of 10 cps during the descent mode and a noise bandwidth of 1 cps for the preentry and landed modes. The bandwidth required for the descent mode will be switched by a programmer. A detailed analysis of the receiver has not been undertaken since it is beyond the scope of this program.

6. RF Electronics

The transponder, exciters, and rf switches will be based on Mariner C designs with only slight modifications.

7. DAS

The Data Automation Subsystem will be slightly modified from the original Mariner C DAS to accomodate more real time and non-real time logic. This modification is reflected in table 29 in the weight volume and power requirements.

8. Command Subsystem

The Command Subsystem will undergo a slight modification in weight, volume and power requirements to accomodate the increase in required command words.

9. Telemetry

An increase in the number of analog measurements will be included in the modified telemetry subsystem. The use of additional commutators will also increase the basic parameters as shown in table 29.

RE-ORDER No. 64-524

5.0 COMMAND AND CONTROL

5.1 GUIDANCE

Guidance of the flyby/bus throughout the interplanetary flight is accomplished by Earth tracking of the spacecraft by the DSIF stations in combination with the application of small discrete velocity increments at two points in the interplanetary flight. The thrust application direction for these midcourse corrections is controlled by the attitude control subsystem.

After tracking the spacecraft for a sufficient period of time, three quantitative commands are transmitted from the DSIF to the flyby/bus and stored in the central computer and sequencer (CC and S). These commands control the midcourse correction; two attitude commands, pitch and yaw, and an engine burn time command. A discrete command transmitted from the DSIF to the flyby/bus initiates a preprogrammed sequence within the CC and S which uses these stored quantitative commands to maneuver the flyby/bus through the required angle in pitch, and then through the required angle in yaw. Both attitude maneuvers are controlled by on-board rate integrating gyros operated in the rate integrating mode. These maneuvers are referenced from the flyby/bus cruise attitude as maintained by cold gas reaction jets controlled by the outputs of a sun sensor and a Canopus tracker to 0.10 degree about all three axes.

The propulsion system then is ignited and burns for a period of time preset by the stored command, to provide a velocity increment accurate to 0.1 ft/sec. The flyby/bus then returns to the cruise mode by reacquiring the sun and Canopus references.

This method of midcourse correction applied twice, 1 and 10 days after launch, provides the guidance necessary to place the flyby/bus on the proper trajectory to fly by Mars at the desired passing distance to an accuracy of 500 to 1,300 kilometers, one sigma. This accuracy, while quite adequate for the flyby/bus mission, would result in a serious dispersion problem for the lander. As the spacecraft approaches the outer bound of the lander separation range, approximately 5 million kilometers from Mars, the tracking information obtained by the DSIF is once again updated. The lander separation range is now adjusted to between 0.5 and 5 million kilometers from Mars to accommodate the most extreme variations in the flyby periapsis distance. If both midcourse maneuvers are successful, the variation in lander separation range need only be between approximately 0.6 and 1.5 million kilometers. Control of the lander impact point in this manner reduces the lander dispersion on the planet's surface from 500 to 1,300 kilometers, one sigma, to less than 300 kilometers, one sigma, making the selection of a specific target area such as Syrtis Major quite feasible.

5.2 FLIGHT COMMAND SUBSYSTEM

Command and control of the Advanced Mariner spacecraft after launch is implemented through the use of on-board operational sequences stored in the Central Computer and Sequencer (CC and S), and by the use of direct commands to the various spacecraft subsystems. These commands and sequences may be either automatically initiated at preselected times throughout the spacecraft flight profile or upon ground command to the spacecraft command system via the DSIF.

The use of existing equipment has been maximized, in that the command detector, command decoder, and CC and S units used on the Mariner C have been incorporated into this design with a minimum of modifications.

1. Command Detector and Command Decoder

The command detector receives the command signal (as sent by the DSIF) from the spacecraft telemetry subsystem. The detector processes the signal synchronization information, acquires phase coherence with the command signal and establishes bit synchronization and the phase reference signal for the command decoder. Since the same modulation and coding scheme is being used on Advanced Mariner as on Mariner C, no apparent change is required in the command detector.

The command decoder receives the command word bits and synchronization signal from the command detector, identifies which command word has been received, error checks the word for proper bit parity and issues the proper output to the spacecraft subsystem affected by the command. The command word coding scheme used is similar to that used on Mariner C, allows a maximum of 30 command addresses, using a six-bit command address location in the command decoder unit and a total serial bit content of 26 locations per command word. Twenty-six discrete commands (DC) and one quantiative command (QC) were used on Mariner C, with three spare command addresses available. Due to the many similarities in equipment between Mariner C and Advanced Mariner, almost all of the existing sequences and discrete operations can be used without alterations. Certain of the Advanced Mariner sequences, however, were not present in the Mariner C profile and require new DC's and additional quantitative data. These can be accomplished by using the available spare commands previously mentioned and by utilizing a notation for the subaddressing of QC's (to allow one QC to be used for the location of several different pieces of data) which is already in use on Mariner C. This scheme can be conveniently expanded to allow sufficient data storage capacity for additional maneuver sequences as well as for read-in and monitoring of commands which must be stored internally to the lander vehicle, in the lander post-separation program control unit(PCU). From a study of the existing command decoder, it appears that only detailed changes are required to handle the additional commands and sequences.

2. Central Computer and Sequencer

The CC and S performs the timing, sequencing, and computational services for all other subsystems on the spacecraft. The major sequences of events are:

a. Launch to initial cruise mode acquisition sequence.

b. Midcourse maneuver sequence.

c. Lander separation and bus slowdown maneuver sequence.

d. Master timer flight profile sequence.

Prior to lander separation from the flyby/bus, the spacecraft CC and S is used to monitor, process, and transfer updated quantitative information to its own internally stored sequences as well as to the lander PCU (through the bus-lander umbilical). Subsequent to lander separation, the CC and S performs preprogrammed functions required for the encounter and post-encounter phases of the mission. A schematic drawing of all of the components in and affecting the CC and S with functional notation is shown on figure 79 for the typical mission profile shown in table 30. A more comprehensive mission profile is to be found in the Systems Analysis Volume, Volume 2.

Addition of a new timer and additional quantitative information storage (for the lander separation and bus slowdown sequence), are required over and above the Mariner C CC and S capacity. No major changes in equipment operation are anticipated.

3. Spacecraft Bus Flight Command Subsystem

External Commands

The prelaunch sequence as accomplished by the ground complex equipment (GCE) for a typical mission is shown in steps 1 through 6 at the left of the figure 79. The GCE-to-spacecraft umbilical connections required to perform these tasks are indicated. After launch, at Centaur shroud removal, step 7, the Centaur-to-spacecraft umbilical carries a signal from the Centaur Guidance and Control to the spacecraft, turning on the cruise science and the radio subsystem. At Centaur/spacecraft separation, step 8, the Centaur-to-spacecraft umbilical is disconnected and the separation sensor/connector switch starts the spacecraft separation initiated timer (SIT). Later, via the DSIF, step 9, discrete commands (DC) and quantitative commands (QC) are received by the spacecraft radio subsystem and processed by the command detector and command decoder and then sent to the appropriate spacecraft subsystems. DC and QC identification and functional distribution are shown next to the command detection and command decoder in figure 79.

Internal Sequences

Just prior to launch, the launch sequence time (LST), and Master Timer (MT), are reset to zero, given a final updating of internal timing data,

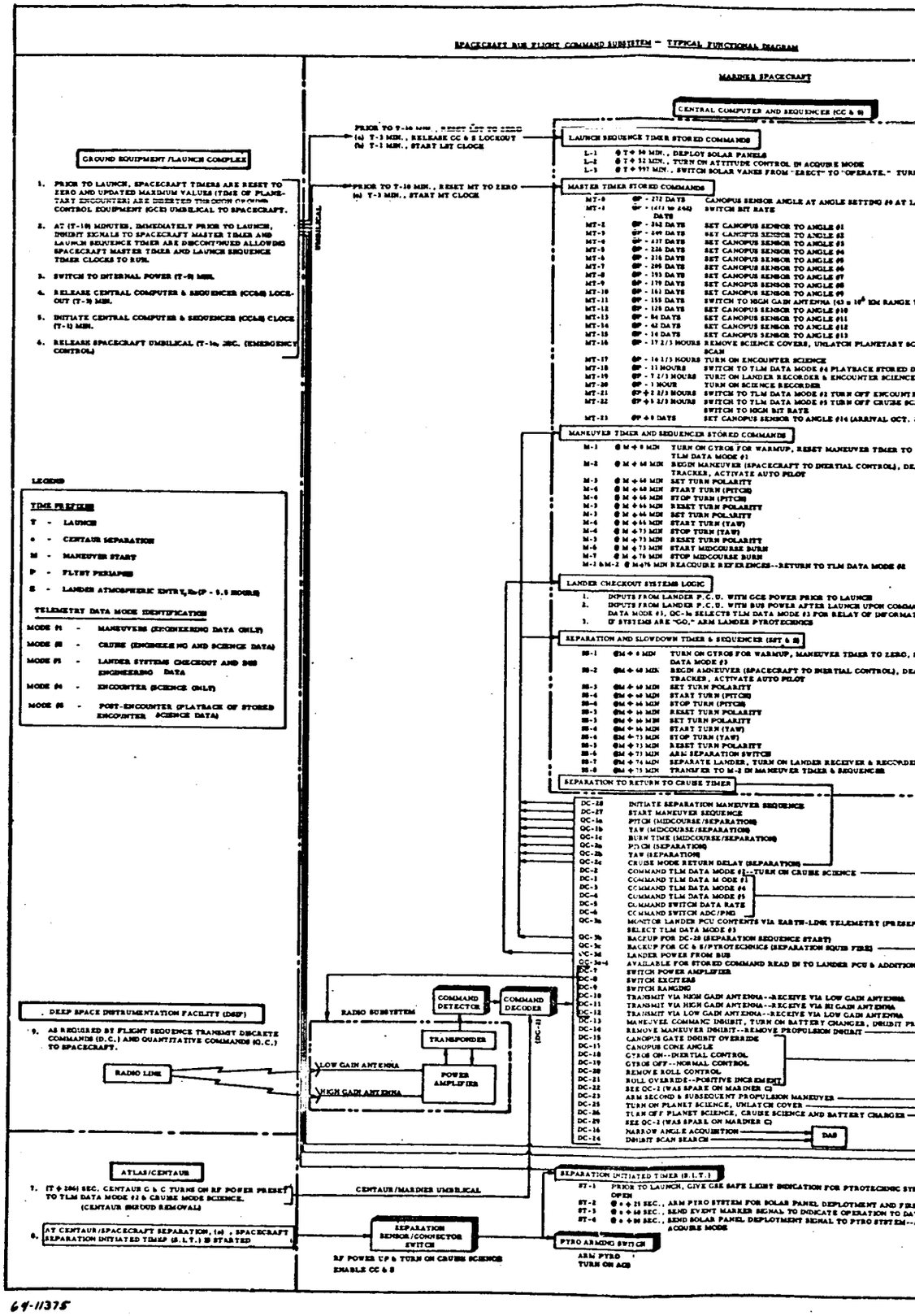

Figure 79 SPACECRAFT-BUS FLIGHT COMMAND SUBSYSTEM - T
FUNCTIONAL DIAGRAM

1#

RE-ORDER No. 64-524

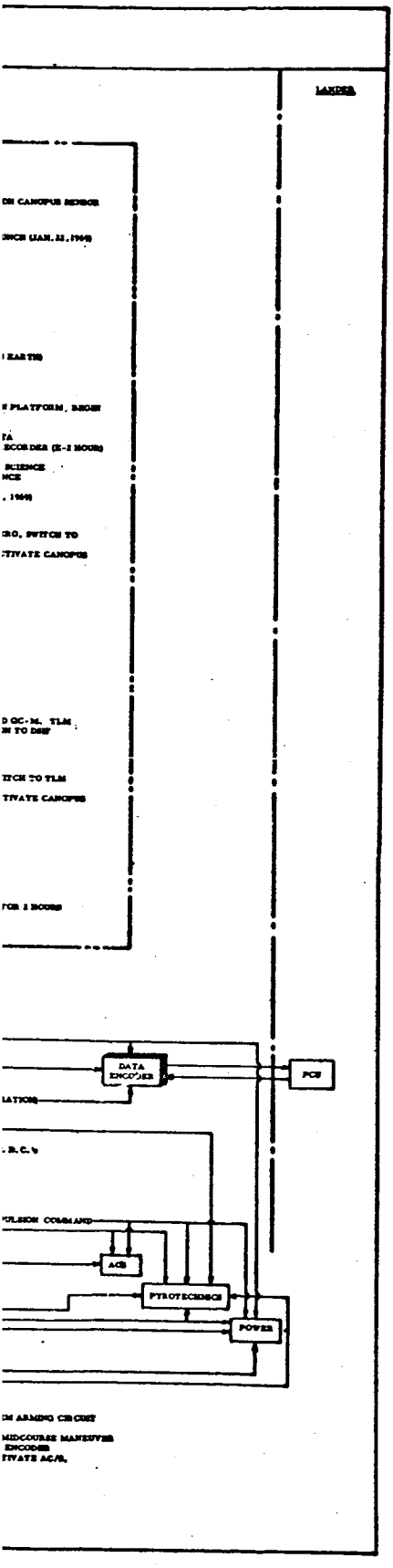

'PICAL

2#

187

RE-ORDER No. 64-524

TABLE 30*

ABRIDGED ADVANCED MARINER SPACECRAFT MISSION PROFILE

Time from Launch (days)	Time Relative to Planetary Periapsis (P) (days)	Event and Comments
0	P - 272	Prelaunch through initial reference acquisition sequence (duration $\leq$ 82.5 minutes.) Begin cruise mode. Turn on cruise science. Initial Canopus sensor cone angle set prior to launch.
1	P - 271	End cruise mode. First midcourse trajectory correction sequence. (duration $\leq$ 42.9 minutes at $\Delta V \leq$ 100 ft/sec). Begin cruise mode.
10	P - 262	End cruise mode. Second midcourse trajectory correction sequence. (duration $\leq$ 40.1 minutes at $\Delta V \leq$ 10 ft/sec). Set Canopus sensor cone angle No. 1. Begin cruise mode.
23	P - 249	Set Canopus sensor cone angle 2.
35	P - 237	Set Canopus sensor cone angle 3.
46	P - 226	Set Canopus sensor cone angle 4.
56	P - 216	Set Canopus sensor cone angle 5.
67	P - 205	Set Canopus sensor cone angle 6.
79	P - 193	Set Canopus sensor cone angle 7.
93	P - 179	Set Canopus sensor cone angle 8.
111	P - 161	Set Canopus sensor cone angle 9.
117	P - 155	Switch to high gain antenna.

TABLE 30* (Concl'd)

Time from Launch (days)	Time Relative to Planetary Periapsis (P) (days)	Event and Comments
144	P - 128	Set Canopus sensor cone angle 10.
188	P - 84	Set Canopus sensor cone angle 11.
230	P - 42	Set Canopus sensor cone angle 12.
258	P - 14	Set Canopus sensor cone angle 13.
269	P - 3	End cruise mode. Lander ejection and bus slowdown sequence (duration $\leq$ 66.2 minutes at $\Delta V \leq$ 912 ft/sec). Five hours slowdown of bus relative to lander. Begin cruise mode.
272	P	End cruise mode. Turn off cruise science. Begin encounter mode; store encounter data. Lander atmospheric entry approximately five hours prior to bus periapsis. End encounter mode. Begin encounter data playback.
280	P + 8	Set Canopus sensor cone angle 14.
282	P + 10	End data playback [illegible]rn on cruise science. Resume cruise mode.

*For explanatory purposes a typical flight sequence has been chosen. For a 22 January 1969 launch date, the time of flight will be 272 days, and the corresponding planetary arrival date will be 21 October 1969.

and then started via the GCE-to-spacecraft umbilical. The timing of these events is shown by the L-series and MT-series of commands. (Time prefix identification is shown in the legend, at the left of the chart, along with the telemetry transmission data mode identification.) The MT commands run throughout the mission, while the L commands are over shortly after launch.

At Centaur/spacecraft separation, the SIT is activated and the ST command sequence begins. For midcourse corrections data sent via the DSIF using QC commands is prestored in the CC and S and then the maneuver timer is started by a ground originating DC to the CC and S at the appropriate time. In a like manner, the lander separation and bus slowdown sequence are implemented by preloading maneuver data into the CC and S, and then initiating the sequence via ground-link telemetry. M and SS commands, respectively, are responsible for subsystem commands in these sequences.

6.0 PROPULSION SYSTEM

6.1 PERFORMANCE AND DESIGN REQUIREMENTS

After completion of parametric studies for the determination of flight trajectories and corresponding mission payload weights, it was possible to define the design and performance requirements that the flyby/bus propulsion system would have to meet. The primary requirements are listed below:

1. Three, start/firing sequences

2. Minimum thrust level 19 pounds.

3. Minimum impulse bit which would result in a vehicle ΔV of < 0.1 ft/sec

4. 100 and 10 ft/sec ΔV capability for a total vehicle weight consisting of flyby/bus and lander (lander weight 500 pounds)

5. 919 ft/sec ΔV capability for a flyby/bus only payload and structure weight of 652 pounds

6. Propellants subjected to a temperature range of 0° to 130° F

7. Envelope limitations

8. Development status to be compatible with January, 1969, flight

Some additional discussion of the above requirements is in order to give more insight into the reasons for and further clarification of a particular item. The three firing periods are composed of two for midcourse correction of the entire vehicle, while the third firing is to slow down the flyby/bus only, after the lander has been separated in the vicinity of Mars. It is possible that the second midcourse correction might require a ΔV as small as 10 ft/sec, thus the requirement for the minimum impulse bit limitation.

The minimum thrust level noted was established after a study of the effect of maneuver sequences on battery weight. It was determined that for thrust levels below 19 pounds the battery weight increased appreciably. Because of this, the minimum allowable thrust level was set at 19 pounds.

A preliminary thermal analysis indicated that the propellants would be subjected to a wide temperature range during the entire flight. The expected propellant temperature could be narrowed by the use of insulation and heaters, but it was desirable not to resort to this type of solution if possible because of the weight penalty and complexity.

The envelope limitations were brought about by the desire to keep the bus height to a minimum so that the lander diameter could be maximized.

6.2 PARAMETRIC DESIGN DATA

To assist in sizing the propulsion system and to determine the effect of specific impulse on propulsion system weight, a set of parametric curves was generated. Velocity increment, ΔV was calculated as a function of propellant weight to vehicle total weight ratio, W_P/W_T for different specific impulses, I_{SP}. The range of specific impulse covered includes monopropellant, bipropellant, and solid propellant systems. This parametric calculation is presented in figures 80, 81, and 82. These figures consider only the propellant weight portion of the propulsion system; therefore, to determine the propulsion system total loaded weight, the system mass fraction must be taken into consideration. To arrive at realistic mass fractions, existing propulsion systems were investigated, and the resulting mass fractions, λ (ratio of mass of propellants to mass of propulsion system) for system total impulses are presented in figure 83 for both monopropellant and bipropellant systems. Mass fraction determination trend for solid propellants was not straightforward, because many of the existing solid propellant engines had primary design requirements other than a high mass fraction

The weight of propellant required to meet the vehicle ΔV requirements was readily determined by using the proceeding parametric curves. For example, the propellant required to give the bus only, a ΔV of 919 ft/sec is obtained from the curve in figure 81. A specific impulse of 280 seconds is used and the W_P/W_T ratio for 919 ft/sec ΔV is 9.7 percent. The total allowable bus weight is 785 pounds which results in 76 pounds of propellant required for bus slowdown. Adding this propellant amount to that required for the other maneuvers, which were determined the same way, results in a total propellant load of 93 pounds. Using this propellant weight and multiplying by the 280 specific impulse determines the total impulse of the system. By using figure 72 and the curve for bipropellants, a total impulse of 26,000 lb-sec results in a system weighing 133 pounds.

After the system concept was defined, the parametric curves were again used to determine the final propulsion system weight.

6.3 PROPULSION SYSTEM SELECTION

1. Propellant Selection

The first item of the propulsion system to be studied was the propellant combination. From the design requirements given, parametric data and actual performance data on various propellant combinations, it was possible to determine the best combination for the application.

192

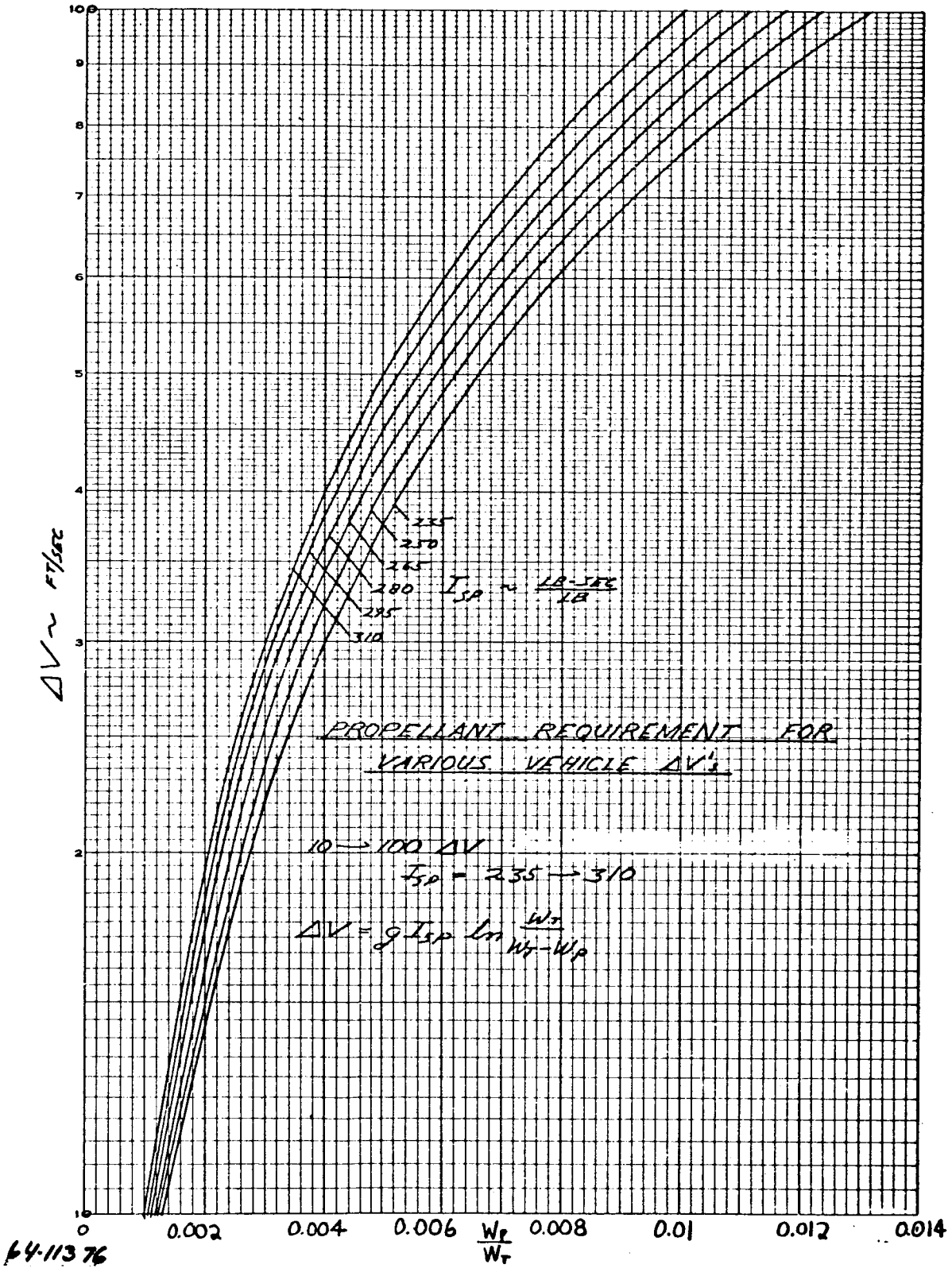

64-11376

Figure 80 PROPELLANT REQUIREMENT - 10 TO 100 FT/ SEC v

193

RE-ORDER No. 64-524

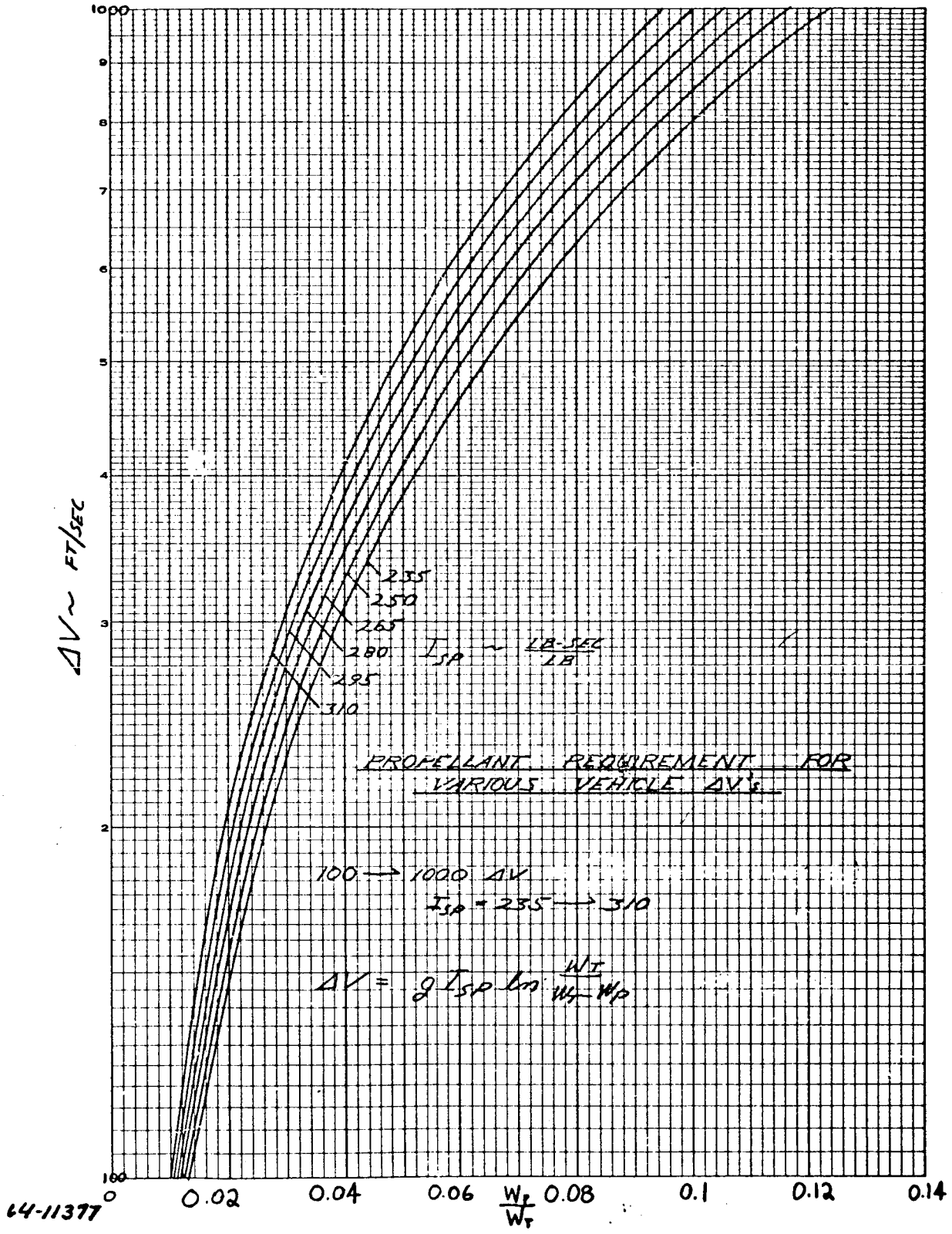

64-11377

Figure 81 PROPELLANT REQUIREMENT - 100 TO 1000 FT/SEC V

194

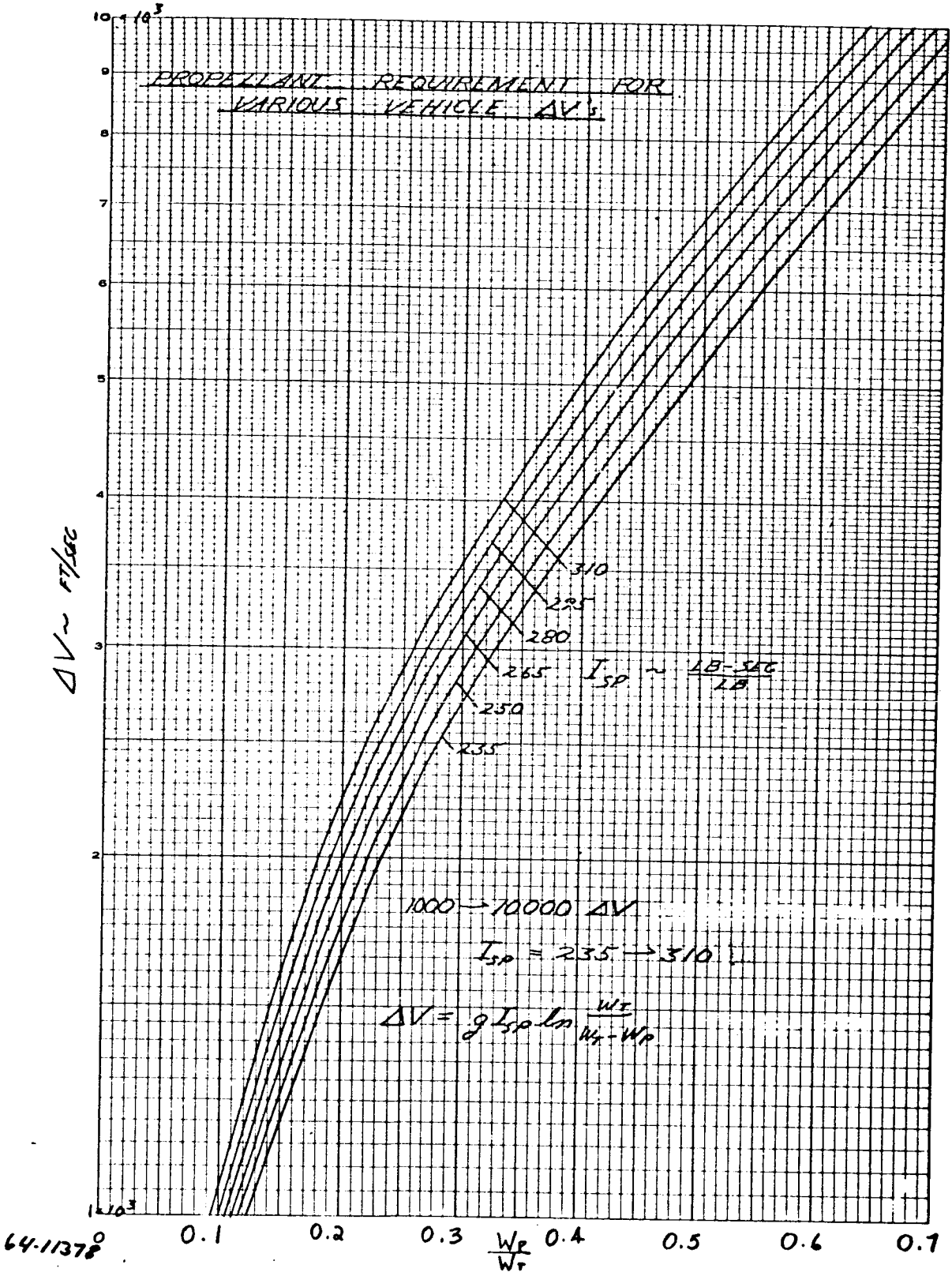

64-11378

Figure 82 PROPELLANT REQUIREMENT - 1000 TO 10,000 FT/SEC V

195

RE-ORDER No. 64-529

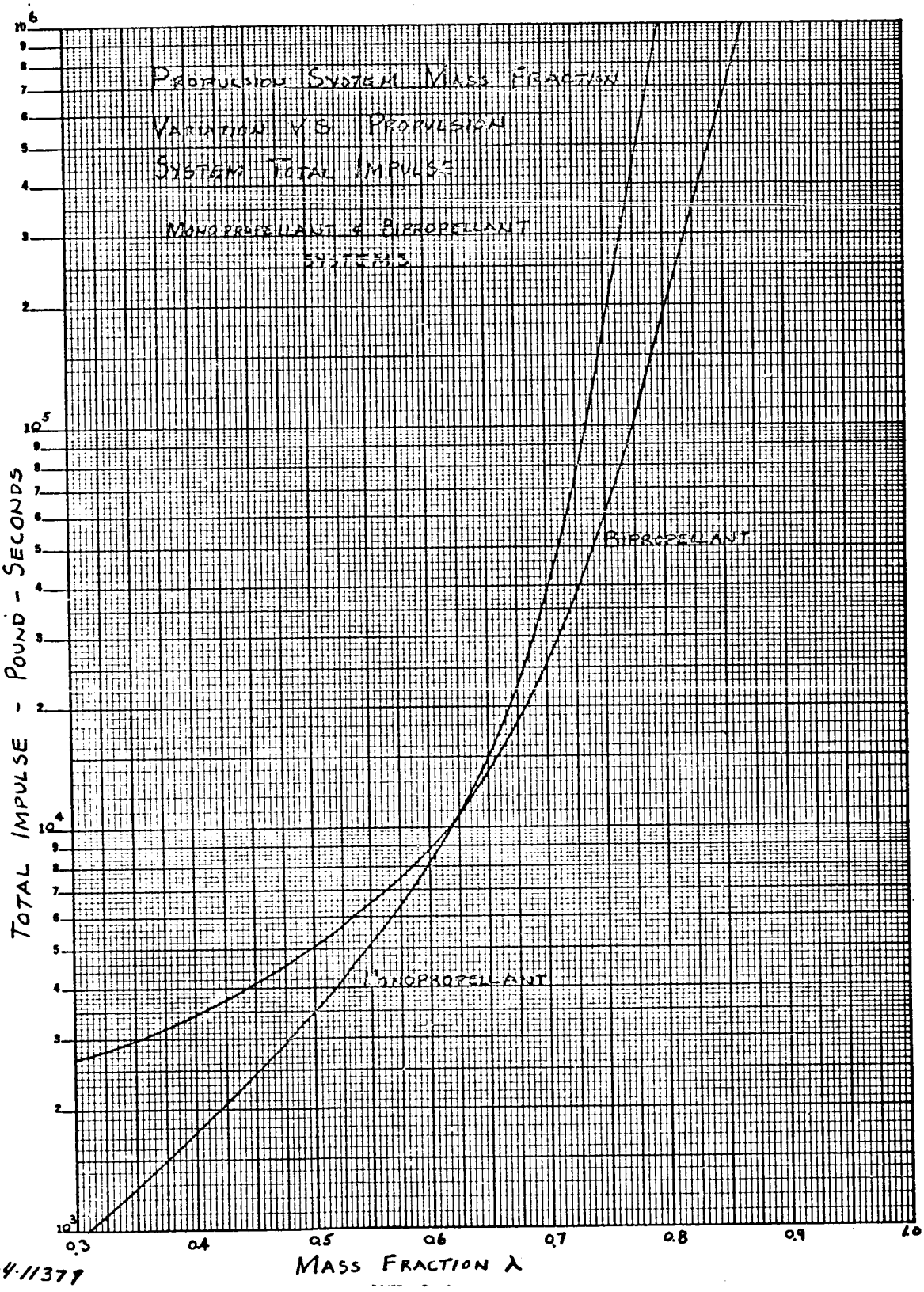

Figure 83 PROPULSION SYSTEM MASS FRACTION

196

Because of the restart requirement the solid propellant was eliminated from consideration immediately. The first cut at sizing the propellant requirement resulted in determining that approximately 80 pounds of propellant were required. From the parametric data it can be seen that the propellant requirement only varies by approximately two per cent from the lowest to the highest specific impulse. Due to this fact and because the total propellant load is small, it was decided that specific impulse would not be a major parameter in slecting the propellant combination to be used.

The next propellant parameter studied was the storability of the propellant in relation to the temperature requirement imposed by the vehicle and flight trajectory. In table 31 several oxidizers and fuels are listed with their respective freezing and boiling points and it should be noted that these propellants are being used in today's rocket engines. It is readily seen that two of the oxidizers meet the 0°F requirement and that MON is marginal. If the preliminary thermal analysis is the least bit optimistic, then there is a good possibility that propellant freezing would occur. In addition, the boiling point for the MON is well below the expected temperature limit, so high vapor pressure would result. The high vapor pressure would mean designing the propellant tanks for higher pressure than normal, and it might be necessary to prepressurize the tanks at filling. Because the IRFNA had a -56°F freezing temperature, well below the 0°F required, and its boiling temperature is above the 130°F requirement, it was decided that IRFNA should be used as the oxidizer.

The fuels that are normally used with IRFNA are also shown in table 31 and both their freezing and boiling temperatures are compatible with the vehicle requirements. They are so similar that IRFNA/UDMH was selected because of its higher specific impulse. Also, the mixture ratio for IRFNA/UDMH is higher than IRFNA/MMH, which results in a slightly higher bulk density. The higher bulk density is an advantage because it allows smaller tanks, thus less system weight.

The characteristics of hydrazine as a monopropellant are also shown, and its freezing point falls far short of meeting the 0°F requirement. Based mainly on this fact, hydrazine was dropped from further consideration. A preliminary propulsion system reliability analysis, appendix B, indicated that the reliability of the mono and bipropellant systems were equal.

2. Thrust Chamber Selection

With the propellant selection made in favor of IRFNA/UDMH, the next propulsion system parameter studied was the thrust chamber. The first decision made was the selection of thrust level. The vehicle requirements limited the minimum thrust level at above 20 pounds and the maximum thrust level that would be compatible with the minimum vehicle ΔV requirement.

TABLE 31

PROPELLANT CHARACTERISTICS

Propellant Combination		Performance Characteristics					
Oxidizer	Fuel	Freezing Point °F	Boiling Point °F	O/F	δ gm/cc^3 77°F	Theoretical I_{sp}	Actual I_{sp}*
N_2O_4	---	12	70	---	1.43	---	---
	MMH	-63	189	1.6	0.87	330	288
	50/50/ N_2H_4/ UDMH	18	170	1.6	0.90	334	292
	UDMH	-72	146	2.4	0.78	328	287
IRFNA	---	-56	148	---	1.54	---	---
	MMH	-63	189	1.6	0.87	307	269
	UDMH	-72	146	2.5	0.78	316	280
MON (10 percent NO)	---	0	50	---	1.43	---	---
	UDMH	-72	146	2.6	0.78	328	287
	N_2H_4 Monopropellant	35	236	---	1.00	---	235

*Assumed - Eff. Nozzle - 94 percent of Shifting C_F.

Eff. C* - 93 percent of Shifting C*.

RE-ORDER No. 64-534

198

This requirement can be met with minimum impulse bit, but this in turn is related directly to thrust level. Therefore, because of this fact it was desirable to have a low thrust level engine.

From inquiries to propulsion companies, it was determined that thrust chambers of the twenty-five-pound thrust level were a rather common development item. Because of the proposed program schedule, it was considered necessary to use components now under development. Based on the above considerations, a thrust level of 25 pounds was selected.

There is a choice of either ablation- or radiation-cooled thrust chambers, and a radiation-cooled chamber was selected. This selection was based on several points. The radiation-cooled chamber would weigh less, which in itself is not a significant system weight reduction, but along with other factors is an advantage. Other features are 1) the engine installation is such that radiation to the vehicle is not a problem; thus an ablative chamber is not reuqired. 2) Ablative thrust chambers are still an unknown quantity from an operational view point and especially in the area of long space storage after firing and then having to be fired again, 3) The Agena vehicle has been using radiation-cooled thrust chambers in this size for years without difficulty.

3. Propellant Expulsion Concept Selection

A propulsion system for a vehicle of the type being considered requires some method of positive propellant expulsion; therefore, various concepts were considered. Because the propellants selected have freezing points as low as -56°F, and the tanks will be exposed to such temperatures it is necessary that the expulsion concept operate at this temperature. The only bladder concepts that are compatible with these propellants are the TFE-FEP composite material bladders. Cycle life at even 30°F has been a real problem, thus bladders were dropped as not being feasible

Tanks with metal diaphragms and bellows are under development. The latter has a very large weight penalty and the other has a cycle life limitation of one. This limited cycle life is considered by most to be unsatisfactory for application of this type because of system checkout requirements. Based on the above reasoning, it was decided not to use either concept.

One positive expulsion concept that has had considerable study by propulsion companies and NASA Lewis during the last two years is surface tension baffles. Most of the work has been done with small tanks, and the tanks required for this application are also small, so it is felt that the data obtained to date is very applicable. In addition, Bell Aerosystems has a contract from the Air Force to develop and determine performance of a 10-inch-diameter tank using surface tension baffles for propellant expulsion. Preliminary

vehicle designs indicate that the propellant tanks would be approximately ten inches in diameter. Because of the work being done on the surface tension concept and its size similarity, it was decided to use this concept for propulsion system propellant expulsion.

4. System Valve Selection

The last major component of the propulsion system to be considered was the control valves. Because the number of engine firings was limited to three, duplicate valving was considered, along with solenoid valves. If duplicate valving was used for each firing, then explosive-actuated valves could be used. By pairing a normally open and normally closed explosive valve in series, the propellant flow could be started and stopped upon electrical signal. Explosive valves were used in the Mariner flight and are planned for the other Mariner flights, so the concept is proven. There is less chance for leakage on valve closing with the explosive valve than a solenoid valve; thus considering the long flight time, it was determined that the explosive valve would result in the most reliable system. There was no apparent weight advantage to the solenoid valve, because of the fewer required; therefore, the explosive valve was selected for all signal-actuated valves.

5. Pressurization Gas Selection

Nitrogen was selected as the pressurizing gas. Because the total weight of nitrogen was less than three pounds, it was felt that the weight saving by going to helium does not offset the possibility of higher leakage. To achieve higher reliability it was decided to use nitrogen as the pressurizing gas.

6. System Installation Concept

After the propulsion system concept was determined, it was found that it would be compatible with the vehicle if it was a prepackaged system. A prepackaged system concept has many advantages over other approaches in the area of reliability and simplicity. Therefore, it was decided to make a prepackaged propulsion system, and the propellant loading could take place in the ground servicing hanger. It should be further noted that the propellants chosen are being used in present prepackaged systems.

7. Propulsion System Schematic

A schematic of the propulsion system is shown in figure 84. The explosive valve package shown consists of three normally open and three normally closed valves, one of each type in series for each firing. There is a package upstream of each propellant tank, because the propellants are

RE-ORDER No. 64-524

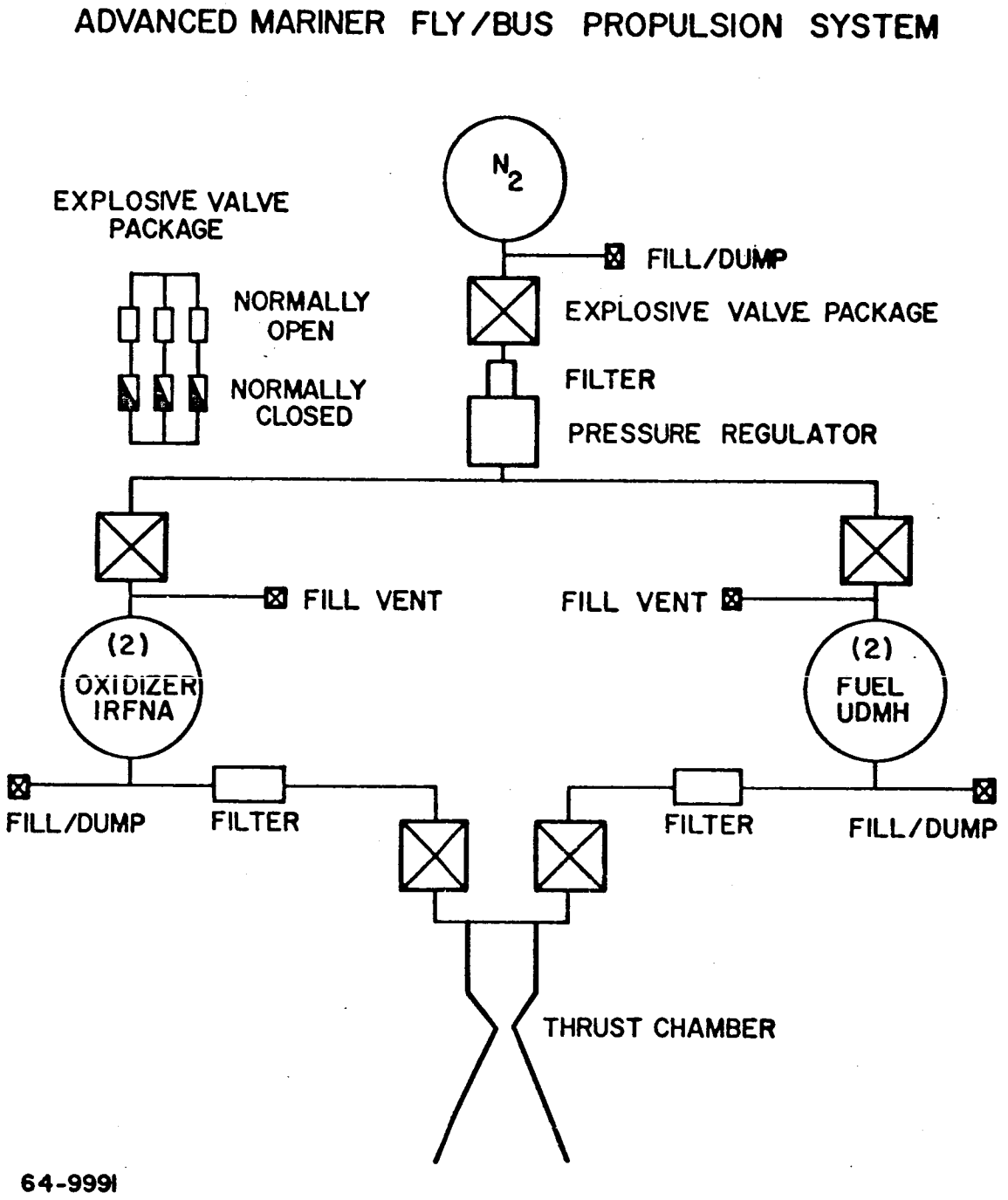

Figure 84 SCHEMATIC OF FLYBY/BUS PROPULSION SYSTEM

201

hypergolic and it is necessary to prevent them from mixing. Some systems use check valves, but it is felt that the positive shutoff is much more reliable with explosive valves. Also if the explosive valve upstream of the regulator did happen to leak internally, the valves upstream of the propellant tanks would prevent the tanks from being overpressured. The explosive valves are also used in place of a thrust chamber bipropellant solenoid valve or valves. No trouble is expected with starting, as the propellant lead is not critical with the propellants being used.

The entire plumbing would have welded joints, and the manual valves would have sealing caps in addition to valve shutoff after the system was filled and pressurized.

As noted in the schematic the system consists of four propellant tanks. Four tanks made for better system packaging within the bus. This more efficient packaging with four tanks was due to the bus height. Becuase four tanks were required, they were placed such that any uneven propellant useage due to mixture ratio shifts would not effect C. G. shift.

8. Propulsion System Design

The flyby/bus propulsion system performance and design characteristics are shown in table 32, and a system weight breakdown in table 33.

TABLE 32

CHARACTERISTICS OF FLYBY/BUS PROPULSION SYSTEM

Performance Characteristics:	
Total Impulse	26,000 lb-sec
Specific Impulse	280 sec.
Propellants	IRFNA/UDMH
Operational Temperature Range	-56°F to +146°F
Start/Burn Periods	3
Thrust Level	25 pounds
Design Characteristics:	
Packaging	Prepackaged
Mass Fraction	0.7
Expulsion Concept	Surface Tension Baffles
Pressurization System	Nitrogen
Mixture Ratio	2.5
Thrust Chamber Cooling	Radiation

RE-ORDER No. 64-524

TABLE 33

PROPULSION SYSTEM WEIGHT BREAKDOWN

Total Loaded System Weight		133.0 pounds
Dry Weight		33.0
Thrust Chamber	2.1	
Explosive Valves (30)	8.4	
N_L Regulator	1.2	
Filters (3)	0.6	
Oxidizer Tanks (2)	7.6	
Fuel Tanks (2)	6.4	
Nitrogen Tank	2.7	
Fill and Vent Valves (5)	2.0	
Plumbing	2.0	
Residuals		7.0
Nitrogen	2.4	
Propellant	4.6	
Usable Propellant		93.0
IRFNA	66.4	
UDMH	26.6	

204

RE-ORDER No. 64-524

7.0 STABILIZATION AND CONTROL SYSTEM

7.1 CHARACTERISTICS OF SELECTED SYSTEM

The characteristics of several attitude control system configurations have been studied in order to define a conceptual design which achieves the desired mission objectives. These objectives include the nulling of initial body rates after separation of the flyby bus from the launch vehicle, holding a sun-Canopus reference attitude throughout the mission, reorienting when required for velocity changes and lander separation, and holding the gyro reference attitude during main engine burn periods.

Through parametric evaluation, it has been possible to select means for attitude and thrust vector control and to establish the operational requirements on the conceptual design which are listed in table 34.

The control system configuration chosen for the conceptual design is compatible with flyby bus system constraints and reliable over long mission times required for the Earch-Mars transfer trajectory. There are four major modes of operation for the ACS, as follows:

1. Acquisition Modes
2. Transit Cruise Mode
3. Orientation Command Mode
4. Thrusting Mode

The first mode is further subdivided into a sun-acquire mode and a Canopus-acquire mode. The conceptual design is built around a cold gas reaction system. Nitrogen jets are used for vehicle attitude control during all phases of the mission. A total of 12 gas jets, 4 per axis, each having a thrust level of 0.01 pound, provide torque couples for pitch, yaw, and roll rotation in either direction during the acquisition, transit cruise, and orientation modes of operation. Eight gas jets, two for pitch, two for yaw, and four for roll, each having a thrust level of 0.1 pound, are used for thrust vector control during the thrusting mode of operation. Performance in each major mode is described in table 35. The components used during each mode are listed in table 36.

During the transit cruise mode of operation, a vehicle-centered coordinate system will be established. The positive (+) Z roll axis of the vehicle will coincide with e_3, the vehicle-sun line. The posi[illegible] (+) Y pitch axis will lie long e_2, normal to the vehicle-sun-Canopus plane, and the positive (+) X yaw axis will lie in the vehicle-sun-Canopus plane, along e_1 and normal to the vehicle-sun line. Figure 85 illustrates the coordinate system.

205

Expressed vectorially,

$$e_3 = \underline{1}_{vs}$$

$$e_2 = e_3 \times \underline{1}_{vc}$$

$$e_1 = e_2 \times e_3$$

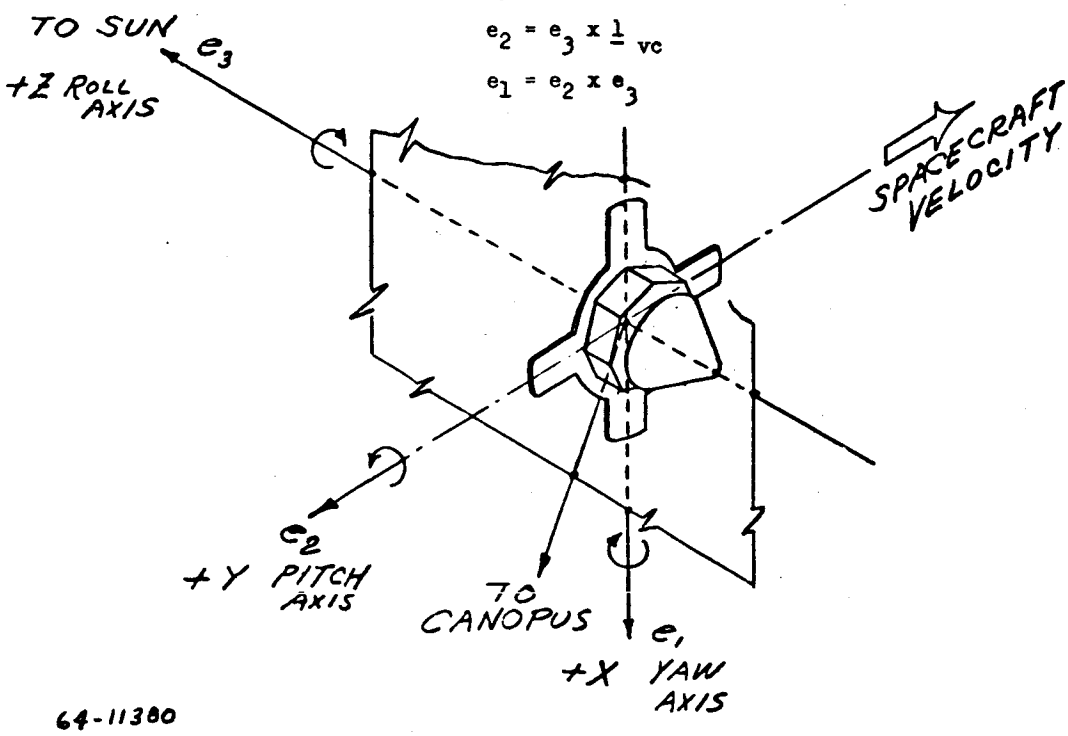

Figure 85 VEHICLE-CENTERED COORDINATE SYSTEM

206

TABLE 34

OPERATIONAL REQUIREMENTS

Parameter	Symbol	Units	Pitch	Yaw	Roll
Moment of Inertia (cruise)	I	slug-ft^2	206	283	284
Moment of Inertia (post lander separation)	I	slug-ft^2	85	55	125
Reaction System Moment Arm	r	feet	3.75	3.75	3.75
Thrust	F	lb/jet	0.01	0.01	0.01
Limit Cycle Amplitude	θ_{LC}	degrees	0.1	0.1	0.1
Jet on Time	Δt	seconds	0.01	0.01	0.1
Initial Separation Rates		deg/sec/ axis	3	3	3
Orientation Rate		deg/sec	0.5	0.5	0.5
Perturbing Momentum Flux	$\frac{QH}{r}$	ft-lb-sec day	---	2.0	2.0
Angular acceleration (thrust on)	a	millirad/ sec^2	0.364	0.265	0.264

TABLE 34 (Concl'd)

Parameter	Symbol	Units	Value
Weight (cruise)	W	pounds	1549
Weight (post lander separation)	W	pounds	706
Cruise mission time	L_1	days	280
Fly by mission time	L_2	days	20
Science platform and antenna inertia factor	---	%	5

In addition, there are the following orientations:

1. Cruise: two ΔV corrections, and one lander separation

2. Post lander separation: one lander separation and one retro thrust

TABLE 35

DESCRIPTION OF ACS MODES

Mode	When Used	Description	Remarks
Sun-Aquire Mode	For initial acquisition of the sun and for acquisition of the sun after a disturbance or occultation.	Acquisition sun sensor sends pitch and yaw error signals to ACS control electronics to actuate reaction jets. Gyros in rate mode for damping.	Steady-state angular rates are set by sun sensor and gyro gains.
Canopus-Acquire Mode	For initial acquisition of Canopus and for acquisition of Canopus after a roll disturbance or occultation.	A constant roll rate is commanded until brightness discriminator commands the Canopus tracker into the roll loop as a reference null. Roll gyro in rate mode for damping, as above.	Steady-state rate, $\dot{\phi}$, for search is preset.
Transit Cruise	For major portion of mission (a quiescent mode).	Vehicle oriented to sun-Canopus frame and solar panels normal to Sun line. Gyros off. Derived rate for damping in all three channels	Limit cycle amplitude examined parametrically, $\Delta\dot{\theta}$'s governed by minimum impulse bit.
Orientation Command Mode	For special maneuvers, such as midcourse velocity correction or Capsule separation.	Use gyros for attitude reference (integrate command rate) and use either lead-leg network or integrated "jet-on" signal for damping. Command rate determined by current to gyro torquer. Command roll first. Then pitch (or yaw), then command reverse maneuvers. If sun and/or Canopus are not required, then go into appropriate Acquisition Mode.	This mode is used to either reorient the vehicle to any arbitrary attitude or to hold the vehicle at any arbitrary attitude.
Thrust Mode	Used only during main engine burn.	Use gyros for attitude reference with zero input commands. Attitude will be maintained with auxiliary reaction jets.	Used only to command a constant attitude during engine burn, i.e., $\dot{\theta}_c = 0$

RE-ORDER No. 64-524

209

TABLE 36

ACS COMPONENTS USED DURING EACH MODE OF OPERATION

Mode	Components								
	Acquisition Sun Sensor	Primary Sun Sensor	Canopus Tracker	Gyros			Control Electronics	Reaction Control System	Auxiliary Reaction Sys. For Thrust Vector Control
				Pitch	Yaw	Roll			
Sun-Acquire Mode	V	-	-	R	R	R	V	V	-
Canopus-Acquire Mode	-	V	V	R	R	R	V	V	-
Transit Cruise Mode	-	V	V	-	-	-	V	V	-
Orientation Command Mode	-	-	-	I	I	I	V	V	-
Thrusting Mode	-	-	-	I	I	I	V	-	V

V = system actively used
- = system not actively used
R = rate mode
I = integrate mode

210

RE-ORDER No. 64-524

7.2 RATING SYSTEM FOR DESIGN ALTERNATIVES

To evaluate the various stabilization and control system alternatives under parametric study, the matrixes presented in tables 37 and 38 were devised. Among the design alternatives considered were cold gas, subliming solid, and cap pistol reaction controls in the basic ACS used for the acquisition, transit cruise, and orientation modes of operation. For thrust vector control during the thrusting mode of operation, jet vanes, gimbaling, and auxiliary reaction jet TVC systems were rated. The trade-off categories which are listed in the tables reflect the feasibility criteria as well as the system design and development areas which were considered. A rating system from 1 to 10 was used in which a "1" was given to the best feature as evaluated in any given category. Each remaining concept was then rated in relation to the best or standard concept with higher numbers reflecting not only less desirable but also less feasible systems. The criteria which were considered included those which could only be evaluated qualitatively at the time. An RMS average was computed and the relative rating based on this average.

1. Rating Used for Basic Cruise Mode ACS Design Selection

a. Vehicle Interface

Areas considered here include mating the reaction system, packaging requirements, prelaunch and launch operational procedures, and the effect of control system dynamics on vehicle stability.

b. System Weight

The total system weight including nozzles, regulators, supply system, etc., to deliver the specified total impulse is the criterion. Relative system weight, as illustrated in figure 86, is determined from the following empirical relationships:

Cold Gas

$$W = 8 \text{ lb.} + (0.034)\, I_t$$

Subliming Solid

$$W = 7 \text{ lb.} + (0.013)\, I_t$$

Cap Pistol

$$W = 9 \text{ lb.} + (0.02)\, I_t$$

where I_t equals the total required impulse in pound seconds.

RE-ORDER No. 64-52

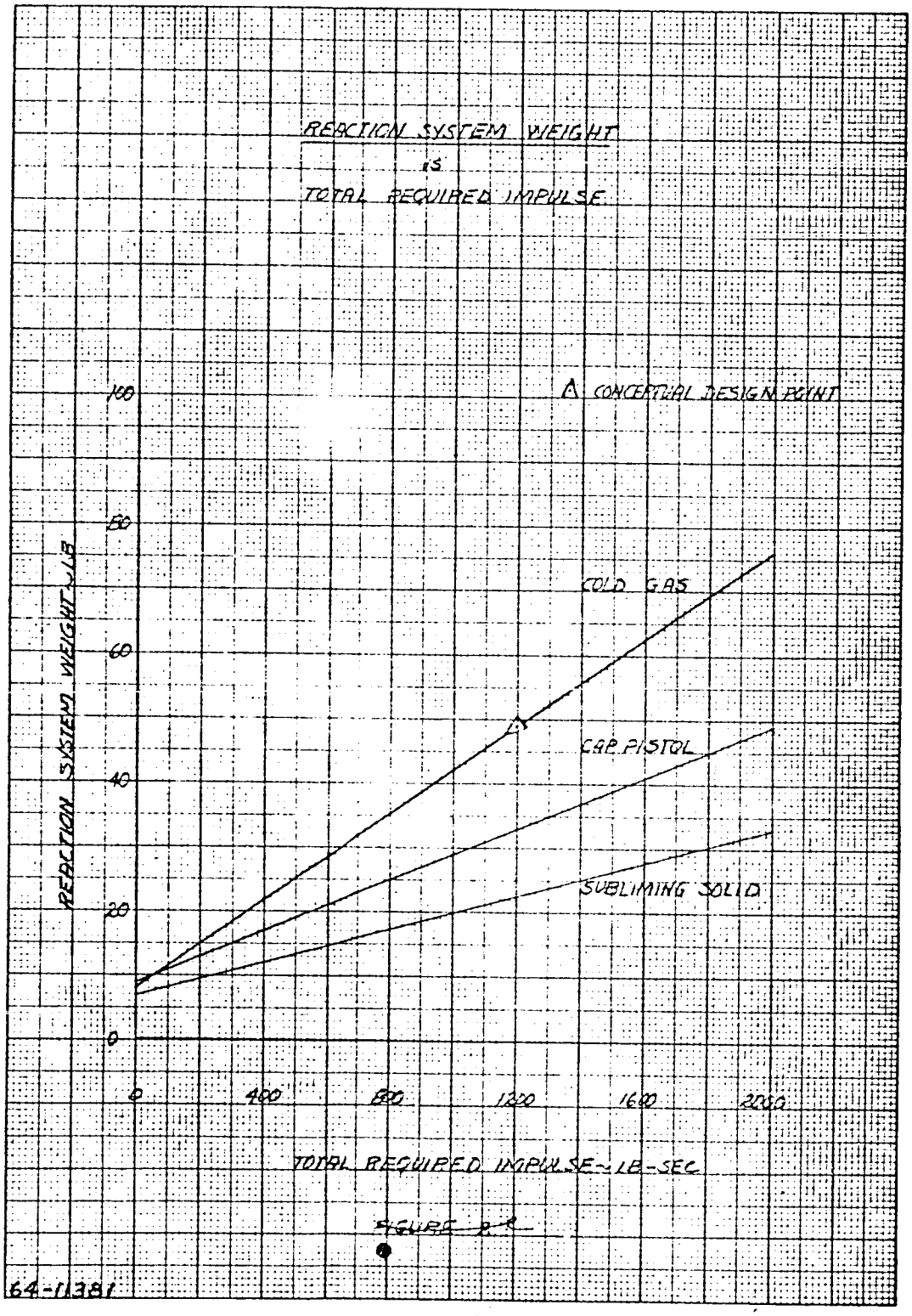

Figure 86 REACTION SYSTEM WEIGHT AS A FUNCTION OF TOTAL IMPULSE

212

TABLE 37

MATRIX USED FOR RATING ACS REACTION CONTROL CONCEPTS

Type of Reaction Control System	Vehicle Interface	System Weight	Power Consumption	Controllability	System Complexity	Reliability	Operating History	Development Time	Development Cost	RMS Average
Cold Gas	1	3	1	1	2	2	1	1	1	1.6
Subliming Solid	4	1	1	2	1	1	5	2	4	2.8
Cap Pistol	3	2	3	3	3	3	5	3	4	3.3

RE-ORDER No. 64-524

RE-ORDER No. 64-524

TABLE 38

MATRIX USED FOR RATING TVC SYSTEM

TVC Parameters	Reaction Jets	Vanes	Gimbaling
Rocket Motor Interface	1	3	2
Vehicle Interface	2	1	3
Reliability	2	1	2
Operating History	1	3	2
System Weight	3	2	1
Power Consumption	1	2	3
System Complexity	2	1	2
Development Time	1	3	2
Development Cost	1	3	2
RMS Average	1.7	2.3	2.2

214

c. Power Consumption

Electronic control logic would be similar for each reaction control system considered, and therefore is not included in the power consumption rating for each system.

Because of the low operating pressure in the subliming system, valve driving power will be somewhat lower than that of a cold gas system. However, the diffenence between the two is negligible, both systems requiring on the order of three watts per solenoid.

The power consumption of a cap pistol system is somewhat higher. Present systems require a 17-watt stepping motor to position each charge and incur a 5 microsecond ignition delay through a 0.6-ohm igniter.

d. Controllability

Areas considered here included switching from one operational mode to another, minimum on-time, rise time, etc. For example, the impulse bit from each charge in the cap-pistol system is invariant, that from a cold gas system is dependent upon regulator operation and therefore subject to fluctuations in pressure and temperature, whereas that of a subliming solid is more loosely controlled because of thrust drop-off due to tank ambient temperature and variation of adiabatic sublimation of propellant with nozzle on-time.

e. Complexity

Here one considers the ease with which the various control system components could be integrated. For example, the need for a pressure regulator is eliminated in a subliming solid system; however, a passive thermally controlled orifice may be necessary to otherwise regulate propellant flow. Although a lighter propellant tank might be used because of lower operating pressures, the tank might have to be made larger in order to store a certain amount of gaseous nitrogen for initial acquisition maneuvers where high propellant flows are required to cancel separation rates. In the case of a cap pistol system, no fluid problems would exist.

f. Reliability

The ratings under this heading are based in part on reliability studies reported in appendix B. Reliability, although closely tied to system complexity, may reflect a different rating because of such factors as the nature of the valves used in cold gas and subliming solid systems, necessity of filters in a subliming system to prevent condensation of

the solid and possible clogging of lines, and differences in system mechanization, i. e., necessity of a stepper motor and magazine in a cap pistol system.

g. Operating History

The operating history of cold gas systems is well established, as evidenced by the developed and proven system to be used on Mariner C. Although no subliming solid or cap pistol system has yet been flown, they now are in an advanced state of development. NASA Goddard has investigated a subliming solid system for use on the Advanced Technological Satellite, and has completed environmental testing of a cap pistol system which is now on PFRT for the TIROS weather satellite.

h. Development Time

The three systems require a development time of six months to one year, depending on the level of effort made. First cold gas, then subliming solid and cap pistol systems could be developed for the Advanced Mariner in respective time intervals.

i. Development Cost

From the vendor's estimate, a subliming solid system could be developed for the spacecraft for $0.5 to $1.5 million. This figure would extend through production of flight items. Cap pistol and cold gas systems are rated respectively from the standpoint of present development status.

2. Rating Used for TVC Design Selection

Jet vanes, gimbaling, secondary injection, and auxiliary reaction jet thrust vector control (TVC) concepts were studied as means of maintaining inertial orientation during motor firing periods. A trade-off among the following categories was made in order to reflect the feasibility criteria as well as the system design and development areas which were considered. Under the assumption that a bipropellant engine is used, reaction jets are best for TVC. If, however, a monopropellant was used, jet vanes would be recommended.

a. Rocket Motor Interface

The prime consideration in the selection of a TVC system will be the type of rocket propulsion system that is chosen for the spacecraft. For example, jet vanes are ideally suited to mono-hydrazine single chamber motors, which develop inherently low flame temperatures; however, they have not been developed for use with liquid bipropellants. Rocket motors incorporating ablative chambers are more compatible

with gimbaled arrangements than are the radiation cooled types because they present less difficulty with hot spot problems due to actuator attachments. Secondary injection systems thus far have been used on large rockets in the booster category, and preliminary investigation thus far has ruled out the application of these systems on the Advanced Mariner. The major interface with the basic propulsion system resulting from the use of an auxiliary reaction control system for TVC would be in the possible sharing of propellant tankage.

b. Vehicle Interface

Areas considered here include mating the system, packaging requirements, prelaunch and launch operational procedures, and the effect of control system dynamics on vehicle stability.

c. Reliability

The ratings under this heading are based in part on reliability studies reported in appendix B. The reliability of reaction jet and gimbaled systems were rated equally whereas the jet vanes were given a preferable rating on the basis of monopropellant operation.

d. Operating History

Reaction jets and gimbaling are proven systems as are jet vanes used with a monopropellant. Jet vanes for use with bipropellants have not been developed.

e. System Weight

The reaction system weights for three axis thrust vector control, illustrated in figure 87, are determined from the empirical expressions,

$$W = 11 + 0.012\, I_T \text{ for hot gas}$$

and

$$W = 8 + 0.1014\, I_T \text{ for cold gas,}$$

where I_T equals the total required impulse in pound seconds.

Further design studies would be required to pin down the weight of specific systems, particularly the hot gas types, which might utilize hypergolic bipropellants or monopropellants such as H_2O_2 of Hydraxine. The relative weights of the jet vane and gimbaled systems were established on the basis of the parametric design information.

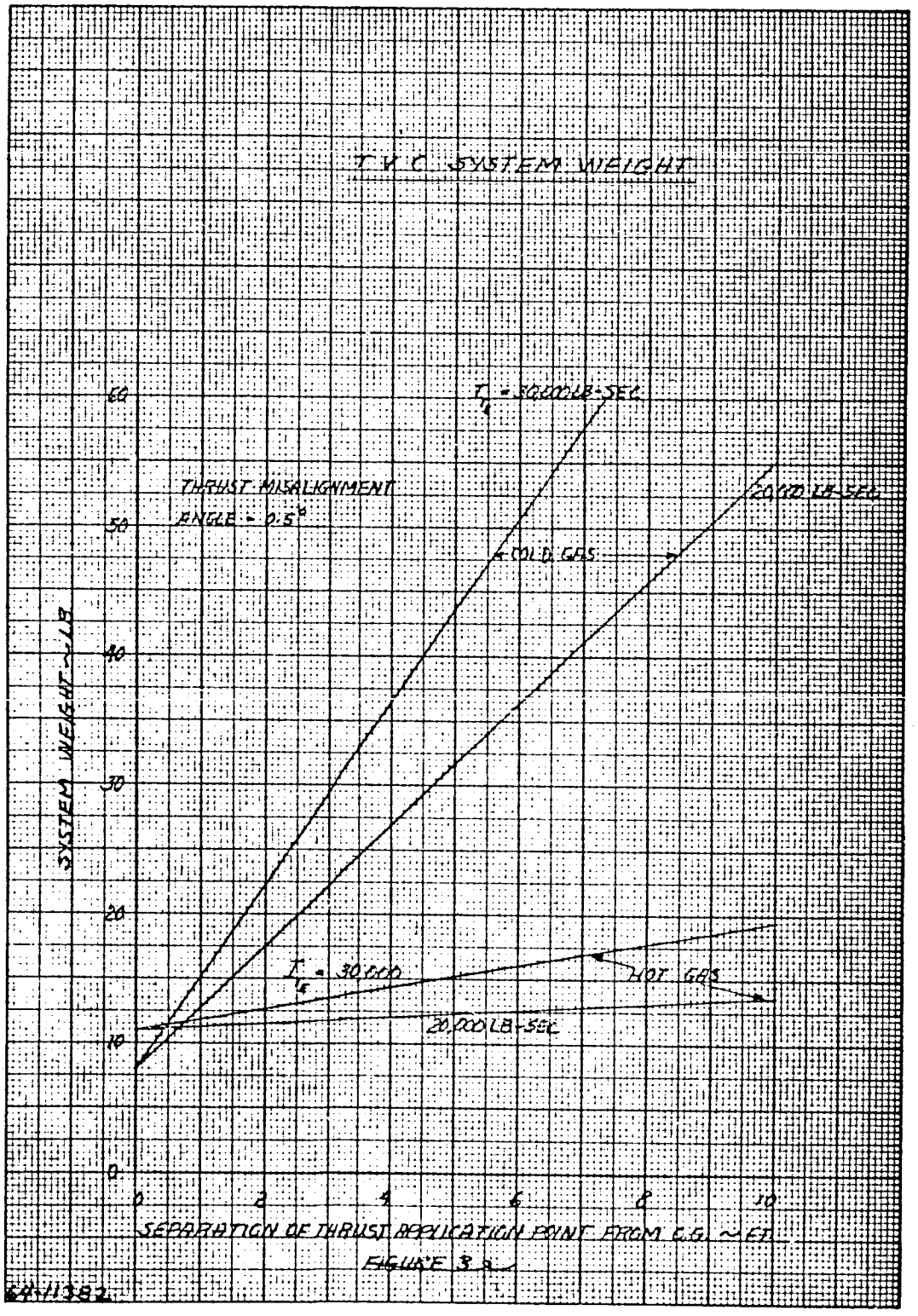

Figure 87 THRUST VECTOR CONTROL SYSTEM WEIGHT

f. Power Consumption

Power consumption, as well as the relative system weight estimate, was based on studies of the thrust vector control system. The analyses yielded maximum control thrust deflections, angular rates, and angular accelerations in response to a unit step in spacecraft angular rate. The gimbaled system consumed appreciable power because of the higher inertia and torque loads presented to the control actuator. Torque input power for jet vanes was considerably less. By comparison, the reaction jets merited the highest rating because of the relatively small amount of power required by the solenoid drivers.

g. System Complexity

The ratings given here were based on the ease with which the various TVC system components could be integrated with respect to other systems to be used on the spacecraft. Judgement of the merits of each system included a consideration of increased complexity in the case of poor interface with either the rocket motor or the spacecraft, and degree of complexity associated with the maintenance of a reasonable level of reliability.

h. Development Time and Cost

Note that similar ratings are given for development and cost efforts. Jet vanes have not been developed for bipropellant use, hence they are rated lowest. If a monopropellant was used, however, they would receive a "1".

7.3 IMPULSE REQUIREMENTS

1. Cruise Mode

In the determination of ACS impulse requirements, error torques due to reaction control system errors, including nozzle location errors, c.g., locaton errors, nozzle thrust angular misalignment, and nozzle thrust level variations, have been considered negligible. A study of these effects, as well as a general three-axis study of acquisition and limit cycle operation would be necessary to analyze cross-coupling effects between control axes and to evaluate single axis performce degradation. However, for the purposes of conceptual design, the cross-coupling effects can be shown to be safely negligible.

The Euler equations for the motion about each of the spacecraft axes can be written as:

$$I_x \dot{\omega}_x + (I_z - I_y)\,\omega_y \omega_z = M_x$$

$$I_y \dot{\omega}_y + (I_x - I_z)\,\omega_z \omega_x = M_y$$

$$I_z \dot{\omega}_z + (I_y - I_x)\,\omega_x \omega_y = M_z$$

The severity of cross-coupling in the attitude motions is dependent upon the inertia mis-match and the magnitude of the rates. The extent to which this cross-coupling will affect single-axis performance calculations can be estimated in terms of expected torques acting on the spacecraft. An examination of the Euler equations reveals that cross-coupling can be ignored if

$$\frac{I_x - I_z}{I_y} \quad \omega_z \ \omega_x \ << \ \frac{M_y}{I_y}$$

or

$$\frac{I_x - I_z}{M_y} \quad \omega_y \ \omega_x \ << \ 1 \ .$$

Using the value of M_y calculated as an approximate value for solar radiation torque, it can be noted that performance based on single-axis calculations will be adequate for the transit cruise mode where the inequality is satisfied. For the acquisition and orientation processes and post lander separation operations, where the inequality is not satisfied, single-axis calculations may be in error. These errors, however, will be minimized by the inclusion of a factor of safety in the following parametric analysis.

a. Initial Acquisition

The total impulse required to stabilize the initial separation rates is estimated by

$$\text{Impulse} = 2F \sum_{i=1}^{3} \frac{\dot{\theta}_i}{\bar{\theta}_i} = \sum_{i=1}^{3} \left(\frac{I}{r}\right)_i \dot{\theta}_i \qquad (1)$$

where

F = thrust for one jet

$\dot{\theta}$ = vehicle initial rate about thrust axis

$\ddot{\theta}$ = vehicle acceleration when a pair of jets are operating

I = vehicle moment of inertia

r = control moment arm

The initial acquisition is not completed until the vehicle has reoriented to the sunline Canopus-line attitude. For orientation, assuming one start/stop is required for each axis, then

$$\text{Impulse} = 2 \times 2F \sum_{i=1}^{3} \frac{\dot{\theta}_i}{\ddot{\theta}_i} \tag{2}$$

The total impulse for initial acquisition is obtained by adding the results of equations (1) and (2), which are plotted in figure 88.

b. Limit Cycling

Limit cycle rates and periods are derived from

$$\dot{\theta}_{LC} = \frac{\Delta t}{2} \ddot{\theta} \tag{3}$$

and

$$\tau_{LC} = \frac{4}{60} \frac{\theta_{LC}}{\dot{\theta}_{LC}} \tag{4}$$

where

$\dot{\theta}_{LC}$ = limit cycle body rate (deg/sec)

$\ddot{\theta}$ = control torque acceleration (deg/sec^2)

θ_{LC} = limit cycle amplitude (degrees)

Δt = jet "on" time (seconds)

τ_{LC} = limit cycle period (minutes)

RE-ORDER No. 64-524

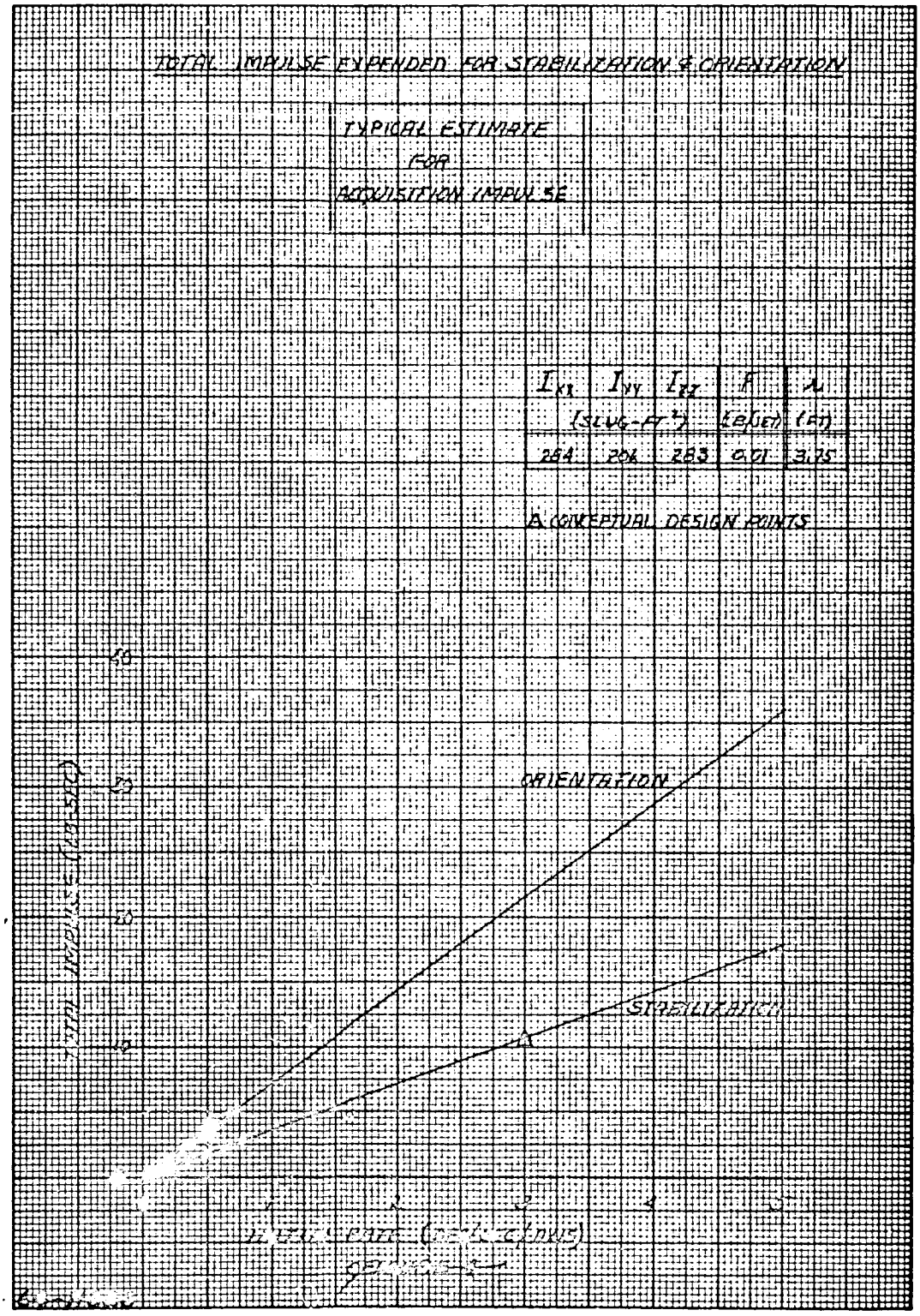

Figure 88 TOTAL IMPULSE EXPENDED FOR STABILIZATION AND ORIENTATION

222

For no disturbance torques the total impulse per axis is found from

$$I_T = (\text{Mission Duration}) \times (\text{Duty Cycle}) \times 2F \tag{5}$$

where the duty cycle $= \dfrac{2\,\Delta t}{60\,\tau_{LC}}$ sec/sec

To allow for the fact that the specific impulse will be lower during the limit cycle due to the effect of transient flow, etc., I_T is modified by the factor $\dfrac{60}{35}$, i.e.

$$I_{T_{equiv}} = \frac{60}{35}\, I_T \tag{5}$$

By combining equations (3), (4), and (5) one obtains

$$I_{T_{LC}} = \frac{L\,r}{I\,\theta_{LC}}\,(F\,\Delta t)^2 \tag{7}$$

which is plotted in figures 89 and 90.

c. Solar Radiation Torques

The impulse required to null solar radiation pressure bias torques is strictly speaking not additive to the limit cycle. A conservative estimate for the total impulse expended during limit cycle can be obtained by such an addition, however, and is treated so herein.

The solar radiation pressure torque is calculated from

$$T_d = PA\,\Delta x \tag{8}$$

where

P = solar radiation pressure (lb. ft^2)

A = effective area (ft^2)

Δx = distance from c.p. to c.g. (feet)

then

$$I_T = 2\,\frac{L T_d}{r} \tag{9}$$

is the total impulse for two axes.

223

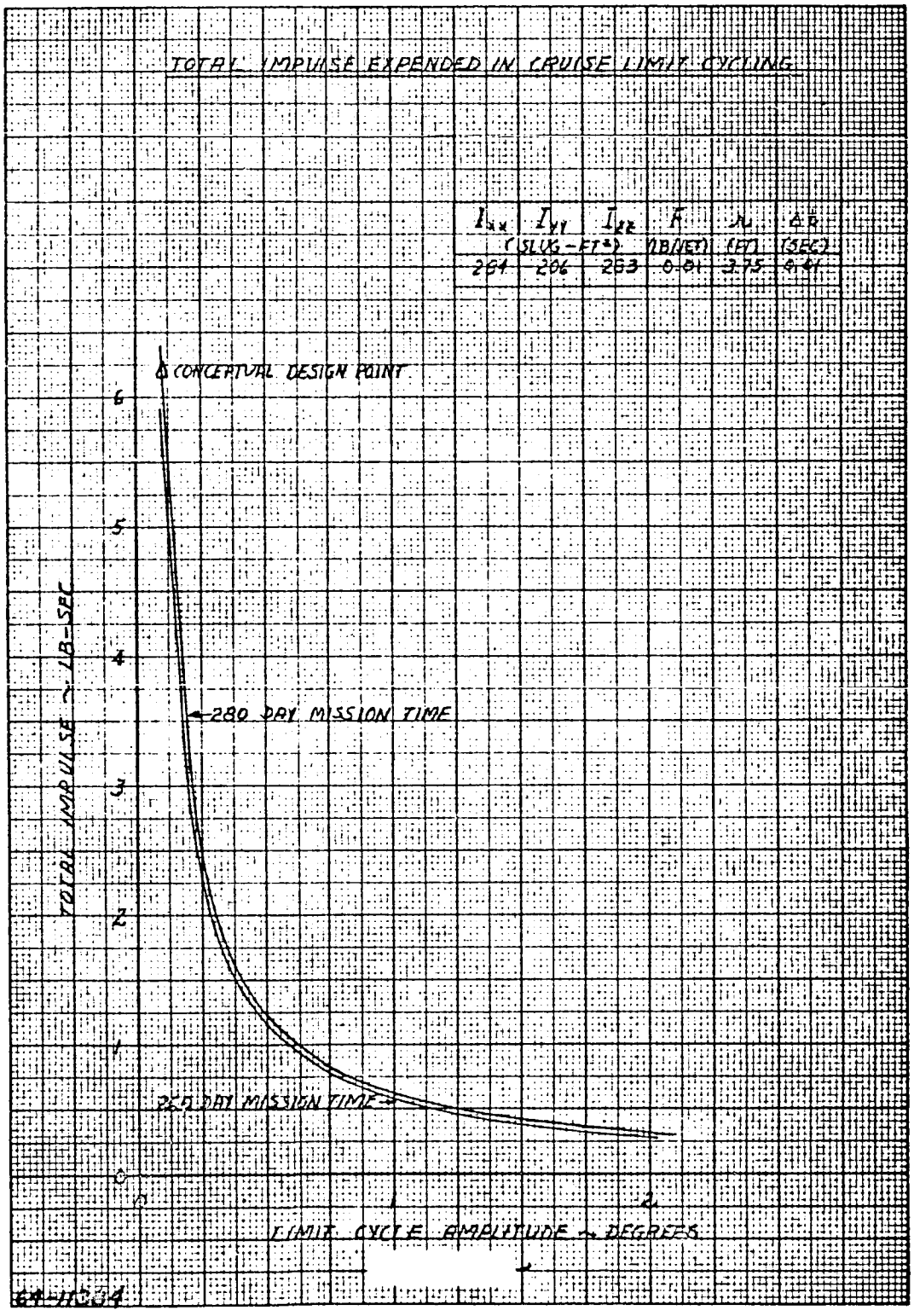

Figure 89 TOTAL IMPULSE EXPENDED IN CRUISE LIMIT CYCLING

224

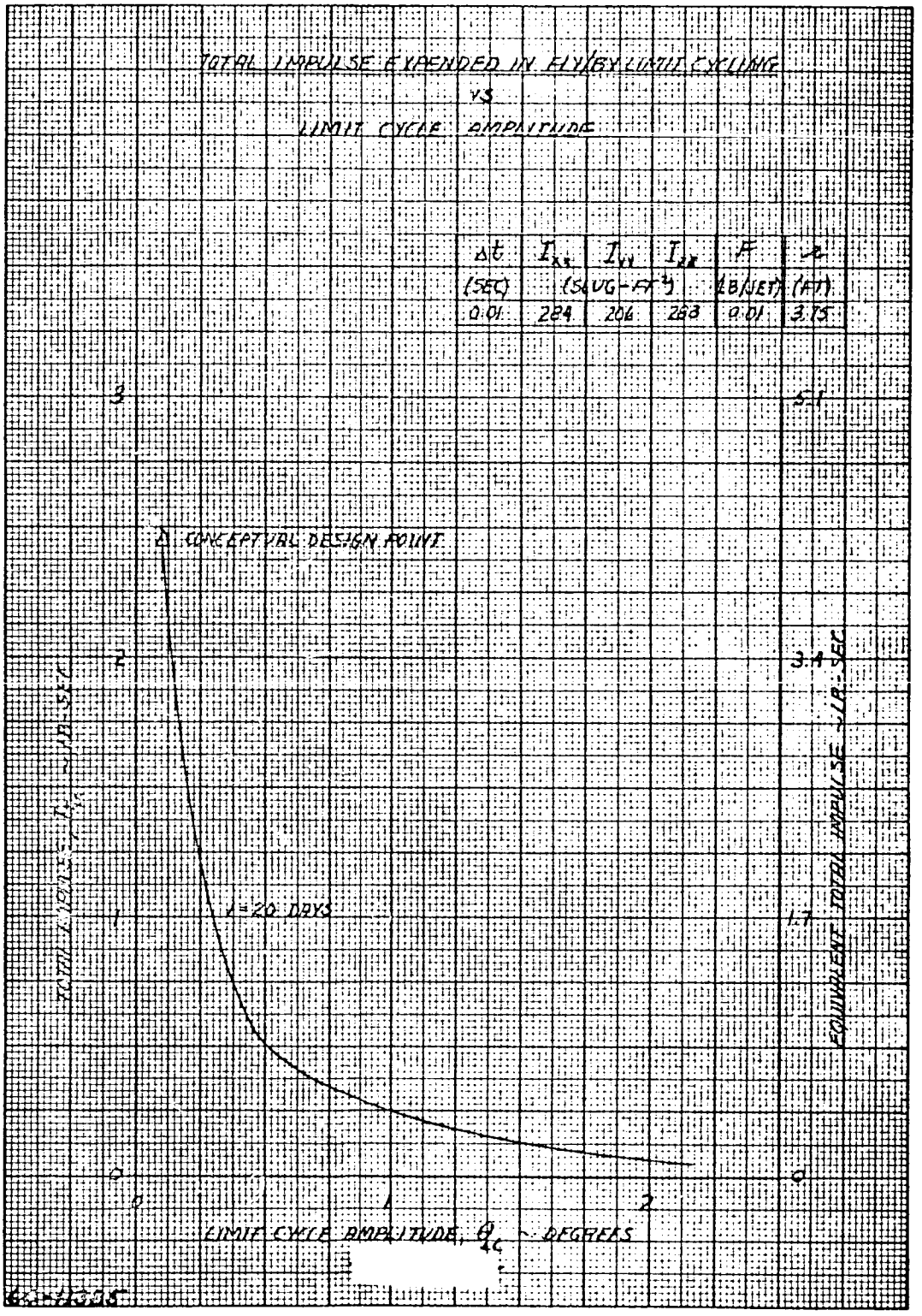

Figure 90 TOTAL IMPULSE EXPENDED IN FLYBY LIMIT CYCLING

d. Orientation

Each maneuver consists of an orientation about the pitch and yaw axes. The jet on-time is determined from

$$\Delta t = \frac{\dot{\theta}_{max}}{\bar{\theta}} \tag{10}$$

The impulse per maneuver is then

$$I_T = 2 \times [2 F t_{pitch} + 2 F t_{yaw}] \tag{11}$$

e. Meteroid Impacts

The angular momentum induced in the vehicle by meteorids per unit time is given by the parameter $\frac{QH}{r}$. The $\frac{H}{r}$ term represents the incoming angular momentum possessed by meteoroids (relative to the spacecraft), and the Q term is a "momentum multiplication factor" which has been determined by a detailed investigation of the high-speed impact process. The $\frac{H}{r}$ term in turn is composed of two parts. One part is the integrated mass per unit area which composes the highly directional meteoroid flux, multiplied by their average velocity. The other part is a function of spacecraft geometry and can be interpreted as a "static margin" (i.e., center-of-pressure to center-of-mass distance) of the vehicle's profile times the area presented to the meteoroid flux.

The Q term, the ratio of induced angular momentum to incoming, was found to be 36 using the most conservative assumptions. This large factor is brought about by the large amount of mass which is expelled from the vehicle when struck by a mereoroid which causes a crater.

The expression obtained using conservative meteoroid flux estimates is

$$\frac{QH}{r} = 0.04 \quad r \quad \Delta a \quad \frac{\text{ft lb/sec}}{\text{day}}$$

where r is the distance in feet to each element, Δa (ft^2), of the total area of the vehicle which is presented to the meteoroid flux. (This presented area is the projected profile of the spacecraft onto a plane normal to the ecliptic plane and containing the sun-line).

The vehicle will have a large perturbation in yaw, due to the fact that the center of mass is located in the bus while the center of pressure is located in the lander.

For the purpose of preliminary design estimates, it is adequate to use the triangular projected profile of the lander as Δa in the equation above and the distance between the center of mass of the vehicle and the centroid of the triangle as the distance r. The remainder of the spacecraft is distributed more or less symmetrically relative to the yaw axis.

Although the basic spacecraft profile is symmetric about the roll axis, there will be a perturbation about this axis due to the antenna.

The total required impulse can be found from

$$I_T = \left[\frac{QH}{r}\right] \frac{L}{t} \tag{12}$$

where

L = mission duration (days)

r = reaction jet moment arm (feet)

This expression is plotted in figures 91 and 92 for the cruise and flyby phases of the mission.

f. Capsule Separation Impulse Torques

The total impulse is given by

$$I_T = \frac{F\ \Delta t}{r} \ (\Delta x + \Delta y) \tag{13}$$

where

F = ejection force

Δt = duration

$\Delta x, \Delta y$ = c. p. to c. g. distances

r = moment arm

g. Science Platform and Antenna Inertia Torques

The magnitude of this impulse is taken to be a certain percentage of the other impulses. It is referred to as the science platform and antenna inertia factor. As a first estimate, this factor was assumed to be 5 percent of the impulse subtotal.

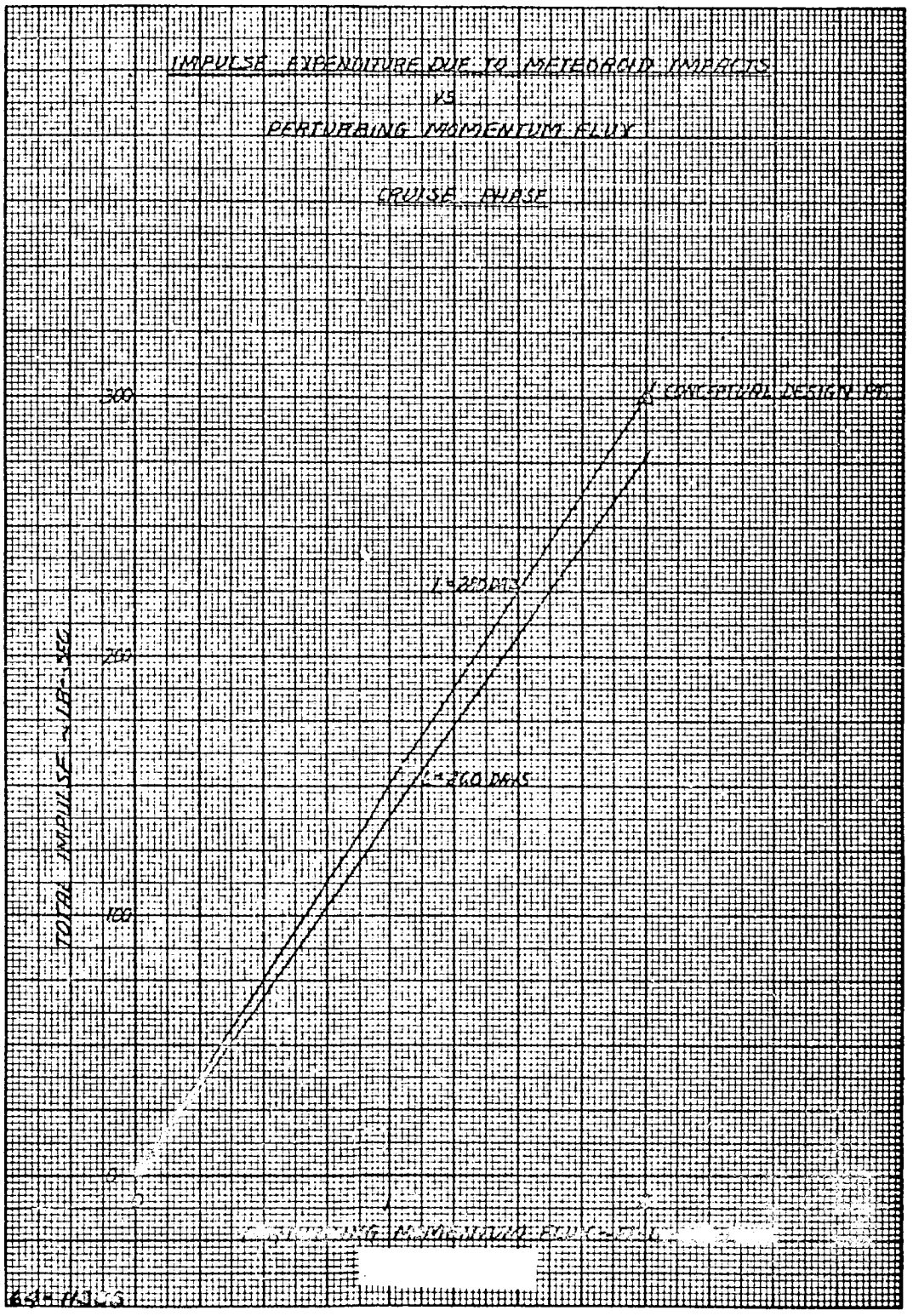

Figure 91 IMPULSE EXPENDITURE DUE TO METEOROID IMPACTS - CRUISE PHASE

228

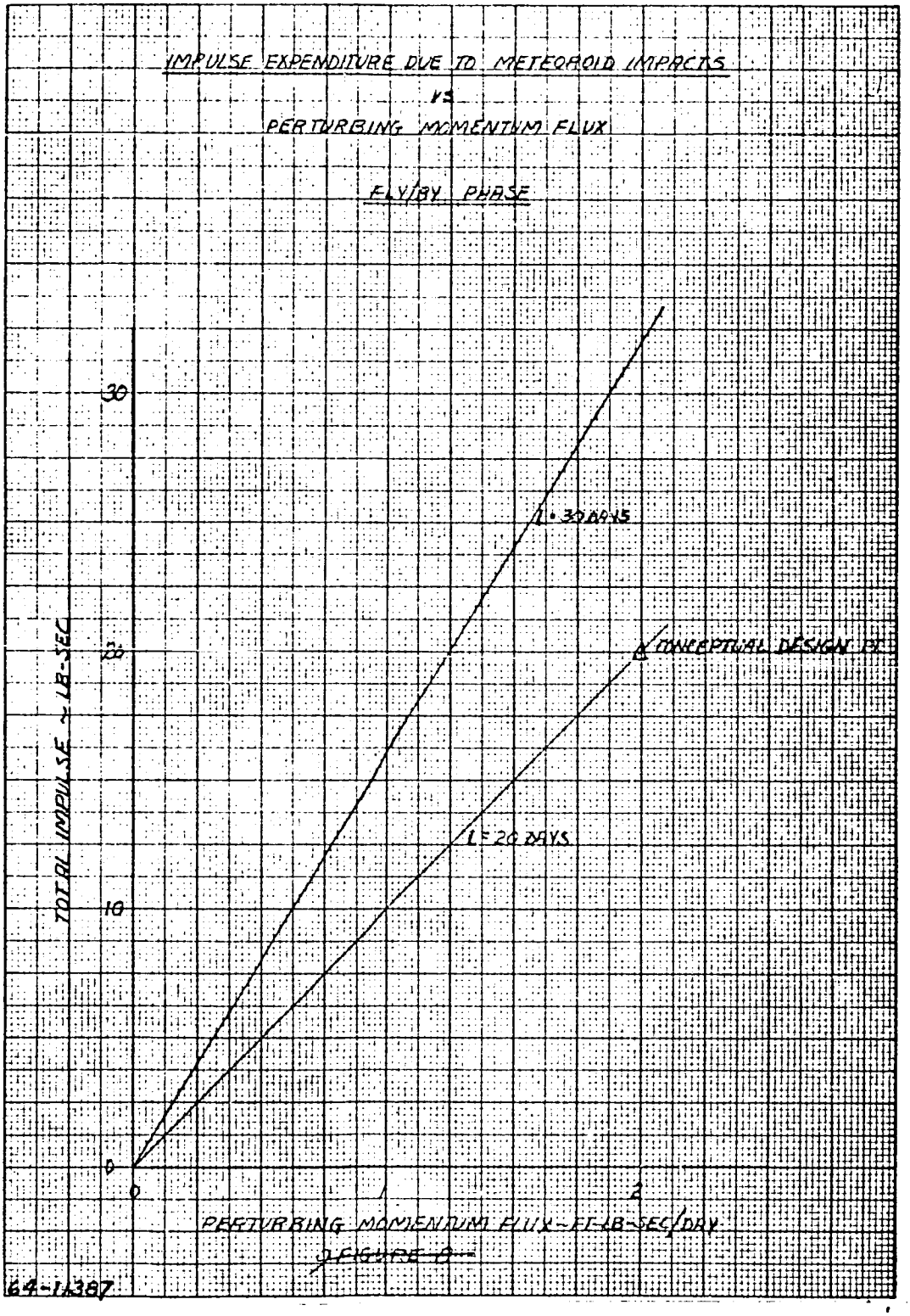

Figure 92 IMPULSE EXPENDITURE DUE TO METEOROID IMPACTS - FLYBY PHASE

h. Total Impulse Estimate

For the operational requirements of the Conceptual Design, the ACS total impulse estimated using the methods of this section is summarized in table 39.

TABLE 39

ACS TOTAL IMPULSE SUMMARY FOR CRUISE MODE ACS OPERATION

Mode	Impulse (lb-sec)
Initial Acquisition	10.9
Limit Cycling	13.0
Solar Torques	22.4
Orientations	12.7
Meteroid Torques	320
Capsule Separation Impulse Torques	1.0
Science Platform and Antenna Inertia Torques	20.3
Total	400.3 lb-sec

2. Maneuver Mode

The minimum control thrust curves of figure 93 are determined from

$$F_N = \frac{F_e \, l \sin \epsilon}{r}$$

where

F_N = control thrust

F_e = engine thrust

ϵ = thrust misalignment angle

l = separation of thrust application point from c. g.

r = control moment arm

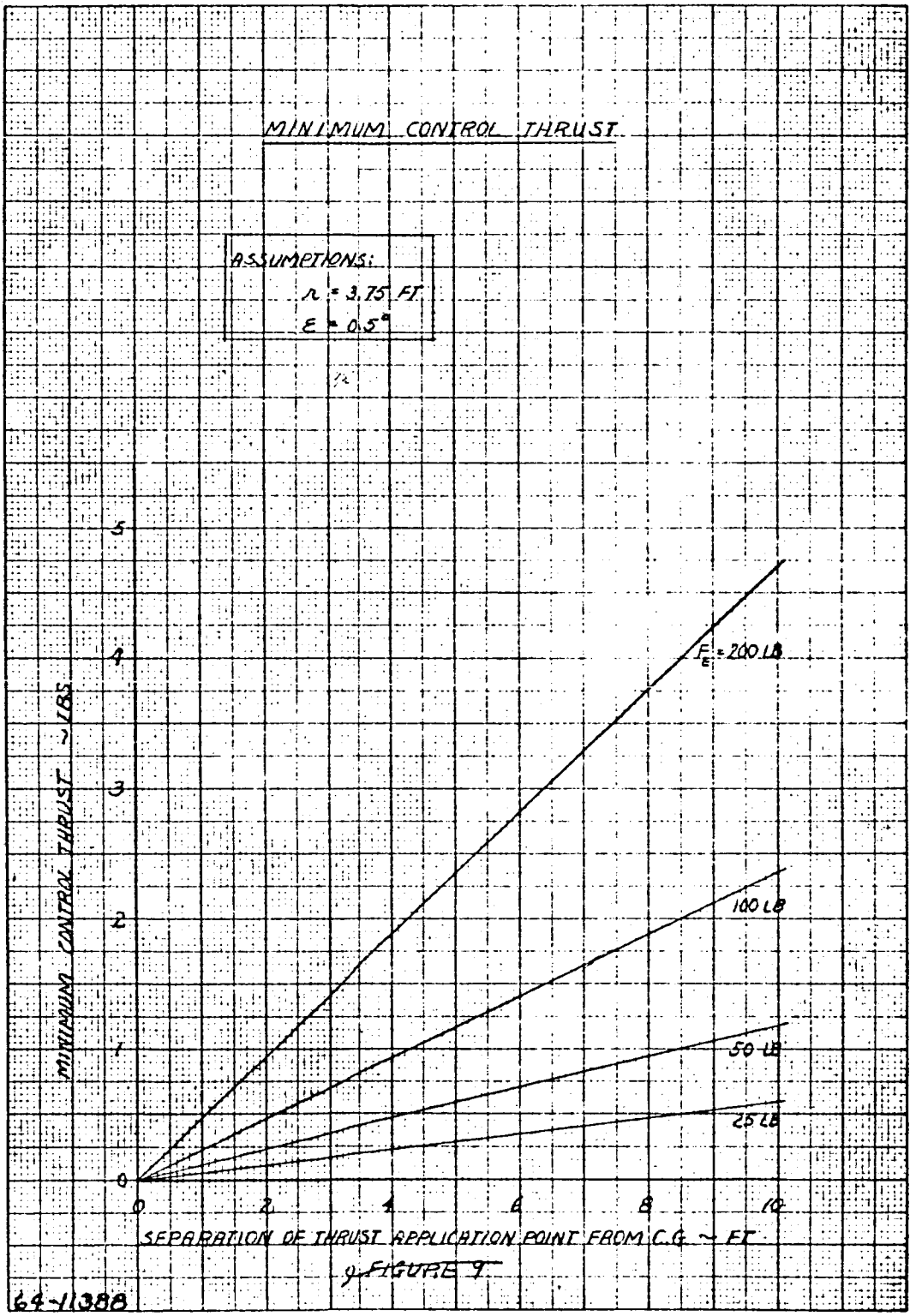

Figure 93 MINIMUM CONTROL THRUST

The total impulse required (per axis) is directly proportional to the magnitude of the unbalance, see figure 94, and is given by

$$I_T = I_{T_e} \frac{l \sin \epsilon}{r}$$

where

I_T = impulse required for control system (per axis)

I_{T_e} = total impulse of engine

7.4 SUBSYSTEM DESIGN

1. Major Components

The ACS consists of the following basic components as installed in the spacecraft: reaction system, gyro/electronics package, control electronics package, Canopus star tracker, coarse acquisition sun sensor, and limit cycle sun sensor. For the purpose of describing the ACS components, the actual physical grouping is ignored. Instead the ACS is regrouped and described in terms of common equipment as follows: sensors, reaction system, and electronics.

Typical functional diagrams for the ACS pitch axis during the acquisition, transit cruise, and orientation command modes, are illustrated in figures 95 through 97.

The major components used in the ACS and indicated on the diagrams are:

2. Sun Sensors

Two separate sun sensor units are used to provide sun acquisition without gimbals or complicated search maneuvers and to provide accurate sun reference attitude when the ACS is holding the vehicle roll axis parallel to the sun line. The sun sensor units are: (a) coarse acquisition sun sensor and (b) limit cycle sun sensor.

a. Coarse acquisition sun sensor

This sensor is used for initial alignment of the spacecraft roll axis to the sun line, and therefore has an unlimited field of view. It initiates pitch and yaw commands to the vehicle so that the field of view of the limit cycle sun sensor can capture the sun line.

The coarse acquistion sun sensor will give attitude indications of the Advanced Mariner spacecraft over a range of 360 degrees in pitch and

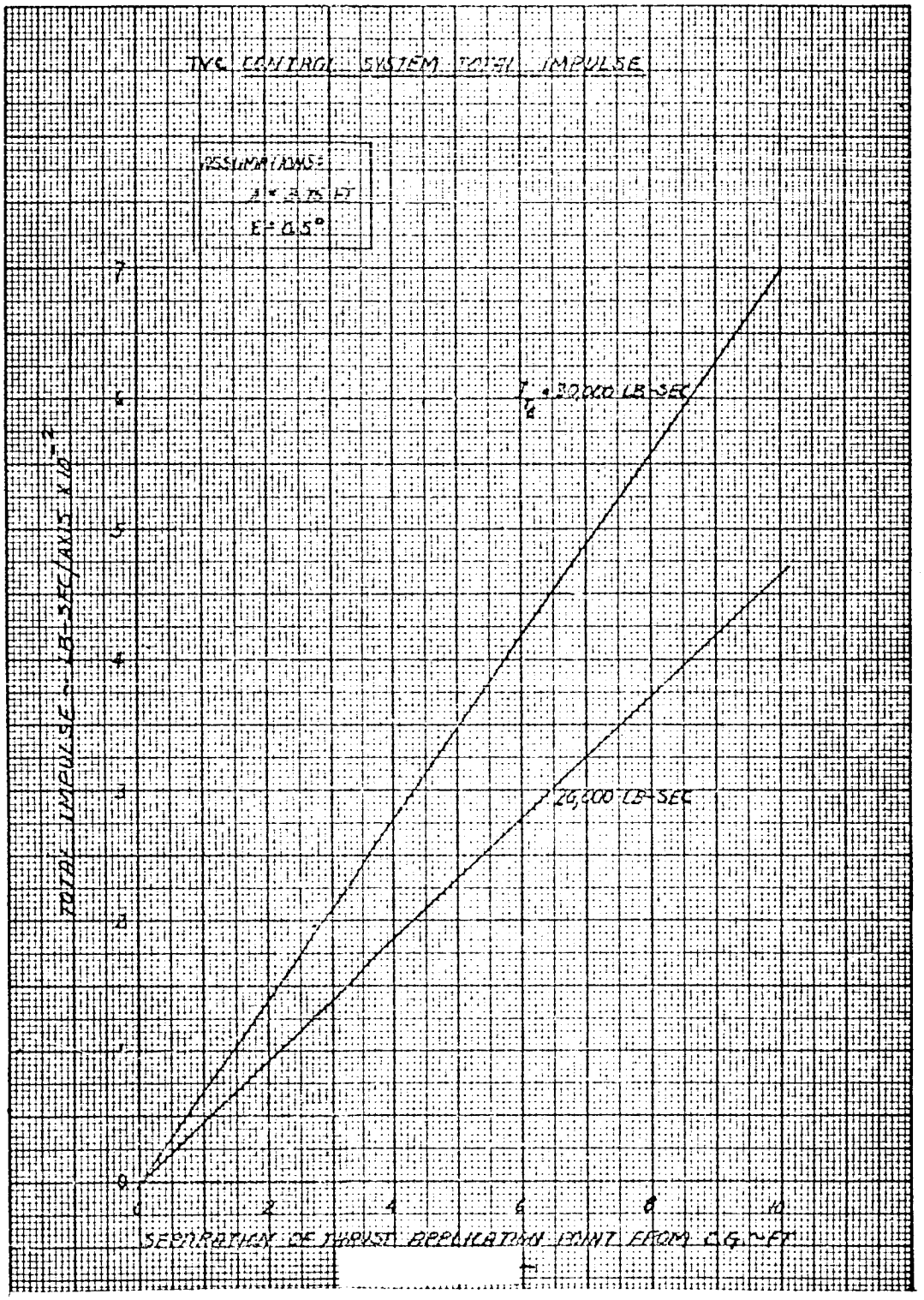

Figure 94 THRUST VECTOR CONTROL SYSTEM TOTAL IMPULSE

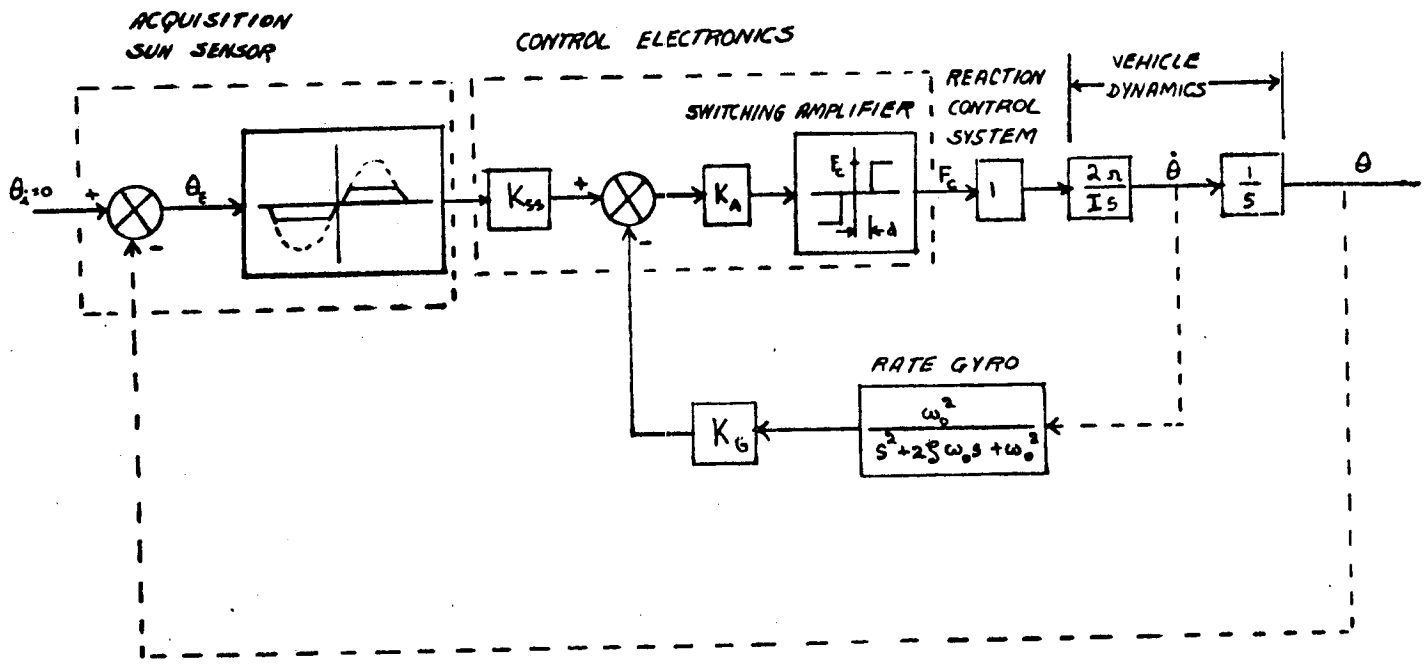

Figure 95 STABILIZATION AND CONTROL SYSTEM BLOCK DIAGRAM - SUN ACQUISITION MODE

64-11390

RE-ORDER No. 64-524

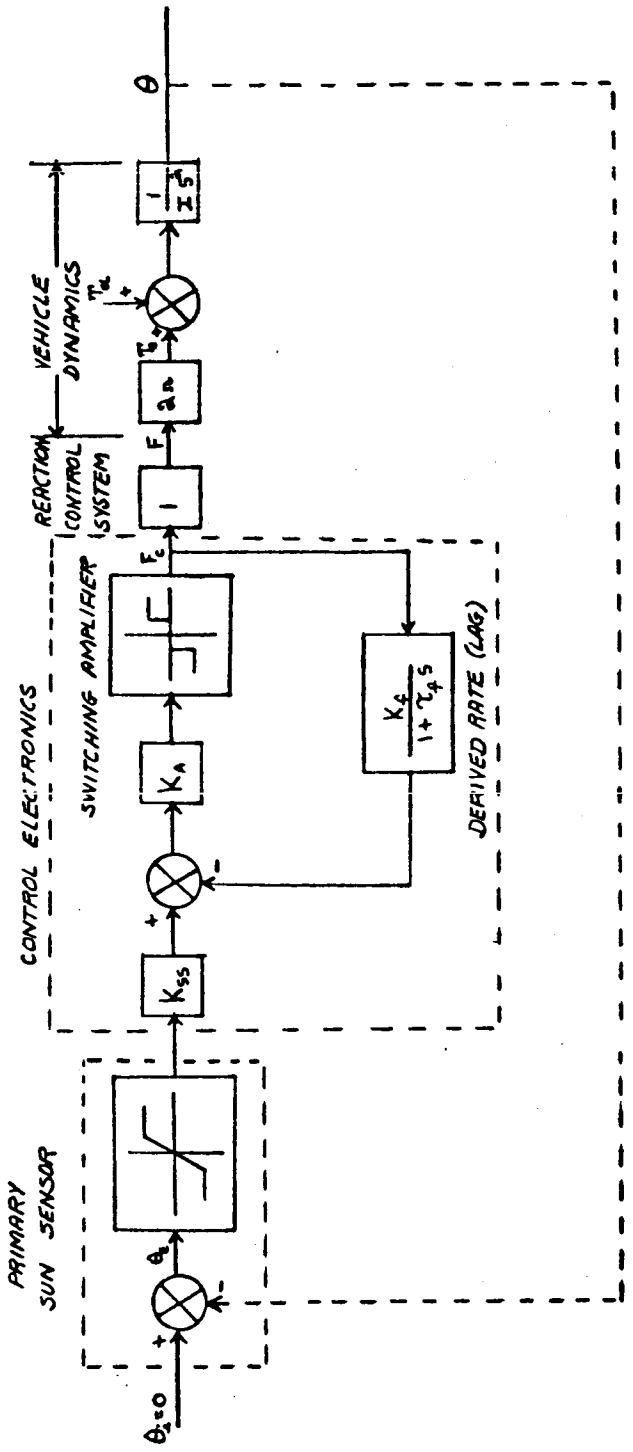

Figure 96 STABILIZATION AND CONTROL SYSTEM BLOCK DIAGRAM - TRANSMIT CRUISE MODE

64-11391

235

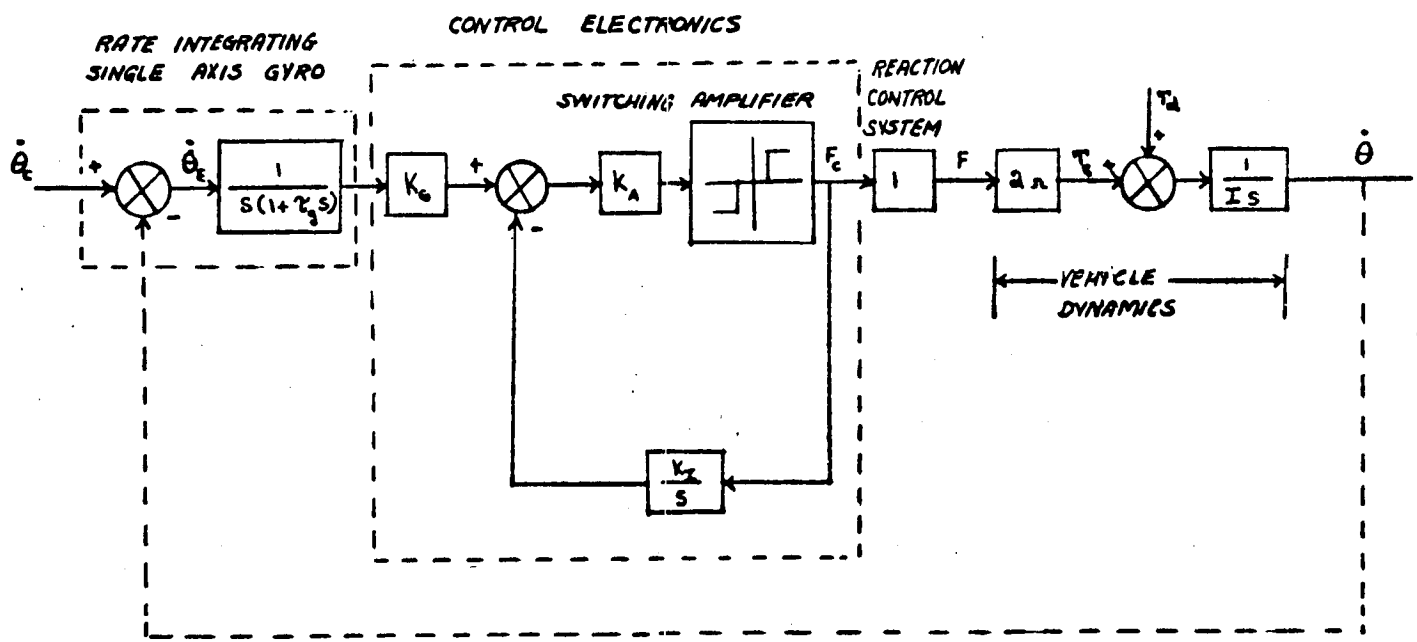

Figure 97 STABILIZATION AND CONTROL SYSTEM BLOCK DIAGRAM - ORIENTATION COMMAND MODE

64-11392

236

RE-ORDER No. 64-524

yaw. The sensor is nearly identical to the acquisition sun sensor to be used on the advanced orbiting solar observatory and will have been developed, qualified, and flown prior to its use in the Advanced Mariner program.

The pitch and yaw configurations are identical. The device consists of four silicon detectors in each axis, connected in a bridge network so that the bridge output is proportional to the sine of the angle between the controlled axis of the vehicle and the line-of-sight to the sun. This type of output signal results fromthe mounting geometry and the fact that individual cell current output into a low impedance load is proportional to illumination, or incident flux, in the sensitive spectral region of the detectors.

The null accuracy of the device, will be about 1 degree, the inaccuracy resulting almost solely from the differences in drift characteristics between detectors.

b. Limit Cycle Sun Sensor

This sensor generates accurate pitch and yaw error signals for precision pointing of the vehicle z-axis along the sun line. High accuracy is obtained at the expense of a limited field of view.

The basic element of the limit cycle sun sensor is a critical angle prism. The prism is of isosceles geometry with the isosceles angles cut approximately at the critical internal reflectance angle of the glass material for the wavelength of maximum detector sensitivity. When the sun's rays enter the prism normal to the front surface, they pass through the prism and strike the lateral faces at the critical angle, causing virtually all the incident radiation to be totally internally reflected.

3. Canopus Star Tracker

The star tracker generates roll error signals for accurate alignment of a preselected vehicle plane with the plane formed by the sun, Canopus, and the spacecraft. This preselected plane passes through the vehicle roll axis and the Canopus star tracker.

The Canopus star tracker performs two functions: (1) provides the ACS with vehicle roll reference, and (2) provides knowledge of Canopus position. Both digital and analog signals are required. This is achieved without complicated A/D or D/A conversion by feeding the components of the scan-generated error signal into both digital and analog signal processing electronics, and utilizing a digital gimbal loop. Thus analog error signals proportional to roll error are fed to the ACS.

4. Cold Gas Reaction System

Nitrogen jets are used for vehicle attitude control during all phases of the mission. Four 0.01-pound jets in each axis provide torque couples for pitch, yaw, and roll rotation in either direction during the acquisition, transit cruise, and orientation modes of operation.

This system is comprised of 12 jets, 2 nitrogen storage tanks, a pressure regulator, pressure transducers, and other necessary plumbing.

In addition, eight 0.1-pound auxiliary cold gas jets are used to afford attitude control during the thrust phases of the mission for TVC.

a. Sizing of the ACS Cold Gas Reaction System

The design presented herein is predicated on a thrust level of 0.01 pound per nozzle. It was indicated in the parametric study that this is adequate to assure an angular acceleration of at least 1/4 millirad/sec^2, thus giving satisfactory performance in the various ACS non-thrusting operating modes.

The nozzle throat diameter is given by

$$D_t = \left[\frac{4F}{\pi P_c \sqrt{\frac{2k^2}{k-1} \left(\frac{2}{k+1}\right)^{R+1/R-1}}} \right]^{1/2} \tag{14}$$

where

D_t = throat diameter (inches)

F = thrust (pounds)

P_c = nozzle pressure (psi)

k = specific heat ratio of gas

so,

D_t = 0.0265 inch

The required nitrogen gas weight flow rate is a function of the thrust, gas temperature, and gas constants and is given by

$$\dot{W} = F \sqrt{\frac{g(k-1)}{2kRT_c}} \tag{15}$$

where

$\dot{W}$ = flow rate (lb/sec)

F = thrust (pounds)

g = acceleration due to gravity (ft/sec^2)

k = specific heat ratio

T_c = gas temperature (°R)

R = gas constant (ft/ °R)

therefore,

$\dot{W}$ = 1.25 x 10^{-4} lb/sec per nozzle.

The maximum number of nozzles firing at any one time is six. Hence, the maximum flow demand of the system is 7.5 x 10^{-4} lb/sec. The maximum permissible downstream pressure for critical flow is

$$P_d = \left(\frac{2}{k+1}\right)^{\frac{k}{k-1}} P_u \tag{16}$$

where

P_d = downstream pressure (psia)

P_u = upstream pressure (psia)

so,

P_d = 15.8 psia.

The equivalent diameter of the solenoid valve for critical flow is given by the following relation,

$$d_o = \sqrt{\frac{4\sqrt{T_u}\,\dot{W}}{\pi C_d P_u \sqrt{\frac{gk}{R\left(\frac{k+1}{2}\right)^{k+1/k-1}}}}} \tag{17}$$

where

d_o = equivalent orifice diameter (feet)

T_u = upstream temperature (°R)

C_d = orifice coefficient,

therefore,

d_o = 0.0329 inch

Leakage values are summarized in table 40

TABLE 40

COLD GAS LEAKAGE SUMMARY

Component	Leakage per Unit (sec/hr)	Number of Units	Leakage per Component (sec/hr)
Regulator	5	1	5
Solenoid Valves	1	12	12
Fittings	0.5	12	6
Fill Valve	0.5	1	0.5
Total System Leakage			23.5

The above total leakage is equivalent to 61.5 in.^{3} of tank volume at 3000 psia for a one year operating period.

The required tank volume for a given total impulse may be calculated from

$$V = \frac{I_t}{P_i - P_f} \sqrt{\frac{g\,RT\,(k-1)}{2k}} \qquad (18)$$

where

V = tank volume (ft^3)

I_t = total impulse (lb-sec)

240

P_i = initial tank pressure (lb/ft^2 absolute)

P_f = final tank pressure (lb/ft^2 absolute)

Using the total impulse from table 39 with a safety factor of 3 to account for the uncertainties involved in the assumptions used in the parametric analysis one has I_T = 1200 lb-sec,

therefore

$$V = 1829 \text{ in.}^3$$

or 914 in.^{3} per tank for two tanks.

Since leakage losses must be allowed for in tank volume, the total required gas volume per tank is

$$V_T = 945 \text{ in.}^3$$

The inner radius of a spherical tank to enclose the gas is given by:

$$r = \sqrt[3]{\frac{3V}{4\pi}} \tag{19}$$

giving r = 6 inches.

Assuming a wall thicknesses of 0.1 inch, the outer diameter of each spherical tank is

$$d = 12.2 \text{ inches}$$

The weight of the gas required is determined from

$$W = \frac{I_T}{I_{SP}} \tag{20}$$

Using a specific impulse of 60 seconds

$$W = 20 \text{ pounds}$$

The weight summary of the cold gas system required for attitude control during nonthrusting phases only is given in table 41.

TABLE 41

SYSTEM WEIGHT WITHOUT TVC

Item	Weight
Gas	20
Tankage	20
Fixed Weight (valves, etc.)	8
Total	48

b. System Sizing Including Thrust Vector Control (TVC)

For TVC us assume

1) a control moment arm, $r = 3.75$ feet

2) a thrust misalignment angle, $\epsilon = 0.5$ degree

3) a midcourse correction total impulse, $I_{T_e} = 31,200$ lb-sec

4) a minimum control thrust level of 0.1 pound from figure 93 for an engine thrust of 25 pounds.

Further, with an engine moment arm of 1 foot and allowing a safety factor of 3, the control impulse per axis as given by

$$I_T = I_{T_e} \frac{l \sin \epsilon}{r} \tag{21}$$

for the stated parameter values yields

$$I_T = 218 \text{ lb-sec per axis}$$

and for conservation the total required impulse assumed for three-axis TVC is

$$I_{T_c} = 654 \text{ lb-sec}$$

242

Combining the TVC total required impulse with that necessary for attitude control during the non-thrusting mode, yields an overall impulse of 1854 lb-sec. Substituting this value into equation (18) gives

$$V = 2826 \text{ in.}^3$$

or 1413 in.^{3} per tank for two tanks. Using the same leakage losses as in the preceding section, the total required gas volume per tank is:

$$V_T \approx 1444 \text{ in.}^3$$

The inner radius of an equivalent spherical tank as given by equation (19) is 7.0 inches. Assuming a wall thickness of 0.1 inch, the outer diameter of each spherical tank is 14.2 inches, and the overall tank volume of each is 1498 in.^{3}.

The weight of the necessary gas is found from equation (20) and is 31 pounds. For a spherical titanium tank, the tank weight is approximately the same as the gas weight, i.e., 31 pounds in this case. A size and weight summary including TVC requirements is given in table 42.

Additional system characteristics are summarized below.

Attitude jet thrust	0.01 lb/jet (12 jets used)
I_{s_p}	60 seconds (steady state) 35 seconds (limit cycling)
Storage pressure	3000 psi
Jet valve power required	approximately 100 ma at 28 volts
Tubing	3/16 inch OD stainless

The proposed reaction system is shown in figure 98.

c. Gyro and Control Electronic Packages

The major blocks of the gyro and control electronics are briefly described in the following paragraphs. At this time it is not practical to exactly define the circuits required for the ACS, but the circuits have been detailed to the extent necessary for realistic size, weight, power, and reliability estimate. The functional block diagrams for the control electronics and the gyro electronics packages are shown in figures 99 and 100 respectively.

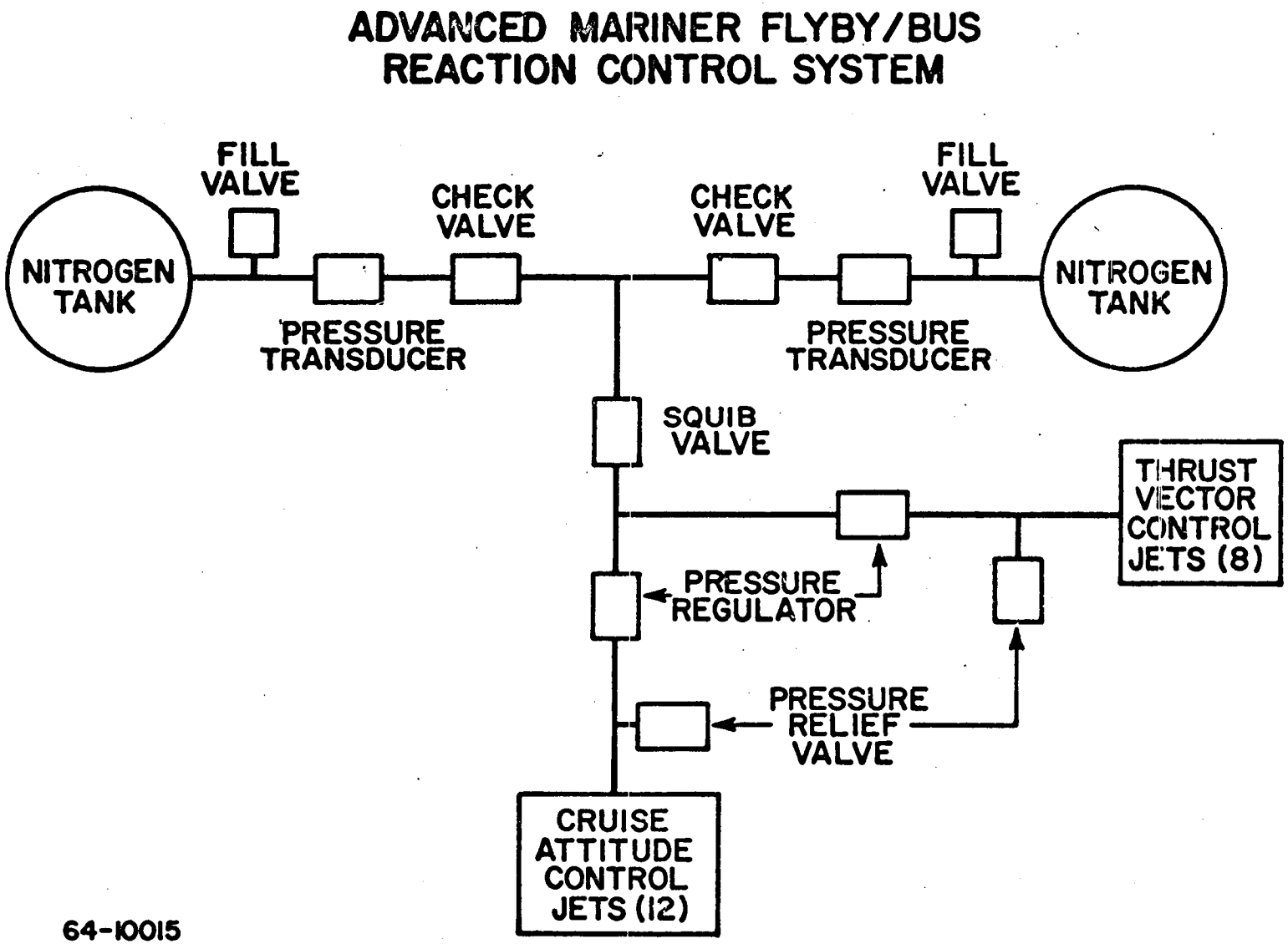

Figure 98 REACTION SYSTEM FUNCTIONAL DIAGRAM

RE-ORDER No. 64-524

244

RE-ORDER No. 64-524

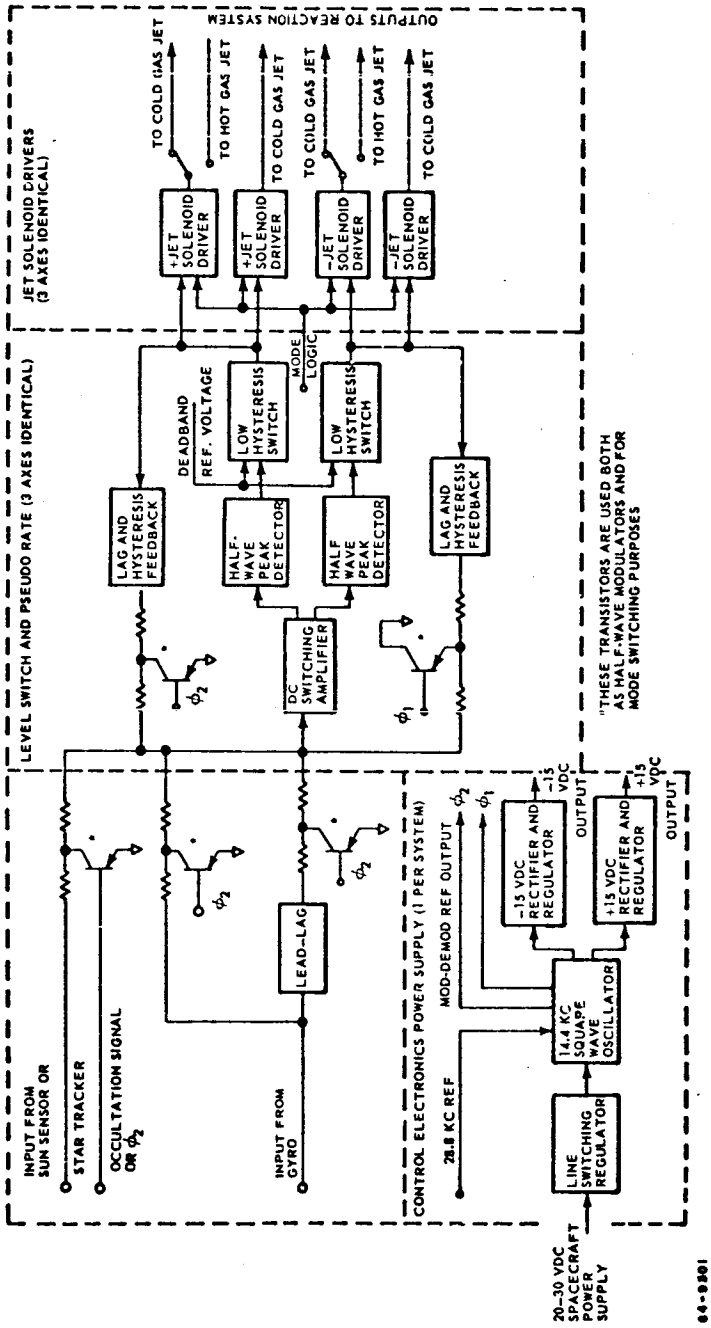

Figure 99 BLOCK DIAGRAM OF CONTROL ELECTRONICS

245

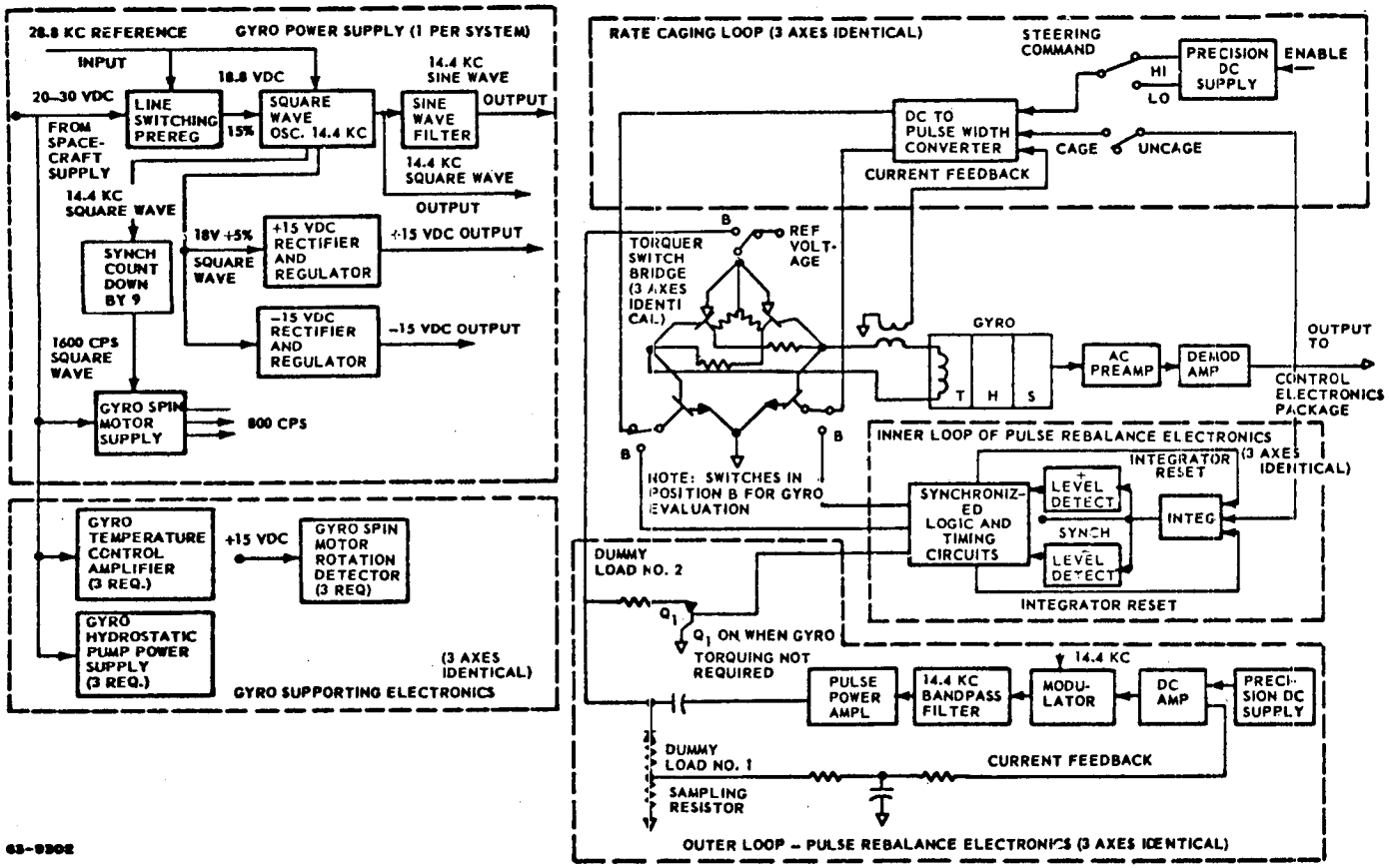

Figure 100 BLOCK DIAGRAM OF GYRO/ELECTRONICS PACKAGE

RE-ORDER No. 64-529

TABLE 42

SIZE AND WEIGHT SUMMARY FOR REACTION CONTROL SYSTEM

Item	No.	Item Weight (pounds)	System Weight (pounds)	Item Volume (in. ^{3})	System Volume (in. ^{3})
Regulator	2	0.50	1.00	15	30
Plumbing		3.00	3.00		12
Pressure relief valve	2	0.25	0.50	2.5	5
Valve, solenoid, and nozzle					
1) Cruise Attitude Control	12	0.25	3.00	2.75	33
2) Thrust Vector Control	8	0.50	4.00	3.00	24
Squib valve	1	0.25	0.25	2.00	2.00
Charge valve	2	0.09	0.18	2.5	5
Transducer	2	0.25	0.50	2.5	5
Check valve	2	0.25	0.50	2.5	5
Tank (Titanium)	2	15.5	31.00	1498	2996
Gas			31.00		
Total			74.93		3117

1) Control Electronics

The control electronics provide the elements necessary to process the error input signals from the gyros or optical sensors and command the appropriate reaction jets when the preset deadband of the on-off level switch is exceeded. The phase of the error signal determines when the deadband is exceeded. The mechanization chosen for the control electronics uses an a. c. (square wave) summing technique at the input to the switching amplifier. The conversion from d. c. to a. c. (square wave) is accomplished by simple, single half-wave chopper transistors which also function as mode control switches when energized continuously.

The following elements make up the control electronics: active lead-lag circuit, switching amplifier, peak reading half-wave voltage detector, low hysteresis switch, lag feedback circuit (for pseudo rate), jet solenoid driver, control electronics power supply, and mode command logic.

The elements of the control electronics package are:

a) Mode command logic

This logic controls the switching necessary to provide the various ACS modes during the mission. Some of these mode command logic circuits are located in the gyro/electronics package.

b) Jet solenoid drivers

On-off commands to the cold gas jet solenoids and the auxiliary TVC gas jet solenoids are directed through these drivers by the on-off level switches and the mode command logic.

c) On-off level switches

These switches pass signals to the jet solenoid drivers when the switch inputs exceed a preset deadband level.

d) Pseudo - rate networks

These networks around the on-off level switches provide system stability during sun and Canopus attitude hold without the necessity for gyro rate information.

e) Lead-lag networks

These active networks on the inputs to the on-off level switches provide system stability during attitude hold with gyros, and during steering phases.

f) Power supply

Provides power to the control electronics, the Canopus star tracker and the sun sensors.

2) Gyro/Electronics

The gyro electronics provide the elements necessary to control the gyros in the rate, attitude, and gyro evaluation configurations and supply an output error signal to the control electronics. The mechanization of these circuits uses ac, dc, and pulse techniques to attain the required accuracy with a minimum of circuits.

The gyro/electronics package includes:

a) Three floated single-degree-of-freedom gyros

These gyros are rate sensors for damping and attitude sensors for attitude hold during spacecraft maneuvering when either the sun or Canopus is occulted.

b) Power supply

This supply provides power to the gyros and their associated electronics.

c) Temperature control amplifiers

These circuits control gyro temperature within close limits to provide the necessary gyro accuracy.

d) Caging electronics

A precision current supply, dc-to-pulse-width converter, and a torquer switch bridge allow caging of the gyros in a rate mode so that their output may be used for rate damping.

e) Evaluation electronics

A current pulse generator, pulse rebalance electronics, and a torquer switch bridge allow an accurate evaluation of gyro drift during flight.

3) Packaging

a) Control electronics package

The control electronics will be packaged as a separate unit. This unit is envisioned as a simple hard-mounted package with the electronics designed as plug-in subassemblies.

b) Gyro electronics package

The gyro electronics will be contained within the outlines of the gyro mounting block. Locating the gyro electronics on the mounting block creates a relatively stable temperature environment compatible with the use of integrated circuits.

c. Summary

The gyro and control electronics package characteristics are summarized in table 43.

TABLE 43

GYRO AND CONTROL ELECTRONICS PACKAGE CHARACTERISTICS

Item	Volume (in.^{3})	Weight (pounds)		Power Required (watts)		
				Steady-State		Peak
Control Electronics Package	125	3.0		2.4		
Gyro/Electronics Package	245	10.0		31.0		
Gyros (3)			3.00		9	
Casting (1)			1.25			
Harness and Mounting			0.50			
Power Supply (1)			1.25		1.0	
Caging Electronics (3)			1.00		2.0	
Pulse Rebalance Electronics (3)			2.00		10.0	
Temperature Control Electronics (3)			1.00		9.0	90*
Totals	470	13.0	10.00	33.5	31.0	

* Gyro warmup power-20 minutes maximum.

d. Summary of Attitude Control System Characteristics

The ACS size, weight, and power characteristics are summarized in table 44.

TABLE 44

ACS SIZE, WEIGHT, AND POWER SUMMARY

Item	Volume (in. ^{3})	Weight (pounds)	Power (watts)
Gyro/Electronics Package	245	10	31.0
Control Electronics Package	125	3.0	2.5
Canopus Star Tracker	350	7.0	7.2
Limit Cycle Sun Sensor	13	1.5	0.5
Coarse Acquisition Sun Sensor	4	0.44	0.35
Reaction Control System			
1) Attitude Control	1975	48	
2) TVC	1142	26.93	
Totals	3854	96.87	41.55

8.0 STRUCTURE

8.1 CONCEPTUAL DESIGN

This section describes the flyby/bus, lander attachment points, and adapter section structure. The lander structure is discussed in the Lander Volume, Volume 3. The procedure followed in developing the structure is essentially the reverse of the parametric approach used in the balance of the study. Structural weight variation does not lend itself to the parametric approach. Therefore, a single basic conceptual, structural design has been developed during the study. During the final stage of the study a firm concept as outlined in the following three sections: lander attachment system, flyby/bus structure, and adapter section, has been developed. After establishment of this basic design, a brief parametric study was performed to show the variation of bus structural weight as a function of lander weight. The results of the study are also included in this section.

The critical design loads occur during booster ascent. Design loads are based on 6 g axial loads and 0.4 g lateral loads occuring simultaneously. A 1.25 safety factor on ultimate loads has been employed to assume structural integrity.

Preliminary structural analysis of the flyby/bus has been limited to basic calculations, usedas necessary for the development of a realistic structural weight breakdown.

The majority of the structural elements are 7075 aluminum alloy with AZ31A magnesium used in some areas for a weight saving. Riveted fabrication has been assumed throughout the structure.

Figure 101 shows the basic structural layout of the spacecraft with the structural number keyed to the text.

1. Lander Attachment Points

The lander and its propulsion system (6) are totally enclosed in an aluminum sterilization canister (11) that protects the lander sterility prior to separation. Attachment of the canister and the lander to the bus structure is through three tie-down bolts. These tie-downs transmit loads from three hard points on the lander to the bus through three adapter angle brackets (4) that include the lander/bus separation mechanism. Details of these joints are discussed in section 10.4.

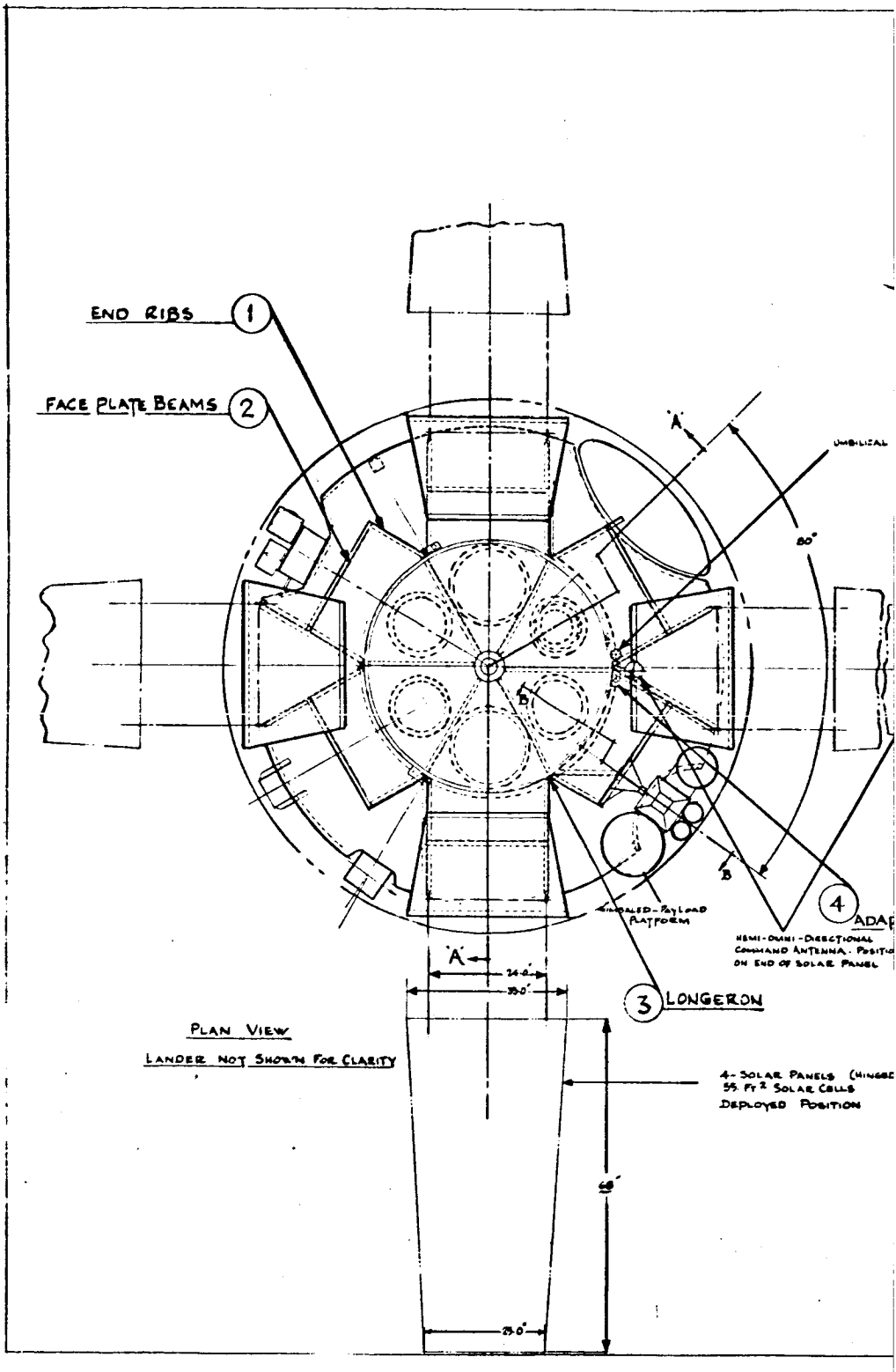
END RIBS
1
FACE PLATE BEAMS
2
'A'
UMBILICAL
80°
'B'
'B'
4
ADAP
HEMI-OMNI-DIRECTIONAL
COMMAND ANTENNA - POSITIO
ON END OF SOLAR PANEL
GIMBALED-PAYLOAD
PLATFORM
'A'
24-0"
35-0"
3
LONGERON
PLAN VIEW
LANDER NOT SHOWN FOR CLARITY
4-SOLAR PANELS (HINGED
55 FT² SOLAR CELLS
DEPLOYED POSITION
68"
25-0"

64-11311

1#

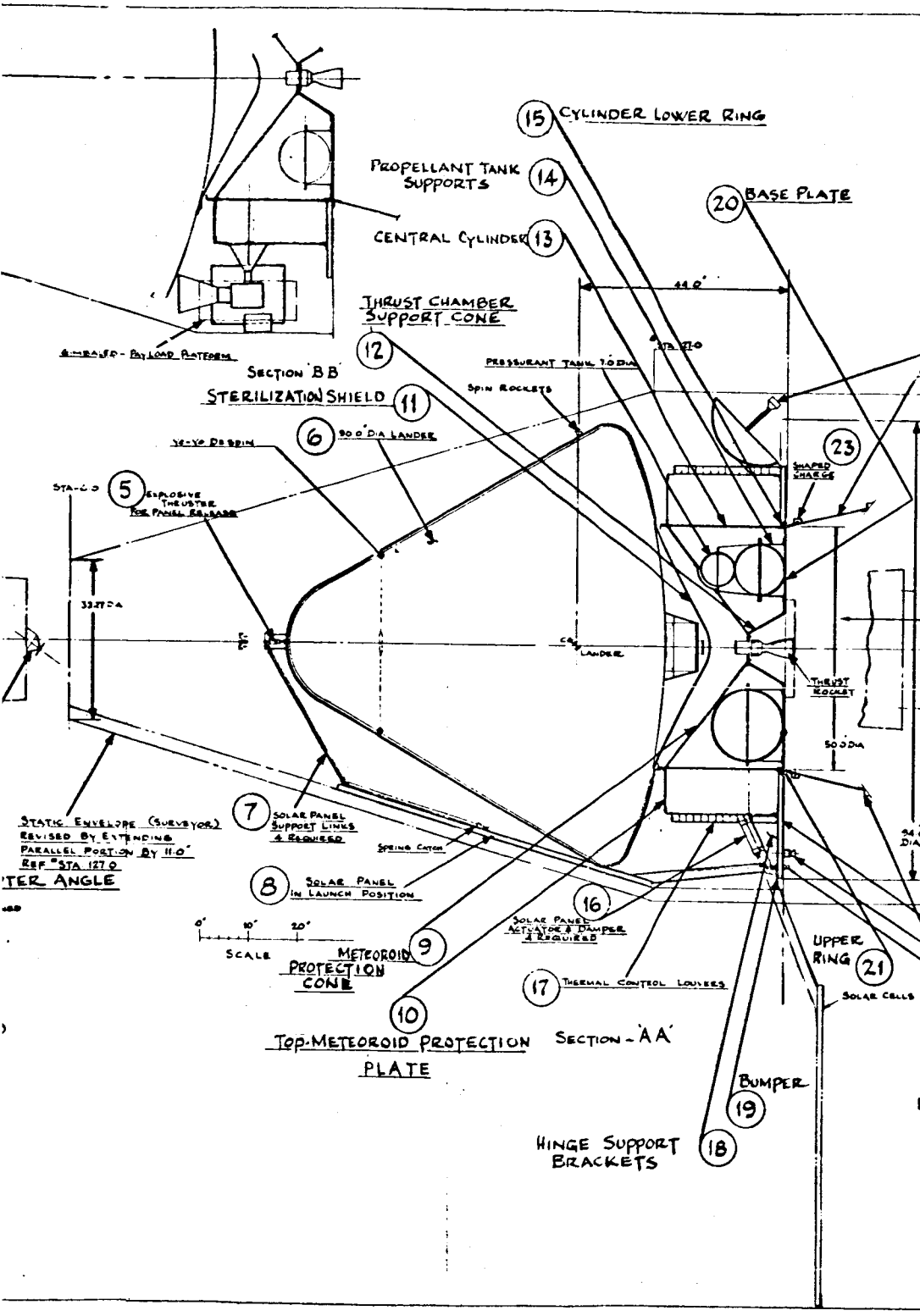

Figure 101 FLYBY/BUS STRUCTURAL ELEMENTS

RE-ORDER No. 64-524

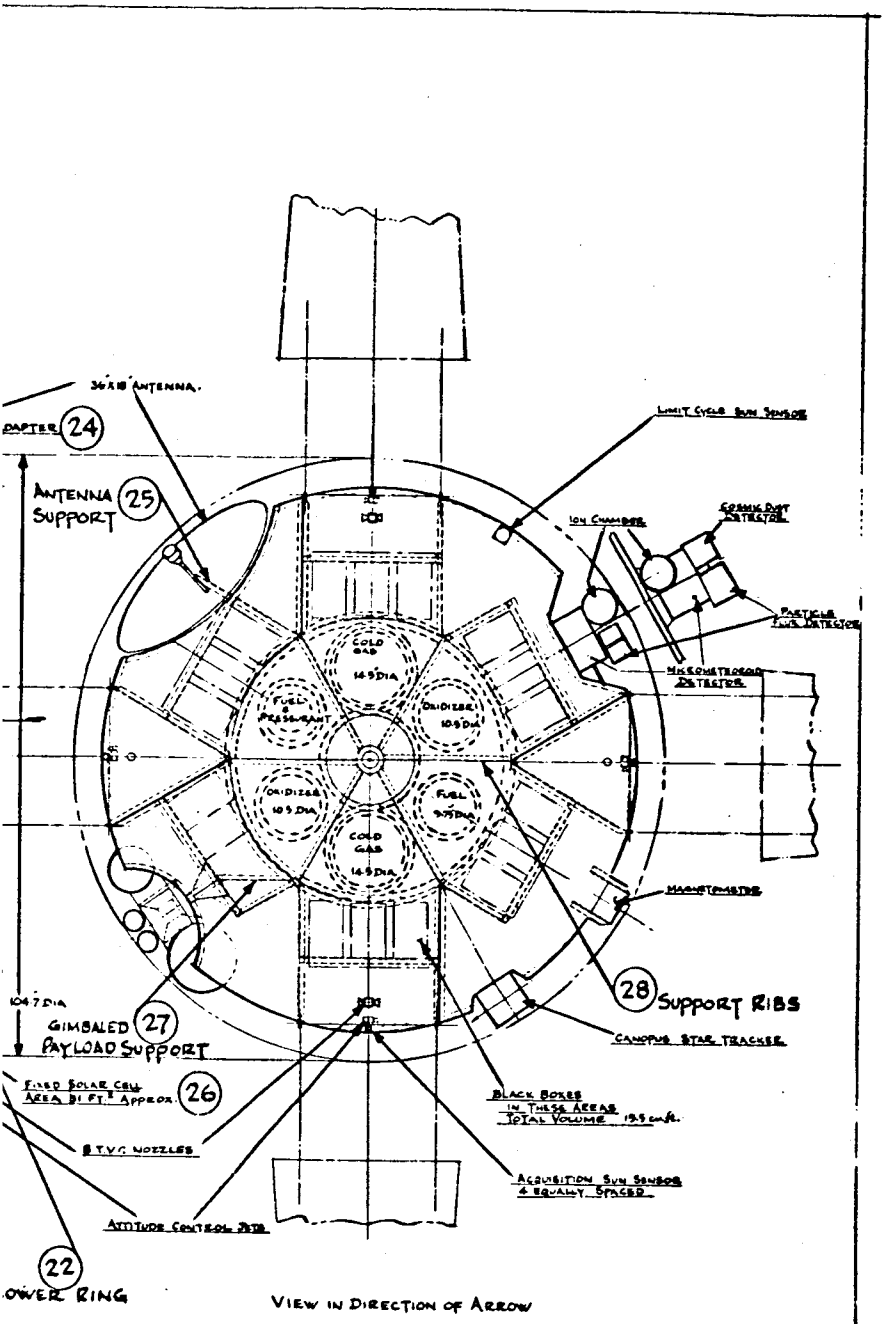

VIEW IN DIRECTION OF ARROW

Avco

(3) ADVANCED MARINER CONCEPTUAL DESIGN OF SPACECRAFT (90" DIA LANDER)

04614 | K4-1358

253

2. Flyby/Bus Structure

The flyby/bus structural arrangement is primarily controlled by the lander and propulsion system, since the lander and the propellant tanks are the major contributors to the bus launch loads.

The basic structure consists of four major elements.

1) Central cylinder structure.

2) Propulsion system support structure.

3) Electronics package.

4) Hinged solar panel support structure.

a. The Central Cylinder Structure consists of a cylindrical aluminum shell (13) with a stiffening flange at the top and a structural ring (15) at the bottom. The cylinder has six extruded longerons (3) that transmit lander loads, propulsion support loads, and electronic package support loads to the bottom structural ring, which, together with the cylindrical shell, redistribute the loads to the top adapter ring (21).

Considering axial and bending loads introduced by the lander and neglecting the effect of the longerons, it has been found that 0.040-inch magnesium sheet thickness is adequate for the cylinder and the failure mode is in compressive buckling. The longerons were checked, neglecting the effect of the cylindrical shell except for stabilization, and assuming 2/3 of the bending and axial load on each longeron. An extruded aluminum section with an area of 0.17 in.^{2} and a moment of inertia of 0.042 inch^4 is required to meet the loading. The failure mode is in bending. An aluminum extruded angle section with a cross-sectional area of 0.14 in.^{2} is required for the bottom ring.

b. The propulsion support structure consists of six main support ribs (28), a base plate (20), propellant tank support brackets (14), and a thrust chamber support cone (12). The six support ribs are made of magnesium and transmit the propellant tank and propulsion rocket loads to the cylinder longerons. The base plate is a reinforced aluminum (7075) plate which is bolted to the support ribs and to the cylinder ring. The propellant tank support brackets are aluminum cylindrical shells and are attached to base plate integral reinforcing rings. For meteoroid protection, a light aluminum cone cover (9) for the propulsion system is provided.

An advantage to this arrangement is that the complete removal of the propulsion system module can be accomplished by simply disconnecting fuel and oxidizer lines at the valves, then removing screw attachments from base plate to support ribs, cylinder ring, and heat sink cone.

The support ribs have been analyzed as cantilever beams, each supporting 1/6 of the total propulsion system loads. Inherently large moments of inertia allow the ribs to be made from 0.04-inch magnesium plate. The base plate was analyzed as a beam transmitting the propellant tank support loads to the ribs. It has been determined that an aluminum 0.07-inch thick plate be used with integral stiffener rings to pick up propellant tank support brackets. The failure mode is in bending.

c. The electronic package structure consists of six box compartments cantilevered from the cylinder longerons by 12 end ribs (1). The electronic packages are mounted on face plate beams (2) which transmit loads to the end ribs. In addition, the face beams have the thermal control louvers (17) mounted on the outer face. The top of the box is covered by a light aluminum sheet (10) for meteoroid protection.

The electronic package structure also provides support for the gimbaled payload platform (27), the fixed antenna (25), and the fixed solar panel (26). The solar panel annulus is fabricated from aluminum honeycomb. In addition to its primary function as a solar cell array, the annulus provides a mounting platform for sensors and scientific instrumentation.

The fixed solar cell array is fabricated in four segments. These segments are supported at the joints by electronic package structure and hinged solar cell panel hinge support brackets (18).

The electronic package structure was analyzed by assuming the front plate beam with a concentrated load at the center simply supported by the end ribs. The offset moment is transmitted to the top and bottom caps in bending by web stiffeners. It then is transmitted in shear in the top plate skin and on the bottom by the fixed solar panel array. For the top and bottom caps a cross sectional area of 0.09 in.^{2} is required, 0.03-inch thick web with stiffeners at approximately 6-inch spacing and having a cross sectional area of 0.03 in.^{2}.

The end ribs were considered to be cantilever beams transmitting the loads to the cylinder longerons. Because of their inherently large moment of inertia, the stress levels are very low and magnesium can also be applied here.

The meteoroid protection top plate can be made from 0.020 aluminum with formed stiffeners coincidental with plate beam stiffeners.

The gimbaled payload support created a need for an additional rib, canted from the center of the gimbal base to the cylinder longeron. The same material as the end ribs proved satisfactory.

d. Hinged Solar Panel Support Structure. There are four hinged, trapezoidal, solar cell array panels with an area of approximately 14 ft^2 each. These are cantilevered from the electronic package structure by eight hinged support brackets. The panel module is constructed of a substrate made up of a single skin reinforced with chord-wise corrugations, backed up with two longitudinal box beams which act as a hinge load path. During the launch mode the panels are supported from a mounting on the apex of the lander sterilization shield by four support links (7). At booster burnout these links are simultaneously released by one explosive thruster (5). The panels are deployed by four liquid spring/damper actuators (16). After deployment the panels are automatically locked in position by an over-center mechanism. In this final position the panel hinge brackets rest against silicone rubber bumpers (19) supported from the fixed solar cell anulus array. One solar cell panel also supports the hemi-omni-directional command antenna on the outer end of the panel.

The fixed and hinged solar panels structural design is based on previous Ryan Aeronautical Company work. The weight of the fixed solar cell panels is assumed to be 0.35 lb/ft^2 and for the hinged panels 0.99 lb/ft^2, (structure only, in both cases).

3. <u>Adapter</u>

The adapter is an aluminum shell frustrum (24) of a cone with a top (21) and bottom ring (22). It transmits the loads from the lander and the flyby/bus to the booster payload support structure.

It also includes a shaped charge ring (23) for booster and spacecraft separation.

The adapter structure transmits loads from the lander and flyby/bus to the booster interface. It was analyzed as a cylinder under axial compression and bending. A 0.040-inch aluminum shell thickness is required with the

critical loading in compressive buckling. The upper and lower adapter rings were analyzed as uniformly loaded along the circumference of the flanges. An aluminum extruded angle section with an area of 0.14 in.^{2} is required for the top ring and 0.16 in.^{2} for the bottom ring.

A structural weight summary is presented in table 45.

TABLE 45

STRUCTURAL WEIGHT BREAKDOWN

Item	Weight (pounds)
Cylinder and Six Longerons	13.50
Six Support Ribs	11.10
Propulsion Support Structure	23.00
Cone Upper (Meteoroid Protection)	3.10
Electronic Package Structure	43.00
Gimbaled Payload Support Structure	2.00
Four Spring Actuators (Solar Panels)	4.00
Thruster-Explosive (Solar Panel Release)	0.39
Four Solar Panel Support Rods	1.41
Eight Hinge Support Brackets	3.00
Antenna Support Bracket	0.50
Adapter and Two Rings	17.00
Shaped Charge (For Bus-Lander Separation From Booster)	2.00
Total	124.00

8.2 PARAMETRIC VARIATION

One of the most significant structural parameters is the variation of bus structural weight as a function of lander entry weight.

Since the bus structural weight is sized to a large extent by launch loads, the total weight of the lander and its associated equipment must be considered. This weight is for all practical purposes equivalent to the ejected weight at lander separation. Table 46 illustrates the variation of lander entry weight and ejected weight (at separation) as a function of lander diameter. Figure 102 shows the variation in bus structural weight as a function of ejected weight at separation. It should be noted that the only significant weight variation is in the primary load path structure. This fact is reflected in the relatively slight variance in total bus structural weight over a wide range of ejected lander weights.

TABLE 46

VARIATION OF LANDER WEIGHT AND EJECTED WEIGHT

Lander Diameter (inches)	Lander Weight (pounds)	Additional Equipment* Weight (pounds)	Ejected Weight (pounds)
70	312.4	68.0	380.4
90 (design point)	516.5	106.7	623.2
110	771.5	155.1	926.6

*Note: Additional equipment includes lander sterilization can, lander propulsion rocket and support structure, spin rockets, despin yo-yo and explosive device, shaped charge for sterilization can cutting, bus-to-lander umbilical, and tie-down bolts.

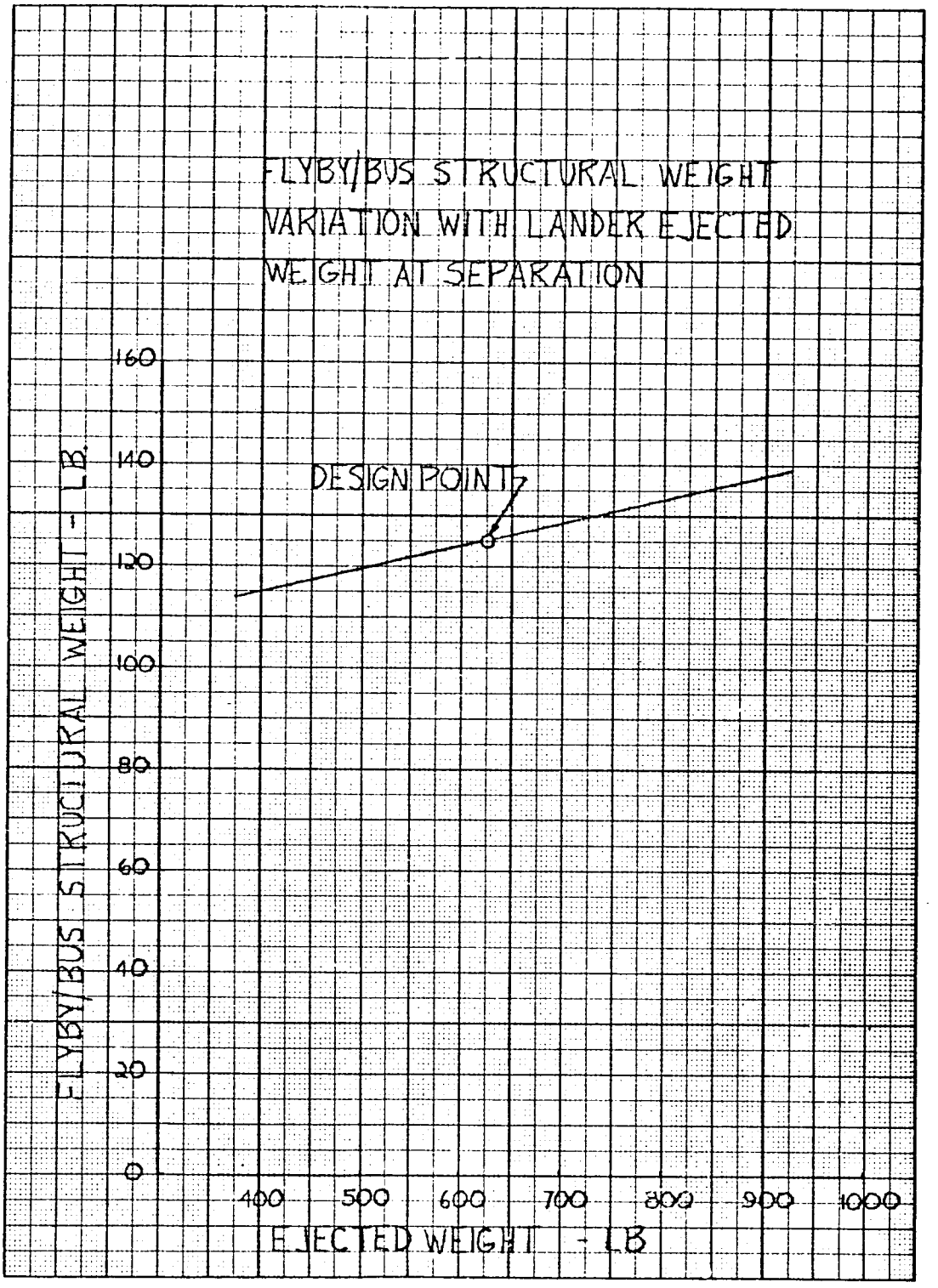

64-11394

Figure 102 BUS STRUCTURAL WEIGHT AS A FUNCTION OF LANDER EJECTED WEIGHT AT SEPARATION

9.0 THERMAL CONTROL

9.1 DESIGN APPROACH

The temperature excursion of the spacecraft must be maintained within prescribed bounds for the duration of the mission. Account must be taken of the multiple modes of operation, which include the following:

1. Launch pad operation.
2. Launch and Ascent.
3. Interplanetary transfer (both cruise mode and maneuver mode).
4. Post-lander separation.

As a general guideline most electronic equipment is designed to operate between 0 °F and +120°F. There are certain exceptions to this generalization, such as gyros, batteries, and cryogenic liquid for the infrared spectrometer detector. For this study only the gross thermal control of the flyby/bus has been considered. Control of temperature has been achieved by use of radiative coatings over the entire surface and by use of louvers adjacent to the black box compartments. Louver operation occurs independent of the spacecraft central computer and sequencer. Louver blade setting is by a bimetallic spring that responds to changes in temperature .

The thermal control study of the spacecraft awaited selection of a spacecraft configuration. Once a configuration was selected, the temperature excursions in the various modes of operation were determined. It was found that with the use of surface coatings and louvers the black box temperatures excursions could be limited to +94°F near Earth and +20°F near Mars.

Some parametric work was accomplished. This work, which is presented herein, shows the influence of the black box loading that is mass per unit area of boxes that are adjacent to louvers in the black box compartments.

It has been assumed that the sources of energy that contribute to the heat load are (1) solar flux and (2) internal power dissipation, which was determined to be 180 watts for the Advanced Mariner spacecraft.

9.2 ANALYTICAL PROCEDURE

Any system can be subdivided into its individual components and for each of these, the fundamental equation is

$$m_n c_n \, dT_n/dt = \sum Q_{e,n} + \sum_{\substack{n=1 \\ j=1}}^{\substack{j=p \\ n=p}} Q_{n,j} \qquad (1)$$

where

m_n = mass of item

c_n = specific heat of item n

dT_n/dt = temperature rise of item n

$Q_{e,n}$ = energy input terms independent of temperatures, e.g., sun, albedo, electric, etc.

$\sum_{\substack{n=1 \\ j=1}}^{\substack{j=p \\ n=p}} Q_{n,j}$ = summation of all heat interchanges between item n and all other equipment, as well as with surroundings (radiation, conduction, and transport interchanges, whether positive or negative).

As both $Q_{e,n}$ and $Q_{n,j}$ may be functions of time, only a digital computer solution of the multitude of differential equations can give the temperature time history of each item in the complete system.

Because of the generality of the above equation, it is possible to apply this expression to individual parts of the structure, as well as within any component, and thus obtain gradients within same.

The general form of the $\sum Q_{n,j}$ term will be:

$$\sum_{\substack{n=1 \\ j=1}}^{\substack{j=p \\ n=p}} Q_{n,j} = A_{n,j} F_{n,j} (T_n^4 - T_j^4) + \frac{A_c \cdot k}{l} (T_n - T_j) \qquad (2)$$

with

$A_{n,j}$ = radiating area from item n towards item j

$F_{n,j}$ = configuration factor from n to j

A_c = cross-sectional area of conductive path from n to j

k = specific conductivity of conductive material

l = length of conduction path.

With respect to the $\sum Q_{e,n}$ term, we have

$$\sum Q_{e,n} = Q_s + Q_a + Q_r + Q_l$$

where

$Q_s = A_s \cdot \alpha \cdot S$ = input from sun on area A_s, having solar absorptivity α, and being the projected area perpendicular to the sun vector.

$Q_a = F_a \cdot A_a \cdot \alpha \cdot \rho \cdot S$ = albedo input on exposed area A_a; ρ is albedo reflectivity of planet: 0.4 for Earth; 0.15 for Mars; F_a is view factor between A_a and that part of the planet acting as reflector.

$Q_r = F_r \cdot E_t \cdot \epsilon A_r$ = input received from planetary thermal emission on area A_r with emissivity ϵ and view factor F_r; E_t is the field strength of the radiation from Earth.

Q_{el} = electrical (or chemical) energy input.

For the present analysis, Q_a and Q_r are of negligible importance during the interplanetary journey and the variation in the solar constant S becomes the most important factor. The expression in (2) can be re-written as:

$$\sum Q_{n,j} = A_{n,j} \cdot F_{n,j} \cdot \sigma (T_n^2 + T_j^2)(T_n + T_j)(T_n - T_j) + \frac{A_c \cdot k}{l} \cdot (T_n - T_j)$$

with

$$F_{n,j} = \frac{1}{\frac{1}{\tilde{F}_{n,j}} + \left(\frac{1}{\epsilon_n} - 1\right) + \frac{A_n}{A_j}\left(\frac{1}{\epsilon_j} - 1\right)}$$

where $\tilde{F}_{n,j}$ is the geometric view factor from surface n to j and ϵ_n and ϵ_j are the emissivities of surface n and j, respectively.

The two right-hand side terms in (2) indicate the thermal couplings effect between n and j; the first shows the radiative coupling term, the second, the conductive.

With Q_{el} being arbitrary functions of time (expressing equipment being turned on or off), a closed solution to equation (1) cannot be obtained. However, a digital computer program was used to provide a temperature-time solution which, when carried sufficiently far out timewise, thus shows steady-state values, in addition to the transient characteristics.

With respect to the term $\tilde{F}_{n,j}$, a separate computer program determined the geometric view factor from one surface to another, each with complex boundaries from one spatial position to the other. Also, the heat interchange between two gray bodies having absorbing or non-absorbing media between them were evaluated by Oppenheimer's radiosity method.

9.3 DESIGN PARAMETERS

With given geometrical sizes and masses of individual components, the operational temperature can be materially influenced by selecting α and ϵ values, as well as arranging changes in conductivity through the term $A_c \cdot k / l$.

Figure 103 shows the change in temperatures for a plate exposed to direct sunlight on one side, while radiating also from the back side during a journey from Earth to Mars. The design philosophy will, therefore, strive to maintain all equipment below the upper operating limit during the first part of the journey and as the vehicle recedes from the sun, the lower operating limits will be approached. During a midcourse maneuver, where any spacecraft attitude could be assumed, the thermal control system also limits the temperature excursions.

It is possible to execute a purely/passive thermal design. However, this philosophy entails a strict constraint upon equipment location and, in order to allow more freedom for placing individual items, it is proposed to arrange electronics and instrumentation in special bays which will be temperature-controlled by placing outward-facing louvers as a cover for these bays.

Figure 104 illustrates a typical effective emissivity characteristic of a louver system as a function of the louver blade angle (reference 1). The sensors actuating the blades will be set for fully closed position at 50°F and fully open at 80°F. From the graph, it is seen that the ratio of heat rejection rate at maximum opening to that at fully closed is 20:1. This is in conformity with measured values, as also shown in figure 104. Equipment can thus be switched on or off, and the resulting effects will be felt mainly by the louvers and not by the complete spacecraft, so long as total power variation stays within the above limits. In the analytical investigation, a conservative range of $0.1 \leq \epsilon \leq 0.7$ has been used.

Special equipment which cannot be mounted in the bays, due to size or placement, must be analyzed separately. Also, in such cases, the essential feature is to balance the heat loss against the internal heat generation and the main parameter is the emissivity of the radiating surface. A range of typical values is given in table 47.

TABLE 47

RADIATIVE PROPERTIES OF TYPICAL SURFACE COATINGS

Material	Surface Treatment	α	ϵ
AL	Polished	0.10	0.05-0.08
AL	Iridized	0.3	0.10-0.15
AL	Anodized	0.6	0.6-0.85
AL	White Paint	0.25	0.9
AL	Oil Paint	0.75	0.85
Aluminized	Mylar	0.16	0.08
Silver	Polished	0.09	0.03

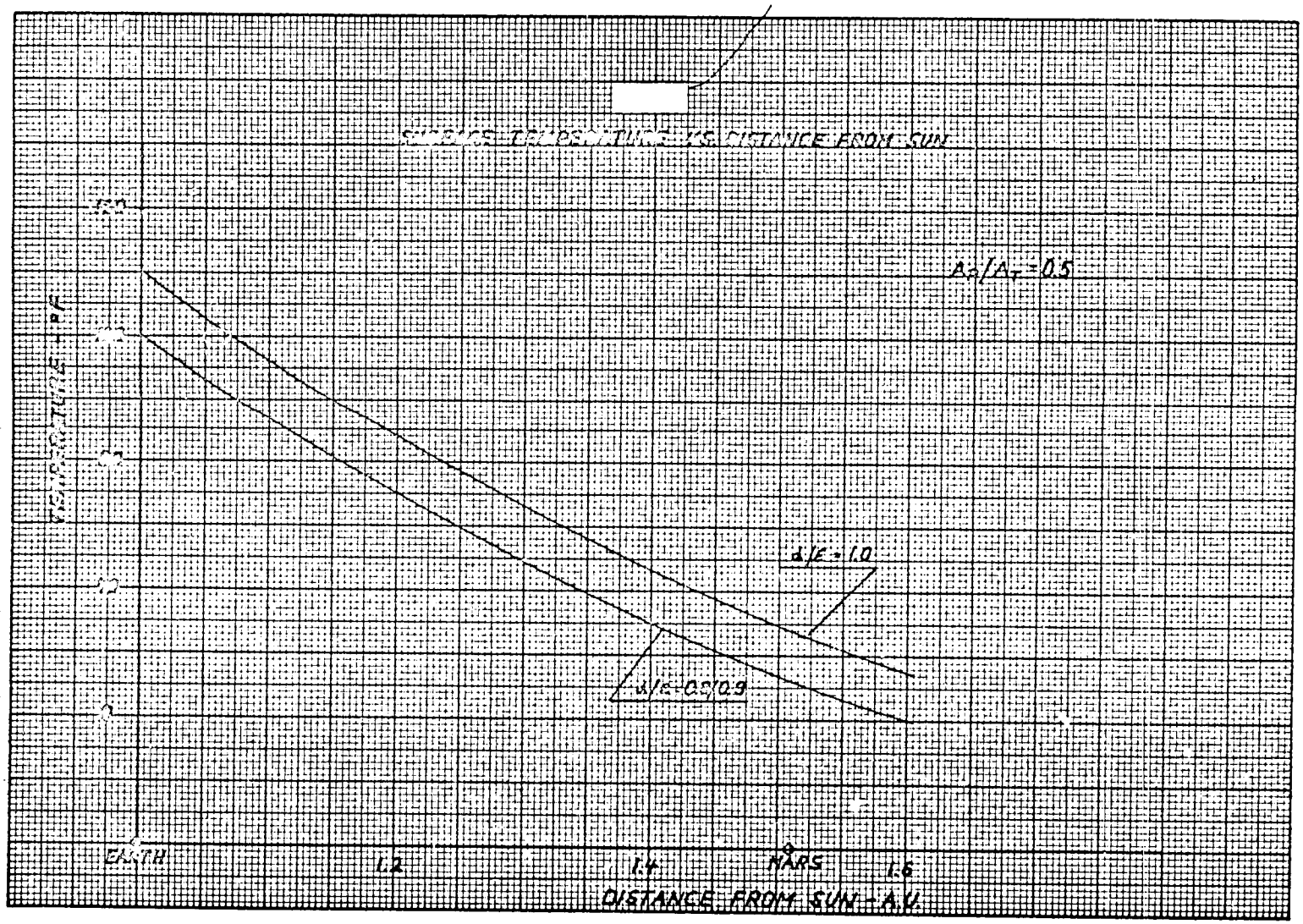

64-11395

Figure 103 SURFACE TEMPERATURE AS A FUNCTION OF DISTANCE FROM SUN

RE-ORDER No. 64-524

265

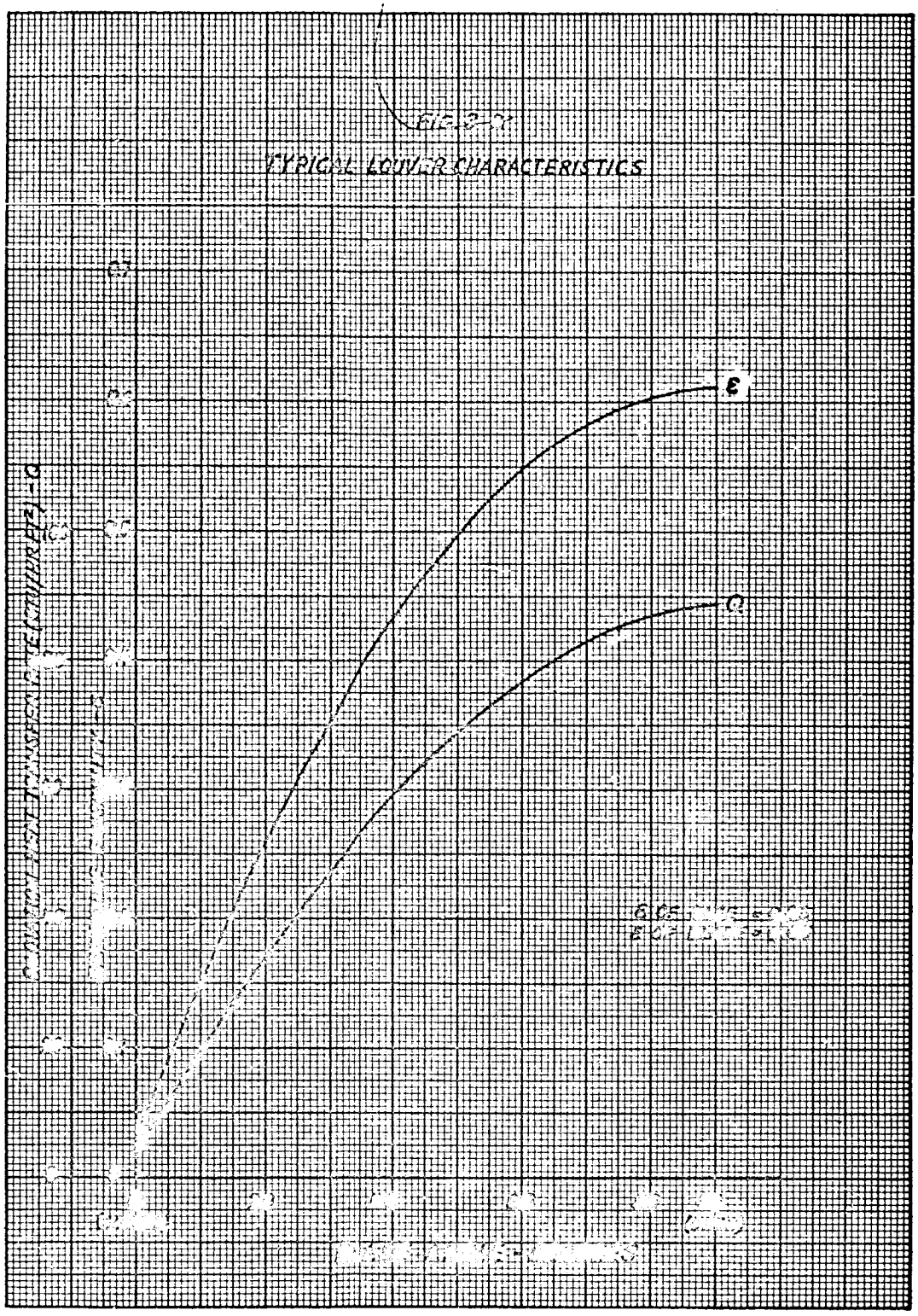

64-11396

Figure 104 TYPICAL LOUVER CHARACTERISTICS

266

In order to influence the conductive coupling effects, the designer can make use of simple insulation techniques, as well as adjusting the contact resistance across joints.

Figure 105 shows the effective conductance (in vacuum) across an insulating bat made up of several layers of superinsulation (aluminized mylar). In figure 106 an illustration of contact resistance for different types of adjoining surface Ref (2) is shown. Naturally, the designer cannot prescribe a specific desired value of the contact resistance, as it would be very difficult to duplicate, during production from one vehicle to the next, the specific data required. However, he can very simply assure a low resistance by having clean and polished surfaces meet each other; conversely, if a section is to be thermally isolated, thin asbestos washers placed between the surfaces will accomplish this.

9.4 THERMAL CONTROL DURING MISSION MODES

1. Pad Operation

In order to allow complete freedom for equipment operations and check-out procedures while the spacecraft is mounted onto the booster on the pad, conditioned air (50-80°F, 50 percent RH) is blown into the interior of the shroud.

From a ground unit or mobile equipment, an air line is carried up along the mast out to the umbilical boom. A flexible rubber hose with light insulation will connect the air line with a quick-disconnect fitting mounted on the shroud. Unless this is done, sun input to the latter may produce interior temperatures of the order of 125°F and higher with equipment operating.

In case of malfunction (or power loss) on the part of the air-conditioning equipment, during daytime operation, all electronics must be switched off. Should it happen during the night, continued operation should be limited to approximately 1/2 hour.

2. Launch and Ascent

By using a lanyard disconnect, in conjunction with the flexible hose, at the moment the boom is retracted, it is possible to maintain prescribed interior temperature levels up to lift-off time and thus be independent of countdown procedures during eventual hold-down extensions.

Both the inlet air fitting, as well as the opening for the exhaust (placed in the upper part of the shroud), are provided with q-doors which will automatically close when the airspeed reaches 70 ft/sec.

The influence of aerodynamic heating during ascent is minimized by proper shroud design. The interior surface temperatures of well-designed shrouds are generally kept below 450-500°F because of structural requirements and

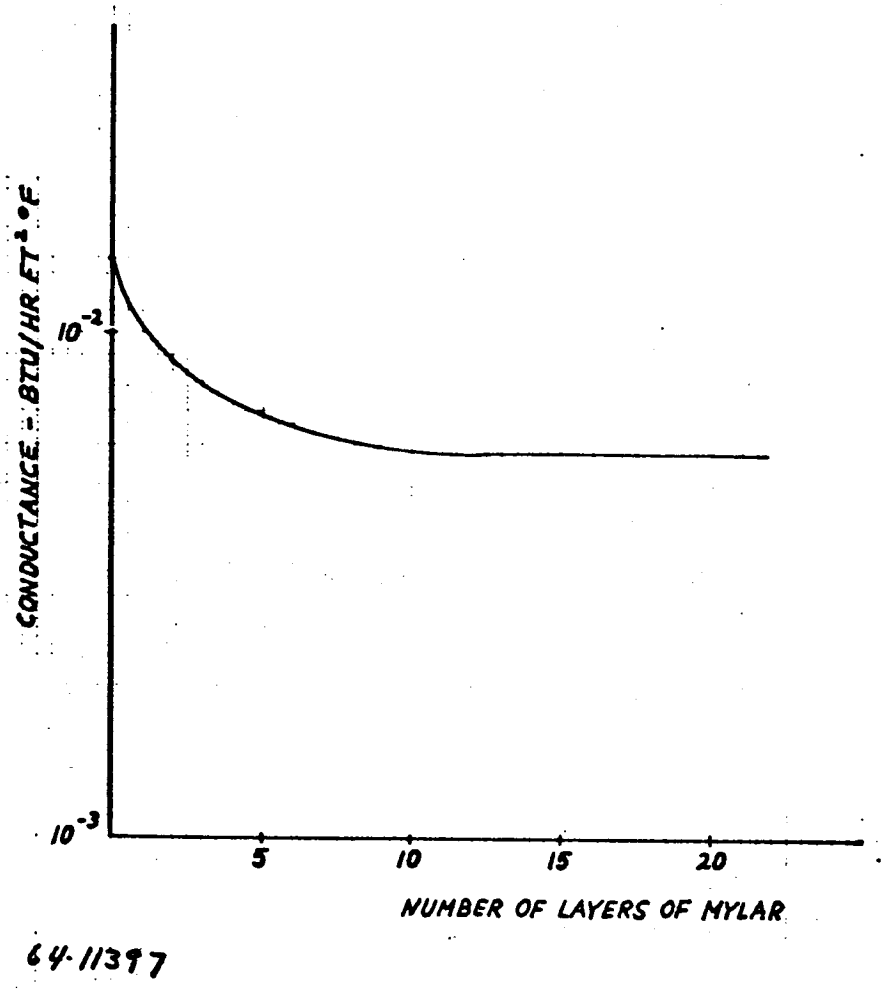

Figure 105 THERMAL CONDUCTANCE AS A FUNCTION OF NO. OF MYLAR LAYERS

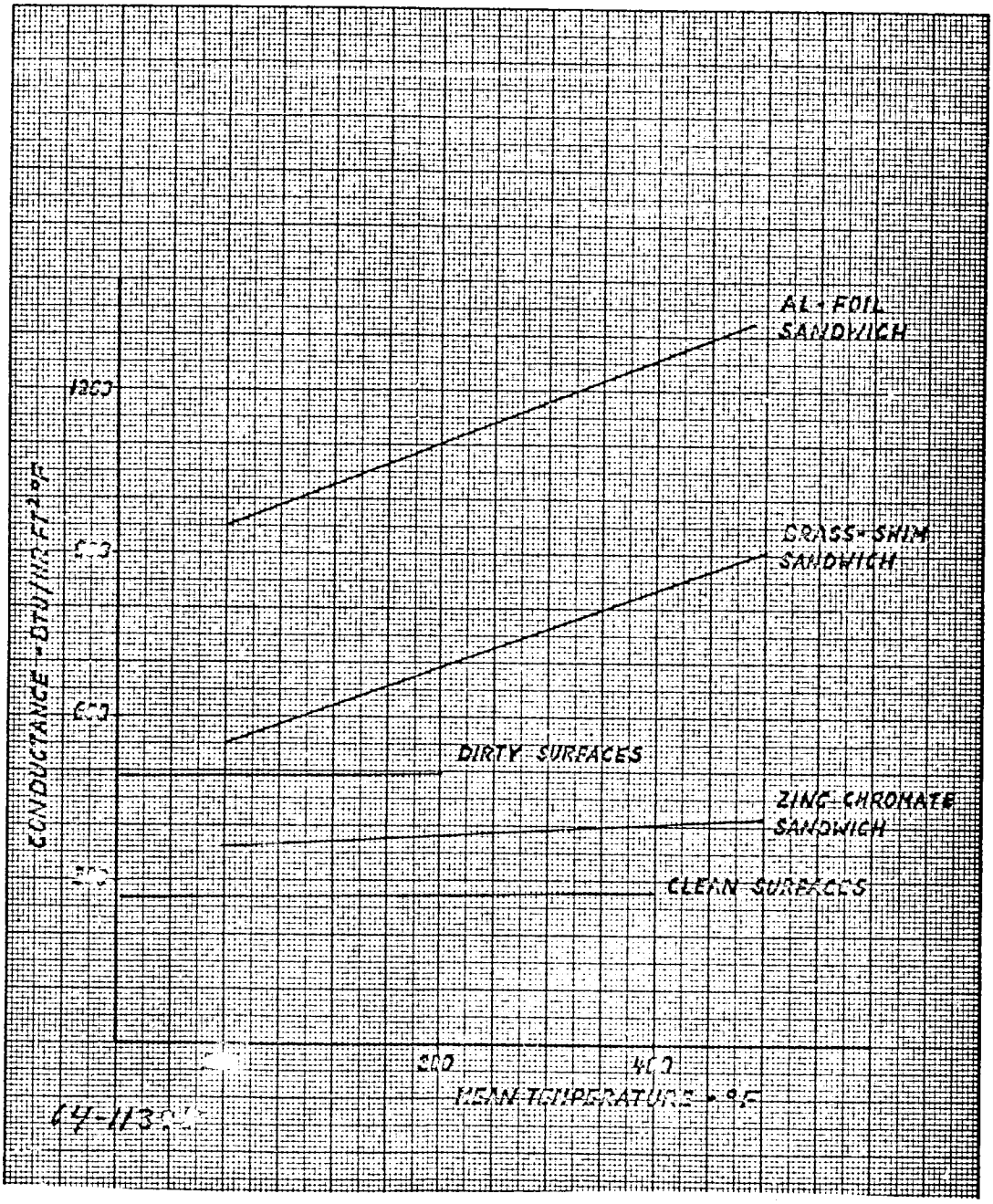

Figure 106 CONTACT RESISTANCE FOR TYPICAL METAL JOINTS

protection for the pyrotechnique subsystems. A low emissivity can be obtained by placing aluminized tape (or vacuum deposited AL-layer) on the inside surface. A simple heat balance for the heat transfer from shroud to vehicle will show the adequacy of this approach. The heat transfer from one surface at 450°F, having an emissivity of $\epsilon \sim 0.1$ to another at 60°F, is 104 Btu/hr-ft^2.

Because the actual duration that the shroud internal surface is at a high temperature is approximately the time interval from peak temperature to fairing ejection i.e. about one minute, it is seen that the integrated energy received per unit area is 1.7 Btu, which is negligible.

3. Interplanetary Journey

Temperature distribution over the spacecraft was determined for cruise mode operation near Earth, near Mars, and near Mars after lander separation. Black box temperature was determined for a maneuver near Earth, and a maneuver near Mars. In both cases it was assumed that solar energy would fall directly on the black box compartments.

a. Cruise Mode

In the cruise mode the Sun is perpendicular to the main panels of the bus, thus causing the lander to be in the shade in the reference configuration. The lander can receive heat by radiation from flyby/bus, and it is assumed that the lander surface, which radiates to the flyby/bus is at -60°F. Figure 107 shows the cross section of the spacecraft and the mode number relation to configuration. In Figure 108 through 110 is shown the steady-state temperature of the Advanced Mariner near Earth, near Mars before lander separation, and near Mars after lander separation.

b. Maneuver Mode

In the maneuver mode the solar energy impinges on the spacecraft perpendicular to the longitudinal axis. The total projected area exposed to the sun is reduced, while the total radiating area remains constant.

A parameter which is important in the analysis of the transient characteristics is the heat capacity of the system, that is the black box loading. Three different cases have also been considered here: nominal unit area weight, 12 lb/ft^2, as well as very light, 4 lb/ft^2, and very heavy, 20 lb/ft^2. With each bay having an effective louver area of 4.6 ft^2, the total mass for 6 bays corresponds to 110, 330, and 550 pounds for light, nominal, and heavy respectively. The total weight of electronic equipment for instruments, power supply, guidance and control, and telemetry for the Advanced Mariner is about 350 pounds.

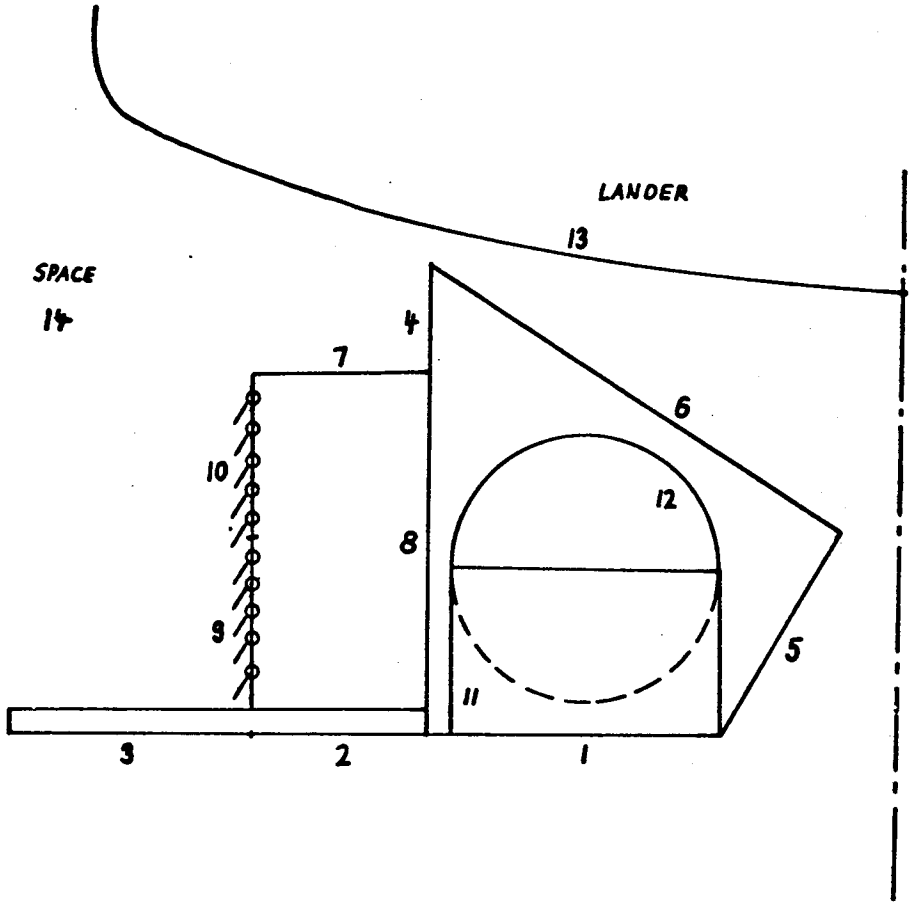

64-11399

Figure 107 NODE NUMBER FOR 60-DEGREE VECTOR

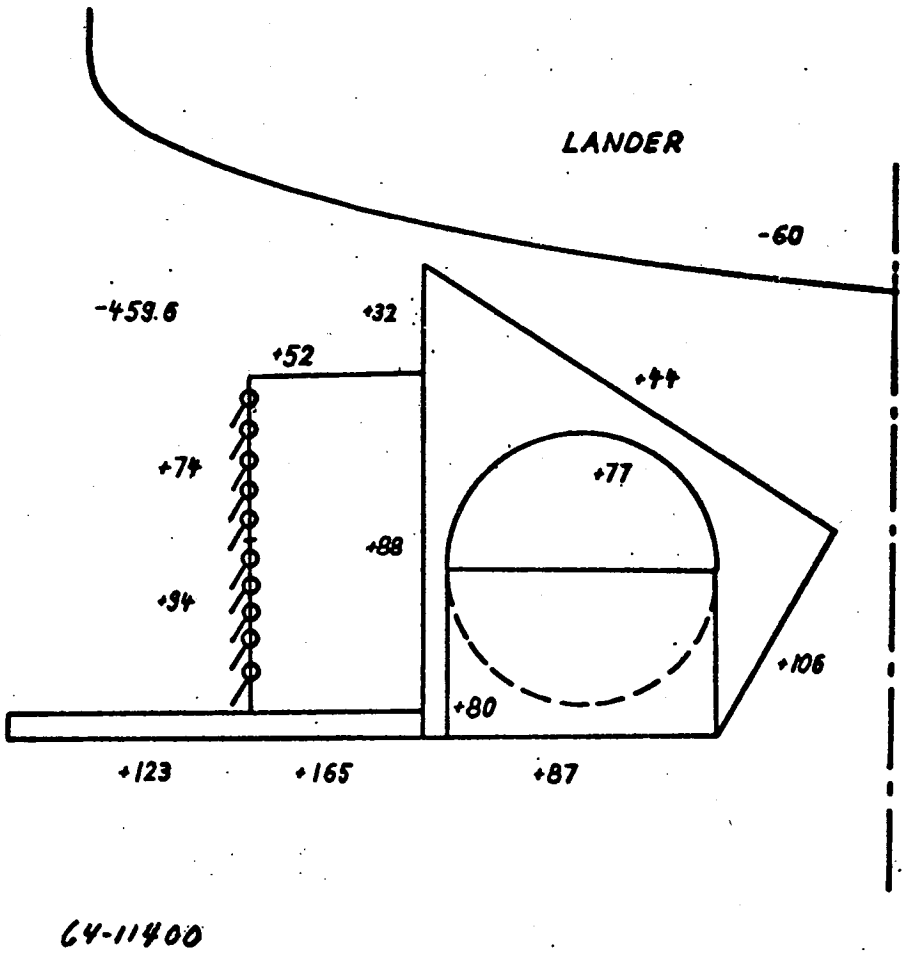

Figure 108 TEMPERATURE LEVELS NEAR EARTH

272

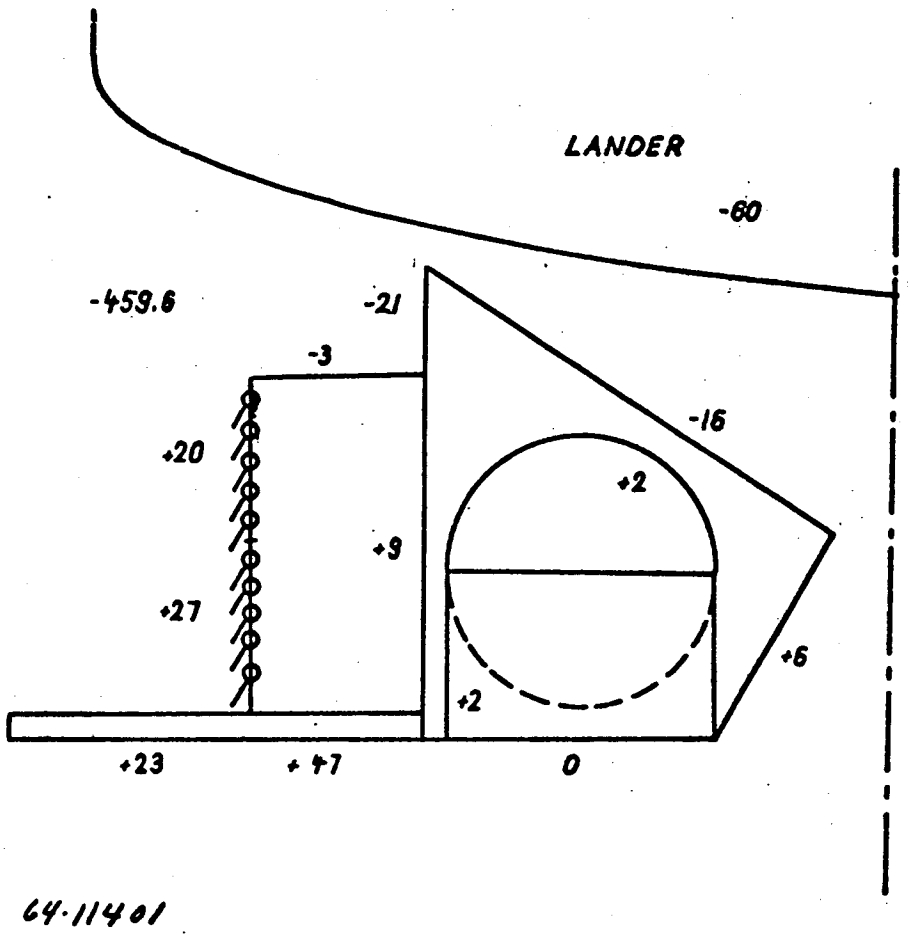

Figure 109 TEMPERATURE LEVELS NEAR MARS

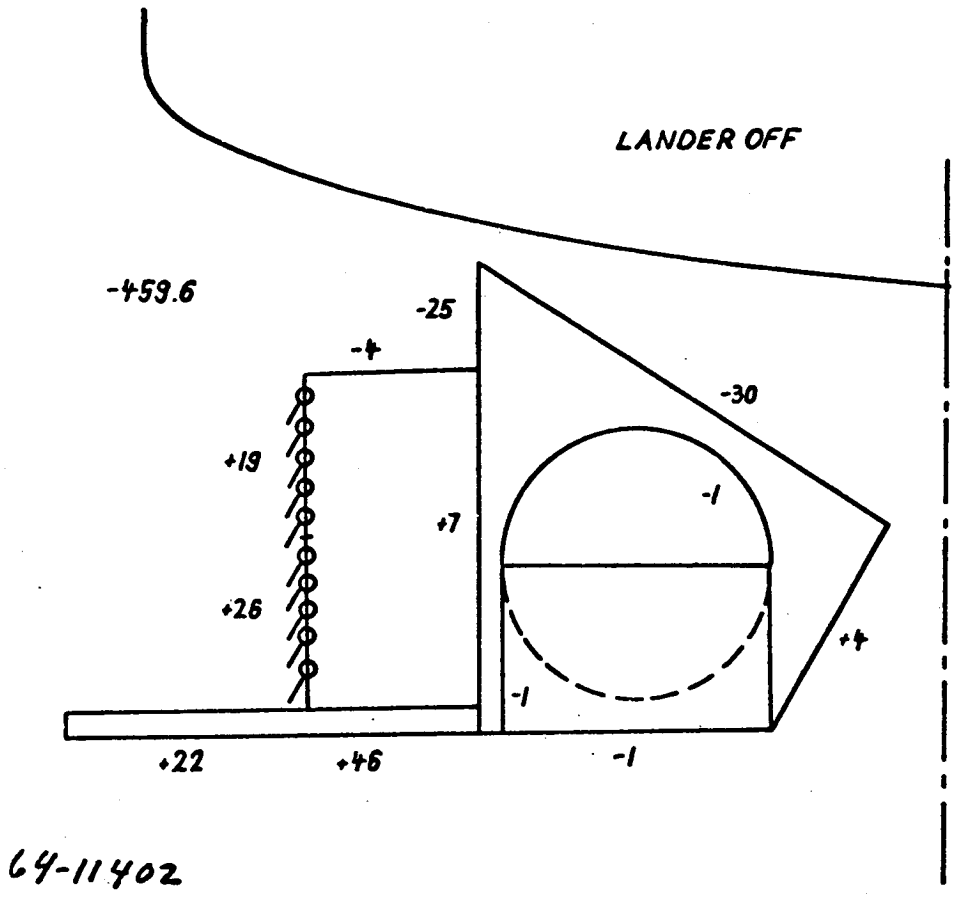

Figure 110 TEMPERATURE LEVELS NEAR MARS PORT SEPARATION

With respect to α and ϵ values, it has been taken for granted that the selected values remain as chosen. In order to study this parameter, some computer runs with 50 percent increase in values were also made. In general, α values will increase due to degradation effects of UV exposure. However, the resultant enlarged input of solar energy is offset by the decrease in solar constant as the vehicle recedes from Earth. The selected ϵ value of 0.1 for most surfaces can be obtained by iridizing those aluminum surfaces which radiate to the universe. These analyses have, therefore, been made with $\epsilon = 0.1$, as well as $\epsilon = 0.15$.

Insight of failure mode characteristics has also been obtained. Although louvers have been perfected to assure high reliability (over 10 million open-close motions), it is of interest to see what happens if the louvers get stuck in either the fully opened or fully closed position. A few runs have thus been made with louvers "fully opened", as well as "fully closed".

Three manuever times were considered. The maneuver was approximated by a sinusoidial variation from spacecraft sun orientation to a 90-degree pitch and return to sun orientation. The time to go from 0° to 90° was taken as 20 minutes for Case A, 15 minutes for Case B, and 10 minutes for Case C.

Figure 111 shows the effect of time upon a light-weight louver system (4 lb/ft^2). The three upper graphs represent the response of a louver which becomes exposed to direct sunlight, whereas the three lower graphs are for a shaded louver. The dashed line is the response of a fully closed louver in the shaded section of the vehicle.

Figure 112 illustrates the mass, as well as the time parameters. The turning maneuver near Mars is of longer duration due to the increased burning time for the slow-down phase. Figure 113 shows the effect of a prolonged exposure time for Node 10 when in shade (lower graphs) or sun exposed (dashed graph).

In figure 114 the response of Node 9 is shown. The curves above the horizontal steady-state line show that acceptable temperature rises will be experienced even for light-weight louvers when exposed to direct sunlight. Node 9 shows less response than Node 10 because the former is a longer time in shadow before the sun rays impinge during the turning motion. The louver in shade all the time, has a response as indicated by the curves below the line.

Figure 115 shows the temperature response of the rear wall of the bay containing the equipment. In reality, the excursions will be much smaller than indicated because of the inertia of equipment attached to it, e.g., boxes, pipes, cables, and clamps.

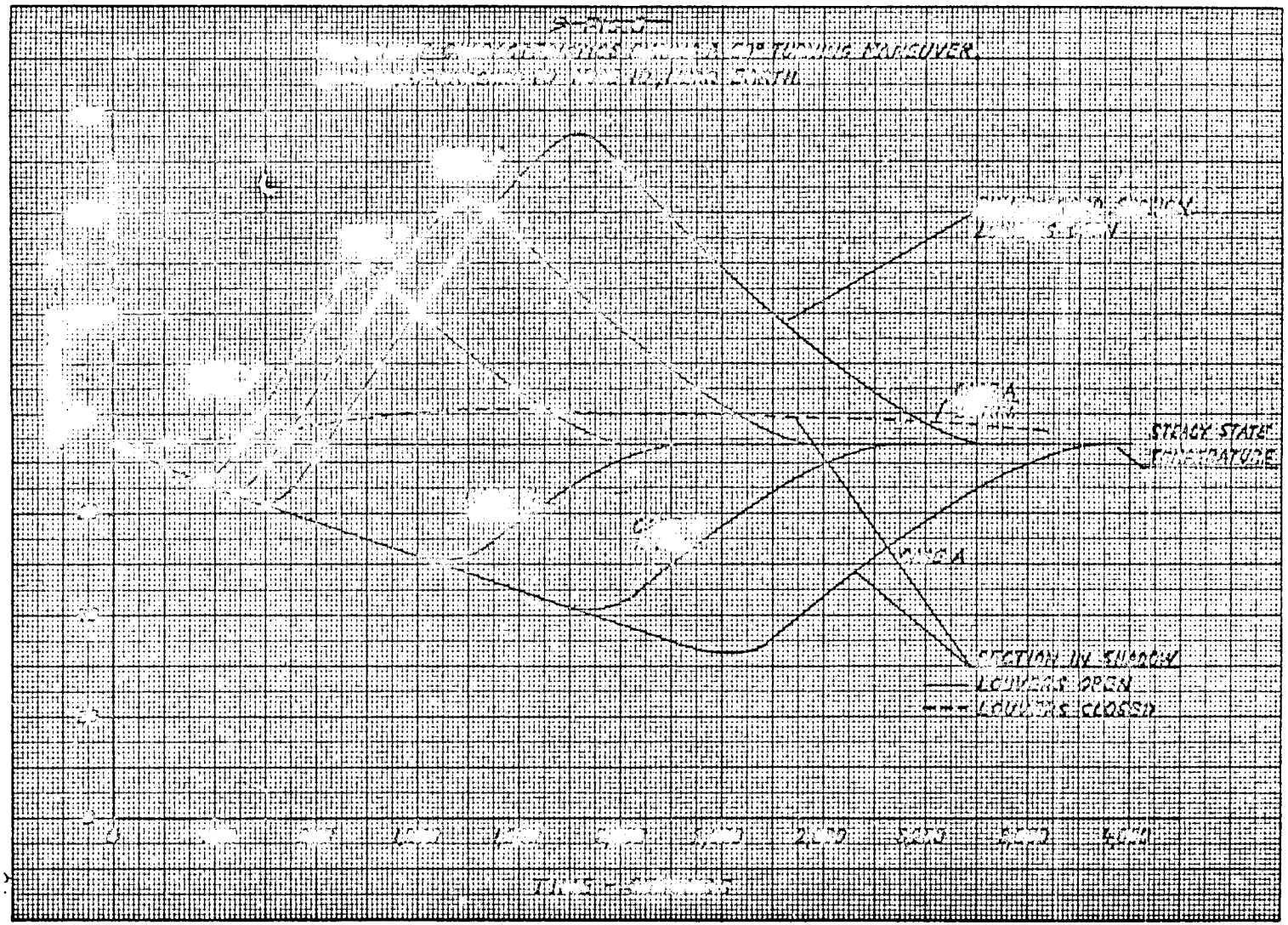

64-11403

Figure 111 TRANSIENT CHARACTERISTICS DURING A 90-DEGREE TURNING MANUEVER m = 4 LB/FT^2 ATTACHED TO NODE 10, NEAR EARTH

RE-ORDER No. 64-524

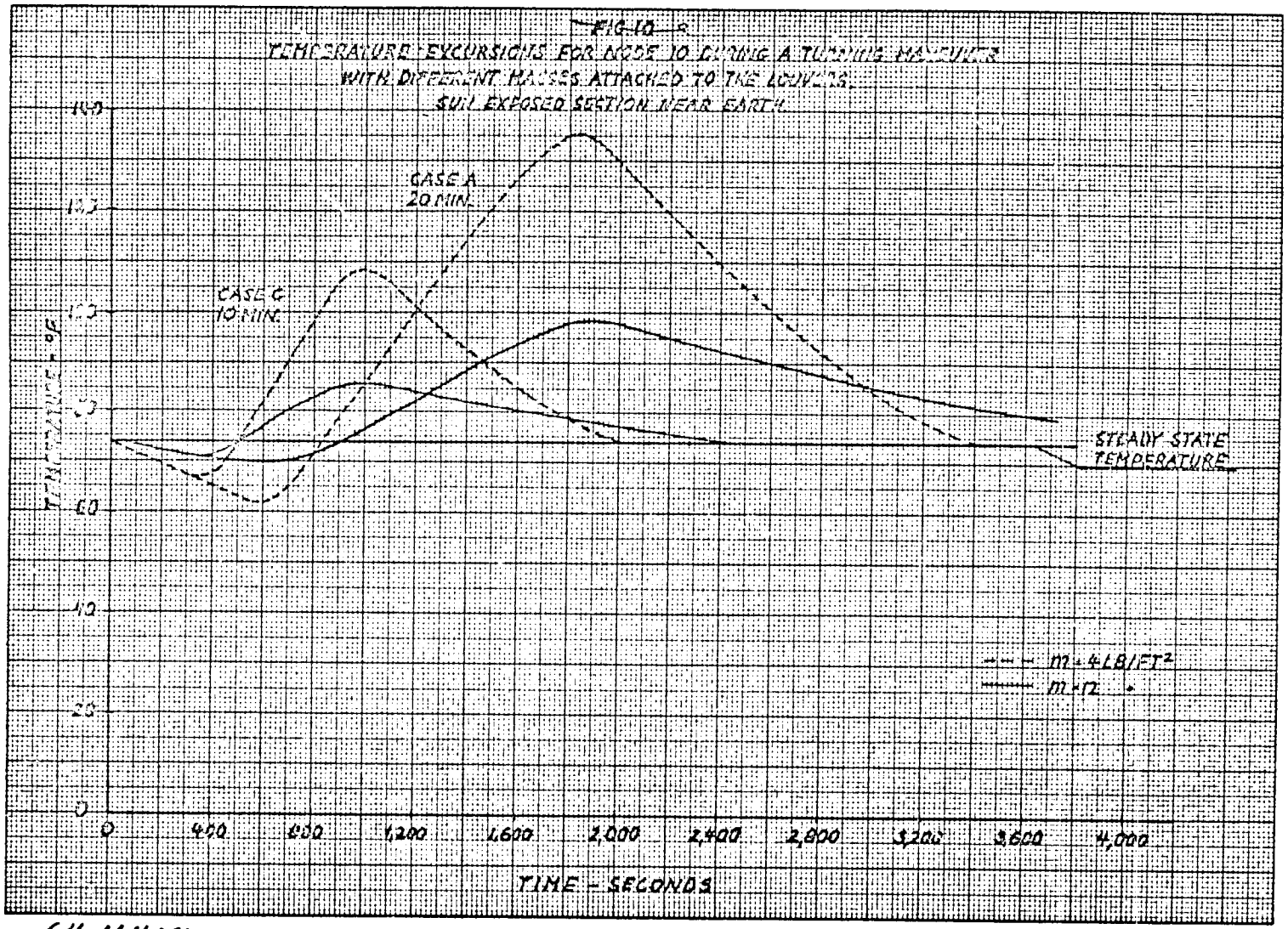

64-11404

Figure 112 TEMPERATURE EXCURSIONS FOR NODE 10 DURING A TURNING MANUEVER WITH DIFFERENT MASSES ATTACHED TO THE LOUVERS, SUN EXPLORED SECTION NEAR EARTH

RE-ORDER No. 64-529

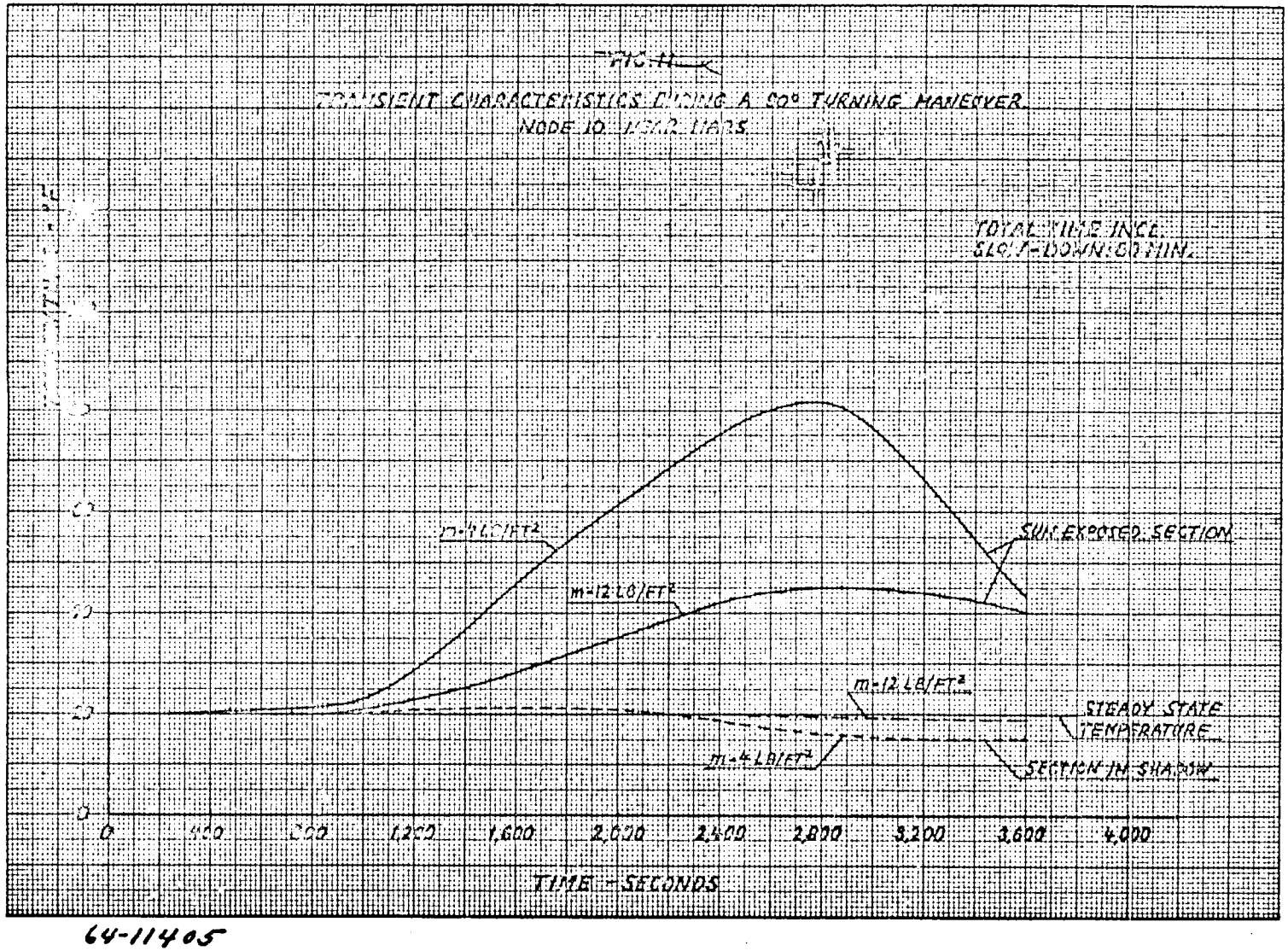

64-11405

Figure 113 TRANSIENT CHARACTERISTICS DURING A 90-DEGREE TURNING, NODE 10, NEAR MARS

RE-ORDER No. 64-524

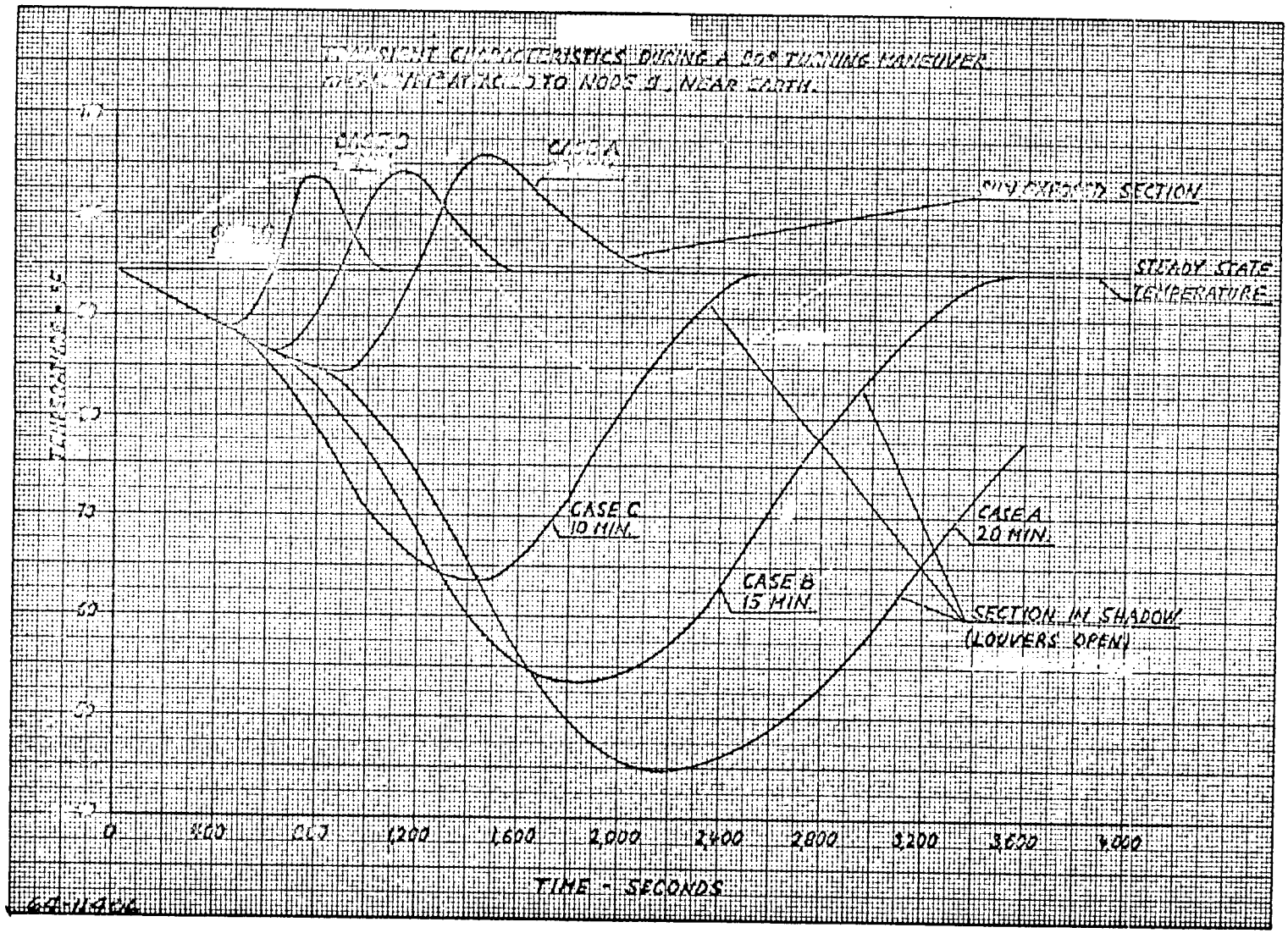

Figure 114 TRANSIENT CHARACTERISTICS DURING A 90-DEGREE TURNING MANUEVER, m = 4 LB/FT^2 ATTACHED TO NODE 9, NEAR EARTH

RE-ORDER No. 64-524

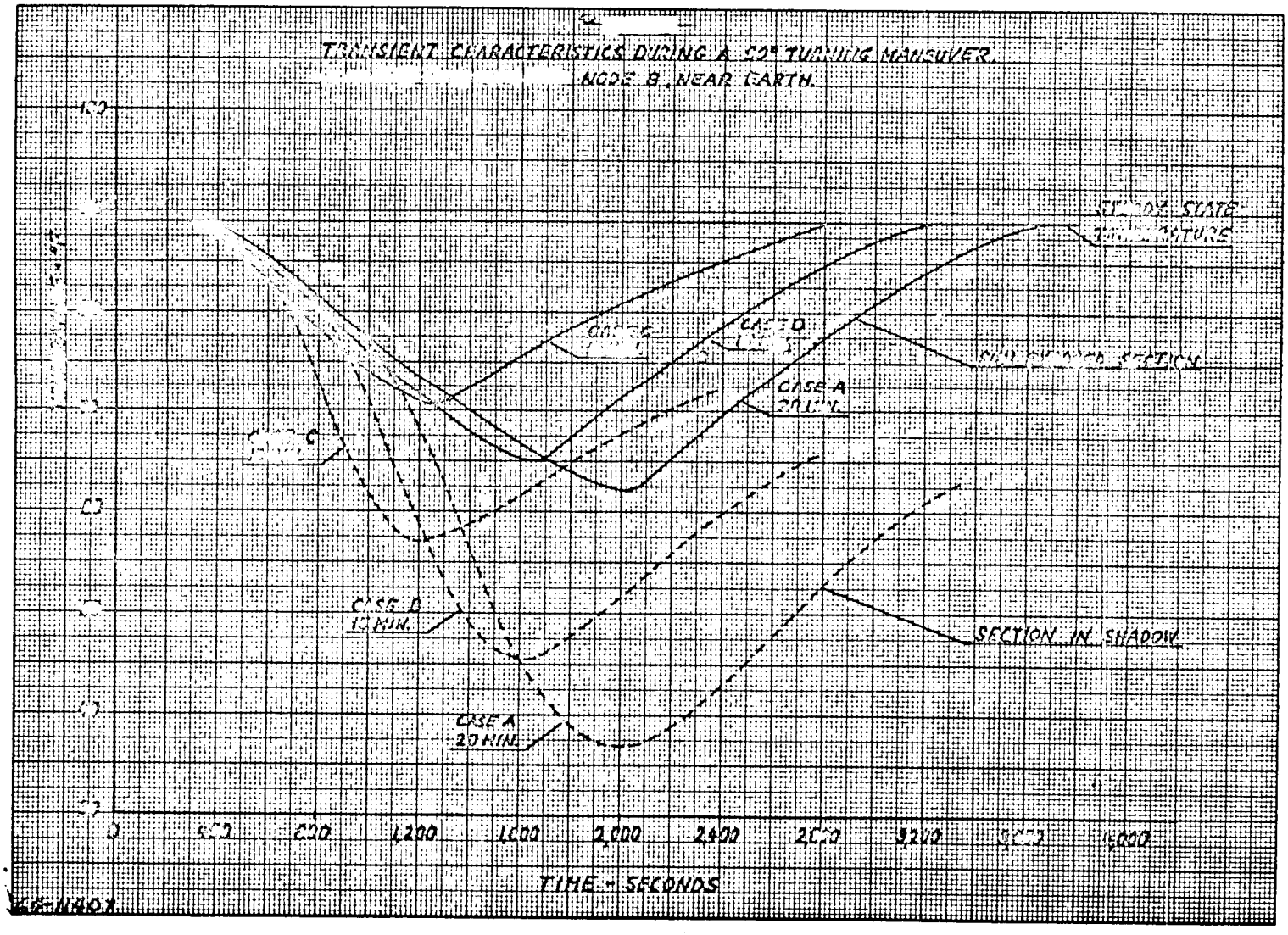

Figure 115 TRANSIENT CHARACTERISTICS DURING A 90-DEGREE TURNING MANUEVER, NODE 8, NEAR EARTH

RE-ORDER No. 64-524

283

Through the many illustrations, the influence of the different parameters have been shown to produce results which are well within acceptable limits. Because the individual instruments and electronic equipment boxes have not been finalized the analytical study had to use parametric values which covered a wide range. Whether the weight per unit area in reality 8.9 or 13.7 lb/ft^2 is of little importance because the study covered the whole range from 4 to 20 lb/ft^2. The designer will therefore be guided by the results which indicate that very light loading of the louvers (mass per unit area) should be avoided. Similarily, the influence of time is easily evaluated irrespective of the actual time taken for a maneuver; as long as the parametric study covers a wide range and its results stay within the requirements the actual maneuver time is of little consequence.

The thermal control weight requirement is:

1)	Surface coating	5 pounds	
2)	Louver assembly	21 pounds	(0.9 lb/ft^2)
3)	Insulation	10 pounds	

REFERENCES

1. J. Plamedon: Analysis of Movable Louvers for Temperature Control, JPL TR 32-555.

2. M. Barzley: Thermal Conductance of Contact in Aircraft Joints, NASA TND-426 and NACA TN-3167.

RE-ORDER No. 64-524

10.0 SEPARATION SYSTEM

10.1 DESIGN CONCEPT

Major considerations in the development of a lander/flyby separation system are as follows:

1. Physical arrangement.
2. Sterilization
3. Separation mechanism.
4. Lander stabilization.
5. Lander propulsion.
6. Lander dispersion.

Lander dispersion error analysis has been treated parametrically and the approach and results are contained in Volume 2, Systems Analysis. Primarily these analyses considered the effect of errors at separation in lander thrust angle of application, lander ΔV magnitude, bus flight path angle, on lander entry angle. An additional analysis evaluated the spin rate requirements of the separated lander. The approach followed in this study for the other major areas and in previous related effort has been to evaluate concepts and tradeoffs qualitatively, using quantitative analysis to confirm major choices. This section considers the overall separation sequence and also describes the pertinent analytical design studies.

The sequence of events and the implementation of these events follow overall guidelines that generally attempt to:

1. Minimize the probability of catastrophic failure (defined as loss of both bus and lander due to the separation maneuver).

2. Minimize the probability of planet contamination.

3. Minimize dynamic disturbance both to the lander and bus during separation.

4. Minimize tip-off errors.

5. Minimize impingement of lander retro exhaust plume field on the bus. A brief study indicated that separation distances greater than 100 feet were adequate to reduce this problem to negligible terms. To be conservative, a separation distance of 1,000 feet at the time of lander retro-ignition has been assumed.)

282

6. Maximize overall system reliability.

It should be noted that the sterility requirement imposes a reliability penalty on the separation subsystem, in that the necessity for canister removal adds extra steps in the sequence and increases the complexity of the separation pyrotechnic system.

The separation system concept is summarized by the following characteristics:

Sterilization--hard canister

lander and canister are separated as a unit.

canister cut into at least 4 "orange peel" segments.

canister jettisoned centrifugally.

Physical arrangement--lander positioned on top of bus (see figure 6).

lander retro rocket attached to lander base.

lander tied down at 3 hard points.

Separation mechanism--explosive nuts and springs.

Lander stabilization-- spin up to 20 rpm immediately after separation, using spin rockets.

yo-yo despin to zero immediately upon completion of retro rocket firing.

The sequence of events during the separation maneuver as shown in figure 116 and figure 117 illustrates the basic events. The weight summary of the separation system concept is persented in table 48.

TABLE 48

LANDER SEPARATION SYSTEM WEIGHT SUMMARY

Sterilization Canister	60.0 Pounds
Separation Joints	3.3
Shaped Charge for Canister Separation	6.5
Spin Rockets	2.8
Propulsion	23.0
Yo-Yo Despin	9.5
Bracketry, Fittings, Leads	5.5
	110.6 Pounds

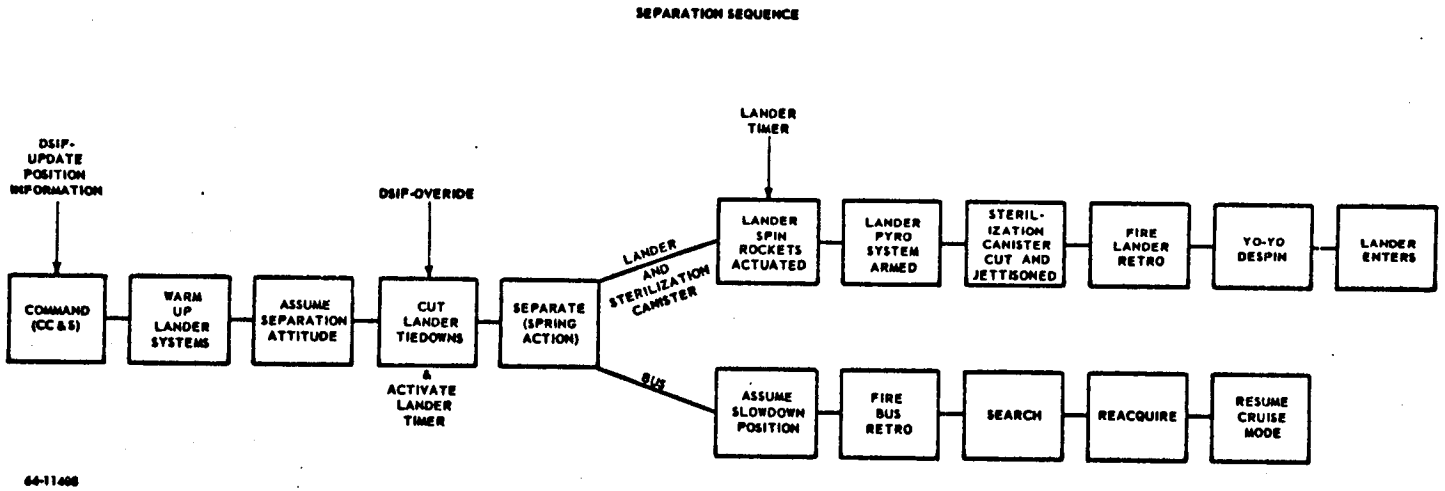

Figure 116 SEPARATION SEQUENCE

RE-ORDER NO. 64-524

284

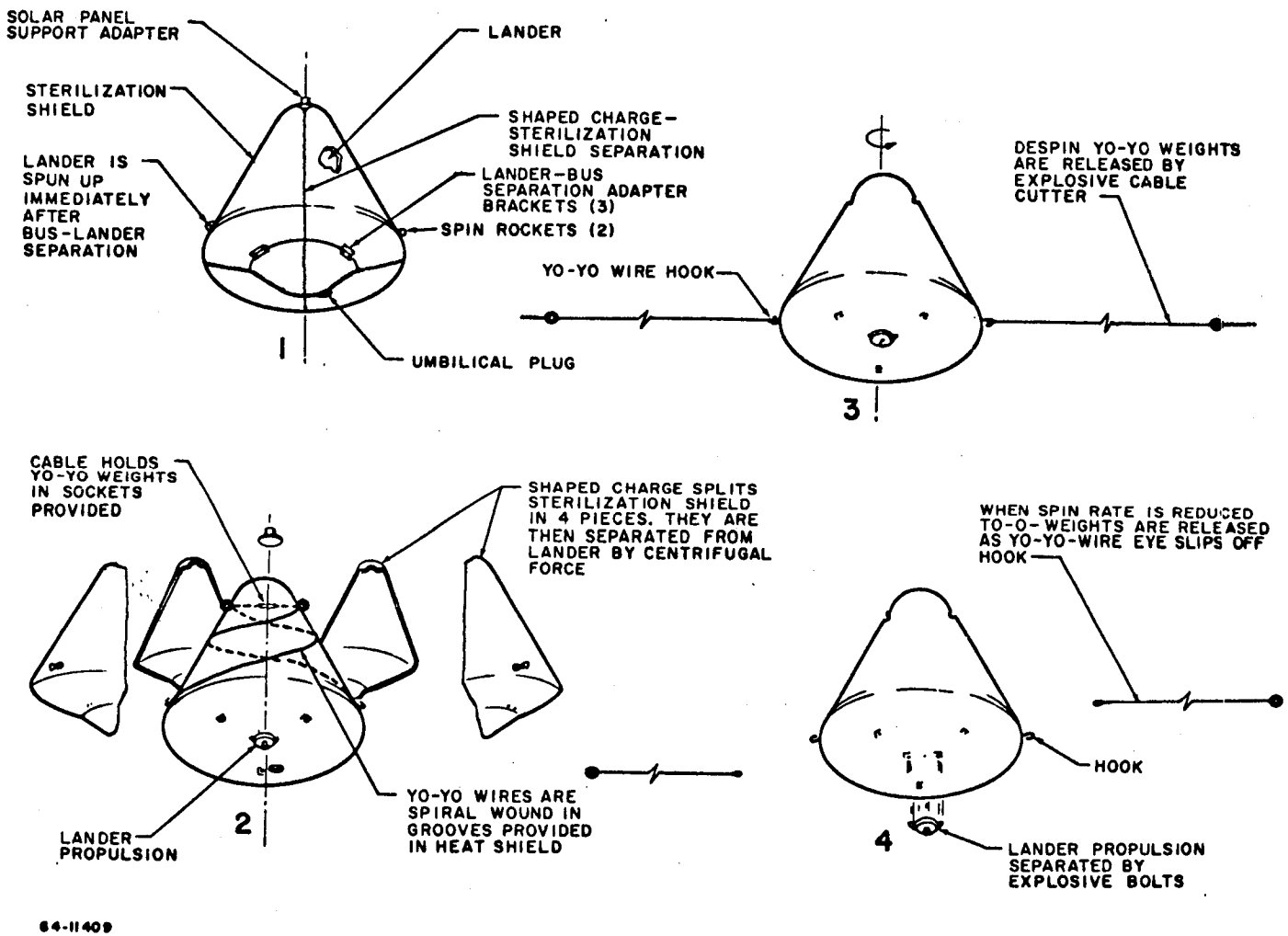

Figure 117 LANDER SEQUENCE AFTER SEPARATION

RE-ORDER NO. 64-524

282

Rationale and analysis used in developing the preceeding system characteristics follow.

10.2 PHYSICAL ARRANGEMENT

The configuration location of the separation system and its components is controlled by tradeoffs between packagingconvenience, payload envelope constraints, and overall system reliability. Several different basic combinations were considered--included were, top mounting of the lander with the retro at either the apex or base of the lander, and central or "bottom" mountings with the retro located again either at the apex or at the base of the lander. These alternatives are shown schematically in figure 118.

Although the "bottom" mounting allows the use of a larger diameter lander capsule, it does so at the expense of complicating launch load path design and additional packaging complexity. "Bottom" mountings were therefore discarded as causing unnecessary complication.

"Top" mountings were then evaluated. Location of the engine at the lander base is undesirable because of packaging, bus/lander interface, canister configuration, and separation system location and actuation problems. However, the most attractive alternative--lander on top of bus with retro-engine at the apex of the lander presents two major problems. With the engine at the apex of the lander, there is a small but finite probability that in case of a severe tipoff error, or failure (or malfunction) of the bus slowdown system, the entire mission could be terminated due to a vehicle collision. In addition, the effect of misalignment errors between the lander c. g. and the lander retro engine thrust vector is magnified by this configuration. (The effect of this magnification on lander spin rate requirement is shown in Systems Analysis Volume, Vol. 2.) It is also probable that a lander structural weight penalty would be incurred by location of the engine at the apex.

The recommended configuration is then a "top" mounting of the lander with the retro engine attached to the base of the lander, inside the sterilization canister. While this arrangement does complicate the packaging of the bus propulsion system and the separation mechanism, the gain in overall system reliability is overriding.

10.3 STERILIZATION

It seems logical to assume that a definite requirement for sterilization of vehicles entering the Martian atmosphere will exist until at least preliminary investigation of possible life forms is completed. Various sterilization modes have been reviewed during this study and previous work. Among the possibilities considered were hard rigid canisters, flexible covers, self-sterilizing coatings,[1]

[1] Willard, M., and A. Alexander, A Self Sterilizing Coating for Spacecraft Surfaces, Nature Vol. 202 (16 May 1964).

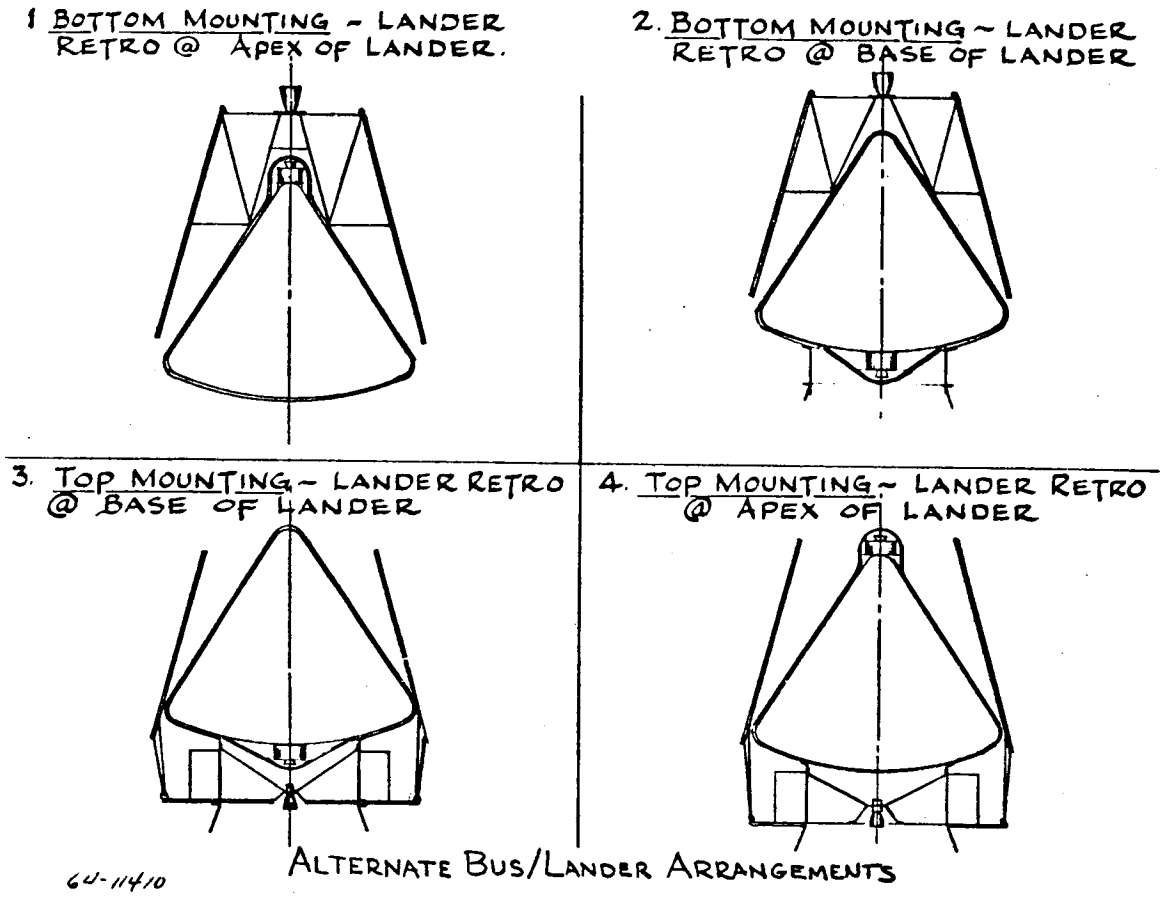

Figure 118 ALTERNATE BUS/LANDER ARRANGEMENTS

and solar sterilization in transit. The "hard" canister imposes a significant weight penalty on the vehicle. However, in view of the high probability of violation of the sterilization barrier during the assembly, checkout, and launch sequence, the "hard" canister seems preferable to flexible covers or self-sterilizing paint. In-transit solar sterilization may prove attractive, but it is currently unproven and its use also leaves open the possibility of contamination of the lander by unsterilized attitude control cold gas products during the flight.

The choice of barrier for sterilization assurance is an aluminum shell with case hardened polyurethane foam on the outside to provide meteoroid protection. Although this choice results in a significant weight penalty, in view of the absolute requirement for lander sterility this mode of protection seems to be the most feasible.

Sequences of Removal

The sequence of operations predicated on canister removal is based on the assumption that the probability of violating lander sterility is less during a remote canister jettison action than in the immediate bus vicinity. That is, if a flux of viable organisms is associated or attached to the bus, presumably the magnitude of this flux decreases with distance. If lander sterility is an overriding criterion then the probability of the lander encountering a viable earth organism must be minimized. A maneuver sequence in which the total canister is jettisoned after separation would then seem to result in the least possibility of lander contamination.

Although to a certain extent this procedure reduces lander mission reliability, it should be noted that it does in some respects simplify the bus/lander separation sequence. The burden of canister removal is completely transferred to the lander at some distance from the bus. Therefore the danger of a catastrophic failure of the overall mission during the separation sequence is reduced.

Cansiter Removal-- several alternative modes of canister removal were considered during the study. The decision to carry the canister with the lander at separation precludes the use of the simplest removal mode, i.e., cutting the spring loaded canister at its largest diameter while attached to the bus. Removal of the whole canister from the lander is complicated by the necessity for imparting minimal disturbance to the lander capsule. A requirement also exists for removal of the canister debris from the path of the lander after rocket firing.

The choice of canister removal mode is to cut the unit into 4 "orange peel" segments with linear shaped charges subsequent to lander spin up. The segments are then spun off centrifugally with a minimum of lander disturbance.

This mode of removal is not without problems, e.g., differential rates of shaped charge burning, possibility of lander contamination by secondary ejecta during cutting process, however it does appear preferable to other alternatives.

This procedure has one other major drawback in that after separation the segments will have residual spin about their own axes, and this spin may cause a corner of the piece to collide with the lander surface, possibly then, violating sterility, perturbing the lander, or chipping the heat shield. A graphical analysis was performed in order to investigate this situation. The results are shown in figures 119 and 120. If the canister is split into 2 or 3 parts, then the pieces will contact the lander. The canister must be cut into at least 4 pieces to avoid this problem. It should be noted that the results of the graphical analysis are independent of the spin rate and of the actual size of the lander and canister. As long as the geometry is the same, the motion will be the same.

10.4 SEPARATION MECHANISM

The choice of separation system mechanism is primarily dictated by a tradeoff between overall system reliability and the levels of position and rate error acceptable to the bus and lander attitude control system. (For study purposes it has been assumed that the bus gyro's can accept instantaneous position errors of up to 5 degrees and rates of 5 deg/sec without becoming saturated. Although these values are somewhat more optimistic than presently available units they are believed to be representative of the near term state-of-the-art.)

A broad spectrum of actuators, separation mechanisms, and possible combination systems were investigated during the study. It proved difficult to rank the system quantitatively without performing detailed design and analysis. The mechanisms were then evaluated qualitatively using relative reliability estimates, operating characteristics, and dynamic effects as guidelines. (Appendix B shows the relative reliability of the candidate separation system components.) Components considered were:

Release mechanisms:	Linear shaped charge.
	Explosive bolts and nuts.
	Ball lock.
	Mechanical latch.
	Marmon clamp.
Actuators:	Spring.
	Gas generator.
	Cartridge actuated device.
	"Fly-away".

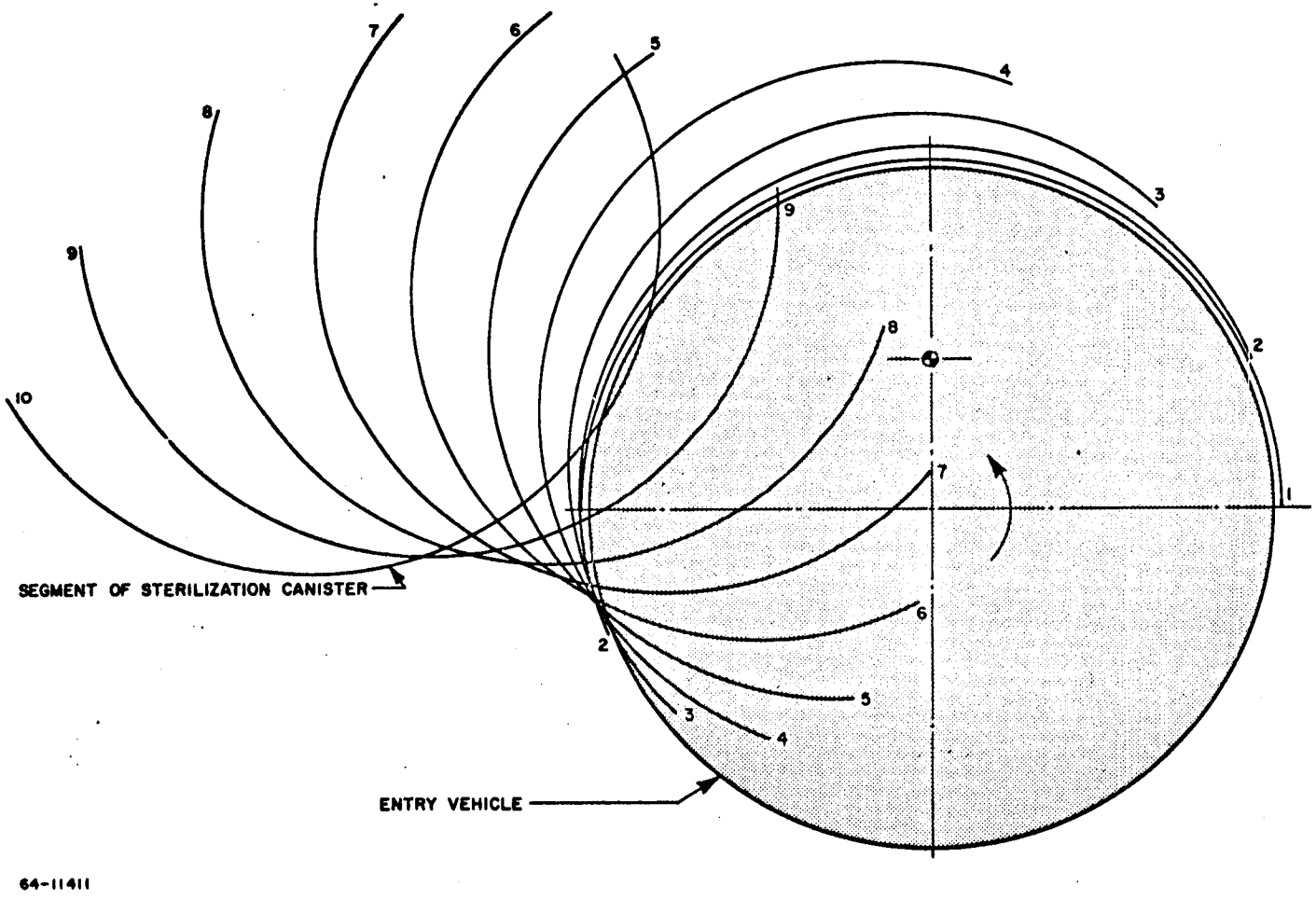

Figure 119 SPIN-OFF OF CANISTER -- TWO PIECES

RE-ORDER No. 64-524

290

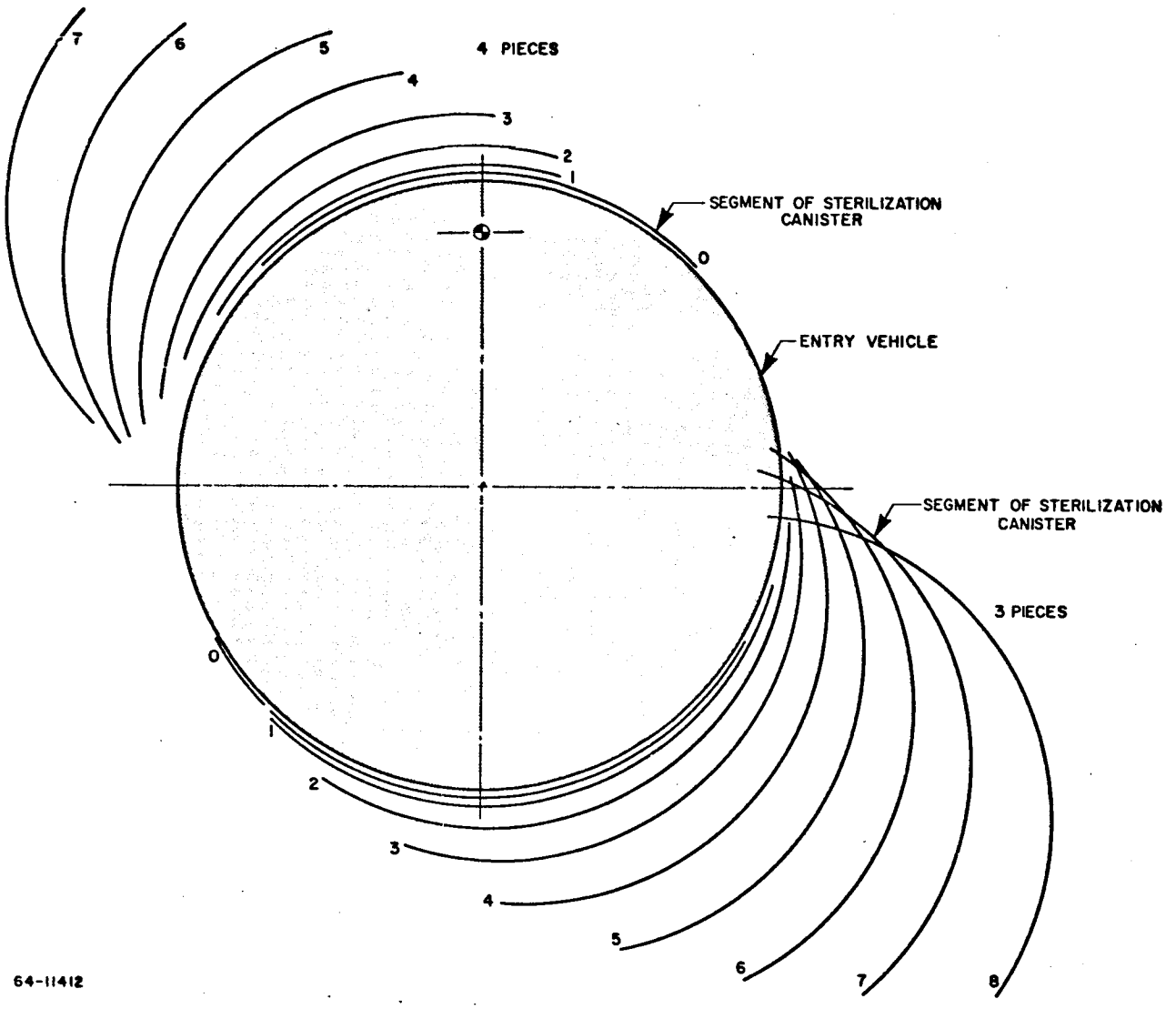

Figure 120 SPIN-OFF OF CANISTER -- THREE PIECES AND FOUR PIECES

The "fly-away" system is one in which the bus and lander are separated with minimal residual momentum imparted to the two vehicles. After separation the bus is "flown" away from the lander by using the bus cold gas system to translate and turn the bus. Although this separation mode appears attractive from the point of view of minimizing bus and lander dynamic disturbances, it has been discarded as being unnecessarily complex.

A review of component operating characteristics and reliability led to the choice of a combination of 3 explosive nuts and springs as the basic separation mechanism. A prime factor in the choice was the necessity for achieving separation without violating the sterilization barrier. The basic release and actuator mechanism is shown in figure 121.

The lander is mounted to the bus at three positions, each joint is identical and has four main items,

1. the adapter bracket

2. bolt catcher

3. explosive separation captive nut

4. separation spring

The adapter bracket is in the form of an angle and serves two functions.

1. To transmit the lander launch loads to the flyby bus.

2. To provide a base for the explosive-captive-type nut, separation spring and housing.

The adapter angle initially is mounted against the lander sterilization shield at hard points provided. It is attached to the lander payload by an attachment bolt from the lander payload bracket to the adapter bracket. A bolt catcher is provided on the lander payload bracket. The lander, including the adapter brackets, power cartridges, and separation springs are sterilized as one unit. After sterilization the lander is mounted to the flyby bus by four attachment adapter bracket.

Separation action is initiated by a signal from the CC & S. The signal activates the dual power cartridges, releasing the captive nuts and forcing the attachment bolt up into the lander bolt catcher. The separation springs exert the required separation force and the lander separates from the bus at a line between the sterilization shield and the adapter brackets leaving the adapter bracket assembly on the flyby bus. Three-point tie down has been chosen over a single central tie down because of the difficulty of packaging a relatively large spring in the already crowded central bus area.

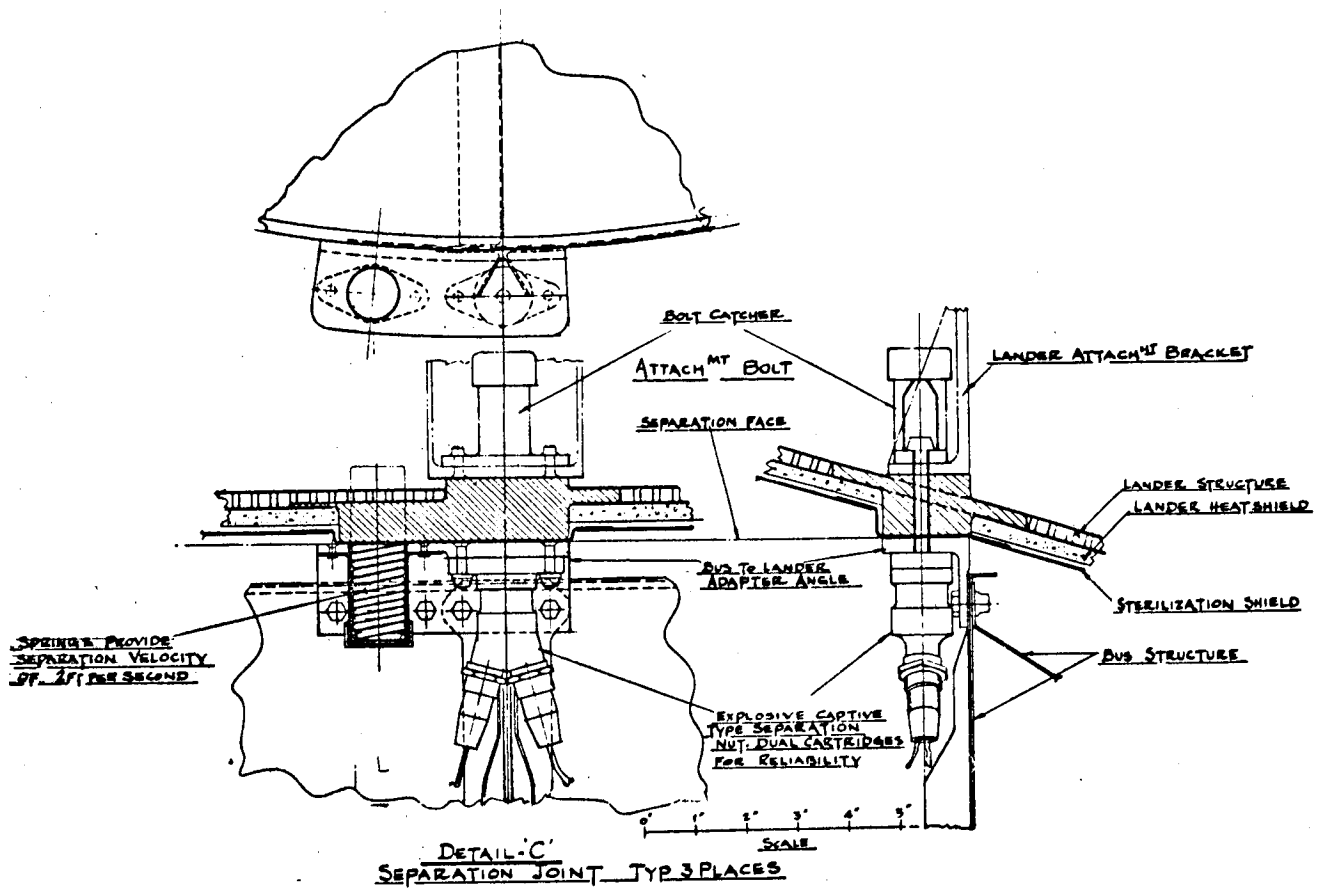

Figure 121 BUS/LANDER SEPARATION JOINT DETAIL

RE-ORDER No. 64-524

293

A brief study was conducted to determine desirable characteristics for the separation spring (see appendix D). This study also compared the system characteristics of one and three spring systems. It was concluded that a soft spring with long strokes is desirable since it tends to minimize tip-off error rates and positional charges for a given offset error.

10.5 LANDER STABILIZATION

Several possible lander stabilization systems were investigated during this study and during earlier related efforts. These combinations were:

spin rockets--spin up after separation.

spin rockets--spin up onboard the bus.

momentum wheels--spin up after separation.

momentum wheels--spin up onboard the bus.

lander attitude control system--sensors, logic, and torquers.

yo-yo system--
despin rockets-- } lander despin.

Appendix B contains reliability figures for spin rockets and an integral attitude control system. As would be expected, spin rockets are inherently more reliable than a complete attitude control subsystem. Spin rockets also would appear to be more reliable than relatively unproven momentum wheels. In addition, the use of a momentum wheel or an attitude control system would impose a considerable weight penalty, packaging problems, and added thermal control problems on the lander.

Spinup of the lander onboard the bus prior to separation significantly improves lander overall mission reliability. However, this procedure imposes a weight penalty and packaging problem on the bus due to the need for a spin table. Preliminary analysis indicates that the dynamic interaction between the spinning lander or momentum wheel and the bus attitude control system limit cycle damping mode may be unstable, creating a situation in which large quantities of attitude control gas are lost.

Lander attitude control prior to retrorocket firing is therefore attained by spinning up the lander to approximately 20 rpm immediately after separation with 2 small solid rockets located in the plane of the lander c. g.

The 20 rpm spin rate results in a requirement for two spin rockets having a total impulse of 59 lbs-sec.

Standard control rockets were investigated and it was determined that the Atlantic Research Corporation MARC-15A1 rocket is suitable for this application.

The rocket characteristics are as follows:

Thrust	32 pounds
Burn Time	0.88 seconds
Total Impulse	30 lbs-sec.
Total Weight	1.4 pounds
Useable Propellant	1.13 pounds
Length	5.27 inches
Diameter	1.53 inches

Despin

Because of the small difference between the lander moments of inertia about the roll, and pitch or yaw axes there is a possibility that the actual spin axis may not coincide with the desired spin axis at the time of entry. This would then lead to the possibility of the despin system causing rotation about the wrong axis. As there is a requirement for despin of the lander prior to entry, if the foregoing condition exists the probability of successful lander entry is diminished. Despin is therefore programmed to occur immediately after lander engine firing to minimize this possibility.

A yo-yo system is used to despin the lander. This system is simple, reliable and offers the additional benefit of exactly cancelling the original spin rate regardless of its value. (A definite bonus if one of the original spinup rockets fails). The yo-yo despin mechanism consists of two weights attached to cables. The weights are spherical and are housed in cup type sockets, one on each side of lander and are held in place during launch by a cable through the center of the lander. The tether cables are spiral wound to hooks that are mounted on each side of lander on the "X" axis through the lander c.g. At a signal from the lander timer, an explosive cable cutter is activated, cutting the cable and releasing the two weights on their tether cables. Over a period of time these weights reduce the spin rate to zero at which time the tether cables slip off the specially designed hooks separating the weights from the lander.

10.6 LANDER PROPULSION

The choice of type and configuration of the lander retropropulsion system is primarily controlled by packaging considerations and reliability. System requirements are as follows:

One firing period.

ΔV capability of 225 ft/sec for a lander weight of approximately 500 pounds.

Envelope restriction:	Maximum Length - 7 inches. Diameter - no restriction.
Temperature Limits:	Operation - -60°F to +130°F. Storage - same.
Sterilization Capability:	Flight engine - temperature soak for 24 hours at 135 °C in an inert atmosphere.

The system requirements were used in conjunction with the propulsion parametric curves to arrive at a required propellant weight of 13 pounds. A liquid propellant system would be unnecessarily heavy and complex for this application. Therefore, a solid propellant engine has been chosen. A survey of the engine vendors produced one engine that would meet the seven-inch length restriction. In this engine it was necessary to off-load the propellant 50 percent to meet the total impulse requirement. By off-loading the engine, the case length was reduced sufficiently to meet the seven-inch length constraint.

It is desirable from both the scheduling and the development cost viewpoints to use an existing or slightly modified engine, if possible. While the designated engine will not operate over the entire specified range of lander temperatures, it is felt that this problem can be overcome by minor development or by the use of propellant heaters in the lander to maintain the engine within its proven operating limits.

Modification of an existing engine results in a relatively inefficient mass fraction. As the weights involved are small, this is not considered to be a major drawback.

As noted in the requirements, the engine must be capable of meeting a temperature soak requirement for sterilization. At this time there is no engine that has been tested under such conditions, but no development problems of major consequence are currently anticipated by the propulsion companies.

The performance and design characteristics for the engine selected are given in table 49.

TABLE 49

CHARACTERISTICS OF LANDER RETROPROPULSION SYSTEMS

Performance Characteristics:	
Total Impulse	3,400 lb/sec
Specific Impulse	270 seconds
Propellants	Solid
Operational Temperature Range	10° - 140°F
Thrust Level	377 pounds
Design Characteristics:	
Mass Fraction	0.53
Weight Loaded	23 pounds
Propellant	13 pounds
Envelope - Length	7 inches
Diameter	10 inches

APPENDIX A

PAYLOAD PLATFORM, GIMBAL ORIENTATION, AND GIMBAL MOTION EQUATIONS

The technique for converting spacecraft-Mars cone and clock angles to a set of gimbal rotations is presented. Typical cone and clock angle variation for the 1969 launch opportunity is shown in figure 8 and 9 for a minimum inclination (to Martian equator) flyby. Also presented are the gimbal angle excursions for the 1969 launch opportunity that are required for the television optical axis to point towards the local vertical during flyby.

A. PROBLEM

When the vehicle is passing the planet on a flyby trajectory; the direction from the vehicle to the planet is defined at any time by the unit vector, $\bar{e}_{vp}$, as showm in figure A-1. The vehicle axes are defined by the orthogonal unit vectors $\bar{e}_1$, $\bar{e}_2$, $\bar{e}_3$ such that:

1. $\bar{e}_3$ is directed toward the sun

2. $\bar{e}_1$ is in the sun-Canopus plane, directed generally toward Canopus

3. $\bar{e}_2$ is directed such that $\bar{e}_1$, $\bar{e}_2$, $\bar{e}_3$ forms a right handed orthogonal set.

Information is available giving the direction of the unit vector $\bar{e}_{vp}$ with respect to $\bar{e}_1$, $\bar{e}_2$, $\bar{e}_3$ as a function of time. This information is presented in two different forms:

1. The cone-clock angles, ν and δ. These are two Euler angles: δ is a rotation about $\bar{e}_3$ and ν about $\bar{e}_2'$ such that $\bar{e}_3'$ is in the direction of $\bar{e}_{vp}$.

2. The direction cosines, a_1, a_2, a_3. These are defined by:

$$a_1 = \bar{e}_{vp} \cdot \bar{e}_1$$

$$a_2 = \bar{e}_{vp} \cdot \bar{e}_2$$

$$a_3 = \bar{e}_{vp} \cdot \bar{e}_3$$

A two-gimballed structure, as shown in figure A-2 is to be attached to the vehicle such that an optical axis on the inner gimbal, $\bar{u}_o$, is servoed to $\bar{e}_{vp}$. The orientation of the gimballed structure with respect to the vehicle axes is to be defined such that the inner gimbal motion is minimized for all possible trajectories, and the resulting gimbal motion for this orientation is to be calculated for nominal and various off-nominal trajectories.

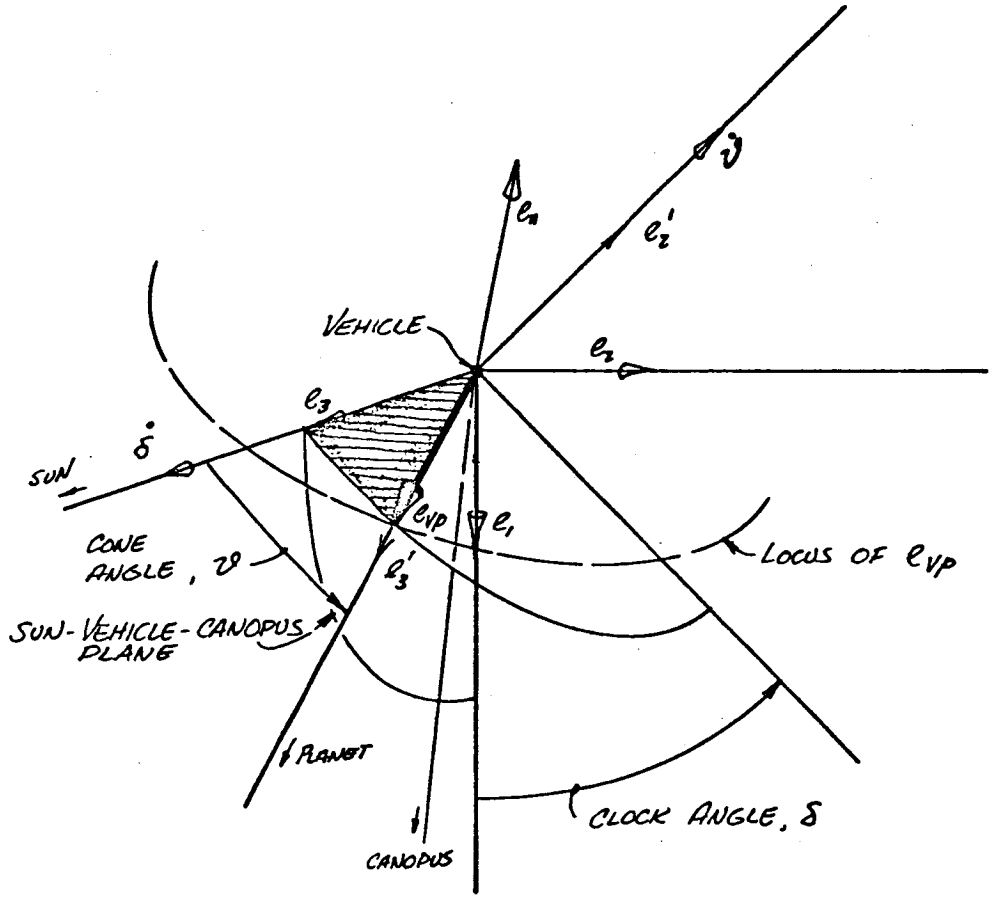

64-11414

Figure A-1 MISSION GEOMETRY

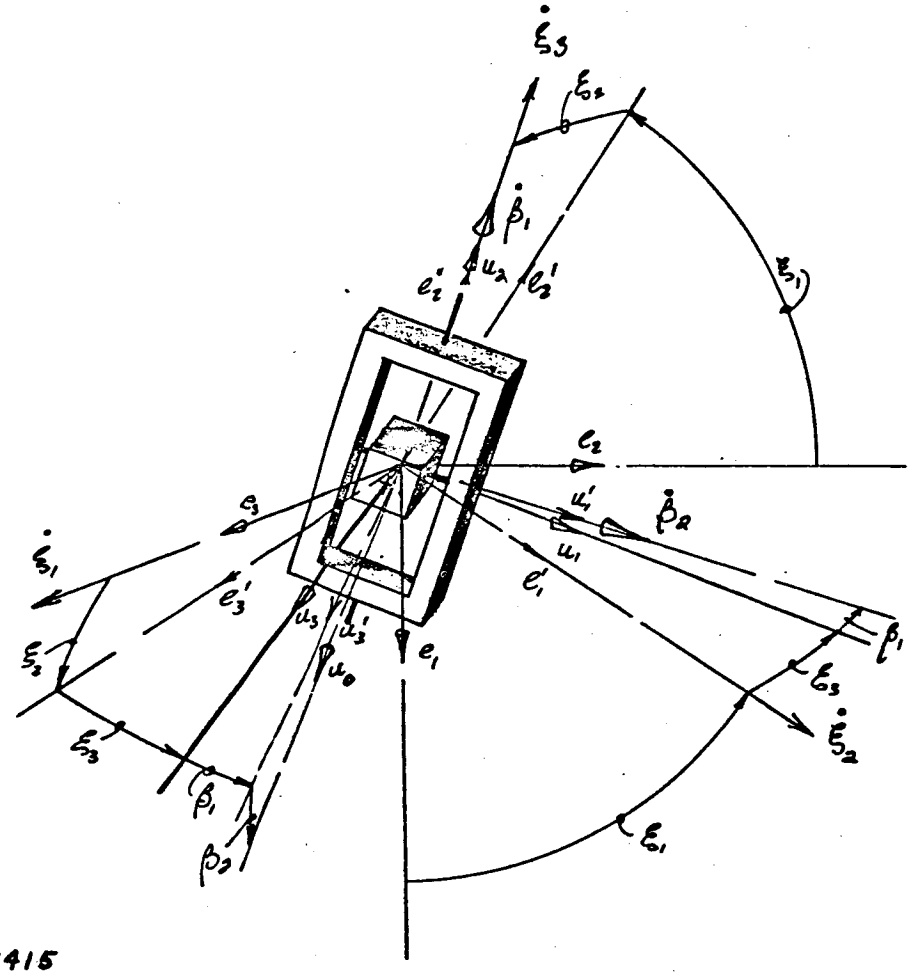

Figure A-2 GIMBAL GEOMETRY

300

B. METHOD

Let u_1, u_2, u_3 be an orthogonal set defining the gimballed structure such that when the gimbal angles, β_1, and β_2, are zero, $\bar{u}_1$ coincides with the inner gimbal axis; $\bar{u}_2$ with the outer gimbal axis; and $\bar{u}_3$ with the optical axis $\bar{u}_o$. The gimbal angles β_1 and β_2 are Euler angles taken with respect to $\bar{u}_1$, $\bar{u}_2$, $\bar{u}_3$: β_1 is a rotation about $\bar{u}_2$ and β_2 is a rotation about $\bar{u}_1'$. β_1 is allowed to rotate continuously, but β is limited to less than ±90° since this is a pole of the system.

Set $\bar{u}_1$, $\bar{u}_2$, $\bar{u}_3$ is defined with respect to $\bar{e}_1$, $\bar{e}_2$, $\bar{e}_3$ by the Euler angles ξ_1, ξ_2, ξ_3:

ξ is a rotation about $\bar{e}_3$

ξ is a rotation about $\bar{e}_1'$

ξ is a rotation about $\bar{e}_2$

as shown in figure A-2.

All of the Euler angle rotations defined above can be represented in the resolver diagram shown in figure A-3a. The direction cosines a_1, a_2, a_3, and c_1, c_2, c_3, are those resulting from the unit vector, $\bar{e}_{vp}$ on the $\bar{e}_1$, $\bar{e}_2$, $\bar{e}_3$, and the inner gimbal axes which contains the optical axis, $\bar{u}_o$, respectively.

Since the direction cosines, a_1, a_2, a_3, are known and ξ_3 and β_1 are rotations about the same axis, the resolver diagram can be simplified as shown in figure A-3b.

In terms of the resolver diagram, the solution proceeds as follows: Given the direction cosines a_1, a_2, a_3, as a function of time during the mission and the gimbal orientation angles, ξ_1 and ξ_2 as defined below (the value of ξ_3 is only a constant bias on the gimbal angle β_1), the time history of the direction cosines, b_1, b_2, b_3, are given as:

$$
\begin{aligned}
b_1 &= a_1 \cos \xi_1 + a_2 \sin \xi_1 \\
b_2 &= -a_1 \sin \xi_1 \cos \xi_2 + a_2 \cos \xi_1 \cos \xi_2 + a_3 \sin \xi_2 \\
b_3 &= a_1 \sin \xi_1 \sin \xi_2 - a_2 \cos \xi_1 \sin \xi_2 + a_3 \cos \xi_2
\end{aligned}
\qquad (1)
$$

The direction cosines, c_1, c_2, c_3, are related to b_1, b_2, b_3 by:

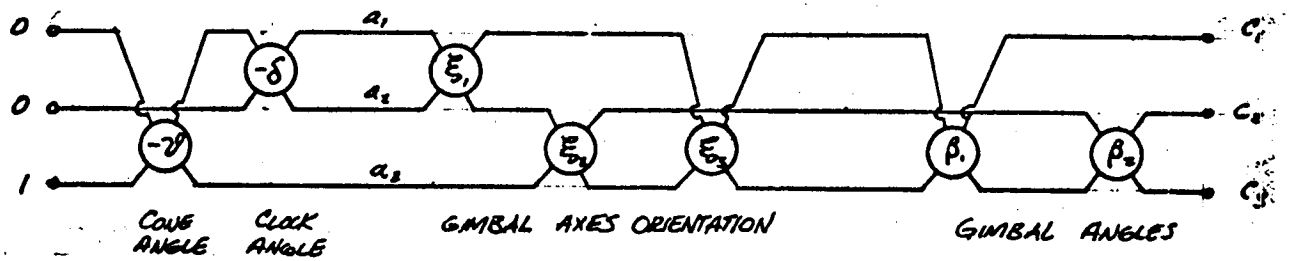

(a) COMPLETE DIAGRAM

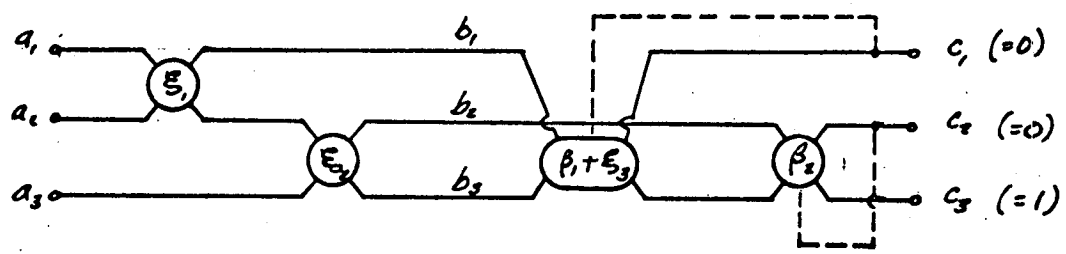

(b) SIMPLIFIED DIAGRAM

64-11416

Figure A-3 RESOLVER DIAGRAMS

RE-ORDER No. 64-524

302

$$c_1 = b_1 \cos \beta_1' - b_3 \sin \beta_1'$$

$$c_2 = b_1 \sin \beta_1' \sin \beta_2 + b_2 \cos \beta_2 + b_3 \cos \beta_1' \sin \beta_2 \qquad (2)$$

$$c_3 = b_1 \sin \beta_1' \cos \beta_2 - b_2 \sin \beta_2 + b_3 \cos \beta_1' \cos \beta_2$$

By virtue of the gimbal servo system, the gimbal angles will adjust themselves so that $c_1 = c_2 = o$ and $c_3 = 1$. Hence, from equation (2):

$$\beta_1' = \xi_3 + \beta_1 = \tan^{-1} b_1/b_3 \qquad (3)$$

$$\beta_2 = \tan^{-1} -b_2/b_1 \sin \beta_1' + b_3 \cos \beta_1' = \tan^{-1} -b_2/(1 - b_2^2)^{1/2}$$

where

$$-90° < \beta_2 < 90°; \text{ and } -90° < \beta_1' < 90° \text{ if } b_3 > 0 .$$

The optimum gimbal orientation angles can be found in the following manner. If the locus of $\bar{e}_{vp}$ as shown in figure A-1 for the nominal trajectory were in a plane with respect to $\bar{e}_1$, $\bar{e}_2$, $\bar{e}_3$, then a vector normal to this plane, $\bar{e}_n$, could be found and the outer gimbal axis, $\bar{u}_2$, aligned with $\bar{e}_n$. In this manner β_2, the inner gimbal angle, would always be zero. However, e_{vp} does not move exactly in a plane, and an average $\bar{e}_n$ must be found. This can be done approximately by taking the cross product of the $\bar{e}_{vp}$'s at two different times centered about periapsis:

$$\bar{e}_{n_{ave}} \cong \frac{\bar{e}_{vp1} \times \bar{e}_{vp2}}{|\bar{e}_{vp1} \times \bar{e}_{vp2}|} = \frac{d_1 \bar{e}_1 + d_2 \bar{e}_2 + d_3 \bar{e}_3}{D} \qquad (4)$$

where:

$$d_1 = a_{2_1} a_{3_2} - a_{3_1} a_{2_2}$$

$$d_2 = a_{3_1} a_{1_2} - a_{1_1} a_{3_2} \qquad (5)$$

$$d_3 = a_{1_1} a_{2_2} - a_{2_1} a_{1_2}$$

$$D = (d_1^2 + d_2^2 + d_3^2)^{1/2}$$

$a_{1_1}\, a_{2_1}\, a_{3_1}$ = direction cosines of $\bar{e}_{vp1}$ in $\bar{e}_1$, $\bar{e}_2$, $\bar{e}_3$ frame.

$a_{1_2}\, a_{2_2}\, a_{3_2}$ = direction cosines of $\bar{e}_{vp2}$ in $\bar{e}_1$, $\bar{e}_2$, $\bar{e}_3$ frame.

The direction cosines d_1, d_2, d_3, expressed in terms of the gimbal orientation angles can be obtained from the following resolver diagram:

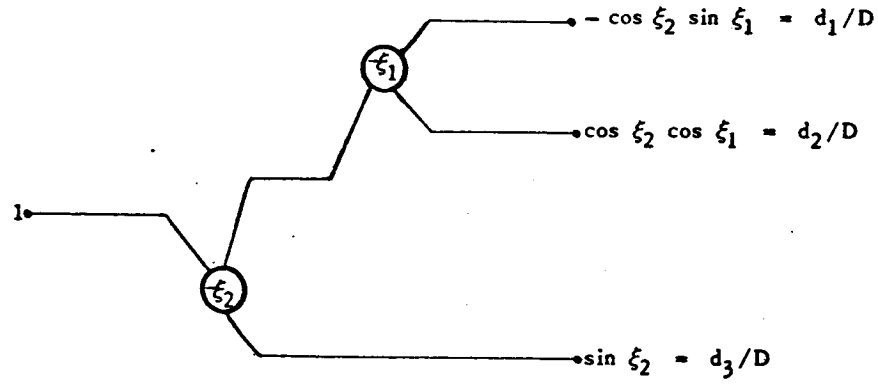

From which

$$\xi_2 = \pm \sin^{-1} d_3/D$$
$$\xi_1 = \tan^{-1} \frac{-d_1}{d_2} \qquad (6)$$

The sign of ξ_2 can be either plus or minus since the direction of $\bar{\epsilon}_{n_{ave}}$ reverses if the angle between $\bar{\epsilon}_{vp1}$ and $\bar{\epsilon}_{vp2}$ exceeds 180 degrees. The proper choice of the angles ξ_1 and ξ_2 is best determined by a sketch of the geometry.

C. EXAMPLE

The method outlined above was used to obtain the outer and inner gimbal angle time histories shown in figures A-4 and A-5 for a launch date of 22 January 1969. The calculations are given below.

The direction cosines at the beginning and end of the hyperbolic trajectory are from digital computer results:

at t = 0:		at t = 6.027:	
a_{1_1}	= 0.1724	a_{1_2}	= −0.2780
a_{2_1}	= 0.9665	a_{2_2}	= −0.9578
a_{3_1}	= 0.1899	a_{3_2}	= 0.0725

304

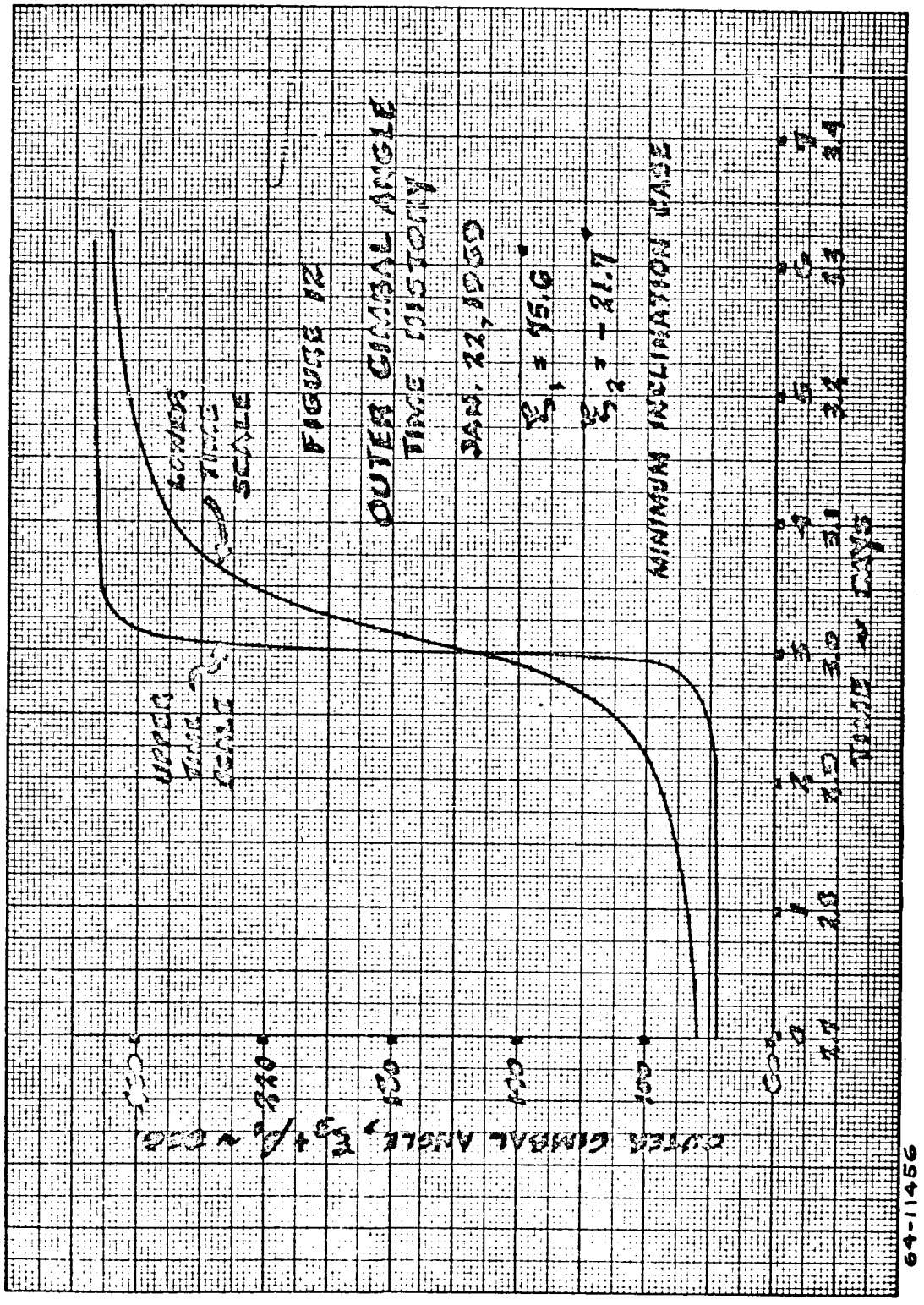

Figure A-4 OUTER GIMBAL TIME HISTORY

305

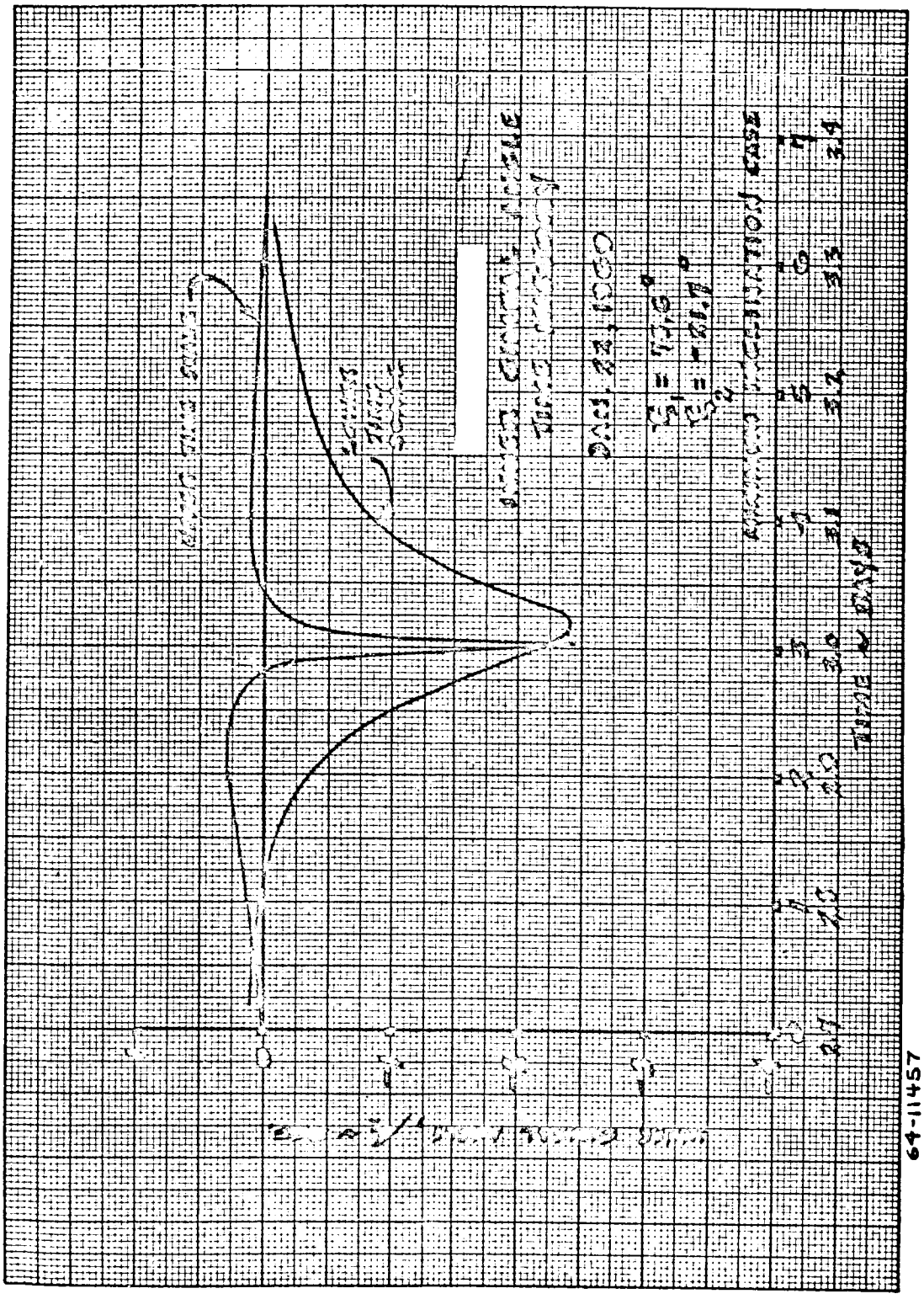

64-11457

Figure A-5 INNER GIMBAL TIME HISTORY

306

From equation (5):

$$d_1 = 0.2520$$

$$d_2 = 0.0653$$

$$d_3 = 0.1036$$

$$D = 0.2802$$

From equation (6):

$$\xi_2 = \pm \sin^{-1} \frac{0.1036}{0.2802} = \sin^{-1} 0.3697 = \begin{cases} \pm 21.7^\circ \\ 180 \pm 21.7^\circ \end{cases}$$

$$\xi_1 = \tan^{-1} \frac{0.2520}{0.0653} = \tan^{-1} 3.859 = \begin{cases} 75.6^\circ \\ 180 + 75.6^\circ \end{cases}$$

From figure A-6 the proper choice for the angles is:

$$\xi_2 = -21.7^\circ$$

$$\xi_1 = 75.6^\circ$$

From equation (1):

$$b_1 = 0.2509\ a_1 + 0.9680\ a_2$$

$$b_2 = 0.8994\ a_1 + 0.2330\ a_2 - 0.3697\ a_3$$

$$b_3 = 0.3579\ a_1 + 0.0928\ a_2 + 0.9291\ a_3$$

and

$$\xi_3 + \beta_1 = \tan^{-1} \frac{b_1}{b_3}$$

$$\beta_2 = \tan^{-1} -b_2/(1 - b_2^2)^{1/2}$$

D. APPLICATION TO THE ADVANCED MARINER CASE

The following curves (figures A-7 through A-22) present the angle changes in the outer- and inner-gimbal axes for eight different approach trajectories for the nominal launch data window of 10 January to 11 February 1969. Both the nominal inclination angle of 45 degrees and minimum inclination angles (no

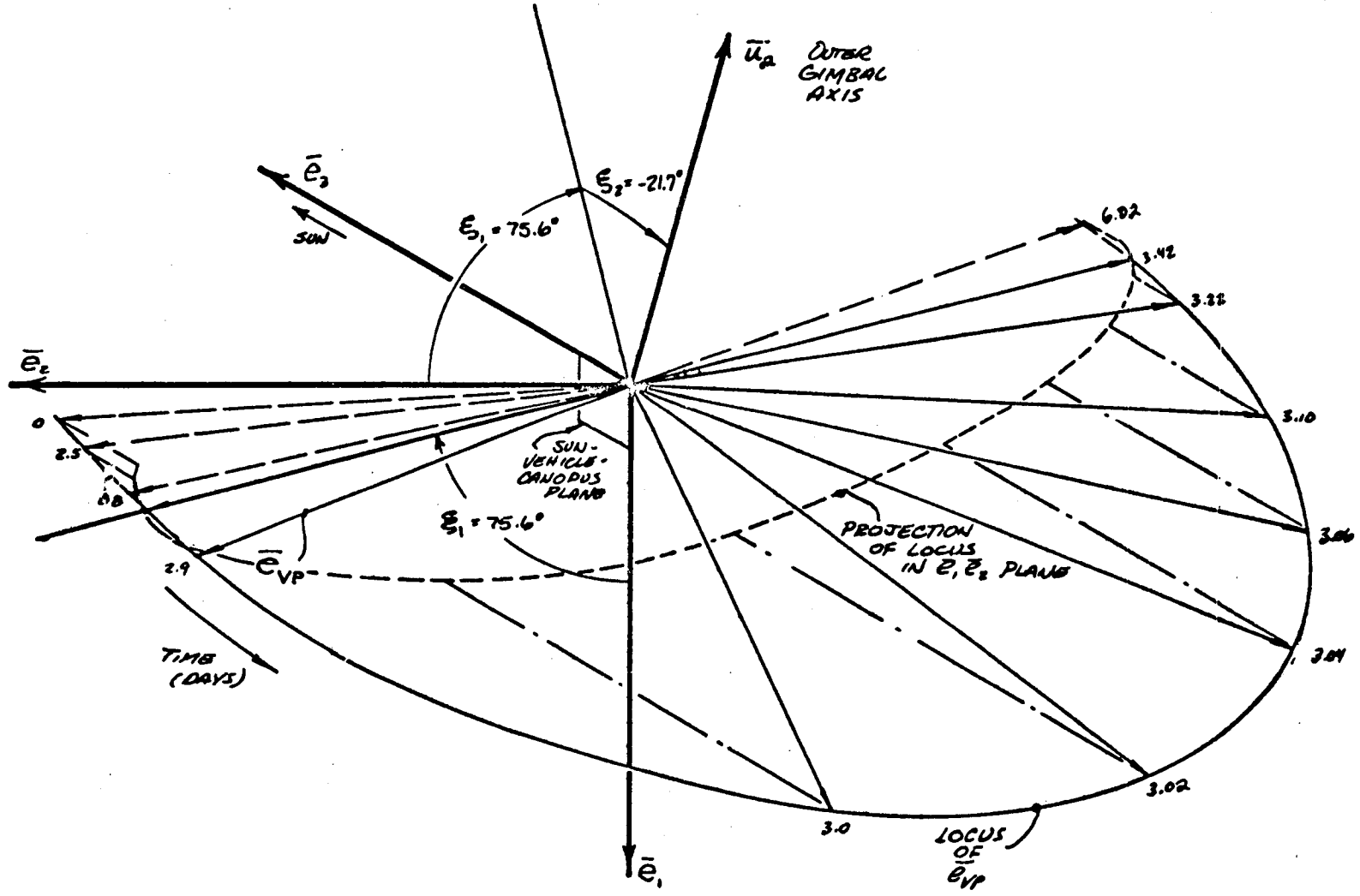

64-11417

Figure A-6 GEOMETRY FOR 22 JANUARY 1969, LAUNCH DATE

RE-ORDER No. 64-524

308

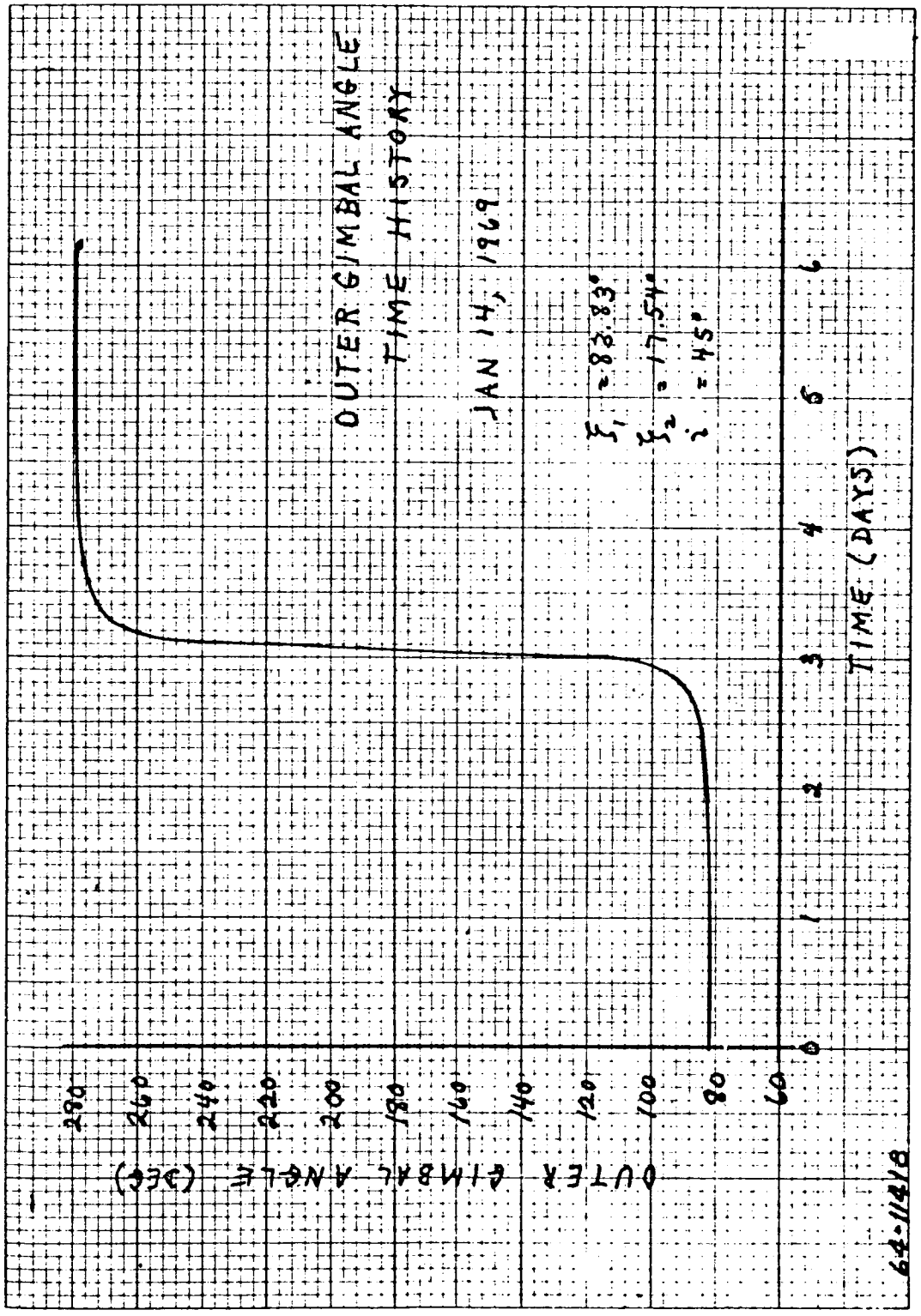

Figure A-7 OUTER GIMBAL ANGLE TIME HISTORY, 14 JANUARY 1969, i = 45°

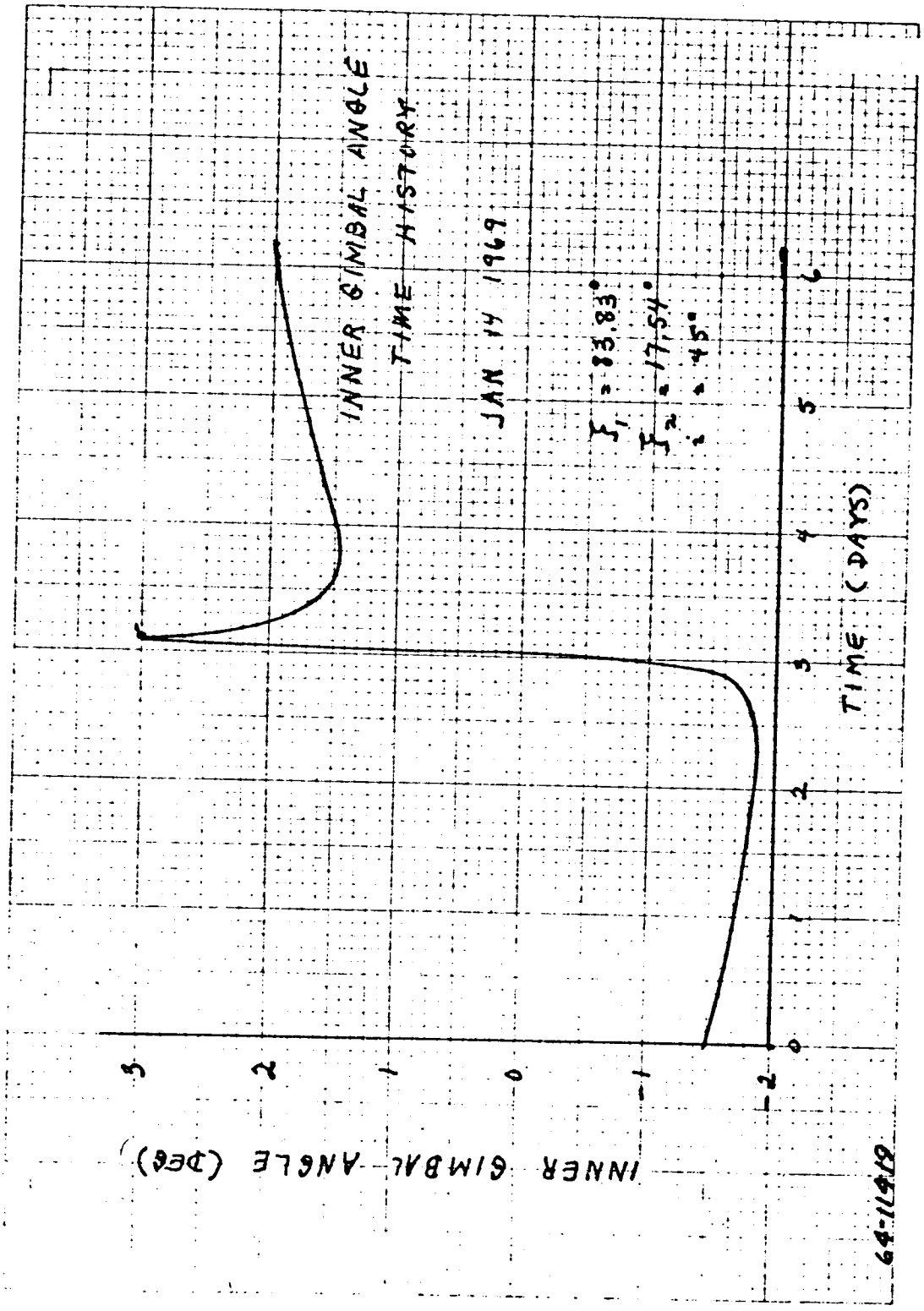

Figure A-8 INNER GIMBAL ANGLE TIME HISTORY, 14 JANUARY 1969, i = 45°

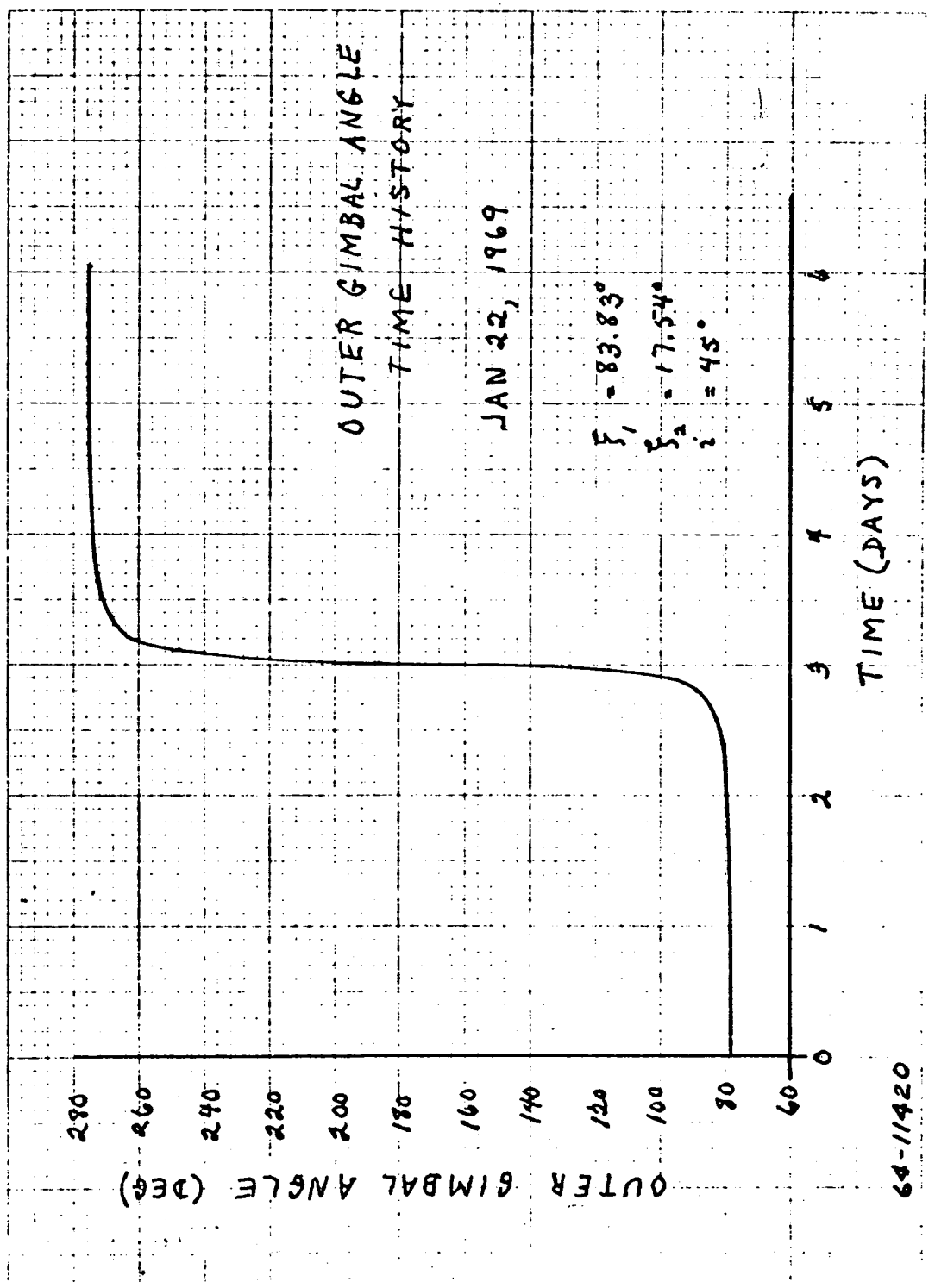

Figure A-9 OUTER GIMBAL ANGLE TIME HISTORY, 22 JANUARY 1969, i = 45°

311

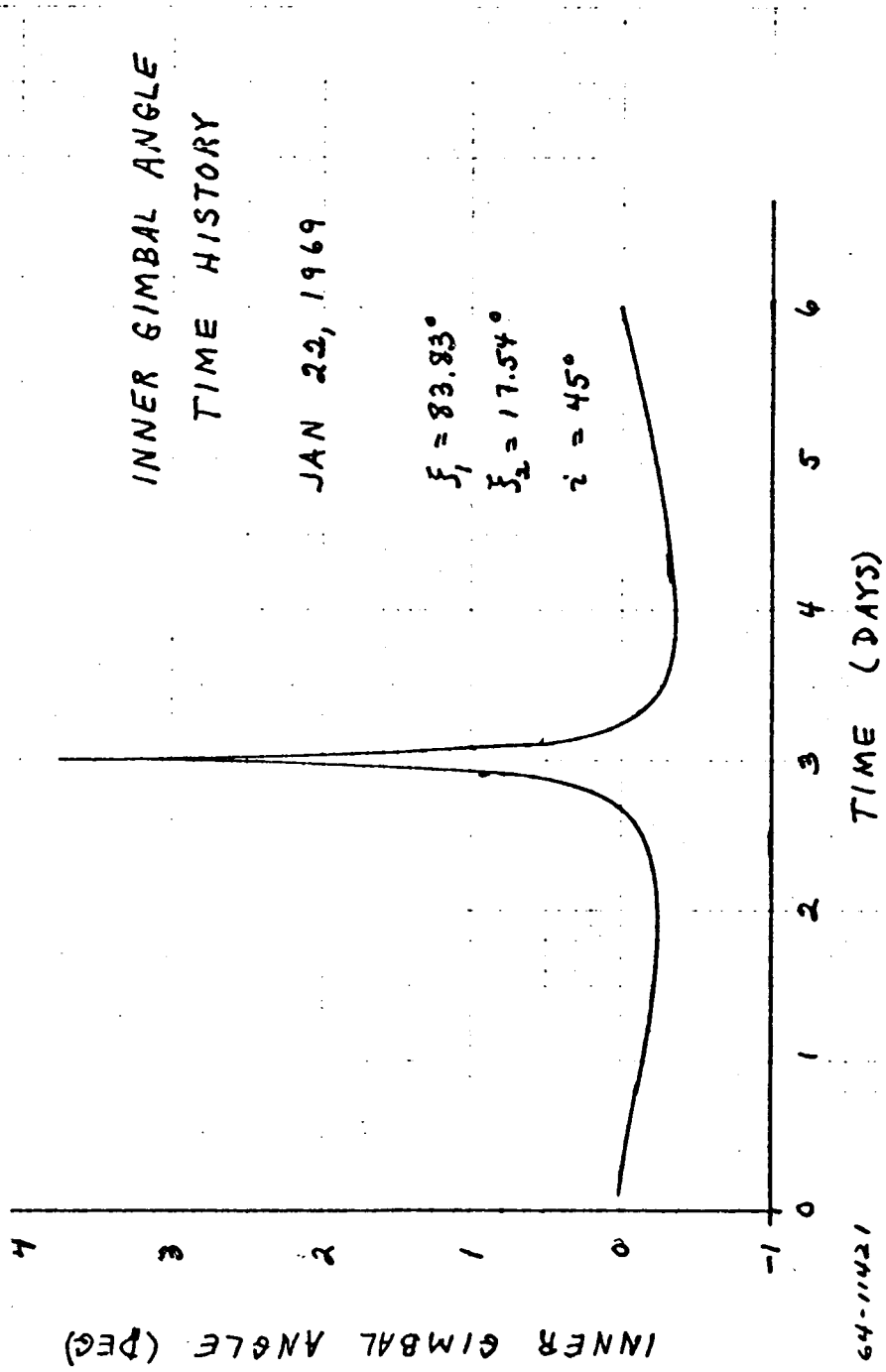

Figure A-10 INNER GIMBAL ANGLE TIME HISTORY, 22 JANUARY 1969, i = 45°

312

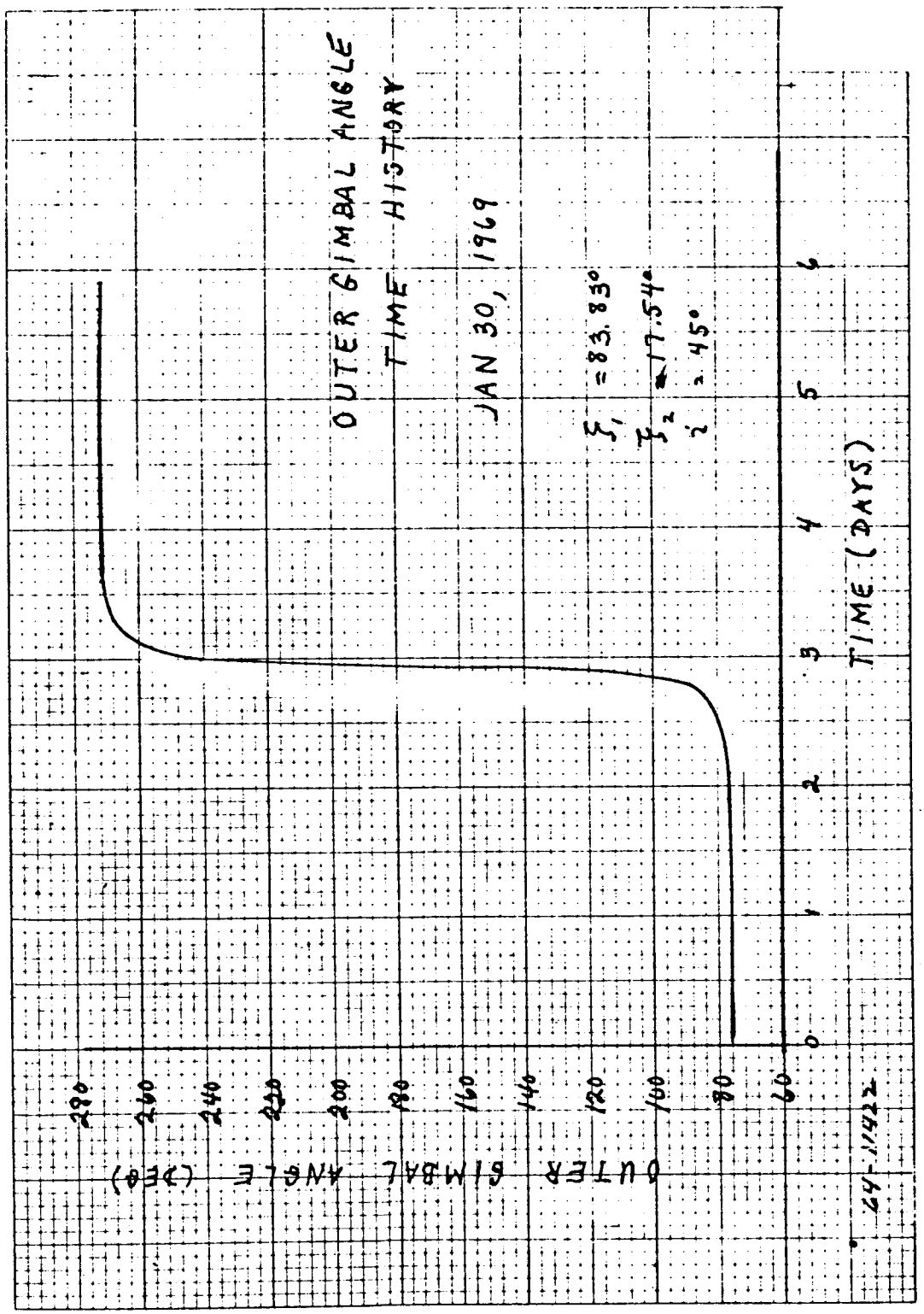

Figure A-11 OUTER GIMBAL ANGLE TIME HISTORY, 30 JANUARY 1969, i = 45°

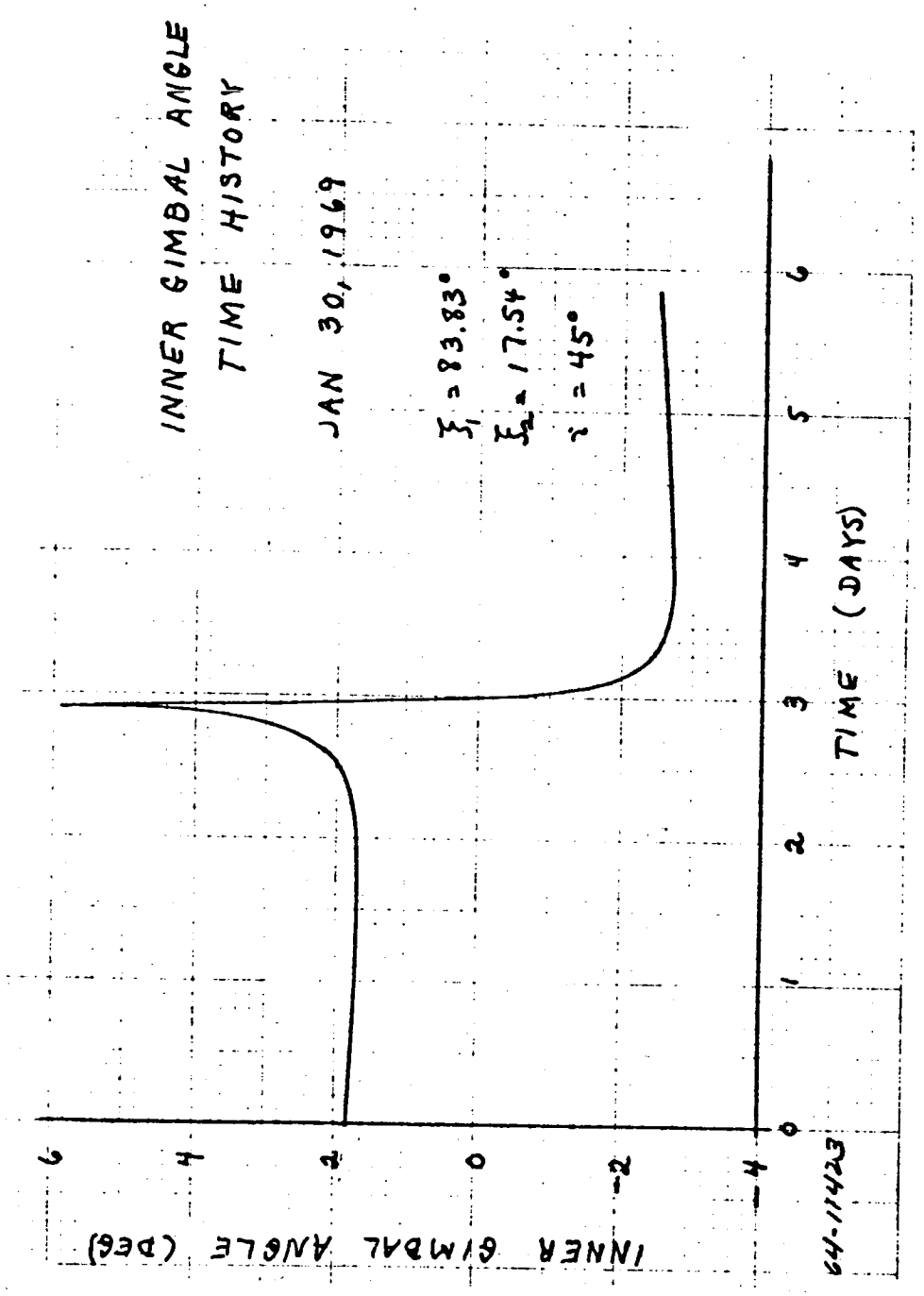

Figure A-12 INNER GIMBAL ANGLE TIME HISTORY, 30 JANUARY 1969, i = 45°

314

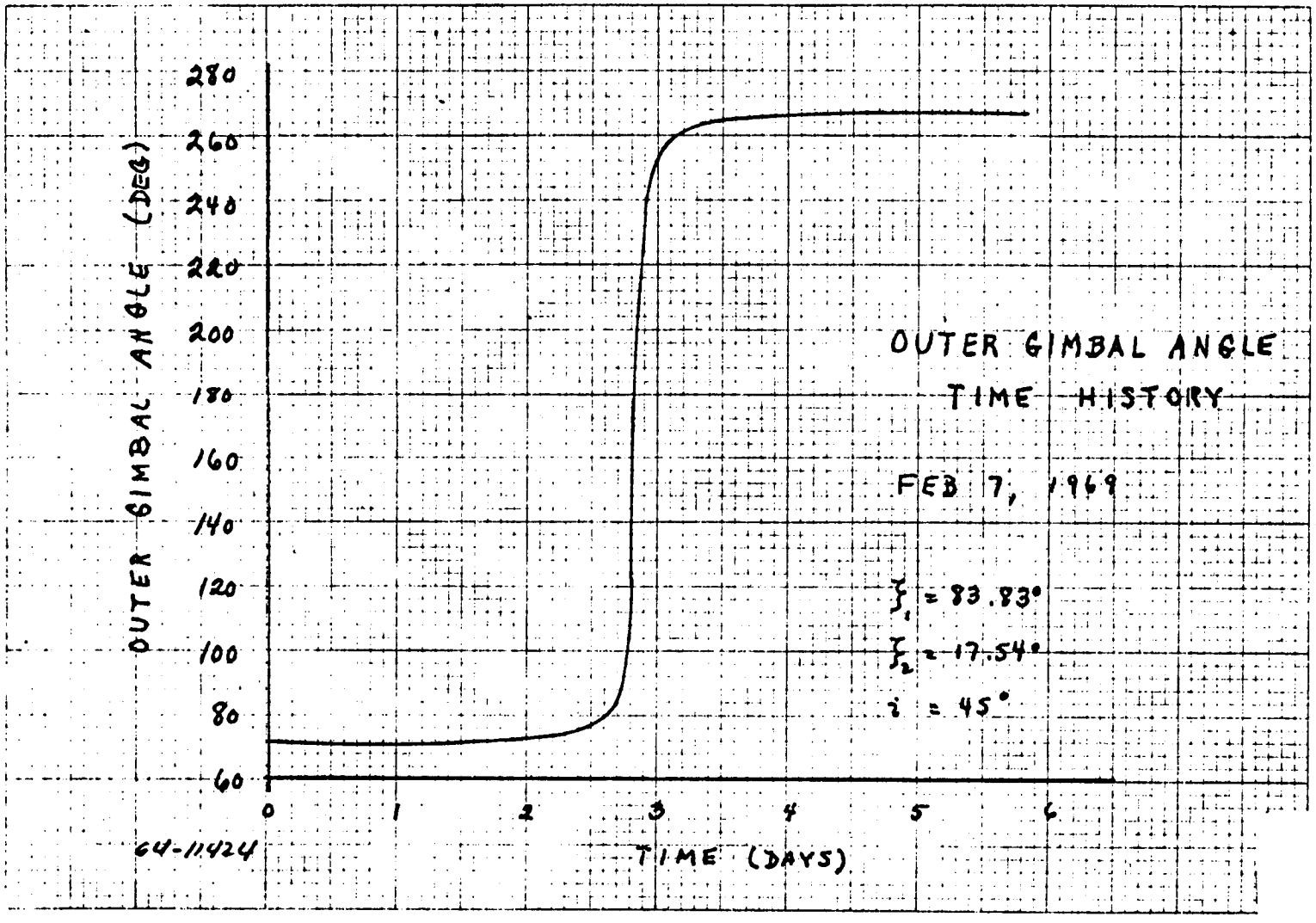

Figure A-13 OUTER GIMBAL ANGLE TIME HISTORY, 7 FEBUARY 1969, i = 45°

RE-ORDER No. 64-524

315

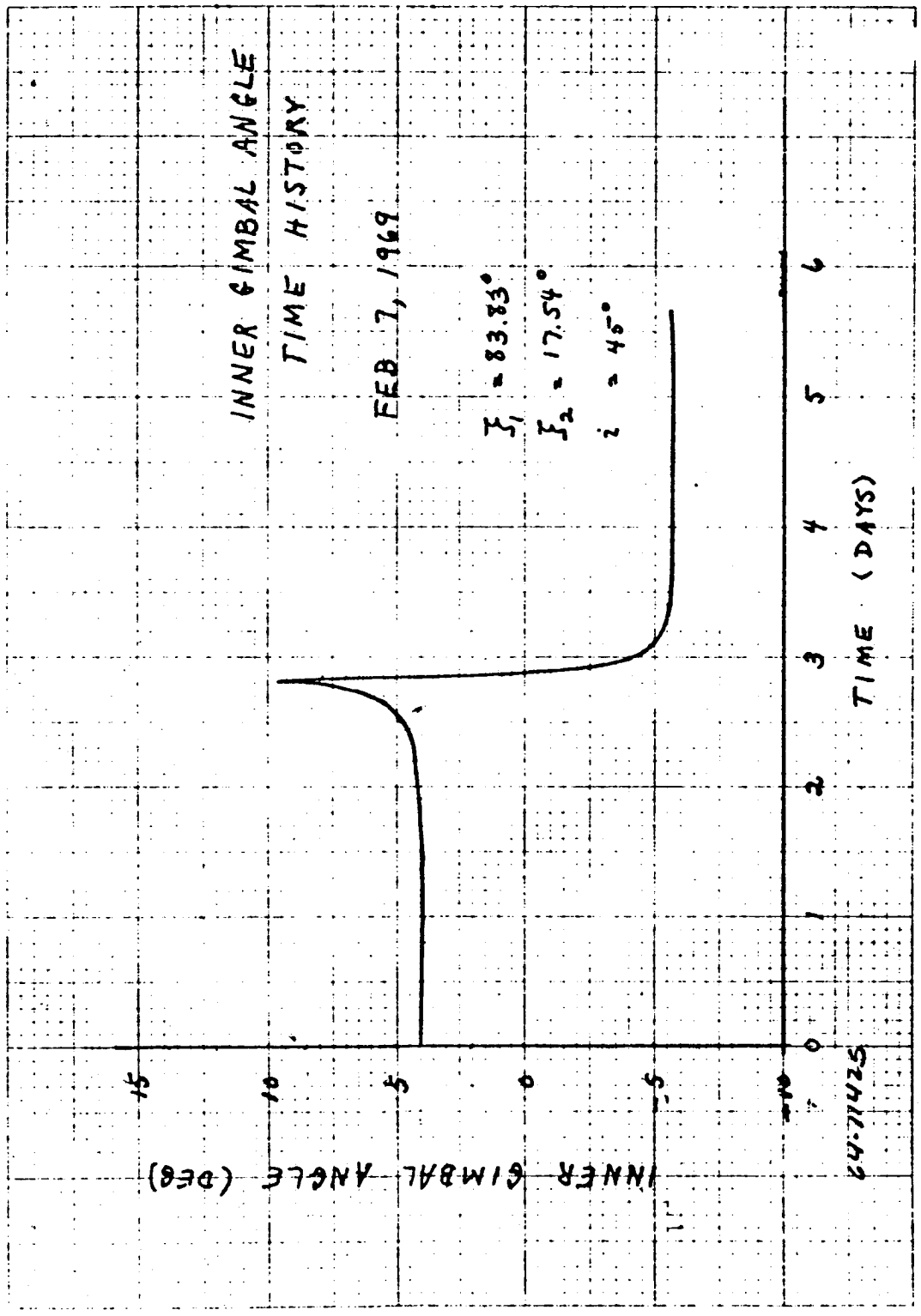

Figure A-14 INNER GIMBAL ANGLE TIME HISTORY, 7 FEBUARY 1969, i = 45°

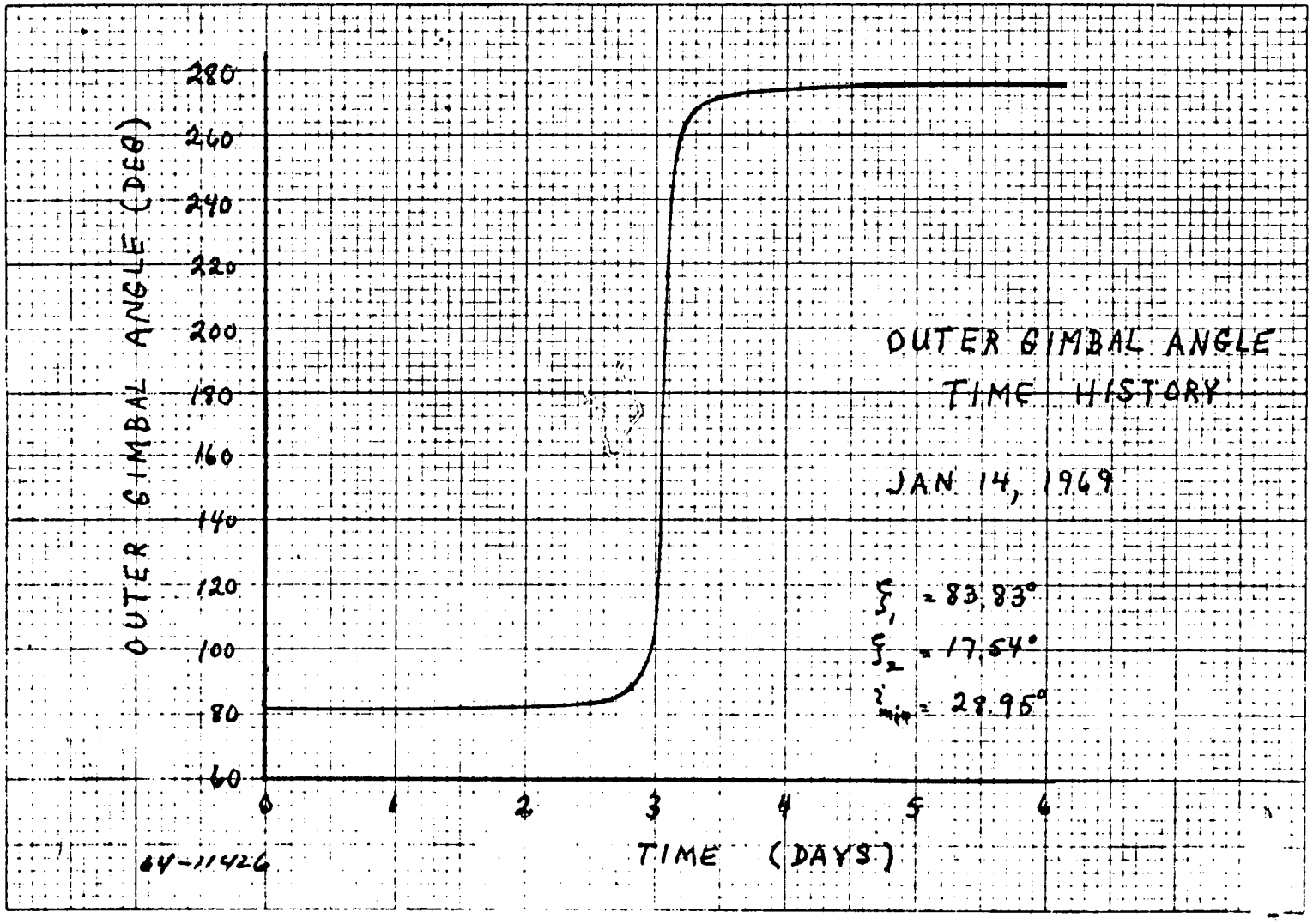

Figure A-15 OUTER GIMBAL ANGLE TIME HISTORY, 14 JANUARY 1969, i = 28.95

RE-ORDER No. 64-524

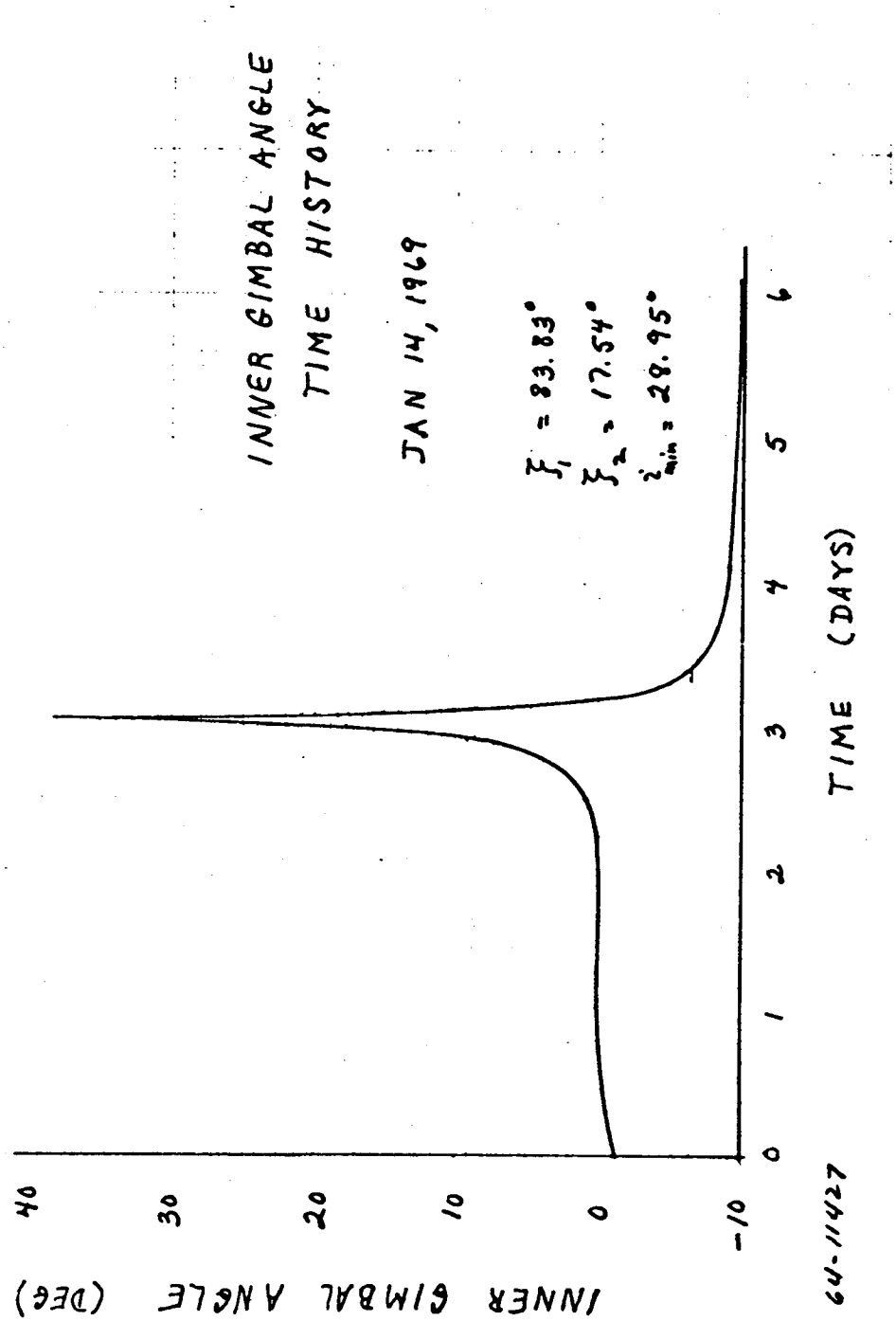

Figure A-16 INNER GIMBAL ANGLE TIME HISTORY, 14 JANUARY 1969, i = 28.95

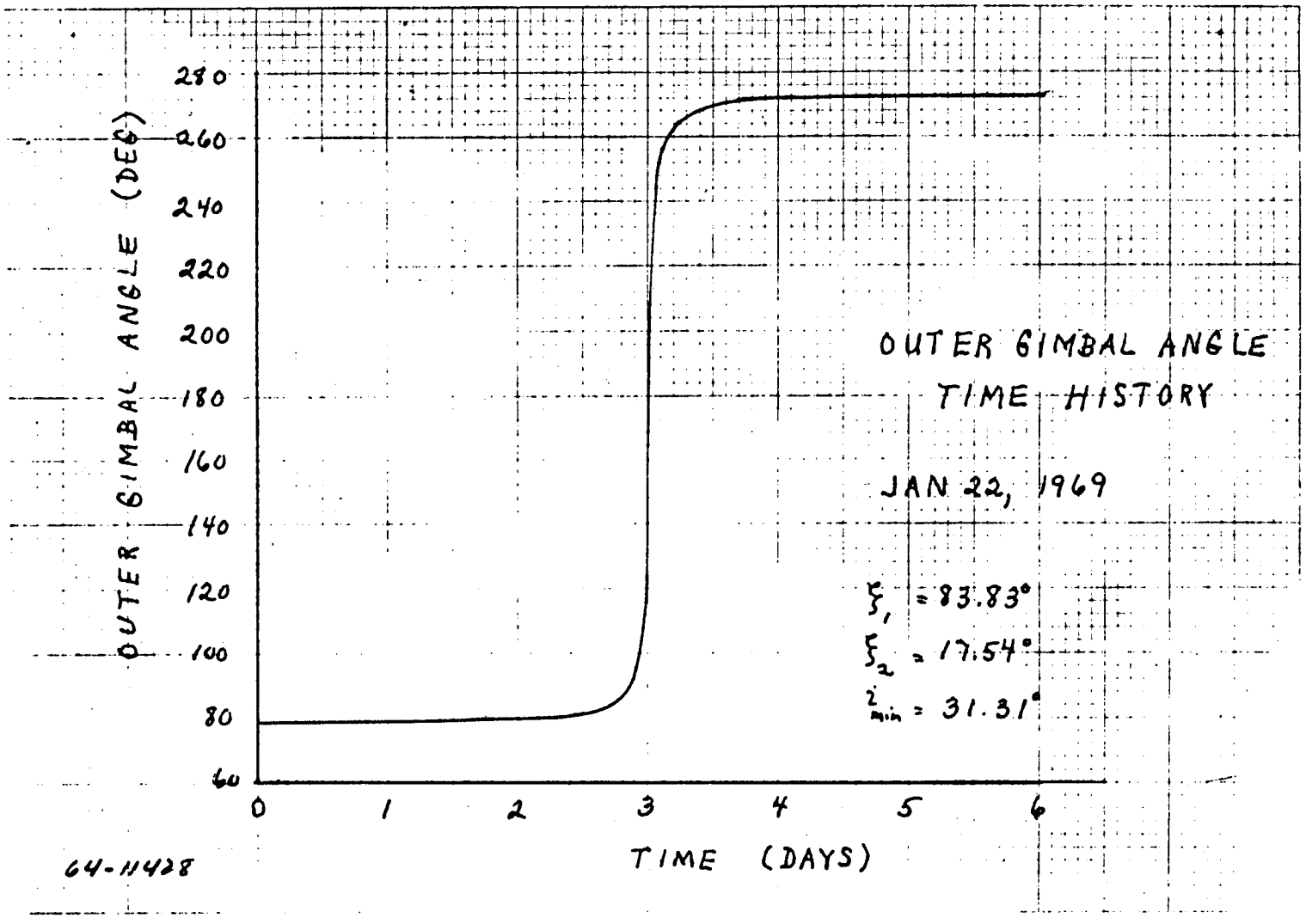

Figure A-17 OUTER GIMBAL ANGLE TIME HISTORY, 22 JANUARY 1969, i = 31.31

RE-ORDER No. 64-524

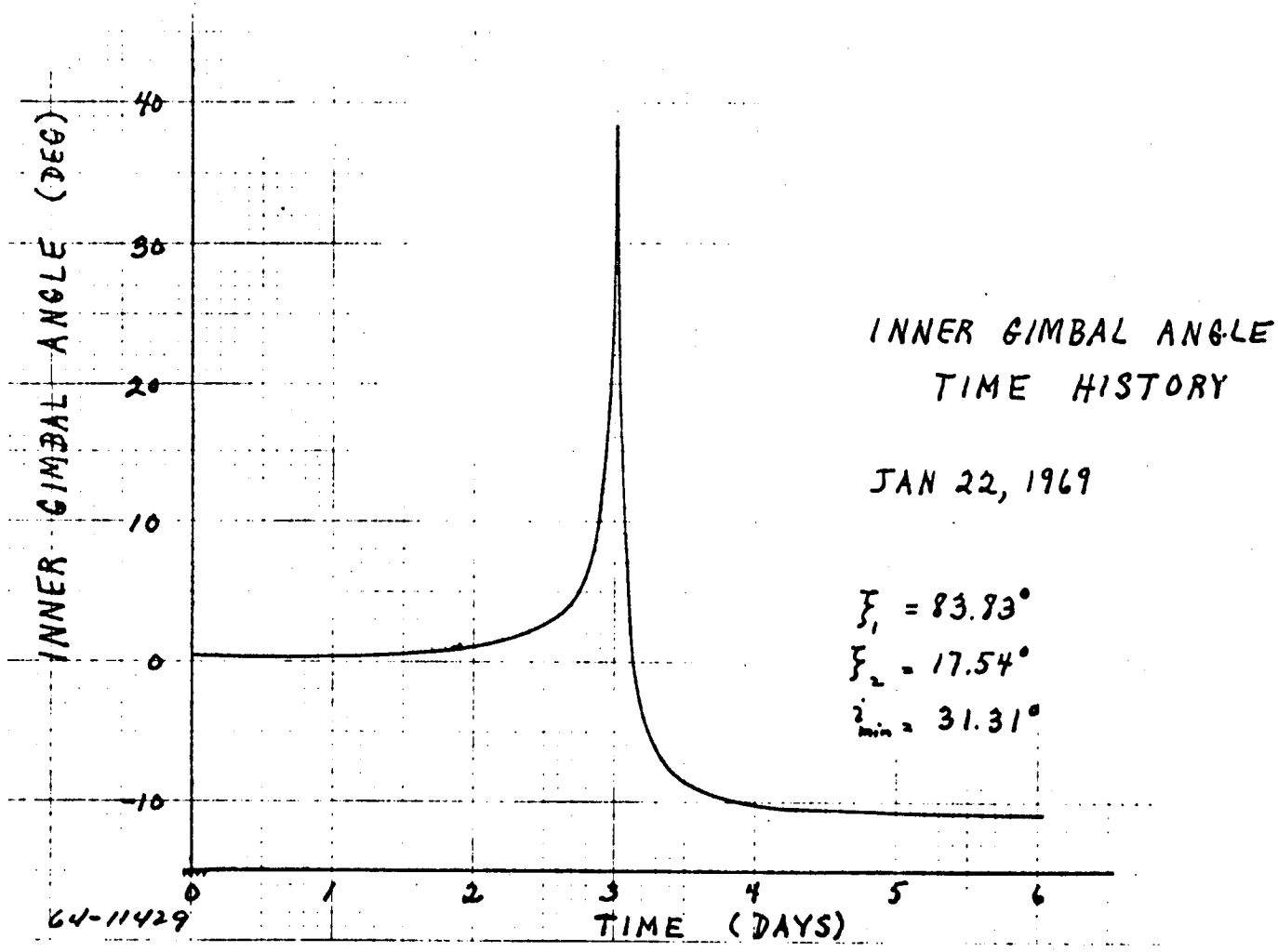

Figure A-18 INNER GIMBAL ANGLE TIME HISTORY, 22 JANUARY 1969, i = 31.31

RE-ORDER No. 64-524

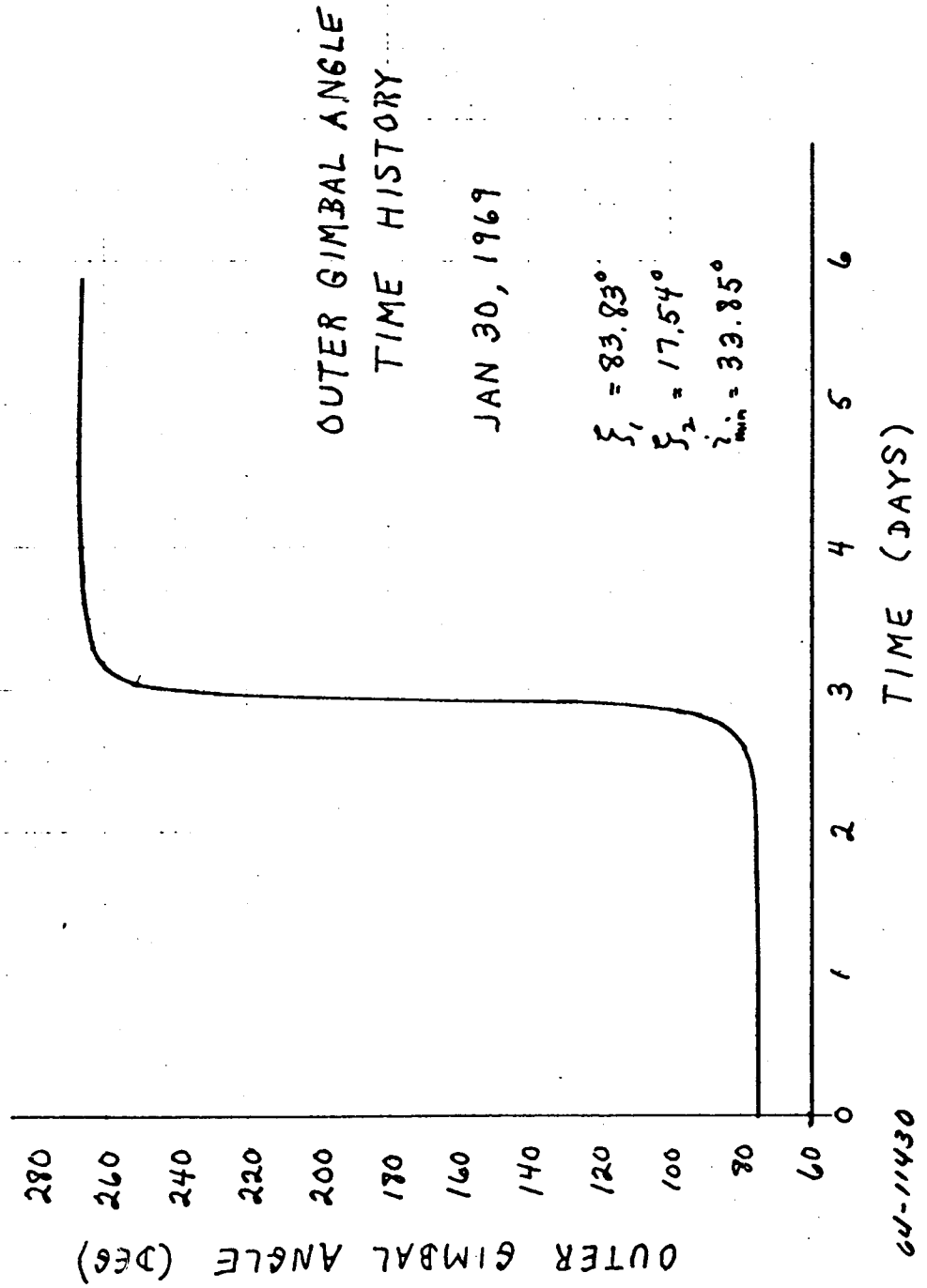

Figure A-19 OUTER GIMBAL ANGLE TIME HISTORY, 30 JANUARY 1969, i = 33.85

321

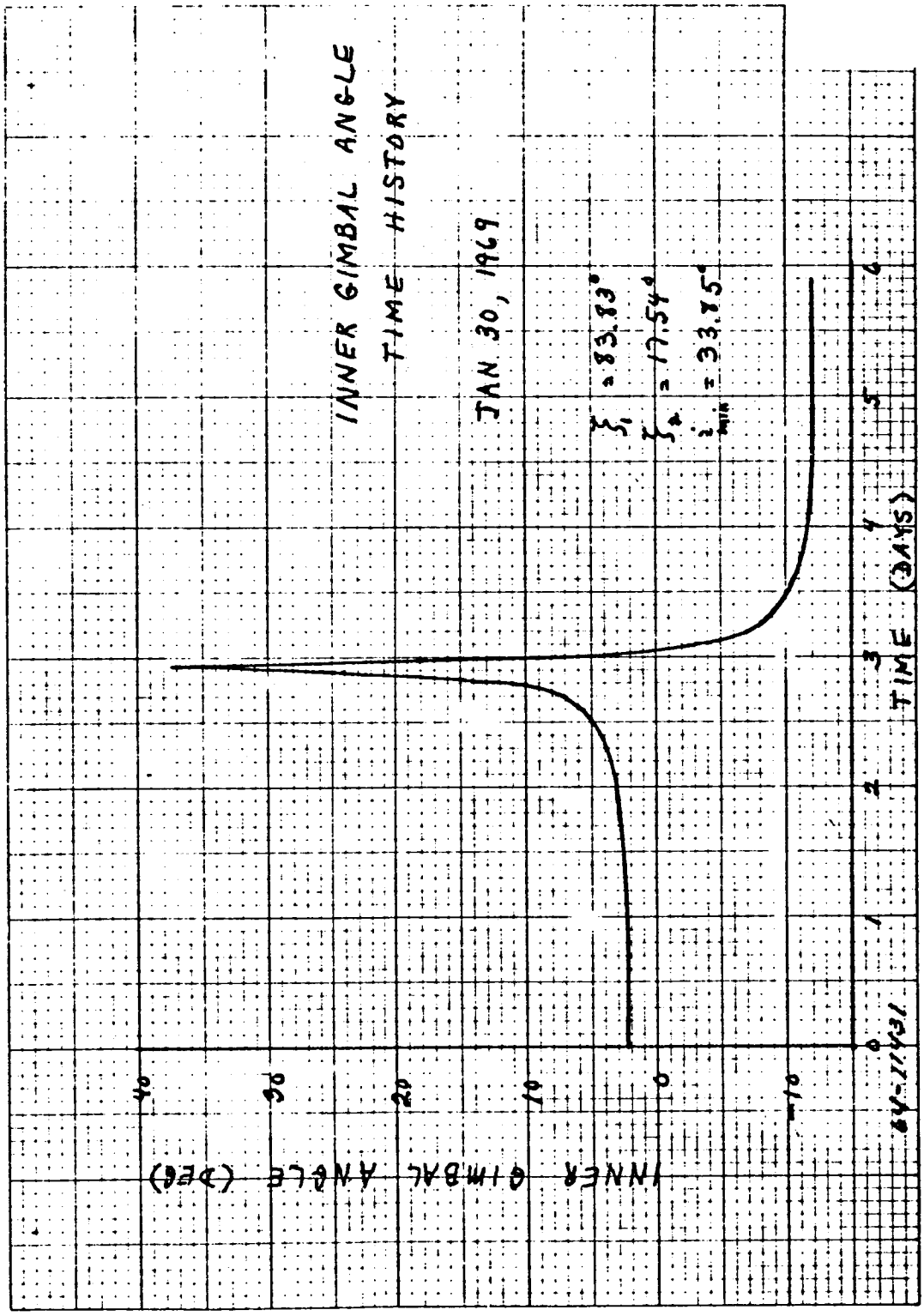

Figure A-20 INNER GIMBAL ANGLE TIME HISTORY, 30 JANUARY 1969, i = 33.85

322

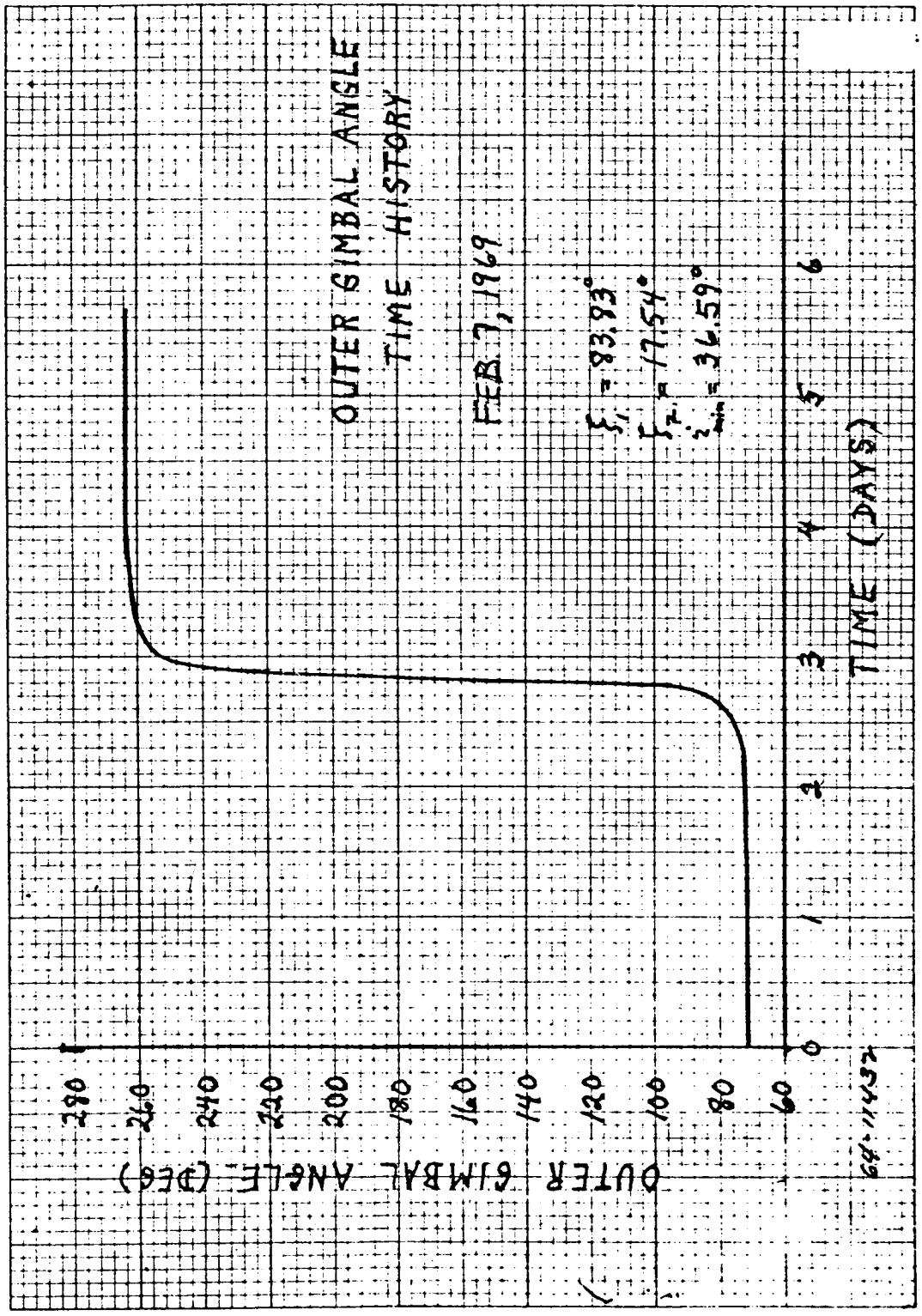

Figure A-21 OUTER GIMBAL ANGLE TIME HISTORY, 7 FEBUARY 1969, i = 36.59

RE-ORDER No. 64-524

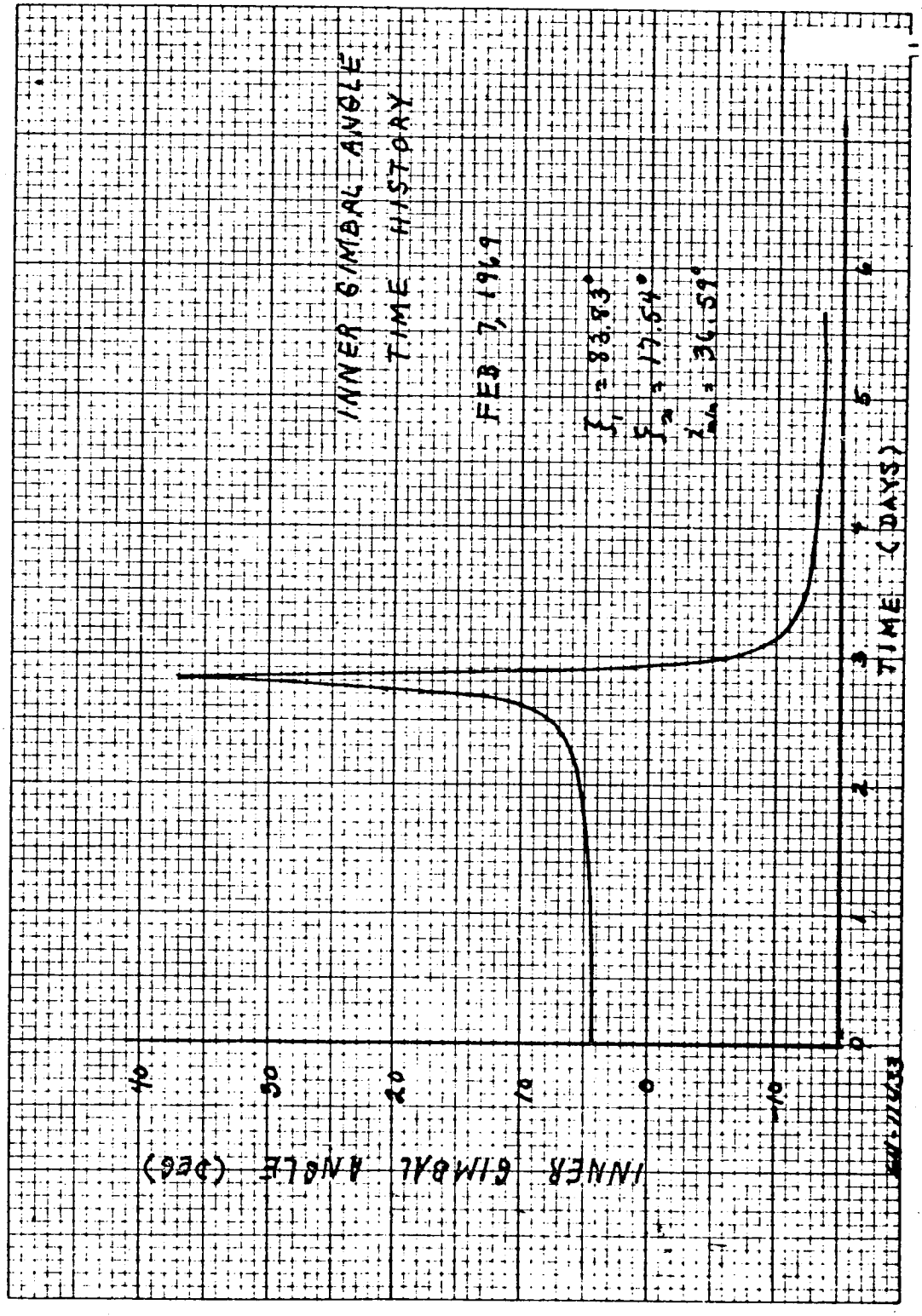

Figure A-22 INNER GIMBAL ANGLE TIME HISTORY, 7 FEBUARY 1969, i = 36.59

324

propulsive correction) are considered. The results are based on the analysis and mission, gimbal geometry outlined above.

There are four constant arrival dates, launch subwindows within the nominal launch window of 10 January to 11 February 1969. Taking the launch subwindow of 22 January with the nominal inclination of 45 degrees as typical, an average plane containing the initial and final vehicle-planet position vectors is established. The gimbal orientation angles ξ_1 and ξ_2, measured with respect to the cone-clock angle coordinate frame and defining the reference inner gimbal and outer gimbal axes, are computed as 83.83 and 17.54 degrees, respectively. Figures A-7 through A-22 present the outer gimbal axis deviation and inner axis deviation for each of the four launch subwindows for the inclination angle of 45 degrees and the minimum inclination angles. The inclination angle is designated by the letter i .

The change in the angle of the inner gimbal axis is the deviation of interest since this excursion is limited by pole stops to ±90 degrees (vehicle structure may impose additional restrictions.) Results show that for any trajectory within the nominal launch window the maximum excursion, which occurs for the minimum inclination angle, is less than 40 degrees. Of course, the average plane, and hence ξ_1 and ξ_2, can be determined by any two vehicle-planet position vectors. For a broad set of trajectory conditions (i , arrival date) the deviations may be better biased about zero for a plane defined by a representative trajectory's pair of position vectors near periapsis.

It is clear that, within the nominal launch window and for the inclination angle for which the average plane has been defined, inner axis angle deviations can be kept small, in this case less than ±10 degrees. By defining the average plane as that containing the initial and final vehicle-planet position vectors, the inner axis deviation is zero at the greatest distance from the planet and increases to maximum value at periapsis, the point on the trajectory where the planet (as seen by the vehicle) has its greatest angular diameter. For the periapsis distance of 10,000 kilometers and Mars radius of 3,412 kilometers, the planet angular diameter is close to 38 degrees or an order of magnitude greater than the inner gimbal axis deviation for the launch subwindow of 22 January and inclination angle of 45 degrees.

325

APPENDIX B

COMPARATIVE RELIABILITY ANALYSES

A. INTRODUCTION

During the parametric evaluation phase, reliability efforts were concerned with the analysis of alternate design concepts and mission approaches. In selecting a particular design concept or mission approach from among several alternatives, such parameters as performance, safety, weight, power requirements, cost, volume, accuracy, information yield, and reliability must be taken into consideration. Depending on the concept or approach being analyzed, the pertinent parameters must be evaluated and factored into a comprehensive systems analysis study of the candidate alternatives. To this end, the purpose of the reliability analyses was to support the overall selection process by providing the necessary reliability inputs.

In support of the selection process, five separate reliability analyses were made. These analyses were used to evaluate the reliability of Systems being considered for:

1. Maneuver mode attitude control,
2. Cruise mode attitude control,
3. Flyby/bus propulsion,
4. Lander separation, and
5. Lander stabilization.

The first three analyses (1, 2, and 3) were performed using a quantitative technique which required system reliability predictions at preselected confidence levels. The last two analyses (4 and 5) were made using a quantitative/ qualitative technique which considered the reliability potential of the candidate systems.

B. QUANTITATIVE SUBSYSTEM RELIABILITY

The following design alternatives were evaluated using a quantitative technique:

1. <u>Maneuver Mode Attitude Control</u>
   a. Jet Vane System
   b. Gimballing System

2. Cruise Mode Attitude Control

   a. Subliming Solid System

   b. Cold Gas System

3. Flyby/Bus Propulsion

   a. Monopropellant System
   b. Bipropellant System

The steps involved in the use of this technique are described below.

a. Selection of a Suitable Evaluation Method

The reliability evaluation of each candidate system was performed at the same, preselected, confidence level. This approach is a departure from the usual method of making reliability predictions. Normally, the reliability of a system is predicted without regard to its confidence level. If several systems are being evaluated, their reliability estimates are associated with different confidence levels. Hence, the comparison of system reliability is not done on an equitable basis -- an advantage gained by evaluating each system at the same confidence level.

Briefly, the method applied here involves the calculation of component failure rates at some confidence level such that the resulting system failure rate is at the preselected confidence level. The confidence level associated with any component type is determined by using the relationship

$$\gamma_k = \sqrt[N]{\gamma_s}$$

where,

γ_k = the confidence level of the kth component type

N = the number of component types

γ_s = the preselected confidence level for the system

b. Description of the Essential Information

The following information is needed for use of this method:

1) System Description (block diagrams, etc.)

2) Component Quantities, by Type

3) Component Histories*

   a) Number of Failures

   b) Total Test/Operational Time

4) Component Operating (Mission) Time

c. Use of the Information

The previously listed information was used (1) to develop the success diagram for each candidate system and (2) to formulate the system mathematical model.

1) Development of success diagrams

Success diagrams were developed for each candidate system to illustrate the one or more of several possible sets of component successes that must occur in order to achieve system success. A review of the system descriptions revealed that, in every case, series operation existed for the design concepts being evaluated. That is, failure of any component would result in a system malfunction.

2) Formulation of mathematical models

The success diagrams were used as the basis for formulating the system mathematical models. Each model expresses the probability of system success as a function of the success of its components. In the case of serial operation, assuming the exponential failure distribution, the general model describing the probability of mission success is

$$P_s = \exp\left[-\left(\sum_{k=1}^{N} n_k \lambda_k t_k\right)\right]$$

*These data were extracted from the Failure Rate Data (FARADA) Handbook which is a compilation of failure rate information for components used in various environments, e.g., laboratory, ground, airborne, shipboard, missile, and space. In these analyses, every effort was made to use only data which pertains to components operated in the missile or space environment.

where,

P_s = mission success probability

N = number of component types

n_k = quantity of the kth component type

λ_k = failure rate of the kth component type

t_k = required (during the mission) operating time of the kth component type

Each failure rate, λ_k, was calculated using the relationship

$$\lambda_k \leq \frac{X^2_{(\alpha_k,\, 2r_k)}}{2T_{r_k}}$$

where

$X^2_{(\,)}$ = chi square value for $2r_k$ degrees of freedom (r_k = number of failures) at the α_k probability level ($\alpha_k = 1 - \gamma_k$)

T_{r_k} = total test/operational time to the r_kth failure

In the above equation, it should be noted that r_k and T_{r_k} are obtained from the FARADA handbook.

3) Quantification of mathematical models

The mathematical models were then quantified using the information described earlier to obtain the mission success probability for each design concept.

4. Summary of Results

Quantifying the reliability mathematical model for each system being evaluated yielded the results summarized in table B-1. As indicated in this table, the probability of mission success is given for each system at varied confidence levels. The reliability assessment was accomplished in this manner to determine whether or not uniformity prevails at various confidence levels. A review of the table shows the results are in fact uniform - the design concept possessing the higher success probability does so at the three confidence levels.

RE-ORDER No. 64-524

TABLE B-1

RELIABILITY EVALUATION OF ALTERNATE DESIGN CONCEPTS
SUMMARY OF RESULTS

	Probability of Mission Success		
	Confidence Level		
	0.50	0.75	0.90
A. Maneuver Mode Attitude Control			
1. Jet Vane System	0.9997	0.9996	0.9996
2. Gimballing System	0.9988	0.9986	0.9984
B. Cruise Mode Attitude Control			
1. Subliming Solid System	0.9984	0.9980	0.9975
2. Cold Gas System	0.9922	0.9914	0.9905
C. Flyby/Bus Propulsion			
1. Monopropellant System	0.9991	0.9990	0.9989
2. Bipropellant System	0.9990	0.9989	0.9988

330

From a reliability point of view, a jet vane system and subliming solid system appear to be more desirable for thrust vector control and reaction control, respectively. In the case of the propulsion system, neither the monopropellant nor bipropellant concepts can be excluded on the basis of reliability alone - other factors such as performance, weight, and safety must be evaluated.

C. QUANTITATIVE/QUALITATIVE SUBSYSTEM RELIABILITY

The following design alternatives were evaluated using a quantitative/qualitative technique:

1. Lander Separation

   a. Release Mechanisms

      1) Explosives (both the use of shaped charges and explosive bolts).

      2) Ball Lock Bolt

      3) Mechanical Latches

      4) Marmon Clamp

   b. Actuator Mechanisms

      1) Spring

      2) Gas Generator

      3) Cartridge Actuated Device

      4) "Fly-away" (using a combination of shaped charges and attitude control jets)

2. Lander Stabilization

   a. Spin Rockets

   b. Momentum Wheels

   c. Attitude Control System

The steps involved in the use of this technique are described below.

a. Synthesis of System Designs

Because of the parametric nature of the systems analysis study, design definition for each alternative was vague. Therefore, the first step was to synthesize system designs which could be employed for each alternative being considered.

b. Estimation of Inherent Reliability

The inherent reliability of the basic (without redundancy) systems was next estimated using reliability data obtained from Avco reliability demonstration tests and the FARADA handbook. Since the synthesized designs lacked firm details, these reliability estimates* were used only as guidelines, rather than as absolute measures of reliability capability. However, as explained later, the estimates are valuable in ranking the candidate systems according to overall reliability potential.

c. Improvement through Redundancy

Redundancy can be added in one form or another to each system being considered. However, the reliability improvement expected by incorporating redundancy is a function of which elements are made redundant. If an unreliable element is given malfunction protection in the form of redundancy, a considerable increase in system reliability can generally be realized; conversely, if a comparatively reliable device is made redundant, the relative improvement in system reliability is somewhat less.

In spite of the fact that some reliability gain can be obtained by redundancy, it is not a simple matter of indiscriminately adding redundant elements to effect reliability improvements. For example, failure sensing and switching elements may be necessary, not to mention the additional weight, volume, power, etc., required by the redundant elements themselves. The practicality or ease with which redundancy can be incorporated then becomes an important consideration. Due to the absence of detailed lander separation/stabilization system designs, the latter consideration becomes difficult to measure. Hence, the approach taken here combines a quantitative and qualitative analysis of system alternatives to obtain a ranking of reliability improvement expected by the use of redundancy.

*Table B-2 is a tabulation of the estimated inherent reliability of the lander separation and stabilization alternatives.

TABLE B-2

INHERENT RELIABILITY* OF LANDER SEPARATION AND STABILIZATION ALTERNATIVES

I. Lander Separation	
A. Release Mechanism	
1. Explosives	
a. Flexible Linear Shaped Charges	0.98200
b. Explosive Bolts	0.99974
2. Ball Lock Bolt	0.99790
3. Mechanical Latches	0.97850
4. Marmon Clamp	Data Not Available
B. Actuator Mechanism	
1. Spring	0.99160
2. Gas Generator	0.99435
3. Cartridge Actuated Device	0.98900
4. "Fly-Away"	0.98188
II. Lander Stabilization	
A. Spin Rockets	0.99070
B. Momentum Wheels	Data Not Available
C. Attitude Control System	0.98430

*Reliability predictions are based on data from Avco reliability demonstration tests and the FARADA Handbook. These estimates have been used as guidelines only.

d. Ranking of Design Alternatives

Each design alternative was then ranked - first, in terms of its inherent reliability and second, on the basis of its expected reliability improvement through redundancy. Lastly, these relative rankings were subjectively weighed to obtain a ranking of the system designs according to overall reliability potential. The latter rankings were used to recommend a technique for lander separation and stabilization.

3. Summary of Results

A summary of results, showing the system rankings, is presented in table B-3. In addition, brief comments describing reliability advantages and disadvantages are given for each alternative. As indicated by their top position in the overall reliability potential ranking, the technique recommended would employ a combination of mechanical latches and gas generators for lander separation and spin rockets for lander stabilization.

TABLE B-3

SUMMARY OF RESULTS
RELATIVE RANKINGS OF LANDER SEPARATION
AND STABILIZATION SYSTEM ALTERNATIVES

System Alternatives	Inherent Reliability Ranking	Reliability Improvement (Redundancy) Ranking	Overall Reliability Potential Ranking	Comments
I. Lander Separation				
A. Release Mechanism				
1. Explosives				
a. Flexible Linear Shaped Charges	4	2	2	Not inherently reliable because of interface between primacord and shaped charge; however, redundant shaped charges and squibs can easily be incorporated to increase reliability.
b. Explosive Bolts	1	3	3	Have the highest inherent reliability, but unless all bolts are sheared, release is not effected; redundancy cannot be simply applied by adding additional bolts; instead, each bolt must be made redundant within itself.

RE-ORDER NO. 64-524

TABLE B-3 (Cont'd)

System Alternatives	Inherent Reliability Ranking	Reliability Improvement (Redundancy) Ranking	Overall Reliability Potential Ranking	Comments
2. Ball Lock Bolt	2	3	4	Is nearly as inherently reliable as explosive bolts; is used on Avo re-entry programs; has essentially the same disadvantages as explosive bolts.
3. Mechanical Latches	3	1	1	Inherently not as reliable as the ball lock bolt or explosive bolts; nevertheless, offers the advantage of easily adding sufficient squibs to make the latch itself virtually failure-free; thus, the use of mechanical latches has the highest reliability potential.
4. Marmon Clamp	-	-	?	Not ranked; reliability information is not readily available.
B. Actuator Mechanism				
1. Spring	1	4	3	Is inherently the most reliable of those alternatives evaluated; offers the advantage of being able to test the same unit to be used on mission; disadvantageous in that the use of redundant springs does not appear to be straightforward and may result in an undesirable weight situation; another

RE-ORDER No. 64-524

TABLE B-3 (Cont'd)

System Alternatives	Inherent Reliability Ranking	Reliability Improvement (Redundancy) Ranking	Overall Reliability Potential Ranking	Comments
				disadvantage might be the problem of creep and possible loss of elasticity after being compressed and subjected to the uncertainties of the space environment during the transit phase.
2. Gas Generator	2	1	1	Is about as inherently reliable as a spring; can be made redundant by incorporating additional units to provide fail-safe situation; gas generators thus offer the highest reliability potential.
3. Cartridge Actuated Device	3	2	2	Not as inherently reliable as either the spring or gas generator, but a substantial increase in reliability can be realized by using redundant elements.
4. "Fly-Away"	4	3	4	Most complex, least inherently reliable and could present a probable weight and volume problem if redundancy is used on a large scale.

RE-ORDER No. 64-524

TABLE B-3 (Concl'd)

System Alternatives	Inherent Reliability Ranking	Reliability Improvement (Redundancy) Ranking	Overall Reliability Potential Ranking	Comments
II. Lander Stabilization				
A. Spin Rockets	1	1	1	Are inherently the most reliable; if necessary, redundant rockets can be added without much difficulty; thus, spin rockets offer the highest reliability potential.
B. Momentum Wheels	-	-	-	Not ranked; reliability information is not readily available.
C. Attitude Control System	2	2	2	Inherently, quite reliable due to the comparatively short mission time from separation; however, may be disadvantageous because of uncertainty concerning turn-on of units after transit phase; redundancy would not solve latter problem since redundant units would also be subjected to essentially the same "storage" environment.

RE-ORDER No. 64-524

338

APPENDIX C

BATTERY WEIGHT REQUIREMENTS AS DETERMINED BY MANEUVER MODE OPERATIONS

The energy storage capacity of the flyby/bus battery must be sufficient to allow battery operation throughout each of the major flight maneuvers and sequences. Evaluation therefore of both the maneuver durations and the power consumption profiles during each of these periods is necessary for the proper battery watt-hour capacity (and hence, battery weight).

A. ATTITUDE CONTROL SYSTEM MANEUVERS (ACS)

The attitude control system philosophy established for Mariner C is used for Advanced Mariner. Attitude control jets are nominally sized at a maximum thrust of 0.01 pound thrust per nozzle. This thrust is adjusted so that with the final vehicle cruise mode inertias, the maximum angular acceleration of the vehicle about pitch, roll, and yaw axes (I_Y, I_Z, I_X, respectively) will be 0.225×10^{-3} rad/sec^2. Accelerations after lander separation due to constant nozzle thrust and different values of vehicle inertia will of course be somewhat higher than in the cruise mode. Using the analysis and notation shown below, maximum angular acceleration can be calculated using $\dot{\theta}_{max} = 0.5$ deg/sec, $r_{jet} = 45.5$ inches and assuming two jet nozzles symmetrically located about each axis, operating additively.

Let

$$\ddot{\theta}_{max} = \frac{2Fr}{I} \qquad \text{(rad/sec}^2\text{)}$$

where

$\ddot{\theta}_{max}$ = Maximum angular acceleration about a particular axis, rad/sec^2.

F = Jet thrust of each nozzle, pounds, (two nozzles are assumed per axis in each direction).

r = Moment arm of a jet about the chosen axis, feet.

I = Mass moment of inertia of the configuration about the chosen axis, slugs-ft^2.

and

$$t_{acc} = \frac{\dot{\theta}_{max}}{\ddot{\theta}_{max}(57.295)} \qquad \text{(seconds)}$$

where

t_{acc} = Time to accelerate to maximum angular rate, ($\dot{\theta}_{max}$), at maximum acceleration, ($\ddot{\theta}_{max}$), seconds.

$\dot{\theta}_{max}$ = Maximum angular rate, as controlled by ACS, deg/sec.

Time for a given angular maneuver of M degrees will then be

$$t_M = \frac{M}{\dot{\theta}_{max}} + t_{acc} \qquad \text{(seconds)}$$

This allows for starting and stopping accelerations of the vehicle at the ends of the maneuver, when the maneuver magnitude, M, is larger than the angle at which maximum angular rate is reached. This angle, θ_{acc}, is defined as

$$\theta_{acc} = \ddot{\theta}_{max}\, t_{acc}^2 \, \frac{(57.295)}{2} \qquad \text{(degrees)}$$

For maneuver evaluation purposes in which the battery operation time requirement is to be maximized, 180-degree maneuvers are assumed. For the vehicle inertias considered, θ_{acc} is less than 20 degrees and the formula shown previously for t_M is used in all calculations. The effect of vehicle inertia on maneuver time is very small, and typical values of vehicle inertia have been used.

B. ATTITUDE CONTROL SYSTEM (ACS) MANEUVER CALCULATIONS

	Axis	X(Yaw)	Y(Pitch)	Z(Roll)
Cruise Mode	Inertia (slug-ft^2)	$I_X = 234$	$I_Y = 234$	$I_Z = 220$
	$\ddot{\theta}_{max}$ (rad-sec^2)	0.225×10^{-3}	0.225×10^{-3}	0.225×10^{-3}
	F_{jet}* (lbs)	6.943×10^{-3}	6.943×10^{-3}	6.528×10^{-3}
	$t_{180°}$ (sec)	398	398	398
Post-Lander Separation	Inertia (slug-ft^2)	$I_X = 101$	$I_Y = 101$	$I_Z = 177$
	F_{jet}* (lbs)	6.943×10^{-3}	6.943×10^{-3}	6.528×10^{-3}
	$\ddot{\theta}_{max}$ (rad/sec^2)	0.5213×10^{-3}	0.5213×10^{-3}	0.2797×10^{-3}
	$t_{180°}$ (sec)	377	377	391

*Adjusted at final assembly from 0.01 pound nominal value, to give proper $\ddot{\theta}_{max}$ in cruise mode configuration.

C. EQUIPMENT

A summary of spacecraft power-consuming equipment has been prepared and is included as table C-1.

D. PROPULSION BURN TIMES AND FLIGHT SEQUENCE EVALUATION

Tables C-2 through C-7 have been prepared using a variable value for the propulsion system thrust level.

A first approximation can be made for the propulsion burn times in terms of the flyby bus rocket motor thrust. Assume the same fixed thrust engine is used for both the midcourse correction maneuver of the combined bus and lander (with a ΔV of 100 ft/sec) and the bus slowdown maneuver after lander separation, with a ΔV of 912 ft/sec. From momentum considerations, neglecting mass loss due to propellant usage:

$$FB = m\Delta V \qquad \text{(lb-sec)}$$

where:

Parameter	Identification	During Midcourse Maneuver	During Bus Slowdown
F	Rocket thrust	1-250 (lbs)	1-250 (lbs)
B	Burn time	B_m (sec)	B_s (sec)
m	Vehicle mass	46.58 (1500 lbs)	24.84 slugs (800 lbs)
ΔV	Velocity increment	100 (ft/sec)	912 (ft/sec)

then:

$$B = \frac{m\Delta V}{F} \text{ (sec)}$$

Using the various computed individual maneuver characteristics in combination, the more important specific flight sequence durations have been obtained. They are:

1. Prelaunch through initial cruise, table C-2 and table C-3.
2. Midcourse correction, table C-4 and table C-5.
3. Separation and bus slowdown, table C-6 and table C-7.

TABLE C-1

POWER CONSUMING EQUIPMENT

System	Item No.	Item Name	No. in System	System Power (watts)	Comments	System Raw Battery Power Multiplier*	System Raw Battery Power (watts)
Stabilization and Control System	1.a.	Gyro/Electronics	1	13.0	Warmup	1.515	19.70
	b.			21.0	Rate Mode	1.515	31.82
	c.			50	Integrate Mode	1.515	75.75
	2.	Gyro/Electronics	1	10		1.718	17.18
	3.	Canopus Star Tracker	1	7.2		1.433	10.32
	4.	Limit Cycle Sun Sensor	1	0.5		1.433	0.72
	5.	Course Acq. Sun Sensor	1	0.35		1.433	0.50
Attitude Control System	6.	Solenoids	12 (4/axis)	6.0	1 Axis, 2 on continuously, except during rocket burn	1.433	8.60
	7.	Control Electronics	1	2.5		1.433	3.58
Thrust Vector Control System	8.	Cold Gas Solenoids	4	10.0	(2 at 5 watts each, on during rocket burn only)	1.433	14.33
Communications System	9.	Power Amplifier Power Supply	1	30.0		1.031	30.93
	10.	S-Band Transponder	1	16.0		1.433	22.93
	11.	Telemetry	1	13.0		1.433	18.63
	12.	D.A.S.	1	8.0		1.433	11.46
	13.	Command Subsystem	1	4.5		1.433	6.45
	14.	CC&S	1	7.0		1.433	10.03
Scientific Instrumentation	15.	Cosmic Dust Detector	1	0.2		1.433	0.29
	16.	Micrometeoroid Detector	1	0.5		1.433	0.72
	17.	Ion Chamber	1	0.1		1.433	0.14
	18.	Particle Flux Detector	1	0.35		1.433	0.50
	19.	Magnetometer	1	5.0		1.433	7.17
Power System	20.	Power Synchronization	1	1.0		1.289	1.29
	21.	Lander Heater	1	15.0		1.031	15.57

*Based on power distribution system efficiencies and power flow diagram shown in power section.

$$\text{Multiplier} = \frac{1}{\text{Total Series Efficiency from Equipment to Battery}}$$

RE-ORDER No. 64-524

342

RE-ORDER No. 64-524

TABLE C-2

PRE-LAUNCH THROUGH INITIAL CRUISE MODE SEQUENCE

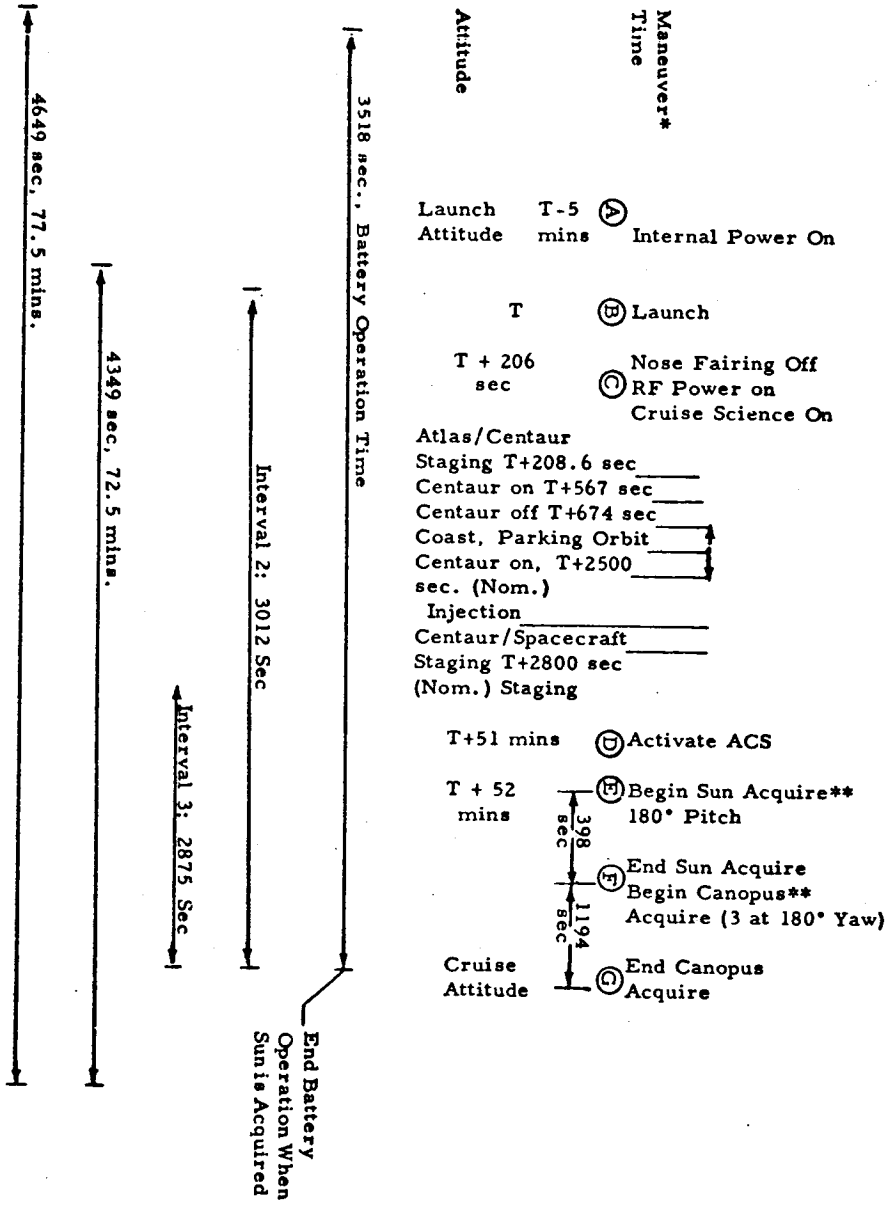

* 180 degree maneuvers are assumed, in order to maximize battery operation time. During Canopus acquisition, 3 such maneuvers are assumed as a worst case.

** See paragraph of ACS Maneuver Characteristics, using appropriate maneuver times for the appropriate mode.

303

RE-ORDER No. 64-524

TABLE C-3

POWER CONSUMPTION ANALYSIS - PRE-LAUNCH THROUGH INITIAL CRUISE MODE SEQUENCE

Event	Event Designation	Time	Power Consuming Equipment**	Raw Power Requirements (watts)	Duration (seconds)	Power (watt-hrs)
Pre-launch	A	T-300 sec.	On: 1a, 2, 3, 4, 5, 7, 10, 11, 12, 13, 14, 20	122.79	506 A to C	17.26
Launch	B	T+0				
Centaur Fairing Ejection	C	T+206 secs.	On: A equipment plus 1b, 9, 15, 16, 17, 18, 19; minus 1a.	174.66	2854 C to D	138.47
Activate ACS	D	T+51 mins.	On: C equipment plus 6	180.66	60 D to E	3.01
Begin Sun Acquire	E	T+52 mins.	On: D equipment	180.66	398 E to F	19.96*
End Sun Acquire Begin Canopus Acquire	F	T+ 58.7 mins.	On: D equipment	180.66		

Total watt-hrs. required from battery 178.70

at 37 watt-hrs./lb., battery weight required = 178.70/37.0 = 4.83 pounds.

*Assume that at event F, sun has been acquired, and battery operation ceases.
**See table C-1.

344

TABLE C-4

MIDCOURSE MANEUVER SEQUENCE

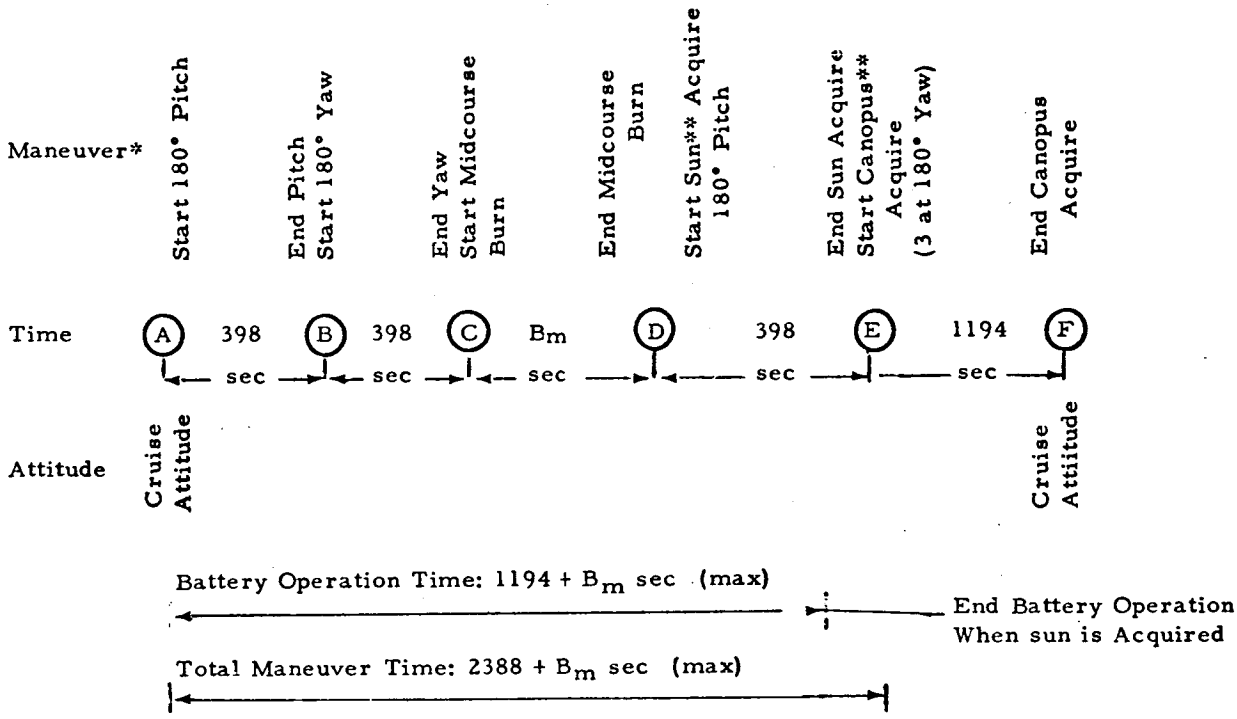

* 180° Degree maneuvers are assumed, in order to maximize battery operation time. During Canopus acquisition, 3 such maneuvers are assumed as a worst case.

** See paragraph of ACS Maneuver Characteristics using appropriate maneuver times for the appropriate mode.

TABLE C-5

POWER CONSUMPTION ANALYSIS - FIRST MIDCOURSE MANEUVER SEQUENCE

Event	Event Designation	Time	Power Consuming Equipment**	Raw Power Requirements (watts)	Duration (seconds)	Power (watt-hrs)
End cruise mode. Start 180° pitch.	A	T = 0 (sec)	On: 1c, 2, 3, 4, 5, 6, 9, 10, 11, 12, 13, 14, 15, 16, 17, 18, 19, 20, 21.	234.06	398 A to B	25.88
End pitch. Start 180° yaw	B	T+398 (sec)	Same as A	234.06	398 B to C	25.88
End yaw. Start mid-course burn.	C	T = 796 (sec)	Same as B, plus 8, 1b; minus 1c.	204.46	B_m C to D	.057 B_m
End mid-course burn Start Sun acquire, 180° pitch.	D	T = 796+B_m (sec)	Same as A	234.06	398 D to E	25.88
End Sun Acquire. Start Canopus Acquire, 3 x 180° yaw.	E	T = 1194+B_m (sec)	Same as A	234.06	1131 E to F	*
End Canopus Acquire. Resume cruise mode.	F	T = 2388+B_m (sec)				

Total watt-hrs. required from battery $77.64 + 0.057\ B_m$

at 37 watt-hrs/lb., battery weight required $= (77.64+0.057B_m)/37.0$ (lbs)

*Assume that at event E, sun has been acquired, and battery operation ceases.
**See table C-1.

346

RE-ORDER No. 64-524

TABLE C-6

SEPARATION AND BUS SLOWDOWN SEQUENCE

Maneuver*	Time**	Configuration
Start 180° Pitch (A)		Cruise Attitude
	398 sec	Bus & Lander Configuration
Stop Pitch, Start 180° Yaw (B)		
	398 sec	
Stop Yaw, Eject Lander, Start 180° Pitch (C)		Separation Attitude
	377 sec	Bus Only Configuration
Stop Pitch, Start 180° Yaw (D)		
	377 sec	
Stop Yaw, Start Engine Burn (E)		Slowdown Attitude
	B_s sec	
Stop Engine Burn, Start 180° Pitch To Acquire Sun (F)		Slowdown Attitude
	377 sec	
Stop Pitch, sun Acquired, Start 3 at 180° Yaw to Acquire Canopus (G)		Sun Oriented
	1131 sec	
End Yaw (H)		Cruise Attitude

Battery Operation Time 1927 + B_s (sec)

End Battery Operation When Sun is Acquired

Total Maneuver Time 3058 + B_s (sec)

796 sec

754 sec

B_s

1508 sec

1550 sec

*180 degree maneuvers are assumed, in order to maximize battery operation time During Canopus acquisition, 3 such maneuvers are assumed as a worst case.

**See paragraph of ACS Maneuver Characteristics using appropriate maneuver times for the appropriate mode.

347

RE-ORDER No. 64-524

TABLE C-7

POWER CONSUMPTION ANALYSIS - BUS/LANDER SEPARATION AND BUS SLOWDOWN SEQUENCE

Event	Event Designation	Time	Power Consuming Equipment**	Raw Power Requirements (watts)	Duration (seconds)	Power (watt-hrs)
End cruise mode. Start 180-degree pitch.	A	T = 0 (sec)	On: 1c, 2, 3, 4, 5, 6, 9, 10, 11, 12, 13, 14, 15, 16, 17, 18, 19, 20, 21	234.06	398 (A to B)	25.88
End pitch. Start 180-degree yaw.	B	T = 398 (sec)	Same as A	234.06	398 (B to C)	25.88
End yaw. Eject lander Start 180-degree pitch.	C	T = 796 (sec)	Same as A minus 21	218.59	377 (C to D)	22.89
End pitch. Start 180-degree yaw.	D	T = 1173 (sec)	Same as C	218.59	377 (D to E)	22.89
End yaw. Start slowdown burn.	E	T = 1550 (sec)	Same as C, plus 8, 1b minus 1c.	188.99	B_s (E to F)	.0525 B_s
End slowdown burn. Start Sun acquire, 180-degree pitch.	F	T = 1550 + B_s (sec)	Same as C	218.59	377 (F to G)	22.89
End sun acquire. Start Canopus acquire, 3 x 180-degree pitch.	G	T = 1927 + B_s	Same as C	218.59	1131 (G to H)	*
End Canopus acquire. Resume cruise mode.	H	T = 3058 + B_s (sec)				
				Total watt-hrs. required from battery		120.43 + 0.0525B_s

at 37 watt-hrs/lb., battery weight required = $\frac{120.43 + 0.0525\ B_s}{37.0}$ (lbs.)

*Assume that at event G, Sun has been acquired, and battery operation ceases.
**See Table C-1.

348

The first-named tables in each of the above-mentioned sequences show maneuver sequence time breakdowns, and the last-named indicate the equipment usage and evaluate the battery capacity and weight requirements.

E. PROPULSION THRUST LEVEL CORROBORATION

Using tables C-2 through C-7 and allowing the propulsion thrust level to vary, thrust level has been selected from a battery weight optimization standpoint. Low thrust levels are desirable, since for fixed burn time errors, low thrust levels minimize velocity increment errors. Figure C-1 shows the battery weight requirements versus thrust level. It can be seen that the flyby/bus-lander separation and bus slowdown sequence, combined with the prelaunch through initial acquisition sequence, determine the optimum thrust level to be 20.5 pounds and that for thrust levels greater than this (such as the 25-pound level chosen) a weight margin exists. The use of conservatively long maneuver excursions and their resultant times further increases this margin. The minimum weight battery, at 25 pounds thrust level is 4.83 pounds and delivers 178.7 watt-hrs. of power (see figure C-1 and table C-3).

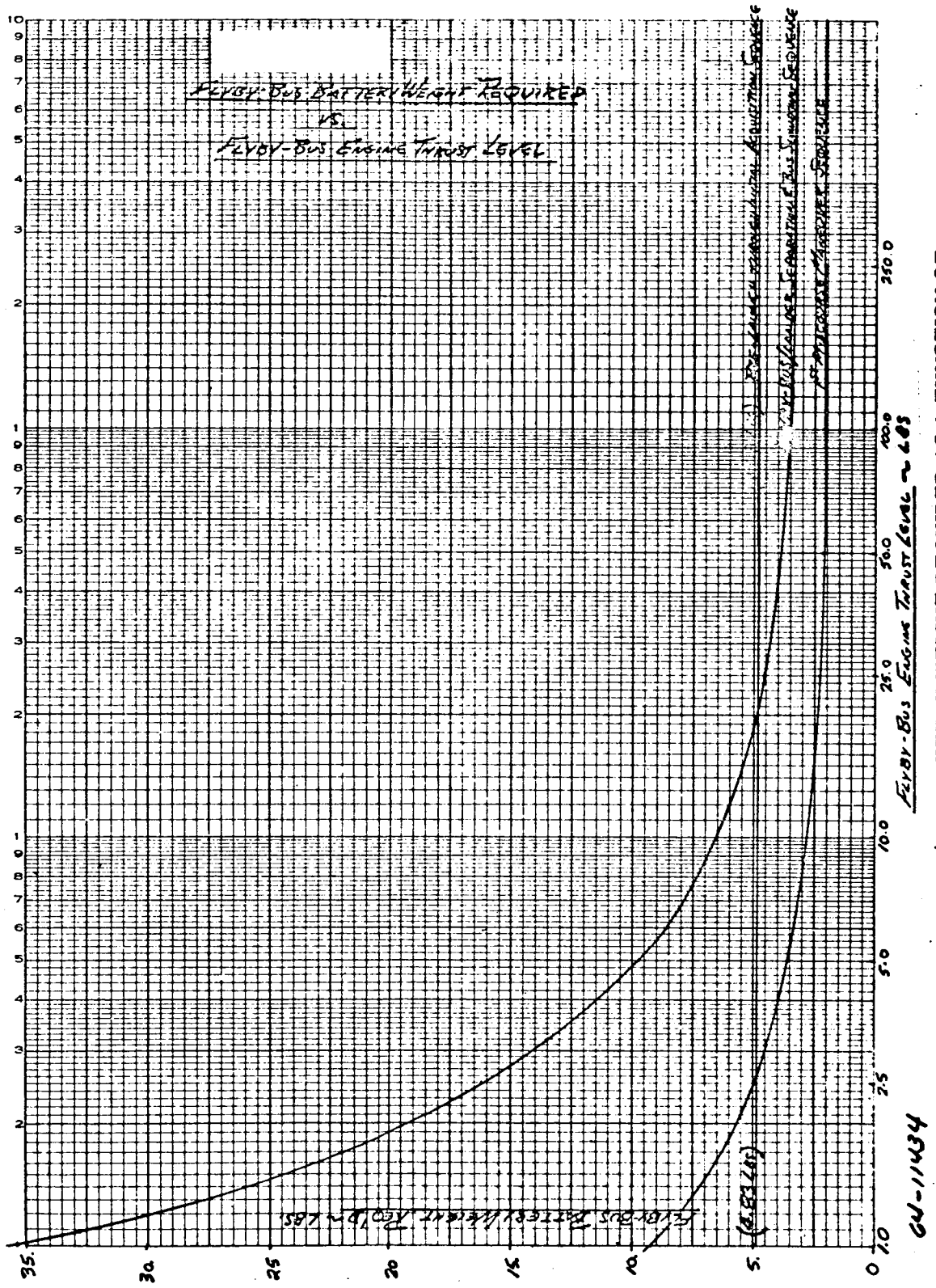

Figure C-1 FLYBY/BUS BATTERY WEIGHT REQUIRED AS A FUNCTION OF FLYBY/BUS ENGINE THRUST LEVEL

APPENDIX D

SEPARATION SPRING ANALYSIS

Assume that the lander and flyby/bus act as a two-mass system, being separated by a central spring, as in Figure D-1.

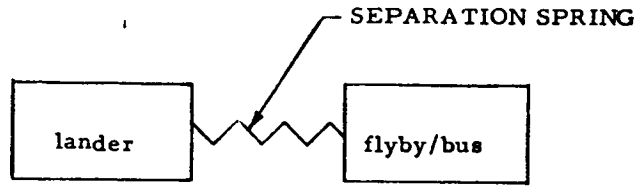

64-11486

Figure D-1 TWO MASS SYSTEM

The lander is assumed to weigh 600 pounds, and the flyby/bus is assumed to weigh 900 pounds (both Earth weights). From momentum considerations the linear momentum of each vehicle of the separated system must be equal. Denoting the lander by subscript L and the bus by subscript B

$$\frac{W_L V_L}{32.2} = \frac{W_B V_B}{32.2} \text{ (lb – sec)}$$

and

$$V_{relative} = V_L + V_B$$

From energy considerations

$$\frac{1}{2} k_T \delta^2 = \frac{1}{2} \frac{W_L V_L^2}{32.2} + \frac{1}{2} \frac{W_B V_B^2}{32.2}$$

where

k_T = total spring constant

P_i = initial total spring force

δ = the spring travel

Substituting

$$k\delta = P_i \quad \text{and} \quad V_B = V_{rel} - V_L = \frac{W_L V_L}{W_B},$$

then

$$P_i\delta = \frac{W_L}{32.2} V_L^2 + \frac{W_B}{32.2}\left(\frac{W_L}{W_B} V_L\right)^2 = 31.02\, V_L^2$$

We shall consider three cases, namely $V_L = 1.0$, 2.0, and 3.0 ft/sec.

Two configurations are investigated: three springs in a plane and equally spaced at 120 degrees to each other in a circle of radius R about the vehicle c.g. with their resultant force through the lander and bus c.g.'s and a single spring (in the previously defined plane), located so that its resultant force is through the lander and bus c.g.'s.

Figures D-2 and D-3 present the results of the calculations using the aforementioned equation for the three-spring and single-spring cases respectively.

Considering the single-spring system, it can be seen that the force diagram of figure D-4 may be used to define the single-plane vehicle dynamics during separation.

Assuming that an offset e occurs in the plane of the minimum vehicle rotational inertia, the maximum values will be obtained for θ_{max} and $\dot{\theta}_{max}$ the vehicle angular excursion and rotational excursion rate at the end of the separation pulse. No attitude control system resistance torques are assumed to be acting during the separation pulse. The spring force will be

$$P = P_i \cos \omega t$$

352

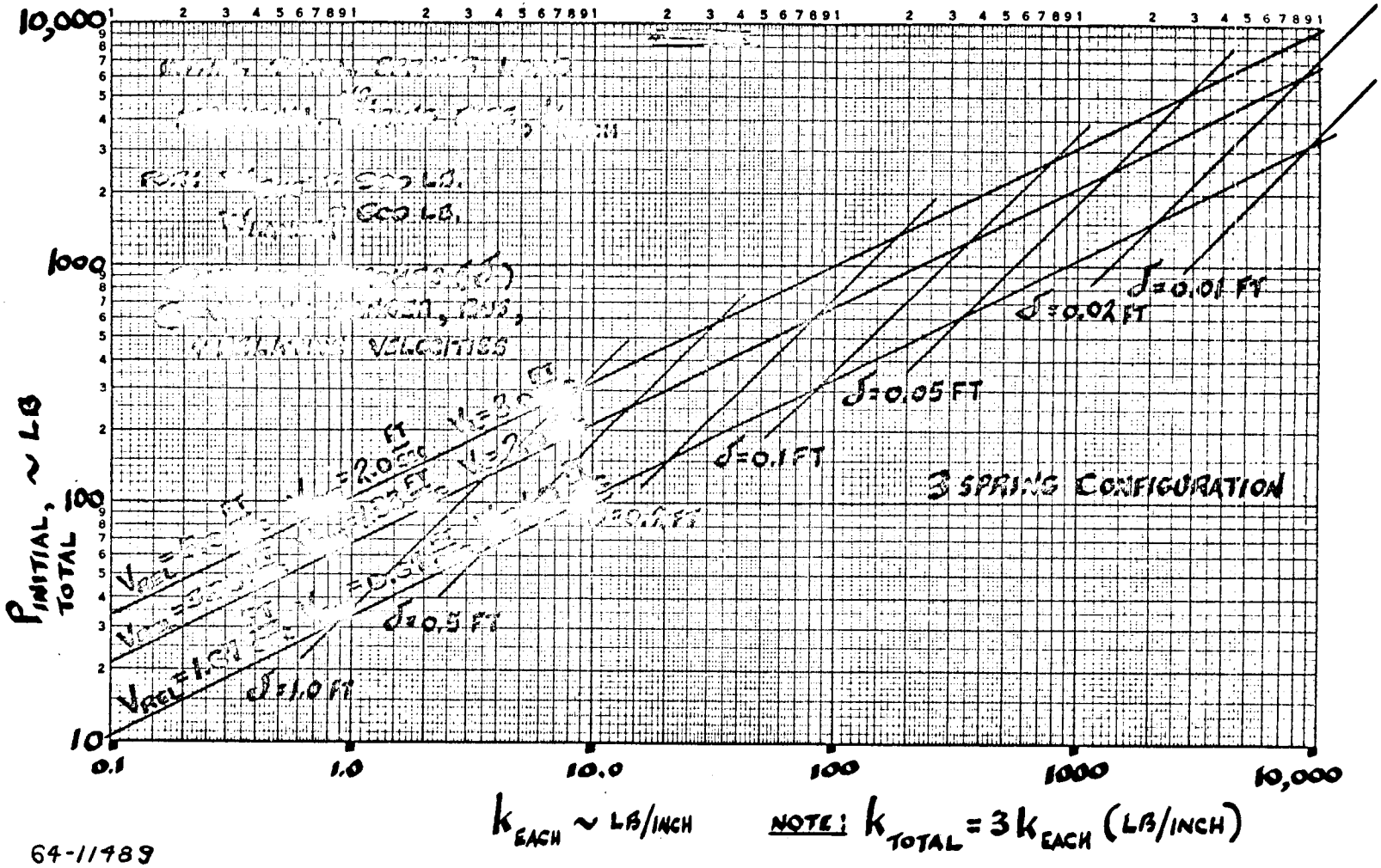

Figure D-2 INITIAL TOTAL SPRING LOAD AS A FUNCTION OF INDIVIDUAL SPRING RATE - 3-SPRING CONFIGURATION

RE-ORDER No. 64-524

353

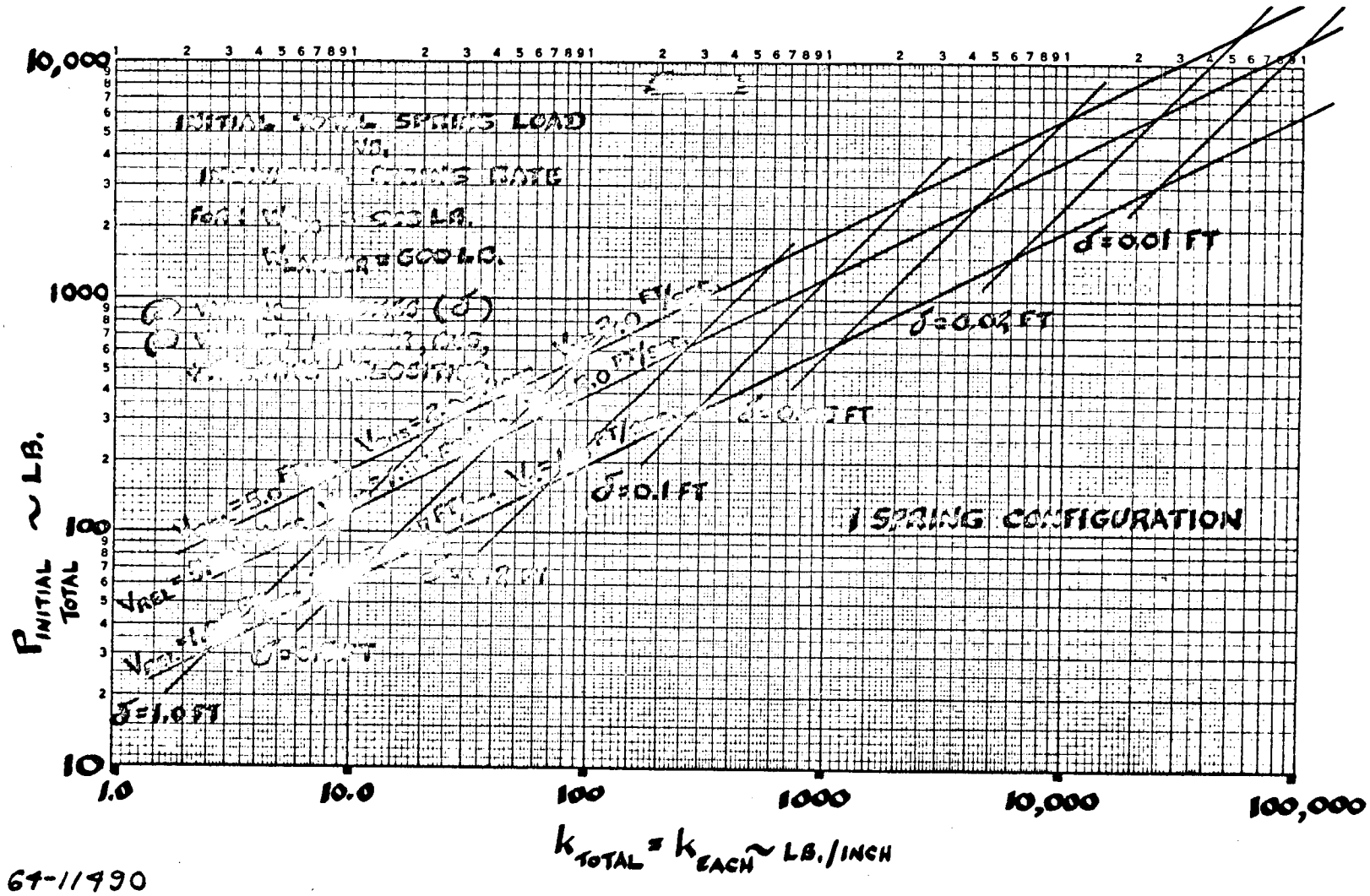

Figure D-3 INITIAL TOTAL SPRING LOAD AS A FUNCTION OF INDIVIDUAL SPRING RATE - 1-SPRING CONFIGURATION

RE-ORDER No. 64-524

354

RE-ORDER No. 64-524

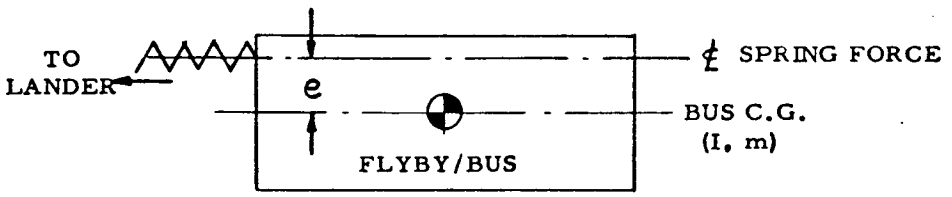

64-11487

Figure D-4 FORCE DIAGRAM

355

where

ω = Flyby/bus-lander system frequency (two mass/central spring configuration, see figure D-1), rad/sec

and

$$\omega = \left(\left[\frac{W_{lander} + W_{bus}}{W_{lander} \times W_{bus}} \right] g k \right)^{1/2} \text{(rad/sec)}$$

where

$g = 32.17 \text{ ft/sec}^2$.

For the values assumed previously,

$\omega = 0.2989 (k_t)^{1/2}$ (rad/sec), k_t in lbs/ft.

This relationship is shown on figure D-5. Let Applied Torque = Inertial Resistance Torque (assume constant e)

$$e P_i \cos \omega t = I \ddot{\theta}$$

or

$$\ddot{\theta} = \frac{e P_i \cos \omega t}{I}$$

If it is assumed that the spring force acts during one quarter of a sinusoidal cycle, as shown in figure D-6, it may be said that at the end of the pulse (if no initial angular velocities or offsets are present):

$$S/B\dot{\theta} = \int_0^{\pi/2} \ddot{\theta} \, dt = \int_0^{\pi/2} \frac{e P_i}{I} \cos \omega t \, dt$$

356

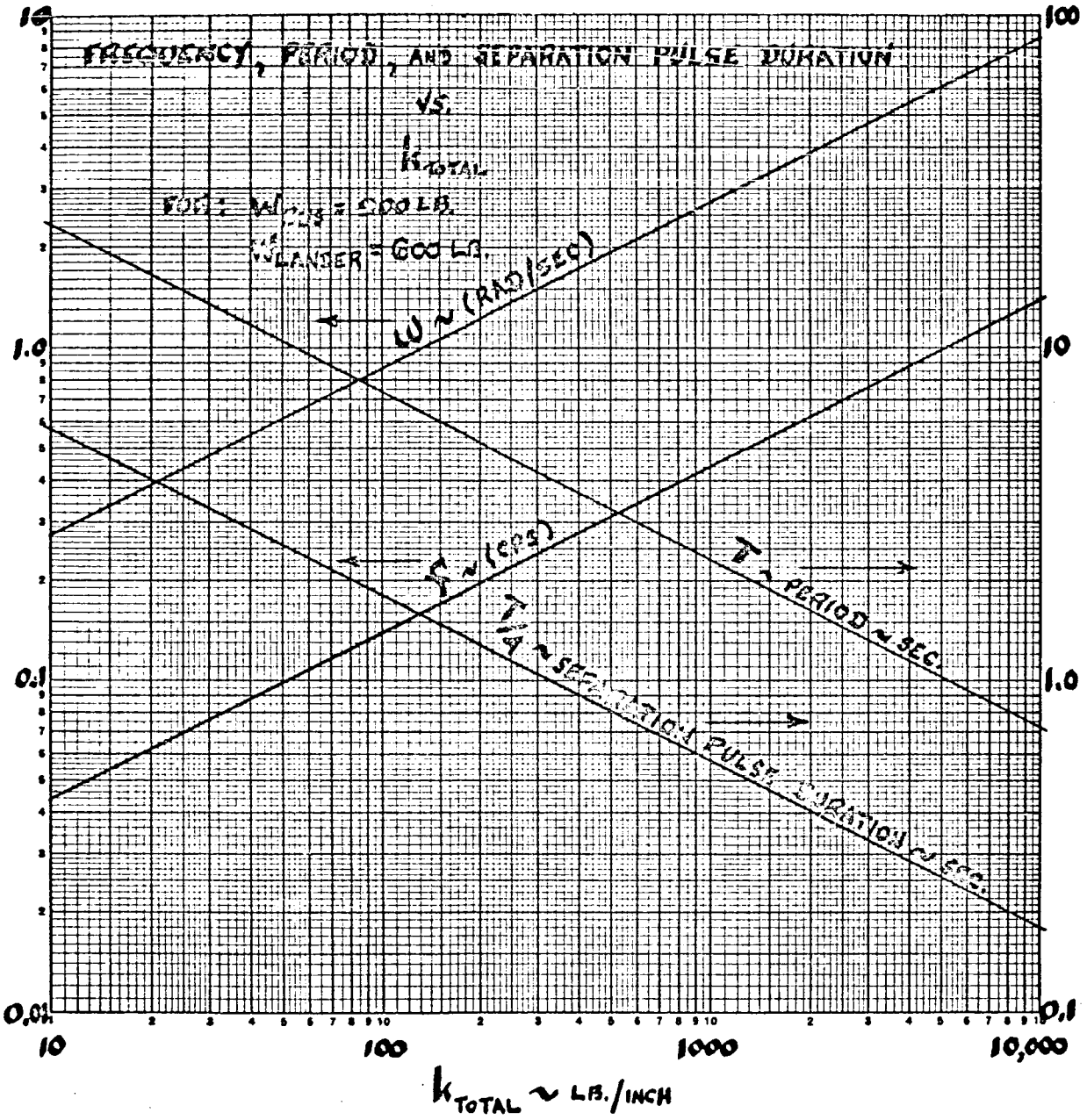

64-11491

Figure D-5 FREQUENCY, PERIOD, AND SEPARATION PULSE DURATION AS A FUNCTION OF SPRING RATE

357

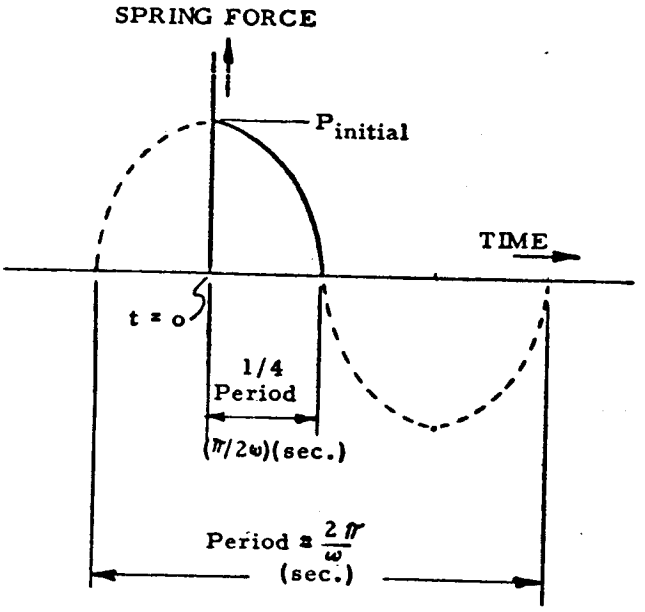

64-11488

Figure D-6 SPRING FORCE AS A FUNCTION OF TIME

Inserting the limits of integration and initial zero boundary conditions and solving for the maximum value, which occurs at the upper limit,

$$\dot{\theta}_{max} = \frac{e P_i}{I\omega} \text{ (rad/sec)}$$

In a like manner, solving for the angular displacement at the end of the spring stroke

$$\theta_{max} = \frac{e P_i}{i\omega^2} \text{ (radians)}$$

Thus $\dot{\theta}_{max} = S/B\,\omega\,\theta_{max}$ figure D-7 shows $\omega^2\theta_{max}$ and $\omega\dot{\theta}_{max}$ plotted versus P_i for several values of e for a typical range of inertias (I values).

358

RE-ORDER No. 64-524

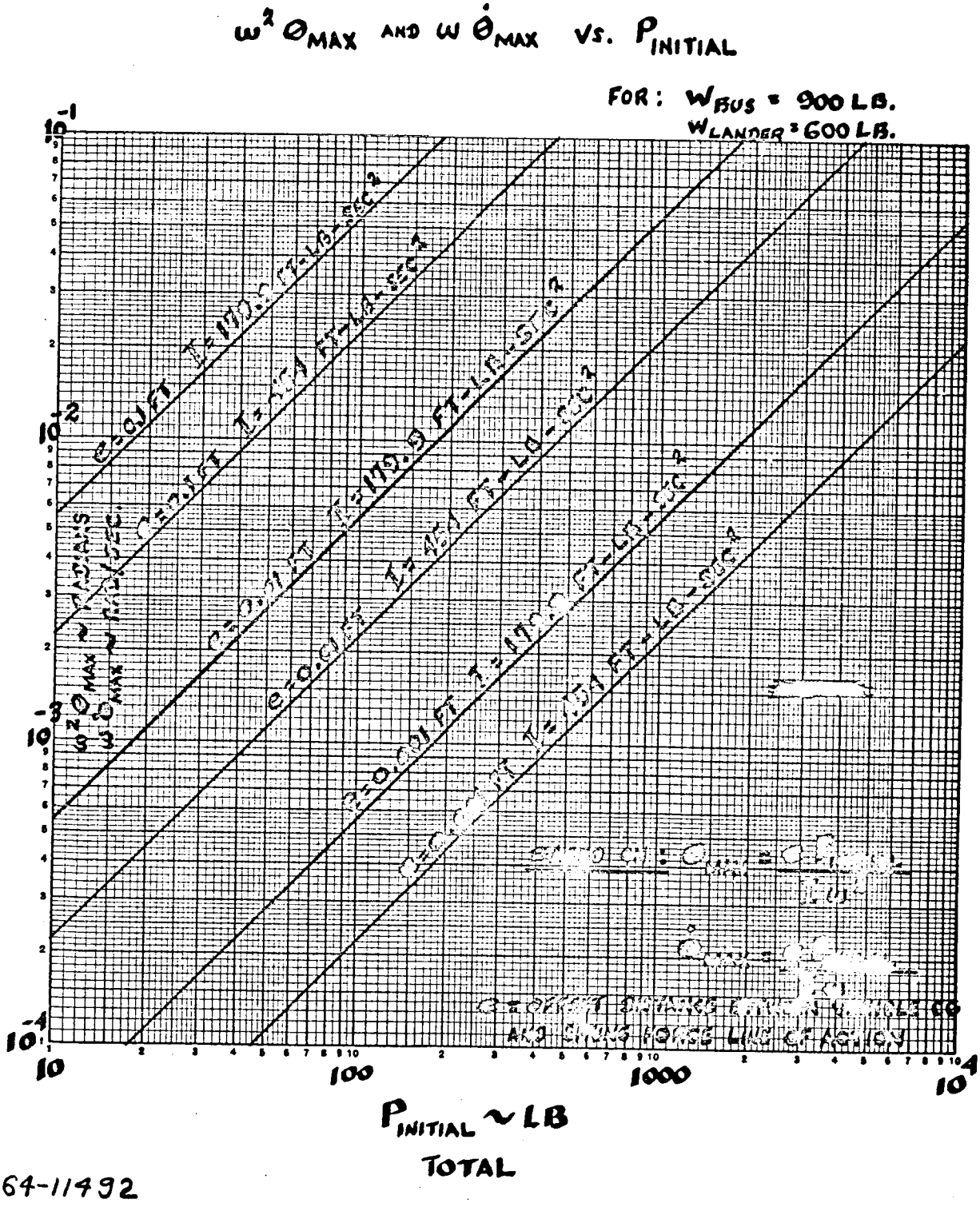

Figure D-7 $\omega^2\theta_{max}$ AND $\omega\dot{\theta}_{max}$ AS A FUNCTION OF INITIAL TOTAL SPRING LOAD

357

Typical Example of Chart Usage -- Single Spring System

From Figure D-3: Choose P_i = 100 lbs, V_L = 1.0 ft/sec. Read k = 26.5 lbs/inch.

From Figure D-5, at k_t = 26.5 lbs/inch, ω = 0.445 rad/sec., and T/4 = separation pulse duration = 3.55 sec.

From Figure D-7, at P_i = 100 lbs, e = 0.01 foot (0.12 inches), I = 179.9 ft-lb-sec^2, read $\omega^2 \theta_{max} = \omega \dot{\theta}_{max} = 5.5 \times 10^{-3}$. Thus: θ_{max} = 1.591 degrees and $\dot{\theta}_{max}$ = 0.708 degrees/second.

It should be noted that for the three-spring case, figures D-2, D-5, and D-7 can be used, if in figure D-7 the offset distance e is taken between the vehicle c.g. and the spring force resultant line of action for the three springs. This analysis of course depends on the geometry of the problem not being such that e varies during the separation stroke.

For the conceptual design the three-spring case was chosen as nominal to better accommodate the flyby/bus and lander design features at the separation plane and to be compatible with the vehicular tie-down system.